UNIVERSITÀ
DEGLI STUDI
FIRENZE

DOTTORATO DI RICERCA IN SCIENZE CHIMICHE

Ciclo XXX

Coordinatore Prof. Piero Baglioni

Polyfunctional Receptors for Ionic Species: Theoretical and Applicative Aspects.

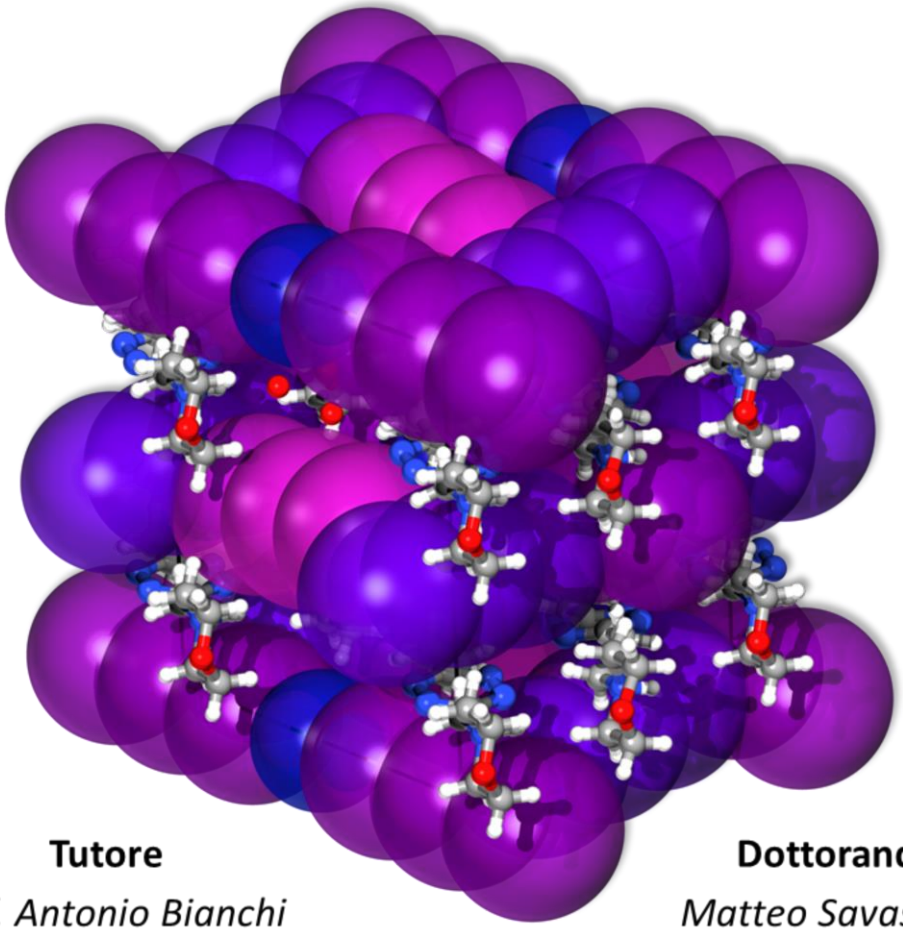

Tutore

Prof. Antonio Bianchi

Dottorando

Matteo Savastano

UNIVERSITÀ
DEGLI STUDI
FIRENZE

DOTTORATO DI RICERCA IN SCIENZE CHIMICHE

CICLO XXX

COORDINATORE Prof. Piero Baglioni

POLYFUNCTIONAL RECEPTORS FOR IONIC SPECIES: THEORETICAL AND APPLICATIVE ASPECTS.

Settore Scientifico Disciplinare CHIM/03

Dottorando
Dott. Matteo Savastano

_____
(firma)

Tutore
Prof. Antonio Bianchi

_____
(firma)

Coordinatore
Prof. Piero Baglioni

_____
(firma)

Anni 2014-2017

Then began I to thrive, and wisdom to get,

I grew and well I was;

Each word led me on to another word,

Each deed to another deed.

Hávamál, 141

1 INTRODUCTION

1.1 CATION AND ANION COORDINATION CHEMISTRY

Among the several possible ways to rationalize the present work, two choices appear as the most significant as well as the most suggestive: One could divide the research herein presented in two branches following either the laws of Nature, distinguishing cations from anions, or following the laws of Man, thus making a distinction between applied and basic research. Interestingly, both ways lead to discriminate cation and anion coordination chemistry.

I confess to be under some kind of fascination, but, if my Reader pleases to bear with me awhile, I think I can make him share, or at least comprehend, my point of view.

Now, please take into consideration any other possible couple of fields of research or objects of study: You will realize that finding a pair which is akin as anion and cation coordination chemistry is not an easy task, especially considering that the two are intertwined from the roots of the fundamental properties of matter upwards, since, apparently, a Demiurge of sort prescribed there should be no plus without a minus and *vice versa*.

Per se, this may not be anything special, yet you should consider that these two twin fields require significantly different approaches and tools from a chemical perspective, making one of them considerably more accessible experimentally: this is bound to appear as a peculiar anomaly to the uninitiated, who is led to ascribe this fact to some weird practical difficulties or theoretical technicalities; in truth, from a chemical point of view, there is far more than a vertical bar distinguishing a plus from a minus.

Finally, to close the gap, you have to know how such long unforeseen differences, with their inner tendency to favour one field over the other, joined spectacularly humanity's contingent needs, leading to an even more asymmetric historical development.

At the end of the day, anion coordination chemistry accumulated almost a century of delay compared to its cationic partner. Such disproportion appears in its full extent if confronted with the whole lifespan of modern chemistry, three centuries at most if we start counting midway between Boyle and Lavoisier, especially considering that modern cation coordination chemistry was not an early bird either (Alfred Werner was its first Nobel prize in 1908), and that, for better or for worse,

the number of scientists increased significantly over time, especially in the last century.

Before we dive into the chemistry of this, I would like to provide a brief historical context to explain the choices made so far by the scientific community. Allow me to say that I undertake this duty very gladly, yet heavy-hearted: a throughout narration, drawing a proper parallel between History and the development of Science, especially in an age of great discoveries like the XIXth and XXth century, when the wildest hypotheses were advanced and often confuted, is unachievable here, deserving far another space and likely a better author.[1]

Cation coordination chemistry, as pointed out above, is experimentally more accessible than anion's, yet the historical reasons for the early blooming of the former should probably be ascribed to mankind compulsion for metals: it is not fortuitous that the term "metal" seems to arise from a Greek verb meaning "to look for".

Since humanity's early days, our ancestors experienced the fascination exerted by small shiny pieces of metal, mainly copper and gold, not impossible to find in veins in their elemental state and very easy to distinguish from the common rocks. Undoubtedly our progenitors used them as ornaments and talismans, crafting them in complex shapes, as metals were so ductile and malleable compared to any other material they possessed: little they know that those tiny glittering trinkets were to end forever the customs and traditions of the Stone Age and start the Ages of metals. It all probably began when somebody realized how easy it was to obtain a cutting edge from a piece of metal compared to the effort required to chip a stone, or how readily a blunt metal blade could be sharpened again: soon bronze-armed warriors conquered vast extent of the known world only to be defeated, in later times, by those possessing the secret of iron smelting.

Drawing a parallel between such ancient times and modern era may seem out of place, yet many of the fantasies which shaped the way of thinking in the past, making their mark on the development of thought, turned out to be feasible.[2] Much of this heritage is probably bound to be relegated forever among the scientific curiosities, like the production of gold from lead, yet some of our contemporary improvements, like the use of metals in medicine, descend directly from ancient beliefs. Notwithstanding the difference between a shaman administering magic

[1] The amateur Reader is gladly addressed to a "Short History of Chemistry" by Isaac Asimov, and his amazing ability to plainly explain scientific matters. The initiated will probably find the books by Salvatore Califano, a renowned scholar who was based here in Florence for many years, more fitting.
[2] "What is now proved, was once only imagined." William Blake.

pieces of metal to the sick and the use of cisplatin in nowadays hospitals for the treatment of certain tumours, [3] one cannot deny the existence of a direct connection, perpetuated through the centuries by the efforts of many unknown charlatans and trailblazing empiricists. Human mind demonstrated unyielding in pursuing his desires.

Now, with a dizzying leap, we are on the brink of the XXth century and modern chemistry is more or less in place to start discovering how charged species behave and interact. Yet, when faced with the choice between cations and anions, the formers were preferred due to the same mindset we demonstrated throughout our history: most metals are found in nature as cations, understanding how cations behave, and mastering them, seemed the key to an unprecedented breakthrough. Although the understanding of the matter was much scarcer than it is now, with chemists and physicists still debating on the nature of charged species while trying to figure why they could "isolate" the atom of electricity bearing the negative charge (nowadays called electron) but not its positive counterpart, some major improvements were made in those years, again coming out on the side of metals: two methods allowed the large-scale production of both aluminium and steel at affordable prices, which, up to date, are still the backbone of our infrastructure and machinery.

Cation coordination chemistry did indeed bear fruit, and it is still blooming in present days: metal extraction from ores, dyes, catalysts, the understanding and use of several electrochemical processes (among which metal electrodeposition), a number of medical uses (*e.g.* complexes as drugs, ligands to cure metal poisoning, contrast agents for imaging) and many more applications arose from this discipline.

Now the questions that come to mind are: "what about anions?", and even "why suddenly people started bothering with anion in the second half of XXth century? Why at that time and not before, or after?".

Concerning the importance of anions and their binding, just citing a simple fact will suffice to do justice on the matter: Life is able to selectively recognize, bind and transform many anionic species, and it has become so good at it that over 70% [1] of all enzymatic substrates or cofactors are of anionic nature.

Let's just take a well-known, although fundamental, pathway: the Krebs cycle. All those weird -ate names, about ten (citrate, cis-aconitate, isocitrate, *et cetera*), each of them is an anion, and if you look closely, you will see that they are strictly related from a structural point of view. Nevertheless, our enzymes are capable to

[3] "Any sufficiently advanced technology is indistinguishable from magic." Arthur C. Clarke.

distinguish among them and operate selectively the required reaction, each on its own designated substrate: the whole thing is carried out so smoothly and efficiently that our cells have the impression of being just breathing.

As to the when, probably my Reader has already smelled out the kind of answer from the nature of the examples, we may say that things followed their natural order, going towards an increasing complexity. By this I do not imply any subordination nor any speculative or pragmatic superiority of one field over the other: I want only to suggest that, unless fate favours a serendipitous discovery much ahead of time, the strongest interactions, the phenomena which manifest more plainly and the starting materials which require the less sophisticated tools are simply more prone to draw attention and be objects of investigation. Without yet entering in the different chemistry of anion and cation coordination, it is safe to say that the latter are generally forming much stronger interactions with their receptors, sometimes displaying striking change in colour upon binding, while often possessing a higher stability even under energetic treatment.

Another good point, concerning the time of development, concerns the feasibility: understanding the possible implication of developing a field of research is a thing, but only when knowledge and technical means are mature enough, theoretical interests may start taking a more pragmatic twist. The milestone signalling that the way has been opened is surely the 1987 Nobel prize to Donald J. Cram, Jean-Marie Lehn and Charles J. Pedersen, for the establishment of Supramolecular Chemistry, of which anion coordination chemistry is but a fraction.

Finally, the world has been changing quite a lot in the last century: the scientific community payed more attention on the biological role of anions, some anthropogenic anions started posing environmental problems [4] and, inevitably, some anionic species found applications or raised special interest.[5]

All of this contributed to increase the awareness of the importance of studying anions and their selective recognition and binding.

[4] *e.g.* phosphate and nitrate used in agriculture, nitrate again and sulphate from fuels combustion, perchlorate from explosives, along with some weird species otherwise non-existent in nature, like the oxyanions of technetium from ^{238}U fission.

[5] *e.g.* the I^-/I_3^- redox couple and its application in solar cells, really polyiodides in general, both from a theoretical point of view and as solid-state conductors for special devices.

1.2 A Statement of Purpose

Contrary to what is commonly done in most thesis, I would like to anticipate the aim of the present work right in the opening, hoping that an early declaration of intent could facilitate the reading.

Following our brief historical excursus, we may say that the main difference between the chemistry of the last 50 years and that of older times, is arguably the fact that theory is developed enough, and in a sufficient number of fields, to allow chemists to make at least informed prediction, if not high-level calculations, on the properties of interest of molecules or compounds.

Whatever the designated destination, designing, simulating and screening became the new North Star to discern the course to follow in a sea of potential molecular candidates.

Surely, knowing where a desired property may hide gives us a head start, yet the increasing demands of specific properties and the continuous endeavour to improve, inborn to research and development for sure, often makes shaping the matter in such a way to squeeze out of it that latent property you strive for, particularly arduous.

Coming to the point, the aims of the current work are perfectly in line with the *Zeitgeist* of modern chemistry: to extend theory whenever possible (read anion coordination chemistry) and apply it, with the elegance of the exquisitely chemical bottom-up approach, to produce new properties and materials (here, both cation and anion coordination chemistry).

1.3 SUPRAMOLECULAR CHEMISTRY [2]

The choice of a deductive organization for this chapter prompts the introduction of Supramolecular Chemistry, which, as a concept, can be and has been defined in several different ways; here, the simplest possible definition would be “The founding and unifying moment of these three years of work”, yet, for the sake of clarity and etiquette, a more orthodox overview on the matter will be presented below.

1.3.1 Definition [3]

“Chemistry beyond the molecules”, “the chemistry of the non-covalent bond”, “non-molecular chemistry” and other striking definitions like “Lego chemistry” are commonly used to sum up what is probably one of the biggest interdisciplinary fields of chemistry.

According to its conceptual father, and 1987 Nobel laureate, Jean-Marie Lehn:

It is a sort of molecular sociology! Non-covalent interactions define the intercomponent bond, the action and reaction, in brief, the behaviour of the molecular individuals and populations: their social structure as an ensemble of individuals having its own organisation; their stability and their fragility; their tendency to associate or to isolate themselves; their selectivity, their "elective affinities" and class structure, their ability to recognize each other; their dynamics, fluidity or rigidity of arrangements and of castes, tensions, motions and reorientations; their mutual action and their transformations by each other. [4]

Supramolecular Chemistry constitutes a true paradigm shift: molecules are designed and prepared with the traditional focus on the molecular level, paying attention on atoms and their covalent connections, then, defocusing to increase the depth of field, the emphasis is laid on the arrangement and properties of the system on a higher level of organisation (***Figure 1.3-1***).

Although the scope of Supramolecular Chemistry is far broader, probably peaking at the degree of complexity of living beings, if not beyond, in the early stages the mutual intermolecular interactions of only two partners at a time were evaluated, as this constituted the most basic and understandable experimental setup: soon enough the community started speaking about host-guest chemistry.

Host-guest chemistry, again, was given many definitions of growing complexity, first in term of relative size, then in terms of mutual arrangement of binding sites, which, in turn, required a definition on their own as molecular regions of one of the two partners capable of taking part in a non-covalent interaction.

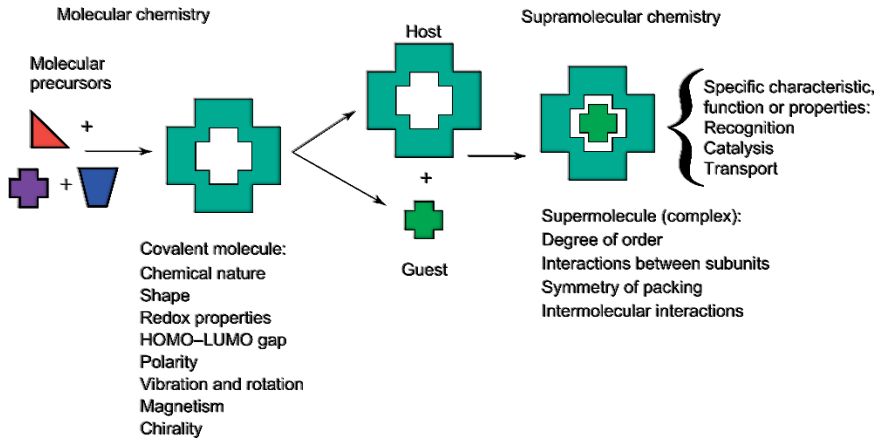

***Figure 1.3-1**.Supramolecular Chemistry definition according to the classic host-guest scheme [3] [4].*

The accepted unifying synthesis, being offered again by one of the 1987 Nobel laureates, Donald Cram, goes as follows:

Complexes are composed of two or more molecules or ions held together in unique structural relationships by electrostatic forces other than those of full covalent bonds… molecular complexes are usually held together by hydrogen bonding, by ion pairing, by π-acid to π-base interactions, by metal-to-ligand binding, by van der Waals attractive forces, by solvent reorganising, and by partially made and broken covalent bonds (transition states)…High structural organisation is usually produced only through multiple binding sites… A highly structured molecular complex is composed of at least one host and one guest component… A host–guest relationship involves a complementary stereoelectronic arrangement of binding sites in host and guest... The host component is defined as an organic molecule or ion whose binding sites converge in the complex… The guest component as any molecule or ion whose binding sites diverge in the complex… [5]

Such a complexes definition, containing both the principles and the toolbox of molecular interactions to put them in practice, will be briefly broken down in the following.

1.3.2 Principles in Host-Guest Chemistry [6]

1.3.2.1 Complementarity and Preorganization: Classical View

The whole of such a complex matter revolves around only two key principles: preorganization and complementarity.

Preorganization refers to a quality of the host, which is possessing the same conformation, in its free form, that the one it will need to assume upon binding of the guest.

Preorganization brings about several consequences: first, the energetic expenditures, both enthalpic, in terms of conformational rearrangement, and entropic, loss of degree of freedom, are reduced, thus favouring the formation of the complex.

A natural consequence of the requirements of preorganization and convergent binding sites for the host, is that, generally, more complex and structured molecules are better fitted as receptors: macrocycles and cage-like ligands with rigid backbones, already possessing a cavity on their own, are generally first choice candidates.

The pre-existence of a cavity, a limited space towards, hopefully, many binding sites converge, explains the second strong point of preorganization: a diminished solvation of the cavity of the host, which means an energetically less expensive desolvation upon binding of the guest, thus promoting the overall association process.

The concept of complementarity is strictly related.

In its most basic and intuitive form, we may speak about geometrical complementarity, addressing the problem of size and shape of the partners.

This is understandable even without delving into chemical concepts: if two pieces were to interlock to keep a complex in place, the joints should fit. If a piece is too big it will not slot in, if it is too small, the junction will be floppy and loose; moreover, as every toddler learned, you cannot fit the square block into the triangular hole.

Unluckily, things are a little bit more complicated, and chemists need to talk about complementarity of binding sites or stereoelectronic complementarity. By this we mean not only that the we need a topological match of donor and acceptor binding sites on the interacting partners, but also a match in a properly chemical way, *e.g.* pairing a hydrogen bond donor on the guest with a reciprocal hydrogen bond acceptor on the host, instead of any other type of interacting group that would cause a mismatch in the interaction pattern of the host-guest complex.

These two different aspects of complementarity, mainly arise from the different nature of the supramolecular forces in play. Some of them are non-directional, or poorly so, while they maintain an inverse dependency on distance. If we take the well-known Lennard-Jones potential as the simplest possible model for this, the size/shape complementarity is evident: forcing the partners too close will cause repulsion, cavity too small for the host, while holding them in a loose contact will result in a scarce stabilization, cavity too big for the host.

Other supramolecular forces exist with a much more directional character and strengths often exceeding those of non-directional interactions; their main advantage is perhaps their main shortfall: they are selective. This means on one hand that one may achieve molecular recognition for a host of choice with the proper selection of its stereochemical properties, and, on the other, that the laborious task of imbuing the required properties to a cavity, both in terms of nature and topology of binding sites, is the only feasible route to confer to the host the ability of discriminating among different binding partners.

1.3.2.2 Complementarity and Preorganization: A Revised Take

Cram's definitions and view, together with that of early days' Supramolecular Chemistry, are heavily influenced by Emil Fischer's 1894 "Lock and Key" model, which explains the impressive level of selectivity exhibited by enzymes for their substrates in living beings. *Mutatis mutandis*, a lock is complementary and preorganized for its key, and the fact that a centenary idea has remained so actual, although somewhat reformulated, says it all about the importance and success of the lock-and-key representation.

As discussed above, preorganization and complementarity, together, contribute to the thermodynamic stability of the host-guest complexes and determine the selectivity of the host for the guest.

Anyhow, at times, chemists are not concerned with the highest possible thermodynamic stability, nor to a recognition that, although selective, causes an irreversible association of the interacting partners. In a sense, this has even more to do with the original systems that inspired Fischer: enzymes do bind selectively a substrate and operate on it, but the binding is reversible and the product released in the cell, if the enzyme-substrate complexes were too stable, the system would stop working; in other words, if one seeks for functions, responses and reactivity, an excess of thermodynamic stability could just make it worse.

A new model, which goes by the name of "induced-fit", equally valid from a chemical point of view (and probably more relevant in a biological sense), was proposed by Koshland in 1958, in which modifications of the host occur upon binding of the guest, the whole host-guest complex reshaping to achieve its final catalytically active form (see ***Figure 1.3-2***).

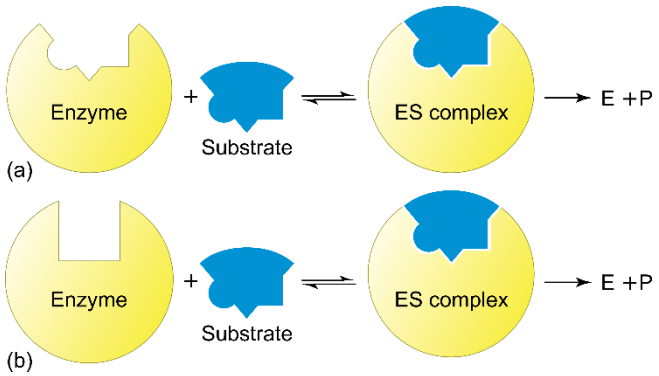

Figure 1.3-2. *Enzyme and substrate interacting to give an enzyme-substrate complex: a) according to the lock and key mechanism; b) according to the induced-fit mechanism [6].*

In this regard, the concept of preorganization, complementarity, and even that of cavity to a certain extent, underwent a sort of paradigm shift when supramolecular stimuli-responsive materials are sought for. The boundaries of cage-like, or even macrocyclic ligands, can be surpassed even maintaining a sort of preorganization and complementarity: prime examples of this, despite the efforts of chemists, are still more common in nature. Deferoxamine here is a case in point, a linear chain molecule which, despite its simplicity, is among the strongest soluble Fe(III) chelators: not only it is able to bind selectively one metal ion, but, as a bacterial siderophore, it manages to scavenge the rare [6] Fe(III) from the extracellular environment making it bio-available, *i.e.* despite the strong binding it can detach from the essential ion, releasing it inside the bacteria.

[6] In terms of Earth abundance iron surely is not a rare element. Rare is to be understood from the perspective of bio-availability of the Fe^{3+} ion, which in general tends to form highly insoluble inorganic species, which many organisms cannot use as a source of this essential ion.

1.3.3 Supramolecular Interactions [7]

Since molecules are the stable and discrete collections of atoms about whose sociology Supramolecular Chemistry is interested in, intermolecular forces, taken individually, must be, and indeed are, significantly weaker than their intramolecular counterparts (see ***Table 1.3-1***).

Table 1.3-1. *Common supramolecular interactions.*

Supramolecular Interactions	Directionality	Bond Energies (kJ mol^{-1})
Ion-Ion	Nondirectional	100 – 350
van der Waals	Nondirectional	< 5
Ion-Dipole	Slightly directional	50 – 200
Dipole-Dipole	Slightly directional	5 – 50
Coordination Bond	Directional	100 – 300
Hydrogen Bond	Directional	4 – 120
Halogen Bond	Directional	10 – 50
π-π Interactions	Directional	2 – 50
Cation-π Interactions	Directional	5 – 80
Anion-π Interactions	Directional	5 – 50

Notwithstanding the fact that they possess only fractions of the energy of a covalent bond, these so called weak forces, can give rise to incredibly stable adducts due to their cooperative nature.

A classic example of this is the marvellous double helix of the DNA.

Keeping it simple, if we exclude any other kind of stabilization, assume hydrogen bonds to have a tenth of the strength of a covalent bond and base pairs to form 2.5 hydrogen bonds on average, it turns out that a binding energy equivalent to that of a covalent bond is provided by the association of every 4 base pairs: now, if one takes in consideration the full extent of the molecule, say about 3 billion base pairs for humans, the overall stability turns out to be astronomical. This has also extraordinary functional implications. Our enzymes are able to fully replicate the molecule without the need of tearing apart the helix, which would be the only way if the two strands were covalently linked: they just need to “unzip” a region of only about 11 base pairs, creating what goes under the name of transcription bubble, which is able to move along one filament replicating it one base at a time.

Cooperativity is an intriguing and debated phenomenon: simple additive models are not always adequate, since synergistic or anti-synergistic phenomena may come in play. Normally we speak about *positive cooperativity* when the overall stability of a complex is higher than the sum of the single interactions that contribute to the

binding of the host; the reverse situation, instead, is termed *negative cooperativity*. Both situations occur, the well-known chelate effect being a prime example of the positive behaviour, while secondary interactions in complexes held together by multiple hydrogen bonds provide examples for both cases.

Now, setting aside the issue of cooperativity, which of course should be held present when coming to the design of receptors and somewhat falls under the preorganization and complementarity principles, the nature and properties of each intermolecular force will be sketched out separately.

The ordering of such a list will follow the criterion of directionality: nondirectional forces tend to be always at work and can be of utmost importance, often sealing the fate of complexes in terms of stability; directional ones, anyhow, are those on which rests most of chemists' attention, since, by controlling their nature and topological arrangement, they offer the chance to obtain the desired selectivity.

1.3.3.1 Nondirectional Supramolecular Forces

1.3.3.1.1 Ion-Ion

Interactions of ions of opposite sign is among the strongest possible intermolecular forces.

As prescribed by the universally accepted Coulomb's law, the spatial dependency of the force is just $F \propto \frac{1}{r^2}$, with r being the distance between the interacting partners: as such, Coulomb's force is perfectly isotropic, fact that is thoroughly mirrored in the uniform lattices of simple salts (*e.g.* NaCl).

Due to their strength ion-ion interactions are not easily overlooked, since they are susceptible to provide an important contribution to the overall stability of a complex. Selectivity can be achieved by organising ions in the framework of a cavity, bringing about both preorganization and a certain degree of size/shape recognition. Receptors based on this concept do exist, but they have their own set of problems: first, ions of the same charge repel each other persistently, as such, they are not easily organized in a scaffold which holds them close. In second instance, there is the problem of counterions and their competition with the designated host. This problem is not easily circumvented: one either renounces to truly charged binding sites for dipolar ones, losing a big share of the overall binding energy (***Table 1.3-1***), or gets rid of the counterions with either synthetical efforts, *i.e.* making the receptor a zwitterionic system of zero net charge, or strategical cunning, *i.e.* designing a receptor specific for an ion-pair, simultaneously able to bind a cation and an anion,

which, although a solution of exquisite elegance, actively doubles the problem of selectivity (***Figure 1.3-3***).

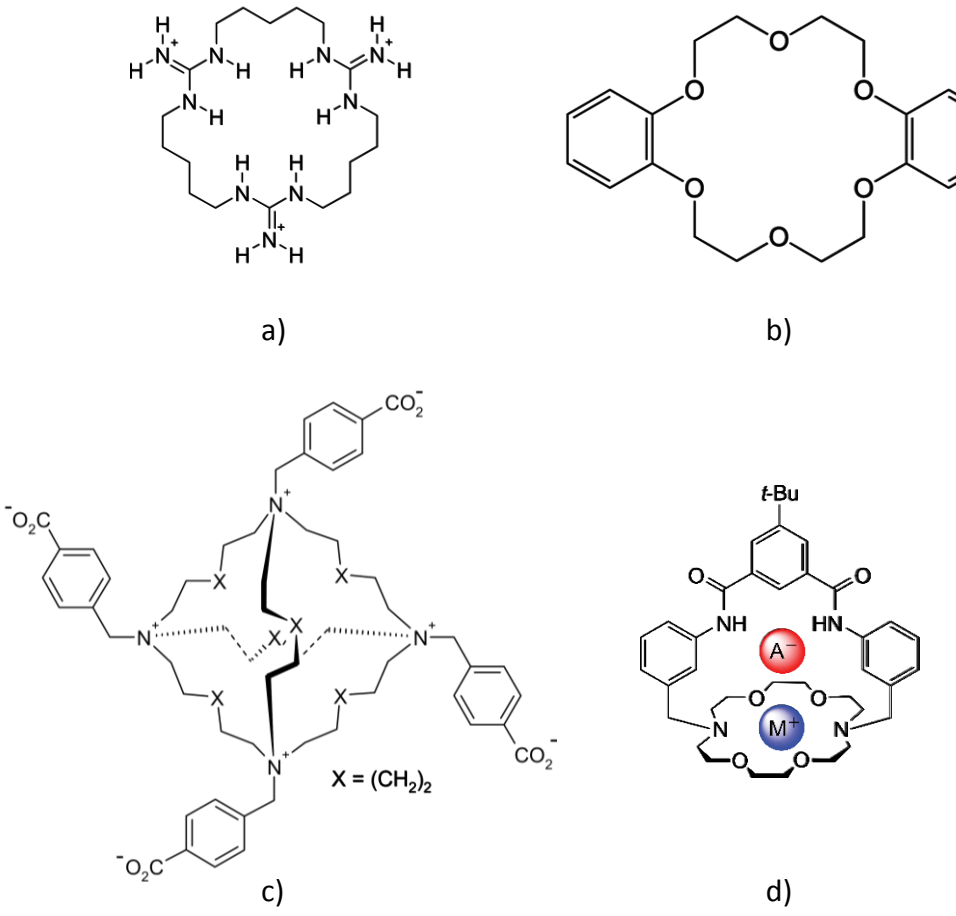

Figure 1.3-3*. a) Macrocyclic receptor for anions with in-built positive charges* [8]*; b) dibenzo 18-crown-6, a classic coordinating dipolar receptor for alkali metals cations* [9]*; c) a zero net charge zwitterionic receptor for anions* [10]*; d) a receptor for ion pairs* [11]*.*

1.3.3.1.2 Van der Waals

Van der Waals forces generally encompass Keesom (dipole-dipole), Debye (dipole-induced dipole) and London (dispersion) forces, directionality and strength of these interactions decreasing in the specified order. As a consequence, Keesom forces occupy a special place among them, since they are both the most intense and directional. As discussed above (see 1.3.3.1.1 and ***Table 1.3-1***) moving from ion-ion interaction to ion-dipole and lastly dipole-dipole means decreasing the interaction energy of two orders of magnitude, yet, since ion-ion is one of the strongest intermolecular forces, even if damped by the loss of real charge separation, Keesom forces end up offering a stabilizing contribution of the same order of magnitude of many other supramolecular interactions, thus their contribution should not be overlooked.

Quite different is the situation for Debye and London forces.

It is not that the contribution of these forces is negligible, in fact they are always present, attractive in nature and, on a basic level, proportional to the extent of surface that host and guest have in contact. The problem is that they overall provide a constant and modest contribution to stability which is totally unspecific, which cannot be object of further enhancing or by itself provide selectivity of any kind, at least in solution.

In the solid state, the situation is partially different, packing forces and close contact between molecules magnifying their overall effect, and at times can be used successfully in crystal engineering.

1.3.3.1.3 Solvent Effect [12]

Although not properly ascribable to the number of supramolecular forces, solvation is a crucial phenomenon for all solution equilibria.

At times, chemists tend to bury its importance in subscripts, for example, when taking into account a complexation equilibrium involving a substrate (S) and its receptor (R) in a given solvent (solv) we could write:

$$S_{solv} + R_{solv} \rightleftarrows RS_{solv} \qquad \text{with} \qquad K_{eq} = \frac{[RS]_{solv}}{[S]_{solv}\,[R]_{solv}},$$

assuming unitary activity coefficients and reference states.

This is fine as long as we are not concerned with a microscopic description of the complexation process, or if we do not care about the effect that the choice of a different working solvent would have on the association of the same two partners.

To remark the centrality of the issue, one of the key concepts of molecular recognition, *i.e.* preorganization (1.3.2), aims partially at reducing the solvation of the host to favour the overall host-guest association process. This, however, does not exhaust the matter.

Traditionally, when presenting solvent effects, the difference between entropic and enthalpic contributions is stressed: this view is proposed below, on the premise that, in real equilibria, both energetic parts may play a significant role at the same time, cooperatively or one against the other.

One of the possible formal ways to explicitly account for the effect of the solvent in a simple association process is constructing an Hess cycle like the one presented in ***Figure 1.3-4***, eventually allowing a quantitative discussion on the relevant energetic parameters.

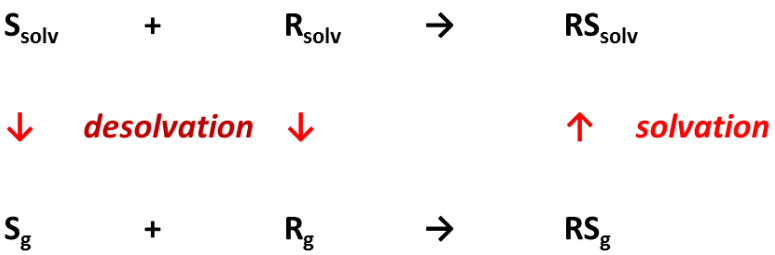

Figure 1.3-4. *One of the possible thermodynamic cycles to specifically account for the energetic contributions of the solvent in a generic association equilibrium. Subscript g for "gas phase".*

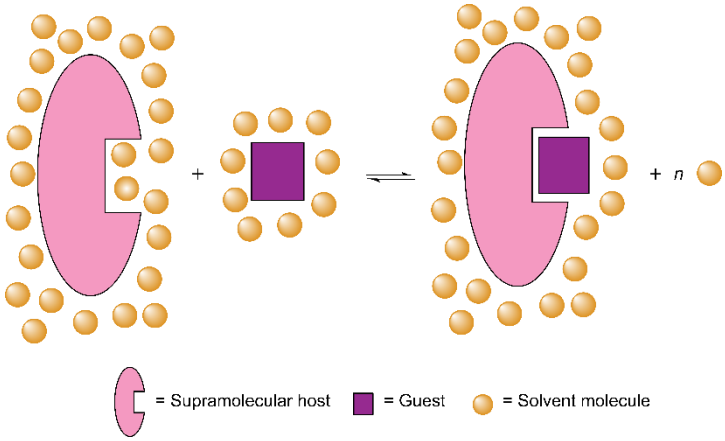

***Figure 1.3-5**. Depiction of host-guest association in a generic non-structured solvent* [12].

A more pictorial view, suitable for a qualitative understanding, is presented in ***Figure 1.3-5***. It is evident that the binding of a guest to a highly preorganized host involves partial desolvation of the two partners and the consequent release of a certain number of solvent molecules, previously solvating the substrate or the receptor, back into the bulk of the solvent. This transition of several solvent molecules, from a bound to a bulk state, is accompanied by an increase of their degrees of freedom, *i.e.* there is an entropic effect due to solvent molecules which promotes the association of the two partners.

There is, however, also an enthalpic contribution due to the solvent, especially in strongly interacting solvents like water: a more detailed picture is proposed ***Figure 1.3-6***.

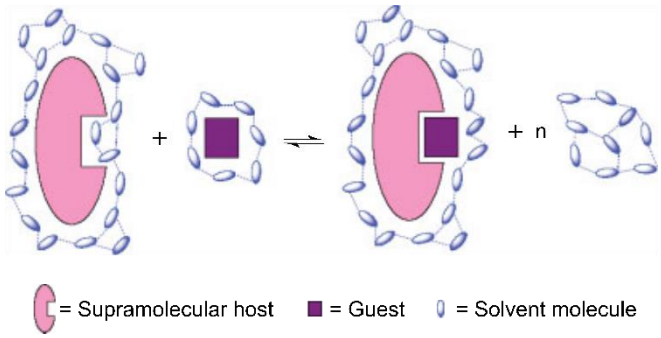

***Figure 1.3-6.** Depiction of host-guest association in a structured water-like solvent* [12].

Surely, upon complexation, there is an enthalpic cost due to the partial desolvation of the host and guest, requiring the breaking solvent-solute interactions, but there is also an enthalpic gain due to the newly formed solute-solute interactions, not to mention that the solvent-host and solvent-guest interactions are not necessarily as intense as those between the solvent and the host-guest complex (*e.g.* the

association of two charged species to give a neutral complex in water, the binding of an apolar guest into the cavity of a cyclodextrin or a calixarene in water). The overall enthalpic gain or loss resulting from the sum of the single contributions is the so-called enthalpic solvent effect.

Even from a qualitative description, one can already understand how the effect of the solvent can hinder or promote the association of two species in solution, at time becoming the prime driving force of the process.

"Similia similibus solvuntur" still applies here, matching or mismatching the polarity of solvent and solutes has a deep impact, and hydrophobicity/hydrophilicity may help rationalize and predict the outcome of the experiments. This view grew so important that many refer to the matter as hydrophobic effect, namely the observed tendency of non-polar solute to aggregate in water, which is but a particular case of solvent effect. Nevertheless, it is worth mentioning here that a specific instrumental and theoretical analysis of the hydrophobic effect (falling out of our general solvent effect overview), involving a clathrate-like first solvation shell depiction (also suggested in ***Figure 1.3-6***) with, among other things, a proper evaluation of residence time and hydrogen bond strength of solvating and bulk water molecules, propend for a chiefly entropic explanation of the phenomenon.

1.3.3.2 Directional Supramolecular Forces

1.3.3.2.1 Coordination Bonds

Coordination bonds are very well-known interactions which have been exploited for the construction of some of the most impressive supramolecular scaffolds and machinery.

This, however, can be a difficult topic, as important distinctions should be made.

Since the natural boundary between traditional and supramolecular chemistry lies in the covalency of the interactions, separating distinct molecular entities from intermolecular assemblies, clarifying the nature of coordination bonds is crucial to understand when and why supramolecular considerations may apply.

Coordination bonds are not “co-valent” in the etymological strict sense of “joint valency”, intended as sharing of a pair of electrons, one for each atom involved in the bond, yet the orbitalic interaction involved in allotting an electron pair of the base into shared molecular orbitals of the acid-base complex is fully covalent in a chemical sense. In this regard, it is not a case that interaction energies for coordination bonds can be of the same order of magnitude as typical covalent bonds.

So, what does supramolecular chemistry has to do with a molecular-like interaction?

Two are the main answers to this question, as coordination bonds can assume both a structural or functional role, and, at times, both.

Structural function is traditionally the domain of cations since Alfred Werner’s pioneering work. If the structure of simple molecules can easily be predicted on the basis of a general electrostatic model (*cf.* early Valence Bond and VSEPR theory), metal complexes demonstrated a marked preference for certain geometries over others, at times even disregarding those simple considerations, with curious recurrence and similarities depending on their position in the periodic table and oxidation state.

Eventually, such features did not go long unnoticed, and a robust theory, featuring orbital-detailed description for the central metal cation while still using an electrostatic depiction for its ligands, was developed: Crystal Field theory (1930s) allowed the correct prediction of several properties, among which geometry, of metal complexes.

The final up-to-date model, which goes under the name of Ligand Field theory (1950s) is but a rearrangement of crystal field theory to overcome the limitation of

the plain electrostatic depiction of ligands, at times simplistic at best: the use of an orbital description for all interacting partners allowed to achieve a detailed description of metal complexes in term of molecular orbitals, favouring the computational evaluation of the properties of interest.

Using metal cations as pinpoints to organize molecular subunits in the desired manner, brought to the development of both discrete and continuous structures (see ***Figure 1.3-7***)

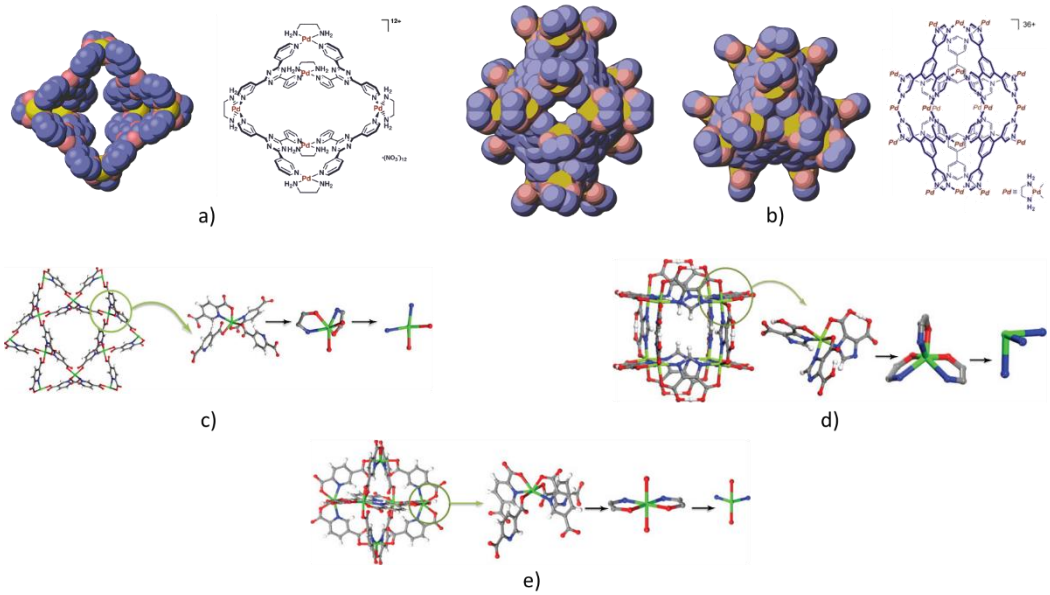

Figure 1.3-7. *Examples of the structural control and variety offered by the use of metal cations as organizing elements: a), b), examples of discrete 3D hollow molecules obtained through the molecular panelling approach* [13]*; c), d) and e) examples of Metal organic frameworks and their detailed features from the overall lattice up to the stereochemistry of the single metal centre* [14] [15].

As one can easily see, both 3D lattices and single molecules thus obtained, may present cavities in which other species can be hosted, both for storage and catalytical purposes, as confinement in a nanoscale interacting environment may promote reactivity: these system, even devoid of this last functional note, although they should be regarded as wholly molecular objects, are perceived as supramolecular systems, since the emphasis is often laid upon their interactions with smaller molecular species.

The functional role of coordination bonds is often more tied to their stability, which, again, a long series of theories and well-described effects allows to predict (*cf.* Pearson's Hard Soft Acid Base theory, Irwing-Williams' series, chelate effect, macrocyclic effect, macrobicyclic effect, *et cetera*).

Reversible coordination bonds are extremely important for several different applications.

Cleavable bonds allow, for example, the use of metal cations in template synthesis (***Figure 1.3-8***), temporarily organizing reacting ligands around themselves in such a way to ensure the formation of selected covalent bonds: many mechanically interlocked molecules, *i.e.* supramolecular structures, can be obtained after removal of the templating ion.

A selection of reversible and irreversible coordination bonds is also used to produce highly structured self-assembled systems, like Fujita's cages shown in ***Figure 1.3-7***: bonds which are irreversible under reaction conditions are used to drive the system towards the geometry imposed by metal centres, while reversible ones allow the system to correct eventual "mistakes" in the bond pattern, so that, at the end of the process, only the most stable structures survive.

Due to the important conformational change that a ligand can undergo upon metal coordination, again a consequence of the high directional character of these interactions, functional applications in molecular machinery and devices have been devised.

Lastly, the functional role of coordination bonds is not limited to the discussed cases: as a directional force upon which we have full control, simply coupling a selective receptor with a molecular moiety possessing any measurable property able to vary upon coordination, means transforming it into a sensor.

As host-guest chemistry, self-assembly, molecular machines, molecular recognition and so on, are rightful parts of the edifice of supramolecular chemistry: the inclusion of coordination bonds into the number of supramolecular forces could not be omitted.

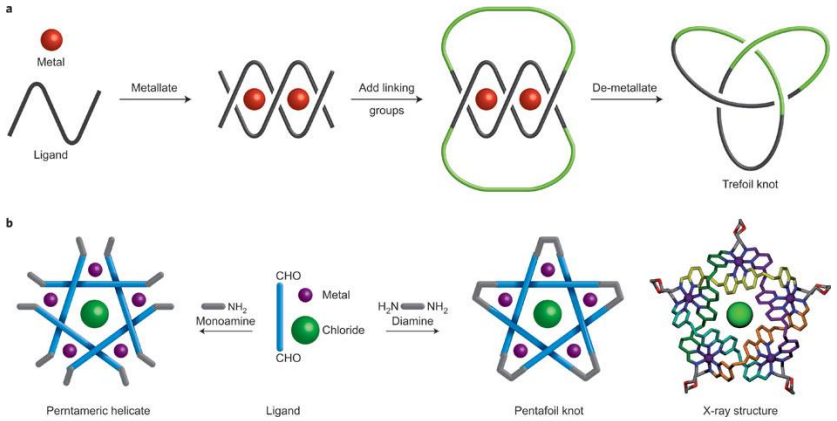

Figure 1.3-8*. From Jean-Pierre Sauvage Nobel-winning synthesis of the trefoil knot (top) up to the highest complexity reached for what concerns interlocked systems* [16].

1.3.3.2.2 Hydrogen Bond [17]

The peculiar features of hydrogen bonding made it recognized as the “masterkey interaction in supramolecular chemistry”. [4]

Hydrogen bond can be defined as the D-H···A interaction occurring between a sufficiently electronegative donor (D), *i.e.* able to withdraw electrons and polarize the bonded hydrogen atom H, and an acceptor (A) possessing lone pairs or polarizable π electrons. Such a definition encompasses all manners of hydrogen bond interaction, from strong covalent-like interactions (*e.g.* in HF_2^-) up to the limit of quasi van der Waals interactions. From a structural point of view, a widely accepted criterion for assessing whether two atoms are hydrogen bonded is measuring the observed D···A distance and compare it to the sum of van der Waals radii of D and A: whenever they are found closer there is a strong indication for hydrogen bonding, nevertheless hydrogen bond on the lower end in terms of interaction energies may not be correctly detected by this method.

The main reasons behind the incredible success of hydrogen bonding in synthetic receptors, not to mention living systems, is tied to three main factors: directionality, cooperativity and tuneable properties, first of all its thermodynamic stability (*cf.* ***Table 1.3-1***), which depends on the chosen donor-acceptor pair.

Directionality in hydrogen bonding is a property chiefly inherited by the partially covalent character of the interaction, and if it is true that the strongest hydrogen bonds tend to be linear or almost linear, there is, for moderate hydrogen bonds, the tendency to align according to the geometric arrangement of the interacting lone pairs of the acceptor. The most commonly encountered geometries are reported in ***Figure 1.3-9***.

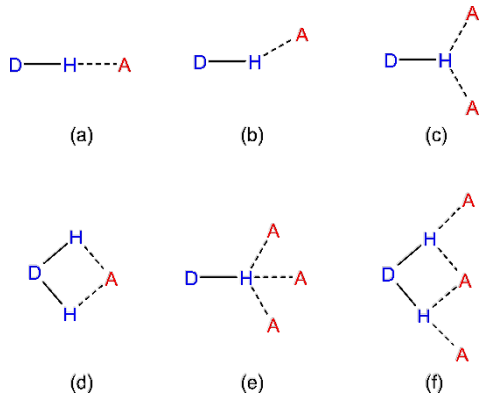

Figure 1.3-9. *Primary hydrogen bonding geometries: a) linear; b) bent; c) bifurcate; d) chelating; e) trifurcated; f) three centre bifurcated* [2].

Cooperativity, although a commonplace for supramolecular forces, is corroborated in hydrogen bonded systems by the so-called secondary hydrogen bond interactions (where the primary interactions are but the direct hydrogen bonds between the donor and the acceptor). Secondary interactions arise whenever different neighbouring groups on the same molecular moiety are engaged in hydrogen bonds: as schematized in ***Figure 1.3-10*** for a simple case, depending on the arrangement of donor and acceptor binding sites we can obtain either an extra thermodynamic stability or disfavour the binding process.

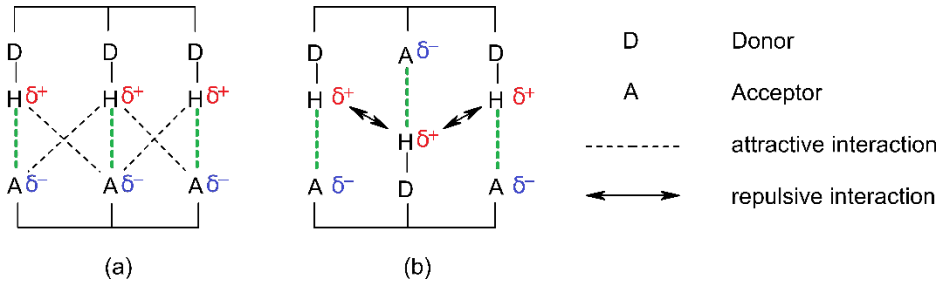

Figure 1.3-10. *Secondary interactions providing attractions between neighbouring groups between DDD and AAA arrays (primary interactions in green) and (b) repulsions from mixed donor/acceptor arrays (ADA and DAD) [2].*

Concerning the intrinsic dependence of the hydrogen bond strength on the chosen donor-acceptor pair, beyond the structural remarks exposed above, one should keep in mind that hydrogen bond formation can be seen as a (partial) proton transfer phenomenon. In this framework, Brønsted-Lowry acid-base character of the involved species comes into play: experimental and computational results confirmed that the stability of hydrogen bonds increases as the proton affinities of donor and acceptor become more and more matching, *i.e.* when the difference between their protonation constants (or pK_a), ΔpK_a gets closer to zero, *viz.* the more the proton is equally shared between the interacting partners. [17] Extension of these results provide useful guidelines, suggesting, for example, that anions which are the conjugate bases of weak acids will be able to engage in stronger hydrogen bonds than those that are conjugate bases of strong acids.

Altogether, the fact that hydrogen bond ranks among the most stabilizing supramolecular interactions, joined to its directional, cooperative and selective character, effectively made it the first-choice intermolecular force for anions receptors and, more in general, for directing and controlling the assembly of the more diverse supramolecular ensembles.

1.3.3.2.3 π-π Stacking

π-π stacking interactions, as the name suggests, regard attractive forces between π-surfaces. According to PBARME[7] rule, apparently one of the pillars of chemistry, the highly prototypical benzene molecule, and its dimer, are the most convenient choice to discuss the nature of these interactions.

The quadrupolar moment of benzene, a representation of its electrostatic surface potential is presented below in ***Figure 1.3-11***, allows for a point charge schematization and the individuation of three idealized geometries for the benzene dimer: the face to face, the parallel displaced and the edge to face orientation (***Figure 1.3-12***). Their stability varies predictably, as depicted in ***Figure 1.3-12***, accounting for the partially directional character of this interaction, edge to face and parallel displaced resulting the most favourable orientations, with the former slightly favoured of a few kJ/mol.

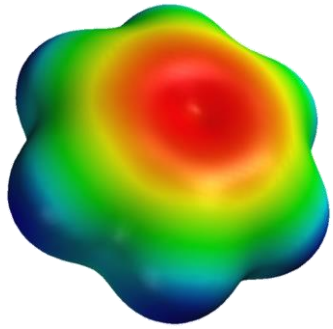

Figure 1.3-11*. Electrostatic surface potential of benzene. Red: negative ESP; Blue: positive ESP.*

Embracing a more general view, π-π stacking can be thought of as a combination of coulombic and van der Waals interactions: the first, heavily influenced by the charge distribution of the interacting partners, justifies the strong interactions observed between aromatic molecules of different polarities up to the limit of charge transfer complexes, while the second, roughly proportional to the extent of the contact surface, accounts for the behaviour of large, polycyclic aromatic systems. The characteristic piling up of aromatic molecules observed in molecular crystals explains the choice of "stacking" as comprehensive name for this kind of interactions.

[7] Pick Benzene As Reference Molecule, Ever!

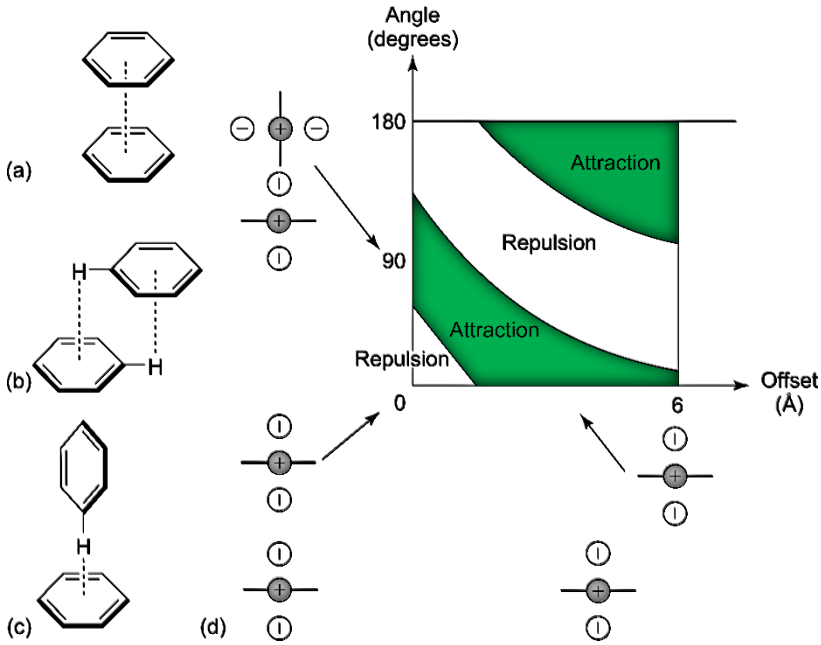

Figure 1.3-12*. Three limit geometries for the benzene dimer: a) face to face, b) parallel displaced, c) edge to face. d) Schematization of the interactions between benzene molecules and their dependence on mutual orientation (angle = angle between the planes of the two rings, offset= linear displacement between ring centres)* [7].

1.3.3.2.4 Cation-π Interaction

The interactions of several transitions metals with olefinic and aromatic compounds have long been reported in the literature (*e.g.* ferrocene, Zeise's salt, *et cetera*), yet their usual colourful nature warned the chemists about the covalent nature of the interaction which is but a form of coordination bond (*cf.* 1.3.3.2.1).

What we refer to with the term cation-π interaction nowadays is a much more non-covalent interaction arising between usually hard cationic species (*i.e.* alkaline or alkaline-earth metal cations) and the quadrupole moment of arenes[8], dominated by the electrostatic attraction between the differently charged surfaces (*cf.* benzene's electronic surface potential, ***Figure 1.3-11***) with very scarce orbitalic contribution.

This kind of interaction is directional, the preferential orientation being the cation sitting right on top of the central negative charge density of the arene.

[8] Think "benzene", PBARME rule.

1.3.3.2.5 Anion-π Interaction

Anion-π interaction is the younger sister of its cationic counterpart. Dismissed by many at the beginning, as the arising of an attractive interaction between a negatively charged species and the negative quadrupole moment of an arene appeared unlikely, is now among the most recently recognized supramolecular forces.

This kind of interaction can be broken down into two main contributions, an electrostatic term, arising from the interaction of the anion with the quadrupole moment of the arene, and an inductive one, arising from the interaction of the anion with the anion-induced ring dipole, although other contributions may play a role in specific cases (*e.g.* the arene induced polarization of the anion with very soft anionic species).

Even in the case of benzene, where the electrostatic interaction is definitely repulsive, the always attractive inductive contribution, reinforced by anions' soft character (1.4.1.1), can provide a sort of compensation (*e.g.* in the case of chloride-benzene interaction the two terms almost cancel out). Thus, making the inductive contribution prevail is a possible route to obtain stabilizing anion-π interactions: generally speaking, this approach involves the use of highly delocalized condensed polycyclic system, which can be easily polarized by the neighbouring charge of the interacting anion. This can be a good idea even for the binding of large delocalized anionic species, even if they are not at all polarizing, since van der Waals and solvophobic effects may furnish an important contribution.

Nevertheless, strong and stabilizing anion-π interactions are generally achieved working on the electrostatic term, making it attractive instead of repulsive via what can be thought of as an *umpolung* approach, aiming to invert the sign of the electrostatic potential above the arene centre from negative (*cf.* benzene, ***Figure 1.3-11***) to positive values. The inversion of polarity can be achieved according to two symmetrical strategies, or with a combination of both, *i.e.* withdrawing electronic density from the centre of the arene towards its periphery or squeezing more positive charge towards the arene centre.

The first methodology is straightforward: the more EWG groups are appended to the arene, the more electron-deficient it will become, up to the point of switching the sign of the vertical component of its quadrupole moment.

The prototypical example is provided by hexafluorobenzene, whose electrostatic surface potential is reported below in comparison to that of the benzene molecule (***Figure 1.3-13***).

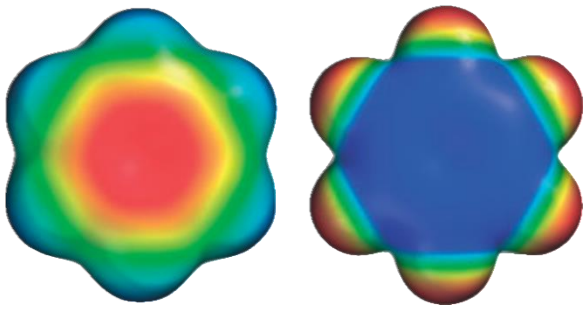

Figure 1.3-13. *Electrostatic surface potential of benzene (left) and of its hexafluoro derivative (right). Scale: -60 kcal mol^{-1} (red), +50 kcal mol^{-1} (blue)* [6].

The other possibility seems a little less obvious, as squeezing positive charge towards the centre of the arene appears a mysterious process. Indeed, this is what happens in substituted systems, with the family of azines as the most classic example.

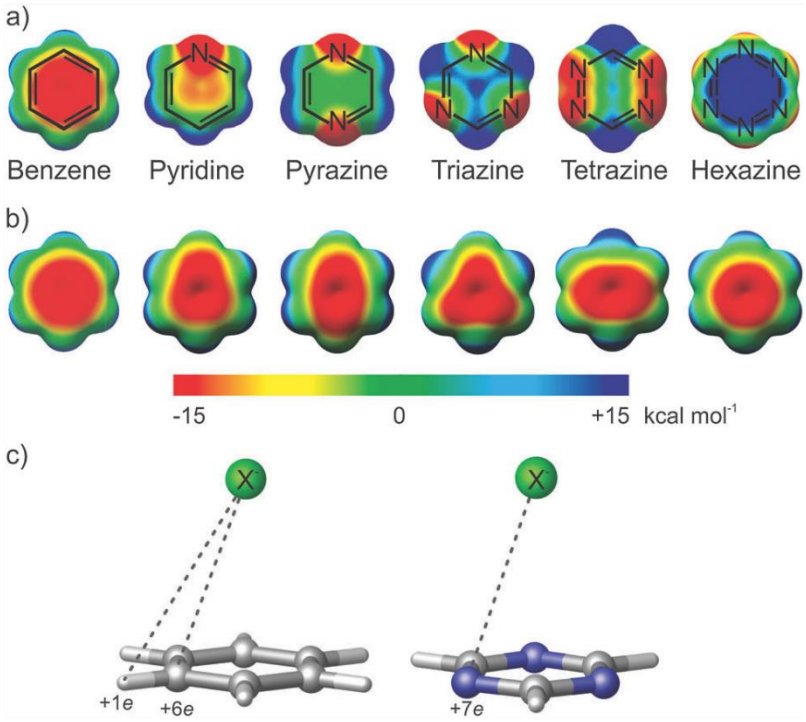

Figure 1.3-14. *a) electrostatic surface potential of benzene and its five azo-derivatives; b) fictitious electrostatic surface potential obtained replacing only the π electron density of benzine with that of the corresponding azine; c) comparison of the proximity of nuclear charges to an anion above the centres of benzene and s-triazine* [18].

Figure 1.3-14, reproduced *in toto* from [18], show the progressive shift from negative to positive potential achievable by gradually introducing heteroatoms in the benzene framework. It should be stressed, as aza-type nitrogen atoms are generally depicted as EWG groups, that the effect on the overall electrostatic potential is not due to π-electron deficiency, as brilliantly illustrated in part b of ***Figure 1.3-14***, but rather to the change in nuclear charge distribution, part c of said figure: *i.e.* azines do not interact favourably with anions due to their π-acidic character, the effect of the aza-type nitrogen on anion-π interactions being primarily replacing a carbon nucleus of charge +6 and its attached hydrogen atom, with a +7 charged nitrogen nucleus, which indeed results in an inversion of the polarization of the arene (*cf.* [18] for further in depth discussion).

As a matter of fact, directional and stabilizing anion-π interactions could be obtained by these *umpolung* approaches, resulting first in an increased appreciation by the scientific community, and finally in a proper recognition of their importance for synthetic receptors [19] and biological systems [20].

1.4 CATIONS AND ANIONS

This section aims to discuss the differences between cations and anions and put them in a coordination chemistry perspective. Anticipated and owed since 1.1, it is presented here, in due time, building on the concepts presented in 1.3.

1.4.1 Effect of Charges of Opposite Sign

1.4.1.1 Dimensions

As clarified in the XXth century, on an atomic level positive charge is confined in the nucleus and it is invariant upon chemical transformation: observed charges of chemical species are due to transfer of negatively charged electrons and namely valence ones, occupying the very periphery of the atom, from one to another. As such, cations are species which have lost one or more valence electrons, while anions are species who have gained some.

Even disregarding quantum chemistry and adopting a simple electrostatic model, it is evident that the charging process has an effect on the size of the atom: a neutral atom will shrink upon loss of an electron, due to the overall electron-electron repulsion decrease while the effective nuclear charge felt by valence electron is effectively increased; on the contrary, gaining an electron implies a dimensional increase with respect to the neutral atom.

From a chemical standpoint, size does matter. Charge to radius ratio is commonly used as an estimation for the strength of the electrostatic interactions to which an ion can be amenable, the more charge dense the ion is, the stronger its interactions; another valid take on the subject is stating that, since the electrostatic potential generated by a point charge is proportional to the ratio between its charge and the distance from it, if an ion is described as a hard sphere with a proper radius and a point charge in its centre, the charge to radius ratio is just a measurement in disguise of the electrostatic potential at the ion's surface.

The numbers, as can be seen in ***Table 1.4-1***, can vary pretty dramatically with charge: finding a cation as big as fluoride, the smallest of halide anions, means going down two periods in the periodic table, up to the potassium ion, not to mention that the same element, with opposite charge, can vary its radius size of more than 50% (*cf.* the sodium ion with its exotic anionic counterpart).

Table 1.4-1. *Properties of some common anions and cations [2].*

Ion	Radius (Å)	$\Delta G_{hydration}$ (kJ mol^{-1})
F^- (6 coord.)	1.33	-465
Cl^- (6 coord.)	1.81	-340
Br^- (6 coord.)	1.96	-315
I^- (6 coord.)	2.20	-275
ClO_4^-	2.50	-430
NO_3^-	1.79	-300
CO_3^{2-}	1.78	-1315
SO_4^{2-}	2.30	-1080
PO_4^{3-}	2.38	-2765
$H_2PO_4^-$	2.00	-465
$PdCl_6^{2-}$	3.19	-695
Na^-	2.2	n/a
Cs^-	3.5	n/a
Li^+ (6 coord.)	0.76	-475
Na^+ (6 coord.)	1.02	-365
K^+ (6 coord.)	1.38	-295
Cs^+ (6 coord.)	1.67	-250
Ca^{2+} (6 coord.)	1.00	-505
Zn^{2+} (6 coord.)	0.74	-1955
Al^{3+} (6 coord.)	0.54	-4525

Overall this has two main consequences: first, hosts for anions should present cavities or binding sites considerably bigger than those for cations; in second instance, valency being equal, cations will give rise to stronger and harder (from a Pearson's HSAB point of view) electrostatic interactions, while anions will behave as softer species, favouring van der Waals type interactions.

1.4.1.2 Ion Hydration

Ion solvation is a fundamental topic subtended to the whole of coordination chemistry.

Although deserving to be explored in all its nuances, for the sake of briefness and clarity, since water is almost the only solvent used in this work and, most of all, in view of the special role water fulfils in biological systems and on a planetary scale, the following discussion will be limited to hydration.

Some of the key structural and electronic properties of water are depicted below in ***Figure 1.4-1***.

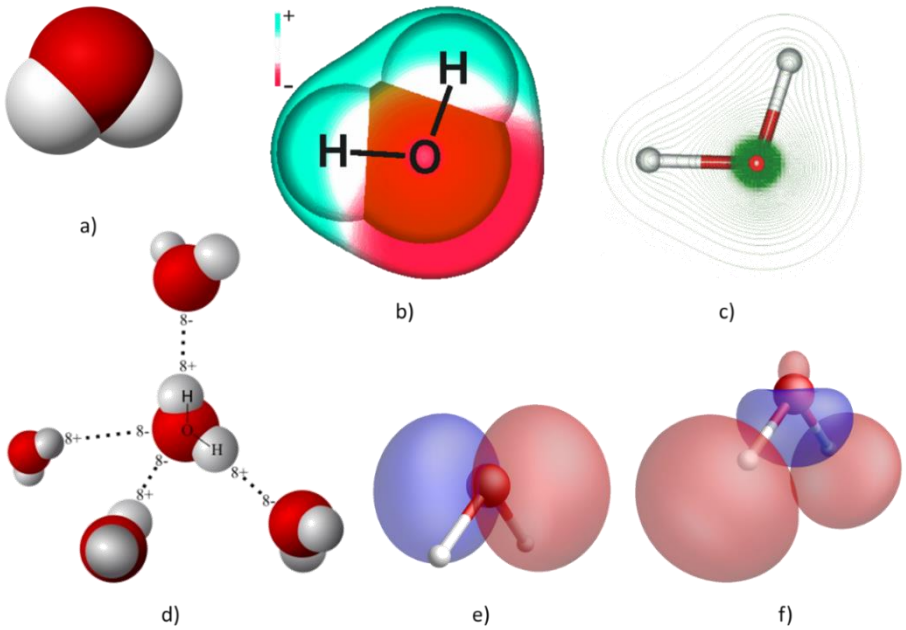

Figure 1.4-1. *Structural and electronic properties of water: a) simple spacefill model; b) electrostatic surface potential; c) electron density distribution; d) ideal tetrahedral structure of water-water hydrogen bonding pattern; e) depiction of the HOMO; d) depiction of the LUMO.*

The dipolar nature of the molecule, the higher negative charge concentrated on the oxygen atom, perfectly aligned with the dipole moment, together with the pronounced amenability of cations to form strong electrostatic interactions, tricked many to believe that cations possess a higher hydration free energy than anions: unluckily nothing could be more wrong. Anions are found to be, for a given charge to radius ratio, much strongly hydrated than cations (*cf.* ***Table 1.4-1***).

Models and theories have been advanced to support the experimental data, with various fortune among the scientific community.

A key point regards the asymmetry of the charge distribution within the water molecule itself: positive charge is located on the H termini, which possess a much smaller radius than the oxygen atom (in absolute terms, van der Waals radii being about 1.0 and 1.7 Å for H and O respectively, plus the difference is surely enhanced in the molecule for the partial charging process, see 1.4.1.1). As such, positive charge ends up occupying a much more superficial area of the molecule, allowing more intimate contacts with negatively charged ions, while the negative charge on the oxygen atom, being buried much deeper in the molecular structure, sees a higher reduction in the electrostatic potential felt by nearby positive ions.

Other justifications, especially when there is a partial charge transfer from or to the water molecule, invoke electronegativity and orbital considerations: whichever the tool we use to picture the situation, oxygen is less prone to cede its electrons and the HOMO symmetry disfavours orbital interactions aligned with the electric dipole of the molecule; on the contrary, H seems more prone to covalent interactions, both in terms of electronegativity and symmetry of the LUMO orbital.

More complex descriptions are possible, partially overlapping with the discussion on the chaotropic or kosmotropic nature of ions and on their overall impact on local water structure: on a microscopical level competition arises between purely electrostatic ion-water interaction and the hydrogen bond network existing among water molecules. Small monovalent cations tend to favour the orientation of water molecules according to their dipolar moment, deviating significantly from the classical tetrahedral hydrogen bond network, while larger ones have a lesser tendency to do so; the reverse is true for anions, with small ones (*e.g.* fluoride) strongly promoting hydrogen bonding. This paragraph does not mean to address the problem properly, which is complex and highly debated, but to stress how pen-and-paper approaches looking at the single interaction of one water molecule with an ion are bound to fall short in describing a complex phenomenon like ion hydration.

Whichever the explanation we decide to adopt, all other things being equal (charge, radius, polarizability, *et cetera*), anions do interact more strongly with water than cations.

If we look at a complexation reaction in aqueous solution as a competition for the guest between the receptor and the solvent, moreover with the former often present in abysmally small concentration compared to the latter, the strength of guest-solvent interactions clearly influences the equilibrium (*cf.* 1.3.3.1.3): this means that, *ceteris paribus*, water will actively compete stronger for anions than for cations, resulting in an intrinsic reduction of the stability of anionic complexes.

Just to provide a quantitative data, which will need to be further discussed in the following since ion hydration alone cannot justify it, for the complexes of a monovalent anion in water (with 1 M as reference state) we may expect stability constants as high as 10^2-10^3, while for a monovalent cation values in the range of 10^5-10^6 (a thousandfold increase!) are still possible.

1.4.2 Basicity

From an acid-base point of view, cations are in general Lewis acids, while anions are Lewis bases, yet the situation is not as symmetrical as it may appear.

Metal cations are coordinatively unsaturated and tend to be strongly acidic, prone of accepting electronic doublets and forming coordination compounds, whose stability, depending on the extent of the orbital contribution to the interaction, can span from typical values for intermolecular adducts up to matching the strength of covalent bonds (*cf.* 1.3.3.2.1).

The contrary is not necessarily true: anions are generally coordinatively saturated and, although some of them really possess a marked Lewis basic character (*e.g.* cyanide), many others have extremely weak coordinating properties, so much that they fall into the so called "innocent anions" commonly used as inert electrolytes during experimental measurements (*e.g.* nitrate, perchlorate, chloride, *et cetera*).[9] This means that many anions will interact only through weak forces, being at best suitable as hydrogen bond acceptors.

Now we can fully understand why several orders of magnitude separate the stability of cationic complexes from that of anionic ones: the basic interactions subtending the formation of the former, *i.e.* coordination bonds, being 2-3 orders of magnitude more intense in terms of bond energies than the properly supramolecular forces (*cf.* ***Table 1.3-1***).

Another direct consequence of this concerns the design of the receptors. Coordination bonds are often highly directional, especially for transition metal cations, and the expected geometry of a given metal complex can be exactly predicted according to ligand field theory (*cf.* 1.3.3.2.1), providing a precious guide for organizing a cavity with the exact number of binding sites arranged in the required manner. The situation of anions is different due to the reduced directionality of several supramolecular forces and, as discussed below in 1.4.3, also in consideration of their geometry.

[9] Not to mention anions like BH_4^- or AlH_4^-, among others, which are not basic in a Lewis sense, since they do not even possess electronic doublets to share.

1.4.3 Geometry

Anions and cations do come in a wide variety of shapes and geometries, yet if we limit ourselves to the simplest and most relevant cases, *i.e.* the classic inorganic species, cations are basically all spherical (just pick any metal on the periodic table and it will exist in solution in at least one ionic form, if not more), while anions really come in a plethora of spatial arrangements: spherical (*e.g.* halides), linear (*e.g.* CN^-, N_3^-), trigonal planar (*e.g.* NO_3^-), tetrahedral (*e.g.* ClO_4^-, SO_4^{2-}), square planar (*e.g.* $PtCl_4^{2-}$), octahedral (*e.g.* PF_6^-) and more.

These structural variety implies an even higher number of possibilities concerning the coordination geometries: if cations (as discussed in 1.4.2) form complexes of definite geometries due to the orbital interactions with the ligands, for anions the situation is more blurred; synthetic receptors based on hydrogen bonding may form from 2 up to 6 hydrogen bonds with the simple halide anions, yet, for polyatomic species, up to three different interactions per terminal atom can be observed.

Overall, the consequence of the increased structural complexity is making complementarity of size, shape and binding sites harder to achieve for anions than for cations, requiring significant synthetic efforts in designing a cavity with a higher number of binding sites and geometric features.

1.4.4 pH Dependence

Ion coordination in solution requires the actual presence in solution of the ion: this may seem a trivial point, yet it turns out to be intriguingly important.

Many metal cations do hydrolyse in "alkaline media",[10] but this is not much of a problem, since the high thermodynamic stability of their complexes tends to favour the complexation to the receptor even under acidic conditions, thus sequestering the cation before the formation of its hydroxo species may hinder the host-guest recognition.

Anions do not find themselves in an equally convenient spot for two main reasons.

The first is their basicity: sufficiently basic anions will undergo protonation in acidic media, meaning that they will lose their negative charge and cease to be anions at all. In a sense, this is the equivalent of cation hydrolysis. However, the thermodynamic stability of anionic complexes is often not even comparable to that of cations (see 1.4.1.1 and 1.4.2), hydrogen bonding, or better salt-bridge formation,

[10] Here "alkaline media" should be understood *cum grano salis*, as for some metal cations hydroxo complex formation and precipitation may already happen in very acidic conditions (*cf.* Fe^{3+}, Al^{3+}, Zr^{4+}, *et cetera*). As a rule of thumb, the higher the charge density of the cation the greater its tendency to form hydroxo species even under acidic conditions.

being the strongest possible interaction they may resort to. Hydrogen bonding to protonable receptors poses another restriction in the useful pH range for anion coordination: if the pH is too high and the host is not protonated it will not be able to work as a hydrogen bond donor, impeding the guest recognition and coordination.

Overall, this create a useful pH window for anion coordination, whose width depends intrinsically from the interacting partners: too acidic conditions will cause anion protonation and loss of its negative charge, too alkaline environment and the receptor, not protonated, will lose both positive charge and hydrogen bond donor behaviour.

1.4.5 Closing Remarks

Not a single instance of those listed above favours anions over cations coordination.

It is worth mentioning, however, that many of the downsides for anions are double edged swords, surely creating difficulties which do not have the parallels for cations, but also adding depth to the research field and possibilities for what concerns the design of selective receptors, which, thanks to chemists untiring efforts, are not as unattainable and far from reality as they may seem.

2 EXPERIMENTAL

2.1 CHEMICO-PHYSICAL TECHNIQUES

2.1.1 Potentiometry

2.1.1.1 Experimental

Potentiometric titrations were performed with an automated system constituted by the following parts:

- Metrohm 713 pH-meter potentiometer;
- Metrohm 665 Dosimat automatic burette;
- Metrohm 728 Stirrer magnetic stirrer;
- Metrohm 6.1414.010 30 cm^3 thermostatic cell;
- Julabo F12 thermocryostat;
- Metrohm 6.0262.100 combination pH electrode;
- Personal computer.

All the solutions employed for potentiometric titrations were prepared from distilled water, further purified with a Millipore system to remove residual ionic species and organic contaminants, deaerated through ebullition and cooled under inert atmosphere to ensure the removal of dissolved CO_2.
Ionic medium, acid (HCl) and basic (NaOH, NMe_4OH) solutions were prepared from commercial products of high purity. Their concentrations were proven according to standard analytical techniques whenever needed. All titrations were performed at 298.1 ± 0.1 K, by thermostating independently the whole room and the measurement cell at said temperature.
A constant flux of N_2 was maintained over the studied solutions during titrations to avoid their carbonation. Before reaching the measurement cell, the gas was bubbled through two separate solutions: first through a concentrated NaOH solution, to ensure the complete absence of CO_2, then through the same ionic medium used in the measurements, to avoid contamination from the strong base solution and pre-saturate the gas in water vapour.
All titrations were performed in 0.1 M NaCl or NMe_4Cl solutions.
Measurements and additions are automated and controlled via a PC interface.
The program requires 7 parameters as an input, which may be regulated to define and adjust the process of data acquisition; namely, they are:

1. Time to wait before starting the titration;
2. Maximum number of readings;
3. Time interval between two successive readings;

4. Time interval between the end of the addition and the beginning of the readings;
5. Tolerance on standard deviation;
6. Tolerance on drift;
7. Volume of titrant initially added;
8. Final volume of titrant to reach;
9. Volume step for titrant injection.

Given these values, the PC starts recording electromotive force (emf) values measured by the potentiometer according to the program's routine outlined below. First the system remains idle for as long as specified (parameter 1), then the titration starts.

With the exception of the very first point of a measurement, for which there is no need of titrant addition, the generic experimental point is collected as follows: if the current volume of added titrant plus the initial titrant volume (parameter 7) is below the set threshold (parameter 8), a fixed volume of titrant (parameter 9) is added to the cell. After the addition, the system waits for as long as specified (parameter 4) before beginning the readings. Once the readings start, single emf values are collected and memorised at regular time intervals (parameter 3) and visualized on the screen accompanied by an incremental number. As soon as a set of 10 readings is generated, the computer checks its standard deviation: if it results higher than the imposed limit (parameter 5) another emf reading is acquired and the test is repeated on the most recent set of 10 readings. The cycle ends either when a set satisfies the condition on standard deviation or when the maximum allowed number of readings (parameter 2) is reached.

Whenever the requirement on standard deviation is satisfied, the test on the drift is performed: the difference between the first and last measurements of the set must be within the tolerance specified (parameter 6) to ensure that equilibrium was reached. Please note that the drift tolerance (parameter 6) is tied to the time interval between readings (parameter 3): setting parameter 6 to X and parameter 3 to Y means that the difference between 2 readings separated by 10×Y time units should be below the threshold value X; this should be held in consideration when faced by kinetical problems. Again, if the set of readings fails the test another reading is performed (if allowed by parameter 2), the new set is evaluated for its standard deviation and eventually for its drift.

Whenever a data set passes both tests the point is accepted, the values are memorized as strings composed of added titrant volume, mean value of emf, number of readings performed, standard deviation and drift; the system then proceeds with the next titrant addition.

If obtaining a data point of the required quality is impossible within the maximum number of readings allowed, the string is recorded as it is at the end, with its parameters signalling that proper criteria were not fulfilled.

Titration curves thus obtained were treated with the HYPERQUAD [21] program to determine equilibrium constants.

2.1.1.2 Determination of the Equilibrium Constants

The determination of equilibrium constants in solution would in principle require the exact measurement of the concentration of each and every species involved in the studied equilibria. Although this would render trivial the ascertainment of the desired constants, such route is rarely frequented, as it proves impractical even for simple cases and almost impossible for complex systems with several simultaneous equilibria.

The most common approach involves mathematically relating the concentration of a single component, the sought set of equilibrium constants and the initial concentration of all the species in solution: in this way, at least in principle, the global composition of the system and the stability constants can be derived by the exact measurement of the concentration of just one species.

Said measurement can be performed by potentiometry, *i.e.* monitoring the potential difference existing between a reference electrode and a selective electrode for the species of interest, for which the relationship between concentration and potential difference is known.

In the case of coordination chemistry, especially when hosts and guests can undergo protonation and/or deprotonation equilibria, the choice of a glass electrode, selective for the hydrogen ion H^+, is very convenient.

The measured potential difference and the concentration of H^+ are related through Nernst equation:

$$E = E^0 + \frac{RT}{F}\ln\left(\frac{a_{H^+}^{in}}{a_{H^+}^{out}}\right) = E^0 + 0.0591 \cdot \left(pH^{out} - pH^{in}\right) = E^{0'} + 0{,}0591\, pH^{out}$$

where E is the measured potential difference, E^0 is the standard cell potential, a_{H+} are the activities of hydrogen ion inside (*in* superscript) or outside (*out* superscript) the glass membrane. Definition of pH is implicitly used.

The value of $E^{0'}$, which factors in also the fixed pH of the solution inside the membrane, is required to assess the concentration of the hydrogen ion from an emf measurement: its accurate experimental determination is thus required right before performing any measurement.

Calibration of the electrode in the chosen experimental conditions is performed by titrating an exactly known amount of strong acid with strong base and evaluating the equivalent point through Gran's method, [22] which provides both the water ionic product (K_w) and $E^{0'}$.

Let us now consider a general case of simultaneous equilibria involving complex formation, *e.g.* the association between an anion A^{n-} and its ligand L to give protonated complexes of various stoichiometries according to the generic equation (charges omitted for clarity):

$$pA + qL + rH = A_pL_qH_r$$

In this way, the range of possible complexes formed by any anion-ligand-proton system is unambiguously associated to a triad of coefficients {*p; q; r*}; for each of them it is possible to define a stability constant in the general form:

$$\beta_{pqr} = \frac{[A_p L_q H_r]}{[A]^p [L]^q [H]^r}$$

Since both anion and ligand may be able to undergo protonation, also the generic protonation equilibria

$$A + iH = H_i A$$
$$L + jH = H_j L$$

with their relative {*i*} and {*j*} indexed protonation constants (or, equivalently, {*1; 0; i*} and {*0; 1; j*})

$$\beta_i = \beta_{10i} = \frac{[AH_i]}{[A][H]^i}$$
$$\beta_j = \beta_{01j} = \frac{[LH_j]}{[L][H]^j}$$

will be taken into consideration.

The total amount of the three associating species A, L and H can therefore be expressed as:

$$T_A = [A] + \sum_{pqr} p\,[A_p L_q H_r] + \sum_i [H_i A]$$
$$T_L = [L] + \sum_{pqr} q\,[A_p L_q H_r] + \sum_j [H_j L]$$

$$T_H = [H] + \sum_{pqr} r\,[A_p L_q H_r] + \sum_i i[H_i A] + \sum_j j\big[H_j L\big] - [OH]$$

Now, by explicitly introducing in the equation the stability constants β_{pqr} and the basicity constants β_{10i} and β_{01j}, we obtain the following system of equations:

$$\begin{cases} T_A = [A] + \sum_{pqr} p\ \beta_{pqr}[A]^p[L]^q[H]^r + \sum_i \beta_{10i}[A][H]^i \\ T_L = [L] + \sum_{pqr} q\ \beta_{pqr}[A]^p[L]^q[H]^r + \sum_j \beta_{01j}[L][H]^j \\ T_H = [H] + \sum_{pqr} r\ \beta_{pqr}[A]^p[L]^q[H]^r + \sum_i i\beta_{10i}[A][H]^i + \sum_j j\beta_{01j}[L][H]^j - [OH] \end{cases}$$

Please note that T_A, T_L and T_H values are exactly known if the initial sample amounts and titrant additions (concentration and volume) are known.

During the titration, the concentration of the hydrogen ion is assessed experimentally, thus obtaining the customary titration curve emf vs added volume of titrant.

For each experimental point, the above system of equations can be written, giving rise to a problem of 3N equations and n+2N unknowns, where N is the number of experimental points and n that of the sought for equilibrium constants, the 2N

added unknowns being the equilibrium concentrations of A and L ([A], [L]) for each experimental point.
Although, provided a sufficient number of experimental points is available, the problem might be straight away soluble, it is important to stress that this is not the general route followed experimentally: good practice demands for a preliminary study of the protonation of A alone and L alone (*i.e.* binary systems consisting only of the proton plus another species), providing much simpler equation systems to solve and largely remediating to the correlation between determined parameters often observed in trying to solve simultaneous equilibria in A-L-H ternary systems at once.
For convenience reasons, we are not concerned with the analytical solution of the system, while, as often happens, iterative algorithms are preferred for a cost-effective solution of the system of equations.
The software HYPERQUAD [21] has been thoroughly used during this thesis project. This program essentially performs a non-linear least square refinement of the experimental data, using as an input the experimental data (titration curve (emf. vs added volume), $E^{0'}$ value, titrant concentration, starting volume, initial amount of each species (T_X)) plus the indication of a model ({*p; q; r*} strings defining the expected species and a starting value for the associated β_{pqr}).
The function to be minimized for solving for the equilibrium constants is:

$$U = \sum_i w_i \, (E_i^{calc} - E_i^{exp})^2$$

where the summation index *i* runs over the experimental point, *w* are weighting coefficients (*vide infra*) and E the calculated (based on the provided model, subject to refinement) and experimental values of the emf.
Weighting coefficient *w*, which account for the statistical relevance of each point, are inversely proportional to the quality parameter σ^2, defined for each point *i* as:

$$\sigma_i^2 = \sigma_e^2 + \left(\frac{dE_i}{dV}\right)^2 \cdot \sigma_v^2$$

where σ_e^2 and σ_v^2 are the variances of the emf reading of the instrument and of titrant addition, respectively, while the derivative is just the slope of the potential vs added volume curve: *i.e.* the higher the slope, the less robust the data towards volume addition errors, *viz.* experimental points collected at or nearby equivalence points will have lower impact than the more certain data originating from buffered regions.
The program solves the matrix equation:

$$\boldsymbol{A^T W A s = A^T W e}$$

where **W** is the statistical weight matrix, **A** contains the partial derivatives of emf with respect to the refined parameters, $\mathbf{A}^T$ is **A**'s transpose, **e** is the vector of residuals on potentials, *i.e.* (E_{calc}-E_{exp}) and **s** the vector containing the deviations to be applied to the refined parameters.

The vector **s**, determined through U minimization, allows to move from the starting arbitrary trial values for the equilibrium constants to the final refined values: the best possible refinement with the available data points is obtained whenever a self-consistent set of values is obtained.
Two statistical parameters are provided by the program to guarantee the goodness of fit, the standard deviation σ and the χ^2, beyond that, the software allows to visualize the (E_{calc}-E_{exp}) residues for each data point.
σ is calculated as:

$$\sigma = \sqrt{\frac{\boldsymbol{e}^T \boldsymbol{W} \boldsymbol{e}}{(N-k)}}$$

with N number of experimental points and k number of refined parameters.
Values of $\sigma \leq 3$ are generally required to ensure proper quality of the data. High values of σ, when not ascribable to experimental problems (*e.g.* formation of precipitates during the titration), demand the insertion or removal of species from the initial trial model, as some equilibria may not have been individuated or an overparameterization of the data may have occurred.
For individuating chemical species missing in the model but actually formed in the measurement cell, one can easily resort to the point by point (E_{calc}-E_{exp}) plot, as characteristic patterns in the error distribution are easily spotted in the case of missing species. The problem of overparameterization is instead resolved following IUPAC's guidelines, which commit to the well-known Occam's razor: thus, whenever a system can be solved invoking a lesser number of equilibria while maintaining the same goodness of fit, the simplest possible solution should be held true; of course, finer statistical analyses on the available data or new experimental investigation can and should be performed in the most doubtful cases.
χ^2 test is run in a traditional fashion to assess whether or not there is a proven incidence of systematic errors in the treatment. To allow the use of a single methodology for all experiments, no matter the number of collected points or that of the refined parameters, data are equally divided in 8 classes according to their distribution around $\sigma = 0$ (*i.e.* no systematic errors exist in the treatment). As such a 7 degrees of freedom test is always obtained, with 12.6 being the critical value for a 95% significant level indication of unbiased results.

2.1.2 Isothermal Titration Calorimetry

Calorimetric measurements were performed with a TA instruments TAM III calorimeter using the same purity grade for starting materials and the same precautions to exclude CO_2 from the media as reported in 2.1.1.1 for potentiometry.
Isothermal Titration Calorimetry allows for the determination of both equilibrium constants and enthalpic components (ΔH^0) of solution equilibria: the knowledge of both allows for the calculation of the entropic term ($-T\Delta S^0$) through the well-known thermodynamic relations

$$\Delta G^0 = -RT \ln K_{eq}$$
$$\Delta G^0 = \Delta H^0 - T\Delta S^0$$

Such a dissection of the stability constants in its thermodynamic parameters, providing vital details for understanding complex formation events and assessing their driving force, is among the strongest points of the technique.
The discussion on calorimetric determination of equilibrium constants, although engaging, is not pertinent to this thesis, where a potentiometric method was adopted: an accessible overview on the matter, with references for in depth discussion, is provided in [23].
In general, previous knowledge of the simultaneous equilibria occurring in a system from potentiometric data, allows for a much easier treatment of calorimetric data: in fact, provided initial concentrations, starting volume, titrant concentration, injection volume and the full set of equilibrium constants are given, the point-by-point equilibrium composition of the system is univocally determined.
This means that the overall observed release or adsorption of heat for each experimental point, ΔQ_k, no matter the complexity of the system, respond to the simple equation:

$$\Delta Q_k = \sum_i x_i \, \Delta H_i^0$$

where x_i is the variation of the concentration of species *i* (negative if the species *i* is consumed) between the experimental points *k* and *k-1* and ΔH^0 the heat associated to the process.
Be *n* the number of discrete equilibria and *N* the number of data points, the problem of determining the *n* unknowns becomes finding a set of *n* ΔH^0 values which minimize the residuals between calculated and measured heats, *i.e.* again a least square refinement.
The program HYPDELTAH, which by the way also allows for the simultaneous determination of the binding constants, has been used for the purpose: it belongs to the HYPERQUAD suite [21] (*cf.* 2.1.1.2) and, *mutatis mutandis*, performs qualitatively the same functions for calorimetric type data.
Cycles of refinement are performed until the systems converges to a self-consistent set of ΔH^0 values with proper quality parameters (*cf.* 2.1.1.2).

2.1.3 Nuclear Magnetic Resonance

NMR data herein presented were recorded on a Bruker Avance III 400 MHz spectrometer.
pH adjustments of the solution were carried out using DCl and NaOD and correlating pH and pD through the pH = pD – 0.4 equivalence.

2.1.4 UV-Visible Spectroscopy

UV-Vis spectra herein presented were recorded on a Jasco V-670 spectrophotometer at 298 K.
Solutions of appropriate concentration for analysis were obtained by dilution, in a weighted amount of CO_2-free MilliQ water, of stock solutions of reagents prepared by direct weighting of the starting materials in said solvent.
Titration were performed either by addition of known small volumes of titrant or, in the case of acid-base curves, by bubbling small amounts of HCl-saturated air or addition of solid NaOH directly in the quartz cuvette to avoid dilution effects as much as possible.

2.1.5 XPS

The XPS spectra have been obtained in a Kratos Axis Ultra DLD spectrometer. Monochromatic Al/Mg K_α radiation from twin anode in constant analyser energy mode with pass energy of 160 and 20 eV (for the survey and high-resolution spectra, respectively) was used. The C1s transition at 284.6 eV was used as a reference to obtain the heteroatoms binding energies. The accuracy of the binding energy (BE) values was ± 0.2 eV.

2.2 Synthetic Procedures

Synthetic approaches are described case-by-case in the dedicated paragraphs of the anion or cation coordination sections. The Reader is gladly addressed to 3.3 and 4.2.1.1.

2.3 Crystallization

Preparation of single crystals suitable for X-ray diffraction analysis was performed in most cases by weighting appropriate quantities (5-10 mg) of ligand, dissolving them in an appropriate solvent, and adding a solution of the substrate, either containing an excess or a stoichiometric amount of it with respect to the ligand, depending on the cases. Water, ethanol or water-alcohol mixed systems were the most commonly used solvents in the framework of this thesis.
The pH was adjusted case by case to favour the host-guest interaction on the basis of the potentiometric data.
When dealing with cationic guest species, the metal cation was oftentimes provided in the form of its perchlorate salt, as the perchlorate counterion is known to favour the precipitation of solutes from polar environment like water.

At times, when dealing with extremely insoluble complexes, which upon mixing would give rise to instant precipitation of amorphous or polycrystalline samples not suitable for analysis, diffusional techniques were employed. The main one is diffusion of two, initially separated, host and guest solutions inside a carefully filled (*i.e.* without mixing) H-shaped sealed tube.
Whenever needed, air-sensitive samples were handled and crystallized in a glove box under an inert (N_2) atmosphere.
For precise experimental detail concerning the preparation of each crystalline sample, the Reader is addressed to the corresponding publication, whose reference is promptly given in the text. The same goes for specifics concerning X-ray diffraction experiments and structure solving methods.

3 CATION COORDINATION CHEMISTRY

3.1 RESEARCH OBJECTIVES

Aim of the cation coordination chemistry part of the present thesis is developing a new methodology for the production of tailored heterogeneous catalysts. Arene-spacer-function (Ar-S-F) (***Figure 3.1-1***) molecular systems, suitable for the task, were then devised and prepared.

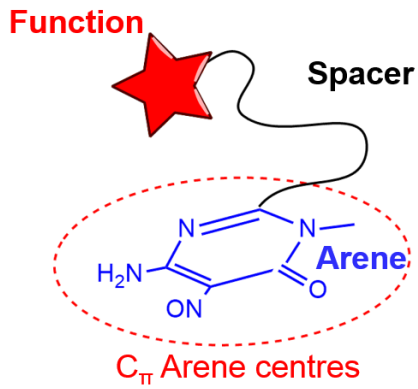

Figure 3.1-1. *General scheme of Ar-S-F ligands, with our signature pyrimidine as the Ar subunit.*

Specific azamacrocycles (F) were designed to recognize and bind metal cations of choice providing, at the same time, enough thermodynamic stability and an activated position in the metal's first coordination sphere, thus granting both resilience and reactivity to the final catalysts. Such molecular moieties, elongated with a spacer (S), were conjugated with a click process to a suitable anchoring group (Ar), capable of grafting them on graphitic surfaces by means of supramolecular interactions. As such, the three tectons [4], *i.e.* the ligand, the metal cation and the graphitic surface, are able to spontaneously self-assemble to produce the final catalyst, consisting in a continuous distribution of single-ion catalytic centres hanging from the graphitic surface in a brush-like fashion. Since the procedure aspires to stand as a general method of wide scope, *i.e.* not restricted to any reaction, the first target to demonstrate its effectiveness was designated, aiming high, as the Sonogashira cross-coupling.

Before delving into the more technical "Result and Discussion" section (*c.f.* 3.4), it is useful to introduce some background knowledge about the developed themes, clarify the choices made and contextualize the research looking at the bigger picture.

3.2 CHOICES EXPLANATION

3.2.1 Polyamines [24]

Polyamines and azamacrocycles are among the most important and well-described metal chelating agents. Recognized early on as widely employed ligands in many different fundamental life processes, ranging from the transport function of Fe(III)-porphyrin complex of the heme group up to the photosynthetic Mg(II)-chlorophyll complex, they became a hot topic starting from the 1960s, when the development of synthetic techniques allowed an in depth study of their coordinative properties, providing useful model systems for understanding and eventually mimicking the biological function of their natural complexes.

A second blooming came in later times due to the advent of Supramolecular Chemistry, a simple change in pH allowing azamacrocycles to become precious hosts for anions, possessing a preorganized cationic cavity capable of strong cooperative interactions with the anionic guest through charge reinforced hydrogen bonds (salt bridges).

Flexibility of use, by virtue of their pH-dependent speciation, together with the tunability offered by perfected synthetic strategies, which allowed the achievement of selective systems, ultimately made the fortune of this class of ligands.

Concerning our purpose, we seek on one hand thermodynamic stability and kinetic inertness for our catalysts, *i.e.* we want them to be stable under reuse, with the metal cation firmly hold in place where it belongs, and a functional behaviour on the other, *i.e.* reactivity, else no catalytic effect could be possible. This is exactly the way Nature uses azamacrocycles, orienting and stabilizing metal ions, within the framework of metal enzymes, in an activated arrangement: favouring the desired reactivity while preserving the active metal centre, whose loss would deprive the enzyme of its functional behaviour. As such, no better candidates than this class of ligands could possibly be devised.

This, together with our group's long expertise in the field (the Reader is encouraged to doublecheck [24]), is what makes azamacrocycles, and polyamines in general, first choice molecular moieties for our study.

3.2.2 Carbon-based Materials

Materials with extensive graphitic surfaces, like activated carbon, are already commonly employed in many industrial applications like purification of liquids or gases, extraction and, of course, in catalytical processes (*e.g.* the most classic Pt/C), mainly due to their specific surface area and the remarkable adsorption properties associated to it.

Although our primary studies in the field involved activated carbon (AC) (*cf.* 3.2.5), we moved to carbon nanotubes (CNTs), essentially seeking a more homogeneous, negligibly functionalized, quasi-molecular substrate, whose surface area is basically wholly exposed.

CNTs are allotropic forms of carbon that can be thought of as extremely elongated fullerenes: Euler's polyhedron formula prescribes the presence of no more and no less than 12 pentagonal faces, yet does not limit the number of the hexagonal ones. As such, a carbon nanotube can be ideally obtained separating the two halves of a base fullerene of choice with an arbitrary number of fused cycloacenic, phenacenic or paracyclophanic molecular belts, depending on the chirality of the nanotube.

A more instructive schematization, although chemically even less feasible as a synthetic route than the previous, is looking at a nanotube as the roll-up product of a graphene sheet, of course with proper bond reorganization to make sure that the formally sp^2-hybridized carbon network is not interrupted by unsatisfied valences (***Figure 3.2-1***).

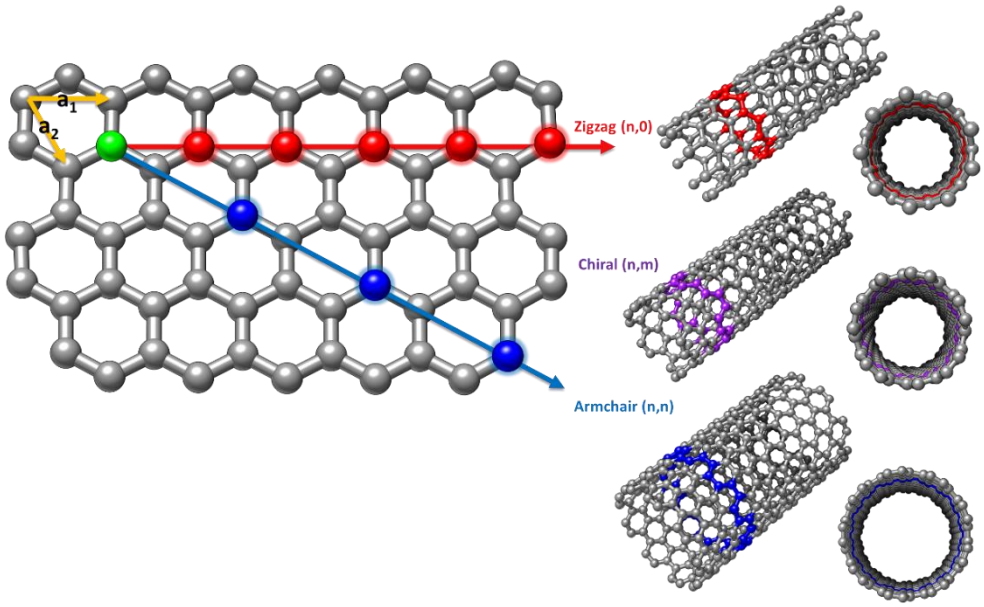

Figure 3.2-1*. Schematization of structural properties of CNTs according to their ideal roll-up formation from a graphene sheet.*

In this way, it is possible to define on the graphitic plane two Bravais lattice vectors ($\underline{a}_1$ and $\underline{a}_2$, ***Figure 3.2-1***) and classifying each possible structure with the associated (n,m) pair of indexes, or equivalently, to the associated chiral angle.

The two (n,m) indexes need to be integer to guarantee the perfect closure of the tubular structure, and allow to distinguish three main classes on nanotubes: the (n,0) or zigzag (due to the pattern of their section, *cf.* ***Figure 3.2-1***), the (n,n) or armchair and the far broader family of the generic (n,m) tubes, called chiral.

What may look like structural notation or nomenclature rules, are indeed fundamental parameters for CNTs' properties: if a graphene sheet would possess a metallic behaviour due to the zero band-gap between its valence (π) and conduction (π*) bands, in CNTs the density of states depends intrinsically on the structure, *i.e.* on its diameter and chirality. This is due to the cylindrical symmetry, which imposes a curvature on the planar network of the π orbitals of graphene, ultimately resulting in a different σ-π hybridization depending on the structural parameters. Alternatively, we can speak of quantum confinement effects due to the mono-dimensionality of these systems: as a matter of fact, metallic or zero band-gap nanotubes (n=m, armchair), semimetallic nanotubes, with band-gaps in the meV region (n-m=3k, with k integer), and semiconducting nanotubes, with band-gaps in the eV range (n-m≠3k, k integer), can be distinguished.

Interesting conduction phenomena, as well as their renowned outstanding mechanical properties, made CNTs attractive materials for a broad spectrum of applications. [25] Such peculiar chemical and physical properties did not go long unnoticed even for catalytic purposes. [26]

Although this will be further discussed in the 3.2.4 section, it is evident that a covalent approach to the surface functionalization of CNTs leads to a vast disruption of the π delocalized systems, ultimately altering the characteristic properties discussed above, which makes CNTs attractive for a plethora of purposes. This, together with the other arguments presented 3.2.4, made us opt for a supramolecular functionalization which does not tamper with the delocalized structure. Beyond the advantages over the use of AC mentioned above (see also 3.2.5), the higher inertness of CNTs should be stressed: this is not a matter of concern for catalytic systems based on adsorbed metal complexes, but opens up the possibility of further manipulation of the material, *e.g.* through a reduction step, to obtain supported metal nanoparticles (*cf.* Appendix A and [27]). In chemical (*e.g.* $NaBH_4$) or physical (*e.g.* hydrogen plasma) reductive processes, AC undergoes much deeper structural modifications than CNTs do and, due to its intrinsic higher

heterogeneity, offers a much less reliable control over the spatial distribution and size dispersion of the resulting particles.

Lastly, carbon-based supporting materials, even the most advanced ones (despite being pricey compared to AC), fall within an environmental friendly and sustainable technology perspective, as many other choices in this work (see also 3.2.3), as shortages of the raw material, *i.e.* carbon, are and will remain out of question.[11]

3.2.3 Target Reaction

Palladium-catalysed coupling reactions, leading to C-C, C-N and C-O bond formation, are highly significant to efficiently access products which would otherwise require far more impractical routes. The advantages they offer are relevant both in terms of costs (yields, reaction rates) and of required synthetic efforts (reaction conditions, selectivity). As all powerful synthetic tools, they found a growing recognition in the scientific community, at present peaking with the 2010 Nobel prize to R. F. Heck, E. Negishi and A. Suzuki: a collection of names that reminds a set of reactions, and not by chance.

Sonogashira cross coupling (*cf.* [28] for the seminal paper) is a carbon-carbon bond forming reaction involving a terminal alkyne and an aryl or vinyl halide according to the general scheme (***Figure 3.2-2***):

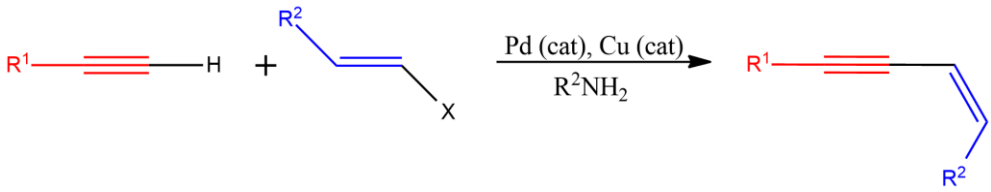

Figure 3.2-2. *General scheme for the Sonogashira cross coupling.*

Mechanism is still partially debated, especially for the Copper free version of the reaction which, incidentally, is the main goal of the experimental part; as such, the Reader is addressed elsewhere for a proper discussion on the topic. [29]

Pd-catalyzed coupling reactions share the common feature of having been developed employing homogeneous catalysts. This has generally been subject to revision, as the difficulty in recovering, and thus re-using, expensive homogeneous catalysts, together with potential purity problems connected to catalyst's residues in the final products, prompted many to attempt at the development of heterogenous systems, capable of overcoming such shortcomings and promoting a

[11] The green aspect is truer the better we manage to perfect CNTs preparation methods and reduce the use of transition metal catalysts. Improvements are still required in this area.

large-scale employment of otherwise costly reactions. This explains the emphasis of this thesis on the heterogeneous nature of the catalysts.

Before receiving the deserved attention by the community, the situation was exactly the same for Sonogashira coupling: industrial application being prevented (or limited to the production of high added value molecules) by the required amount of catalyst and by the air sensitive nature of the used Pd complexes (*i.e.* phosphine complexes), requiring an inert atmosphere.

This primarily made this reaction a suitable target for our study.

One of the strong points of the Sonogashira reaction is that it requires relatively mild conditions, allowing a certain tolerance towards other functionalities, thus enabling the synthesis of complex molecules. In view of this, design and preparation of the catalysts (*cf.* 3.2.4 and 3.4.3.1) were performed to make them water-compatible, enabling the use of water as solvent for the coupling process. Furthermore, the uniform dispersion and ready availability of active sites at the surface (*cf.* 3.2.4) as an expedient to hopefully limit the required thermal energy, *viz*. the working temperature, for the formation of the catalyst-reagent activated complexes. The effort was on raising the bar on reaction conditions, making them even more gentle, having in mind both the potential synthetic advantage and the fact that power-saving processes and green solvents are also of global interest from an environmental perspective.

Finally, the choice of the Cu-free version of the reaction is self-explanatory: since Copper can promote the here undesired Glaser oxidative homocoupling of the terminal alkyne, considering that quite a few Pd catalysts (many of which homogeneous, though) capable of promoting the reaction in the absence of Copper were reported, there was no reason not to assay the Cu-free Sonogashira cross coupling first.

3.2.4 Supramolecular Approach

The signature chemical strategy[12] for the production of nanoscale materials is the bottom-up approach, where Supramolecular Chemistry, through molecular recognition and self-assembly, plays a major role. [30]

When speaking about surface decoration, however, it should be stressed that covalent procedures, both according to a “grafting to” or a “grafting from” strategy, are available for a broad range of materials (*e.g*. silyl derivatives for glass or silica decoration, direct or defective sites strategies for graphitic walls, and a whole world

[12] Although it was inspired by a physicist… (*cf.* “There’s Plenty of Room at the Bottom” (1959) by Richard P. Feynman)

of processes involving polymers, many of which nowadays owe to the development of click-chemistry).

At times, self-assembly is presented as a life saver: why bothering to devise a synthetic route involving a set of high yield orthogonal reactions to decorate a surface, as in a "grafting from" approach, when thiols on gold self-assemble so smoothly forming an even monolayer on their own? Although there may be a point in these arguments, no surface decoration method can disregard the chemical nature of the partners involved and the recognition of an interaction mechanism granting the desired junction. As such, covalent approaches, each on its own merits, in view of the chemical identity of the concerned species and target application, have their pro and con cases with respect to an equivalent non-covalent methodology.

Since a supramolecular approach was adopted in the present thesis, it is useful to discuss its advantages for our objectives.

First, looking from the Pd-complex perspective, the stabilizing and activating function of the polyaminic ligand (*cf.* 3.2.1), necessarily involves a supramolecular design and understanding of the host-guest interactions and of the resulting properties of the final supermolecule, not to mention an estimate of its possible interplay with the reagents of the Sonogashira cross coupling (see 3.2.3) to grant the desired catalytic effect. That is to say that, set aside surface decoration, an intrinsic supramolecular component exists in this project.

The second reason, as partially addressed in 3.2.2, is surface-dependent, aiming to maintain electronic and structural properties of CNTs which would otherwise be disrupted by a covalent approach.

This, however, is not the whole story.

Covalent approaches, either direct methods engaging the graphitic wall or exploiting defective sites or heteroatomic functions, rarely offer the spatial control and homogeneity of functionalization achievable through a self-assembly process. Defective sites or heteroatoms do not have any reason to be evenly distributed on a surface, eventually requiring harsh pre-emptive surface modifications to introduce them: direct methods, instead, requiring reactive species (*e.g.* peroxides, fluorine, carbenes, nitrenes, *et cetera*) or activated organic substrates (*e.g.* azomethine ylides, *cf.* Prato reaction, diethylbromomalonate, *cf.* Bingel reaction, *et cetera*), will net statistically polyfunctionalized products.

Here the focus is on homogeneity, which is mandatory especially for the choice of single ions as catalytic centres, instead of, say, nanoparticles: this is an important

point to stress, since supported single molecule active sites are not widespread, but they could potentially allow to spare precious catalytic metals, again falling into the aforementioned (see 3.2.2 and 3.2.3) green chemistry trend.

Homogeneity oftentimes proceeds from spontaneous self-assembly, therefore in this work a π-π stacking non-covalent functionalization of CNTs was selected: although the approach is not new, being well-established and widely exploited for the purpose, there are some further advantages in our case which should be discussed.

First, the availability of a molecular moiety of proven effectivity with which we were, moreover, already familiar ([31], *cf.* Appendix B and 3.2.5), *i.e.* the 6-amino-3,4-dihydro-3-methyl-5-nitroso-4-oxopyrimidine (*the* pyrimidine hereafter) (***Figure 3.2-3***), which due to its marked electron-deficient character gives rise to strong chemisorption on graphitic surfaces. Furthermore, this heterocycle possesses the intriguing property of being a building block easily incorporated in any of our Ar-S-F type systems (*cf.* ***Figure 3.1-1***).

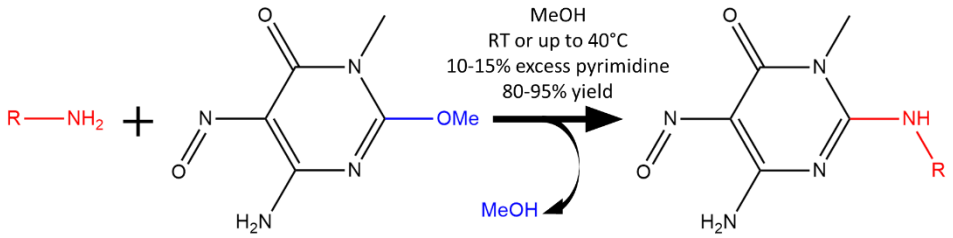

Figure 3.2-3*. Structure and reactivity towards primary amines of 6-amino-3,4-dihydro-3-methyl-5-nitroso-4-oxopyrimidine.*

It was important for us to devise a way of introducing the grafting Ar function that could be used effectively for a wide spectrum of functional groups F, whatever their chemical nature, for the sake of the universality of the method and in view of its possible applications to other problems. In this light, the pyrimidine was chosen as it can be used to selectively functionalize any primary amine in a click-like fashion according to the scheme proposed in ***Figure 3.2-3***, notably under very mild conditions, which, beyond the environmental concerns, are crucial for a broad compatibility with the functional groups of the chosen F moiety.

Accordingly, transformation of any functional group F into an Ar-S-F type molecule, suitable for our approach, only involves the insertion of a desired spacer function S, possessing a primary amine, and its facile conjugation with the pyrimidine, thus providing a wider scope perspective to the whole work.

A second reason to pick up the supramolecular functionalization route, resides in the simplicity of functionalization.

Sure, time and synthetic efforts are required to adequately prepare the tectons, but once everything is in place, surface functionalization happens spontaneously in water at room temperature through chemisorption of the arene centres of Ar-S-F molecules on the CNTs, while the hydrophilic azamacrocyclic F functions work as dispersing agent, segregating bundles and allowing the full exposure of the CNTs surface to the procedure. Beyond the obvious advantage of being a self-process, a key point is again the mildness of the process, which allows to confer the designed molecular properties to the surface without resorting to harsh conditions, which may alter either the adsorbate or the CNTs properties. Preservation of the engineered properties results in a more homogeneous nature of the final products in terms of chemical identity (*cf.* the importance of homogeneity for these systems, *vide supra*) and allows the preparation of the Pd-loaded system again by dispersing the receptor-functionalized nanotubes in a solution of the metal cation.

As discussed above for our specific case, the advantages of a supramolecular functionalization approach can be summarized as follows:

1. It allows the preservation of CNTs structural and electronical properties;
2. It allows the surface functionalization step to happen according to a spontaneous self-process, in mild conditions and promoting an even distribution of sites;
3. It allows the subsequent metal binding step to happen in the same favourable conditions;
4. It is a general process, which through a careful choice of the F function, allows for a ready extension of the developed methodology to other systems;
5. It harmonizes with the overall efforts to develop a new method in an environmental friendly manner.

3.2.5 Previous Experiences

This section aims to spend a few words on the origins of the present work, collocating it within the ongoing research line and providing some useful references, as this appears beneficial to its overall comprehension.

My experience with decoration of carbonaceous surfaces ([31], *cf.* Appendix B) began with AC as supporting material, which was later abandoned, as anticipated in 3.2.2, in favour of carbon nanotubes. Since recovery of target ionic species from their aqueous solution was the goal, AC was selected as an inexpensive substrate with some innate good adsorption properties. The transition to finer applications,

i.e. catalysis, required the switch to CNTs: irregularity and random functionalization present on the material were detrimental for our purposes. Beyond that, also the issue of porosity should be mentioned. Pore size-distribution, heavily depending on the preparation of the AC, had a heavy influence over the final properties of the hybrid materials: open meso- and macro-pores are required for the proper functionalization and functioning of the material, else ligand adsorption will cause pore occlusion or not happen properly due to the stereochemical constrains imposed by narrow pore size. Among the main advantages of CNTs, the fact the surface is basically wholly external should be stressed in view of the above.

As pointed out above (*cf.* 3.2.4), the pyrimidine moiety has been in use for a while, allowing us to grow confident with it both as anchoring group [31] and as anion-binding function ([32], *cf.* 4).

Nevertheless, the explored F functional groups (*cf.* ***Figure 3.1-1***) were linear or branched polyamines. That research line forked in the work presented in this thesis and in an extensive study of hyperbranched or dendrimeric molecules as candidates for F groups ([33] [34] [35], *cf.* Appendix C, D and E). This work, although did not lead to tangible results in surface decorations or catalysis, partially due to the facts that dendrimeric systems tend to elude the developed functionalization strategy, is both valuable on its own and relevant to the present study, being parallel, when not preparatory, to it: as such, the Reader is warmly encouraged to consult this further material at his convenience.

Lastly, most of the material presented in this section is published in two papers, ref. [27] and [36], whose full texts are provided in Appendix A and F: hopefully, the following exposition will prove clear enough not to urge my Reader to consult them, however they contain many valuable references, which could not be fully accommodated throughout the text, that may help clarifying doubts or simply refer to other selected researches.

3.3 STUDIED LIGANDS

Several new ligands were prepared and studied in the course of this thesis project.

HL1 and HL2 (***Figure 3.3-1***) devised as Pd(II) binding agents and assayed as heterogeneous catalysts for the Cu-free Sonogashira cross-coupling, were the main focus of the study.

A third ligand, *i.e.* HL3 (***Figure 3.3-1***), inspired by the interesting coordination properties of the others towards Cu(II), was prepared and investigated as a mean of obtaining Cu-decorated CNTs, either possessing Cu(II) complexes or Cu(0) nanoparticles at the surface.

Each of the obtained ligands has been prepared from the parent macrocyclic polyamine (**1**, **2** and **3**, respectively, *cf.* ***Figure 3.3-1***) according to a click-like conjugation with 6-amino-3,4-dihydro-3-methyl-5-nitroso-4-oxopyrimidine (*cf.* ***Figure 3.2-3*** and 3.2.4)

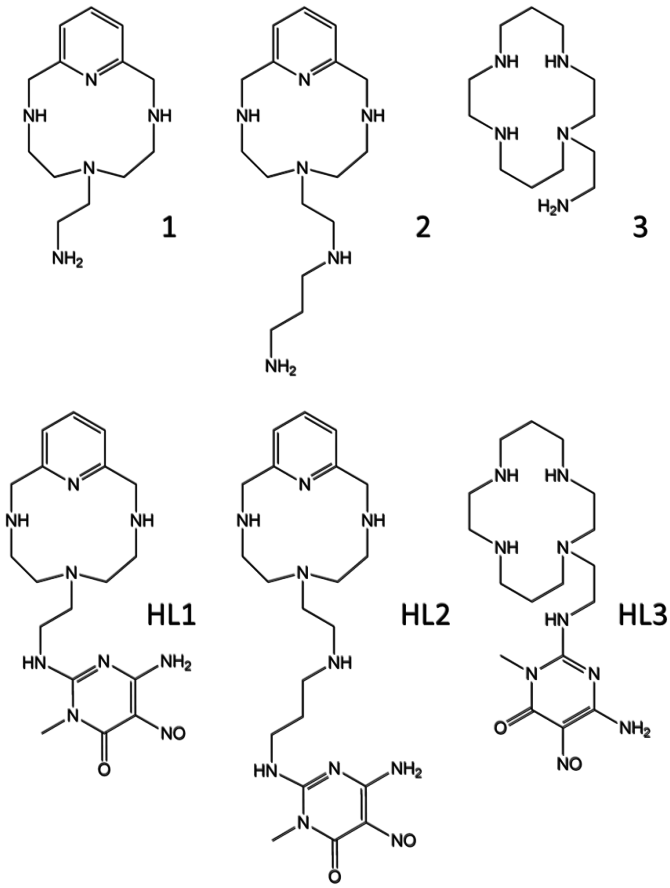

Figure 3.3-1. *The HL1, HL2 and HL3 ligands with their precursor molecules 1, 2 and 3.*

3.3.1 Synthesis of HL1

0.38 g (1.52 mmol) of 6-(2-aminoethyl)-3,6,9-triaza-1-(2,6)-pyridinecyclodecaphane (**1** in ***Figure 3.3-1***) [37] dissolved in 20 cm^3 of methanol were reacted at room temperature with 0.35 g (1.73 mmol) of 6-amino-3,4-dihydro-3-methyl-2-methoxy-5-nitroso-4-oxopyrimidine. The latter dissolves slowly over 8 h under stirring. The excess of pyrimidine was then converted into the insoluble 2,4-diamino-1-methyl-5-nitroso-6-oxopyrimidine derivative by reaction with ammonia (5 drops of 37% aqueous ammonia). After standing overnight in a fridge, the resulting suspension was filtered and the solution was evaporated to dryness under vacuum at room temperature to obtain HL1 as a deep purple solid compound. Yield 95%.

$C_{18.5}H_{31}N_9O_{3.5}$ (HL1·0.5MeOH·H_2O): calculated C 51.02, H 7.18, N 28.94; found C 50.93, H 7.19, N 28.70.

^{1}H NMR D_2O: δ (ppm) 2.62-3.46 (m, 13H), 3.74 (t, 2H), 4.55 (s, 4H), 7.37 (d, 2H), 7.88 (t, 1H).

3.3.2 Synthesis of HL2

HL2 was prepared by reaction of 6-(7-amino-3-azahexyl)-3,6,9-triaza-1-(2,6)-pyridinecyclodecaphane (**2** in ***Figure 3.3-1***) [38] with 6-amino-3,4-dihydro-3-methyl-2-methoxy-5-nitroso-4-oxopyrimidine according to the procedure adopted for the synthesis of HL1. Yield 73%.

$C_{22}H_{37}N_{10}O_4$ (HL2·MeOH·H_2O): calculated C 51.95, H 7.93, N 27.53; found C 52.30, H 7.68, N 27.68.

^{1}H NMR D_2O: δ (ppm) 2.90-3.28 (m, 15H), 3.34 (s, 3H), 3.66 (t, 2H), 4.56 (s, 4H), 7.38 (d, 2H), 7.88 (t, 1H).

3.3.3 Synthesis of HL3

HL3 was prepared by reaction of 1, 4, 8, 11-tetraazacyclotetradecane-1-ethanamine (**3** in ***Figure 3.3-1***) [39] with 6-amino-3,4-dihydro-3-methyl-2-methoxy-5-nitroso-4-oxopyrimidine according to the procedure previously described for the synthesis of HL1 and HL2. Yield 95%.

$C_{18.5}H_{31}N_9O_{3.5}$ (HL3·0.5MeOH·H_2O): calculated C 51.02, H 7.18, N 28.94; found C 50.93, H 7.19, N 28.70.

^{1}H NMR D_2O: δ (ppm) 2.62-3.46 (m, 13H), 3.74 (t, 2H), 4.55 (s, 4H), 7.37 (d, 2H), 7.88 (t, 1H).

3.4 Results and Discussion

As discussed in 3.1, the aim of the work is producing heterogeneous catalyst through a bottom-up approach, engineering their properties from the molecular level upwards and conferring them to the final materials through an Ar-S-F design (*cf.* ***Figure 3.1-1***) and a supramolecular approach to surface decoration (*cf.* 3.2.4).

As such, candidate F functions were recognized in the azamacrocycles of **1**, **2** and **3** parent ligands (***Figure 3.3-1***). The chosen macrocycles were used in the form of their scorpiand aminic derivatives, *i.e.* possessing a spacer S of variable length terminating in a primary amine function, in order to attach them in a one-pot high yield reaction to our pyrimidinic moiety Ar, which enables their chemisorption on graphitic surfaces.

In-depth characterization of their solution behaviour was pre-emptively performed both to ascertain the maintenance of the properties of interest throughout the derivatization process, and to be used as a basis for the further characterization of the ligand-CNTs and metal-ligand-CNTs hybrid materials.

Protonation was evaluated in view of the reported properties of the parent ligands and of analogous polyaminic systems, while metal coordination studies were oriented towards cations implicated in catalytic process (*e.g.* Zn(II) and Cu(II)), which could be used as a model for Pd(II) coordination, whose experimental assessment, although undertaken to some extent for HL1 and HL2, is hindered by kinetic inertness.

3.4.1 Choice of the F Functions

A brief account for the choice of the selected azamacrocycles will be given in this section, for a general discussion on the advantages of these kind of ligands see 3.2.1.

The shared macrocyclic unit of the **1** and **2** precursor molecules (***Figure 3.3-1***), here used as Pd(II) binding agent, was selected due to its supposed inability to adapt to the square planar geometry demanded by this d^8 metal cation. In fact, reported crystal structures of the $[CuL]^{2+}$ complexes of the precursor molecules **1** and **2**, show that the metal is coordinated to all four nitrogen atoms of the macrocycle and to all the nitrogen atoms of the pending arm, moreover not fully available for coordination in HL1 and HL2 due to the conjugation with the pyrimidine. [37] [38] The crystal structures of the $[ML]^{2+}$ (M = Mn(II), Ni(II), Zn(II)) [40] complexes of **2** are isostructural to $[Cu\mathbf{2}]^{2+}$, *i.e.* in all the reported structures the macrocycle is found to be bent in an incompatible manner with respect to a square planar geometry. This idea was further reinforced by the structure of $CuHL1(ClO_4)_2$, obtained during this thesis and reported below ***Figure 3.4-1*** (discussion in 3.4.2.3) to help visualize the bent conformation invariably exhibited by the chosen macrocycle, ultimately due to

its size and rigidity. The importance of leaving an activated position in the first solvation shell of the ion, lies in its increased reactivity which in turn should promote the catalytic behaviour (3.2.1).

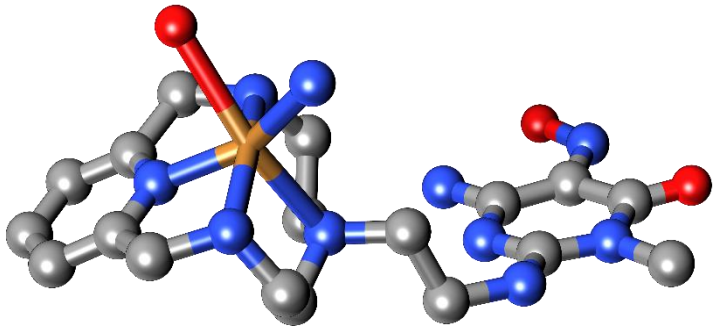

***Figure 3.4-1**. Detail of the conformation of the macrocycle in the crystal structure of CuHL1(ClO$_4$)$_2$.*

Development of the ligand HL3 owes much to the good results obtained both with Cu(II) binding and overall stability of the of the hybrid materials. In view of this, we decided to incorporate cyclam (1,4,8,11-tetraazacyclotetradecane), the most typical tetraazamacrocyclic moiety, well-known for the formation of extremely stable complexes with a series of cations (including Cu(II)) in our Ar-S-F systems. This was an important step, since addressing other catalytic processes is but a way to demonstrate the broad applicability of the whole methodology.

3.4.2 Solution Studies

3.4.2.1 Acid-Base Properties of the Ligands

Potentiometric (pH-metric) titrations performed in aqueous solution (0.1 M NMe_4Cl, 298.1 K) in the pH range 2.0-11.5 showed that HL1, HL2 and HL3 contain, respectively, four, five and four basic groups undergoing protonation, as well as an acidic group that starts being deprotonated above pH 10. The equilibrium constants determined for these processes are reported in ***Table 3.4-1*** in the form of protonation constants.

Table 3.4-1. *Protonation constants of ligands HL1, HL2 and HL3 (L) in 0.1 M NMe_4Cl at 298.1 ± 0.1. Values in parenthesis are the standard deviations on the last significant figure.*

Equilibria	***log K***		
	HL1	***HL2***	***HL3***
$L^- + H^+ = HL$	*11.13(4)*	*11.21(5)*	*11.22(3)*
$HL + H^+ = H_2L^+$	*9.28(5)*	*9.71(4)*	*10.43(3)*
$H_2L^+ + H^+ = H_3L^{2+}$	*7.83(7)*	*8.64(6)*	*8.55(4)*
$H_3L^{2+} + H^+ = H_4L^{3+}$	*2.3(1)*	*7.51(6)*	*3.23(5)*
$H_4L^{3+} + H^+ = H_5L^{4+}$	*1.6(5)*	*2.2(1)*	*1.99(5)*
$H_5L^{4+} + H^+ = H_6L^{5+}$		*1.6(5)*	

Species distribution diagrams for each ligand are reported below in ***Figure 3.4-2***.

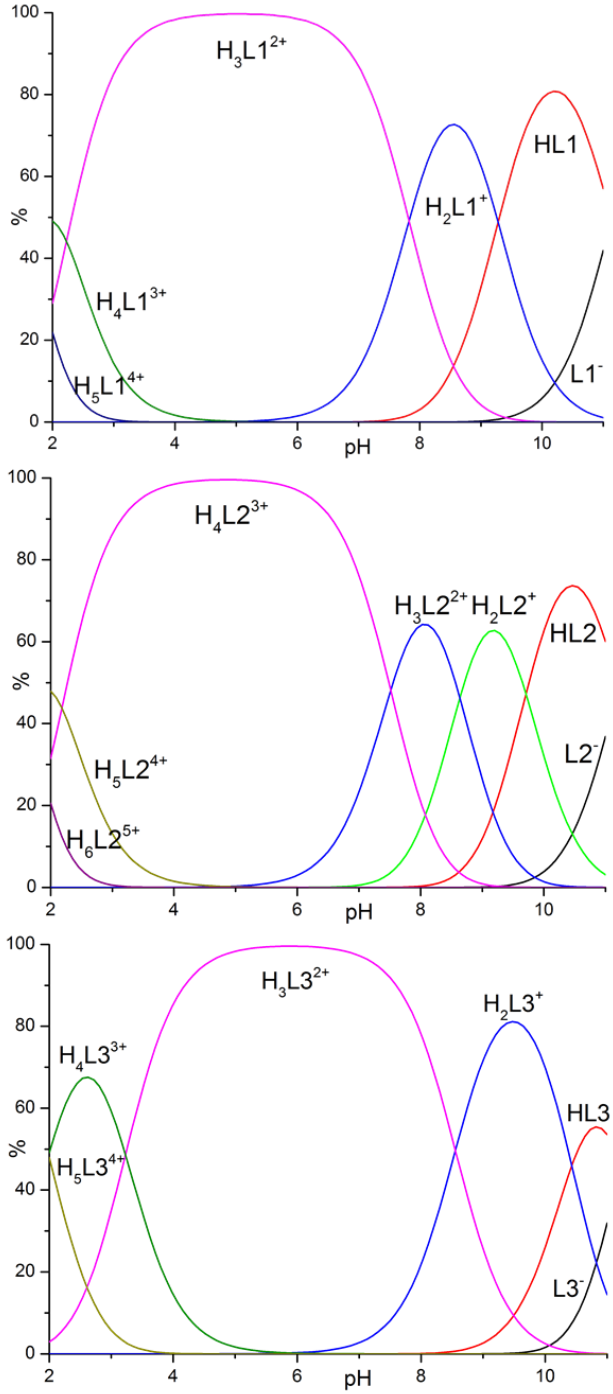

Figure 3.4-2. *Distribution diagrams for the protonated species of HL1, HL2 and HL3 as a function of pH. [ligand] = 1 10^{-3} M.*

According to the properties of other amine derivatives with the same pyrimidine residue, the protonation stages occurring at the highest pH values (log *K* = 11.13, 11.21, 11.22 ***Table 3.4-1***) should involve the amine groups directly connected to the pyrimidine ring, which are expected to be deprotonated at high pH, while the protonation stages corresponding to the log *K* values of 2.3, 2.2 and 1.99 (***Table 3.4-1***) should involve the pyrimidine nitroso groups.

This assignment of the protonation sites is confirmed by the pH dependence of the adsorption spectra of the three ligands.

As shown in ***Figure 3.4-3*** for HL1 and in ***Figure 3.4-4*** for HL2, their near-UV spectra are characterized by three bands centred at about 230, 265 and 330 nm corresponding to allowed π/π^* transitions between π-orbitals of the pyrimidinic group and overlapping with the band at about 265 nm of the pyridinic one. The spectra of both HL1 and HL2 display a marked pH dependence in acidic and alkaline solution, when protonation involves the pyrimidine chromophore, while in the intermediate pH region (4.0-9.0 approximately) they are almost invariant since protonation takes place on the non-chromogenic aliphatic amine groups. Interestingly, the equilibrium constants for the protonation stages involving the chromophores of the two ligands are equal, or almost equal within the experimental errors, in agreement with protonation occurring on almost identical sites; for the remaining proton binding processes, HL2 demonstrates a greater basicity, in terms of values and number of the protonation constants, according to the presence of one more amine group in its structure.

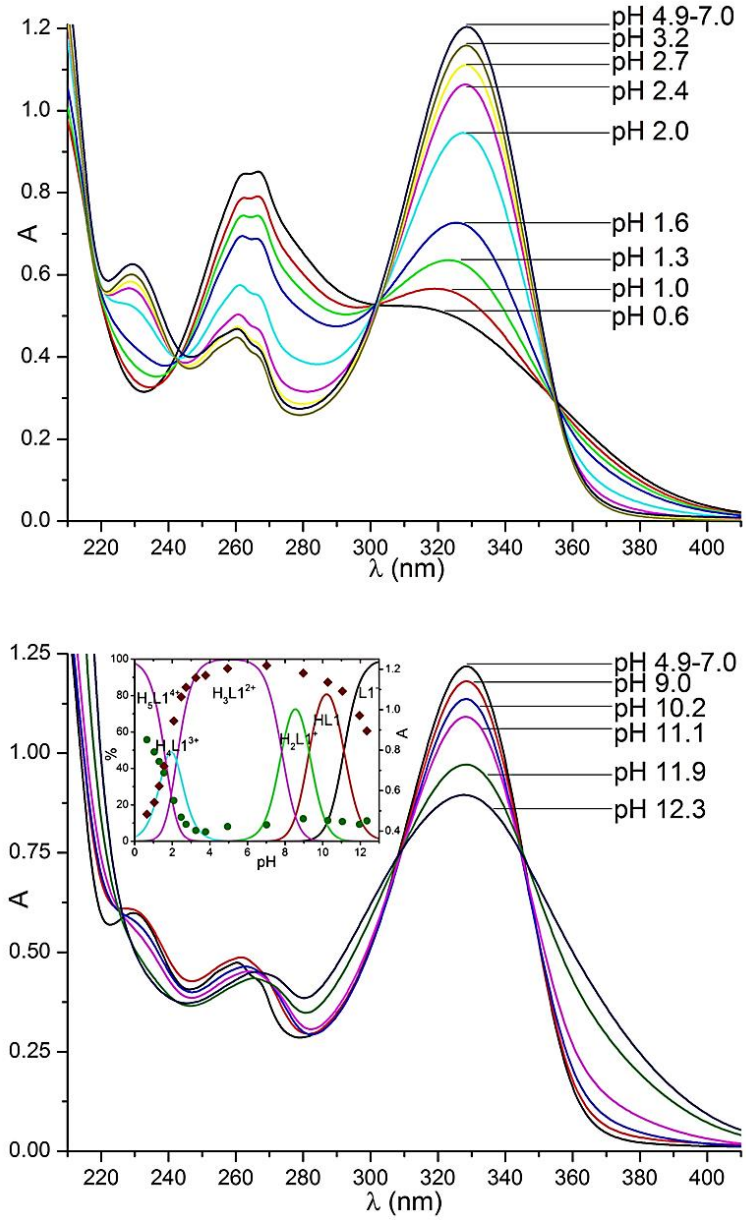

Figure 3.4-3. *UV absorption spectra of HL1 at different pH in aqueous solution: top pH 0.6-7.0, bottom pH 4.9-12.3. Inset: pH dependence of the 330 nm (red diamonds) and 265 nm (green dots) absorbances.*

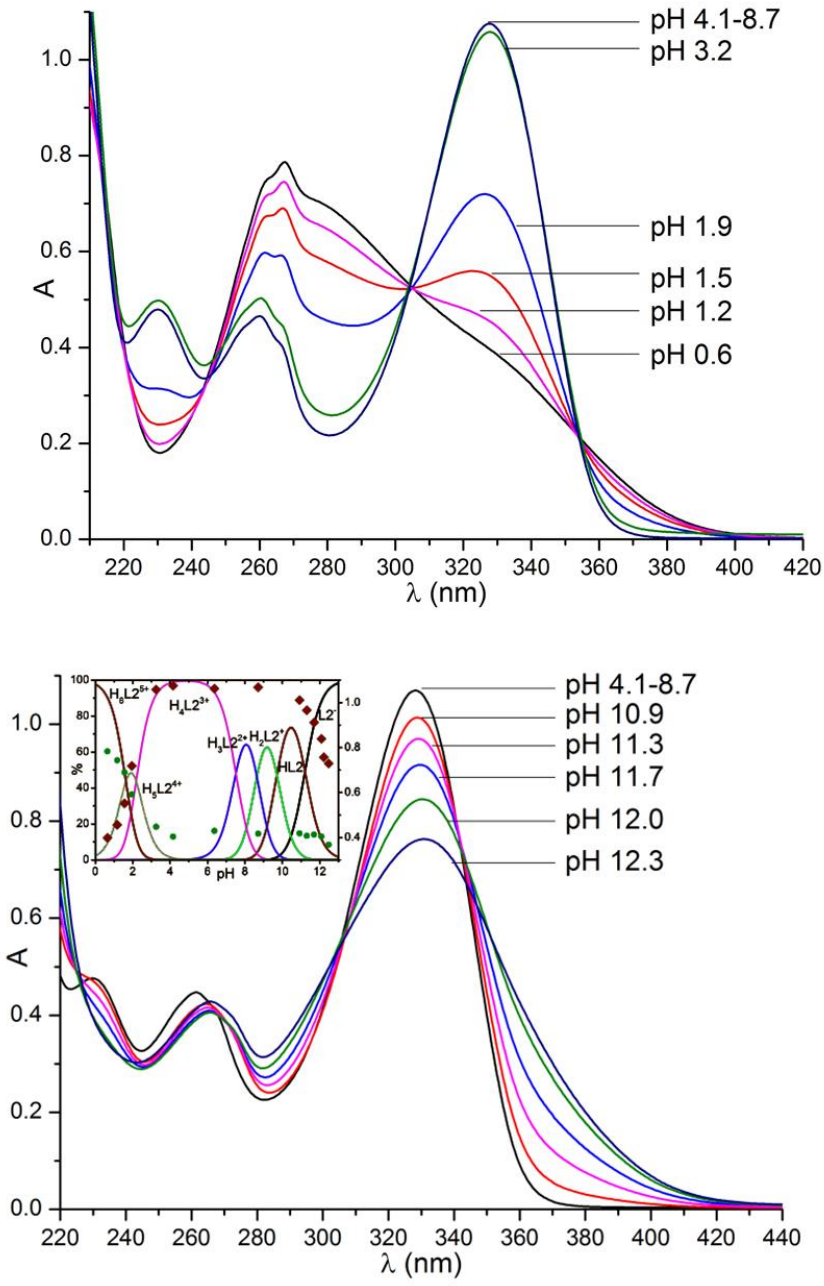

Figure 3.4-4. *UV absorption spectra of HL2 at different pH in aqueous solution: top pH 0.6-8.7, bottom pH 4.1-12.3. Inset: pH dependence of the 330 nm (red diamonds) and 265 nm (green dots) absorbances.*

The spectra of HL3 differs from the other two, mainly due to the absence of the pyridinic band and to a slight shift of the three bands of the pyrimidine at 328, 276 and 230 nm (***Figure 3.4-5***). As for HL1 and HL2, the main spectral variations are found in alkaline and acidic media, associated with protonation steps involving the chromophore, while equilibria involving the polyaminic chain do not affect the absorption.

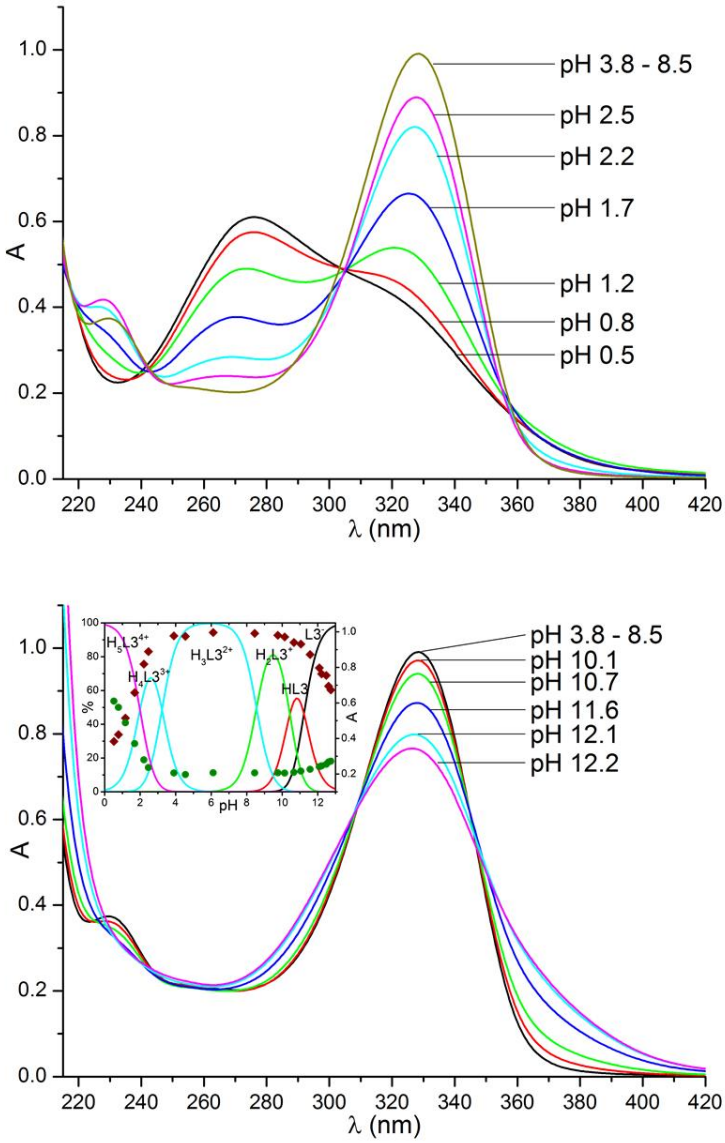

Figure 3.4-5. *UV absorption spectra of HL3 at different pH in aqueous solution: top pH 0.5-8.5, bottom pH 3.8-12.2. Inset: pH dependence of the 330 nm (red diamonds) and 270 nm (green dots) absorbances.*

The highly protonated H_5L1^{4+}, H_6L2^{6+} and H_5L3^{4+} species are formed only in small amounts in the lower pH region we have investigated (*cf.* ***Figure 3.4-2***). Nevertheless, the discovery of their formation reveals that three out of the four nitrogen atoms of both macrocyclic rings of three ligands can undergo protonation in the studied pH range.

3.4.2.2 Formation of Metal Complexes in Solution: Cu(II) and Zn(II)

The equilibrium constants for the formation of Zn(II) and Cu(II) complexes with HL1, HL2 and HL3, determined in aqueous solution (0.1 M NMe_4Cl, 298.1 K) by means of potentiometric (pH-metric) titrations are listed in ***Table 3.4-2***.

Table 3.4-2. *Stability constants of the complexes formed by HL1, HL2 and HL3 with Cu^{2+} and Zn^{2+} in 0.1 M NMe_4Cl at 298.1 ± 0.1 K. Values in parenthesis are the standard deviations on the last significant figure.*

Equilibria	***log K***		
	HL1	***HL2***	***HL3***
$L^- + Zn^{2+} = [ZnL]^+$	*16.3(1)*	*17.8(1)*	*19.0(1)*
$HL + Zn^{2+} = [ZnHL]^{2+}$	*12.62(5)*	*16.65(6)*	*13.1(1)*
$H_2L^+ + Zn^{2+} = [ZnH_2L]^{3+}$	*7.1(1)*	*11.3(1)*	*7.8(1)*
$[ZnL]^+ + H^+ = [ZnHL]^{2+}$	*7.4(1)*	*10.1(1)*	*5.3(1)*
$[ZnHL]^{2+} + H^+ = [ZnH_2L]^{3+}$	*3.8(1)*	*4.4(1)*	*5.1(1)*
$[ZnL]^+ + OH^- = [ZnLOH]$	*4.4(1)*	*2.8(1)*	*7.0(2)*
$L^- + Cu^{2+} = [CuL]^+$	*22.59(6)*	*21.2(1)*	*26.0(3)*
$HL + Cu^{2+} = [CuHL]^{2+}$	*15.65(5)*	*20.21(9)*	*18.6(3)*
$H_2L^+ + Cu^{2+} = [CuH_2L]^{3+}$		*14.74(7)*	
$H_4L^{3+} + Cu^{2+} = [CuH_4L]^{5+}$	*3.6(2)*		
$[CuL]^+ + H^+ = [CuHL]^{2+}$	*4.19(6)*	*10.2(1)*	*3.9(5)*
$[CuHL]^{2+} + H^+ = [CuH_2L]^{3+}$		*4.2(1)*	
$H_5L^{4+} + Cu^{2+} = [CuH_5L]^{6+}$		*3.7(2)*	
$[CuL]^+ + OH^- = [CuLOH]$	*4.16(8)*		*7.2(5)*

Due to the known inertness often exhibited by cyclam in forming metal complexes, assessment of HL3 coordination properties required special attention and sample handling. Both complex formation and dissociation processes appeared to be very slow, although dissociation was studied as it appeared to be much faster: for this reason, measurements were performed following complex dissociation, that is, by performing the potentiometric titrations from alkaline to acidic conditions. In the case of Zn(II), the alkaline solution of the complex was prepared into the potentiometric cell and the pH variation was monitored until the equilibrium was reached (2 hours). Then the solution was titrated with standardized HCl solution. 45 minutes were necessary to reach the equilibrium after each addition. In the case of Cu(II), two days were necessary to reach the equilibrium of the starting solution. Accordingly, the alkaline complex solution was prepared in a separate vessel, stored under inert atmosphere and left to equilibrate for 2 days at 298 K, then it was transferred into the titration cell. The measurement was performed as in the case of Zn(II), but with an elapsed time of 2 hours between successive titrant (acid) additions. The issues posed by kinetic reflect themselves on the stability constants in terms of larger errors and, in the case of Cu(II), also in a restriction of the studied pH range to 2.5-8.0.

Also, in view of the above remarks and of the intrinsic inertness often exhibited by the metal cation in forming complexes, Pd(II) coordination studies with HL3 were not undertaken due to the unfavourable kinetic restraints.

Distribution diagrams for the formation of these complexes can be found below in ***Figure 3.4-6***.

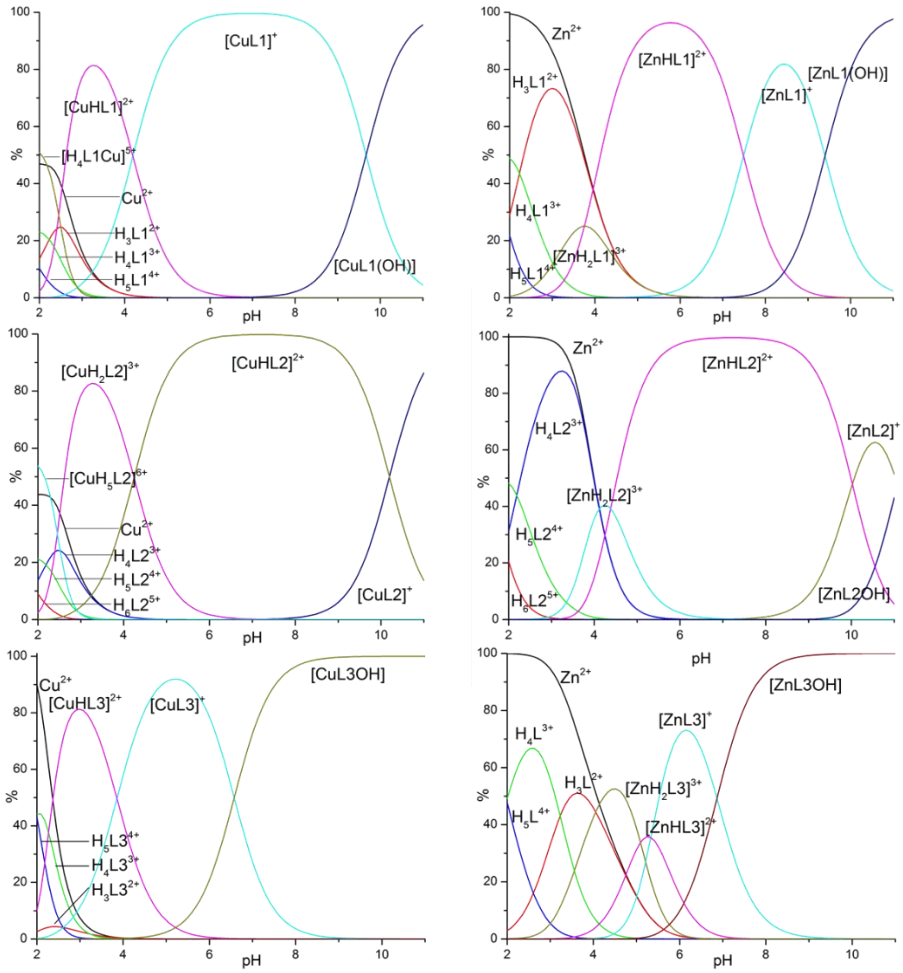

***Figure 3.4-6**. Species distribution diagrams for the complexes formed by HL1 (top), HL2 (middle) and HL3 (bottom) with Cu^{2+} (left) and Zn^{2+}(right).*
$[M^{2+}] = [L] = 1\ 10^{-3}$ M.

In terms of the species formed, the three ligands (HL = HL1, HL2, HL3) give rise to identical complex systems with Zn(II), constituted by ZnL^{+}, $ZnHL^{2+}$, ZnH_2L^{3+} and ZnLOH species, while in the case of Cu(II) there are some differences. Namely, HL1 forms $CuL1^{+}$, $CuHL1^{2+}$, CuH_4L1^{5+} and CuL1OH, while HL2 forms $CuL2^{+}$, $CuHL2^{2+}$, CuH_2L2^{3+} and CuH_5L2^{6+}. HL3 forms the same species of HL1 with the exclusion of the tetraprotonated one. Such differences are justified by the different numbers of donor atoms in the ligands and, in the case of Cu(II), by the greater stability of the complexes with HL3. Indeed, HL1 and HL3, which can provide at most five donor atoms, are not able to fulfil the coordination sphere of the metal ions and deprotonation of a coordinated water molecule gives rise to MLOH complexes in alkaline media. On the other hand, HL2, containing one more donor atom, does not form a similar hydroxylate species with Cu(II) while the corresponding Zn(II) species is significantly less stable then the hydroxylated complexes formed by HL1 and HL3 (***Table 3.4-2***).

The most peculiar feature of these complex systems, however, is the gap of protonation states observed for the Cu(II) systems between $CuHL1^{2+}$ and CuH_4L1^{5+}, in the case of HL1, and between CuH_2L2^{3+} and CuH_5L2^{6+}, for HL2 (*cf.* ***Table 3.4-2***, ***Figure 3.4-6***). In CuH_4L1^{5+} and CuH_5L2^{6+}, the metal ion is expected to be bound by the pyrimidine group in a chelating mode similar to that observed in the crystal structure of $CuHL1(ClO_4)_2$ (*cf.* 3.4.2.3), the macrocyclic ring, being triprotonated, is not able to bind metal ions. As a matter of fact, these highly protonated complexes are formed in very acidic solutions. When the pH is increased and the macrocycle starts releasing the most acidic proton, Cu(II) migrates from the pyrimidine binding site to the macrocycle forcing the deprotonation of the remaining ammonium groups. Most likely, such triple deprotonation process does not occur in a single step but takes place through successive equilibria occurring in a pH range so tight that they are not distinguishable, at least by means of the potentiometric method. This is a case of pH-controlled metal translocation similar to those observed with macrocyclic ligands containing divergent binding sites.

The UV spectra of the ligands in the presence of metal ions, recorded at various pH values, are shown in ***Figure 3.4-7*** for HL1, ***Figure 3.4-8*** for HL2 and ***Figure 3.4-9*** for HL3.

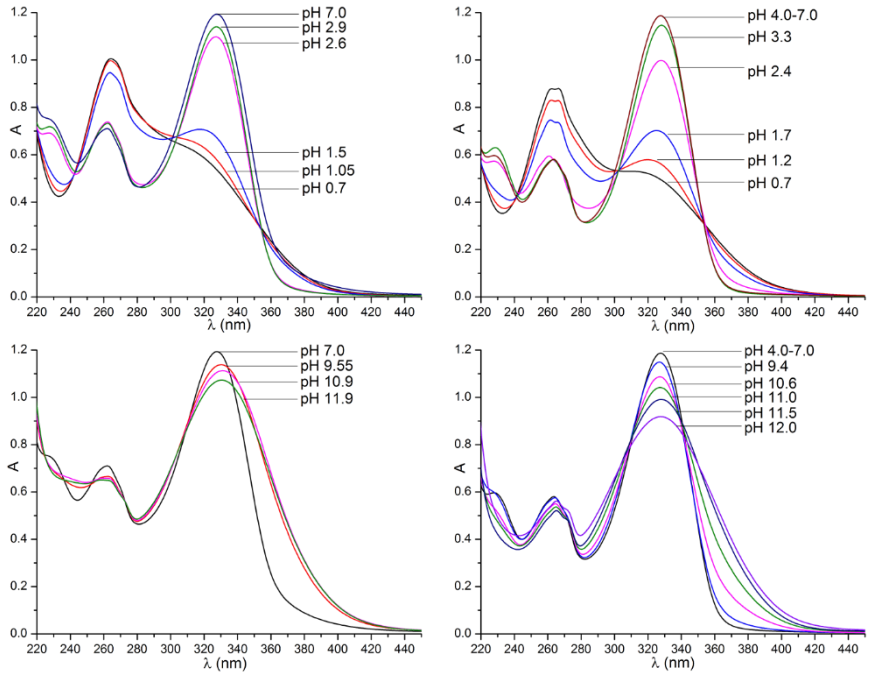

Figure 3.4-7. *UV spectra of HL1 complexes with Cu^{2+} (left) and Zn^{2+} (right) at different pH values. $[M^{2+}] = [HL1] = 5\times10^{-5}$ M.*

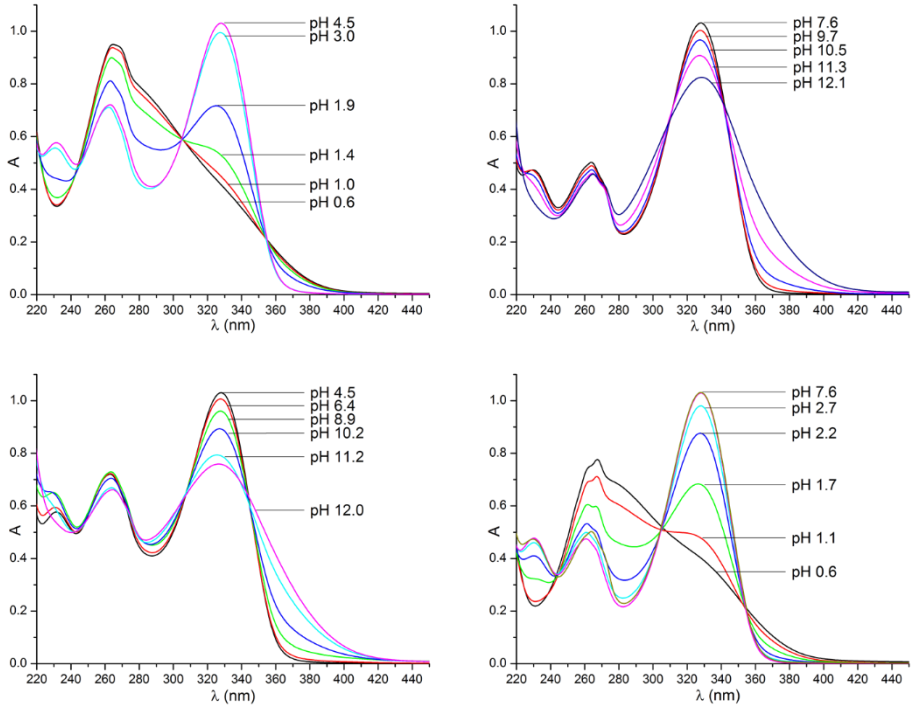

Figure 3.4-8. *UV spectra of HL2 complexes with Cu^{2+} (left) and Zn^{2+} (right) at different pH values. $[M^{2+}] = [HL1] = 5\times10^{-5}$ M.*

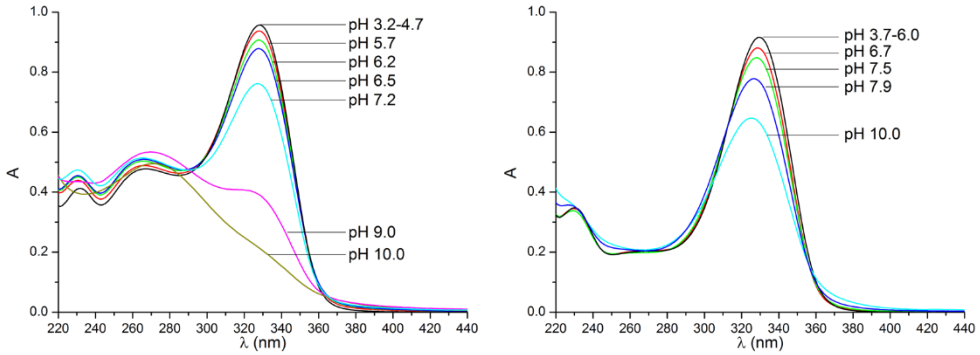

Figure 3.4-9. *UV spectra of HL3 complexes with Cu^{2+} (left) and Zn^{2+} (right) at different pH values. $[M^{2+}] = [HL1] = 5\times10^{-5}$ M.*

In the case of HL1 and HL2, a comparison of complex spectra with those of the metal free ligands shows that the 330 nm absorbance is insensitive to the presence of metal ions, while the band at 265 nm, due to the pyridine moiety, is enhanced within the entire pH region in which metal complexation takes place, indicating that the pyridine nitrogen atom is involved in the formation of all complex species (***Figure 3.4-10***). In the case of Cu(II) complexes (***Figure 3.4-10*** top), however, this enhancement is present even in very acidic solutions: under such conditions, the formation of CuH_4L1^{5+} and CuH_5L2^{6+}, in which the metal ion is coordinated to the pyrimidine residue, enhances the absorbance due to this chromophoric group also occurring at about 260 nm. The profile of the pH dependence of this band is indicative of metal translocation occurring from pyrimidine to the macrocyclic (pyridine) sites with increasing pH.

As already noted above, for HL3 we did not observe the formation of Cu(II) complexes in a high protonation state, such as CuH_4L1^{5+} for HL1, in which the metal ion is chelated by the pyrimidine group. Due to the greater stability of the complexes formed by HL3, release of the Cu(II) ion from the macrocyclic ring takes place in more acidic solutions (below pH 3), relative to HL1. Accordingly, the hypothetical CuH_4L3^{5+} species, is not expected to form in appreciable amounts above pH 2.5, which is the lower pH limit useful for our pH-metric titrations. Nevertheless, we cannot exclude the formation of such species below pH 2.5, although, under similar acidic conditions, protonation of the nitroso group becomes an additional impediment.

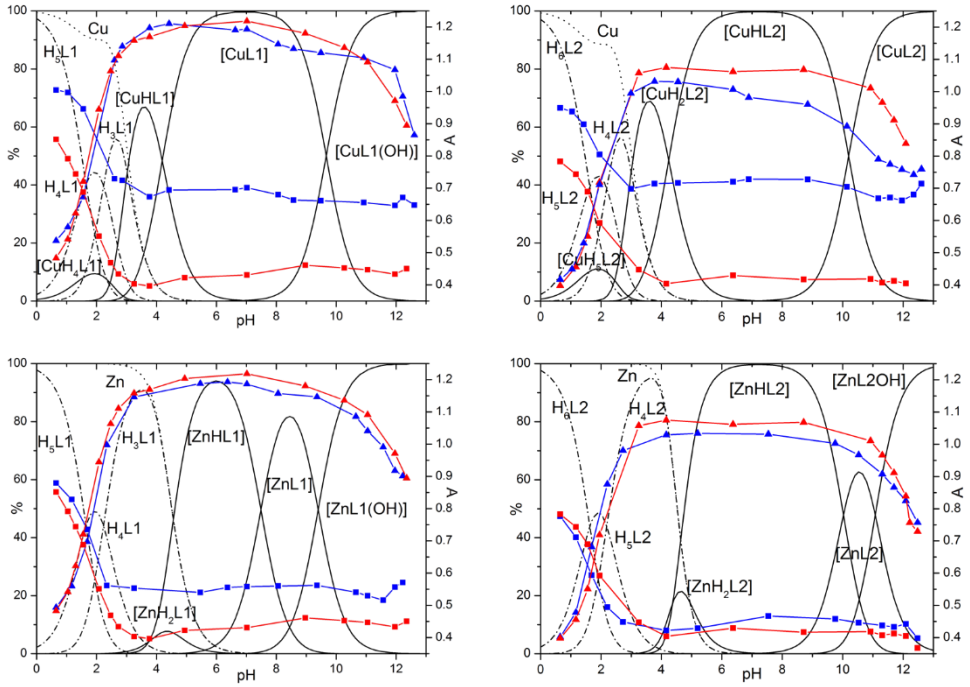

***Figure 3.4-10**. pH dependence of the 330 nm (triangles) and 265 nm (squares) absorbances of HL1 (left) and HL2(right) in the absence (red) and in the presence (blue) of Cu^{2+} (top) and Zn^{2+} (bottom) superimposed to the relevant species distribution diagrams. $[M^{2+}] = [L] = 5\times10^{-5}$ M. Species charges have been omitted for simplicity.*

HL2 binds the two metal ions forming more stable complexes than HL1 and HL3 (***Table 3.4-2***), in agreement with the presence of one more amine group in its lateral chain. In the case of HL1, it is possible to perform a comparison with the coordination properties of the parent ligand **1** [37] [41], evidencing that the stability of the $ZnHL1^{2+}$ (log *K* = 12.6) and $CuHL1^{2+}$ (log *K* = 15.48) complexes is significantly smaller than that of the analogous complexes $Zn\mathbf{1}^{2+}$ (log *K* = 17.42) [41] and $Cu\mathbf{1}^{2+}$ (log *K* = 20.43) [37], in agreement with a loss of coordinating ability experienced by the primary nitrogen of **1** (***Figure 3.3-1***) upon functionalization with the pyrimidine residue. As a matter of fact, in the crystal structure of $CuHL1(ClO_4)_2$ (*cf.* 3.4.2.3) this amine group is not involved in the coordination of the metal ion, which completes its coordination environment by chelate binding of the pyrimidine residue of an adjacent complex molecule. Nonetheless, when this functionalized nitrogen undergoes deprotonation, enhancing its coordinating ability, the complex stability increases (***Table 3.4-2***). This phenomenon is much less evident for HL2, as the additional amine group in the lateral chain is already coordinated when the nitrogen atom directly bound to the pyrimidine group becomes deprotonated. The involvement of this deprotonated amine group in metal coordination can be assessed by comparing the equilibrium constants for protonation of free and

complexed ligands according to the general equilibria $L^+ + H^+ = HL$ and $ML^+ + H^+ = MHL^{2+}$ (L = L1, L2, L3; M = Zn, Cu). In the case of HL2, complex protonation constants (log *K* = 10.42 for $ZnL2^+$, log *K* = 10.5 for $CuL2^+$, ***Table 3.4-2***) are very close to the protonation constant of $L2^-$ (log *K* = 11.25, ***Table 3.4-1***), indicating that the group being protonated is free, while in the case of HL1 a similar comparison shows that complex protonation takes place on a coordinated group (log *K* = 7.4 for $ZnL1^+$, log *K* = 4.02 for $CuL1^+$, log *K* = 5.3 for $ZnL3^+$, log *K* = 3.9 for $CuL3^+$, versus log *K* = 11.13 for $L1^-$ and log *K* = 11.22 for $L3^-$).

3.4.2.3 Crystal Structure of $CuHL1(ClO_4)_2$

The crystal structure consists of a 1D coordination polymer $\{[CuHL1]^{2+}\}_n$ built up by repeats of complex units. A segment of the 1D polymer is shown in ***Figure 3.4-11***, evidencing the metal coordination sphere (crystallographic parameters and selected bond angles and distances are listed in ***Table 3.4-3*** and ***Table 3.4-4*** respectively).

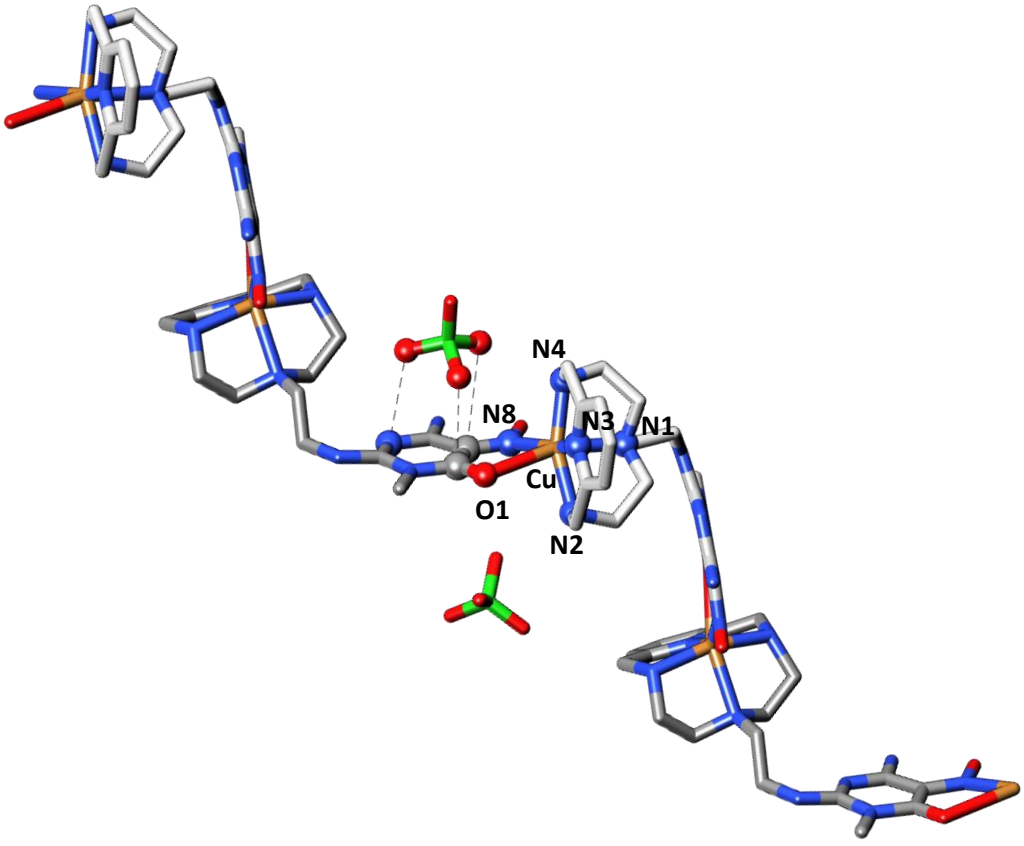

Figure 3.4-11. *A segment of the 1D polymer in the crystal structure of $CuHL1(ClO_4)_2$ showing the metal coordination environment and the anion-π interaction of a perchlorate anion with the pyrimidine function of the ligand.*

***Table 3.4-3**. Crystal data and structure refinement for $CuHL1(ClO_4)_2$.*

Empirical formula	$C_{18}H_{27}Cl_2CuN_9O_{10}$
Formula weight	*663.93*
Temperature (K)	*150*
Crystal system, space group	*Orthorhombic, Pbca*
a (Å)	*14.2264(4)*
b (Å)	*18.2109(5)*
c (Å)	*18.9638(5)*
Volume ($Å^3$)	*4913.1(2)*
Z	*8*
Independent reflections / R(int)	*3770 / 0.0450*
μ (mm^{-1})	*3.938/ (Cu-kα)*
R indices [I>2σ(I)]*	*R1 = 0.0595*
	wR2 = 0.1408
R indices (all data)*	*R1 = 0.1010*
	wR2 = 0.1675

The copper atom is hexacoordinated by the four nitrogen atoms of the macrocycle and by the carbonyl oxygen and the nitroso nitrogen belonging to the nitroso-amino pyrimidine group of a contiguous, symmetry related ligand. The coordination sphere can be best described as a strongly distorted octahedron, whose axial distances, defined by the nitroso oxygen O1 and the macrocyclic tertiary nitrogen N1, are strongly elongated (***Table 3.4-4***). The equatorial plane is defined by the pyridine and the two secondary nitrogen atoms of the macrocycle, together with the nitroso nitrogen from the pyrimidine ring of the contiguous symmetry related ligand. It is to be underlined that, while the coordination of the nitroso nitrogen clearly acts on the electron distribution in the pyrimidine ring system, giving a remarkable shortening of the N=O bond and a lengthening of the N-C bond, coordination of the carbonyl oxygen does not determine the weakening of the C=O bond, whose bond length is even shorter than the corresponding mean value for the free C=O (1.205(7) Å vs 1.22(2) Å for – C=O – and 1.26(3) Å - C=O-M bonds).

The head to tail disposition of the ligands in the chain is due to the 2_1 screw axes, running parallel to the *b* axis and determining an overall helical fashion for the coordination polymer.

Table 3.4-4. *Selected bond angles (deg) and distances (Å) for the crystal structure of [Cu(HL1)]$(ClO_4)_2$. Symmetry relation for primed atoms: 1-x, y-0.5, 1.5-z; e.s.d. in parentheses.*

Cu - N4	*2.068(5)*
Cu - N1	*2.324(5)*
Cu - N3	*1.933(5)*
Cu - N2	*2.060(6)*
Cu - N8'	*2.003(5)*
Cu - O1'	*2.534(4)*
N4 - Cu - N1	*82.7(2)*
N4 - Cu - N3	*82.3(2)*
N4 - Cu - N2	*157.6(2)*
N4 - Cu - N8	*107.6(2)*
N4 - Cu - O1	*81.5(2)*
N1 - Cu - N3	*97.4(2)*
N1 - Cu - N2	*84.0(2)*
N1 - Cu - N8	*108.4(2)*
N1 - Cu - O1	*163.6(2)*
N3 - Cu - N2	*81.7(2)*
N3 - Cu - N8	*153.2(2)*
N3 - Cu - O1	*84.9(2)*
N2 - Cu - N8	*93.6(2)*
N2 - Cu - O1	*112.4(2)*
N8 - Cu - O1	*72.4(2)*

Similarly to the crystal structures previously reported for metal complexes obtained with the 3,6,9-triaza-1-(2,6)-pyridinecyclodecaphane macrocycle functionalized on its 6 position [37] [38] [40] [41], the macrocycle adopts a bent conformation which leaves the metal coordination sphere unsaturated. In these structures, however, the macrocycle and the pendant arm containing donor atoms are involved in the coordination of the same metal centre, and isolated complexes are invariably formed. Instead, in the $\{[CuHL1]^{2+}\}_n$ polymer, the pendant arm and the macrocycle do not coordinate to the same metal ion, so that the pyrimidine ring protrudes outside, and the metal coordination positions not saturated by the macrocycle are occupied by exogenous species.

Electro-neutrality is achieved by the presence of two perchlorate anions in the asymmetric unit. One of them strongly interacts with the nitroso pyrimidine group via anion-π interactions with three out of four oxygen atoms (***Table 3.4-5***). Remarkably, one of the strongest anion-π interactions ever observed was reported for a ligand (L) containing this nitroso-amino pyrimidine group functionalized with a tren (tris(2-aminoethyl)amine) moiety. In the crystal structure of the $\{H_4L[Co(CN)_6]\}\cdot 2H_2O$ compound, the nitrogen atom of a cyanide ion of $[Co(CN)_6]^{3-}$ was found 2.786 Å apart from the ring centroid [32]. In this structure, as well as in those obtained for the same ligand with $HgCl_4^{2-}$, $HgBr_4^{2-}$ and CdI_4^{2-}, the anions are pretty well localized above the ring centroid [42], while in $[Cu(HL1)](ClO_4)_2$, the ClO_4^--pyrimidine interaction appears dominated by the contact of one perchlorate oxygen with the carbonyl C atom of the pyrimidine ring. The O11···C17 contact distance (2.872(8) Å) is almost coincident with the O···ring plane distance (2.882 Å). The O13 and O14 oxygen atoms are 3.238 and 3.813 Å apart from the ring centroid, and can be considered localized on the ring periphery, having offsets of 0.81 and 2.13 Å, respectively.

Table 3.4-5. *Geometrical parameters describing the anion-π interaction between the ClO_4^- anion and the pyrimidine ring in the crystal structure of $[Cu(HL1)](ClO_4)_2$.*

	O11	***O13***	***O14***
d1[a] (Å)	*3.229*	*3.328*	*3.813*
d2[b] (Å)	*2.872 (C17)*	*3.211 (N6)*	*3.287 (C16)*
α[c] (°)	*26.9*	*14.5*	*34.1*
β[d] (°)	*27.0*	*25.0*	*21.0*

[a]) Distance from the ring centroid, [b]) distance from the nearest ring atom indicated in parenthesis, [c]) angle between the d1 vector and the normal to the ring plane, [d]) angle between d1 and d2 vectors.

3.4.2.4 Formation of Pd(II) Complexes in Solution (HL1 and HL2)

The complexation of Pd(II) by the two ligands HL1 and HL2 takes place very slowly, however, once such complexes are formed, their protonation can be studied without kinetic problems above pH 2.5. Accordingly, we were able to determine the protonation constants for these complexes, shown in ***Table 3.4-6***, by means of potentiometric (pH-metric) titration in aqueous solution (0.1 M NMe_4Cl, 298.1 K). Distribution diagrams concerning these equilibria can be found in ***Figure 3.4-12***.

Table 3.4-6. *Protonation constants of the $[LPd]^+$ complexes formed by HL1 and HL2 in 0.1 M NMe_4Cl at 298.1±0.1 K. Values in parenthesis are the standard deviations on the last significant figure.*

Equilibria	***log K***	
	HL1	***HL2***
$[PdL]^+ + H^+ = [PdHL]^{2+}$	*9.46(6)*	*10.19(7)*
$[PdHL]^{2+} + H^+ = [PdH_2L]^{3+}$	*2.2(2)*	*7.0(1)*
$[PdH_2L]^{3+} + H^+ = [PdH_3L]^{4+}$		*2.5(2)*

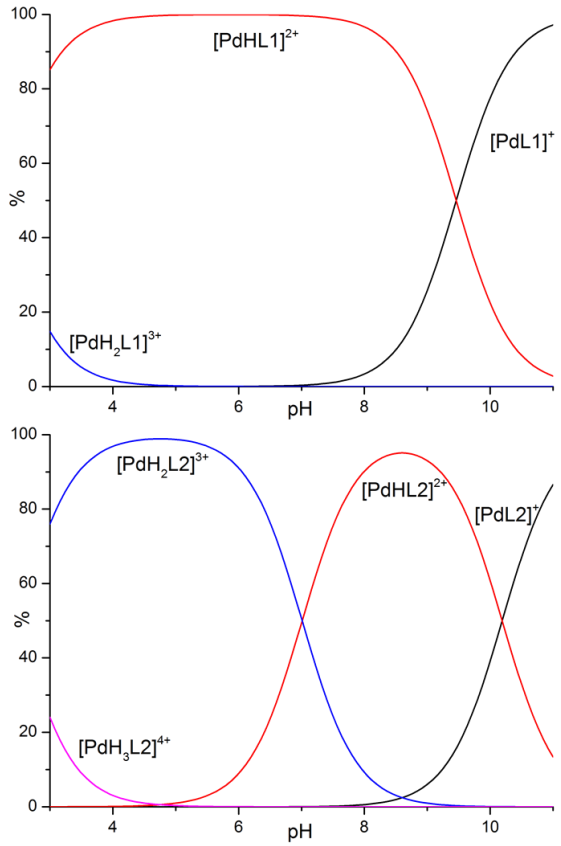

Figure 3.4-12*. Distribution diagrams for the protonated complex species formed by HL1 (top) and HL2 (bottom) with Pd^{2+}. $[M^{2+}] = [L] = 1\ 10^{-3}$ M.*

$[PdL1]^+$ and $[PdL2]^+$ are involved in two and three protonation steps, respectively. The equilibrium constants corresponding to log *K* = 9.46 and log *K* = 10.19 for $[PdL1]^+$ and $[PdL2]^+$, respectively, are too high to be associated with protonation of metal-coordinated amine groups while they can be assigned to protonation of metal-free deprotonated amine groups, in agreement with the UV spectral variations observed for these complexes in the alkaline zone (***Figure 3.4-13***). UV spectra also show that, in the acidic region, protonation corresponding to the smallest equilibrium constants (log *K* = 2.2 and 2.5, Table 2) occurs on the pyrimidine group. In the case of $[PdL2]^+$, there is an intermediate protonation step (log *K* = 7.0) corresponding to protonation of the additional amine group in the chain connecting the macrocycle and the pyrimidine moieties of HL2, which is expected not to be coordinated, as the basicity of this amine group in the complex is relatively close to that of the same group in the free ligand (log *K* = 8.64, ***Table 3.4-1***).

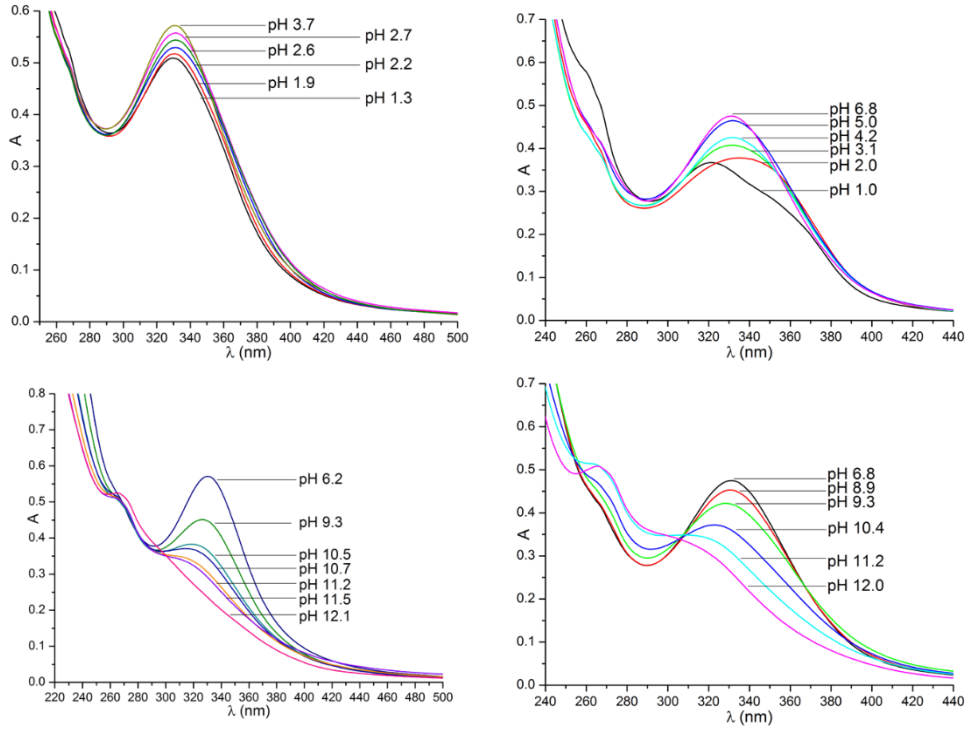

Figure 3.4-13. *UV spectra of HL1 (left) and HL2 (right) complexes with Pd^{2+} at different pH values. $[M^{2+}] = [HL1] = 5\times10^{-5}$ M.*

An interesting point regards the number of donor atoms used by HL1 and HL2 to bind Pd(II). As pointed out before (*cf.* 3.4.1), all the solved $[ML]^{2+}$ crystal structures for metal complexes of the parent ligands **1** (M = Cu(II)) and **2** (M = Mn(II), Ni(II), Cu(II), Zn(II)), together with the structure of $[Cu(HL1)](ClO_4)_2$ (*cf.* 3.4.2.3), show the macrocycle in a folded conformation. As observed above, in the case of the square planar Pd(II) complexes it seems that there is no participation of donor atoms of the appended chains in metal coordination, thus, if the macrocyclic ring of the ligand would assume the expected folded conformation, only three out of the four macrocyclic nitrogen atoms would be coordinated to Pd(II) (***Figure 3.4-14***).

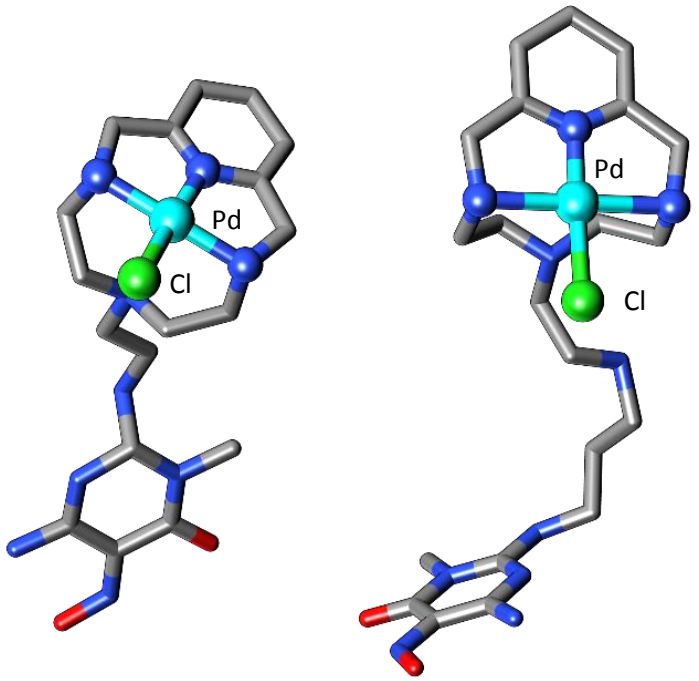

Figure 3.4-14*. Proposed coordination scheme for Pd(II)- HL1 and Pd(II)-HL2 complexes.*

To get information on this point, solutions containing equimolar quantities of ligand and $[PdCl_4]^{2-}$ were equilibrated at pH 4.0 and 298 K within ten days, for both HL1 and HL2. The UV-Vis spectra of the mixtures were monitored daily: no variations were observed after four days. The concentration of free Cl^- was then determined by means of ion chromatography evidencing that only three chloride anions were released by $[PdCl_4]^{2-}$ upon coordination. Accordingly, we must assume that in these complexes Pd(II) is coordinated to three macrocyclic nitrogen atoms and one Cl^- anion, as sketched out in ***Figure 3.4-14***.

3.4.3 Surface Decoration of CNTs

3.4.3.1 Experimental

The work herein presented was performed using thin multi-walled CNTs (MWCNTs) with metal oxides content ≤ 5%, purchased from Nanocyl (Ref 3100) and used as received. Since the substrate has been characterized in previous studies, its properties will be only briefly examined in the following: the eager Reader is addressed to ref [43].

HL1 and HL2 were the focal point of the adsorption studies, HL3 being set aside, at present, mainly due to the kinetic inertness toward metal ion complexation exhibited in the preliminary solution studies.

3.4.3.1.1 HL1 and HL2 Adsorption on MWCNTs

The equilibrium time for the adsorption of HL2 on CNTs was determined experimentally by kinetic measurements, reasoning that, since the three ligands share the same pyrimidinic anchoring group and HL2 possesses the most hydrophilic and conformationally flexible functional unit, its kinetic behaviour would offer guidance also for the other ligands. The data points were obtained by mixing 0.0250 g of the adsorbent with 25 mL of a 10^{-3} M aqueous solution of the adsorbate at a given initial pH value. The obtained suspension was kept at 298.1 K under continuous shaking while concentration of the adsorbate was regularly monitored by checking its UV-absorbance at the isosbestic point (304 nm for HL2, *cf.* ***Figure 3.4-4***) until the equilibrium was reached.

As it can be seen from the obtained data, reported in ***Figure 3.4-15***, the adsorption process is quite rapid for HL2, taking place in the hour time scale, nevertheless we decided to wait 3 days as a precautionary timespan to make sure that the adsorption of the ligands completely segregates CNTs' bundles, thus allowing for the functionalization of the whole surface.

The adsorption isotherms were obtained under the same conditions (298.1 K, 0.0250 g of adsorbent suspended in 25 mL of the appropriate solution of the adsorbate at the chosen pH value). The ligand concentration values ranged from 8×10^{-5} M to 2×10^{-3} M. The samples were shaken in a thermostatic air-incubator until the determined equilibrium time was reached. Desorption isotherms of the ligands from the MWCNT/HL1 and MWCNT/HL2 hybrid materials were obtained point-by-point from the adsorption isotherms, recovering, drying, weighting and re-suspending the solid in water, maintaining a 1 mg of material/1 mL water ratio, then following a similar procedure to that described for the adsorption isotherms.

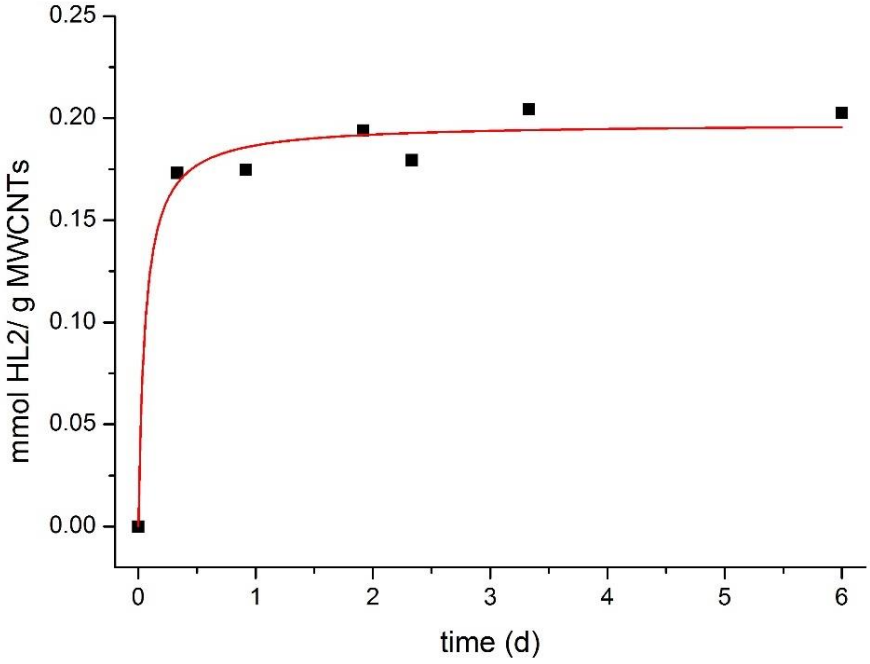

***Figure 3.4-15**. Kinetic plot for the adsorption of HL2 onto MWCNTs.*

3.4.3.1.2 Determination of the Surface Charge Density of MWCNT/HL1 and MWCNT/HL2

The surface charge density (Q in mmol H^+/g of adsorbent) of both materials was determined by a method based on potentiometric titration data, following an already described procedure. [42]

Q was calculated by means of the equation $Q = \frac{1}{m}(V_0 + V_t)([H]_i - [OH]_i - [H]_e + [OH]_e)$, where V_0 and V_t are the volumes of initial solution and titrant, respectively, and m is the mass of the adsorbent. Subscripts i and e refer to the initial and equilibrium concentration of protons or hydroxyl ions. The proton isotherms are obtained by plotting Q vs equilibrium pHs.

3.4.3.1.3 Preparation of the MWCNTS/HL1-Pd and MWCNTs/HL2-Pd Catalysts

The two catalysts, MWCNT/HL1-Pd and MWCNT/HL2-Pd, were prepared following a two-step procedure (*cf.* 3.2.4). First, we prepared MWCNT/HL1 and MWCNT/HL2 materials, adsorbing the ligands on commercial CNTs (Thin MWCNTs Nanocyl, Ref 3100, Spain, with metal oxides content ≤ 5%). This was accomplished according to the following procedure for both ligands: 0.5 g of the adsorbent were mixed with 500 mL of 10^{-3} M aqueous solution of the ligand at pH = 7.5 in a plastic flask. This pH value was proved to be the optimum for the highest irreversible loading of the ligand. The flask was shaken in an air-thermostated bath at 298.1 K until the adsorption equilibrium was reached (3 days). The obtained solids, MWCNT/HL1 and MWCNT/HL2, were separated by filtration, washed repeatedly with distilled water and dried into a desiccator. The final amount of adsorbent per gram of adsorbate was quantified in 0.36 mmol of HL1 and 0.31 mmol of HL2 per g of CNT, respectively.

In the second step, MWCNT/HL1-Pd and MWCNT/HL2-Pd catalysts were prepared by coordination of Pd(II), as K_2PdCl_4, on the appropriate CNT/ligand material. Accordingly, 0.5 g of the corresponding CNT/ligand material were mixed in a suitable plastic flask with 500 mL of a 1 M KCl aqueous solution containing K_2PdCl_4 5×10^{-4} M, whose pH had been adjusted to 5.0 through HCl addition. pH 5.0 was selected as the best compromise between the minimization of proton competition towards the coordination of Pd(II) with the amino groups of the ligands and the avoidance of the formation of Pd(II) hydroxy-species, that, at this pH value, are not yet formed (*i.e.* all the Pd(II) is present as $[PdCl_4]^{2-}$). The suspensions were shaken in an air-thermostated bath at 298.1 K within four days until the adsorption equilibrium was reached (*i.e.* when the UV absorbance of the Pd(II) solution at λ = 474 nm remained constant over time). Finally, the amount of adsorbed Pd(II) was determined as the difference between the initial and final absorbances at λ = 474 nm: 0.45 mmol of Pd per gram of CNT/HL1 and 0.40 mmol per gram of CNT/HL2 were assessed.

3.4.3.1.4 General Procedure for the Sonogashira Reaction

A mixture of iodobenzene (1 mmol), phenylacetylene (1 mmol), Et_3N (2 mmol), H_2O (1 mL) and the catalyst (22 mg of MWCNT/HL1-Pd or 25 mg of MWCNT/HL2-Pd, relationship reactants/Pd(II) = 100) was stirred under aerobic conditions at a constant temperature (30, 50 or 70 °C). The progress of the reaction was monitored by gas chromatography (GC). After completion, $CHCl_3$ (10 mL) was added to the reaction mixture and the catalyst was recovered by filtration and washed with $CHCl_3$ (2 x 5 mL) and H_2O (2 x 5 mL). The aqueous and organic layers were separated through a separatory funnel. The organic layer was dried over anhydrous $MgSO_4$. The analysis of the reaction products in the organic phase was performed by GC using a 7820A Agilent GC System chromatograph, with an Agilent 190915-433 column, 30 m × 250 µm × 25 µm and a flame ionization detector (FID). The recovered catalyst was reused for another batch of the same reaction. The process was repeated for three additional runs.

3.4.3.1.5 Cu(II) and Zn(II) Adsorption on MWCNTs/HL1

Adsorption isotherms of Cu(II) and Zn(II) ions on MWCNTs and MWCNT/HL1 adsorbents were carried out at 298.1 K, according to a previously reported experimental procedure [44]. In typical conditions, 0.050 g of each adsorbent were put in contact with 25 mL of an aqueous solution of the corresponding metal-dichloride at pH 5.0. The samples were shaken in a thermostated air-incubator until the equilibrium was reached (5 days). The adsorbate concentration ranged from 1×10^{-4} M to 1.7×10^{-3} M. The concentration of the ions was determined by atomic absorption spectrometry, using a Perkin-Elmer Aanalyst 800 equipment. The analysis of the equilibrium solutions allowed us to check that HL1 was not desorbed when the MWCNT/HL1 hybrid material was used as adsorbent.

3.4.3.1.6 Preparation of MWCNT/HL1-Cu(0)

43.9 mg of MWCNT/HL1-Cu (containing 0.157 mmol of Cu^{2+}/g MWCNT/HL1), obtained from the adsorption isotherm experiment (see above), were suspended in 10 mL of water and added 22 mg of $NaBH_4$, (molar $Cu^{2+}/NaBH_4$ = 1/80). The mixture was left to react under stirring during 2 hours at room temperature. Afterwards, the resulting solid was separated by filtration, washed repeatedly with doubly distilled water and dried in a desiccator under silica to constant weight.

3.4.3.2 Results and Discussion

3.4.3.2.1 Characterization of the MWCNTs/HL1-Pd and MWCNTs/HL2-Pd Catalysts

The data on the bare graphitic support are sketched below: for a detailed analysis of the properties of the employed MWCNTs the Reader is addressed to a previous paper [43]. The used MWCNTs have C as the main constituent (≈96.0 %), H (≈0.3%) and little oxygen content as the only heteroatomic component (≈3.6%). Negligible amounts of various metal oxides residues, such as chromium, nickel and cobalt, are also present.

The adsorption-desorption isotherms of N_2, determined at 77 K, on MWCNT/HL1-Pd and MWCNT/HL2-Pd, together with the one for the bare MWCNT, appear in ***Figure 3.4-16***.

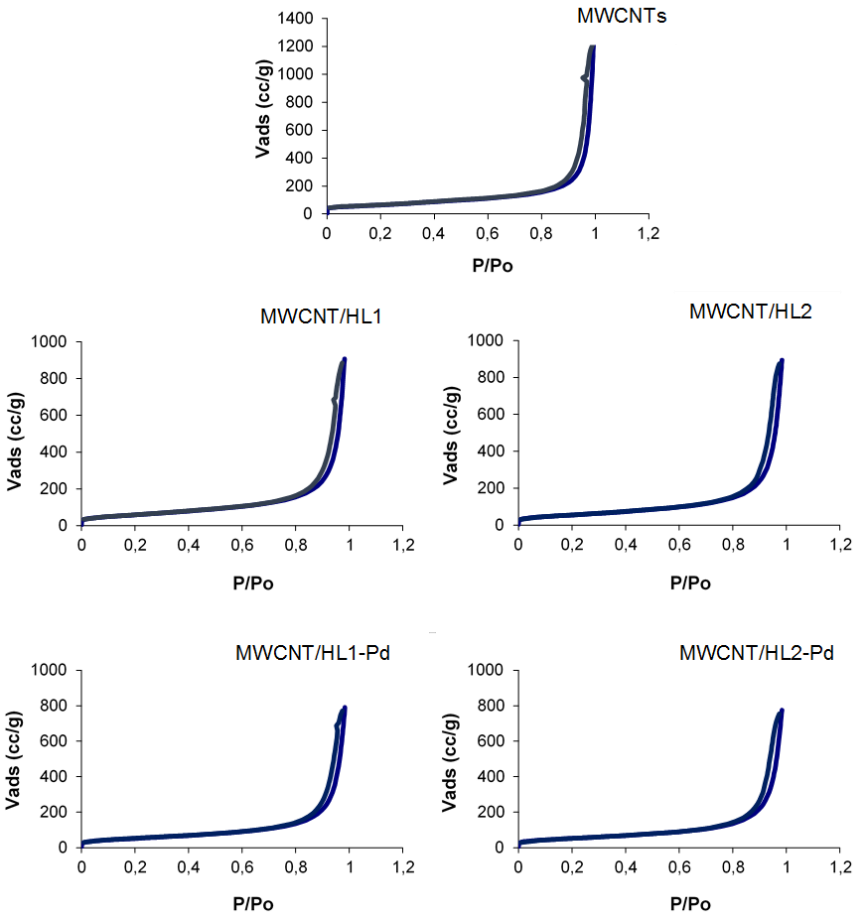

Figure 3.4-16. *Nitrogen adsorption-desorption isotherms for selected preparation stages of the hybrid materials.*

Although little N_2 adsorptions are observed at very low pressures, as in type I isotherms, they are of no account, indicating that the microporosity of the material is irrelevant. Instead, a strong increasing adsorption prevails with a hysteresis loop at high relative pressures, which is typical of type II isotherms, indicating the existence of meso- and macropores with wide distribution sizes, which is consistent with the aggregation of CNTs in bundles. The BET external surface area (determined by applying the BET equation to the N_2 adsorption data) associated to the wide pores of the pristine CNTs, 221 m^2/g, decreases upon adsorption of the ligands, to 198 m^2/g in the case of HL1 and 188 m^2/g in the HL2. These data are consistent with the adsorption of the ligands by π-π interactions of their pyrimidine residues with the arene centres of the external surface of the CNTs. Despite the slightly smaller molar amount of adsorbed HL2 per gram of CNTs (0.31 mmol/g) compared to HL1 (0.36 mmol/g), the larger molecular size of the former determines the observed lower BET surface area of MWCNT/HL2 in respect to MWCNT/HL1.

The adsorption and desorption isotherms of HL1 and HL2 on CNTs at pH 4.0 and 7.5 are reported in ***Figure 3.4-17***: the manifest high irreversibility of the adsorption processes indicates strong ligand-CNT surface interaction.

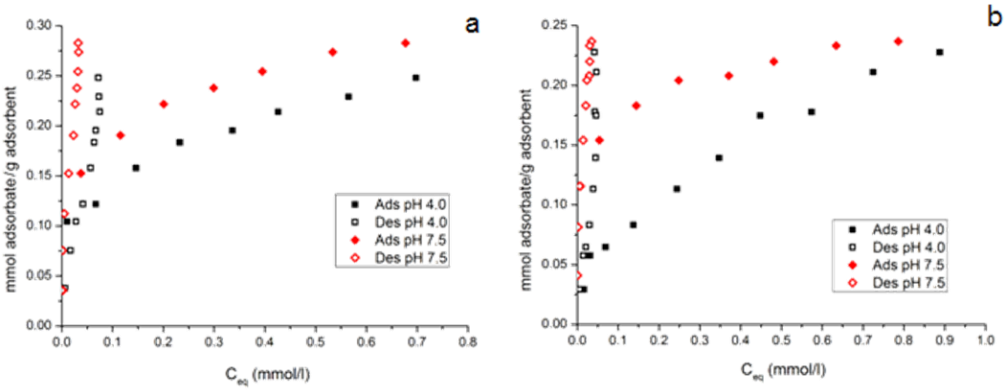

Figure 3.4-17. *Adsorption-desorption isotherms of HL1 (a) and HL2 (b) on MWCNTs at selected pH values.*

All adsorption isotherms fit the type 1 of the Giles classification, indicating a predominant adsorption mechanism. One can also see how the adsorption capacity of CNTs increases slightly with pH for both ligands: this is due to the number of protonated groups in the polyaminic chains attached to the pyrimidine, which decrease, along with the strength of the ligand-solvent interaction, as the pH increases. These features are consistent with the adsorption of the ligands by π-π interactions between the heterocyclic moiety of the ligands and the arene centres, C_π, at the CNT surface as previously observed for analogous ligands on graphitized ACs.

Profile of surface charge density Q (mmol(H^+)/g) versus pH are reported in ***Figure 3.4-18*** for both functionalized materials, MWCNT/HL1 and MWCNT/HL2, and pristine MWCNTs. Applying the SAIEUS method the respective pK_a versus pH profiles were obtained.

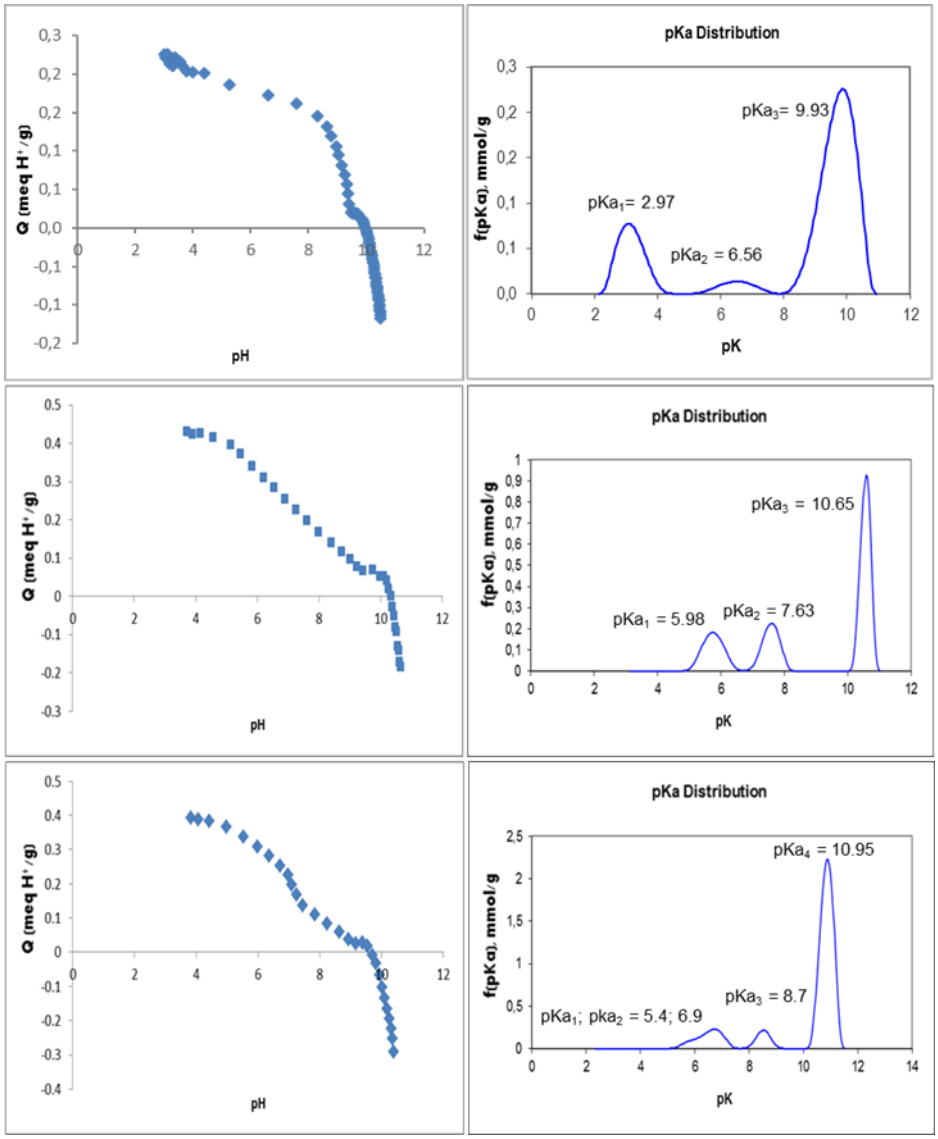

Figure 3.4-18. *Plots of surface charge density Q (mmol H^+/g) vs pH and corresponding distributions of acidity constants, f(pK_a), for MWCNTs (top), MWCNTs-HL1 (middle) and MWCNTs/HL2 (bottom).*

The plot obtained for pristine CNTs is consistent with the existence of carboxyl groups (pK_a ≈ 3) and weakly acidic phenol, lactone and anhydride functions (pK_a ≈ 9-10). Furthermore, the peak at pK_a ≈ 6.5 is due to the protonation of the arene centres of the CNTs surface. Concerning the hybrid materials, the Q vs pH plots already show how their positive surface charge densities are higher than that of the bare CNTs in a wide pH range (3.0-10.0), due to the protonation of the polyamine functions of the anchored ligands. The pKa *vs* pH profiles of MWCNT/HL1 and MWCNT/HL2 (***Figure 3.4-18***), approximately investigated in the 3.0-10.5 pH range, show no signs of the protonation of C(5)- NO groups of the pyrimidine moieties of the adsorbed ligands (log *K* 2.3 and 2.2 for the free ligands HL1 and HL2, respectively, see ***Table 3.4-1***): such evidences suggest that the protonation of those sites is probably hindered due to π-π interactions. Concerning the other protonation steps of the polyamine moieties of the adsorbed ligands, they take place at substantially lower pH values than those observed for the free molecules in solution, indicating a decreasing of the overall basicity of such moieties (*cf.* ***Table 3.4-1*** and ***Figure 3.4-18***). This can probably be rationalized in terms of different conformation of the ligands in solution and at CNTs surface, where an elongated arrangement is required to optimize the stacking interactions, thus hampering to some extent the protonation of such groups.

The XPS spectra of the ligands in the N1s region (***Figure 3.4-19***) consist of a main peak at about 397.0 eV, pertaining to the aliphatic nitrogen atoms, with shoulders (398.1 eV and 397.5 eV for HL1 and HL2 respectively) relating to the aromatic nitrogen atoms.

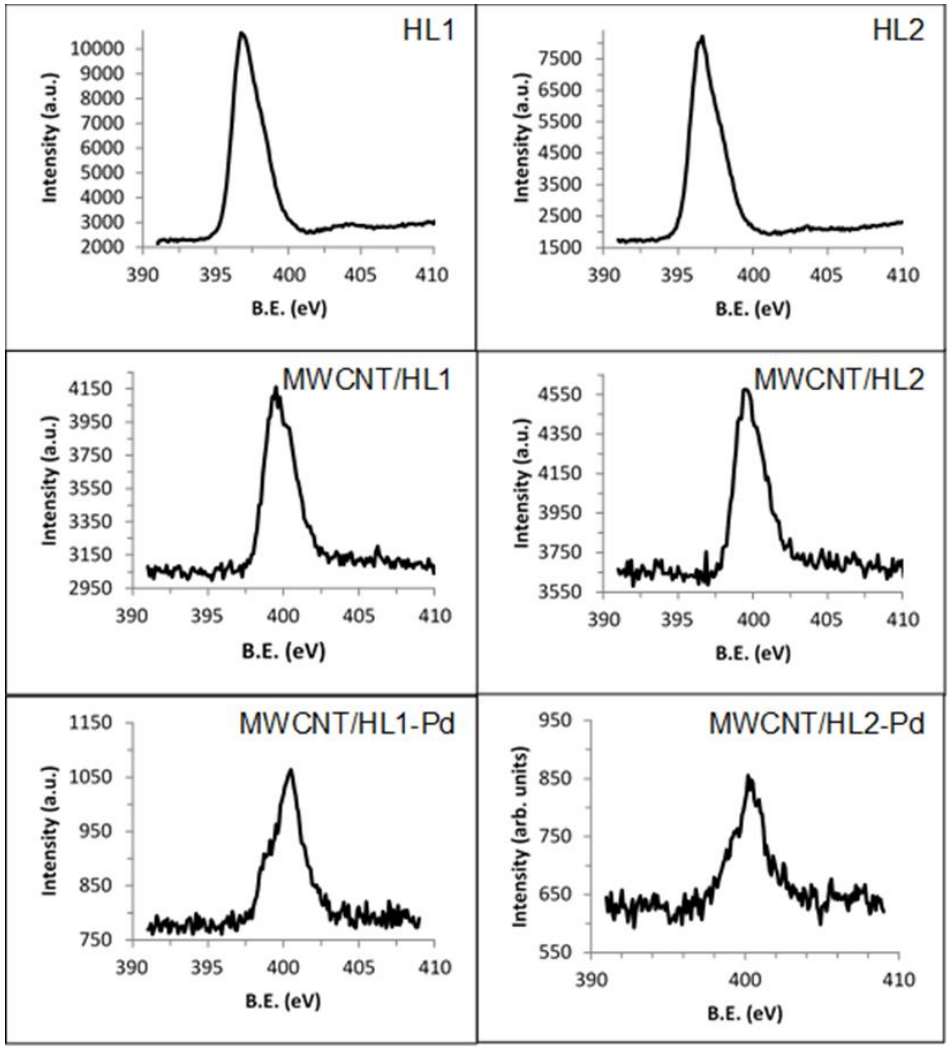

Figure 3.4-19. *High resolution N1s XPS spectra for selected preparation steps of the catalysts.*

After adsorption of the ligands on CNTs surface, both components of the N1s signal shift to higher binding energy values (***Figure 3.4-19***). In the case of the aromatic components, referring to both the pyridine and pyrimidine rings, the shift may indicate a strong plane-to-plane Cπ-pyrimidine interaction, the interacting sites being compressed one onto the other resulting in local repulsion of the adjoined π clouds of both moieties, thus deshielding the N atoms of the pyrimidine. This hypothesis is reinforced by the observation of similar shifts in the binding energies of the C and O atoms of the pyrimidinic ring. These effects are similar to those previously observed with other analogous ligands when adsorbed on graphitized ACs and CNTs. The shift of the aliphatic N atoms, together with the pyridinic

component of the aromatic ones, indicates a change in their chemical environments due to the adsorption process, suggesting changes in the protonation degree of such moieties.

After adsorption of $[PdCl_4]^{2-}$ on the hybrid materials, the binding energy values of the aromatic subunits are almost unmodified, whereas those of the aliphatic moieties increase from 399.6 eV to 400.6 eV for MWCNT/HL1 and from 399.7 eV to 400.6 eV for MWCNT/HL2 (***Figure 3.4-19***). This points out that Pd(II) ions are complexed by the polyaminic portions of the adsorbed ligands, the increased deshielding of the aliphatic nitrogen atoms being due to the coordination of the metal cations.

Concerning the oxidation state of Pd, XPS spectra of MWCNT/HL1-Pd and MWCNT/HL2-Pd (***Figure 3.4-20***) show two signals in the Pd 3d region (343.5 and 338.2 eV) which are characteristics of Pd(II), discarding any reduction to Pd(0).

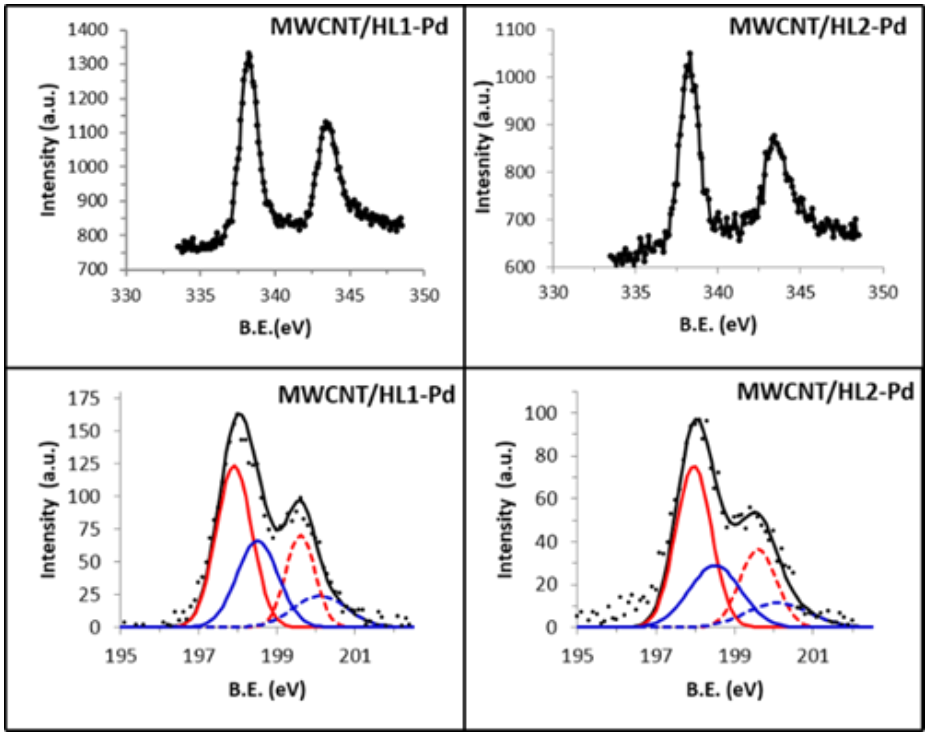

Figure 3.4-20. *High resolution XPS spectra of the catalysts useful for the assessment of the nature of the anchored Pd-complex species: top, spectra in the Pd $3d_{5/2}$ and Pd $3d_{3/2}$ regions, bottom, spectra in the Cl $2p_{3/2}$ and Cl $2p_{1/2}$ regions, showing the deconvolution of the twofold peaks into distinct signals.*

As the molar amounts of adsorbed Pd(II) are always close to those of adsorbed ligand, for both HL1 and HL2, it is safe to conclude that most, if not all, $[PdCl_4]^{2-}$ is adsorbed via complexation of the palladium ion to the polyamine moieties of the ligands. Inspection of Cl/Pd molar ratio, from Pd and Cl signals of the XPS spectra of both catalysts (***Figure 3.4-20***), reveals that such ratio is invariably very close to 2, reinforcing the idea that the metal is bound to the ligand. Moreover, further insight into the nature of the formed complex could be gained by close inspection of Cl XPS spectra. The two peaks at 198.0 and 199.6 eV, assigned to electrons from $2p_{3/2}$ and $2p_{1/2}$ states respectively, both possess a shoulder peak of higher energy (198.5 and 200.1 eV severally) (***Figure 3.4-20***); the twofold nature of such peaks correlates with the presence of two distinct chloride anions: the first bound to Pd(II) ion, acting as its fourth donor, the latter being retained upon complexation of Pd(II) to guarantee charge neutrality. This, corroborated by the evidences from the coordination behaviour observed in the solution studies of the free ligands, proofs that both HL1 and HL2, adsorbed on CNTs or not, function as N-tridentate ligands towards Pd(II), leading to complexes with an activated position occupied by a chloride anion.

The values of the BET surface areas of the functionalized materials reveal changes in the conformations of the polyaminic chains upon Pd(II) complexation. In the case of MWCNT/HL1, the BET surface area diminishes significantly after the coordination of the metal (from 198 m^2/g of the precursor to 179 m^2/g), while for MWCNT/HL2 there is barely a detectable difference (from 188 to 183 m^2/g). This can be rationalized considering the tendency of the formed square-planar Pd(II) complexes to interact with CNTs surface by Cπ-dπ interactions, which should result in a decrease of the BET surface area. Such interaction justifies both the data for HL1 and HL2: for the first ligand, the required folding of the polyaminic chain is not hindered, resulting in the interaction of the Pd(II)-macrocycle complex with the graphitic surface which actively reduces the surface area; in the case of HL2, the possible formation of such interactions is thought to be hindered both by the electrostatic interaction with the additional ammonium group in the side chain, which in Pd(II) adsorption conditions (pH 5.0) is expected to be protonated (log *K*=7.0 for the free complex, see ***Table 3.4-1***), and by the higher loss of conformational entropy of the chain required to establish Cπ-dπ contacts compared to the shorter HL1. Thus, in this latter case, the variation of the BET surface area upon Pd(II) complexation is found to be very modest.

3.4.3.2.2 The Sonogashira Carbon-Carbon Coupling Reaction

The catalytic activity of MWCNT/HL1–Pd and MWCNT/HL2–Pd materials towards the copper-free Sonogashira reaction between iodobenzene and phenylacetylene (1:1 molar relationship) using water as solvent and triethylamine as base was tested at three different temperatures (30, 50 and 70° C). The catalysed process proceeds in all cases, although with significant differences (see ***Table 3.4-7***).

Table 3.4-7. *Catalytic assays of the two catalysts towards the Cu-free Sonogashira coupling between iodobenzene and phenylacetylene (1 mmol of each, 1 ml H_2O, 2 mmol Et_3N, 1% mol Pd).*

Catalyst	***T(° C)***	***Cycle***	***Time***	***Yield (%)***
	30	*1*	*3 d*	*88*
	50	*1*	*2 h*	*90*
MWCNT/HL1-Pd		*2*	*8 h*	*86*
		3	*8 h*	*80*
		4	*24 h*	*80*
	70	*1*	*2 h*	*84*
MWCNT/HL2-Pd	*30*	*1*	*3 d*	*87*
	50	*1*	*2 h*	*94*
		2	*16 h*	*92*
		3	*24 h*	*76*
		4	*24 h*	*66*
	70[a]		*2 h*	*83*

[a] At this temperature desorption of the anchored HL2-Pd complex was observed.

At 30° C, the reaction was not completed until 3 days. This high reaction time could be attributed to the extreme insolubility of the reactants in water, preventing their diffusion to the polar active-centres. Then, the reaction was assayed at 50° C. At this temperature, although the solubility of the reactants in water is still poor, probably acting as a limiting kinetic factor, the C-C coupling reaction was completed in 2 hours: 90% of conversion of the reactants into diphenyl acetylene was achieved in the case of MWCNT/HL1-Pd and 94% for MWCNT/HL2-Pd, moreover without formation of any other by-product. Kinetic plots for the reaction at this temperature are reported in ***Figure 3.4-21***.

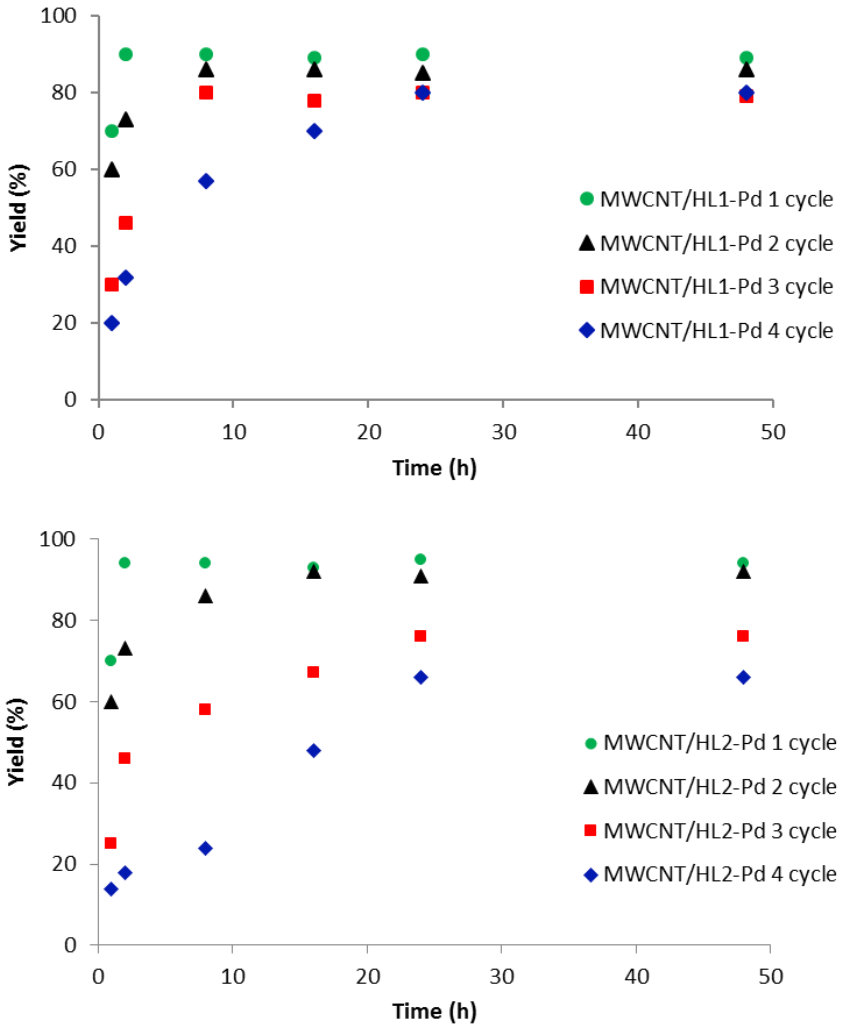

Figure 3.4-21. *Kinetic plots for fresh and reused catalysts, assessing their catalytic performances towards the Cu-free Sonogashira Cross coupling at 50° C.*

The calculated TOF values (mmol of reactants/mmol Pd(II)-amino complexes transformed per second) were 0.021 s^{-1} and 0.024 s^{-1} for MWCNT/HL1-Pd and MWCNT/HL2-Pd, respectively. The shortened equilibrium times, even at lower temperature, than most proposed Pd(II)-based heterogeneous catalysts, (*cf.* Appendix F) along with the high yields obtained, are probably due to the easy accessibility of the catalytic active centres, reinforced by their homogeneous dispersion over the whole external surface of the CNTs.

It should also be mentioned that, after recovering the catalysts by simple filtration methods and washing them with chloroform and water, their XPS spectra still showed traces of adsorbed iodobenzene. This points out that the partial adsorption

of iodobenzene on the CNTs surface likely prevents reaching 100% conversion in both cases.

To explore the influence of higher temperatures on the coupling, tests were also carried out at 70° C. In the case of both catalysts, neither the yields nor the equilibrium times improved from the 50° C assay. Moreover, in the case of MWCNT/HL2-Pd, a significant lixiviation of the anchored complex was observed, which became evident as a pink colour appeared in the aqueous phase. For these reasons, the catalysts were not reused for additional cycles at this temperature. Nevertheless, this should be regarded as an important result, since such behaviour demonstrates the heterogeneous nature of the catalyst, as an increased desorption of the Pd-HL2 complex not only does not improve the yield, but lowers it.

The studied C-C coupling reaction, was also carried out i) without any catalyst, ii) with the MWCNTs used as support of the catalysts, iii) with MWCNT/HL1 and MWCNT/HL2, but no reaction was observed in any of such cases. In addition, the catalytic activity of a MWCNT/$[PdCl_4]^{2-}$ material, consisting of $[PdCl_4]^{2-}$ directly adsorbed on CNTs, was assessed at 50° C. In this case, the C-C coupling reaction did take place, with an equilibrium time of 24 hours, after which a 78% of conversion of the reactants in diphenylacetylene was reached.

3.4.3.2.3 Reusability of the Catalysts

The re-usability of the two heterogeneous catalysts was tested for the above Sonogashira coupling reaction under the same conditions: three additional runs were carried out after the first one. After each cycle, the catalysts were separated by filtration, washed thoroughly with chloroform and water and dried before reusing. As one can see in ***Table 3.4-7***, the catalysts maintain a good catalytic activity through the four reaction cycles. In the second reaction cycle the yields of the reactions are close to those of the first run. For MWCNT/HL1-Pd catalyst, the yield decreases to 80% in the third cycle, value which is maintained in the fourth reaction. In the case of MWCNT/HL2-Pd, a higher decrease of the catalytic activity is observed after the second reaction, as the yields start to decrease with each cycle. Parallel to the above, a significant increase of the equilibrium times was observed for both catalysts after the first run (***Figure 3.4-21***), this effect being again sharper for MWCNT/HL2-Pd than for MWCNT/HL1-Pd.

To get insight into the possible causes of this behaviour, the catalysts were characterized after each cycle to detect any possible modification occurring under their repeated use. The elemental analyses of the catalysts reveal nitrogen losses with each use, obviously involving the corresponding ligands HL1 and HL2, which are more substantial for MWCNT/HL2-Pd than for MWCNT/HL1-Pd (***Table 3.4-8***).

Table 3.4-8. *Correlation between the elemental analyses of the two catalysts and their catalytic properties under repeated use.*

Catalyst	*T(° C)*	*Time (h)*	*Cycle*	*Yield (%)*	*N (%)*	*C (%)*	*H (%)*
MWCNT/HL1-Pd	*50*	*2*	*1*	*90*	*3.15*	*88.4*	*0.81*
	50	*8*	*2*	*86*	*2.47*	*91.9*	*1.04*
	50	*8*	*3*	*80*	*2.04*	*92.0*	*0.94*
	50	*24*	*4*	*80*	*1.96*	*89.4*	*0.93*
MWCNT/HL2-Pd	*50*	*2*	*1*	*94*	*3.20*	*89.2*	*0.79*
	50	*16*	*2*	*92*	*2.02*	*90.0*	*0.93*
	50	*24*	*3*	*76*	*1.98*	*88.1*	*0.95*
	50	*24*	*4*	*66*	*1.70*	*88.6*	*0.93*

Such decreasing is sharper in the earliest cycles, after which the nitrogen content almost remains stable. It should be noted how the catalytic activities of the material decreases in parallel with the nitrogen losses they suffer. Very scarce amounts of Pd(0) nanoparticles were observed in the TEM images of reused MWCNT/HL1-Pd catalyst, while none could be found in the case of MWCNT/HL2-Pd (***Figure 3.4-22***): this might be due to the superior stability of HL2-Pd complexes or to the different number of donor atoms in the ligands. According to the proposed mechanism for the copper-free Sonogashira reaction, the presence of Pd(0) should be related to the formation of a Pd(0) complex as an intermediate species during the catalyzed process.

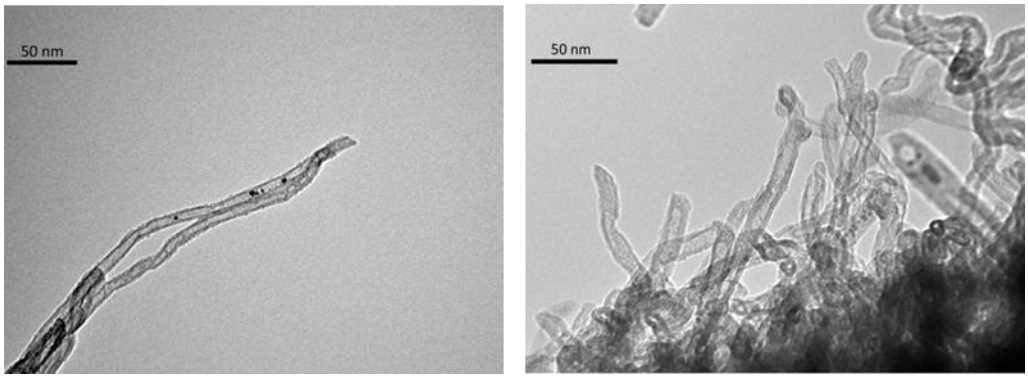

Figure 3.4-22*. TEM Images of MWCNT/HL1-Pd 4th cycle (left) and MWCNT/HL2-Pd 4th cycle (right).*

Nevertheless, the XPS spectra of the materials in the Pd region, collected after each cycle (***Figure* 3.4-23**), show signals at similar values than in the fresh catalysts, *i.e.* 343.5 and 338.2 eV, discarding the reduction of Pd(II) to Pd(0) as a possible cause of the deactivation of the catalysts, which seems better to be related to nitrogen losses.

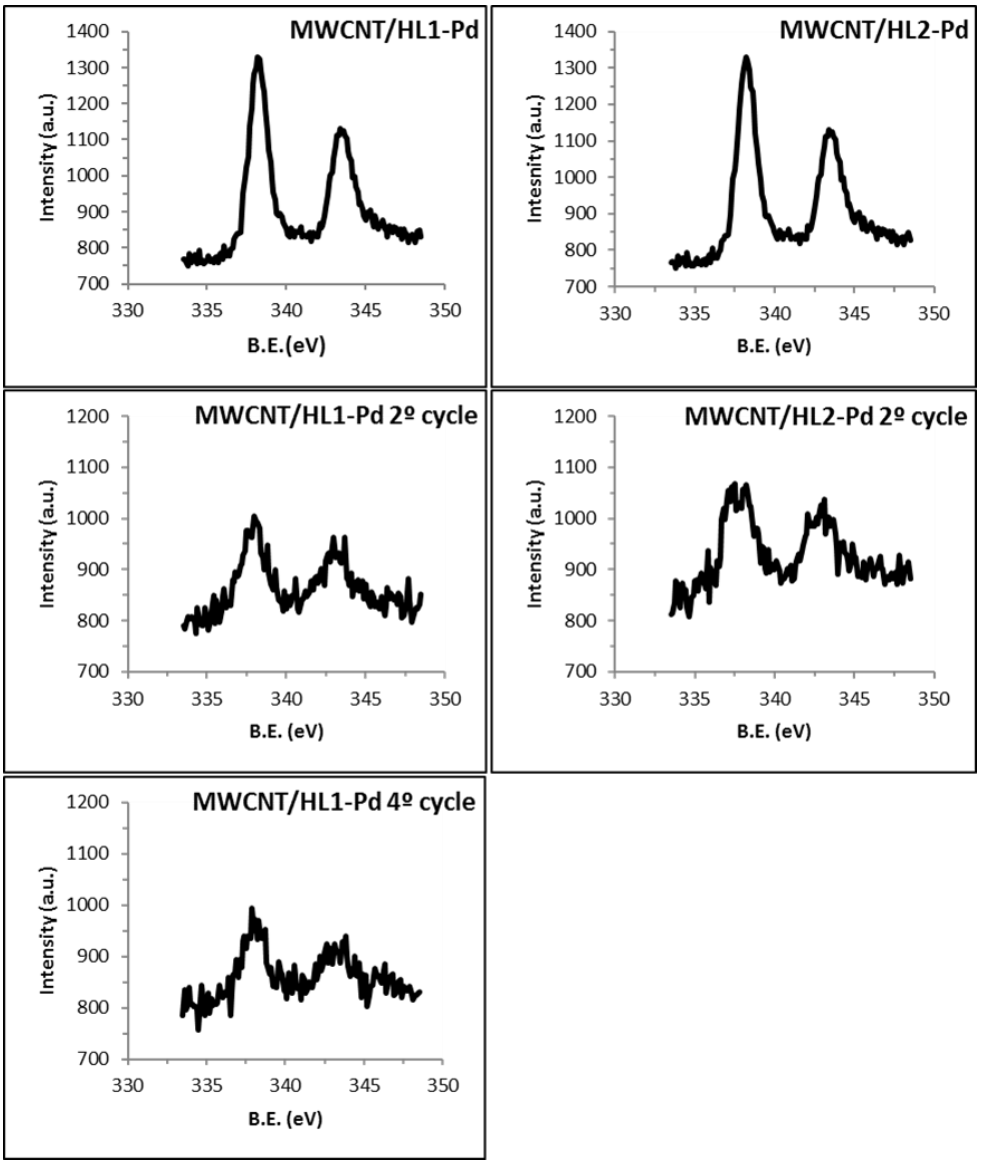

Figure 3.4-23. *High resolution XPS spectra in the Pd $3d_{5/2}$ and Pd $3d_{3/2}$ of fresh and re-used catalysts.*

Furthermore, the ratio between the intensities of N 1s and Pd 3d signals in the XPS spectra of re-used catalysts remains similar to that of the fresh ones. This clearly suggests that the deactivation of the catalysts is due to the lixiviation of the anchored HL1-Pd and HL2-Pd complexes during the reactions. The mechanism of loss of catalytic centres, however, appears different from what some of us previously observed in the case of hydrogenation reactions with AC-supported Pd(II) amino complexes, where pyrimidine residues stuck to the graphitic walls while the appended chain was partially lost due to solvolysis of the $C(2)_{Pyrimidine}$-NH bond. In those cases, the solvolysis was thought to be promoted by the stereochemical restrictions suffered by molecules adsorbed in the micropores of the carbonaceous support. The lack of microporosity in our CNTs-based systems, along with the steady N/Pd ratio observed, lead to the conclusion that the partial lixiviation of catalytic centres observed in this study should be attributed to the competition of the hydrophobic molecules (phenylbenzene, iodobenzene and phenylacetylene) with the adsorbed HL1-Pd and HL2-Pd complexes for the C_π centres of the CNT surface.

3.4.3.2.4 Adsorption of Cu(II) and Zn(II) by MWCNT/HL1

To explore the ability of MWCNTs functionalized with these macrocyclic ligands to adsorb metal ions other than the already discussed Pd(II), which forms very stable and inert complexes, we checked the MWCNT-HL1/Cu(II) and MWCNT-HL1/Zn(II) systems. According to the procedure described above (*cf.* 3.4.3.1), hybrid MWCNT-HL1 material, containing 0.36 mmol of HL1 per g of MWCNT, was prepared by shaking at 298 K a suspension of MWCNT (0.5 g) in an aqueous 10^{-3} M HL1 solution (500 cm^3) at pH 7.5 during three days to reach the maximum load of HL1. The MWCNT-HL1 material, resulting after filtration of the equilibrated suspension, water washing and drying, was employed for the Cu(II) and Zn(II) adsorption tests.

The adsorption isotherms of Cu(II) and Zn(II) ions on MWCNTs and MWCNT-HL1 adsorbents, obtained in water at 298.1 K and pH = 5.0 are shown in ***Figure 3.4-24***. The analysis of the equilibrium solutions allowed us to check that HL1 was not desorbed in the experiments involving MWCNT-HL1. All the adsorption isotherms were fit to the linear form of the Langmuir Equation (except that of the MWCNT/Zn(II) system, see below), where C_e is the adsorbate equilibrium concentration, X is the amount adsorbed, X_m is the maximum adsorption capacity and K_L is the Langmuir constant, defining the position of the adsorption equilibrium.

$$\frac{1}{X} = \frac{1}{K_L X_m C_e} + \frac{1}{X_m}$$

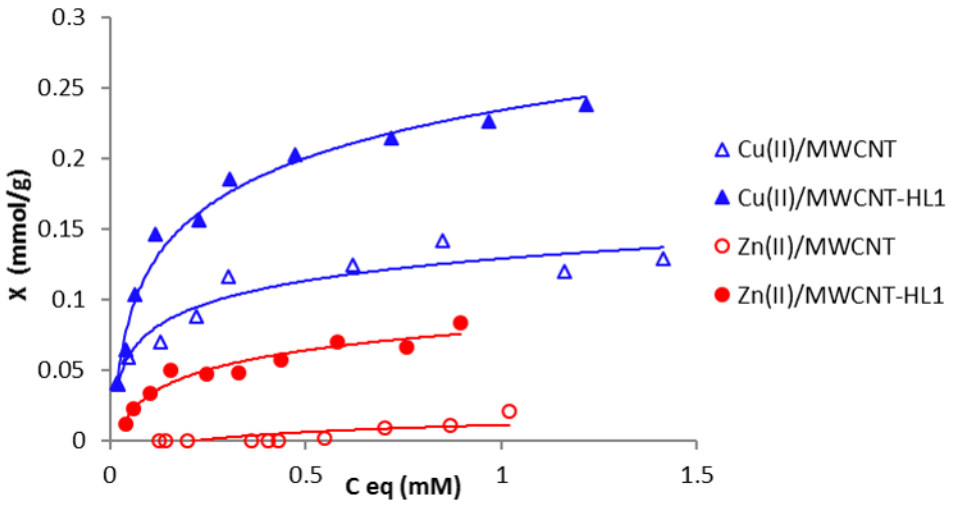

Figure 3.4-24. *Adsorption isotherms of Cu(II) and Zn(II) on MWCNT and MWCNT/HL1 adsorbents at pH 5.0.*

As shown in ***Figure 3.4-24***, at pH = 5.0, the pristine MWCNTs bind Cu(II) at a significant extent, with a maximum adsorption capacity, calculated from the above equation, X_m = 0.13(1) mmol per gram of adsorbent. In contrast, in the case of Zn(II) the adsorption is insignificant. The results can be explained by considering that the adsorption of a metal ion from aqueous solution onto a graphene surface takes place by interactions of Cπ(a soft base)-dπ type which is expected to be stronger for the acidic Cu(II) than for Zn(II).

The Cu(II) and Zn(II) loads increase significantly upon functionalization of the MWCNTs with HL1. In the case of Cu(II), the X_m value increases up to 0.24(1) mmol/g, relative to MWCNT-HL1, while in the case of Zn(II) it also increases significantly from *c.a.* zero to 0.080(4) mmol/g (***Figure 3.4-24***). As discussed above (*cf.* 3.4.3.2.1), the characterization of MWCNT-HL1 showed that π-π stacking interaction of the pyrimidine moiety of the adsorbed HL1 with the Cπ centres of MWCNT results in the loss of (Brönsted) basicity by the pyrimidine-conjugate C(5)-NO group, while the basicity of the polyamine function is preserved to a good extent, allowing the adsorption, *via* complexation, of Pd(II) ions by MWCNT-HL1. Accordingly, also the adsorptivity enhancement observed for MWCNT-HL1 with Cu(II) and Zn(II), relative to pristine MWCNT, is owed to metal coordination to the macrocyclic moiety of HL1. Indeed, like in the case of Pd(II), upon adsorption of Cu(II) by MWCNT-HL1, the aliphatic component of the XPS N 1s signal corresponding to the polyamine moiety (***Figure 3.4-25***) shifts to higher B. E. values, compared with the metal-free MWCNT-

HL1, in agreement with the high strength of the Cu(II)-polyamine interaction (***Table 3.4-2***). On the contrary, in the case of MWCNT-H1L-Zn(II), the N1s component of the XPS spectrum shifts to lower B. E. values. The latter effect, which is opposite to those observed with Cu(II) and Pd(II), can be ascribed to the fact that the binding of Zn(II) to HL1 polyamine nitrogen atoms in MWCNT-HL1-Zn is weaker than the binding of protons by MWCNT-HL1 at the working pH (5.0). In fact, the equilibrium data for the HL1-Zn(II) system (*cf.* ***Table 3.4-2*** and ***Figure 3.4-24***) show that, at pH = 5.0, ligand protonation competes efficiently with Zn(II) coordination.

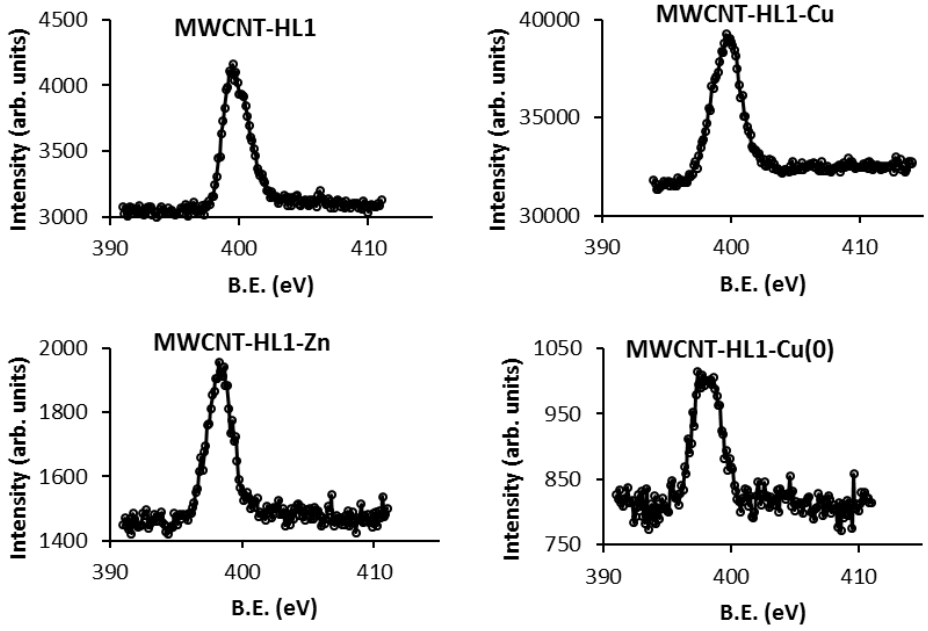

Figure 3.4-25. *High resolution N 1s spectra of MWCNT/HL1 and its prepared Cu and Zn derivatives.*

The presence, in the Cu 2p range of the XPS spectrum of MWCNT-HL1-Cu(II), of a single peak at 933.6 eV with a satellite at 944.0 eV (corresponding to the release of Cu $2p_{3/2}$ electrons) and of another peak at 953.9 eV (assigned to Cu $2p_{1/2}$ electrons), typical of Cu(II), discards any metal reduction during the adsorption process and suggests that all copper is adsorbed as Cu(II) coordinated to the polyamine (***Figure 3.4-26***). In the case of MWCNT-HL1-Zn(II), the presence of Zn(II) is confirmed by a well-defined XPS signal at 1020.1 eV corresponding to the release of Zn $2p_{3/2}$ electrons (***Figure 3.4-27***).

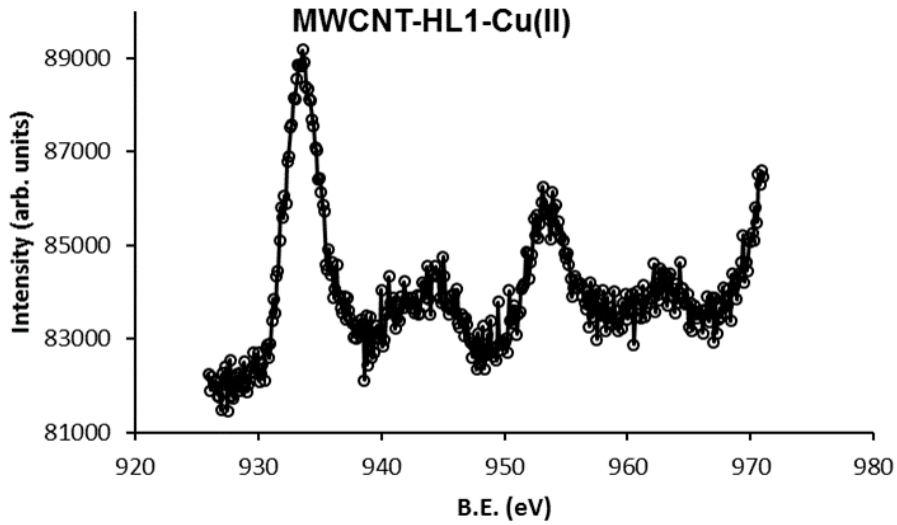

Figure 3.4-26. *High resolution XPS spectrum in the Cu 2p region of MWCNT/HL1/Cu.*

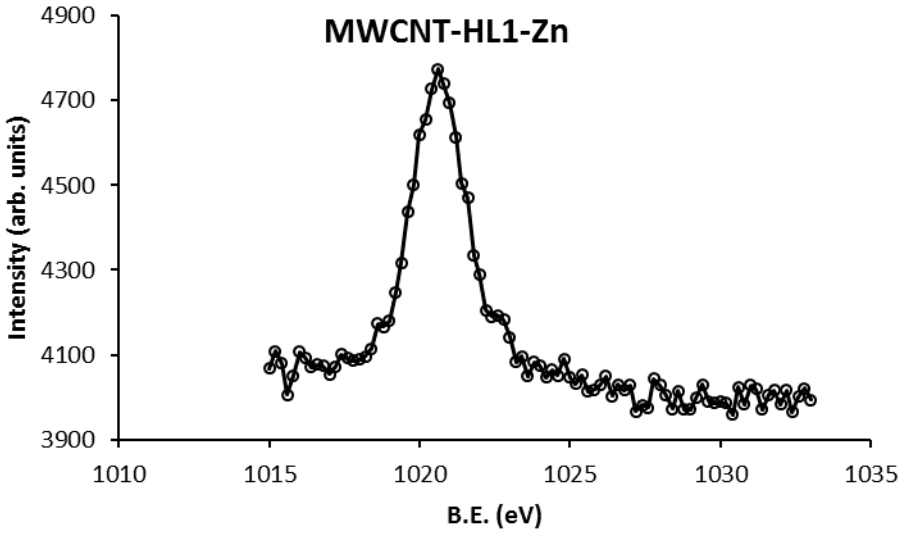

Figure 3.4-27*. High resolution XPS spectrum in the Zn 2p region of MWCNT/HL1/Zn.*

According to the equilibrium data (***Table 3.4-2***) for the formation of HL1 complexes with Cu(II), the ligand environment of the coordinated Cu(II) in MWCNT-HL1-Cu(II) should be formed by four polyamine nitrogen atoms, which leave space for the additional coordination of water molecules or/and hydroxyl groups. The presence of hydroxyl ligands coordinated to Cu(II) in MWCNT-HL1-Cu(II) is suggested by the quantitative analysis of its XPS spectrum, which provides an atomic relationship Cu/Cl ≈ 2/1. As charge neutrality requires two negative charges for each Cu(II) in the sample, it seems likely that the missing Cl^- ions were replaced by OH^- groups upon the repeated washing of MWCNT-HL1-Cu(II) performed in the final stage of its preparation (*cf.* 3.4.3.1). A similar conclusion is reached in the case of MWCNT-HL1-Zn(II), for which the Zn/Cl atomic relationship obtained from its XPS spectrum is also ≈ 2/1. Thus, Zn(II) adsorbed in this material should be complexed by the ligand polyamine moiety (although less strongly coordinated than in the case of Cu (II)) and by additional water molecules and/or hydroxyl groups.

Metal ions adsorption by a polyamine-complexation mechanism explains that the X_m values of MWCNT-HL1 with Zn(II) and Cu(II) at pH = 5.0, follow the same trend of the corresponding effective stability constants (K_{eff}) at this pH (log K_{eff} = 4.48 for Zn(II) and log K_{eff} = 9.33 for Cu (II)). In the case of other metal ions such as Pd(II), which is expected to form more stable complexes with HL1 than Zn(II) and Cu(II), the adsorption capacity of MWCNT-HL1 is also much higher.

3.4.3.2.5 Formation of Cu(0) Nanoparticles Supported onto MWCNTs

As observed in the case of Pd(II) for MWCNTs/HL1 and MWCNTs/HL2, as well as in other previous studies [45], the catalytic efficiency and the robustness of the catalysts increase with the binding ability of surface functions. On this basis and on account of the implication of Cu-based nanoparticles as catalysts in a wide range of reactions, we found it interesting to test the possibility of obtaining functionalized MWCNTs with surface-stabilized Cu(0) nanoparticles by using our hybrid materials. To this purpose, a MWCNT-HL1-Cu(II) sample was treated with $NaBH_4$ by following the procedure described in 3.4.3.1. The XPS of this sample showed the lack of Cu(II) peaks and the appearance of two peaks at 951.0 eV and 930.1 eV corresponding to Cu(0) $2p_{1/2}$ and Cu(0) $2p_{3/2}$, respectively, indicating quantitative reduction of Cu(II) to Cu(0) (***Figure 3.4-28***).

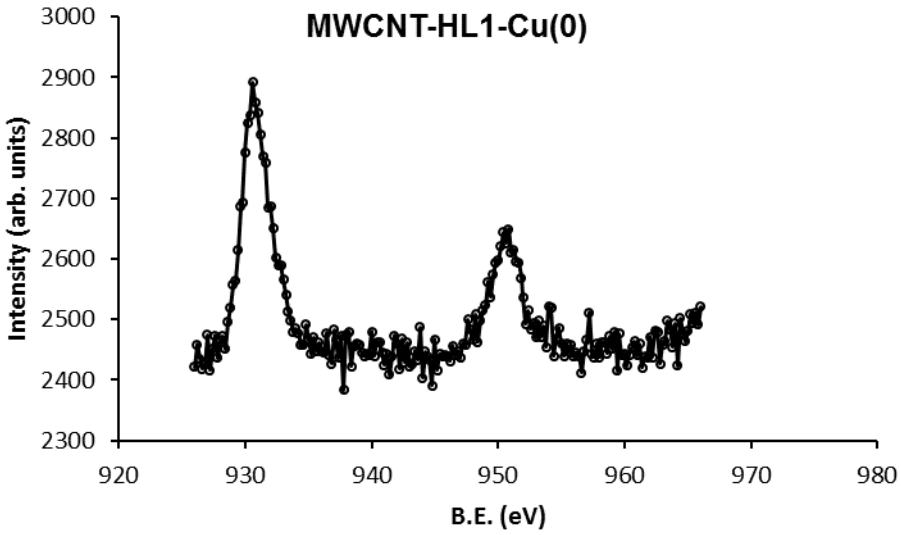

Figure 3.4-28. *High resolution XPS spectrum in the Cu 2p region of MWCNT/HL1/Cu(0).*

Reduction is also accompanied by a loss of oxygen from 2.75 to 2.15 atomic percent, which can be ascribed to the removal of water and hydroxyl ligands. It is very significant that the nitrogen content after reduction remains unchanged (3.09 and 3.04 atom percent for unreduced and reduced MWCNT/HL1-Cu, respectively) as also occurs for the Cu one (0.35 and 0.34 atom percent for unreduced and reduced MWCNT/HL1-Cu, respectively). This shows that, despite the relatively drastic conditions used for the reduction, neither HL1 nor Cu lixiviate during sample reduction and successive repeated washing, pointing out a significant stability of the material. This is not surprising, according to the proven stability of the π-π interactions in similar systems. Concerning the Cu(0) nanoparticles, their interactions with the MWCNT surface, illustrated by the TEM images in ***Figure 3.4-29***, are reinforced by interaction with the polyamine residue of HL1 molecules protruding from the surface. As a matter of fact, shifting of the XPS N 1s signal to significant lower B.E., relative to MWCNT/HL1, suggests that the unprotonated polyamine residues of MWCNT/HL1-Cu(0) interact with the surface Cu(0) nanoparticles. It is noteworthy that the result obtained by XPS analysis for the Cu(0) content of the reduced sample is equal to the Cu(II) content of the parent MWCNT/H1L-Cu(II), meaning that such Cu(0) nanoparticles should be very small in size. Actually, due to the low penetrating power of the radiation used in the XPS analysis, an accurate quantitative determination of metal from nanoparticles, by this technique, is only possible for very small nanoparticles (the bigger the nanoparticle size, the lower the metal amount detected compared to the real one). Indeed, the detected nanoparticles are of size smaller than 5 nm.

This is illustrated in ***Figure 3.4-29***, which also shows the uniformity of their size and distribution on the external surface of the MWCNTs.

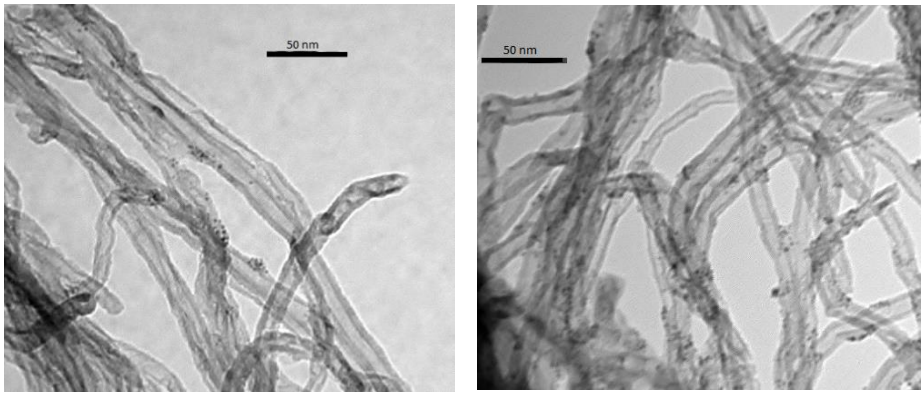

Figure 3.4-29*. TEM Images of MWCNT/HL1-Cu(0).*

The whole results obtained in this section show that the structural characteristics and the stability of both MWCNT/H1L-Cu(II) and MWCNT/H1L-Cu(0) make them promising Cu-based materials to be assayed as potential active and robust solid catalysts.

3.5 Conclusions and Future Perspectives

On the Palladium side, the gathered experimental evidences strongly support the assayed MWCNT/HL1-Pd and MWCNT/HL2-Pd materials as valuable catalysts for the Cu-free Sonogashira coupling reaction: as one can easily see comparing the obtained results with other candidates (*cf.* Appendix F), our systems not only rank among the first in terms of yields and reaction times, but the conditions (solvent and temperature) in which they are capable of such performances are unprecedented; such finding deserves to be underlined, especially in an era striving for green, sustainable and energy-saving chemical processes. Accordingly, also the choices of a carbonaceous support and of a single Pd(II) ion as catalytic active site should be stressed as environmentally friendly solutions, adding to the convincing heterogeneous nature of our catalysts.

As documented above (3.4.3.2), the strong points underlying their striking catalytic activity reside in the uniformity of the catalytic sites, both in terms of surface distribution and chemical environment, which is granted by the supramolecular preparation method (*cf.* 3.2.4).

Another feature worth mentioning is the choice of the polyaminic ligands, which are not only capable of coordinating Pd(II) strongly, forming a macrocyclic complex which is mostly stable under re-use even under stern alkaline conditions, but also manage to maintain an activated position, occupied by a chloride anion in the free complex and in the fresh catalyst, in the metal's first coordination sphere, which is probably crucial for the observed catalytic activity (*cf.* 3.2.1).

These promising results encourage the extension of this research to ligands possessing more than one pyrimidine moiety to ensure a firmer sorption and improve the overall re-usability of these materials, while maintaining the observed high catalytic performances.

Concerning Zn(II) and Cu(II), the adsorption results show how the reactivity of the polyamine function of HL1 toward Zn(II) and Cu(II) determines the preferential adsorption of these ions on MWCNT/HL1 *via* coordination to HL1. This determines the higher adsorption capacity for Cu(II), than for Zn(II), and gives rise to hybrid materials consisting of MWCNTs containing HL1-Cu(II) and HL1-Zn(II) complexes homogeneously distributed on the external graphene surface of the MWCNTs.

In view of the high catalytic efficiency of the Pd(II) derivative, and taking into account the high thermodynamic stability of the Cu(II) complex, we expect that MWCNT/HL1-Cu(II) might behave as a robust and reusable catalyst for reactions in which Cu(II)-based catalysts have proven their efficiency.

Moreover, reduction of MWCNT/HL1-Cu(II) provides a Cu(0) nanostructured MWCNT hybrid material whose structure and stability are very promising for its application in reactions requiring Cu(0)-based catalysts. This will be the focus of further research work.

As a final remark, it should be stated again (*cf.* 3.1) that the focus of the project lies on the methodology, *i.e.* in demonstrating that proper knowledge of the coordination properties of the functional F units with respect to the stereo-electronic preferences of the metal ion of interest, together with a supramolecular attention in designing tectons capable of self-organizing (thus providing an accessible way to homogeneously-functionalized surfaces) and a much required synthetic simplicity (expressing itself in the Ar-S-F design and the involvement of a click-like conjugation to a pyrimidine derivative available on a multigram scale), can lead to advancements in most applications requiring the organized decoration of graphitic walls.

What has been done within the framework of this thesis is an important basis to affirm this approach, yet, I believe, it was nothing but scratching the surface. The goal is having a method to transfer the molecular properties of interest selectively to a surface, metal cations do not need to be there, azamacrocycles do not need to be there, catalysis may not be the target: once the technique is in place you just have your CNT or graphene surface, with all its electrical, mechanical, and whatsoever fancy properties intact, and you functionalize it with the molecule of choice, also retaining its properties. The limit is in the mind.

4 ANION COORDINATION CHEMISTRY

4.1 RESEARCH OBJECTIVES

Aim of the anion coordination chemistry part of the present thesis is shedding light on the thermodynamic and structural features of anion-π interactions (*cf.* 1.3.3.2.5) in aqueous solution.

Although the anion-π interaction is nowadays widely recognized and demonstrated to play an important role in living beings [46], obtaining conclusive evidences on the role of this interaction or clarify the dependence of its thermodynamic parameters on the system properties has been proved very difficult, especially in solution.

This is primarily not a matter of stability, despite the strength of anion-π interaction having been underestimated for a while: the problem lies in its own supramolecular nature, which makes it cooperative and solvent-dependent (*cf.* 1.3.3.1.3), thus making observing and evaluating a pure, isolated, anion-π interaction, very difficult.

Concerning the choice of the solvent, one could argue that receptors for anions should work better in organic solvents of low polarity, especially when charged ligands are employed, due to the reduced solvation of charged species (*cf.* 1.3.3.1.1).

On one side, this is surely true, but there are a few objections that should be raised. The first one is that, by reducing the dielectric constant of the medium, the countercation becomes a strong competitor, introducing a marked dependence of the results on its nature. In second instance, most of the future applications of anion recognition and coordination, be it biomedical or environmental, are expected to be in water. This *per se* may not be a valid argument, as thinking outside the box is generally a good idea in Science. Yet, if we couple it with the observation that anion recognition and binding is routinely performed *in vivo*, namely in water and in a very selective manner, and admit that mankind has yet much to learn from and about the functioning of its own cellular mechanisms, undertaking the study in aqueous media appears as the most interesting choice.

Accordingly, we decided to prepare new aromatic hosts, suitable as model systems, containing the 1,2,4,5-tetrazine ring as the binding site, being both very amenable to anion-π interactions (*cf.* 1.3.3.2.5) and almost unprecedented concerning its study in water due to the poor water solubility of the unfunctionalized heterocycle.

The study involves anions of various nature, geometry and basicity, with special attention devoted to the effect of the solvent.

Potential applications, whenever they stem from this chiefly theoretical work, were investigated, often revealing intriguing possibilities: I cannot keep myself from playing the devil's advocate and joining the systematically-unheeded cry of recognition of that investors' scarecrow, fund-leeching, autotelic exercise that goes under the name of pure research, as a righteous and praiseworthy mean to progress theory and stimulate new applications.

In the following, the material will be organized as follows:

First, a new family of homologous tetrazine-based ligands will be introduced and their own properties will be examined in terms of series.

In the second instance, an in-depth study of the anion-binding properties of the two parents of the series towards typical inorganic anions will be presented.

In the third place, the same two ligands will be examined concerning their interactions with selected organic anions.

In the fourth case, a case-study involving only one of the ligands and its interactions with the whole series of halide anions will be presented.

Lastly, owing much to the study with iodide, the interactions of said ligands with polyiodide species will be debated, also in view of their possible technological applications.

On a final note, much of the data showcased below are still unpublished, however a few papers disclosing some of the research results were already published and are here re-proposed as reference material in Appendix G, H and I.

4.2 STUDIED LIGANDS

Building on our seminal study on the strength of anion-π interactions in water involving a pyrimidinic host [32] and in view of the broad interest in introducing anion−π interactions into the making up of receptors, carriers, catalysts, and new functional systems in general, we undertook the development of a new class of model system ligands.

The 1,2,4,5-tetrazine (s-tetrazine) aromatic nucleus was chosen, as it possesses a high and positive quadrupole moment (Q_{zz} = 10.7 B) and a high molecular polarizability ($\alpha_{\|}$ = 58.7 au); therefore, both electrostatic and ion-induced polarization terms should contribute to its anion binding ability (*cf.* 1.3.3.2.5).

Unluckily, tetrazines generally possess an abysmally low solubility in water, which makes them unsuitable for study. Accordingly, we resorted to functionalization with the aim of conferring to this heterocycle water solubility and sites amenable to protonation, to make its study manageable through our potentiometric technique, without inserting strong hydrogen bond donor groups (*cf.* 1.3.3.2.2), which could potentially interfere with the observation of the anion-π interaction.

Eventually, the choice fell on morpholine pendants, which, due to protonation, rendered well soluble our systems especially in acidic media, where protonation of the morpholines' tertiary nitrogen atoms takes place. The idea that strong salt bridges may arise and dominate the overall anion-ligand interaction, although disproved even from the earliest data, prompted us to prepare a series of homologous ligands with morpholine pendants located further and further away from the s-tetrazine core.

As such the ligands L1, L2, L3 and L4 (***Figure 4.2-1***) were prepared and studied.

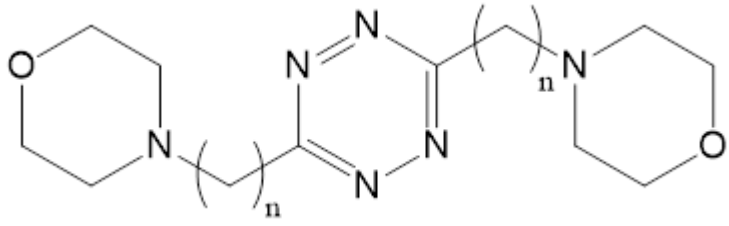

n = 1, L1; n = 2, L2; n = 3, L3; n = 4, L4.

Figure 4.2-1. *The family of tetrazinic ligands studied in this work.*

In principle, this was meant to give us the chance of observing the interaction with the same anion with a decreasing involvement of salt bridges. Furthermore, there is also a scale of degree of preorganization, running parallel and opposite to the

flexibility of these molecules: anion binding to weaker π-acids (a broad term, refer to discussion in 1.3.3.2.5) generally demands a high degree of preorganization and cooperativity, while here, interestingly, anions show a widespread marked preference for the tetrazine binding site over the formation of salt bridges (*cf. 4.3, 4.4, 4.5 and 4.6*)

For this reason, together with a synthetic easiness of preparation, L1 and L2, the most preorganized and, when fully protonated, the most charge dense receptors of the series, where investigated first and more in detail.

4.2.1 Synthesis

The preparation of ligands L1-L4 (**Figure 4.2-2**) was achieved following a two-step, classical Pinner's synthesis, consisting in a reaction of the morpholinyl-nitriles **1** with hydrazine hydrate to generate the corresponding dihydro-1,2,4,5-tetrazine intermediates **2**, which upon easy (though slow) air oxidation yielded the fully aromatic s-tetrazines. Notably, the synthesis of these ligands is one of the few non-metal catalysed Pinner synthesis of 3,6-dialkyl-s-tetrazine derivatives reported to date. Indeed, it is historically accepted that Pinner's procedures are of general applicability to the preparation of 3,6-diaryl-substituted s-tetrazines, but not to the synthesis of 3,6-dialkyl derivatives. Only recently, a variant of the Pinner synthesis to prepare 3,6-dialkyl-s-tetrazines with a wide scope of application was reported, but it was based on the use of anhydrous hydrazine and a metal Lewis acid catalyst, with the drawback of needing intensive purification to remove metal traces in the case of products containing good transition metal binding moieties, such as the morpholinyl groups in our molecules. On the other hand, in our preparations, the safer hydrazine hydrate is used together with N-acetylcysteine (NAC) as catalyst, with acceptable results in terms of isolated yields. Since the catalytic effect of NAC in the general preparation of amidines from primary amines and both alkyl and aryl nitriles is known, we attribute the success of our preparations to the role of NAC as a catalyst in the reactions between the morpholinyl-nitriles, **1**, and hydrazine to give the corresponding amidrazone intermediates. The subsequent formation of dihydro-1,2,4,5-tetrazine derivatives by dimerization of amidrazones is a well-known process that, in our case, leads to the isolable intermediates **2**.

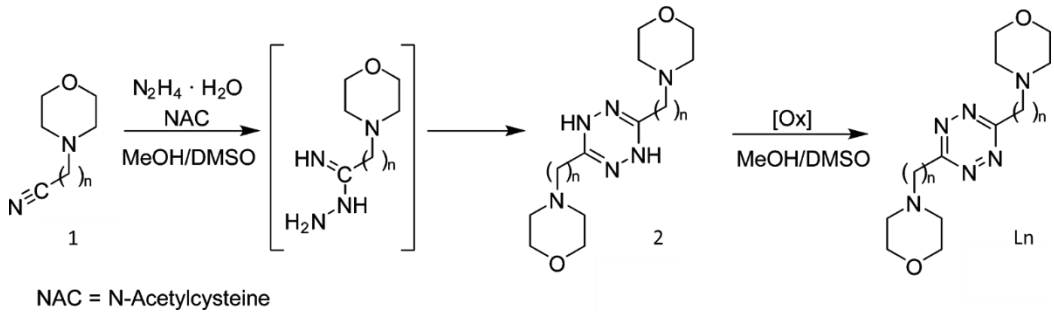

Figure 4.2-2. *Synthetic scheme of the preparation of tetrazine ligands L1-L4.*

4.2.1.1 Experimental

Tetrazine-based ligands were prepared according to a Pinner´s synthetic scheme from the corresponding mopholinyl-nitriles (***Figure 4.2-2***). The morpholinyl-nitrile derivatives, **1** and **2**, were prepared according to literature procedures (*cf.* experimental section of Appendix G).

4.2.1.2 Synthesis of 3,6-bis(morpholin-4-ylmethyl)-1,2,4,5-tetrazine, L1

Hydrazine (50 % aq. soln., 1.9 mL, 30.5 mmol) was dropwise added to a solution of morpholin-4-ylacetonitrile **1** (n = 1) (1.500 g, 11.9 mmol) and N-acetyl-L-cysteine (1.942 g, 11.9 mmol) in methanol (12 mL), and the resulting solution was stirred at r.t. under Ar atmosphere for 48 h. The solid in suspension was collected by filtration, washed with methanol and dried to afford 0.711 g (2.5 mmol, 42 %) of a white compound identified as the dihydrotetrazine intermediate **2** (n = 1). M.p. 194° C (dec.). IR (neat, ATR), ν/cm^{-1} 3285, 2972, 2926, 2901, 2860, 2812, 1661, 1450, 1398, 1111. ^{1}H NMR (DMSO-d_6, 400 MHz): δ 7.71 (s, 2 H), 3.57 (t, J = 4.5 Hz, 8 H), 2.95 (s, 4 H), 2.40-2.32 (m, 8 H). ^{13}C NMR (DMSO-d_6, 100 MHz): δ 147.1, 66.0, 56.7, 52.9. This solid was subjected to air oxidation without further purification. Thus, a suspension of **2** (n = 1) (0.511 g, 1.8 mmol) in DMSO (5 mL) was stirred at r.t. under an air atmosphere for 4 days. The resulting red solid was filtered, washed with methanol and dried to afford **L1** (0.417 g, 83 % referred to **2**. M.p. 145 °C (dec.). IR (neat, ATR), ν/cm^{-1} 2970, 2951, 2891, 2878, 2855, 2812, 2801, 1460, 1443, 1331, 1105. UV-Vis (H_2O, pH 2) λ_{max}/nm (ε) 520 (430), 298 (290, sh), 267 (2,475). ^{1}H NMR ($CDCl_3$, 400 MHz): δ 4.22 (s, 4 H), 3.77 (t, J = 4.6 Hz, 9 H), 2.75-2.70 (m, 8 H). ^{13}C NMR ($CDCl_3$, 100 MHz): δ 167.0, 66.8, 60.9, 53. HRMS (EI) m/z: $M^{+\cdot}$Calcd for $C_{12}H_{20}N_6O_2$ 280.1642; Found 280.1648.

4.2.1.3 Synthesis of 3,6-bis(morpholin-4-ylethyl)-1,2,4,5-tetrazine, L2

Hydrazine (50 % aq. soln., 3.0 mL, 48.2 mmol) was dropwise added to a solution of 3-(morpholin-4-yl)propanenitrile **1** (n = 2) (1.400 g, 10.0 mmol) and N-acetyl-L-cysteine (1.632 g, 10.0 mmol) in a methanol-DMSO 1:2 (v:v) mixture (6 mL), and the resulting solution was stirred at r.t. under Ar atmosphere for 72 h. The resulting solid was filtered, washed with a MeOH-Ethyl ether mixture (1:2, v:v) and pump dried to afford **2** (n = 2) containing some DMSO residue as shown by NMR spectra. ^{1}H NMR ($CDCl_3$, 400 MHz): δ 7.76 (s, 2 H), 3.68 (t, *J* = 4.6 Hz, 8 H), 2.54 (t, *J* = 6.1 Hz, 4 H), 2.50-2.41 (m, 8 H), 2.29 (t, *J* = 6.1 Hz, 4 H). ^{13}C NMR ($CDCl_3$, 100 MHz): δ 151.4, 66.7, 55.3, 53.3, 26.1. This solid was subjected to oxidation without further purification. Thus, a suspension of **2** (n = 2) in a mixture of MeOH (3 mL) and DMSO (0.2 mL) was stirred for two days under air atmosphere. The resulting pink solid was collected by filtration, dissolved in chloroform and filtered to remove insoluble impurities. The filtrate was evaporated to dryness to afford **L2** as a pink solid (0.612 g, 2.0 mmol, 40 %, referred to **2**). M.p. 110° C. IR (neat, ATR), ν/cm^{-1} 2961, 2922, 2878, 2845, 2824, 1460, 1443, 1414, 1115. UV-Vis (H_2O, pH 7) λ_{max}/nm (ε) 518 (435), 329 (300, sh), 275 (2,550). ^{1}H NMR ($CDCl_3$, 400 MHz): δ 3.63 (t, *J* = 4.6 Hz, 8 H), 3.50 (t, *J* = 7.1 Hz, 4 H), 3.01 (t, *J* = 7.2 Hz, 4 H), 2.54 (t, *J* = 4.6 Hz, 8 H). ^{13}C NMR ($CDCl_3$, 100 MHz): δ 169.0, 66.9, 56.5, 53.3, 32.2. HRMS (EI) m/z: $M^{+\cdot}$ Calcd for $C_{14}H_{24}N_4O_2$ 308.1961; Found 308.1964.

4.2.1.4 Synthesis of 3,6-bis(morpholin-4-ylpropyl)-1,2,4,5-tetrazine, L3 and 3,6-bis(morpholin-4-ylbutyl)-1,2,4,5-tetrazine, L4

Ligands L3 and L4 were synthesized according to the same general scheme followed for the preparation of their smaller homologues L1 and L2. Full description of the synthetic procedure, as well as their main characterization, will briefly appear in the literature.

4.2.2 Acid-Base Properties of the Ligands

Ligands in the L1-L4 series undergo protonation on the nitrogen atoms of the morpholine pendants: it is interesting to discuss their protonation properties in the light of their serial behaviour. Protonation constants determined through potentiometric (pH-metric) titration in aqueous solution (0.1 M NMe_4Cl, 298.1 K) are reported below in ***Table 4.2-1***.

Table 4.2-1. *Protonation constants of the series of tetrazine-based ligands L1-L4 determined in 0.1 M NMe_4Cl at 298.1 ± 0.1 K. Literature value for the protonation of the free N-methyl morpholine is included as reference. Values in parenthesis are the standard deviations on the last significant figure.*

Equilibria	***log K***				
	L1	*L2*	*L3*	*L4*	*N-methyl morpholine*
$L + H^+ = HL^+$	*4.45(3)*	*6.19(1)*	*7.19(3)*	*7.65(2)*	*7.38*[a]
$HL^+ + H^+ = H_2L^{2+}$	*3.45(3)*	*5.37(1)*	*6.54(3)*	*6.88(2)*	-

[a] Data taken from ref [47].

As one can easily see there is a net reduction of overall basicity in the order L4 > L3 > L2 > L1 associated to the electron withdrawing effect of the tetrazine nucleus, the nearer it is from the aminic function the less its basicity. Second protonation, although always happening in more acidic conditions due to the presence of a positive charge on the molecule, follows qualitatively the same trend.

N-methyl morpholine is a useful reference compound, revealing that the first ligands of the series suffer a reduction of their basicity of several orders of magnitude compared to the reference value of log *K* = 7.38. It should be stressed however, as clearly observed in the case of L4, that this value is not the limit of the series, lacking of convergence being due to the fact that ligands L1-L4 possess two identical protonable sites instead of just one: as such, statistical effects are expected to slightly raise the observed basicity.

Plateauing of the series is manifest from ***Figure 4.2-3***.

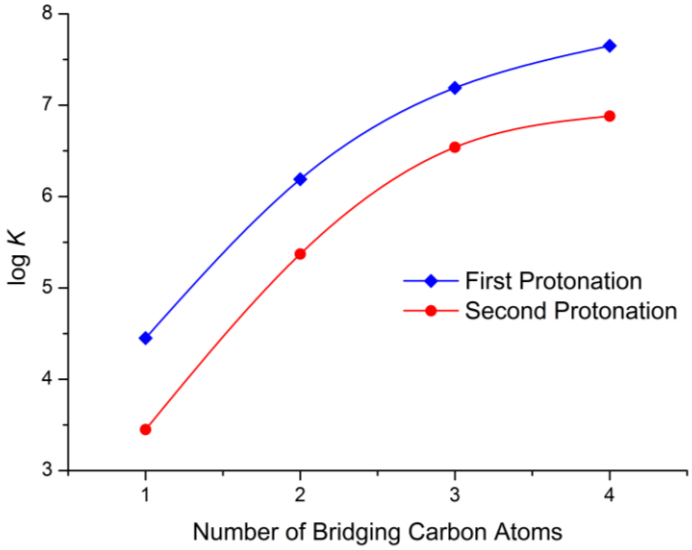

Figure 4.2-3. *Tendency of the first and second protonation constants for the L1-L4 series.*

Although 4 points are a limited set, fitting with a generic hyperbolic function, reported in ***Figure 4.2-4***, provides log K_1 = 7.73 ± 0.01 and log K_2 = 6.89 ± 0.02 as the asymptotic values for the first and second series of protonation constants respectively (R_1^2 = 0.99994, $\chi_1^2 = 1.13 \cdot 10^{-4}$; R_2^2 = 0.99976; $\chi_2^2 = 5.65 \cdot 10^{-4}$).

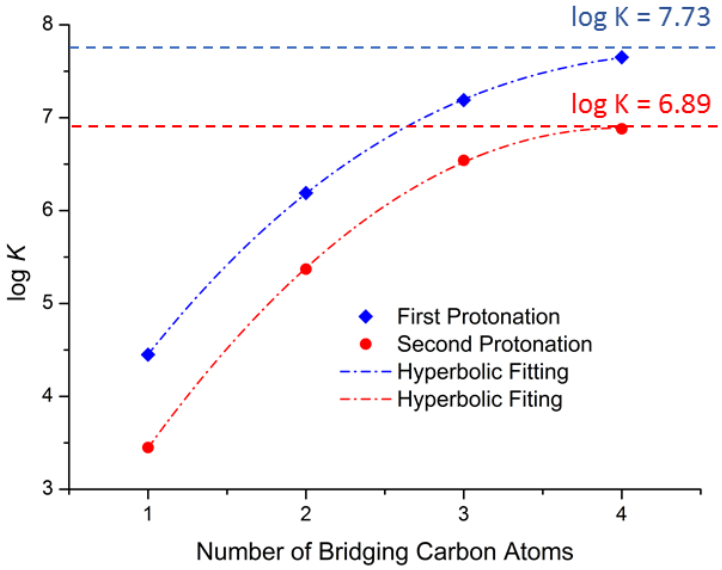

Figure 4.2-4. *Hyperbolic fitting for the first and second series of protonation constants of the tetrazinic ligands L1-L4.*

It should be noted that in the case of L4 we are already very close to the forecast of the asymptotic values: beyond mathematics, this is to be expected on a chemical ground, as the stereoelectronic influence of even the strongest electron withdrawing group is lost when it is located too far away, 5 covalent bonds appearing as a reasonable distance to flat out the effect of the tetrazine.

A point worth mentioning is the relative increment of basicity along the first and second series of protonation constants: as showed in ***Figure 4.2-5***, where the second protonation series was offset to make it start with the same value of the first, the stepwise increase of basicity of the ligands in the second protonation stages due to the spacer elongation is always more marked than that of the first protonation stages. As anticipated in 4.2, there is a flexibility issue here, with the smallest ligands being the most conformationally rigid, with scarce possibility of folding to minimize the charge-charge repulsion between protonated groups: if the trend observed for the first protonation step is primarily to be ascribed to the increased distance from the electron withdrawing tetrazine, in the case of the second protonation step the increased folding possibility and minimization of the repulsion plays a role. Reversing the argument, the first ligands of the series can be viewed as the most preorganized, both due to their rigidity and to their lesser capability of reducing intramolecular repulsion if not resorting to the binding of negatively charged species.

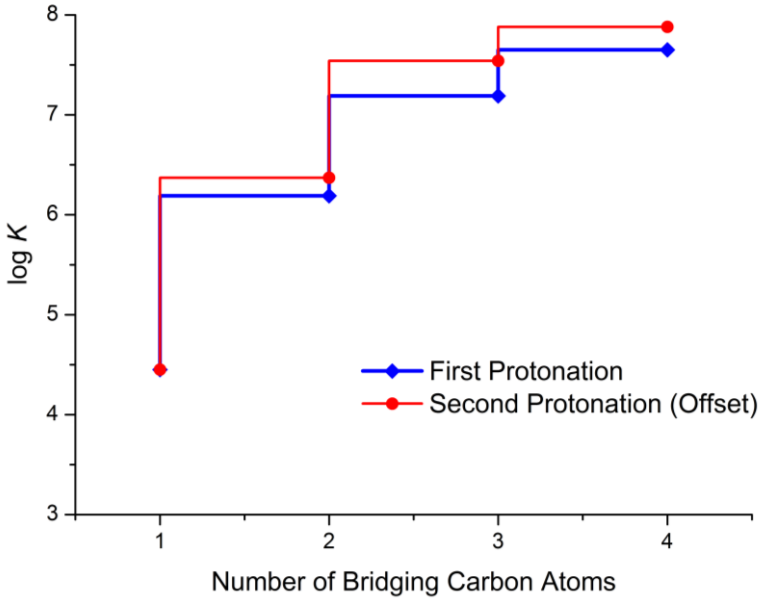

Figure 4.2-5*. Comparison between the stepwise increase in basicity of the first and second protonation equilibria along the series of L1-L4 ligands.*

4.2.3 Crystal Structures of the Free Ligands

Crystal structures of the free ligands (crystallographic parameters in ***Table 4.2-2***) help corroborating the trends observed in the protonation studies and the fitness of these molecules to work as anion receptors by virtue of anion-π interactions.

Several short contacts are recognizable in the solved structure, nevertheless the most striking features are invariably exhibited by the interactions established between the tetrazine ring and morpholinic electron rich atoms (O or N) of a neighbouring ligand molecule. This kind of contacts, which goes under the name of lone pair-π interactions, are to anion-π interactions as hydrogen bonds are to salt bridges: the charge reinforcement of the interplay is lacking, and as such the stability is much less, though their ultimate nature is similar. In this remark, it is noteworthy that, in the absence of other possible partners, ligands of the L1-L4 series organize themselves in the solid state maximizing the intrinsically weak lone pair-π interaction, and do so to different extents.

Having a few van der Waals radii in mind as reference values (C 1.77 Å, N 1.66 Å, here useful also as a rough estimation for the aromatic ring, O 1.50 Å, C-N sum 3.43 Å, N-N sum 3.32 Å, N-O sum 3.16 Å [48]), one can get a feel for the strong polarization of L1, which folds to bring a morpholinic oxygen atom right on the centroid of the tetrazine ring and separated from it by only 2.96 Å (***Figure 4.2-6***).

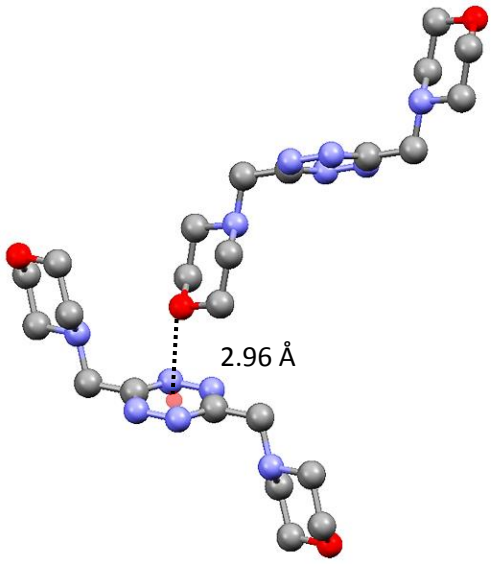

Figure 4.2-6. *Crystal structure of L1 evidencing a strong lone pair-π interaction with the morpholinic oxygen atom of a neighbouring molecule.*

The structure of L2 confirms the observed tendency of the tetrazine moiety to interact with electron rich atoms. Here we can see that the ligand prefers to lie almost planar giving rise to a T-shaped arrangement, instead of bending in the chair-like conformation observed for L1, probably because of its increased conformational freedom. Yet, a strong lone pair-π interaction still arises involving the morpholinic nitrogen atom, which is found 3.24 Å away from the tetrazine's centroid (***Figure 4.2-7***).

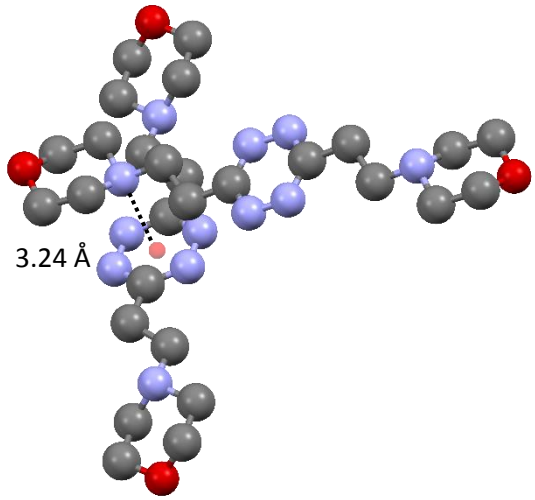

Figure 4.2-7*. Crystal structure of L2 evidencing a strong lone pair-π interaction with the morpholinic nitrogen atom of a neighbouring molecule.*

The crystal structure of L3 somewhat confirms what observed also from the protonation data (*cf*. 4.2.2): the extreme polarization observed for the first members of the series of ligands starts to fade out for the superior homologues. In fact, van der Waals forces starts to predominate, with the lone pair-π contact, although existent, extremely reduced in strength: this time the morpholinic oxygen atom is located 3.69 Å away from the centroid (*cf.* the 2.96 Å for L1) and slightly off-centre, its closest contact being $O^{\cdots}C_{tetrazine}$ 3.36 Å, just slightly below the sum of van der Waals radii (*vide supra*) (***Figure 4.2-8***). This arrangement seems to be a sort of compromise between bringing together the oppositely polarized groups and the required folding of the propylenic spacer, resulting in the head-to-tail disposition observed in the crystal.

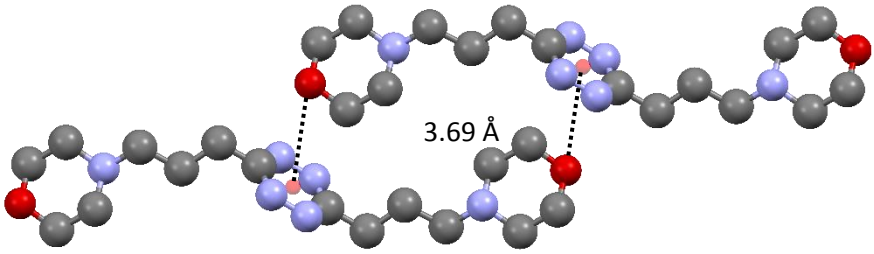

Figure 4.2-8. *Crystal structure of L3 evidencing a weak lone pair-π interaction with the morpholinic oxygen atom of a neighbouring molecule.*

L4 prosecutes the observed trend, with the lone pair-π interaction completely lost in the solid state, crystal structure containing only fully elongated ligands molecule giving rise to van der Waals contacts with one another, with the head to tail disposition observed for L3, and already hindered in that case by the length of the propylenic spacer, now completely lost upon further addition of a carbon atom in the spacer (***Figure 4.2-9***).

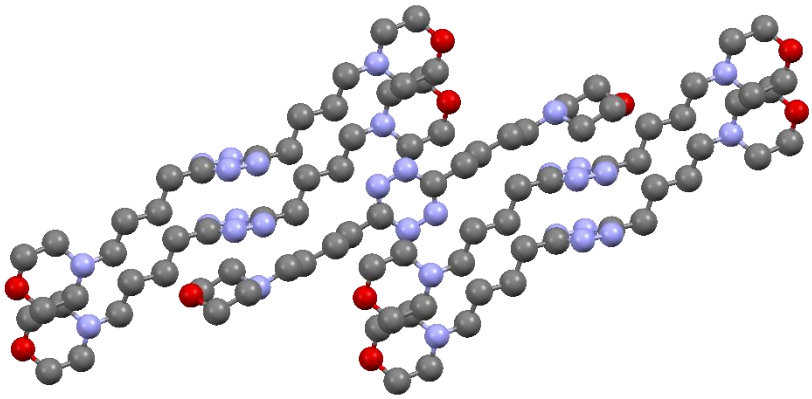

Figure 4.2-9*. Crystal structure of L4 evidencing no lone pair-π interactions.*

Overall, from the inspection of the crystal structures of the free ligands, we can conclude that there is a certain polarity trend, closely mirroring the situation observed for the protonation constants (*cf*. 4.2.2), and that the tetrazine ring is a formidable binding site for electron rich centres, even when they do not possess a net charge. This is especially true for the smallest receptors of the series, which are the most ill-equipped to mitigate the heterocycle electronic effect.

***Table 4.2-2**. Crystallographic information for the structures of the free ligands L1-L4.*

Structure	***L1***	***L2***	***L3***	***L4***
Empirical Formula	$C_{12}H_{20}N_6O_2$	$C_{14}H_{24}N_6O_2$	$C_{16}H_{28}N_6O_2$	$C_{18}H_{32}N_6O_2$
Formula Weight	*280.34*	*308.38*	*336.43*	*364.48*
Temperature (K)	*150*	*150*	*150*	*150*
Crystal System	*Monoclinic*	*Monoclinic*	*Triclinic*	*Monoclinic*
Space Group	$P2_1/n$	$P2_1/c$	*P-1*	$P2_1/c$
a (Å)	*6.2753(4)*	*11.690(1)*	*6.6983(6)*	*13.5805(3)*
b (Å)	*13.9813(8)*	*6.834(1)*	*8.6859(8)*	*5.1482(1)*
c (Å)	*7.4837(4)*	*10.73(2)*	*8.7604(9)*	*14.2994(3)*
α (°)	*90*	*90*	*109*	*90*
β (°)	*97*	*117*	*95*	*104*
γ (°)	*90*	*90*	*110*	*90*
Volume (Å³)	*651.5457*	*761.52*	*440.994*	*967.343*
Z	*2*	*2*	*1*	*3*
R	*0.055*	*0.082*	*0.070*	*0.042*
λ	*1.5418*	*1.5418*	*1.5418*	*1.5418*

4.3 Anion Binding Properties Towards Inorganic Anions

In this section, results concerning the interactions of our model hosts with inorganic anionic guests will be discussed. L1 and L2, which according to the above (*cf.* 4.2) are expected to give rise to the most stable complexes, are the main focus of the study, with a few side notes on the possible behaviour of their superior homologues.

The Reader will understand a little resource management, for his or her own sake, in presenting the material: data and crystal structures for the interaction of L2 with halide anions different from fluoride, which with its marked basic character is helpful for the overall discussion, will be presented in a dedicated section (*cf.* 4.5). Discussion of data involving the thiocyanate anion are also postponed and can be found in the polyiodides section (*cf.* 4.6), where, owing to the pseudohalogen character of this anion, it provides a useful substitute model for the interaction.

4.3.1 Crystal Structures

4.3.1.1 Crystal Structure of $H_2L1(PF_6)_2{\cdot}2H_2O$

In this crystal structure, the diprotonated H_2L1^{2+} ligand lies on an inversion centre and assumes an overall symmetric chair conformation (***Figure 4.3-1***). The tetrazine ring forms two anion-π interactions with the symmetry related PF_6^- ions, one of the fluorine atom of these anions being only 2.94(9) Å apart from the ring centroid. Interestingly, the ammonium groups of the ligand are not involved in the binding of the PF_6^- anions but interact via hydrogen bonding with co-crystallized water molecules (N···OW 2.686(5) Å). Therefore, the anion is held in the crystal packing by the anion-π interaction with contributions from CH···F bonds (2.469(3) Å) and van der Waals interactions.

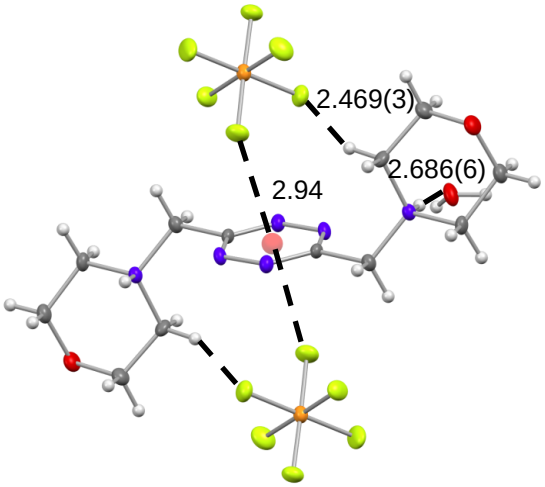

Figure 4.3-1. *Crystal structure of $H_2L1(PF_6)_2{\cdot}2H_2O$. Distances in Å.*

4.3.1.2 Crystal Structure of $H_2L1(ClO_4)_2 \cdot 2H_2O$

In this complex, the ligand assumes a boat-like conformation, both morpholine pendants protruding from the same side of the tetrazine ring (***Figure 4.3-2***). The aromatic group forms anion-π interactions with the oxygen atoms of two symmetry related ClO_4^- anions. As in the previous structure, the anions are located almost above the centre of the tetrazine ring with O···centroid distances of 2.96(3) and 2.78(3) Å, respectively. Accordingly, this anion is sandwiched between tetrazine rings of two ligand molecules, while the other ClO_4^- anion, not shown in ***Figure 4.3-2***, is H-bonded to water molecules interacting with ligand ammonium groups (NH···OW 1.88(3) Å, NH···OW 1.90(3) Å). It is noteworthy that, also in this complex, the sandwiched anion is held in place only by anion-π interactions and CH···O hydrogen bonds (***Figure 4.3-2***).

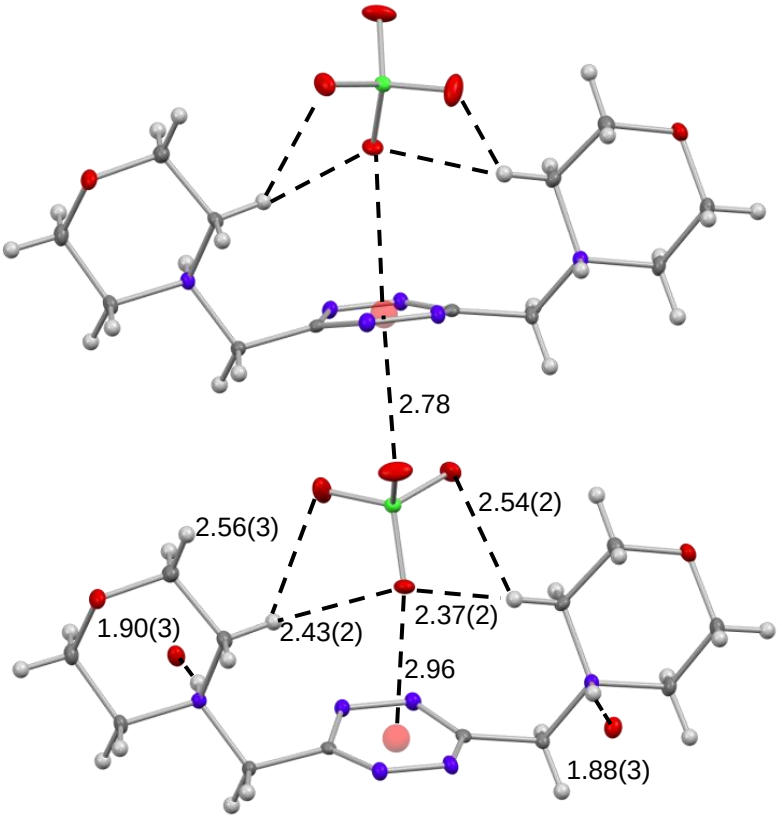

Figure 4.3-2*. Crystal structure of $H_2L1(ClO_4)_2 \cdot 2H_2O$. Distances in Å.*

4.3.1.3 Crystal Structure of $H_2L2(PF_6)_2 \cdot H_2O$

The crystal structure of the PF_6^- complex with H_2L2^{2+} contains two centrosymmetric crystallographically independent ligand molecules (***Figure 4.3-3***). One of them assumes a chair conformation similar to that found in the structure of $H_2L1(PF_6)_2 \cdot 2H_2O$, while the other one is almost planar. Also in $H_2L2(PF_6)_2 \cdot H_2O$ the tetrazine rings give rise to anion-π interactions with PF_6^-. Different kinds of interactions are established between the fluorine atoms of PF_6^- and the tetrazine groups. Actually, one of the fluorine atoms is located pretty well above the tetrazine ring centroid of the planar ligand (F···centroid 2.87(6) Å, ***Figure 4.3-3a***), governed by the ion-dipole attraction, while three cofacial fluorine atoms face the other tetrazine ring forming F···N, F···C and F···N-N contacts (3.110(5), 3.092(5) and 3.07 Å, respectively, ***Figure 4.3-3b***). Due to the enhanced flexibility of the ethylenic chains connecting tetrazine and morpholine rings, the ligand in chair conformation is able to form a salt bridge with the anion (NH···F 2.10(5) Å), in contrast to the behaviour of L1 featuring shorter methylenic chains. It is to be underlined, however, that in this structure only one PF_6^- is in contact with tetrazine rings, bridging the two ligands to form infinite zig-zag chains of anion-π contacts (***Figure 4.3-3c***). The second PF_6^- anion only interacts with a water molecule H-bonded to an ammonium group of the planar H_2L2^{2+} ligand form.

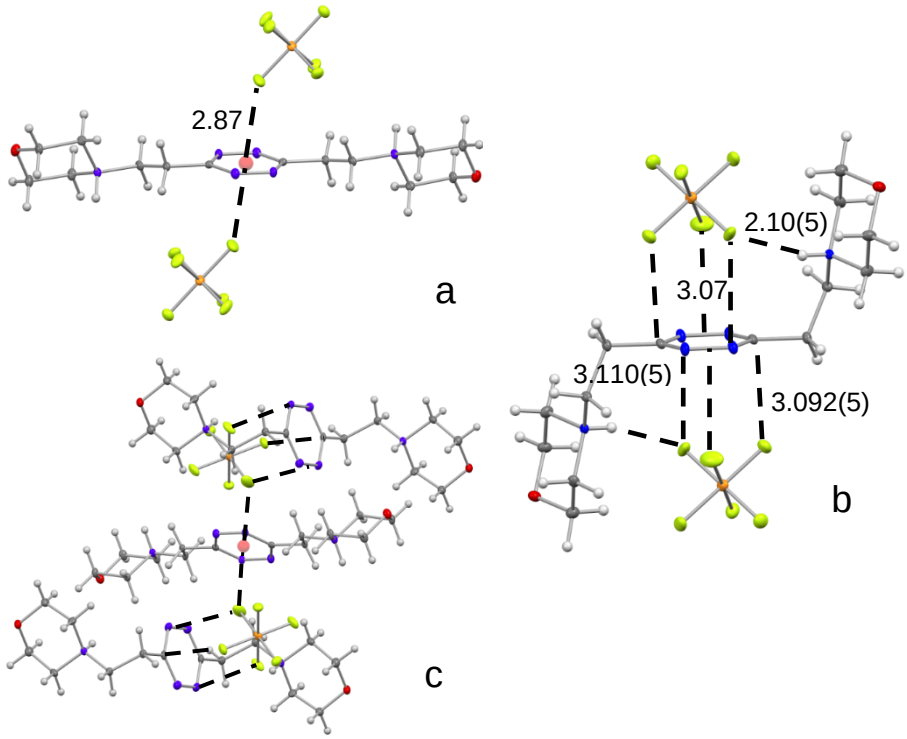

Figure 4.3-3. *Crystal structure of $H_2L2(PF_6)_2 \cdot H_2O$. Distances in Å. Views of the ligand and of its anion···π contacts: (a) planar and (b) chair conformations, (c) portion of the crystal packing.*

4.3.1.4 Crystal Structure of $H_2L2(ClO_4)_2 \cdot H_2O$

This crystal structure contains three crystallographically independent diprotonated ligand molecules H_2L2^{2+}. One of them assumes an almost planar arrangement (***Figure 4.3-4a***), while the other two, lying around a crystallographic centre, adopt chair conformations (***Figure 4.3-4b, c***). Like in the crystal structure of $H_2L2(PF_6)_2 \cdot H_2O$, several types of anion···tetrazine interactions contribute to stabilize the crystal (O···centroid, O···C and O···N in ***Figure 4.3-4***) and the overall crystal packing contains infinite zig-zag chains of alternating ligand and perchlorate units (***Figure 4.3-5***). In particular, in the adducts shown in ***Figure 4.3-4a, c*** one of the anion oxygen atoms is located almost above the ring centroid. However, while in the case of the planar ligand no other relevant interactions are observed in addition to such O···centroid contact (***Figure 4.3-4a***), in the case of the complex in ***Figure 4.3-4c*** additional O···C interactions contribute to strengthen the anion-tetrazine binding. As in the previous structure, each ligand molecule in chair conformation forms a salt bridge with ClO_4^- (NH···O 2.31(6), 2.46(5) Å, ***Figure 4.3-4b***; NH···O 2.18(5) Å, ***Figure 4.3-4c***). The crystal packing is further stabilized by additional hydrogen bonds involving the two remaining ClO_4^- and lattice water molecules.

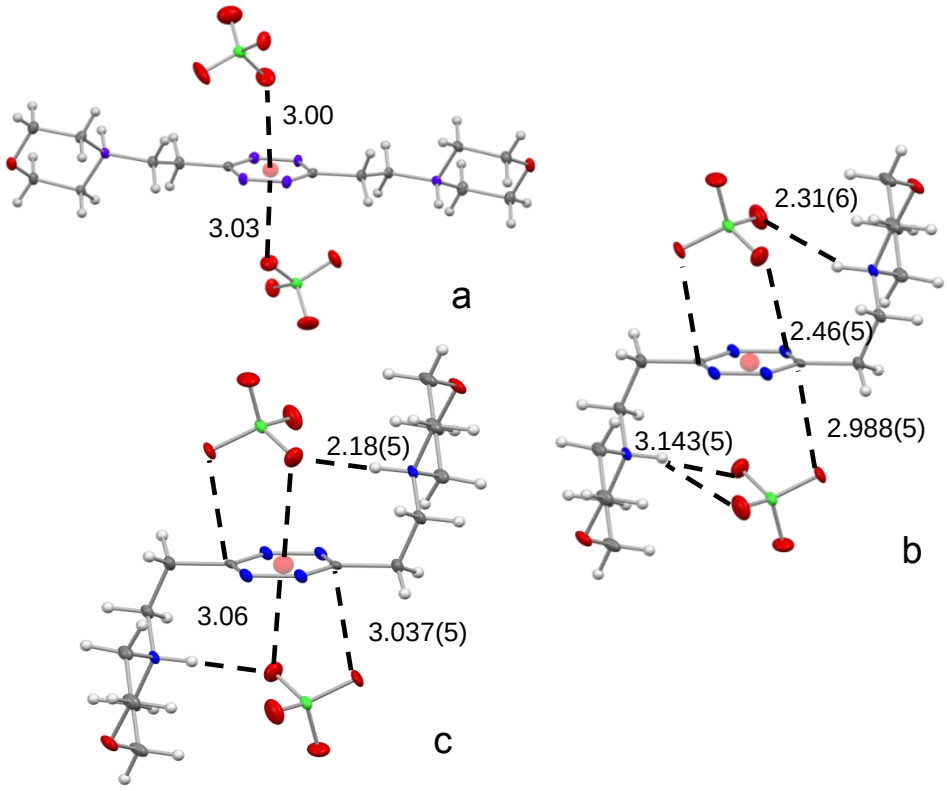

Figure 4.3-4. *Crystal structure of $H_2L2(ClO_4)_2 \cdot H_2O$. Distances in Å. Views of the ligand and of its anion···π contacts: (a) planar and (b, c) chair conformations.*

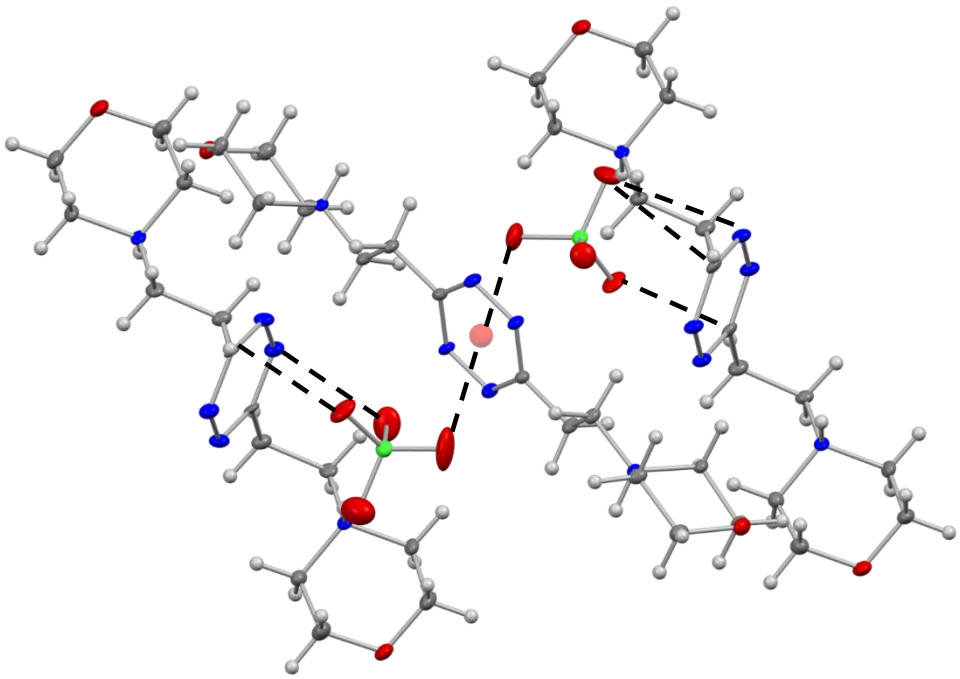

Figure 4.3-5. *A portion of the infinite zig-zag chains of alternating ligand and perchlorate units constituting the crystal structure of $H_2L2(ClO_4)_2 \cdot H_2O$.*

4.3.1.5 Crystal Structure of $H_2L2(NO_3)_2$.

Among the crystal structures obtained for anion complexes with L2, the NO_3^- complex is the one having more similarities with the structures seen for the shorter L1 ligand. Actually, the packing contains a single centrosymmetric ligand molecule in chair conformation, interacting with NO_3^- through the tetrazine ring (***Figure 4.3-6***). The planar anion is arranged almost parallel above the tetrazine group (dihedral angle 21.9(2)°), with an oxygen atom close to the ring centroid (O···ring centroid 2.850(2) Å). The same oxygen atom forms a salt bridge with a ligand ammonium group (NH···O 1.881(2) Å). Obviously, all groups and interactions are duplicated below the tetrazine ring by the inversion centre, but no chains based on repeated anion-π interactions are observed in this crystal.

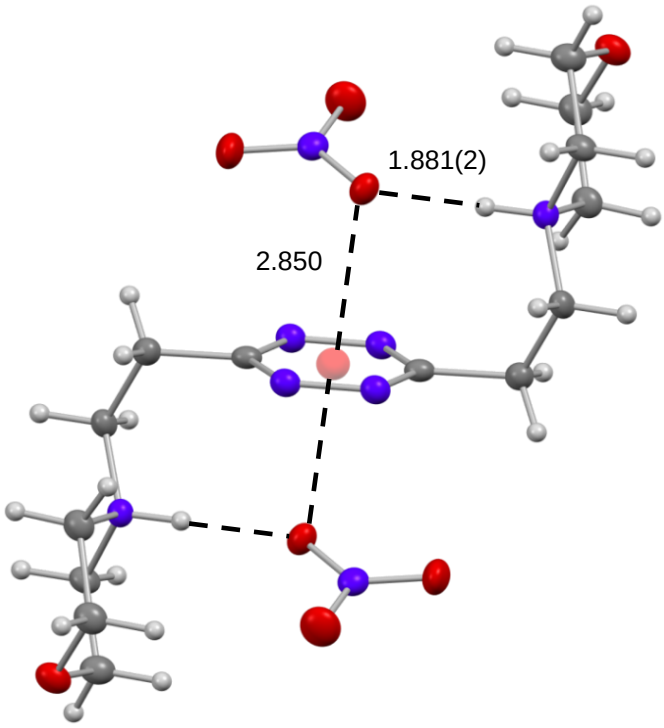

***Figure 4.3-6**. Crystal structure of $H_2L2(NO_3)_2$. Distances in Å.*

4.3.1.6 Crystal Structure of $H_2L3(ClO_4)_2{\cdot}2H_2O$

This crystal structure is found to be much simpler than its analogous for L1 and L2, resembling that of $H_2L2(NO_3)_2$; in fact, the tetrazine ring is located on an inversion centre, with a perchlorate anion above and below it, hydrogen bonded to a co-crystallized water molecule (***Figure 4.3-7***). Although short HN···O_{anion} (3.115 Å, *i.e.* just 0.04 Å shorter than the sum of the van der Waals radii) contacts exist in the structure, the hydrogen bond between the receptor and the anion appear to be mediated by the solvent molecule (HN···O_W 2.753 Å, O_W···O_{anion} 2.845 Å). Beyond that, the anion appears to be well-placed on the tetrazine ring, with at least one of its oxygen atoms giving rise to a strong interaction (O···centroid 3.118 Å).

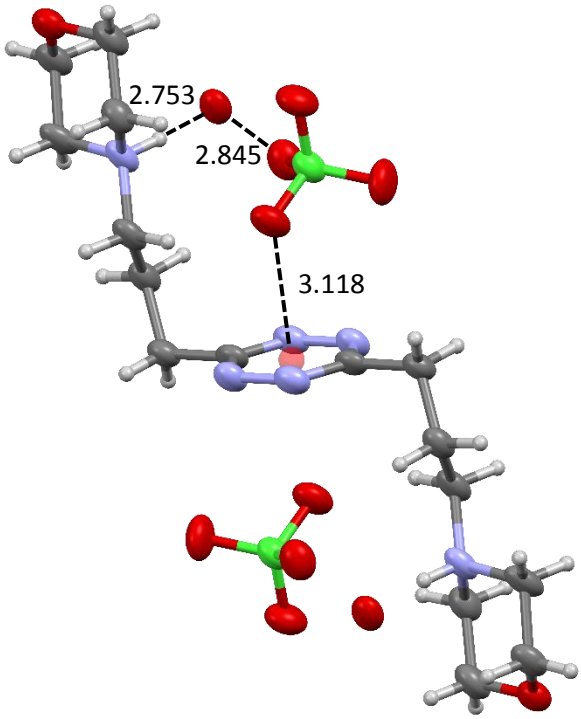

Figure 4.3-7. *Crystal structure of $H_2L3(ClO_4)_2{\cdot}2H_2O$. Distances in Å.*

4.3.1.7 Crystal Structure of $H_2L3(PF_6)_2{\cdot}2H_2O$

Crystals of $H_2L3(PF_6)_2{\cdot}2H_2O$ (***Figure 4.3-8a***) show again the centrosymmetric ligand strongly interacting through anion-π interaction with the octahedral anion (shortest F···centroid distance 3.027 Å). A noteworthy feature is the fact that the anion places itself right on the tetrazine ring, as in all the other cases, despite the fact that the stability contribution due to salt bridges is fading, even in comparison with the structure of $H_2L3(ClO_4)_2{\cdot}2H_2O$. Here, in fact, the solvent molecule is mainly found bridging the protonated morpholine nitrogen atom with the morpholinic oxygen atom of an adjacent ligand molecule (HN···O_W 2.810 Å, O···O_W 2.791 Å), while the involvement of the anion in the hydrogen bond network appears modest (shortest F···O_W distance 2.943 Å) (***Figure 4.3-8b***). As such, this structure strongly corroborates the observation that, although hydrogen bonding and salt bridges are generally the primary forces governing anion binding with ammonium-based receptors, in the case of our ligands, a net preference for the tetrazine binding site is invariably showed.

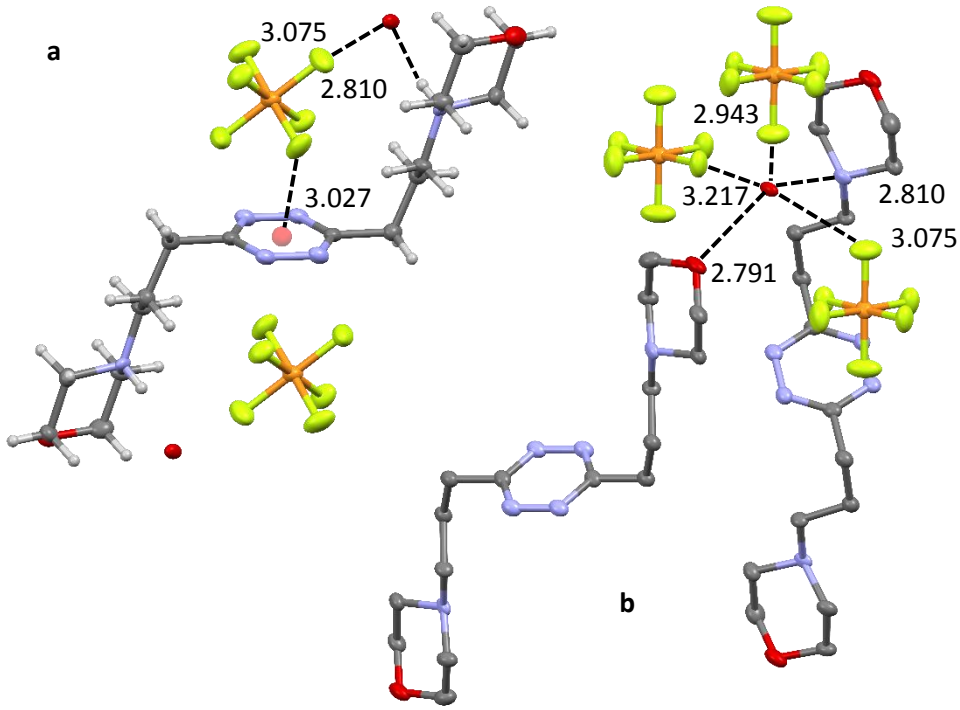

Figure 4.3-8. *Crystal structure of $H_2L3(PF_6)_2 \cdot 2H_2O$. Distances in Å. a) view of the anion-π interaction; b) detail of the environment of the co-crystallized water molecule.*

4.3.1.8 Crystal Structure of $H_2L3(PF_6)_2$

Crowning glory of the series of structures and of the above observations, is the crystal structure of $H_2L3(PF_6)_2$, whose crystals were obtained jointly with those of the diaquo complex from the same crystallization batch (***Figure 4.3-9***).

The structure is indeed very similar to the other, again showing a centrosymmetric ligand forming strong anion-π interactions with the anions above and under the plane of the aromatic ring: the fact is that, in this case, salt bridges do not contribute at all to the positioning of the anion, which is only held in place by the anion-π interaction and a number of CH···anion contacts (namely 12). This may resemble the analogous structure with L1, although in that case the polarization of the ligand and its inability to fold to orient the ammonium groups towards the anion (*cf.* ***Figure 4.3-1***), caused the establishment of extremely strong CH···F contacts (up to 2.469 Å), while in the case of L3 the range of distances observed for CH···F contacts indicates much looser interactions (12 CH···F contacts, medium distance 3.2 ± 0.2 Å, minimum 2.934 Å, median 3.312 Å, maximum 3.610 Å). As a matter of fact, anion-π contacts are preferred to salt bridges, hydrogen bond network regarding only ligand molecules (HN···O 2.935 Å).

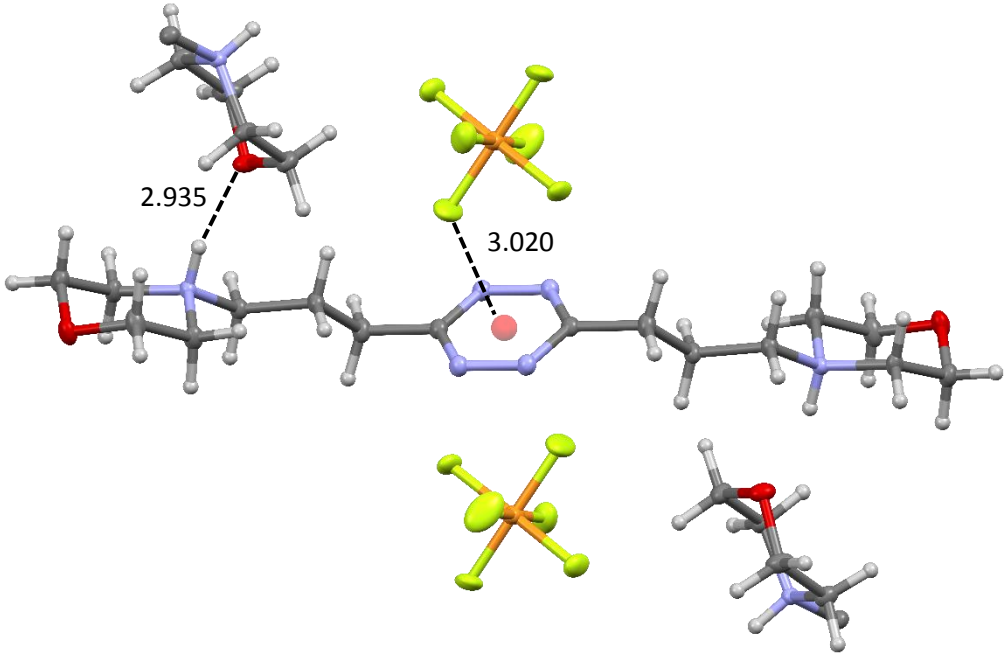

Figure 4.3-9*. Crystal structure of $H_2L3(PF_6)_2$ showing the anion-π interaction and the hydrogen bond network involving only ligand molecules. Distances in Å.*

4.3.1.9 Analysis and Discussion

Three are the central features brought to light by the crystallographic part of this study: the involvement of anion-π interactions, that of salt-bridges and the trends within the family of ligands.

First, anion-π interactions are invariably found as prime elements in all the studied complexes, demonstrating their key role in the anion binding properties of these systems.

Since both centred and off-centred interaction modes can be found in the case of anion-arene interactions, the former indicating a chiefly supramolecular interaction, while the latter is often associated to charge transfer towards the ring or its substituents, a brief analysis indicating the observed tendency of the studied anions to place themselves towards the tetrazine centre or at its periphery is presented below.

According to ***Figure 4.3-10***, three relevant distances, namely the anion-centroid distance $d_{centroid}$, the distance from the ring plane d_{plane} and the in-plane displacement from the centroid (*i.e.* the distance between the centroid of the ring and the projection of the anion on the ring plane) d_{offset}, were collected in ***Table 4.3-1*** for all anion-centroid contacts within 4.0 Å. It should be noted that 0 and 1.4 Å are standard reference values for the offset parameters, the former indicating a perfect alignment between the interacting anion and the ring centre, while the latter meaning that the anion is placed over one of the ring atoms (assuming a benzene model for the generic arene).

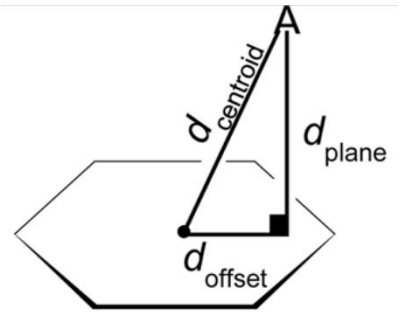

Figure 4.3-10*. Relevant distances used for assessing the anion-π interaction.*

***Table 4.3-1**. Relevant distances for the assessment of the anion-π interaction in the solved structures. Upper limit for anion-centroid distance 4.0 Å.*

	$d_{centroid}$ (Å)	d_{plane} (Å)	d_{offset} (Å)
$H_2L1(PF_6)_2 \cdot 2H_2O$	2.938	2.870	0.628
$H_2L1(CLO_4)_2 \cdot 2H_2O$	2.771	2.727	0.492
	2.968	2.966	0.109
$H_2L2(PF_6)_2 \cdot H_2O$	2.869	2.845	0.370
	3.287	3.066	1.185
	3.326	3.099	1.208
	3.426	3.043	1.574
$H_2L2(CLO_4)_2 \cdot H_2O$	3.002	2.938	0.617
	3.034	3.004	0.426
	3.055	3.008	0.534
	3.187	3.082	0.811
	3.369	2.948	1.631
	3.483	2.959	1.837
	3.997	3.661	1.604
	4.004	3.523	1.903
$H_2L2(NO_3)_2$	2.850	2.839	0.250
$H_2L3(CLO_4)_2 \cdot 2H_2O$	3.118	3.002	0.843
	3.801	3.523	1.427
	3.917	3.300	2.110
$H_2L3(PF_6)_2 \cdot 2H_2O$	3.027	2.995	0.439
	3.446	2.915	1.838
	3.832	3.300	1.948
$H_2L3(PF_6)_2$	3.020	2.957	0.377
	3.547	3.021	1.859
	3.750	3.357	1.671

As shown in ***Figure 4.3-11*** top, the rough data do not show an immediate preference for the centre or the periphery of the ring, indeed showing two peaks both in central and in peripheral regions. However, it should be noted that this kind of analysis was originally devised for halide anions, where the spherical geometry of the anions granted the absence of ambiguities when picking the contacts.

Here, owing to the polyatomic nature of the considered anions, one may argue that hexafluorophosphate, for instance, is able to bring within the chosen threshold distance of 4.0 Å more than one fluoride atoms, even if only one of them gives rise to a strong interaction.

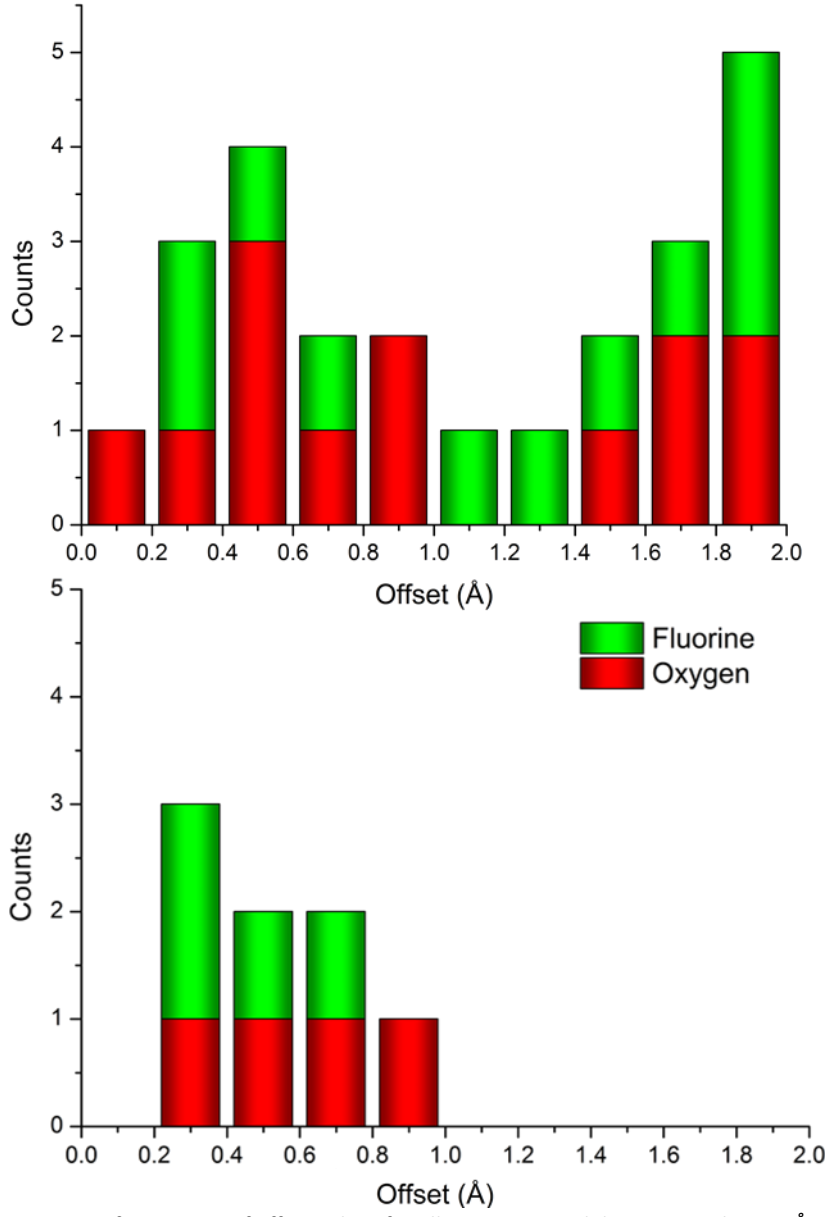

Figure 4.3-11. *Top: frequencies of offset values for all anion-centroid distances within 4.0 Å. Bottom: frequencies of offset values computing only the shortest anion-centroid contact in each structure.*

In view of this, the shortest anion-centroid contacts of each structure where selected and plotted in ***Figure 4.3-11*** bottom. As one can easily see, this plot shows that close anion-centroid distance results in centred interaction, *i.e.* that strong supramolecular interactions arises between the tetrazine and the anions with negligible contributions from charge transfer processes. As this argument may appear as an easy approach to data interpretation, 3D plots with the distributions of all contacts are showed in ***Figure 4.3-12***: the first, d_{offset} vs d_{plane}, is but the projection of the anion distribution on the plane of the aromatic ring, while the latter demonstrates the postulated correlation between $d_{centroid}$ and d_{offset}.

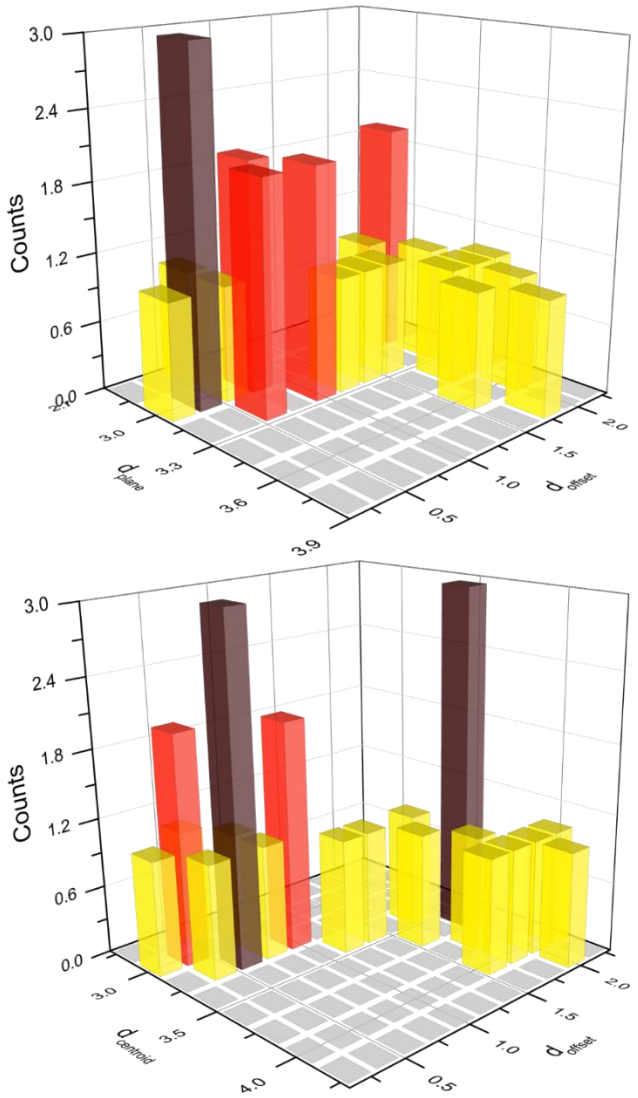

Figure 4.3-12. *Frequencies of anion-ring contacts in the d_{plane} vs d_{offset} and $d_{centroid}$ vs d_{offset} planes, showing their spatial distribution.*

No matter how we look at the data, anions closer to the centroid (*viz.* strongly interacting with the tetrazine) show small offset values, and anions closer to the ring plane (*viz.* also strongly interacting with the tetrazine) show small offset values: therefore, contacts displaying large offset values do not represent the main anion-π interactions, but are found there because of the geometries of the polyatomic anions and, of course, due to the other forces (hydrogen bonding, van der Waals, packing, *et cetera*) which make the anions assume the exact orientation observed in the crystal.

As a final remark, it should also be stressed that, whenever contacts falling within a certain radius from a given point are evaluated and plotted as a function of radius, assuming a spherical distribution, *i.e.* removing the chemistry from the problem, more contacts will invariably be found at the periphery than at the centre. This is ultimately due to the cubic scaling of the volume of a spherical shell of fixed thickness with the radius. This, together with the loss of specificity due to the fading of any interaction at longer distances, foreshadows the fact that, for higher radii, is both more likely to found contacts and that these are anticipated to be less and less dense of chemical sense. Coming to the point, this kind of spherical distribution analyses tends to be biased the more we move from the centre towards finding an excess of contacts: in our case, this probably leads to the quasi exponential growth of contacts observed above offset values higher than 1.4 Å in ***Figure 4.3-11*** top. Overall, this scales down the peaks observed in all diagrams for high offset values, reinforcing the notion that strongly interacting atoms are found in centred positions in the case of our ligands.[13]

Assessment of the possibility of charge transfer was also explored *in silico* though DFT calculations in the case of the diprotonated L1 and L2: although the lowest-unoccupied molecular orbital (LUMO) of the free ligands is localized on the tetrazine ring (***Figure 4.3-13***), which might accept the electronic charge of the interacting anions, a natural population analysis indicates that the charge transfer contribution is modest in our systems, thus confirming the above arguments.

[13] The puzzled or curious Reader is invited to do the following "experiment": perform a search in the Cambridge Structural Database demanding that, say, an oxyanion be in contact within the centroid of a C_6 aromatic ring at a distance (1.4 + VdW_{C+O} + 0.5) Å, where 1.4 Å is the centroid-C distance and 0.5 Å a suggestion for the tolerance, which my Reader can freely modify. The vast majority of contacts will be located at the far periphery. Now ask that the anions be at least in contact with one of the carbon atoms of the ring within (VdW_{C+O} + 0.5) Å, note that if this does not happen the anion is not interacting with the ring at all. Now please confront the new distribution with the previous one: you will realize how many non-specific contacts were picked for high values of the radius.

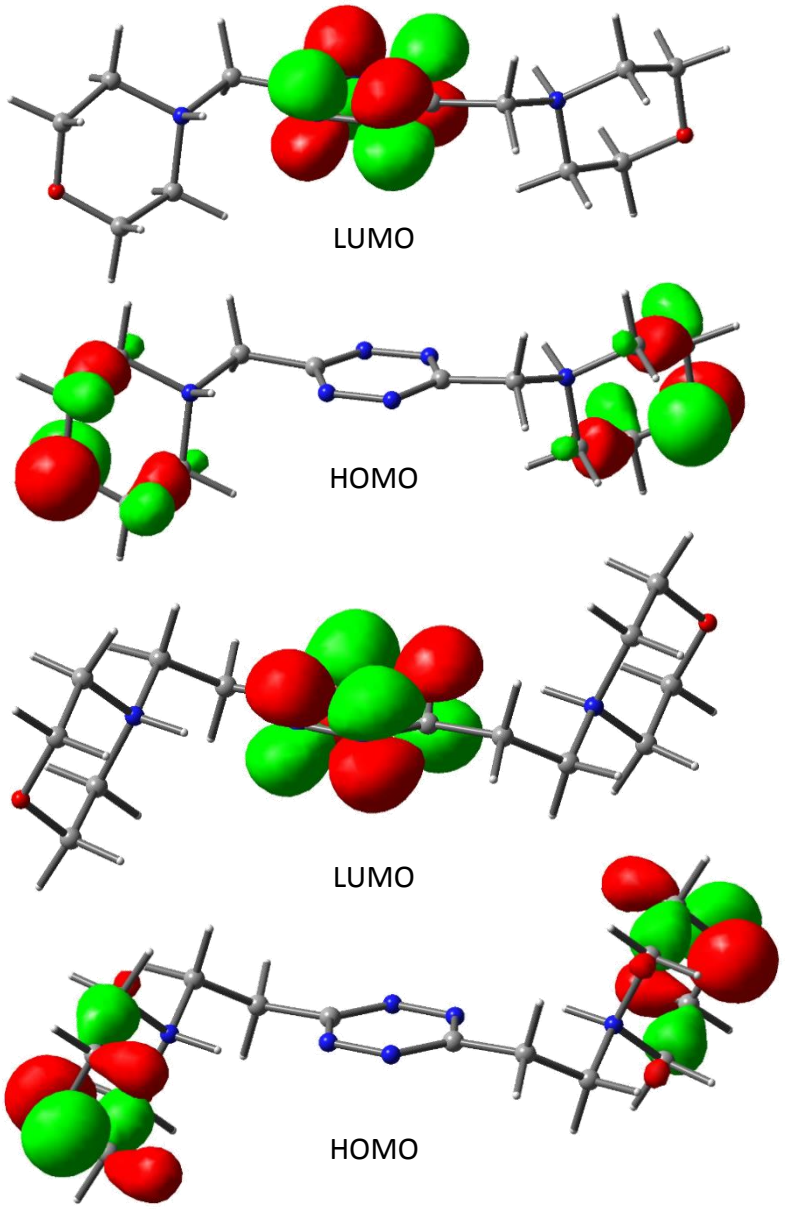

Figure 4.3-13. *HOMO and LUMO Kohn-Sham orbitals of H_2L1^{2+} (top) and H_2L2^{2+} (bottom) calculated at the B3LYP/6-31G(d,p) level. The isovalue is 0.04.*

Concerning salt-bridges and hydrogen bonding in general, although they are universally recognized as fundamental interactions for the anion-binding properties of polyammonium receptors, in our cases they are somewhat underperforming. Whenever anions are forced to choose between establishing strong interactions with the tetrazine ring or giving rise to strong salt bridges, the former choice is always preferred. This is especially important as these receptors were devised for the study of anion-π interaction with the least possible interference from other supramolecular contacts.

The observed interplay of anion-π and salt-bridges lead us to the last focal point, *i.e.* the trends exhibited by the family of receptors.

In fact, both L1 and L3 do never form direct salt bridges with any of the anions.

L1 appears to be too small and resorts to extremely short CH···anion contacts (as short as 2.4 Å) due to its high polarization, owed both to the tetrazine and to the double protonation, and the impossibility to fold forming both salt bridges and anion-π interactions with the same guest.

L3, on the contrary, appears too big to completely wrap around the anion: with the octahedral hexafluorophosphate, with or without the presence of a water molecules, the hydrogen bond network mainly concerns the ammonium groups and the morpholinic oxygen atoms of neighbouring ligand molecules. Partially different is the situation for the tetrahedral perchlorate, when the anion is involved in a solvent mediated salt-bridge, which anyhow indicates the subordinate character of the charge-charge interaction, in this case, with respect to the anion-π contact, else the opposite charges would be found squeezed together.

L2 appears as the best compromise and probably the best anion receptor of the series: chair like conformations in which two anions are held above and under the ring with the contribution of one direct salt-bridge each, are found in all L2 crystal structures, which are moreover the only cases in which a cooperative behaviour of anion-π and direct salt-bridge is manifest. As such, L2 appears as the best candidate to provide anion complexes of the upmost stability.

It is interesting how the above remarks follow quite naturally the observed trends in protonation constants (*cf.* 4.2.2) and the features observed in the crystal structures of the free ligands (*cf.* 4.2.3), allowing to predict weaker binding and scarce contribution of salt-bridges for the analogous crystal structures with L4, at present not available.

Crystallographic parameters for the solved structures conclude the crystallographic part of the study (**Table 4.3-2**).

Table 4.3-2. *Crystal data and structure refinement for the crystal structures of the anionic complexes discussed above.*

	$H_2L1(PF_6)_2{\cdot}2H_2O$	$H_2L1(ClO_4)_2{\cdot}2H_2O$	$H_2L2(PF_6)_2{\cdot}H_2O$	$H_2L2(ClO_4)_2{\cdot}H_2O$
Empirical Formula	$C_{12}H_{26}F_{12}N_6O_4P_2$	$C_{12}H_{26}Cl_2N_6O_{12}$	$C_{14}H_{26}F_{12}N_6O_3P_2$	$C_{14}H_{28}Cl_2N_6O_{11}$
Formula Weight	608.32	517.28	616.35	527.33
Temperature (K)	150	150	120	150
Space Group	*P -1*	*P $2_1/c$*	*P -1*	*P -1*
***a* (Å)**	6.953(1)	12.2843(5)	8.7208(7)	8.3437(7)
***b* (Å)**	9.516(2)	15.5942(7)	10.0766(9)	13.2569(8)
***c* (Å)**	9.768(2)	11.5901(5)	14.263(1)	20.6313(14)
α (°)	89.90(2)	90	96.712(6)	85.306(5)
β (°)	70.24(2)	100.024(4)	107.641(7)	85.170(6)
γ (°)	76.64(2)	90	96.880(7)	77.709(6)
Volume (Å³)	589.7(2)	2186.4(2)	1170.2(2)	2217.0(3)
Z	1	4	2	4
R1 Indices	0.0567	0.0544	0.0506	0.0707
	$H_2L2(NO_3)_2$	**$H_2L3(ClO_4)_2.H_2O$**	**$H_2L_3(PF_6)_2{\cdot}2H_2O$**	**$H_2L3(PF_6)_2$**
Empirical Formula	$C_{14}H_{26}N_8O_8$	$C_{16}H_{34}Cl_2N_6O_{12}$	$C_{16}H_{34}F_{12}N_6O_4P_2$	$C_{16}H_{30}F_{12}N_6O_2P_2$
Formula Weight	434.42	573.38	664.41	628.38
Temperature (K)	150	150	150	150
Space Group	*P $2_1/c$*	*P $2_1/c$*	*P $2_1/c$*	*P $2_1/n$*
***a* (Å)**	6.386(1)	13.7608(5)	13.4690(4)	7.7907(3)
***b* (Å)**	12.583(1)	7.3316(3)	7.8954(2)	8.8430(3)
***c* (Å)**	12.600(2)	13.3194(7)	13.6108(4)	18.2505(8)
α (°)	90	90	90	90
β (°)	98.41(1)	111.655(5)	112.191(4)	96.454(4)
γ (°)	90	90	90	90
Volume (Å³)	1001.5(2)	1248.94	1340.21	1249.37
Z	2	2	2	2
R1 Indices	0.0664	0.0878	0.0627	0.0429

4.3.2 Solution Studies

Protonated forms of L1 and L2 and, in some cases, even the neutral ligands, give rise to detectable interactions with anions in water. Analysis, by means of the computer program HYPERQUAD (*cf.* 2.1.1) of potentiometric (pH-metric) titrations performed for the various ligand/anion systems afforded the stability constants of the anion complexes reported in ***Table 4.3-3***. Since these measurements were performed in the presence of 0.10 M NMe_4Cl, we must assume that all the equilibria in this table are potentially affected by the competitive ligand interaction with Cl^- (*cf.* 4.5.2).

Table 4.3-3*. Equilibrium constants (log K) for ligand protonation and anion complex formation determined at 298.1 ± 0.1 K in 0.1 M NMe_4Cl aqueous solution or water/ethanol 80:20 (v:v) mixture. Values in parenthesis are the standard deviations on the last significant figure.*

	H_2O		H_2O/EtOH
	L1	**L2**	**L2**
$L + H^+ = HL^+$	4.45(3)	6.19(1)	6.04(2)
$HL^+ + H^+ = H_2L^{2+}$	3.45 (3)	5.37(1)	5.19(2)
$HL^+ + F^- = [HLF]$	n.d.	1.58(8)	1.16(7)
$H_2L^{2+} + F^- = [H_2LF]^+$	n.d.	1.97(3)	1.26(5)
$HL^+ + NO_3^- = [HL(NO_3)]$	1.43(5)	1.8(1)	1.72(7)
$H_2L^{2+} + NO_3^- = [H_2L(NO_3)]^+$	1.66(6)	2.32(4)	2.18(3)
$L + SO_4^{2-} = [L(SO_4)]^{2-}$		2.18(3)	
$HL^+ + SO_4^{2-} = [HL(SO_4)]^-$	1.65(8)	2.31(3)	1.68(7)
$H_2L^{2+} + SO_4^{2-} = [H_2L(SO_4)]$	2.08(3)	2.48(3)	2.29(3)
$L + ClO_4^- = [L(ClO_4)]^-$		1.98(5)	
$HL^+ + ClO_4^- = [HL(ClO_4)]$	2.07(9)	2.26(5)	1.55(8)
$H_2L^{2+} + ClO_4^- = [H_2L(ClO_4)]^+$	2.31(8)	2.51(4)	1.83(5)
$L + PF_6^- = [L(PF_6)]^-$	1.96(8)	3.07(8)	
$HL^+ + PF_6^- = [HL(PF_6)]$	2.67(7)	3.17(7)	1.67(9)
$H_2L^{2+} + PF_6^- = [H_2L(PF_6)]^+$	2.98(7)	3.39(8)	2.22(8)

Although the crystal structures of the anion complexes previously described (*cf.* 4.3.1) show the diprotonated ligand forms (H_2L^{2+}) interacting with pairs of anions, the 1:1 stoichiometry of the complexes in solution was unambiguously ascertained by the computer analysis of the titration curves. The stability of these complexes invariably increases with ligand protonation (increasing positive charge), even though the relevant association processes are poorly controlled by electrostatic forces. As a matter of fact, the mean increment of the complexation free energy change associated with the variation of a single positive charge of the ligand, 1.8 kJ/mol (0.4 kcal/mol), is considerably smaller than the literature value 5 ± 1 kJ/mol expected for the formation of a single salt bridge in water [17]. Accordingly, other forces than salt bridges, are expected to provide the decisive contribution, making favourable such association events. This correlates well with the previously described crystal structures of anion complexes, showing that, in the solid phase, the ligands can bind anions without resorting to salt bridges, while the contribution of the anion-π interaction is always prominent: such preference of the anions for the tetrazine as a binding site, despite the presence of two ammonium groups, is both the most surprising and the most recurring feature among the solved crystal structures.

It is interesting to note that L2 forms complexes of greater stability than L1, contrary to what should be expected in terms of charge density and loss of conformational degrees of freedom upon anion binding. This, however, at least for the protonated complexes, is in line with what observed in terms of serial properties of the L1-L4 receptors in the crystal structures of their anionic complexes (*cf.* 4.3.1.9). Concerning the neutral ligands, the comparison between the stability of their complexes is unfortunately only possible for PF_6^-, since complexes of the neutral receptor L1 were not detected with other anions. Most likely they are formed in very small amounts, not detectable with our potentiometric method. The fluoride-L1 system needs a special mention here, as it could not be studied due to the low basicity of the ligand, which forms protonated species in a pH region which already triggers the reactivity of F^- towards the glass components of the measurement cell.

Greater insight into the thermodynamic aspects governing the formation of these complexes was gained by dissecting the complexation free energy changes into their enthalpic and entropic contributions by means of isothermal titration calorimetry (*cf.* 2.1.2). The determined enthalpy changes are reported in ***Table 1.3-1*** along with the derived entropy terms. Regrettably, only few calorimetric data were obtained for the anion complexes with L1 owing to insufficient solubility of the ligand and its complexes.

Table 4.3-4. *Thermodynamic parameters (kJ/mol) for ligand protonation and anion complex formation determined at 298.1 ±0.1 K in 0.1 M NMe_4Cl aqueous solution. Values in parenthesis are the standard deviations on the last significant figure.*

	$\Delta G°$	$\Delta H°$	$T\Delta S°$
$L1 + H^+ = HL1^+$	-25.4(2)	-4.6(4)	20.8(4)
$HL1^+ + H^+ = H_2L1^{2+}$	-19.7(2)	4.6(4)	24.3(4)
$L2 + H^+ = HL2^+$	-35.32(6)	-26.8(4)	8.5(4)
$HL2^+ + H^+ = H_2L2^{2+}$	-30.64(6)	-18.4(4)	12.2(4)
$H_2L1^{2+} + ClO_4^- = [H_2L1(ClO_4)]^+$	-13.2(5)	-0.8(4)	12.4(6)
$L1 + PF_6^- = [L1(PF_6)]^-$	-11.1(5)	n. d.	n. d.
$HL1^+ + PF_6^- = [HL1(PF_6)]$	-15.2(4)	-5.9(4)	9.3(6)
$H_2L1^{2+} + PF_6^- = [H_2L1(PF_6)]^+$	-17.0(4)	0.8(4)	17.8(6)
$HL2^+ + NO_3^- = [HL2(NO_3)]$	-10.3(6)	9.1(3)	19.4(7)
$H_2L2^{2+} + NO_3^- = [H_2L2(NO_3)]^+$	-13.2(2)	6.4(3)	19.6(4)
$L2 + SO_4^{2-} = [L2(SO_4)]^{2-}$	-12.4(2)	-0.6(3)	11.8(4)
$HL2^+ + SO_4^{2-} = [HL2(SO_4)]^-$	-13.2(2)	27.2(4)	40.4(4)
$H_2L2^{2+} + SO_4^{2-} = [H_2L2(SO_4)]$	-14.12(2)	17.0(4)	31.1(4)
$L2 + ClO_4^- = [L2(ClO_4)]^-$	-11.3(3)	-2.3(2)	9.0(4)
$HL2^+ + ClO_4^- = [HL2(ClO_4)]$	-12.9(3)	9.6(4)	22.5(5)
$H_2L2^{2+} + ClO_4^- = [H_2L2(ClO_4)]^+$	-14.3(2)	6.7(4)	21.0(4)
$L2 + PF_6^- = [L2(PF_6)]^-$	-17.5(5)	-0.5(3)	17.0(6)
$HL2^+ + PF_6^- = [HL2(PF_6)]$	-18.1(4)	12.5(3)	30.6(5)
$H_2L2^{2+} + PF_6^- = [H_2L2(PF_6)]^+$	-19.3(5)	5.5(3)	24.8(6)

Data in ***Table 4.3-4***, however, clearly show that these anion binding equilibria are invariably promoted by large and favourable entropic contributions, while the relevant enthalpy changes are mostly unfavourable (endothermic). However, in the cases of anion binding by the neutral (not protonated) L2 ligand, in which anion-π interactions should make the major contribution, the complexation reactions are not hampered by thermal effects, since the measured enthalpy changes are favourable, although very small ($\Delta H°$ in the range -0.5 to -2.3 kJ/mol). A similar enthalpy and entropy dependence of binding equilibria is typical of association processes controlled by desolvation phenomena. Indeed, charge neutralization occurring upon interaction of charged specie causes an important release of solvent molecules, that is an endothermic process accompanied by a large entropy increase. When the anion binds an uncharged ligand, a smaller desolvation is expected to occur with respect to the association with a charged one and, accordingly, the reaction is expected to be less endothermic and less exoentropic, as actually found for our systems (***Table 4.3-4***).

To get more information on solvent effects, the formation of anion complexes with the more soluble[14] L2 ligand was also studied in the water/ethanol 80:20 v:v mixture, displaying a lower dielectric constant (ε = 69.05 at 25°C) with respect to pure water (ε = 78.56 at 25°C). The stability constants of the complexes formed in the solvent mixture are listed in ***Table 4.3-3***. These data show that the addition of ethanol to water causes a general lowering of stability for complexes with protonated ligand forms, while complexes of the unprotonated, uncharged ligand were not detected. At first glance, these results might be surprising, since one could reasonably expect that the association between charged species becomes stronger as the polarity of the solvent decreases. Nevertheless, when the association takes place between charged and neutral species, the stability of the assembly may increase with increasing solvent polarity. As a matter of fact, protonation constants of L2 are smaller in water/ethanol 80:20 v:v than in pure water, as it generally happens for many other amines. Instructive examples, in this sense, are given by the protonation properties of molecules containing both neutral and negatively charged protonation sites, such as amino acids. In these cases, as the solvent polarity decreases (upon addition of ethanol to water), protonation constants of carboxylate groups increase while protonation constants of amine groups decrease, as a consequence of the selective solvation occurring in the solvent mixture, water

[14] Although not as relevant as other properties discussed with more attention in this thesis, also solubility shows a trend along the L1-L4 series, L1 being the most insoluble receptor of the family. It should also be noted that this is partially due to the trend in protonation constants: L3 and L4, capable of undergoing one or even two protonation equilibria even in pure water (pH = 7.0), appearing much more readily soluble than their shorter counterparts.

and ethanol molecules being preferentially attracted, respectively, by charged groups and by neutral functionalities. Accordingly, the lower stability of our anion complexes in the solvent mixture corroborates our previous conclusion that in pure water the anion complexation processes here studied are essentially controlled by other forces than charge-charge attractions.

Also anions are subjected to selective solvation. F^-, for instance, in water/ethanol 80:20 v:v is selectively hydrated, with no ethanol molecules in its first solvation sphere. Upon increase of the anion size, also the involvement of ethanol molecules in anion solvation increases, and for ClO_4^- the composition of the first solvation sphere approaches the composition of the bulk solvent [49]. Taking into account, however, that in the water/ethanol 80:20 v:v mixture there is one ethanol molecule every thirteen water molecules, even for ClO_4^- the participation of ethanol molecules in the solvation sphere is still modest. Then, anion desolvation occurring upon interaction with L2 is not expected to be at the origin of the difference of complex stability between water and the water/ethanol mixture and, accordingly, different ligand solvation should be responsible for the observed difference in the binding constants. Consistently with this general drop of stability, complexes of anions with the neutral L2 ligand are not formed or their formation is too scarce to be detected.

Unfortunately, our attempts to identify significant changes in the NMR spectra (^1H, ^{13}C, ^{15}N and also ^{19}F and ^{31}P for PF_6^-) of the species involved in the anion-π complexation equilibria were unfruitful both in D_2O and acetonitrile-d_3. However, interesting information about the formation of such anion complexes in water was obtained by PGSE ^{19}F and ^1H NMR diffusion spectroscopy, following the variation of the diffusion coefficients of PF_6^- and H_2L2^{2+} occurring upon complexation. Since the exchange between complexed and uncomplexed species in the anion-π complexation equilibrium is a fast process on the time scale of the (relatively slow) NMR measurements, the diffusion coefficient measured by PGSE NMR for a particular species is the weighted average of the diffusion coefficients of its uncomplexed and complexed forms.

That is, for the equilibrium $\mathrm{H_2L2^{2+} + PF_6^- \leftrightarrow [H_2L2(PF_6)]^+}$, the observed diffusion coefficient for PF_6^-, $\bar{D}_{PF_6}$, can be expressed as $\overline{D}_{\mathrm{PF_6}} = (1-\alpha)\cdot D_{PF_6} + \alpha \cdot D_{L2PF_6}$, where D_{PF_6} and D_{L2PF_6} represent the diffusion coefficients of the uncomplexed and complexed forms of PF_6^-, respectively, and α is the mole fraction of complexed PF_6^-.

As shown in ***Figure 4.3-14a***, addition of increasing amounts of H_2L2^{2+} to a solution of PF_6^- causes a significant decrease of the observed diffusion coefficient of the anion.

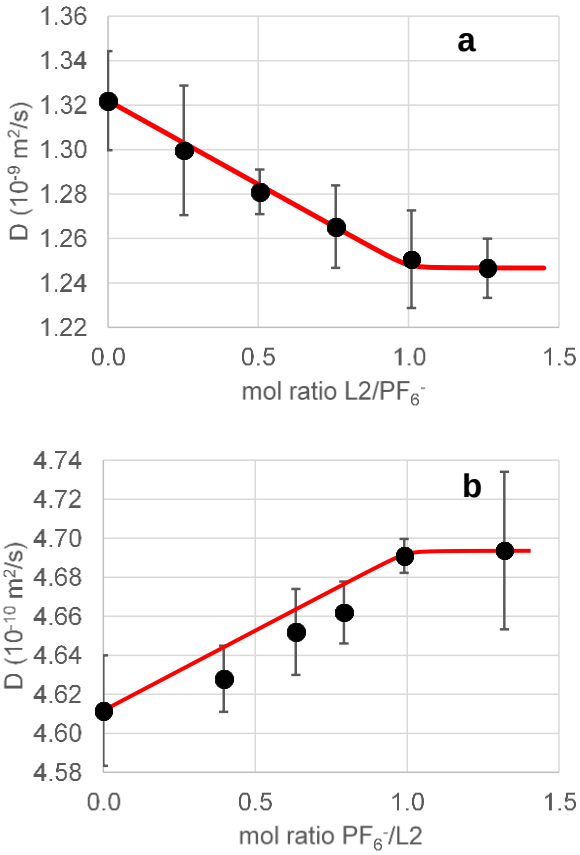

Figure 4.3-14*. Average diffusion coefficients of a) PF_6^- in the presence of increasing concentration of H_2L2^{2+}, measured by means of ^{19}F NMR; b) H_2L2^{2+} in the presence of increasing concentration of PF_6^-, measured by means of ^1H NMR. Red lines represent the trends expected on the basis of the stability constant (log K = 3.39,* ***Table 4.3-3****) measured for the $[H_2L2(PF_6)]^+$ complex.*

According to the Stokes-Einstein equation $\overline{D} = \frac{k_B T}{6\pi\eta r}$, such variation of $\overline{D}$ can be ascribed to the increase of the hydrodynamic radius (*r*) of the measured species as PF_6^- is increasingly associated to H_2L2^{2+}. Furthermore, this figure also reveals a good agreement between the evolution of the observed diffusion coefficient $\overline{D}_{PF6}$ upon increasing concentrations of H_2L2^{2+} (black dots) and the evolution expected according to the value of the stability constant (log *K* = 3.39, ***Table 4.3-3***) measured by potentiometry for the $[H_2L2(PF_6)]^+$ complex, represented by the red line. This line was calculated by assuming D_{PF_6} equal to the value of $\overline{D}_{PF_6}$ measured for the sample

containing pure PF_6^- (*i.e.* α = 0), and D_{L2PF_6} equal to the value of $\bar{D}_{PF_6}$ obtained for a $[H_2L2^{2+}]/[PF_6^-]$ ratio greater than 1:1, at which $\bar{D}_{PF_6}$ appears to become invariant (***Figure 4.3-14a***).

The evolution of the average diffusion coefficient of H_2L2^{2+}, $\bar{D}_{L2}$ (***Figure 4.3-14b***), gives rise to a less accurate fitting of the expected trend (red line calculated according to the procedure above described for $\bar{D}_{PF6}$), but it shows a noteworthy feature. When PF_6^- is gradually added to H_2L2^{2+}, the average diffusion coefficient of H_2L2^{2+} increases denoting that the complex has a smaller size than the free ligand, a phenomenon that can be rationalized by considering that an extensive desolvation occurs upon interaction of the two oppositely charged species, the volume of lost water molecules being greater than the gained volume of the bound anion, in agreement with the important entropy increase derived for anion binding from the above thermodynamic data. Alternatively, another rationalization could be related to a conformational change of the ligand upon complexation: the two ligand arms might fold inwards to interact with the anion giving rise to a smaller hydrodynamic radius. Nevertheless, although the occurrence of a similar conformation change is possible, its contribution to the overall phenomenon appears to be modest as it would be accompanied by a loss of entropy in contrast to the highly exoentropic character of the complexation process.

Furthermore, taking into account that both theoretical and experimental works in the literature coincide in affirming that the interaction of PF_6^- with water molecules is extremely weak, the observed phenomenon occurring upon the formation of the $[H_2L(PF_6^-)]^+$ complex should be mostly due to ligand desolvation.

4.3.3 Conclusions

Crystallographic data obtained for eight crystal structures of anion complexes formed by the diprotonated forms of L1, L2 and L3 show that the anions invariably choose the tetrazine ring as preferential binding site, forming short anion-π contacts, despite the presence of two ammonium groups. Nevertheless, weak anion contacts with aliphatic CH groups and, in few cases, mainly encountered in L2 structures, salt bridge interactions with the ammonium groups also contribute to complex stability in the solid state. According to DFT calculations, the lowest-unoccupied molecular orbital (LUMO) of the free ligands is localized on the tetrazine ring, which is able to bind anions *via* anion-π interactions even in the absence of supplementary binding groups.

Equilibrium data for L1 and L2 reveal that anion binding takes place in aqueous solution with the ligands in different protonation states. In some cases, even the neutral (unprotonated) ligands form stable anion complexes. The main

characteristic of these binding events is that the stability of the formed complexes is poorly related to the ligand charge, indicating that formation of these complexes is not governed by the dominating charge-charge attraction that is normally observed in the formation of anion complexes with positively charged ligands. The enthalpic ($\Delta H°$) and entropic ($T\Delta S°$) parameters for the binding equilibria, experimentally determined by dissecting the complexation free energy changes ($\Delta G°$) by means of ITC measurements, clearly show that these anion binding processes are invariably promoted by large and favourable entropic contributions, while the relevant enthalpy changes are mostly unfavourable (endothermic). A similar enthalpy and entropy dependence of binding equilibria is typical of association processes controlled by desolvation phenomena (desolvation is typically endothermic and exoentropic). The occurrence of a significant desolvation occurring upon the formation of these complexes is corroborated by diffusion NMR spectroscopy data, that led to the unprecedented observation that the ligand undergoes a significant shrink in size (increase of diffusion coefficient) upon interaction with PF_6^-.

A somewhat different behaviour is observed for anion binding by the neutral ligands, in which anion-π interactions should make the major contribution. In this case, the complexation reactions ($-\Delta G°$ in the range 11.1 to 17.5 kJ/mol) are still favoured by dominant entropic contributions ($T\Delta S°$ in the range 9.0 to 17.0 kJ/mol) but are accompanied by favourable, although very small, enthalpy changes ($\Delta H°$ in the range -0.5 to -2.3 kJ/mol). Interestingly, these thermodynamic parameters are strongly consistent with previous values ($-\Delta G°$, 9 to 12 kJ/mol; $\Delta H°$, -2 to 3 kJ/mol; $T\Delta S°$, 8 to 15 kJ/mol) [32] experimentally determined in water for the formation of various anion complexes with receptors based on nitroso-amino-pyrimidine, which are thought to be almost exclusively stabilized by anion-π interactions.

Equilibrium data for the formation of anion complexes in a 80:20 (v:v) water:ethanol mixture, showed that a decrease of the dielectric constant of the medium (ε = 78.56 for pure water and ε = 69.05 for the mixture at 25°C) causes a general lowering of stability for complex with protonated ligand forms, while complexes of the unprotonated ligand are no longer detectable. Taking into account that the presence of 20% of ethanol affect very little the solvation sphere of the anions, the loss of stability observed in the aqueous-ethanolic solution, relative to pure water, can be reasonably ascribed to a stronger ligand solvation in the mixed solvent. Once again, solvation effects seem to play a fundamental role.

4.4 Anion Binding Properties Towards Organic Anions

As extensively discussed above (*cf.* 1.3 and 1.4), the binding of anions in solution generally revolves around a combination of weak forces, properly selected incorporating the required structural features within the receptor during its design stage: although individually weak, such interactions can collectively furnish enough stabilization to afford polyfunctional ligands capable of strong and selective anion binding.

This part of the study, although maintaining its focus on anion-π interactions and solvent effects, builds on the primary investigation addressing inorganic anions by adding to the mix more possibilities concerning the strength and type of forces in play. To some extent, it can be considered an exercise in understanding the interplay of selected molecular forces. The task is ambitious, as plain additivity of forces is never granted, with both cooperative and competition effects coming into play to produce a non-linear response of the system.

A new list of interesting substrates was brewed up with the explicit intention of playing with the following parameters:

1. Basicity of the anions;
2. Capability of establishing π-π stacking interactions;
3. Stereochemistry of the interacting groups;
4. Dependence on host-guest mutual sizes.

Basicity of the anions is an important parameter to tune the strength of salt bridges and hydrogen bonds in general. As discussed in 1.3.3.2.2, when formation of a hydrogen bond is perceived as a partial proton transfer from an acid to a base, the highest stability of the donor-acceptor complex is achieved when the proton is equally shared (*i.e.* when $\Delta pK_a = 0$). In our original work with inorganic anions, all the studied substrates were indeed conjugate bases of strong acids, as such, in water there was scarce discrimination between them on this basis. The obvious exception was fluoride, yet this anion, set aside its marked basicity, is also the smallest and the most charge dense of the monovalent species, thus would probably be an outlier in any data set for a series of reason.

In the new set of anions, the simplest homologous compounds from the carboxylate and sulfonate series were investigated: acetate and methanesulfonate.

Accordingly, the effect of π-π stacking interaction was considered by comparing their methyl and phenyl derivatives: benzoate and benzenesulfonate. Establishment of π-π stacking interactions was initially thought as a way to strengthen the effect of the solvent, giving rise to a truly hydrophobic effect, with the aromatic moieties brought together by their energetically favourable desolvation.

Lastly, the effect of the insertion of a second charge was considered with the dicarboxylate anions phthalate and isophthalate, examining the observed differences in view of their regiochemistry.

Effect of the mutual size of host and guest was implicitly considered by prosecuting the study with both L1 and L2, the best receptors, in terms of complex stability, in our tetrazine-based family of molecules.

Needless to say, a complicated picture emerged, demanding further analyses and demonstrating, once again, how shedding light on the subtleties of the interplay of so many different effects, even within the framework of simplified model systems, still remains an ambitious task.

4.4.1 Crystal Structures

4.4.1.1 Crystal Structure of $H_2L2(C_6H_5SO_3)_2 \cdot H_2O$

As showed in ***Figure 4.4-1***, two symmetrically non-related benzenesulfonate anions are present in this structure. Both form a salt bridge with the protonated nitrogen atom of the ligand, however only the first one exhibits a marked interaction with the tetrazine ring, bringing one of the sulfonate oxygen atoms at 3.422 Å from the ring centroid, the interaction being particularly strong with one of the tetrazine nitrogen atoms (O···N 3.049 Å, O-N-centroid angle 93.56°) (***Figure 4.4-2***).

The other two oxygen atoms of the sulfonate group are found either giving rise to salt bridge interaction (NH···O 2.657 Å), as said above, or involved in multiple (namely 7) CH···O contacts.

The second anion, required to guarantee the electroneutrality of the system, but probably too bulky to be accommodated in proximity of the tetrazine ring, is found mainly interacting through hydrogen bonds with the co-crystallized water molecule (O···O_W 2.869 Å) and the protonated nitrogen atom of the morpholine moiety (NH···O 2.690 Å), although several CH···anion contacts are recognizable.

As evidenced in ***Figure 4.4-3***, π-π stacking interaction offers a modest contribution to the overall stability of the structure, three carbon atoms of the benzene ring being in the 3.4-3.6 Å range from the tetrazine. The relative positions of the two rings, probably imposed by their sizes, by the non-planarity of the sulfonate group, by the geometry imposed by the hydrogen bond network and maybe by the preference of the tetrazine for the anionic head rather than the aromatic portion of the anion, impose a 13.27° angle between the ring planes, limiting their superimposition.

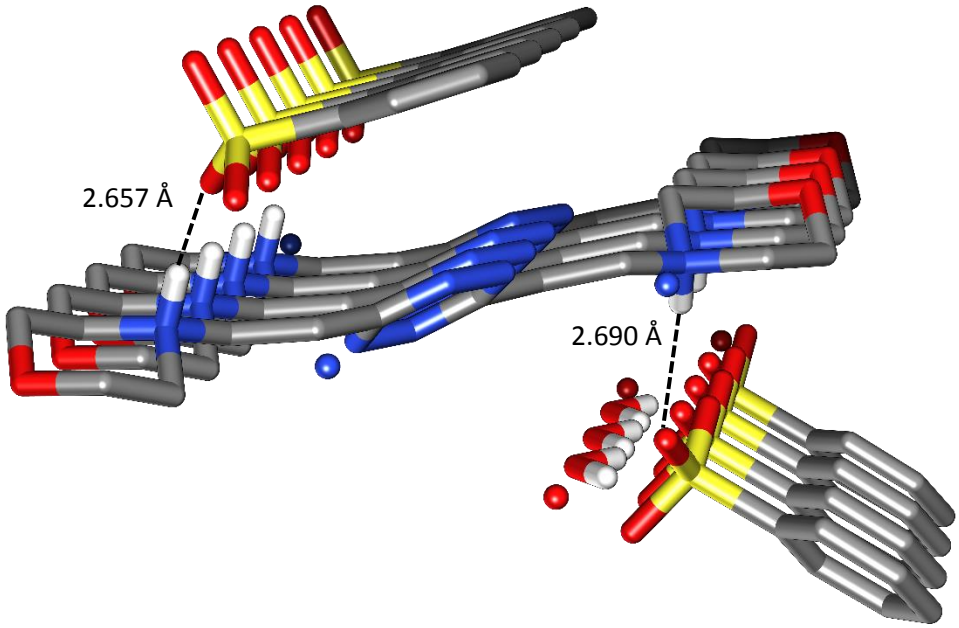

Figure 4.4-1. *Cell content of $H_2L2(C_6H_5SO_3)_2{\cdot}H_2O$ with overview of the hydrogen bond network.*

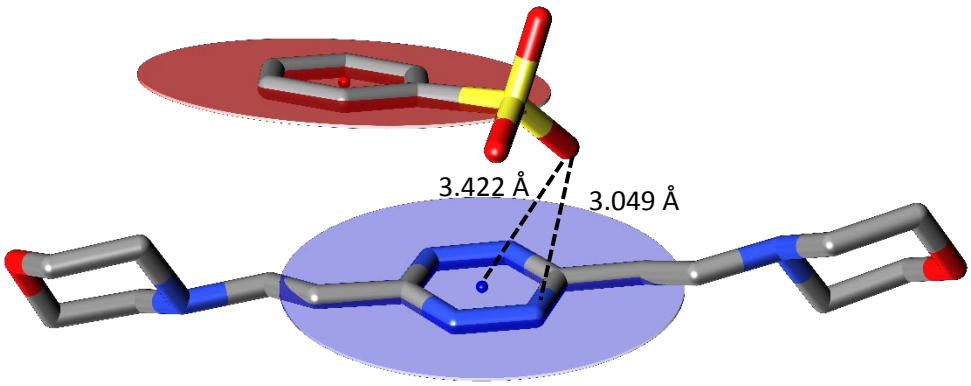

Figure 4.4-2. *Detail of the anion-π interaction in the structure of $H_2L2(C_6H_5SO_3)_2{\cdot}H_2O$.*

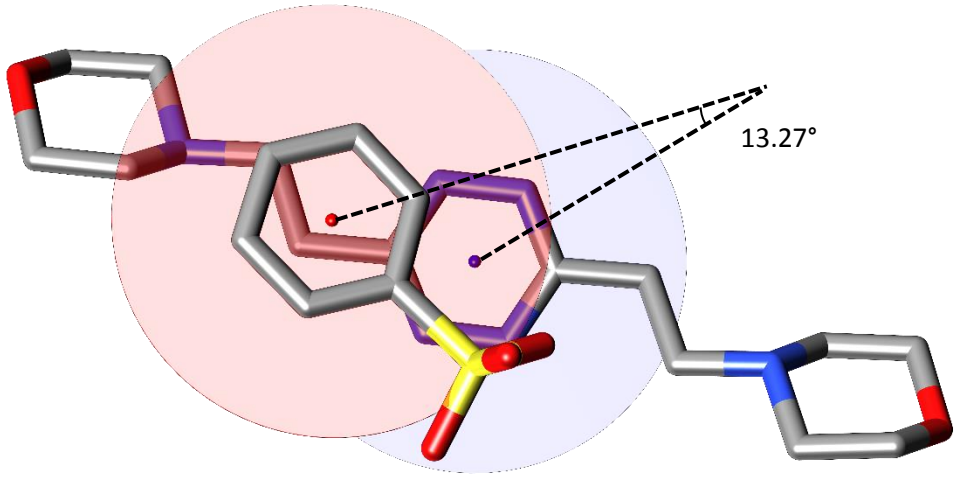

Figure 4.4-3. *Detail of the π-π stacking contribution to the host-guest interaction.*

The argument is much more valid for the second benzenesulfonate anion, with an angle in-between the ring planes of 53.47°, which, in fact, does not give rise to contacts with the tetrazine ring.

4.4.1.2 Crystal Structure of $H_2L2(HIsophthalate)_2$

Considerably different is the situation encountered with the isophthalate anion, which was found in the crystal in its monoprotonated form.

As showed in ***Figure 4.4-4***, the crystal structure consists of zig-zag ribbons of anions and ligand molecules held together by salt bridges and hydrogen bonds. Despite the undisputed importance of these interactions for the overall arrangement of the structure, the tetrazine ring remains an important binding site, with the anion well-placed above its centroid (***Figure 4.4-5***). This time, however, the interaction is markedly of the π-π stacking type (***Figure 4.4-6***), the two ring planes being almost coplanar and 6 out of 6 carbon atoms of the benzene ring placed at 3.4 Å from at least one atom of the tetrazine. Contrary to what observed for benzenesulfonate, only one symmetry independent anion is found in the crystal structure, which is once again centrosymmetric with the inversion centre overlapping with the centroid of the tetrazine ring.

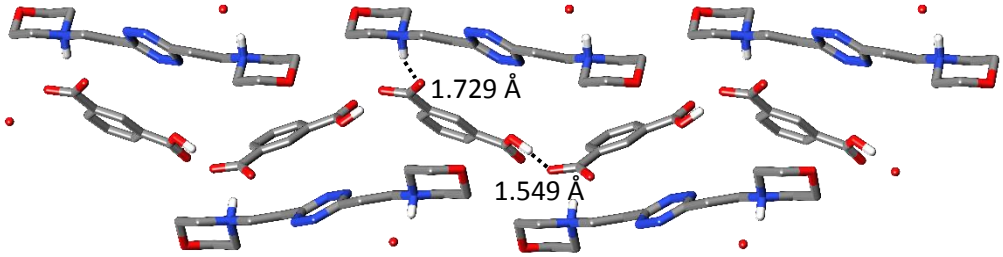

Figure 4.4-4. *Crystal structure of $H_2L2(HIsophthalate)_2$, evidencing the ribbon arrangement of the molecules governed by hydrogen bonding and salt bridge formation.*

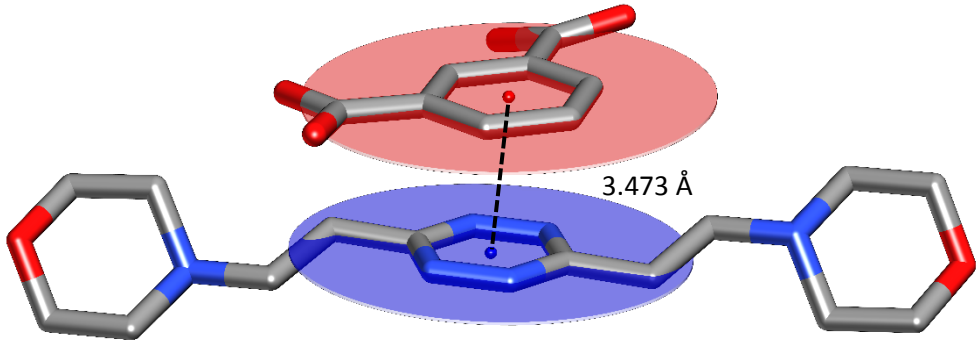

Figure 4.4-5*. Detail of the ring-ring contact in the structure of $H_2L2(HIsophthalate)_2$.*

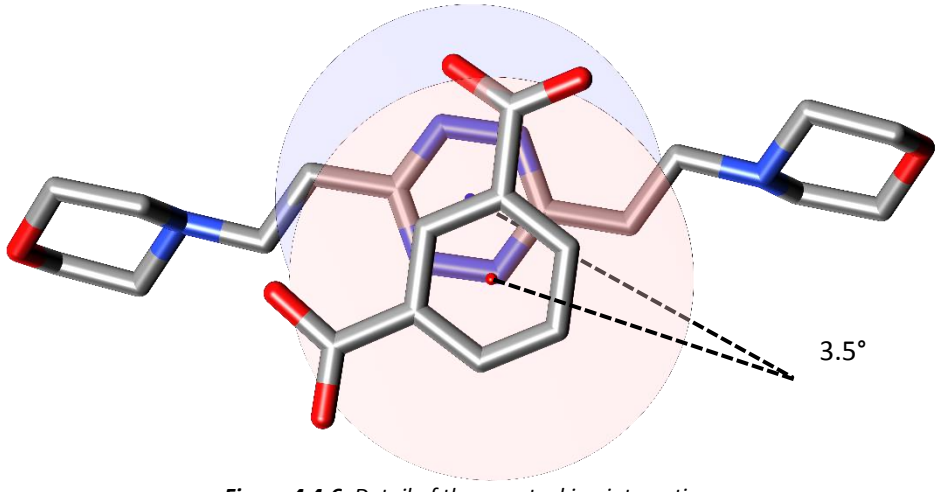

Figure 4.4-6. *Detail of the π-π stacking interaction.*

Crystallographic information for both benzenesulfonate and isophthalate complex structures are reported below in ***Table 4.4-1***.

Concerning crystallization conditions, pink crystals of $H_2L2(C_6H_5SO_3)_2 \cdot H_2O$ were obtained upon evaporation at room temperature of an aqueous solution of L2 (0.01M) at pH 4.0 containing an excess of benzenesulfonate. Crystals of $H_2L2(HIsophthalate)_2$, were obtained by dropwise addition of an ethanolic solution of the dicarboxylic acid to a solution of the ligand in the same solvent without further pH adjustment. Slow evaporation at room temperature led to pink crystals of the complex.

Table 4.4-1. *Crystal data and structure refinement for the crystal structures of the organic anion complexes discussed above.*

	$H_2L2(C_6H_5SO_3)_2 \cdot H_2O$	$H_2L2(HIsophthalate)_2$
Empirical Formula	$C_{26}H_{38}N_6O_9S_2$	$C_{30}H_{36}N_6O_{10}$
Formula Weight	642.74	640.64
Temperature (K)	150	150
Space Group	P n a 2_1	P 2_1/n
a (Å)	15.1627(5)	6.8698(1)
b (Å)	6.4915(4)	14.4541(3)
c (Å)	29.4057(9)	14.7842(3)
α (°)	90.00	90.00
β (°)	90.00	95.204(2)
γ (°)	90.00	90.00
Volume (Å^3)	2894.36	1461.97
Z	1	2
R1 Indices	0.0622	0.0513

4.4.2 Solution Studies

As in the case of their inorganic counterparts, the investigated series of organic anions does give rise to detectable interactions with our receptors in water. Stability constants of the anion complexes, obtained through potentiometric titrations performed in 0.10 M NMe_4Cl at 298.1 ± 0.1 K, are reported in ***Table 4.4-2*** for L1 and in ***Table 4.4-3*** for L2.

Table 4.4-2*. Equilibrium constants (log K) for L1 anion complex formation determined at 298.1 ±0.1 K in 0.1 M NMe_4Cl aqueous solution. Ligand and anion protonation constants included as references.*

Equilibrium	***log K***
$H^+ + L1 = HL^+$	4.45(3)
$H^+ + HL1^+ = H_2L1^{2+}$	3.45(3)
$HL1^+ + CH_3SO_3^- = [HL1(CH_3SO_3)]$	2.21(9)
$H_2L1^{2+} + CH_3SO_3^- = [H_2L1(CH_3SO_3)]^+$	1.6(2)
$HL1^+ + C_6H_5SO_3^- = [HL1(C_6H_5SO_3)]$	2.49(5)
$H_2L1^{2+} + C_6H_5SO_3^- = [H_2L1(C_6H_5SO_3)]^+$	2.48(5)
$H^+ + CH_3COO^- = CH_3COOH$	4.51(1)
$L1 + CH_3COO^- = [L1(CH_3COO)]^-$	2.71(8)
$L1 + CH_3COOH = [L1(CH_3COOH)]$	3.27(5)
$HL1^+ + CH_3COOH = [HL1(CH_3COOH)]^+$	3.09(3)
$H^+ + C_6H_5COO^- = C_6H_5COOH$	4.15(3)
$L1 + C_6H_5COO^- = [L1(C_6H_5COO)]^-$	3.02(1)
$HL1^+ + C_6H_5COO^- = [HL1(C_6H_5COO)]$	3.16(3)
$H_2L1^{2+} + C_6H_5COO^- = [H_2L1(C_6H_5COO)]^+$	2.95(4)
$H^+ + Pht^{2-} = HPht^-$	5.10(3)
$H^+ + HPht^- = H_2Pht$	2.78(3)
$L1 + Pht^{2-} = [L1(Pht)]^{2-}$	2.88(2)
$L1 + HPht^- = [L1(HPht)]^-$	2.87(3)
$HL1^+ + HPht^- = [HL1(HPht)]$	2.56(3)
$H_2L1^{2+} + HPht^- = [H_2L1(HPht)]^+$	2.60(3)
$H^+ + IPht^{2-} = HIPht^-$	4.32(1)
$H^+ + HIPht^- = H_2IPht$	3.28(1)
$HL1^+ + IPht^{2-} = [HL1(IPht)]^-$	3.40(5)
$HL1^+ + HIPht^- = [HL1(HIPht)]$	2.73(8)
$H_2L1^{2+} + HIPht^- = [H_2L1(HIPht)]^+$	3.45(5)

Table 4.4-3. *Equilibrium constants (log K) for L2 anion complex formation determined at 298.1 ±0.1 K in 0.1 M NMe_4Cl aqueous solution. Ligand and anion protonation constants included as references.*

Equilibrium	***log K***
$H^+ + L2 = HL^+$	6.19(1)
$H^+ + HL2^+ = H_2L^{2+}$	5.37(1)
$HL2^+ + CH_3SO_3^- = [HL2(CH_3SO_3)]$	1.41(8)
$H_2L2^{2+} + CH_3SO_3^- = [H_2L2(CH_3SO_3)]^+$	1.8(3)
$HL2^+ + C_6H_5SO_3^- = [HL2(C_6H_5SO_3)]$	1.44(6)
$H_2L2^{2+} + C_6H_5SO_3^- = [H_2L2(C_6H_5SO_3)]^+$	1.84(2)
$H^+ + CH_3COO^- = CH_3COOH$	4.51(1)
$HL2^+ + CH_3COO^- = [HL2(CH_3COO)]$	2.33(9)
$H_2L2^{2+} + CH_3COO^- = [H_2L2(CH_3COO)]^+$	2.0(1)
$H_2L2^{2+} + CH_3COOH = [H_2L2(CH_3COOH)]^{2+}$	2.67(6)
$[H_2L2(CH_3COOH)]^{2+} + CH_3COO^- = [H_2L2(CH_3COOH)(CH_3COO)]^+$	2.74(6)
$H^+ + C_6H_5COO^- = C_6H_5COOH$	4.15(3)
$L2 + C_6H_5COO^- = [L2(C_6H_5COO)]^-$	1.82(9)
$HL2^+ + C_6H_5COO^- = [HL2(C_6H_5COO)]$	2.18(5)
$H_2L2^{2+} + C_6H_5COO^- = [H_2L2(C_6H_5COO)]^+$	2.62(3)
$[H_2L2(C_6H_5COO)]^+ + C_6H_5COO^- = [H_2L2(C_6H_5COO)_2]$	2.69(7)
$H^+ + Pht^{2-} = HPht^-$	5.10(3)
$H^+ + HPht^- = H_2Pht$	2.78(3)
$HL2^+ + Pht^{2-} = [HL2(Pht)]^-$	2.27(2)
$H_2L2^{2+} + Pht^{2-} = [H_2L2(Pht)]$	2.6(3)
$H_2L2^{2+} + HPht^- = [H_2L2(HPht)]^+$	2.0(7)
$H_2L2^{2+} + H_2Pht = [H_2L2(H_2Pht)]^{2+}$	1.9(1)
$[H_2L2(Pht)] + Pht^{2-} = [H_2L2(Pht)_2]^{2-}$	2.16(9)
$[H_2L2(Pht)] + HPht^- = [H_2L2(HPht)(Pht)]^-$	1.64(3)
$[H_2L2(HPht)]^+ + H_2Pht = [H_2L2(H_2Pht)(HPht)]^+$	2.97(7)
$[H_2L2(H_2Pht)]^{2+} + H_2Pht = [H_2L2(H_2Pht)_2]^{2+}$	2.42(3)
$H^+ + IPht^{2-} = HIPht^-$	4.32(1)
$H^+ + HIPht^- = H_2IPht$	3.28(1)
$L2 + IPht^{2-} = [L2(IPht)]^{2-}$	1.75(6)
$HL2^+ + IPht^{2-} = [HL2(IPht)]^-$	1.79(6)
$H_2L2^{2+} + IPht^{2-} = [H_2L2(IPht)]$	2.37(1)

Despite being conspicuous, the amount of gathered data fails to produce a clear-cut picture, reinforcing the notion that unravelling the interplay of different supramolecular forces in a structured solvent like water is not easily accomplished.

It should also be mentioned here, despite the accuracy and the appreciable detection limits of the technique, that potentiometry alone may not provide, in some cases, a clear speciation of the system. The generic complex species $H_xL_yA_z$ is univocally described by a {x; y; z} triad of numbers (*cf.* 2.1.1.2), however location of the protons on the anion or on the ligand is not necessarily taken for granted, especially when deliberately exploring host-guest pairs with $\Delta pK_a \approx 0$ (*e.g.* pK_{a1}(L1) = 4.45 vs $pK_a(CH_3COOH)$ = 4.51). Accordingly, data reported in ***Table 4.4-2*** and ***Table 4.4-3***, have been presented following both a logic order in terms of the relative basicity of the involved partners and the guidance offered by computer simulations. Anyhow, the coexistence of two species in solution possessing the same $H_xL_yA_z$ formula, but differing for the localization of protons (*viz.* a sort of supramolecular tautomerism, if one looks at the host-guest complex as a supermolecule) cannot be ruled out in some cases, potentially resulting in a weighted averaging of the observed binding constant.

Nevertheless, several trends emerge from the data and will be further discussed also in view of the aforementioned *in silico* simulations, namely:

1) Electrostatic forces alone do not correlate well with the observed stability of the complexes;
2) L1 tends to form more stable complexes than L2;
3) The species formed by L1 and L2 with the same guest can differ beyond the differences in basicity, L2 being inclined to form readily 1:2 ligand-anion complexes;
4) The occurrence of anion complexes with neutral ligands is higher for aromatic guests;
5) The occurrence of anion complexes with neutral ligands is higher for carboxylate anions than for sulfonates;
6) Relative positions of anion sites on dicarboxylate anions influences the stability of the complexes.

As in the case of the studied inorganic anions, there is a poor correlation between electrostatic forces alone and the observed binding constants (*cf.* 4.3.2), *i.e.* increasing charge separation between host and guest does not lead to the increase in complex stability expected for purely electrostatic interactions. Since this was already encountered for simpler inorganic species, and somewhat reinforced in

view of the increase in the number of possible interactions the organic anions series may engage in (π-π stacking above all), this observation should not surprise.

In second instance, L1 tends to form more stable complexes than L2. Although in line with preorganization (or at least with a lesser decrease in conformational degrees of freedom upon complex formation) and charge density considerations, the fact that this is found in contrast with what observed for inorganic anions demands attention. Molecular modelling, performed using the empirical forcefield provided with the Hyperchem [50] package, proved relevant to assess the point.

The calculated conformation for the benzoate complexes of both ligands, one of the cases in which L1 and L2 different basicity do not prevent the formation of the same species, reported below in ***Figure 4.4-7*** and ***Figure 4.4-8***, are useful to provide a possible explanation of this trend reversal.

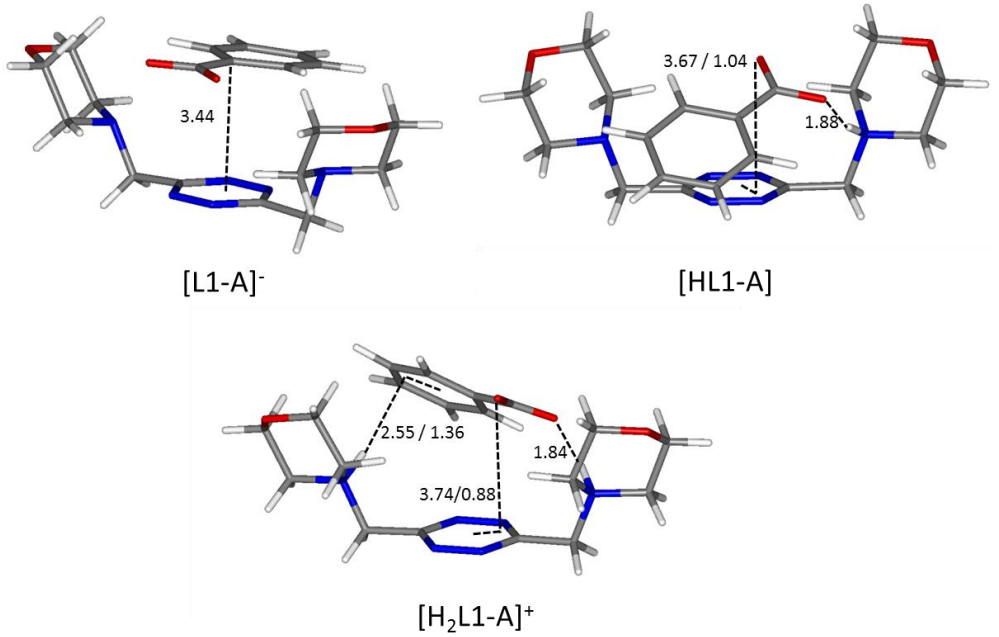

Figure 4.4-7*. Calculated solution conformations of L1 complexes with benzoate (A). Distances in Å.*

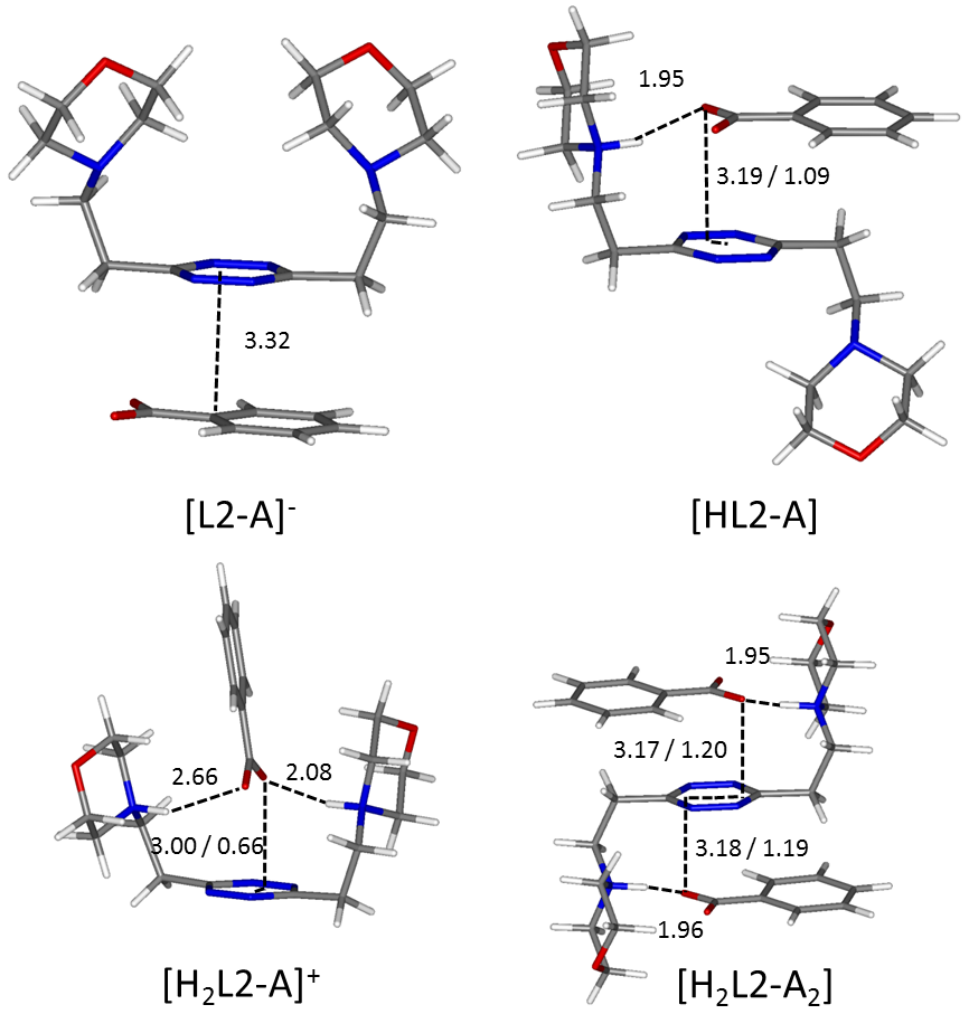

***Figure 4.4-8**. Calculated solution conformations of L2 complexes with benzoate (A). Distances in Å.*

Although it should be stressed that this kind of simulations is not perfect, treating water with polarizable continuum model overall resulting in the loss of the atomic details justifying the entropic contribution due to desolvation, the inspection of the minimum energy configurations are nevertheless revealing, at least for what concerns the enthalpic part of the interaction.

In fact, L1 is always found U-shaped, with all the binding sites converging towards the anion, while for L2 this is not always the case. Also, the shorter methylenic spacer allows for a throughout contribution of the anion arenic portion to the interaction, which is found scarce in all the minimum energy conformations of L2.

This is also found to be true for another series of homologous complexes, that of benzenesulfonate.

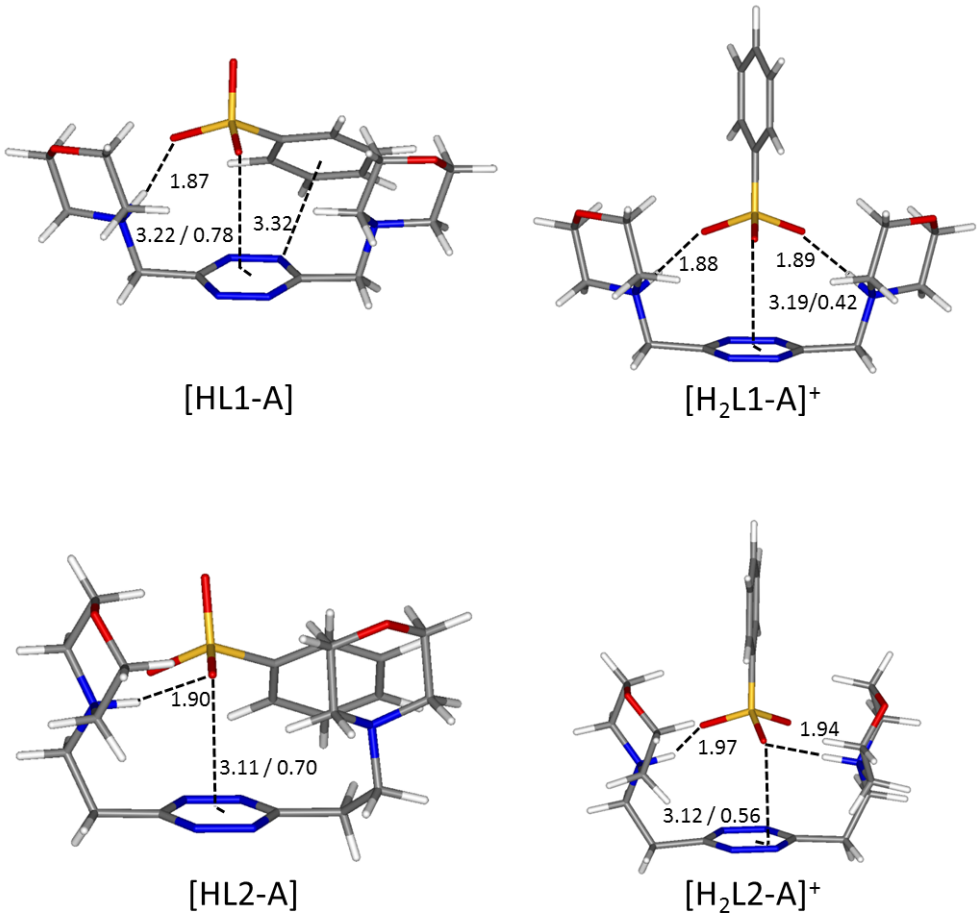

***Figure 4.4-9**. Calculated solution conformations of L1 and L2 complexes with benzenesulfonate (A). Distances in Å.*

As one can see in ***Figure 4.4-9***, the more curled-up structure of L1 invariably results in an increase of involvement of the benzenic ring in the overall host-guest interaction. A point worth mentioning here, is that deprotonated complexes of benzenesulfonate are found to be marginally more stable than their monoprotonated counterparts (log *K* values 2.48 vs 2.49 for L1, 1.44 vs 1.84 for L2, ***Table 4.4-2*** and ***Table 4.4-3***), in agreement with what observed in the minimum energy conformations, where the second protonation brings not only stronger enthalpic contributions but also entropic losses due to the exposure of the hydrophobic part of the anion to the solvent.

For the reasons discussed above, the higher overall stability observed for L1 complexes indeed appears to be related to its more rigid character and the closer localization of its binding sites, favouring the cooperativity of the individual supramolecular forces.

One could wonder why the trend is reversed compared to the inorganic anion series: the answer here gets speculative, yet a main reason comes to mind: the geometry of the anions. Octahedral or tetrahedral anions offer the more flexible L2 the possibility to wrap around them more easily than the flat aromatic anions of the new series (*cf.* the case of benzoate ***Figure 4.4-8***), offering several electron-rich binding sites amenable of accepting salt bridges or interacting with the tetrazine ring. On the contrary, L1, which with inorganic anions was obliged to resort to CH···anion contacts (*cf.* 4.3.1), now manages to maintain host and guest aromatic portions in contact while giving rise to salt bridges with the anionic groups protruding from the benzene ring. This, reinforced by the magnified importance of solvation effects, the hydrophobicity of the anions being greatly increased in comparison to the inorganic ones, seems to lead to the observed difference in relative stability of the complexes among the two series of studied anions.

The third point, *i.e.* the greater tendency of L2 to form 1:2 ligand:anion complexes, was already partially addressed. As one can observe for example in ***Figure 4.4-8***, monoprotonated complexes are found in the signature chair conformation, leaving out the other face of the tetrazine ring and the additional morpholine group for the interaction with a second anion, resembling the centrosymmetric arrangement observed in the crystal structures of inorganic anion complexes (*cf*. 4.3.1). Such conformation is not amenable for L1, which, in fact, sticks to the 1:1 stoichiometry.

Interestingly, only carboxylate anions (acetate, benzoate, phthalate, isophthalate) do give rise to 1:2 complexes with L2. This correlates well with the discussion on the influence of the anion geometry: carboxylate groups lay coplanar to their benzenic ring, allowing the charged groups to form salt bridges while the aromatic moieties can freely engage in parallel displaced π-π stacking interactions, which ultimately lead to the chair conformation observed for the ligand in L2 complexes (*cf.* ***Figure 4.4-8***). This is not the case for sulfonate anions, the umbrella shape of the charged group forces the system to choose: if a linear strong salt-bridge is formed, imperfect matching in the π-π stacking interaction is not avoidable; else, if the stacking interaction is preferred, the contribution of charge-charge interaction is greatly sacrificed. As a matter of fact, when the ligand is diprotonated it probably wraps around the anion as portrayed in ***Figure 4.4-9***, two salt bridges taking the upper hand over π-π stacking, leaving no possibility of other stoichiometries but 1:1 even for the flexible L2.

A borderline, and thus interesting, case is offered by acetate, which surely maintains the geometrical features of the other carboxylate anions, yet lacks entirely of the aromatic portions, partially invalidating some of the above arguments.

In fact, without the stabilizing contribution of π-π stacking, the $[H_2L2(acetate)]^+$ is predicted to be in a folded conformation by our simulations, closely resembling the situation encountered for sulfonate anions. Differently from them, however, acetate is a base, although of modest strength, thus it can undergo protonation: in the calculated conformation of $[H_2L2(Hacetate)]^{2+}$ the ligand opens up once more in the familiar chair conformation, again resulting in the possibility of 1:2 stoichiometry, which is indeed empirically encountered (***Figure 4.4-10***).

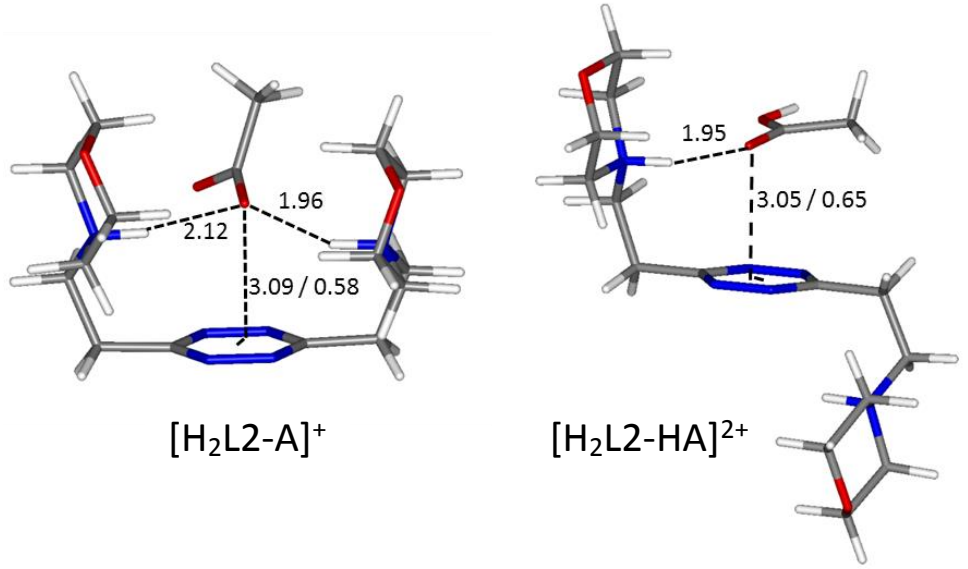

Figure 4.4-10*. Calculated solution conformations of selected L2-acetate (A) complexes. Distances in Å.*

As a side note, the $[H_2L2(Hacetate)]^{2+}$ is a true species experimentally detected in solution, ambiguity in proton location being non-existent here, since host and guest cumulatively possess 3 protonable sites and exactly 3 protons are found in the complex.

Overall, L2 tendency to form 1:2 ligand:anion complexes is due to its increased flexibility compared to L1, but it is subject to the geometry of the anions and their basicity, which ultimately lead to discriminate the tetrahedral and essentially non-basic sulfonates from their carboxylate counterparts.

The more we delve into the discussion, the more giving up pieces of information ahead of time is unavoidable: as a matter of fact, the observation at points 4 and 5 have already been partially addressed.

The fact that complexes of the neutral, non-protonated, ligands are more common for aromatic guests, to the point that they are exclusively found with them (with the exception of the L1-acetate complex) (point 4), and for carboxylate anions over sulfonates, again exclusively (point 5), appears to be tied to three familiar concepts: π-π stacking interaction, solvent effect and geometry.

Spontaneous association of non-polar solutes in water is commonplace, and it is well-known to be driven by the hydrophobic effect, here reinforced by anion-π and stacking interaction. The studied aliphatic anions are both missing any contribution from stacking interaction and far less hydrophobic than their aromatic counterparts, resulting in non-detectable, at least by means of our potentiometric method, association equilibria. This reinforces the notion that direct interaction of the π clouds is a factor in play for our complexes.

Concerning the preference for carboxylates over sulfonates, it is once more a matter of geometry: flat carboxylates just sit on the tetrazine and stick to it (*cf.* ***Figure 4.4-7*** and ***Figure 4.4-8***) causing extensive desolvation of both host and guest surfaces; things are a little more complicated with the three-dimensional sulfonates, which have to choose between anion-π or stacking interactions, and, even if the second is preferred, manage to accommodate their bulkier polar head without getting too close to the electronegative morpholine atoms.

Coming to the sixth and last point of our analysis, regiochemistry of the two examined dicarboxylate anions, phthalate and isophthalate,[15] matters towards their binding properties, phthalate being preferred by L2 and isophthalate by L1. Invoking a single explanation here is much more difficult due to the increased number of parameters to take into account: sure, there is a size and geometry complementarity due to the ortho and meta position of the anionic heads, but also solvation, which due to the PCM eludes our simulations, may play an important role, especially considering the differences that may exist between solvated proximal and distal sites. Computational work is still ongoing in this area.

[15] Although marginal and easy to guess, the para- member of this isomers' family was not blatantly set aside. The fact is that terephtalate is somewhat temperamental, unwilling to get along with practically any solvent: as such, its study was not feasible due to its extreme insolubility.

4.4.3 Conclusions

The anticipated notion that this study was bound to result in a complicate picture was not disattended.

Beyond chemistry, I think this is much revealing about (basic) research in general: at times, we set forth to go fishing in the pool in the garden (our simplified model systems) and we come back home with a basket of exotic seafood.

Sure, importance and true contribution to the stability of complexes of the newly added π-π stacking interaction has invariably been demonstrated. However, additivity of supramolecular forces here is not granted, it happens in many cases, but, on occasion, the geometry restraints of the system force it to choose between π-π stacking and anion-π interactions. As such, a clear trend in the determined binding constants is hard to recognize, the only possible rationalization being a case-by-case inspection of each complex species at the microscopic level.

Observed differences in salt-bridge strength due to the matching of pK_as of the interacting partners is barely detectable, yet a major distinction is found between sulfonates and carboxylate anions, both in terms of stoichiometry of the complexes and relevance of π-π stacking interaction. As discussed above, the main reason for it appears to lie in the geometry of the negatively charged groups.

Lastly, effects of the increased flexibility of the L2 ligand are here limited to the possibility of 1:2 ligand:anion stoichiometries, but they do not imply a higher thermodynamic stability of L2 complexes over those of L1 as observed for the inorganic anions series. This also appears mainly as a consequence of the relative size and mutual arrangement of binding sites between host and guest.

4.5 L2 Binding Properties Towards The Series Of Halide Anions

In the following, the case study of L2 interacting with the whole series of halide anions, featuring solution, solid state and computational data, will be presented.

Personally, I consider this as the most interesting piece of work herein presented for two reasons: first, our research could not get more basic than this, to the point that we are back to periodic properties. Being able to explore the structural and thermodynamic features of the very same anion-π interaction as the periodic properties of halide anions vary dramatically from the small hard and basic fluoride up to the bulky soft and polarizable iodide, with everything that goes with it, is a fantastic opportunity. In second instance, this work once again raises the awareness on solvation problems, on the effect that solvent has on each and every association equilibria: the gigantic binding constants of cations holding back the recognition of these effects for a long time.

Since this is very important to me, and apparently at times I cannot avoid showing passion for my work, I will make sure that my Reader understands the state of the art on the subject.

The observation of different behaviours of charged species in solution is normally addressed in one of two ways.

The first, and sadly still more common, is resorting to the Hofmeister series. I do not mean to challenge its importance, it surely is a milestone in understanding ion solvation and has had beneficial influences on the development of the research field; yet it has three shortcomings: first, it is 129 years old, and some fancier descriptions start to be available; second, it is a qualitative ranking involving, in its original form, no more than 20 ions, as such its universality should be taken *cum grano salis*; lastly, it has a strong tie with protein behaviour, and really there is no need for proteins in a modern take on ion solvation, *i.e.* ions behave in solvents the way they do, involvement of proteins in the study is superfluous. By this, I just want to say that in 1888 Franz Hofmeister did not provide us with a universal definitive answer, the series does not even get close to explain everything, else this research field would be long gone. As such, Hofmeister series should not be invoked blindly and lightly, but only in pertaining cases.

The second approach, or better the modern one, more incline to produce new experimental or simulation data in search of models for solvation of increasing validity, is, in my humble opinion, disgraced by a revealing name: the broad family of these studies going under the name of ion specific effects.

The name reveals that the foundation and novelty of the discipline lies in the acknowledgement that ions do behave differently from one another. But why did we ever think they would not? Is the periodic table not an orchestra or a chorus, each element being a performer with his own unique timbre?

Yet we had been warned. The best science book ever[16] says it plainly:

"You must not trust the almost-the same (…), the practically the same, the nearly, the or, any surrogates or stopgaps. The differences may be small but can lead to radically diverse results, like railroad switches".[17]

Now that the state of the art on the matter has been sketched out, my Reader can fully appreciate the need of raising the awareness towards ion solvation and its implications in complex formation equilibria.

4.5.1 Crystal Structures

Crystal structures for L2 interacting with halide anions were obtained from aqueous (I^-) or alcoholic media (water-methanol, for F^-, pure methanol for Cl^- and Br^-). Interestingly, all of them are found to interact with the L2 ligand through two main contacts: the anion-π interaction, always found to be strong and centred, and one salt bridge involving the protonated nitrogen atom of the morpholinic pendants, as usual.

4.5.1.1 Crystal Structure of $(H_2L2)F_2{\cdot}3H_2O{\cdot}MeOH$

In this first crystal structure, displayed in ***Figure 4.5-1***, the ligand is found in a flat conformation, with the fluoride anion placed right above the centroid of the tetrazine forming anion-π interaction (F···centroid distance 3.003 Å). As the anion is probably too small to force the folding of the ligand and forming both salt bridge and anion-π interaction with the same receptor molecule, the salt bridge, although extremely strong (HN···F 2.604 Å), as expected for fluoride, is found within the anion and an adjacent ligand molecule.

[16] According to the Royal Institution of Great Britain.
[17] From *Potassium*, in *The Periodic Table* by Primo Levi (1975).

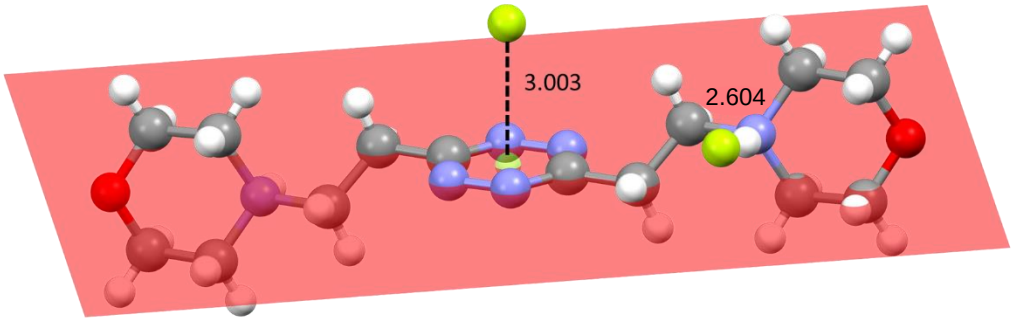

***Figure 4.5-1**. Crystal structure of $(H_2L2)F_2 \cdot 3H_2O \cdot MeOH$. Distances in Å.*

4.5.1.2 Crystal Structure of $(H_2L2)Cl_2$

Chloride, apparently due to its size increase, enables the bending of the L2 ligand in its chair conformation, already encountered or several inorganic anions (cf. 4.3.1), and the simultaneous establishment of both anion-π and salt bridge interactions with the same ligand molecule (***Figure 4.5-2***).

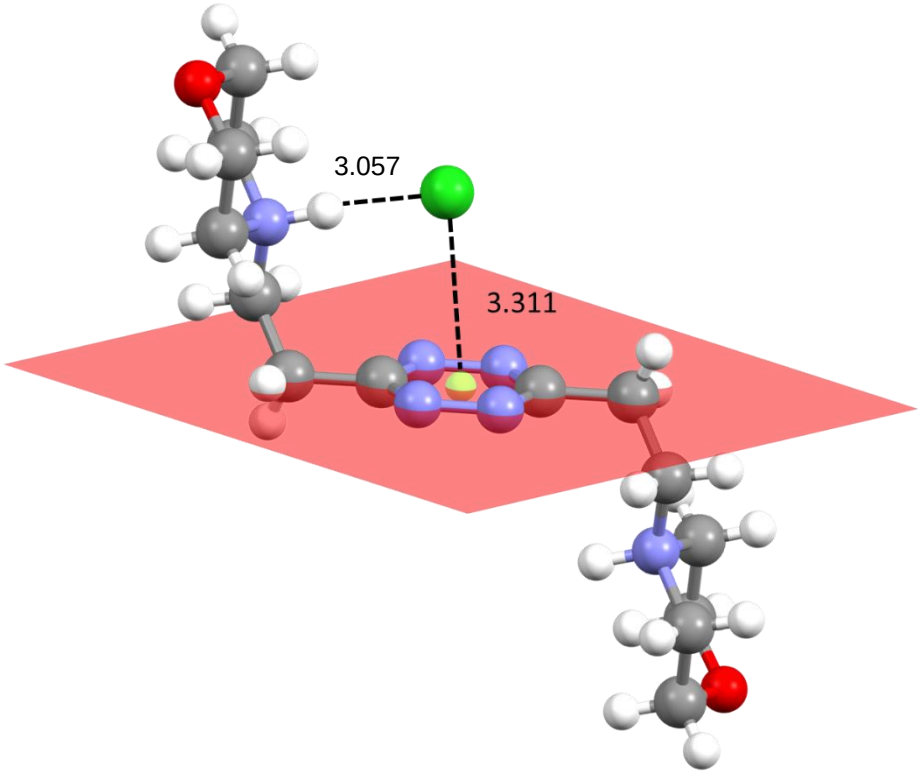

***Figure 4.5-2**. Crystal structure of $(H_2L2)Cl_2$. Distances in Å.*

4.5.1.3 Crystal Structure of $(H_2L2)Br_2$

Bromide gives rise to an almost isomorphic structure to that of chloride, with subtle barely appreciable differences, which will be further analysed in the analysis section (*cf.* 4.5.1.5). The crystal structure is reported in ***Figure 4.5-3***.

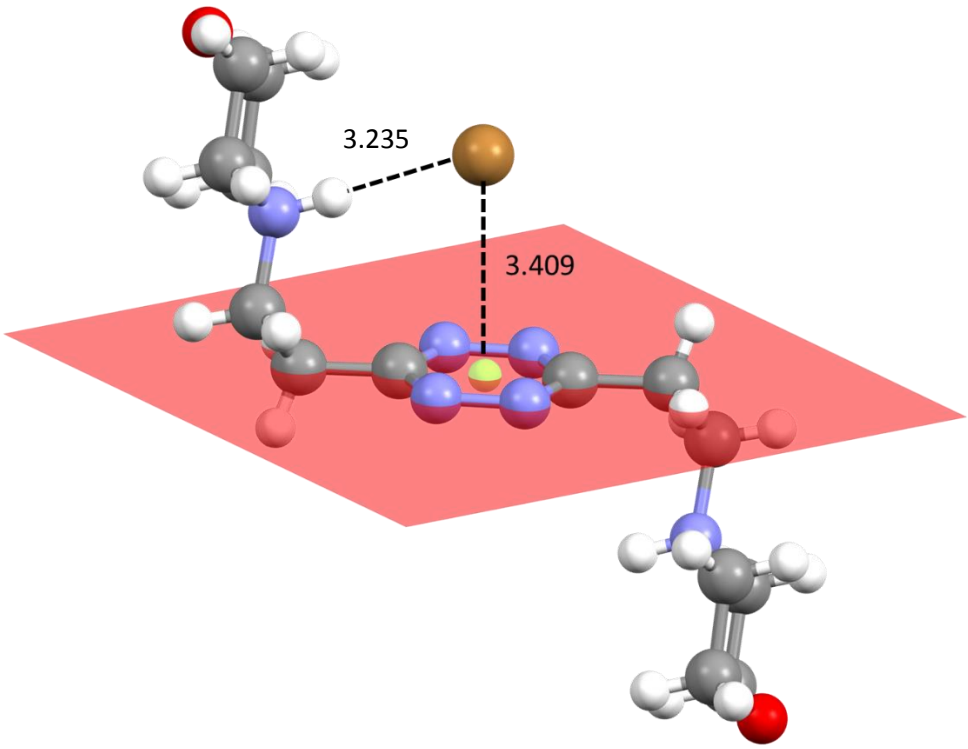

Figure 4.5-3*. Crystal structure of $(H_2L2)Br_2$. Distances in Å.*

4.5.1.4 Crystal Structure of $(H_2L2)I_2{\cdot}H_2O$

The crystal structure of the iodide complex is the most diverse, including two non-symmetry related ligand molecules interacting with the same number of non-identical anions. Differences between the two distinct complexes found in the crystal are almost non-existent (HN···I distances 3.451 and 3.465 Å, I···centroid and offset values 3.70/0.32 and 3.67/0.27 Å respectively), with the absence of further crystallographic symmetries being due to the stronger interaction of the co-crystallized water molecule with one of the two complexes. In depth discussion on the matter is postponed to the polyiodide section (*cf.* 4.6.1.1), as these crystals are the progenitors of the series and the argument much more relevant in that context.

Here we will take as reference the stronger interacting iodide anion (the other one being so similar that one could easily use the same image and change the displayed distances of few hundredth of Å) and discuss the host-guest arrangement.

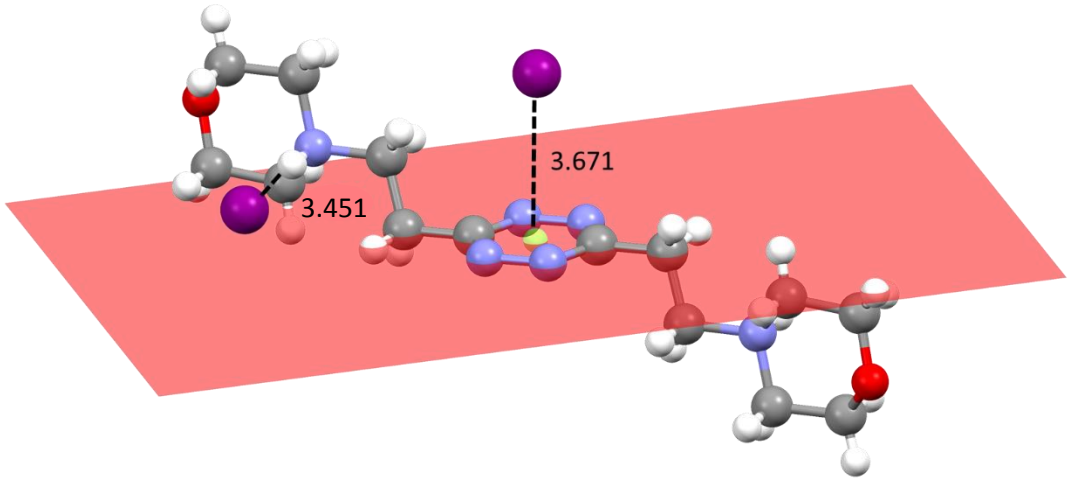

***Figure 4.5-4**. Crystal structure of $(H_2L2)I_2 \cdot H_2O$. Distances in Å.*

As showed in ***Figure 4.5-4***, the interaction pattern resembles that encountered for fluoride, though arguably for the opposite reason: iodide seems too bulky to form both anion-π and salt bridge interaction with just one ligand molecule, as such it prefers to stick to the tetrazine molecule of one receptor while forming a salt bridge with the protonated nitrogen atom of an adjacent ligand molecule.

4.5.1.5 Analysis and Discussion

Relevant geometric parameters useful for the assessment of the anion-π and salt bridge interactions have been extrapolated and gathered in ***Table 4.5-1***.

***Table 4.5-1**. Relevant distances useful for the assessment of the main host-guest interaction encountered in the crystal structure of L2-halide complexes.*
† Values corrected for relative ionic radii.

Anion	***Anion-Centroid***	***Anion-Centroid†***	***Offset***	***Salt Bridge Length HN···X***
F^-	*3.003*	*1.67*	*0.363*	*2.604*
Cl^-	*3.311*	*1.50*	*0.452*	*3.057*
Br^-	*3.409*	*1.45*	*0.246*	*3.235*
I^-	*3.671*	*1.47*	*0.271*	*3.451*

At first sight, and much unsurprisingly, fluoride is recognized as the anion forming the strongest salt-bridges, the other halide anions following, as expected, in their natural order.

More interesting are data on the anion-π interaction. Although moving down along the group anion-centroid distance just seems to increase, taking in consideration

the actual size of the anions, *i.e.* correcting the data for the relative ionic radii, a different trend may be discerned, indicating that tetrazine-anion contacts could be, in truth, getting more and more intimate moving down along the group.

Chloride and bromide complexes, due to their quasi-isomorphism, offer the chance of an in-depth comparison of the relevant geometric parameters for the interactions, impossible, with the same trustworthiness, for complexes showing different overall conformations. As one can see, moving from chloride to bromide we have a weakening of the salt bridge (this time not ascribable to the difference in ionic radii, as the observed change is almost double if compared to the difference between their sizes) accompanied not only by a shortening of the anion-centroid distance, but also by a shift of the anion towards more centric position on the tetrazine, chloride being, in fact, the anion showing the highest offset value.

This peculiar transition situation for the chloride anion, which seems to form both far weaker salt bridges than fluoride and meeker anion-π interactions than bromide or iodide, will be further discussed also in view of the results of the solution study.

Crystallographic parameters for the four structures of halide complexes are provided below in ***Table 4.5-2***.

Table 4.5-2. *Crystal data and structure refinement for the crystal structures of the halide anion complexes discussed above*

	$(H_2L2)F_2·3H_2O·MeOH$	***$(H_2L2)Cl_2$***	***$(H_2L2)Br_2$***	***$(H_2L2)I_2·H_2O$***
Empirical Formula	$C_{15}H_{36}N_6O_6F_2$	$C_{14}H_{26}N_6O_2Cl_2$	$C_{14}H_{26}N_6O_2Br_2$	$C_{14}H_{26}I_2N_6O_3$
Formula Weight	*434.48*	*381.30*	*470.20*	*580.21*
Temperature (K)	*150*	*150*	*150*	*150*
Space Group	*C 2/c*	*P 2_1/n*	*P 2_1/c*	*P -1*
a (Å)	*12.1360(5)*	*5.8409(2)*	*6.0275(6)*	*7.7303(6)*
b (Å)	*8.6567(4)*	*13.9837(7)*	*13.5630(9)*	*7.7864(6)*
c (Å)	*19.1395(7)*	*11.5093(5)*	*11.9342(9)*	*22.022(2)*
α (°)	*90.00*	*90.00*	*90.00*	*86.949(7)*
β (°)	*92.145(4)*	*103.017(4)*	*104.374(8)*	*87.158(7)*
γ (°)	*90.00*	*90.00*	*90.00*	*60.575(8)*
Volume (Å^3)	*2009.34*	*915.893*	*945.091*	*1152.5(2)*
Z	*2*	*2*	*2*	*2*
R1 Indices	*0.0786*	*0.0484*	*0.0377*	*0.0517*

4.5.2 Solution Studies

Once more, we were able to determine a few thermodynamic parameters for halide complexation with L2 through our potentiometric technique. The gathered data, again obtained in 0.10 M NMe_4Cl aqueous solution at 298.1 K, are reported below in ***Table 4.5-3***.

Table 4.5-3. *Equilibrium constants (log K) and associated ΔG° for ligand protonation and L2-halide anions complex formation determined in 0.1 NMe_4Cl aqueous solution at 298.1 ± 0.1 K.*

Equilibrium	*log K*	*-ΔG° kJ/mol*
$L2 + H^+ = HL^+$	6.19(1)	35.3(1)
$HL2^+ + H^+ = H_2L2^{2+}$	5.37(1)	30.6(1)
$HL2^+ + F^- = (HL2)F$	1.58(8)	9.0(5)
$H_2L2^{2+} + F^- = [(H_2L2)F]^+$	1.97(3)	11.2(2)
$H_2L2^{2+} + Br^- = [(H_2L2)Br]^+$	1.3(1)	7.6(6)
$HL2^+ + I^- = (HL2)I$	2.03(7)	11.6(4)
$H_2L2^{2+} + I^- = [(H_2L2)I]^+$	2.35(4)	13.4(2)

Before proceeding, let us deal with the point which may seem an unbearable major fallacy for the goodness of the data: why would we ever work in a chloride ionic medium when striving to determine halide anions binding constants? Is it not obvious that we could not determine binding constants for chloride itself in these conditions?

When we started this discussion on anion-binding in solution (*cf.* 4.3.2), possible bias of the data due chloride competition for the ligand was foreshadowed to avoid omitting anything. Yet three main reasons support our choice for NMe_4Cl as our ionic medium and put its eventual influence into perspective.

First, maintaining unaltered the same experimental conditions appears as a requirement for the comparability of different data sets, ultimately contributing to the oneness of the work as a whole.

In second instance, although non-interacting anions, the so-called innocent anions, are indeed recommendable as ionic media, presumption of innocence does not apply in chemistry: if existence of an expected interaction is not proven, we still have to take its possibility into consideration until the real presence of an interplay is confirmed or otherwise confuted. It is worth mentioning here, that several anions commonly used as non-interacting ionic media (*e.g*. perchlorate and nitrate) have been reported to interact with L2 in water (*cf.* 4.3) (and to do so in the presence of a hundredfold excess of chloride, considering 0.10 M NMe_4Cl was used in the measurements); as such, they would have made into far worse choices than

chloride, although, right off the bat, this was not manifest at all. The point of the discussion however, is not presenting chloride as the only anion for which there are no proven interactions in water, although this is perfectly in line with the data, but questioning the existence of truly non-interacting anions and consequently the possibility of completely ruling out the hypothetical bias induced by the ionic medium, whatever its nature.

Lastly, it is important to reassure the Reader that the observed lack of interaction between chloride and L2 is not artificial. In principle, HYPERQUAD (*cf.* 2.1.1.2) treatment of protonation curves of the ligand alone in 0.10 M NMe_4Cl, may result in values for the two protonation constants which somehow encompass the presence of scarce amount of L2 chloride complexes in solution, not detectable *per se,* but potentially causing little adjustments of the protonation constants values during the refinement process to account for their presence. This possibility has been taken into account and addressed experimentally by varying NMe_4Cl concentration by ±10% (*i.e.* repeating the measurements in 0.11 and 0.09 M NMe_4Cl aqueous solution). This was done to explore the effect of altering chloride concentration (together with its L2 complexes eventually formed) without changing significantly the ionic strength (which has its own proven impact on the determined equilibrium constants): if chloride complexes formation do really exist in solution and alter the observed protonation constants of L2, discrepancies between the protonation constant determined in different conditions should manifest. This was found not to be the case, demonstrating, if not the non-interaction of chloride with L2, its extremely weak character, which places it far below the detection limit of our potentiometric technique.

Overall, this means that the lack of data on chloride should be regarded as the proof of this anion being the most weakly bound anion in the series, if bound at all, the other halides being all appreciably interacting with L2 despite a hundredfold excess of chloride present in the measurement cell.

Two are the general trends observed from the available binding constants: first, we have again scarce correlation between stability and charge. When binding constants with the mono- and di-protonated L2 ligand are available, the rise in stability is only about 2 kJ/mol, about 40% of what is expected for the formation of a single salt bridge in water. This is a common feature invariably observed with our tetrazine-based ligands, indicating forces other than electrostatic as the most important for these system, *i.e.* the anion-π interaction, which dominates L2 complexes with halide anions in the solid state (*cf.* 4.5.1), and the effect of the solvent, which should be reckoned with in solution studies.

The second trend is that of the overall complex stability encountered moving along the halide series: the tendency is highlighted below in ***Figure 4.5-5***.

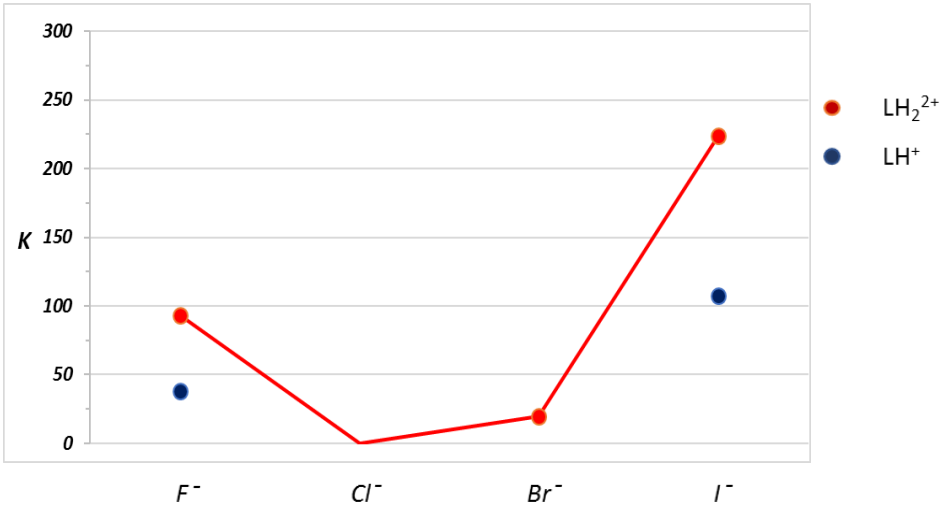

Figure 4.5-5. *Stability trends observed for mono- and di-protonated complexes of the ligand L2 with halide anions. K value for the formation of $[H_2L2(Cl)]^+$ complex arbitrarily set to 0, as it is expected to be around this value.*

Assuming minima of stability for the undetectable chloride complexes, a non-obvious curve is obtained featuring maxima of complex stability for anions at the extreme of the series, a decreasing for bromide, and the reaching of the aforementioned minima for chloride.

A possible rationalization of data involves invoking two opposite tendencies: on one side, the basicity and charge density which strengthen the interactions with the ligand, decreasing in the fluoride to iodide direction, and solvation free energy and solvent effect on the other, the larger and more poorly solvated the anion the stronger its tendency to desolvate and stick to the ligand, this contribution to association decreasing in the iodide to fluoride direction.

Another, equivalent, point of view is that of discriminating an entropic and enthalpic driving force: replacement of anion-water interaction with the more stabilizing salt bridges being the reason for the strong association of fluoride; on the contrary, iodide simply replaces the weak anion water interactions with anion ligand ones with no necessity of huge stability gains, as the entropy gained in the release of a large number of water molecules back into the bulk solvent is more than enough to promote the overall process.

Justifying what happens in between the series, properly addressing the effect of the solvent, the role of the host and guest size, as well as charge density and polarizability, will require further in-depth study.

DFT (ωB97X-D) optimized geometries for diprotonated complexes in PCM water with the 6-31+G(d, p) and LANL2DZ basis sets (the latter for iodide) are showed below in ***Figure 4.5-6***.

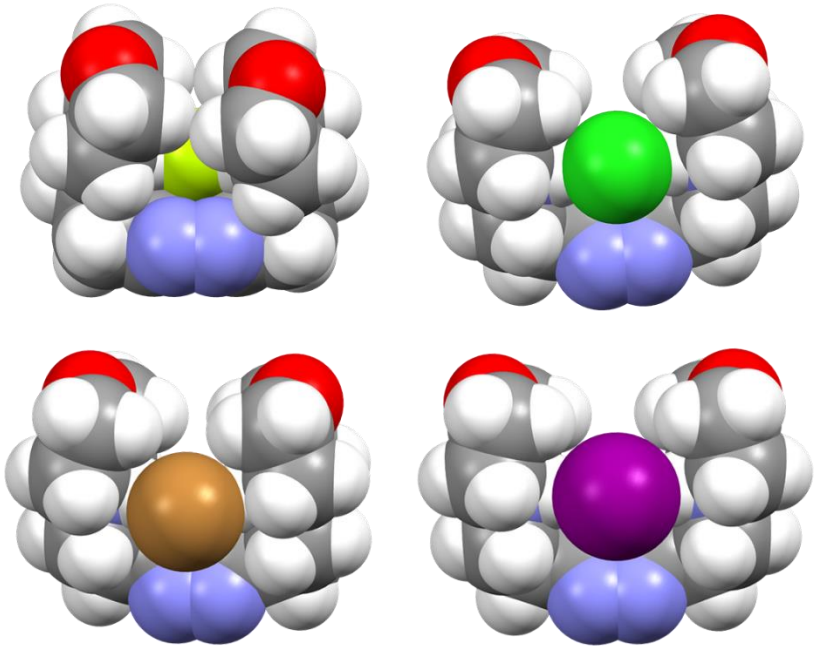

Figure 4.5-6*. DFT optimized geometries for fluoride, chloride, bromide and iodide H_2L2^{2+} complexes in PCM water.*

Although finer simulation with explicit water molecules would be needed, we can observe how the overall geometry of the complex does not differ significantly, having the ligand in an U-shaped conformation with the morpholine pendants more and more spread as the guest ion becomes bigger and bigger. Also differences in solvation are appreciable, with fluoride totally engulfed by the ligands while other halide anions still manage to expose some surface to the solvent also in their complexed forms.

Relevant parameters, displayed in ***Table 4.5-4***, mirrors the aforementioned observations: salt bridges are found prominent for fluoride, and decreasing in strength down along the group, while anion-π interaction becomes of increasing importance, especially in the case of iodide where a certain degree of charge delocalization could strengthen the interaction of the anion with the tetrazine.

Table 4.5-4. *Relevant geometric parameters for halide-H_2L^{2+} interactions in the DFT optimized complexes.*

Anion	*Anion-Centroid*	*Salt Bridge Length*	*Mulliken Charge (au)*	*N-X-N Angle*
F^-	*2.731 Å*	*2.537 – 2.542 Å*	*-0.69*	*166.28°*
Cl^-	*3.307 Å*	*3.103 – 3.103 Å*	*-0.71*	*141.26°*
Br^-	*3.374 Å*	*3.203 – 3.200 Å*	*-0.73*	*125.23°*
I^-	*3.695 Å*	*3.541 – 3.541 Å*	*-0.55*	*119.50°*

4.5.3 Conclusions

Periodic properties of halide anions and their influence upon complex formation with the L2 ligand have been explored. Both crystal structures and solution studies confirm the central role of the tetrazine moiety as a fundamental anion binding site for these complexes, together with salt bridge formation involving the protonated nitrogen atoms of the morpholinic pendants.

Both salt bridges and anion-π contributions showed a dependence on the properties of the halide in their solid complexes, tendency to form strong salt bridges decreases from fluoride to iodide, while the reverse seems to hold for anion-π interactions.

The overall trend exhibited by the complex formation constants, however, is not at all linear, suggesting the working hypothesis of two competing trends subtending the observed behaviour: an enthalpic drive for fluoride-like species which give rise to strong interactions with the ligand, and an entropic one, ultimately due to solvent effect, for softer species like iodide.

Both solution and solid-state data indicate chloride as the least interacting anion of the series, having lost most of the basic and polarizing character of fluoride and not yet gained the bigger dimensions and softer behaviour of bromide and iodide.

Even our preliminary *in silico* calculation agree with the overall picture and seem to point out differences in solvation and hydration free energies as a discriminating factor.

Unsurprisingly, each anion is found to behave in its own specific way.

4.6 Stabilization of Polyiodides Through Anion-π Interactions: Towards Solid-State Conductors

Within the multifaceted chemistry of anions, the behaviour of iodide and polyiodides occupies a special position, as a wide spectrum of structures, ranging from isolated units to complicated three-dimensional networks, passing through linear chains and two-dimensional assemblies, can be generated from three simple building blocks: I_2, I^- and I_3^-. This kind of structural features are made possible by the ability of iodine to concatenate *via* donor-acceptor interactions, the character of each assembly being regulated by its chemical environment. In the solid state, for instance, polyiodides of variable structures can be generated by using different countercations.

The understanding of such a structural variety is an interesting challenge, especially when considering that the hypervalency exhibited by several large polyiodides is not easily justified by simple covalent bonding models and, accordingly, the nature of bonding in polyiodide anions has been the object of intense theoretical consideration. Furthermore, the particular electrical conductivity and redox properties of polyiodide systems have gathered interest toward their application for the development of dye-sensitised solar cells and solar batteries, where they have been incorporated in many different forms, including aqueous solutions, ionic liquid electrolytes, gel polymer electrolytes or even solid state crystalline conductors.

In view of this, polyiodide binding appeared as a new intriguing testing ground for our receptor molecules, to which we were also driven by the unusual behaviour observed for L2-Iodide crystallization media, which yields different types of crystals, recognizable to the naked eye, depending on the conditions (*vide infra*).

Although among our strongest interacting receptors, L1 and L2, only the latter could be studied, L1 undergoing degradation in even slightly acidic media in the presence of I^-, two of the solved crystal structures, $(H_2L2)_2(I_3)_3I\cdot 4H_2O$ and $H_2L2(I_3)_2\cdot 2H_2O$, proved extremely interesting as a complete segregation of ligand and anion in discrete planes was observed, fostering their proposal as potential solid-state conductors. Electrical conductivity and spatial arrangement are closely related for polyiodide systems, as conduction generally happens through a Grotthuss-like mechanism, in which charge (*i.e.* electrons) alone are transferred through an internal reversible rearrangement of intra- and inter-molecular bonds, *i.e.* without mass transport.

Studies concerning thiocyanate binding are also reported within this section with the aim of providing a background on the solution behaviour of these systems. Since triiodide-containing complexes proved of extreme insolubility in water, the

pseudohalogen SCN^- ion, the only one of linear geometry so far addressed in our solution studies, was devised as a possible model for the interaction in solution.

4.6.1 Crystal Structures

4.6.1.1 Crystal Structure of $(H_2L2)I_2 \cdot H_2O$

Crystals of $(H_2L2)I_2 \cdot H_2O$ (**1**) suitable for single crystal X-ray analysis were obtained by slow evaporation of an aqueous solution containing L and I^- at pH 3, in an anaerobic atmosphere at room temperature. Microcrystalline samples of the same compound can be obtained even under aerobic conditions provided that crystallization occurs in a few hours, otherwise complex $(H_2L2)_2(I_3)_3I \cdot 4H_2O$ (**2**) is obtained. The crystal packing of **1** is built up by alternate planes of two sets of symmetry independent H_2L2I_2 adducts developing in the (001) and the (002) crystallographic planes, respectively. In each H_2L2I_2 adduct (***Figure 4.6-1*** and ***Figure 4.6-2***), the ligand is placed around an inversion center, giving rise to anion-π interactions with two iodide anions placed one above and one below its tetrazine ring (I···ring centroid /offset distances 3.70 /0.32 Å –(001) plane– and 3.67/0.27 Å –(002) plane–).

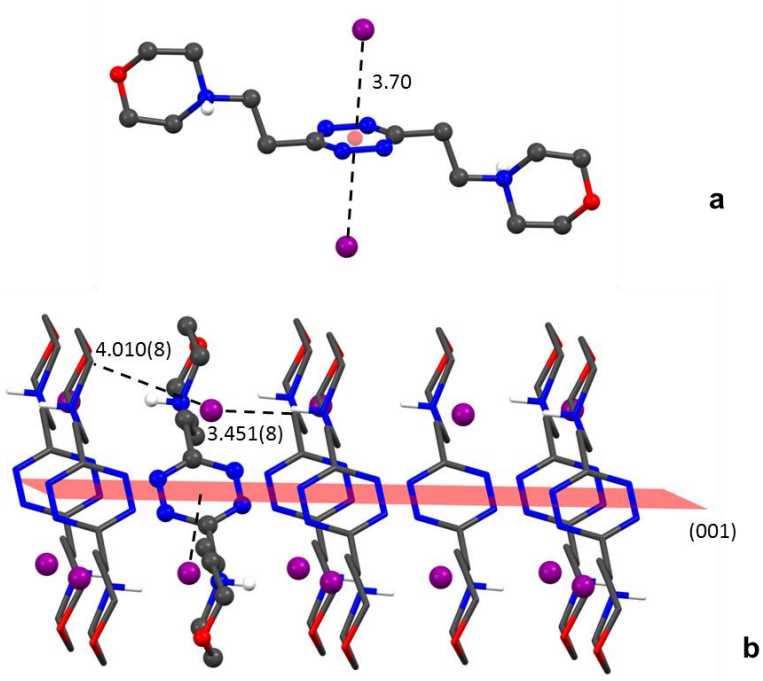

Figure 4.6-1. *Crystal structure of $(H_2L2)I_2 \cdot H_2O$ (**1**): ligand conformation and anion-π contacts (a) in H_2L2I_2 adduct developing in the (001) crystallographic plane (b). Distances are in Å.*

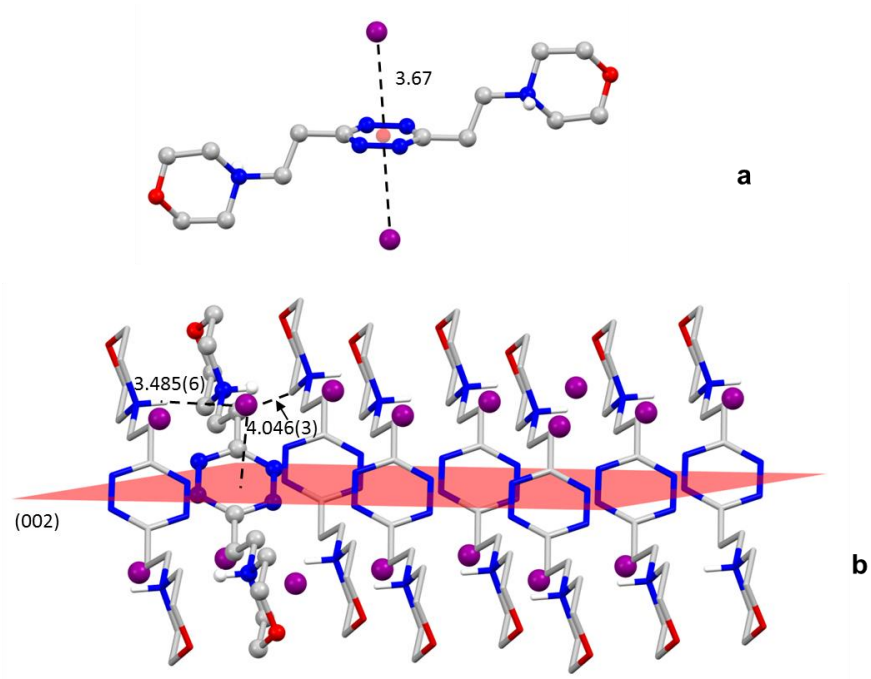

***Figure 4.6-2**. Crystal structure of $(H_2L2)I_2{\cdot}H_2O$ (**1**): ligand conformation and anion···π contacts (a) in H_2L2I_2 adduct developing in the (002) crystallographic plane (b). Distances are in Å.*

Moreover, each iodide is H-bonded to two adjacent ligand molecules, through the protonated morpholine nitrogen on one side and a CH hydrogen bond on the other one (N···I 3.451(8) Å and C···I 4.010(8) Å –(001) plane, ***Figure 4.6-1***– and N···I 3.485(6) Å and C···I 4.046(3) Å –(002) plane ***Figure 4.6-2***–). In the (001) plane, the NH···I contacts are directed along the *b* axis, while, in the (002) plane, the analogous contacts point in the [100] direction. Actually, both ligand conformations and relative anion/receptor spatial dispositions are very similar, and the major reason for the lack of additional crystallographic symmetries is the presence of a co-crystallized water molecule which joins the two H_2L2I_2 systems, forming stronger interactions with the one developing in the (002) plane (OW1···C9 3.68(1) Å, ***Figure 4.6-3***).

In both planes, the conformation assumed by the ligand can be considered intermediate between the planar and the chair conformations previously observed in the crystal structures of H_2L2^{2+} complexes with ClO_4^-, PF_6^- and NO_3^- anions. Interestingly, in most of these complexes, as well as in all crystal structures solved up to now for the anion complexes with L1 and L3, anion and receptor almost exclusively form anion-π contacts, without the contribution of additional H-bonds from the protonated nitrogen atoms, which, instead, are very often in contact with water solvent molecules. In analogy with the behavior seen in these structures, we

can hypothesize that, even in H_2L2I_2, the anion-π interaction strongly contributes to stabilize the complex. As a matter of fact, the anion is very well placed above the ring centroid, and the anion···centroid distance (3.67 and 3.70 Å) is significantly short with respect to the iodide ionic radius (2.20 Å).

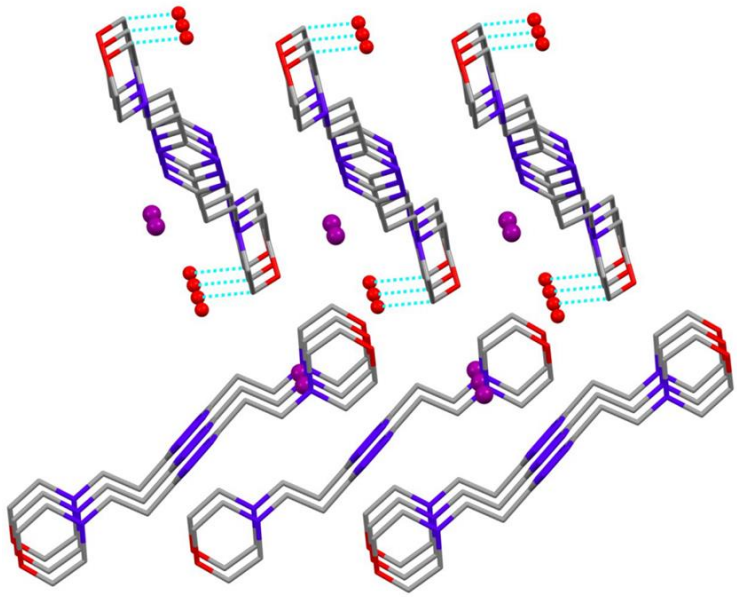

***Figure 4.6-3**. Crystal packing of compound **1**. Water···carbon (OW1···C9) contacts with the H_2L2I_2 molecular system developing in the (002) plane.*

4.6.1.2 Crystal Structure of $(H_2L2)_2(I_3)_3I{\cdot}4H_2O$

When crystals of **1** are left in contact with the mother liquor and exposed to the air, they slowly re-dissolve while crystals of $(H_2L2)_2(I_3)_3I{\cdot}4H_2O$ (**2**) are formed as a consequence of the spontaneous air oxidation of I^- to I_2 (I_3^-). Crystals of **2** are also the product of slow evaporation of acidic solutions of L2, not protected from the air, in the presence of I^-. No further air oxidation of this compound was observed over several months.

In the structure of **2**, the three symmetry independent triiodide anions lie on crystallographic inversion centers. Two of them are in contact with the ligand tetrazine ring, both giving a side-on interaction (***Figure 4.6-4a***). Nevertheless, while one of them is very well placed above the ring centroid (I···ring centroid/offset distances 3.57/0.30 Å), the other one is more displaced toward the ring periphery (I···ring centroid/offset distances 3.61/0.80 Å). Interestingly, this second triiodide places its central iodine just above a C-N aromatic bond, giving an η^2-type binding.

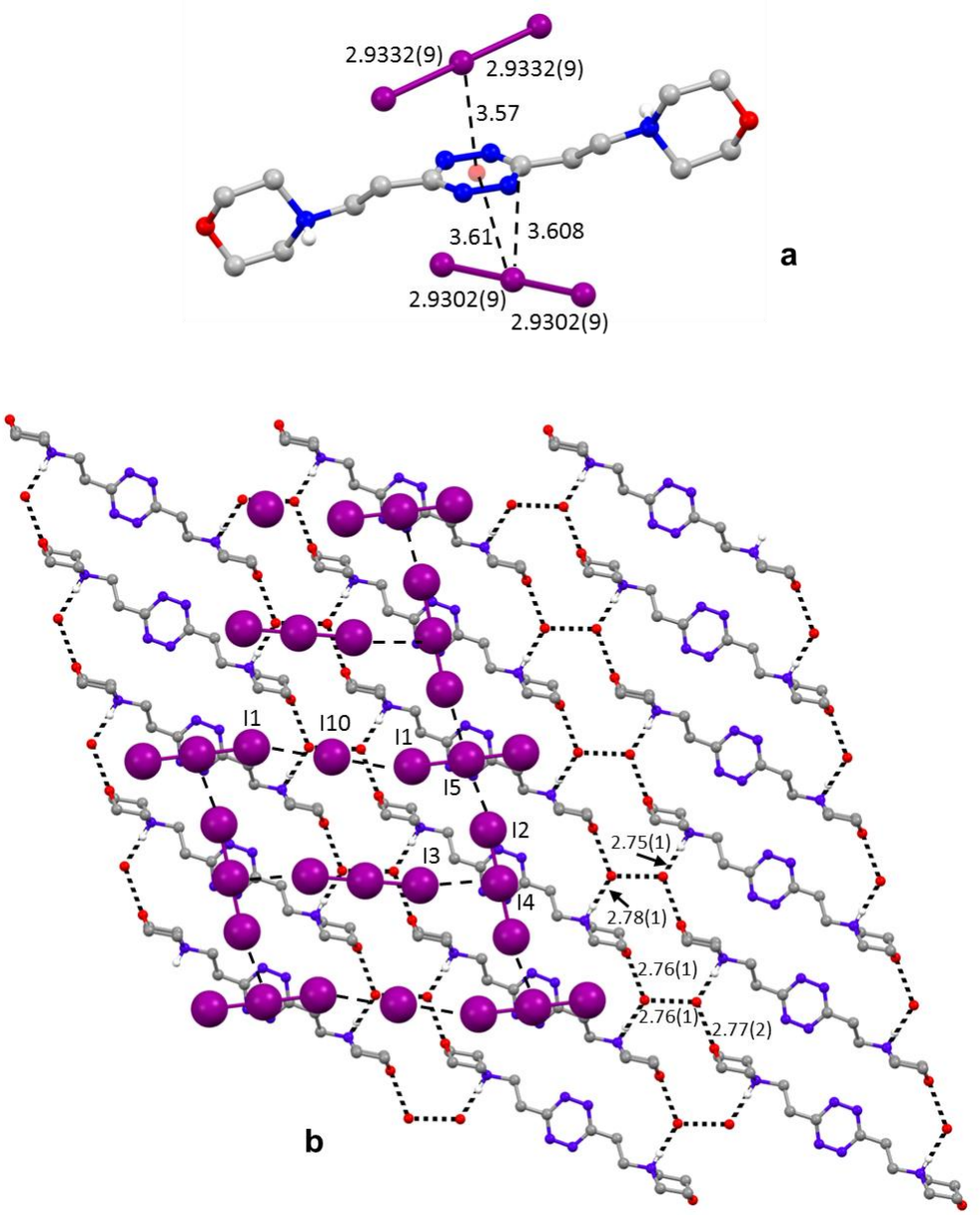

***Figure 4.6-4**. Crystal structure of $(H_2L2)_2(I_3)_3I{\cdot}4H_2O$ (**2**): ligand conformation and $I_3^-\cdots\pi$ contact (a); honeycomb-like network given by protonated ligands and co-crystallized water molecules and T-shaped pattern of triiodide anions (c). Distances are in Å.*

Crystallographic symmetry imposes both linearity and equal I-I bond distances to all anions, which are indeed found very similar (I-I bond distances in the three triiodides are 2.930, 2.933 and 2.937 Å). Alternation of triiodide and iodide anions gives rise to the overall honeycomb-like T-shaped structure portrayed in ***Figure 4.6-4b***.

4.6.1.3 Crystal Structure of $H_2L2(I_3)_2{\cdot}2H_2O$

The very insoluble $H_2L2(I_3)_2{\cdot}2H_2O$ (**3**) complex was obtained from the components by using a diffusion method (*cf.* 2.3). In its crystal structure, the asymmetric unit contains two half ligand molecules, each interacting with triiodide through the tetrazine ring. In particular, as shown in ***Figure 4.6-5a,b***, both end-on (a) and side-on (b) binding modes are found. In the case of triiodide (a), the I···ring centroid distance is 3.60 Å with an offset of 0.45 Å. This triiodide is almost symmetric and linear (I-I 2.94(2) and 2.91(2) Å, I-I-I angle 178.28(6)°). Instead, the anion (b) is strongly asymmetric, bent (I-I 2.796(2) and 3.098(2) Å, I-I-I angle 174.25(6)°) and almost aligned along the C–C axis. The central iodine atom is almost perfectly placed above a tetrazine nitrogen. The I···N distance is only 3.64(2) Å, significantly shorter than the sum of the van der Waals radii (3.7 Å) and, together with the overall asymmetry of the anion and its remarkable deviation from linearity, could be a consequence of charge-transfer or coulombic interactions taking place within the crystal. Parallel zig-zag chains are formed by the head-to-tail disposition of the anions (***Figure 4.6-5c***).

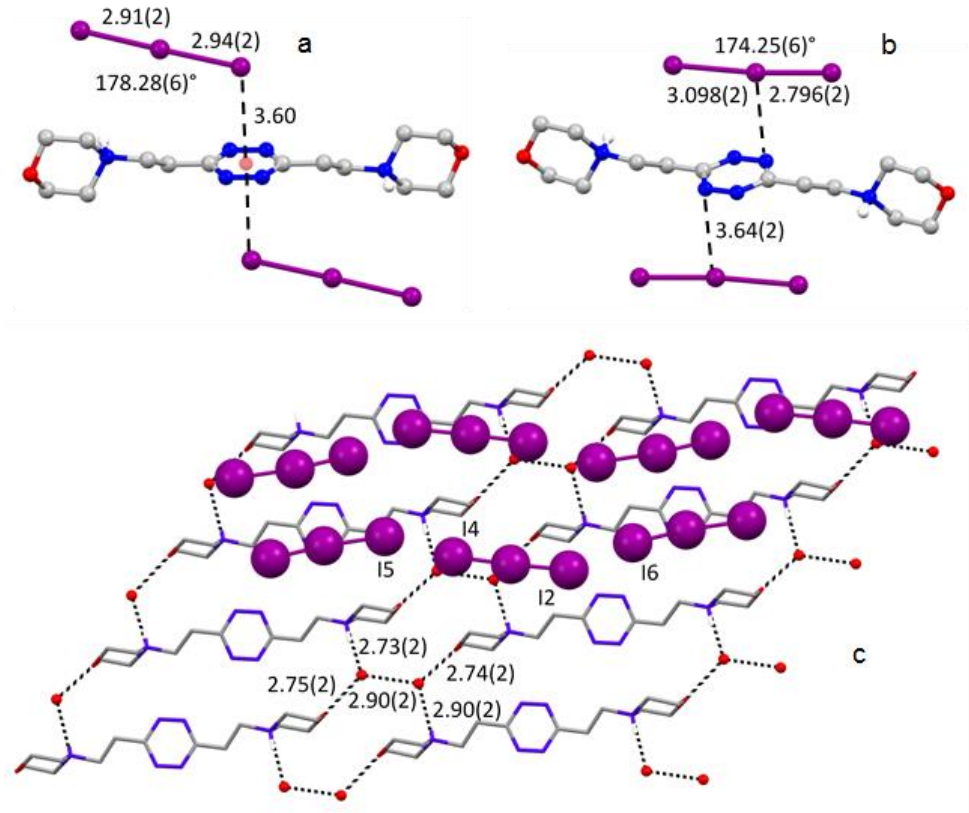

***Figure 4.6-5**. Crystal structure of $H_2L2(I_3)_2{\cdot}2H_2O$ (**3**): end-on (a) and side-on (b) $I_3^-\cdots\pi$ contacts; honeycomb-like network given by protonated ligands and co-crystallized water molecules and zig-zag chains of triiodide anions (c). Distances are in Å.*

4.6.1.4 Crystal Structure of $H_2L2(SCN)_2$

The crystal structure of the $H_2L2(SCN)_2$ compound contains centrosymmetric diprotonated ligand molecules interacting with two symmetry related thiocyanate anions (***Figure 4.6-6***). The ligand assumes a chair-type conformation, similar to that previously reported for its ClO_4^-, NO_3^-, PF_6^- complexes, in which the morpholine pendant arms are in trans position with respect to the tetrazine ring. The two SCN^- anions are localized in a side-on conformation just above, and below, the tetrazine ring, almost aligned along the C–C axis. The projection of the sulphur atom of each anion on the tetrazine plane lies completely outside the ring, while both nitrogen and carbon positions are representative of an anion-π interactions with the electron-poor aromatic group (distances from ring centroid/offset 3.19/0.46 Å for N and 3.35/0.72 Å for C). Furthermore, the thiocyanate nitrogen forms a strong H-bond (H···N distance 1.75(7) Å, N-H···N angle 174(6)°) with the morpholine protonated nitrogen. Interestingly, the H···N-C angle featuring the H-bond (161(2)°), as well the N-C intra-ion bond distance (1.187(8) Å), strongly suggest the presence of a triple bond between nitrogen and carbon in the thiocyanate anion. This connectivity implies that the negative charge is formally associated to the sulphur atom, which, as a matter of fact, is in contact with a hydrogen atom of a CH_2 group linked to the tetrazine ring (H···S distance 2.861(1) Å).

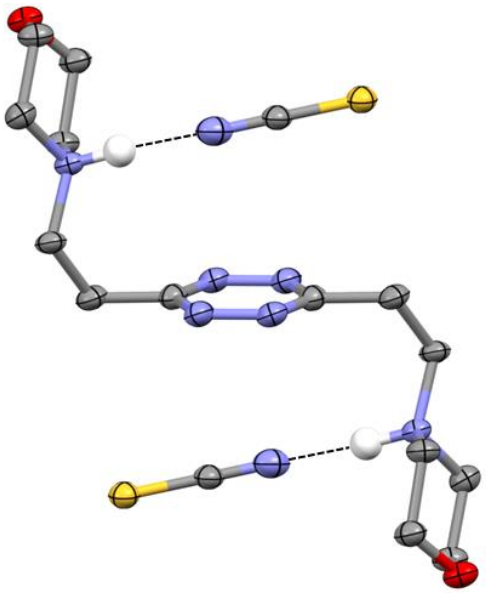

Figure 4.6-6*. ORTEP drawing of $H_2L2(NCS)_2$. Thermal ellipsoids plotted at 40% probability level.*

4.6.2 Analysis and Discussion

The crystal structures of **2** and **3** show close analogies, despite crystals of these complexes belong to different space groups and crystal systems (***Table 4.6-1***).

Concerning the possibility of their use, the most important similarity between them is the segregation of ligands and anion in discrete infinite planes, fostering the opportunity, at present under evaluation, of electrical conductivity along the planes of anions according to a Grotthuss-like mechanism. Depictions of the planes of anions found in structures **2** and **3** are reported below in ***Figure 4.6-7*** and ***Figure 4.6-8***, together with an analogous depiction of structure **1** (***Figure 4.6-9***), which appears unfit to conduction studies due to the presence of the iodine species only as single ligand-separated centres with no communication between one another.

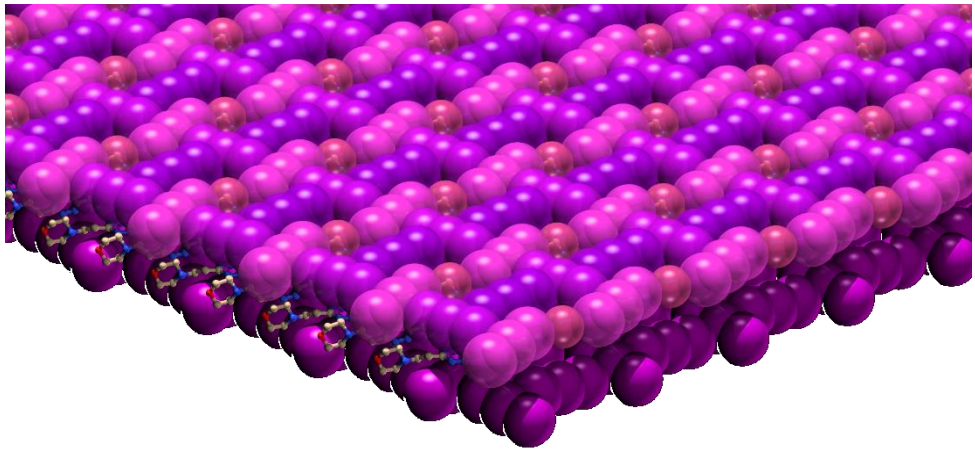

Figure 4.6-7. *Depiction of the anion planes in $(H_2L2)_2(I_3)_3I{\cdot}4H_2O$ (**2**). The three non-equivalent triiodide and the iodide anions are shaded differently to appreciate their mosaic.*

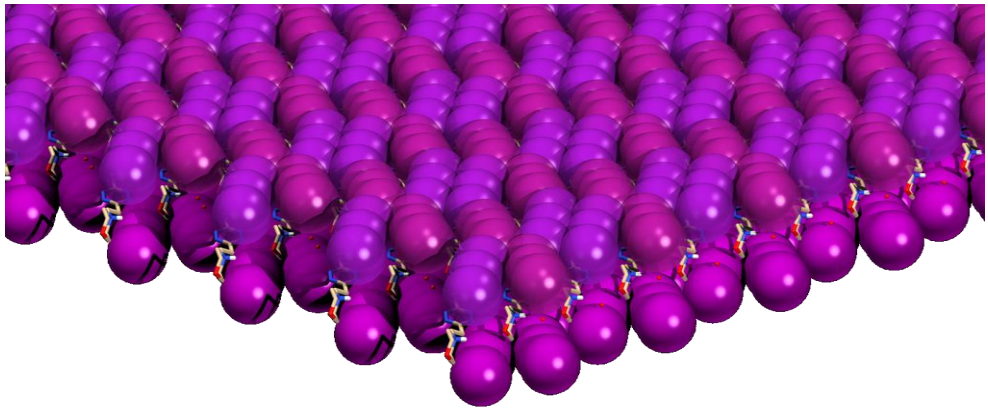

Figure 4.6-8. *Depiction of the anion planes in $H_2L2(I_3)_2{\cdot}2H_2O$ (**3**). The two non-equivalent anions are shaded differently to appreciate their mosaic.*

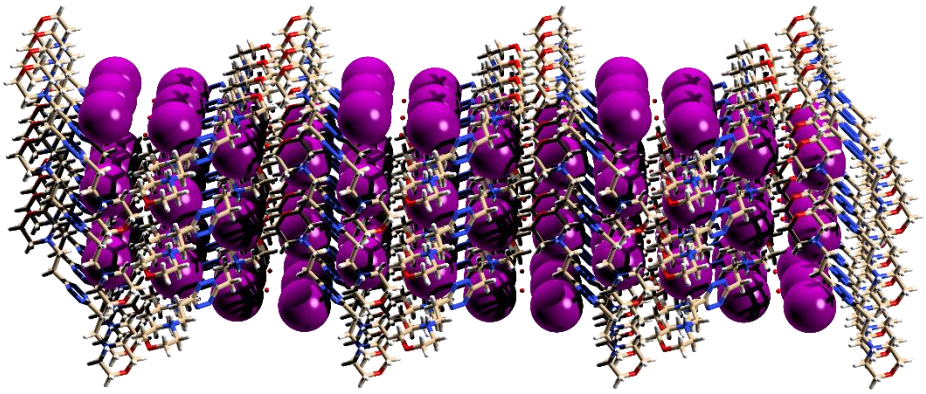

***Figure 4.6-9**. Depiction of the crystal structure of $(H_2L2)I_2 \cdot H_2O$ (**1**) showing no close contacts between iodine species.*

***Table 4.6-1**. Refinement and crystallographic parameters for **1**, **2**, **3** and $H_2L(NCS)_2$ structures.*

	(1)	***(2)***	***(3)***	***$H_2L2(NCS)_2$***
Empirical Formula	$C_{14}H_{26}I_2N_6O_3$	$C_{14}H_{26}I_5N_6O_4$	$C_{14}H_{26}I_6N_6O_4$	$C_{16}H_{26}N_8O_2S_2$
Formula Weight	*580.21*	*976.91*	*1103.81*	*426.57*
Temperature (K)	*150*	*100*	*100*	*293*
Space Group	*P -1*	*P $2_1/c$*	*P -1*	*P $2_1/c$*
a (Å)	*7.7303(6)*	*14.3403(3)*	*7.5053(6)*	*12.334(2)*
b (Å)	*7.7864(6)*	*14.3161(2)*	*13.5410(7)*	*6.816(1)*
c (Å)	*22.022(2)*	*13.8619(3)*	*14.5928(9)*	*12.497(2)*
α (°)	*86.949(7)*	*90*	*99.590(5)*	*90*
β (°)	*87.158(7)*	*106.228(2)*	*102.045(6)*	*96.61(1)*
γ (°)	*60.575(8)*	*90*	*94.974(5)*	*90*
Volume (Å^3)	*1152.5(2)*	*2732.42(9)*	*1418.74(16)*	*1043.5(3)*
Z	*2*	*4*	*2*	*2*
R Indices	*R1 = 0.0517*	*R1 = 0.0660*	*R1 = 0.1013*	*R1 = 0.1013*

Analogies between the structures **2** and **3** are not limited to this, in fact in both crystalline structures the ligand assumes almost the same conformation, the protonated nitrogen atoms of the morpholine rings pointing toward opposite directions and establishing water assisted contacts with the oxygen atoms of adjacent ligands (***Figure 4.6-4b*** and ***Figure 4.6-5c***). Protonated ligands and co-crystallized water molecules define honeycomb-like networks developing parallel to the (100) planes both in **2** and **3**. The similarity between these two structures goes even further, since the tridimensional arrangement attained by the ligand molecules is practically the same in both of them, as evidenced by the graphical

superimposition of the ligand components of the crystalline structure (***Figure 4.6-10***). Thus, the prime differences between structures **2** and **3** are the number of iodine atoms and their arrangement into discrete anions, leading to different interhalogen contact networks in the anionic planar layers sandwiched between two successive planes of protonated ligands. Some contacts of the iodine anions with the aliphatic hydrogen atoms (H···I distances in the range 3.0-3.21 Å) contribute to stabilize the interplanar interaction. In **3**, parallel zig-zag chains are formed by the head-to-tail disposition of the anions (***Figure 4.6-5c***). Interestingly, the I···I contacts in these chains (I2···I6 3.530(2) and I4···I5 3.578(2) Å) can be regarded as secondary bonds, being the van der Waals contacts about 3.8-3.9 Å. In the mixed I^-/I_3^- system **2**, iodide and triiodide anions alternate giving the T-shaped pattern shown in ***Figure 4.6-4b***. This structure features longer I···I contacts ranging from 4.0230(9) to 4.3413(9) Å.

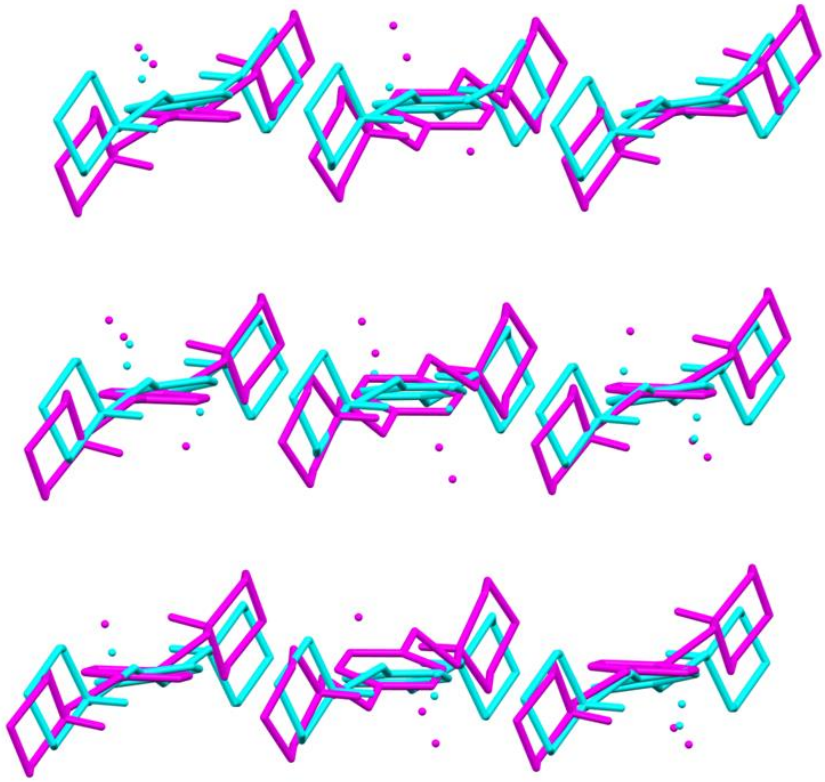

Figure 4.6-10. *Superimposition of ligand and water molecules of the crystalline structures **2** and **3**.*

Further information about geometries and structures of the different triiodide anions of **2** and **3** were acquired by the analysis of their Raman spectra (***Figure 4.6-11***) in the frequency region below 250 cm^{-1} which is characterized by vibrations involving the I_3^- units.

In complex **2**, a single prominent band is observed at 110 cm^{-1} (***Figure 4.6-11a***), although, as shown by the inset, a lower intensity structure is present with weak shoulders at 60, 75 and a broad one at 154 cm^{-1}, respectively, and an additional very weak band at 221 cm^{-1}. Crystals of **3** show a more structured spectrum, where the main band centred at 112 cm^{-1} is surrounded by few medium intensity peaks, indicating that I_3^- anions have lower symmetry than in the case of **2**.

In crystals of **2** ($(H_2L2)_2(I_3)_3I{\cdot}4H_2O$, ***Figure 4.6-4***), three kinds of I_3^- anions were identified, displaying linear and symmetric structures but with slightly different I-I bond lengths. For each anion, three vibrational modes are expected (one twofold), among which only the symmetric stretching is Raman active. Therefore, the intense band at 110 cm^{-1} can be assigned to this vibration (ν_1). The presence of the very weak band at 221 cm^{-1}, assigned as $2\nu_1$, supports the linear structure of the ions. However, small deviations from linearity, when randomly occurring, can be compatible with an observed overall centrosymmetric lattice. In such a case, bending and asymmetric stretching would become Raman active, even though with very weak intensities. Most likely, the shoulders at about 75 cm^{-1} and 154 cm^{-1} have a similar origin and can be related to the bending (ν_2) and asymmetric stretching (ν_3), respectively. The latter has been previously observed around 140-145 cm^{-1}. The difference with the present data may be ascribed to the difficulty in accurately locating the maximum position because of the convolution with the very intense ν_1.

The 60 cm^{-1} shoulder can be attributed considering that, at room temperature, excited low frequency vibrational modes may be populated, hence also ν(1-2) vibrational transitions other than the fundamental ν(0-1) can be observed. For this reason, the 60 cm^{-1} is probably a hot band transition of the bending vibration ν_2. Alternatively, it could be considered a lattice vibration (*i.e.* I_3^- with respect to the ligand), but in our opinion 60 cm^{-1} is a too high value for lattice modes.

As shown before, crystals of **3** ($H_2L2(I_3)_2{\cdot}2H_2O$, ***Figure 4.6-5***) contain two differently conformed I_3^- anions, (a) and (b), featuring end-on and side-on interaction modes, respectively, with the tetrazine ring. Both are non-linear, the bending angle of (b) being larger than that of (a). Moreover, the I-I distances are not symmetric with respect to the central atom and this is more evident in (b) than in (a), the latter being more similar to the symmetric I_3^- anions of complex **2**. Due to the loss of symmetry of (a) and (b), all three vibrational modes become Raman active accounting for the higher number of bands in the spectrum and for their increased intensities (***Figure 4.6-11***, ***Table 4.6-2***). Furthermore, the deviation from linearity of these anions causes a lowering of the force constant of bending vibrations, justifying, in the (a) case, the frequency shift toward lower energies (75/70 cm^{-1}; 145-140/136 cm^{-1}) observed for the relevant bands.

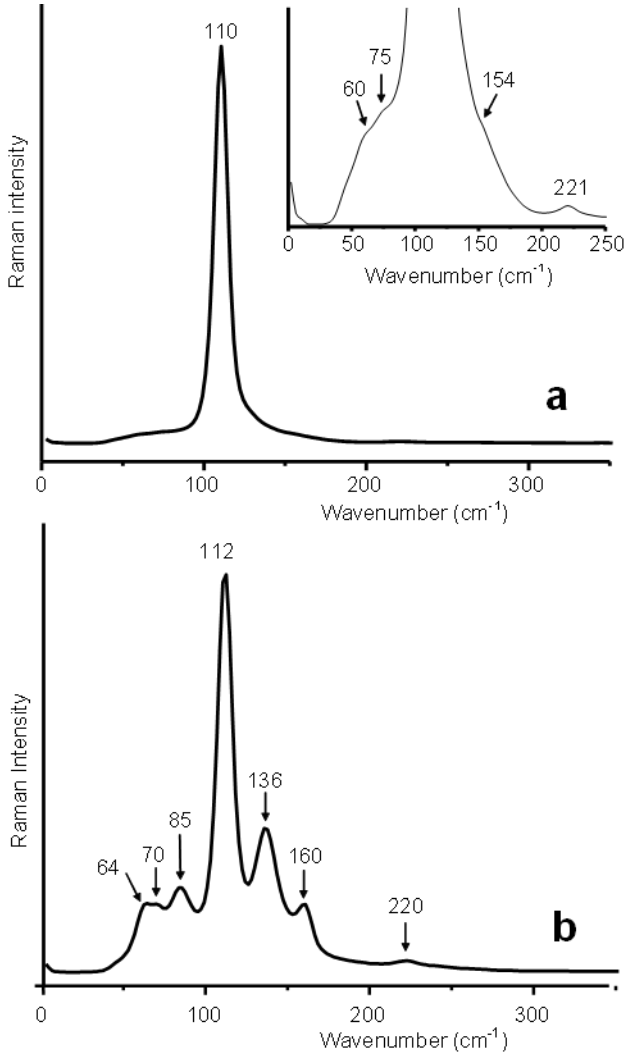

***Figure 4.6-11**. Raman spectra of **2** $(H_2L2)_2(I_3)_3I{\cdot}4H_2O$ (a) and **3** $H_2L2(I_3)_2{\cdot}2H_2O$ (b).*

Table 4.6-2. *Observed Raman frequencies of crystalline $H_2L2(I_3)_2{\cdot}2H_2O$ (**2**, (a) and (b)) and $(H_2L2)_2(I_3)_3I{\cdot}4H_2O$ (**3**) complexes.*

2	***3****(a)*	***3****(b)*	***Assignment***
60 vw	*64 mw*		***Bending ν_2 υ(1-2)***
75 vw	*70 w*		***Bending ν_2 υ(0-1)***
110 vs	*112 s*		***Symmetric Stretch ν_1***
154 bs	*136 ms*		***Asymmetric Stretch ν_3***
221 vw	*220 w*		***$2\nu_1$***
		85 m	***Stretching $I_2\cdots I^-$***
		160 m	***Stretching I-I$\cdots I^-$***

In (b), the I-I bond distances from the central iodine atom, although still below the limit reported for intramolecular distances in polyiodide systems (3.3 Å), are rather different, giving this triiodide anion some similarity with a $I_2\cdots I^-$ system. This may help in the assignment of the 160 cm^{-1} and 85 cm^{-1} bands. Actually, the band at 160 cm^{-1} can be assigned to an I-I stretching "perturbed" by the presence of a close I^- ion, as already reported for systems with I-I distances comparable to (b), while the $I_2\cdots I^-$ stretching should be found at lower frequency because of its longer bond distance (3.098 Å vs 2.796 Å, ***Figure 4.6-5***). The 85 cm^{-1} band can be attributed to this vibration. The bending is not observed, being likely hidden under this low frequency spectral feature.

In order to compare the relative strength of interaction of iodide and triiodide anions with the tetrazine moiety of L2, we investigated the four complexes shown in ***Figure 4.6-12***.

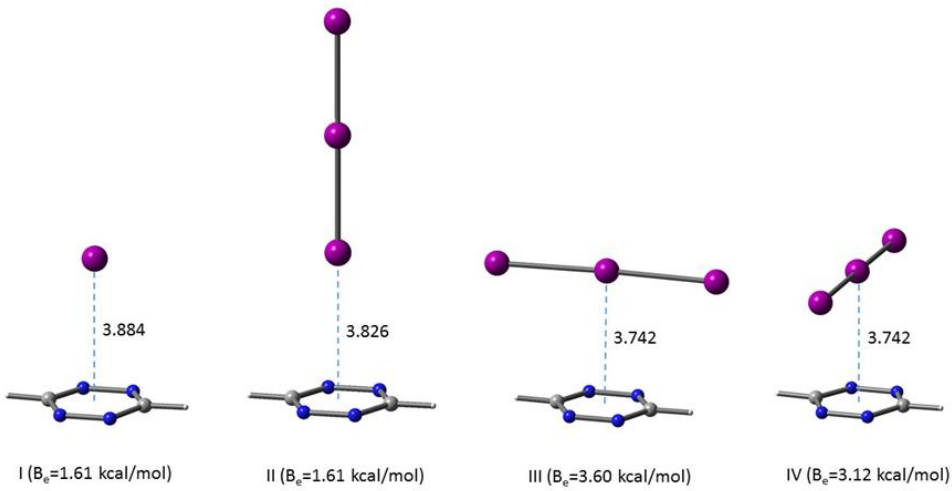

Figure 4.6-12*. DFT-optimized geometries of four tetrazine-anion complexes. Distances are in Å.*

Complex I is characterized by a binding energy (B_e) of 6.7 kJ/mol which results from the anion-π interaction established between iodide and tetrazine with a I^-···centroid distance of 3.884 Å. Regarding the triiodide anion, three high-symmetry orientations above the molecular plane of the tetrazine were conceived: one where I_3^- is oriented normal to the plane (complex II), a second one (complex III) where I_3^- is oriented parallel to the plane and aligned along the C–C axis, and a third one (complex IV) where the bond axis of I_3^- bisects the N-N bonds of tetrazine. Interestingly, complex III possesses both the lowest total electronic energy and the highest value of B_e (15.1 kJ/mol) among the triiodide complexes shown in ***Figure 4.6-12***. A rotation of the I_3^- anion about the (central I)-centroid axis by 90.0° yields complex IV which, in spite of having the same I-centroid distance of 3.742 Å of complex III, is characterized by a slightly lower B_e value (13.1 kJ/mol) with respect to the former. The most disfavored orientation is the vertical one corresponding to complex II which is characterized by a B_e value (6.7 kJ/mol) that is same as that of the complex with iodide anion.

As far as the possibility of a charge transfer process is concerned, the results of our natural population analysis indicate that almost no charge is transferred from the anion to the tetrazine. For instance, $q(I^-)$ = -0.99e in complex I, while similar net charges were calculated for the complexes with triiodide anion. Interestingly, however, the negative charge accumulates on the terminal iodine atoms of I_3^-, while the charge of the central atom is close to zero. This result suggests that the terminal iodine atoms of I_3^- are likely favored to interact electrostatically with the counter-cations both in solution and in the crystals. Nevertheless, it is to be underlined that the contacts found in our models are longer than the sum of the van der Waals radii and always significantly longer than those found in the solid state.

To unravel the nature of the intermolecular interactions that are operative within the I_3^- complexes both in the solid-state and in water, we have performed a topological analysis of the computed electronic charge density of the trimeric $(H_2L2^{2+})(I_3^-)_2$ complex displayed in ***Figure 4.6-5b*** . The molecular graph obtained for the geometry corresponding to the crystal structure is shown in ***Figure 4.6-13a***. Each I_3^- anion interacts with the deprotonated ligand *via* five bond paths, four of which are concerned with C-H···I interactions and the fifth one with an N···I interaction. The latter is likely associated to an anion-π interaction rather than to halogen bonding interaction since it occurs in the direction normal to the tetrazine plane which is populated by π-electrons. The values of the electronic charge densities at the BCP(3,-1) indicates that the complex in the crystal is C_i symmetric. The binding energy associated to the interaction of two I_3^- anions with the dicationic ligand corresponds to 65.2 kJ/mol. Hence, half of this energy (32.6 kJ/mol) corresponds to the interaction of one I_3^- anion with the ligand. Upon replacement of both

morpholinic arms with hydrogen atoms, the binding energy associated to the interaction of one I_3^- anion to the ligand becomes 10.2 kJ/mol, which approximately double the mean contribution from the four CH···I contacts. This value is slightly lower than those calculated for complexes III and IV in ***Figure 4.6-12***. Hence, this result indicates that the parallel orientation of the I_3^- anion with respect to the tetrazine plane is still favored over the vertical orientation (complex II) even when the triiodide anion is translated away from its centroid.

As above noted, we were not able to get information about I_3^- complexes in aqueous solution because they are poorly soluble. To remedy this lack of information, details of the possible geometry of the complex in water were obtained by optimization at the IEF-PCM(H_2O)-ωB97X-D/DGDZVP level of theory of the trimeric $(H_2L2^{2+})(I_3^-)_2$ complex and of the same system solvated by two explicit water molecules. Both calculations were followed by QTAIM analysis of the electronic charge densities. The molecular graph of the DFT-optimized not solvated complex is shown in ***Figure 4.6-13b***.

Each I_3^- anion is now characterized by six bond paths connecting it to the diprotonated ligand. The new bond path topology results from the translation of the I_3^- anions in opposite directions, toward the positive ligand charges, nearly oriented along the C-C axis of the tetrazine ring. In addition to four C-H···I bond paths, each I_3^- anion is now characterized by two I···C bond paths connecting the central and one terminal iodine atoms of I_3^- with the carbon atoms of the tetrazine ring. The increased number of bonding interactions in this model is in line with the enhancement of the computed binding energy, by ≈10 kcal/mol, from 15.58 kcal/mol to 25.25 kcal/mol. However, it noteworthy that, in the solvated system (***Figure 4.6-13c***), the charge assisted NH···I hydrogen bonds are lost and replaced by water bridged bonds, while the I···π and CH···I interactions still have a role in stabilizing the adduct.

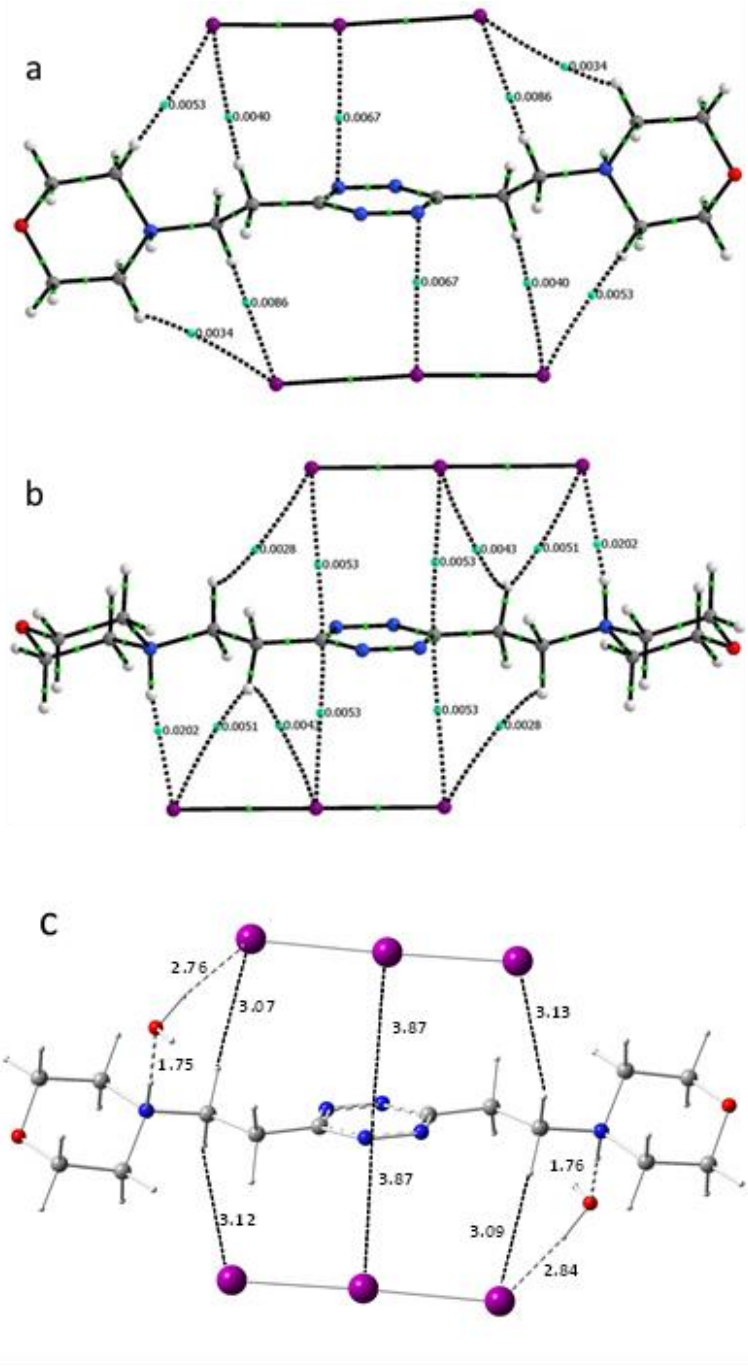

Figure 4.6-13. *Molecular graphs for (a) the $H_2L2(I_3)_2$ complex in the molecular crystal and (b) the same complex after geometry optimization in a continuum water environment. The values of the charge density at selected BCP(3,-1) are reported (in a.u.) whereas RCPs and CCPs are not shown. (c) The same complex with two explicit water molecules. Distances are in Å.*

The thiocyanate complex crystal structure somewhat bridges the gap between I_3^- and the crystal structures of other anions such as ClO_4^-, NO_3^-, PF_6^- (*cf.* 4.3.1), as interesting comparisons can be made among them.

Figure 4.6-14, for instance, shows the SCN^- ion superimposed to the side-on (a) and to the end-on (b) H_2L2I_3 species found in the crystal of $H_2L2(I_3)_2{\cdot}2H_2O$ (**3**). As in the case of the SCN^- anion, also the end-on I_3^- is approximately aligned along the C-C interatomic axis of the tetrazine, while the side-on one is displaced toward the N-N side edge of the tetrazine ring. Notably, in the end-on $H_2L2I_3^+$ adduct, the main force taking triiodides in place is the anion-π interaction, while in the case of the side-on $H_2L2(SCN)^+$ an additional salt-bridge interaction, linking together the morpholine protonated nitrogen with the nitrogen atom of SCN^-, contributes to strengthen the assembly. Most likely, the stronger propensity to form H-bonds of nitrogen induces the H_2L2^{2+} ligand to assume the chair conformation, which in the adduct with triiodide seems less favoured than the planar one. Nevertheless, such considerations do not take into account the effect of crystal packing forces, that could be important in determining the overall arrangement of these anion complexes.

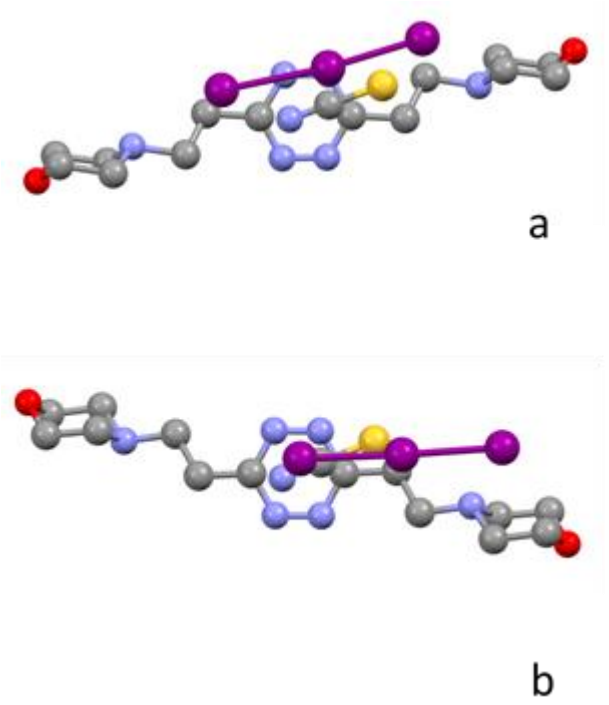

Figure 4.6-14*. NCS^- ion superimposed to the side-on (a) and the end-on (b) H_2L2I_3 species found in the crystal of $H_2L2(I_3)_2{\cdot}2H_2O$ (**2**). Superimposition obtained overlapping the tetrazine rings.*

Conversely, in H_2L2X^+ complexes with ClO_4^-, NO_3^- or PF_6^-, H_2L2^{2+} assumes the chair conformation, in analogy with the SCN^- complex. ***Figure 4.6-15*** offers an overlaid vision of H_2L^{2+} molecules from SCN^- and PF_6^- complexes. The superimposition has been calculated for all the non-hydrogen atoms, except the tetrazine rings. It is evident that the pendant arms in the two structures are almost equal, but the similarity is even greater for ClO_4^- and NO_3^- compounds. Actually, the calculated Root Mean Square Deviation is 0.48 Å in the case of PF_6^- and at most 0.2 and 0.1 Å for NO_3^- and ClO_4^-, respectively. The tetrazine rings are never coplanar, dihedral angles ranging from 11.2° for NO_3^- to 21.4° for ClO_4^-. For all these adducts as well as for the SCN^- one, H-bonds involving the protonated morpholine nitrogen atoms and anion-π interactions are recognized.

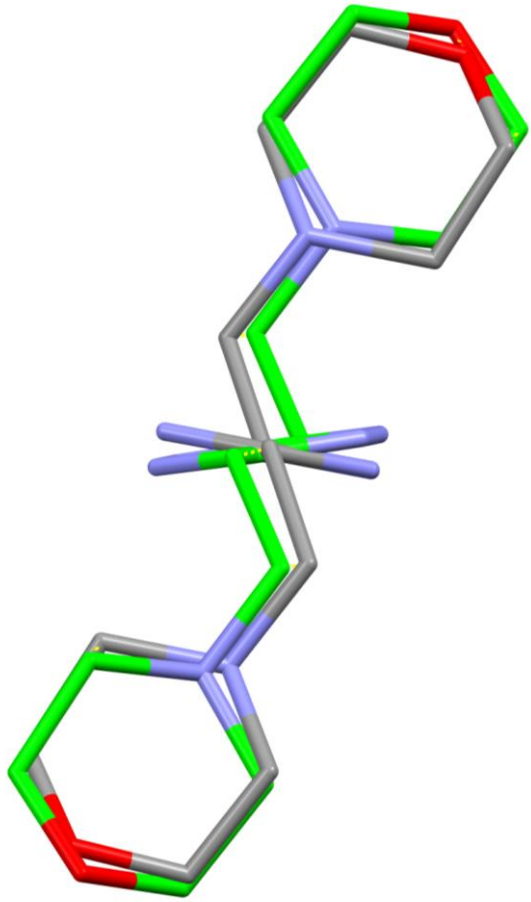

Figure 4.6-15. *L2 from the SCN^- complex (gray carbons) overlaid on ligand L2 from the PF_6^- complex (cf. 4.3.1.3) (green carbons). Superposition calculated for all the non-hydrogen atoms, except the tetrazine rings.*

To our knowledge, no crystal structures of SCN^- complexes with tetrazine ligands have been reported so far, while only two papers containing crystallographic structures includes receptors expressly selected for involving anion-π interactions in the binding of SCN^- [51] [52]. The most reliable comparison can be made with thiocyanate complexes with s-triazine, although, even in this case only three structures are available in the CSD [51] [53]. It is noteworthy, however, that the anion is invariably found pinched between different aromatic rings *via* concomitant end-on interactions of both N and S atoms.

Further information on the SCN^--L2 interaction was obtained by performing a series of DFT calculations on complexes of SCN^- with the bare tetrazine ring, that is with L2 deprived of the morpholine residues. The calculations performed in a simulated implicit water environment showed that in the most stable adduct the anion forms an end-on anion-π interaction with the electron-deficient ring *via* the N atom (***Figure 4.6-16a***) characterized by a B_e of 10.04 kJ/mol. This complex, which also possesses the lowest energy, is characterized by a tetrazine centroid (X)···N atom distance of 3.168 Å; the SCN^- anion is almost parallel to the tetrazine ring as evinced by the ∠XNC angle of 93.4° formed by the anion with the N-centroid line. When the SCN^- anion is oriented normal to the tetrazine molecular plane (∠XNC = 180°), the X···N distance (2.962 Å) is slightly shorter than the above value but B_e reduces to 7.11 kJ/mol (***Figure 4.6-16c***). This result indicates that the complex shown in ***Figure 4.6-16c*** lacks the extra-stabilization due to the π-π interaction that operates in the complex of ***Figure 4.6-16a***.

The same trend is observed for the interaction of thiocyanate via the terminal S atom *(**Figure 4.6-16b,d***). Interestingly, the parallel complex (***Figure 4.6-16b***) has only a slightly smaller B_e than the complex with the N-interacting anion (***Figure 4.6-16a***), while the XS distances are always longer than 3.5 Å

Finally, the natural population analysis indicates that there is practically no charge transfer from the anion to the tetrazine ring, being the natural charges of the three atoms of free thiocyanate anion almost the same as those of the anion in the complexes shown in ***Figure 4.6-16***. The negative charge within the (free) SCN^- anion, however, is localized mainly on the terminal atoms with q(N) = −0.597*e* and q(S) = −0.460*e*. The larger magnitude of q(N) thus favours the end-on coordination of SCN^- via the nitrogen atom which results in the formation of a stronger monopole-quadrupole interaction with the tetrazine ring.

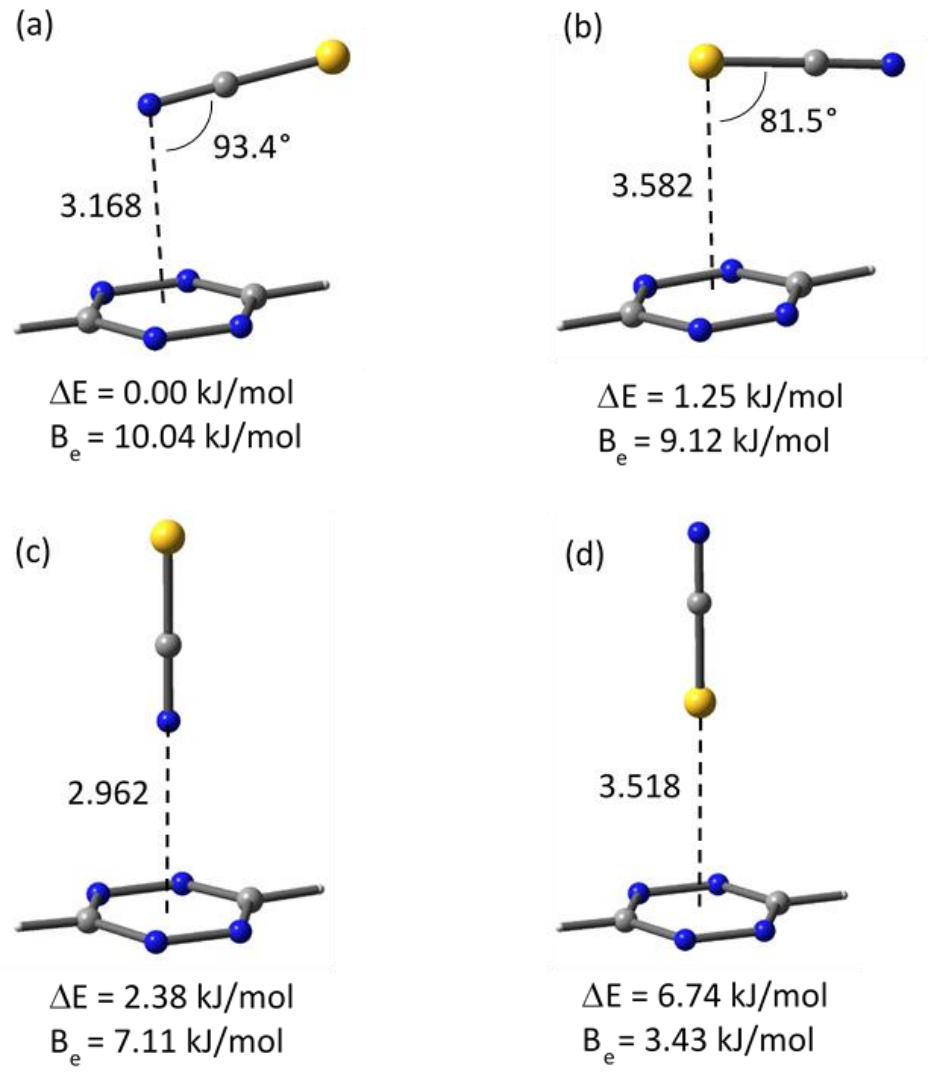

Figure 4.6-16. *DFT-optimized geometries of four tetrazine-SCN^- complexes. Distances are in Å.*

DFT and crystallographic results denote an important interplay of salt bridge, hydrogen bond and anion-π interactions in stabilizing the thiocyanate complex. Nevertheless, salt bridge interactions seem to have no effect when the complex is formed in aqueous solution. Equilibrium data determined for the formation of SCN^- complexes with neutral L2 and its protonated (charged) forms ($HL2^+$, H_2L2^{2+}) in water furnished association free energies that are almost independent of ligand charge, being 9.5(5), 10.7(5) and 10.8(4) kJ/mol for the formation of $[(L2)SCN]^-$, [(HL2)SCN] and $[(H_2L2)SCN]^+$, respectively (***Table 4.6-3***).

Table 4.6-3. *Equilibrium constants and relevant -ΔG° values for anion complex formation determined at 298.1 ± 0.1 K in 0.1 M NMe_4Cl aqueous solution. Values in parentheses are standard deviation on the last significant figure.*

Equilibrium	***log K***	***-ΔG° kJ/mol***
L2 + SCN^- = $[(L2)SCN]^-$	*1.66(8)*	*9.5(5)*
$HL2^+$ + SCN^- = [(HL2)SCN]	*1.87(8)*	*10.7(5)*
H_2L2^{2+} + SCN^- = $[(H_2L2)SCN]^+$	*1.90(7)*	*10.8 (4)*

A similar behaviour, although not so marked, was previously observed for the binding of other anions by L2 and the analogous L1 molecule, and suggests that anion-π interactions afford a prominent contribution to the interplay of weak forces stabilizing these complexes in a solvent, such as water, which has a high dielectric constant and is very competitive in the formation of hydrogen bonds. SCN^- ranks among the most hydrophobic anions of the Hofmeister series and, accordingly, its association with the aromatic ligand moiety, resembling a π-π stacking interaction, is not expected to be much hampered by the polar solvent. As a matter of fact, it was previously shown that lowering the dielectric constant of water by addition of ethanol results in a drop of stability of L2 complexes with several anions (*cf.* 4.3.2).

4.6.3 Conclusions

Protonated forms of the tetrazine-based ligand L2 are able to form I^-, I_3^-, mixed I^-/I_3^- and SCN^- anion complexes in the solid state. X-ray structures of these complexes showed that the anions are invariably located over the positive electrostatic potential of the ligand's tetrazine ring forming anion-π interactions. In the I^- and SCN^- complexes, further noncovalent forces contribute to hold the anions in place, while in the case of I_3^- solid complexes, constituted by alternated segregated planes containing only protonated ligands and co-crystalized water molecules or only iodide and triiodide anions forming halogen-halogen contacts, forces other that anion-π interactions appear to make a modest contribution to the anion-ligand association. In the solid complexes, the triiodide anion displays both end-on and side-on interaction modes with the tetrazine moieties, the I_3^- axis being aligned parallel to the ligand axis. DFT calculations substantiated that the side-on arrangement of I_3^- over the tetrazine ring corresponds to the most stable interaction mode among those computationally explored. Furthermore, calculations evidenced that, even when the ligand is deprived of the two morpholinium residues and in the presence of a simulated implicit water environment, the tetrazine ring is still able to promote the association with I^- and I_3^-, the side-on orientation of I_3^-, relative to the aromatic ring, remaining the most stable conformation. The infinite two-dimensional networks established between I_3^- and I_3^-/I^- anions through I···I short

contacts makes theses crystalline structures good candidates to behave as solid conductors.

Both in terms of observed arrangement in the solid state and DFT optimized geometries, thiocyanate gives somewhat different results, as although the geometry is linear as well, the electronic situation is not quite the same compared to triiodide. Tetrazine alone is still found to promote the association with the anion in PCM water, but this time the most stable orientation resembles a π-π interaction within host and guest, with the N terminus of the anion centred on the ring in an end-on fashion. This same arrangement, also thanks to the establishment of a strong straight salt bridge between the negatively charged N tip of the anion and the protonated nitrogen atom of the morpholinic pendant, is indeed found in the crystal structure of the thiocyanate complex. Solution studies, although possible only for I^- (*cf.* 4.5.2) and SCN^- due to the poor solubility of triiodide complexes, showed once more that the stability of the resulting complexes is poorly correlated with ligand charge, further suggesting that anion-π interactions give a prominent contribution to the stability of these complexes in water. In the case of I_3^-, the formation of solution complexes was simulated by means of computational methods, showing that the anion lays at short distance over the tetrazine ring and shifted toward a protonated morpholine nitrogen to form, this time, a salt bridge interaction. Addition of explicit water molecules, however, leads to their insertion in the salt bridges, which become solvent mediated, while the anion-π interaction remains untouched, indicating its prominent role in the formation of triiodide complexes.

4.7 Conclusions and Future Perspectives

A new family of ligands containing the tetrazine aromatic nucleus were prepared and an extensive study of their anion binding properties was undertaken.

Much of the above discussion was devoted to investigating and explaining the subtleties, addressing ion specific behaviours, justifying effects due to the modest differences among the ligands: this is indeed the peculiar habit of chemists, which dealing with so tiny objects are well-aware that devil is in the detail.

Nevertheless, a big picture emerges on top of that which deserves as much consideration, finding a home only in these final lines.

The long-lasting perception of anion-π interaction as, at best, a valid auxiliary force to keep together or orient host-guest assemblies, appears incredibly dated and out of place after seeing 17 out of 17 crystal structures invariably exhibiting strong anion-π interactions, at times even disregarding its majesty hydrogen bond, prince of all supramolecular interactions, even its charge reinforced variant.

The objection that the effective usage of stacking forces, to which anion-π interaction can be related, is already reported for crystal design and engineering, subtending a magnified importance of these kind of interactions in the solid-state due to packing forces and overall desolvation conditions which may alter their comparison with hydrogen bonding, is irrelevant here. In the case of our ligands even solution studies demonstrated poor correlation between ligands' charge and the observed stability of the complexes, again pointing out that forces other than salt bridges contribute to the association phenomena, anion-π interaction being the prime.

In this regard, the inclusion of the tetrazine moiety had surely played a role: a heterocycle with great positive Q_{zz} quadrupole moment so marginally explored in the literature for anion-π interactions, both in general and in aqueous solution in particular, was indeed hiding a great potential.

Solvent effects were no less prominent, studied complexation events being invariably entropically driven according to important desolvation effects. Even the notion that polar solvents should hinder the association of oppositely charged species was challenged by the results of L2 complexation studies in water:ethanol mixed solvent: whether we want to ascribe the decreasing of the association constants to an essentially non electrostatic control of the process or to selective solvation phenomena, the gathered evidences challenge the common beliefs.

No selectivity was sought for in designing the L1-L4 ligands, truly aiming for simple model systems, this is probably what allowed the detection of preferences determined by the host properties, or so-called ion-specific effects, even in the case of halide anions. As a matter of fact, specificity was not looked for in the design stage, but irremediably found: as such the possibility, already fostered and invariably strongly rejected, that anion-π interactions may be discriminating tools providing selectivity for the target anionic species in specifically designed hosts, appears once more tangible.

Basic research, however, is not limited to challenging common beliefs or giving scholars matters of discussion, it is really all about making something new, all the better if it can be put to use in a practical manner. Polyiodide crystals foreshadow a possibility of re-reading part of the work for real-world applications, herein included most of the other crystal structures with both different ligands and different anions, which are not far away from a sample case that could be used in further crystal engineering.

We end the way we started by re-reading the inspiring work of J. M. Lehn, which a few decades ago accidentally provided the material for our little circular ending, in the framework of the present thesis work:

"Although anionic species play a very important role in chemistry and in biology their binding features went unrecognized, whereas the complexation of metal ions and, more recently, of cationic molecules was extensively studied. The coordination chemistry of anions may be expected to yield a great variety of novel structures and properties of both chemical and biological significance. To this end, anion receptor molecules and binding subunits for anionic functional groups have to be devised. Research has been increasingly active along these lines in recent years and anion coordination chemistry is progressively building up as a new area in coordination chemistry." [4]

5 REFERENCES

[1] A. Bianchi, K. Bowman-James and E. García-España, “Aspects of Anion Coordination from Historical Perspectives,” in *Anion Coordination Chemistry*, Wiley-VCH Verlag GmbH & Co. KGaA., 2012, pp. 2-73.

[2] J. W. Steed and J. L. Atwood, Supramolecular Chemistry, Second Edition, Online: John Wiley & Sons, Ltd., 2009.

[3] J. W. Steed, J. L. Atwood and P. A. Gale, “Definition and Emergence of Supramolecular Chemistry,” in *Supramolecular Chemistry: From Molecules to Nanomaterials*, Online, John Wiley & Sons, Ltd., 2012.

[4] J.-M. Lehn, Supramolecular Chemistry: Concepts and Perspectives, New York: John Wiley & Sons, 2006.

[5] D. J. Cram, *Angew. Chem. Int. Ed. Engl.,* vol. 27, p. 89, 1988.

[6] J. B. Wittenberg and L. Isaacs, “Complementarity and Preorganization,” in *Supramolecular Chemistry: From Molecules to Nanomaterials*, Online, John Wiley & Sons, Ltd., 2012.

[7] D. B. Varshey, J. R. G. Sander and T. Friščić, “Supramolecular Interactions,” in *Supramolecular Chemistry: From Molecules to Nanomaterials*, Online, John Wiley & Sons, Ltd., 2012.

[8] J. M. Lehn, B. Dietrich, D. L. Fyles and T. M. Fyles, “Anion coordination chemistry – polyguanidinium salts as anion complexones.,” *Helv. Chim. Acta,* vol. 62, p. 2763–2787, 1979.

[9] C. J. Pedersen, “Cyclic polyethers and their complexes with metal salts.,” *J. Am. Chem. Soc,* vol. 89, p. 7017–7036, 1967.

[10] K. Worm, F. P. Schmidtchen, A. Schier, A. Schafer and M. Hesse, “Macrotricyclic borane-amine adducts – the first uncharged synthetic host compounds without Lewis-acid character, for anionic guests,” *Angew. Chem., Int. Ed. Engl.,* vol. 33, pp. 327-329, 1994.

[11] J. M. Mahoney, J. P. Davis, A. M. Beatty and B. D. Smith, *J. Org. Chem.,* vol. 68, p. 9819, 2003.

[12] M. Rekharsky and Y. Inoue, "Solvation Effects in Supramolecular Recognition," in *Supramolecular Chemistry: From Molecules to Nanomaterials*, Online, John Wiley & Sons, Ltd., 2012.

[13] M. Fujita *et al*., "Molecular paneling via coordination," *Chem. Commun.,* pp. 509-518, 2001.

[14] Y. Liu, V. C. Kravtsov, D. A. Beauchamp *et al.*, *J. Am. Chem. Soc.,* vol. 127, p. 7266–7267, 2005.

[15] Y. Liu, V. C. Kravtsov, Walsh, R. D. *et al.*, *Chem. Commun.,* vol. 24, pp. 2806-2807, 2004.

[16] M. J. Hardie, "Interlocked molecules: One-pot pentaknot," *Nature Chemistry,* vol. 4, pp. 7-8, 2012.

[17] A. Bianchi and E. García-España, "Thermodynamic Aspects of Anion Coordination," in *Anion Coordination Chemistry*, Online, Wiley-VCH Verlag GmbH & Co. KGaA, 2012.

[18] S. E. Wheeler and J. W. G. Bloom, "Anion–π interactions and positive electrostatic potentials of N-heterocycles arise from the positions of the nuclei, not changes in the π-electron distribution," *Chem. Commun.,* vol. 50, pp. 11118-11121, 2014.

[19] D. Quiñonero, A. Frontera and P. M. Deyá, "Anion–π Interactions in Molecular Recognition," in *Anion Coordination Chemistry*, Online, Wiley-VCH Verlag & Co., 2012.

[20] X. Lucas, A. Bauzá, A. Frontera and D. Quiñonero, "A thorough anion–π interaction study in biomolecules: on the importance of cooperativity effects," *Chem. Sci.,* vol. 7, pp. 1038-1.50, 2016.

[21] P. Gans, A. Sabatini and A. Vacca, *Talanta,* vol. 43, p. 1739–1753, 1996.

[22] G. Gran, *Analyst (London),* vol. 77, p. 661–671, 1952.

[23] F. P. Schmidtchen, “Isothermal Titration Calorimetry in Supramolecular Chemistry,” in *Supramolecular Chemistry: From Molecules to Nanomaterials*, Online, John Wiley & Sons, Ltd, 2012.

[24] A. Bianchi and E. García-España, “Azacycloalkanes and Azacyclophanes,” in *Supramolecular Chemistry: From Molecules to Nanomaterials*, Online, John Wiley & Sons, Ltd, 2012.

[25] G. P. Kotchey and A. Star, “Advances in Supramolecular Chemistry of Carbon,” in *Supramolecular Chemistry: From Molecules to Nanomaterials*, Online, John Wiley & Sons, Ltd., 2012.

[26] P. Serp and B. Machado, “Heterogeneous Catalysis on Nanostructured Carbon Material Supported Catalysts,” in *Nanostructured Carbon Material for Catalysis*, Cambridge, The Royal Society of Chemistry, 2015.

[27] M. Savastano, P. Arranz-Mascarós, C. Bazzicalupi, M. P. Clares, M. L. Godino-Salido, L. Guijarro, M. D. Gutiérrez-Valero, A. Bianchi, E. García-España and R. López-Garzón, “Polyfunctional Tetraaza-Macrocyclic Ligands: Zn(II), Cu(II) Binding and Formation of Hybrid Materials with Multiwalled Carbon Nanotubes,” *ACS Omega,* vol. 2, no. 7, pp. 3868-3877, 2017.

[28] K. Sonogashira, Y. Tohda and N. Hagihara, “A convenient synthesis of acetylenes: catalytic substitutions of acetylenic hydrogen with bromoalkenes, iodoarenes and bromopyridines,” *Tetrahedron Lett.,* vol. 16, p. 4467–4470, 1975.

[29] R. Chinchilla and C. Nájera, *Chem. Soc. Rev.,* vol. 40, p. 5084–5121, 2011.

[30] P. Iqbal, J. A. Preece and P. M. Mendes, “Nanotechnology: The “Top-Down” and “Bottom-Up” Approaches,” in *Supramolecular Chemistry: From Molecules to Nanomaterials*, Online, John Wiley & Sons, Ltd, 2012.

[31] M. Savastano, P. Arranz-Mascaros, C. Bazzicalupi, A. Bianchi, C. Giorgi, M. L. Godino-Salido, M. D. Gutierrez-Valero and R. Lopez-Garzon, “Binding and removal of octahedral, tetrahedral, square planar and linear anions in water by means of activated carbon functionalized with a pyrimidine-based anion receptor,” *RSC Adv.,* vol. 4, pp. 58505-58513, 2014.

[32] P. Arranz-Mascarós, C. Bazzicalupi, A. Bianchi, C. Giorgi, M. Godino-Salido, M. Gutiérrez-Valero, R. López-Garzón and M. Savastano, "Thermodynamics of Anion-π Interactions in Aqueous Solution," *J. Am. Chem. Soc.,* vol. 135, no. 1, pp. 102-105, 2013.

[33] E. Salvador-Serrano, M. Savastano and A. Bianchi, "Inorganic Mercury Sequestration by a Poly(ethylene imine) Dendrimer in Aqueous Solution.," *Molecules,* vol. 20, pp. 3783-3790, 2015.

[34] C. Bazzicalupi, A. Bianchi, C. Giorgi, M. Savastano and F. Morales-Lara, "ATP dephosphorylation can be either enhanced or inhibited by pH-controlled interaction with a dendrimer molecule.," *Chem. Commun.,* vol. 51, pp. 3907-3910, 2015.

[35] M. Savastano, C. Bazzicalupi, C. Giorgi, P. Gratteri and A. Bianchi, "Cation, Anion and Ion-Pair Complexes with a G-3 Poly(ethylene imine) Dendrimer in Aqueous Solution," *Molecules,* vol. 22, no. 5, p. 816, 2017.

[36] M. Savastano, P. Arranz-Mascarós, C. Bazzicalupi, M. P. Clares, M. L. Godino-Salido, M. D. Gutíerrez-Valero, M. Inclán, A. Bianchi, E. García-España and R. Lopez-Garzón, "Construction of green nanostructured heterogeneous catalysts via non-covalent surface decoration of multi-walled carbon nanotubes with Pd(II) complexes of azamacrocycles," *Journal of Catalysis,* vol. 353, pp. 239-249, 2017.

[37] B. Verdejo, A. Ferrer, S. Blasco, C. E. Castillo, J. González, J. Latorre, M. A. Máñez, M. García Basallote, C. Soriano and E. García-España, *Inorg. Chem.,* vol. 46, p. 5707–5719, 2007.

[38] M. Inclán, M. T. Albelda, J. C. Frías, S. Blasco, B. Verdejo, C. Serena, C. Salat-Canela, M. L. Díaz, A. García-España and E. García-España, *J. Am. Chem. Soc.,* vol. 134, p. 9644–9656, 2012.

[39] P. S. Pallavicini, A. Perotti, A. Poggi, B. Seghi and L. Fabbrizzi, *J. Am. Chem. Soc.,* vol. 109, p. 5139, 1987.

[40] M. P. Clares, C. Serena, S. Blasco, A. Nebot, L. del Castillo, C. Soriano, A. Domènech, A. V. Sánchez-Sánchez, L. Soler-Calero, J. L. Mullor, A. García-España and E. García-España, *J. Inorg. Biochem.,* vol. 143, p. 1–8, 2015.

[41] J. González, J. M. Llinares, R. Belda, J. Pitarch, C. Soriano, R. Tejero, B. Verdejo and E. García-España, *Org. Biomol. Chem.,* vol. 8, p. 2367–2376, 2010.

[42] P. Arranz, A. Bianchi, R. Cuesta, C. Giorgi, M. L. Godino, M. D. Gutiérrez, R. López and A. Santiago, *Inorg. Chem.,* vol. 49, pp. 9321-9332, 2010.

[43] F. Morales-Lara, M. J. Perez-Mendoza, D. Altmajer-Vaz, M. García-Roman, M. Melguizo, F. J. Lopez-Garzón and M. Domingo-García, *J. Phys. Chem. C,* vol. 117, p. 11647−11655, 2013.

[44] M. L. Godino-Salido, A. Santiago-Medina, P. Arranz-Mascarós, R. López-Garzón, M. D. Gutiérrez-Valero, M. Melguizo and F. J. López-Garzón, " Novel active carbon/crown ether derivative hybrid material for the selective removal of Cu(II) ions: the crucial role of the surface chemical functions," *Chem. Eng. Sci.,* vol. 114, pp. 94-104, 2014.

[45] M. L. Godino-Salido, M. D. Gutiérrez-Valero, R. López-Garzón, P. Arranz-Mascarós, A. Santiago-Medina, M. Melguizo, M. Domingo-García, F. J. López-Garzón, V. K. Abdelkader-Fernández, C. Salinas-Martínez de Lecea and M. C. Román-Martínez, "New hybrid materials based on the grafting of Pd(II)-amino complexes on the graphitic surface of AC: preparation, structures and catalytic properties," *RSC Advances,* vol. 6, pp. 58247-58259, 2016.

[46] X. Lucas, A. Bauzá, A. Frontera and D. Quiñonero, "A thorough anion–π interaction study in biomolecules: on the importance of cooperativity efects," *Chem. Sci.,* vol. 7, pp. 1038-1050, 2016.

[47] R. Smith and A. Martell, "NIST Stability Constants Database," Washington, 1997.

[48] S. Alvarez, "A cartography of the van der Waals territories," *Dalton Trans.,* vol. 42, pp. 8617-8636, 2013.

[49] Y. Marcus, *J. Chem. Thermodyn,* vol. 39, pp. 1338-1345, 2007.

[50] Hypercube Inc., "Hyperchem, Release 7.51 for Windows MM System," Gainesville, FL, USA, 2002.

[51] W. De-Xian and W. Mei-Xiang, *J. Am. Chem. Soc.,* vol. 135, pp. 892-897, 2013.

[52] H. Bing, L. Jianjiang and K. Jay, *Cryst. Growth Des.,* vol. 8, pp. 1327-1334, 2008.

[53] A. Reed, L. Curtiss and F. Weinhold, *Chem. Rev.,* vol. 88, pp. 899-926, 1988.

6 APPENDIX

In the following, full-texts of published papers within the framework of this thesis are provided.

The listing is in order of appearance of their quotations in the text, however a table of contents providing the title of each piece of research and the relative page number is provided below for the Reader's convenience.

ACS OMEGA

Article

http://pubs.acs.org/journal/acsodf

Polyfunctional Tetraaza-Macrocyclic Ligands: Zn(II), Cu(II) Binding and Formation of Hybrid Materials with Multiwalled Carbon Nanotubes

Matteo Savastano,[†] Paloma Arranz-Mascarós,[‡] Carla Bazzicalupi,[†] Maria Paz Clares,[§] Maria Luz Godino-Salido,[‡] Lluis Guijarro,[§] Maria Dolores Gutiérrez-Valero,[‡] Antonio Bianchi,*[,†] Enrique García-España,*[,§] and Rafael López-Garzón*[,‡]

[†]Department of Chemistry "Ugo Schiff", University of Florence, 50019 Sesto Fiorentino, Italy

[‡]Department of Inorganic and Organic Chemistry, University of Jaén, 23071 Jaén, Spain

[§]Institute of Molecular Science, University of Valencia, 46071 Valencia, Spain

Supporting Information

ABSTRACT: The binding properties of HL1, HL2, and HL3 ligands toward Cu(II) and Zn(II) ions, constituted by tetraaza-macrocyclic rings decorated with pyrimidine pendants, were investigated by means of potentiometric and UV spectrophotometric measurements in aqueous solution, with the objective of using the related HL-M(II) (HL = HL1−HL3; M = Cu, Zn) complexes for the preparation of hybrid MWCNT-HL-M(II) materials based on multiwalled carbon nanotubes (MWCNTs), through an environmentally friendly noncovalent procedure. As shown by the crystal structure of $[Cu(HL1)](ClO_4)_2$, metal coordination takes place in the macrocyclic ring, whereas the pyrimidine residue remains available for attachment onto the surface of the MWCNTs via $\pi-\pi$ stacking interactions. On the basis of equilibrium data showing the formation of highly stable Cu(II) complexes, the MWCNT-HL1-Cu(II) material was prepared and characterized. This compound proved very stable toward lixiviation processes (release of HL1 and/or Cu(II)); thus, it was used for the preparation of its reduced MWCNT-HL1-Cu(0) derivatives. X-ray photoelectron spectroscopy and transmission electron microscopy images showed that MWCNT-HL1-Cu(0) contains Cu(0) nanoparticles, of very small (less than 5 nm) and regular size, uniformly distributed over the surface of the MWCNTs. Also, the MWCNT-HL1-Cu(0) material proved very resistant to detachment of its components. Accordingly, both MWCNT-HL1-Cu(II) and MWCNT-HL1-Cu(0) are promising candidates for applications in heterogeneous catalysis.

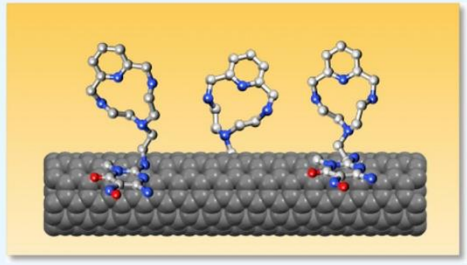

INTRODUCTION

In a recent work, we performed the synthesis of HL1 and HL2 ligands obtained via functionalization of the tetraaza-macrocyclic molecules **1** and **2** with a 6-amino-3,4-dihydro-3-methyl-5-nitroso-4-oxopyrimidine group (Figure 1).[1] Thanks to the ability of such pyrimidine residues to form strong $\pi-\pi$ stacking interactions with arene centers,[2] HL1 and HL2 were irreversibly absorbed onto the surface of multiwalled carbon nanotubes (MWCNTs) and the resulting hybrid materials (MWCNT-HL1, MWCNT-HL2) were further decorated with Pd(II) ions coordinated to the macrocyclic rings. The final products (MWCNT-HL1-Pd, MWCNT-HL2-Pd) were assayed as heterogeneous catalysts for the Cu-free Sonogashira coupling reaction, in which respect they revealed high efficiency, ranking among the best Pd(II)-based heterogeneous catalysts in terms of yields and reaction times, and an unprecedented ability to work under environmentally friendly conditions, such as in water at 50 °C and in an aerobic atmosphere.[1] Macrocyclic ligands were chosen to retain Pd(II) on the surface of MWCNTs because they form complexes with high thermodynamic stability and high kinetic inertness toward demetallation processes, characteristics that contribute to the robustness of the catalysts and favor their reusability.

In addition to their efficiency as active centers in many catalytic processes, metal ions fixed into the frames of macrocyclic ligands have proven useful for a variety of applications, including the construction of large self-assembled structures, molecular sensors, switches, motors, and machines; for mimicking biological processes; and for tissue and organ imaging, among others.[3] For this reason, and in consideration of the successful results given by the Pd(II)-based heterogeneous catalysts with HL1 and HL2, we decided to assay the

Received: June 6, 2017
Accepted: July 7, 2017
Published: July 25, 2017

DOI: 10.1021/acsomega.7b00736
ACS Omega 2017, 2, 3868−3877

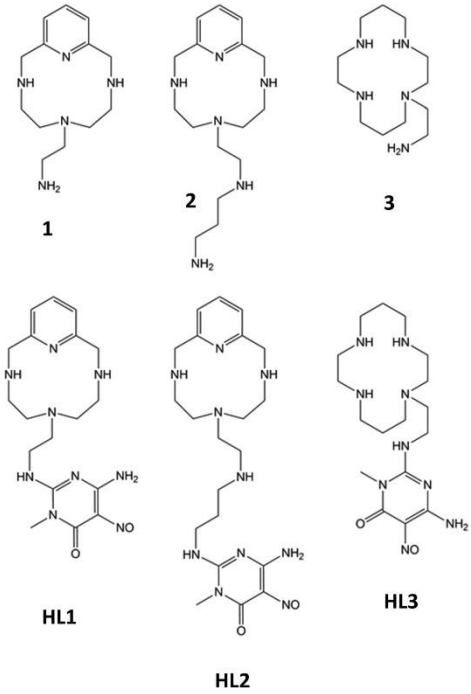

Figure 1. HL1, HL2, and HL3 ligands with their precursor molecules 1, 2, and 3.

binding ability of HL1 and HL2 toward other metal ions, and Zn(II) and Cu(II) were chosen, in view of their possible applications and on account of their implication as catalysts in a variety of reactions.[4−6] In this respect, the ability of a hybrid material of the MWCNT-HL1 type to adsorb Cu(II) and Zn(II) metal ions from aqueous solution was also tested. For the same purpose, we synthesized the analogous ligand HL3 (Figure 1), containing cyclam (1,4,8,11-tetraazacyclote-tradecane), the most typical tetraaza-macrocyclic molecule, and extended to this new ligand the coordination study with Zn(II) and Cu(II). Among tetraaza-macrocycles, cyclam is the one able to form metal complexes with utmost stability with many metal ions.[7] A potential catalyst based on Cu(0)-supported nanoparticles was generated from MWCNT-HL1-Cu(II).

RESULTS AND DISCUSSION

Crystal Structure of $[Cu(HL1)](ClO_4)_2$. The crystal structure consists of a one-dimensional (1D) coordination polymer, $\{[CuHL1]^{2+}\}_n$, built up by repeats of complex units. A segment of the 1D polymer is shown in Figure 2, evidencing the metal coordination sphere (selected bond angles and distances are listed in Table 1).

Table 1. Selected Bond Angles (deg) and Distances (Å) for the Crystal Structure of $[Cu(HL1)](ClO_4)_2$[a]

Cu−N4	2.068(5)
Cu−N1	2.324(5)
Cu−N3	1.933(5)
Cu−N2	2.060(6)
Cu−N8	2.003(5)
Cu−O1	2.534(4)
N4−Cu−N1	82.7(2)
N4−Cu−N3	82.3(2)
N4−Cu−N2	157.6(2)
N4−Cu−N8	107.6(2)
N4−Cu−O1	81.5(2)
N1−Cu−N3	97.4(2)
N1−Cu−N2	84.0(2)
N1−Cu−N8	108.4(2)
N1−Cu−O1	163.6(2)
N3−Cu−N2	81.7(2)
N3−Cu−N8	153.2(2)
N3−Cu−O1	84.9(2)
N2−Cu−N8	93.6(2)
N2−Cu−O1	112.4(2)
N8−Cu−O1	72.4(2)

[a]Symmetry relation for N8 and O1 atoms: $1 - x, y - 0.5, 1.5 - z$; e.s.d. in parentheses.

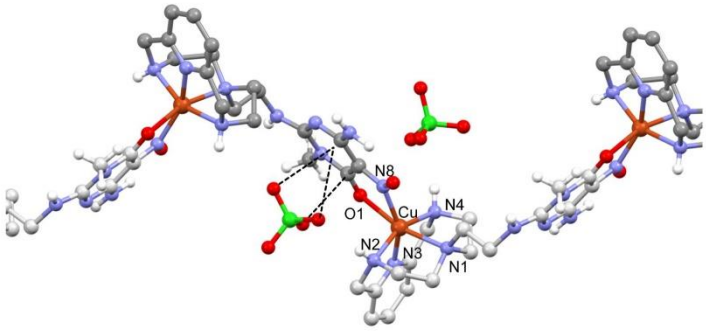

Figure 2. Segment of the 1D polymer in the crystal structure of $CuHL1(ClO_4)_2$ showing the metal coordination environment and the anion−π interaction of a perchlorate anion with the pyrimidine function of the ligand.

DOI: 10.1021/acsomega.7b00736
ACS Omega 2017, 2, 3868−3877

The copper atom is hexacoordinated by the four nitrogen atoms of the macrocycle and by the carbonyl oxygen and nitroso nitrogen belonging to the nitroso-amino pyrimidine group of a contiguous, symmetry-related ligand. The coordination sphere can be best described as a strongly distorted octahedron, whose axial distances, defined by the nitroso oxygen (O1) and the macrocyclic tertiary nitrogen (N1), are strongly elongated (Table 1). The equatorial plane is defined by the pyridine and the two secondary nitrogen atoms of the macrocycle, together with the nitroso nitrogen from the pyrimidine ring of the contiguous symmetry-related ligand. It is to be underlined that although the coordination of the nitroso nitrogen clearly acts on the electron distribution in the pyrimidine ring system, giving a remarkable shortening of the N=O bond and a lengthening of the N−C bond, the coordination of the carbonyl oxygen does not determine the weakening of the C=O bond, which is even shorter than the corresponding mean bond length of free C=O (1.205(7) Å vs 1.22(2) Å for C=O and 1.26(3) Å for C=O−M bonds). The head-to-tail disposition of the ligands in the chain is due to the 2_1 screw axes, running parallel to the *b* axis and determining an overall helical fashion for the coordination polymer.

Similarly to the crystal structures previously reported for metal complexes obtained with the 3,6,9-triaza-1-(2,6)-pyridinecyclodecaphane macrocycle functionalized on its 6 position,[8] the macrocycle adopts a bent conformation, which leaves the metal coordination sphere unsaturated. In these structures, however, the macrocycle and the pendant arm containing donor atoms are involved in the coordination of the same metal center and isolated complexes are invariably formed. Instead, in the $\{[CuHL1]^{2+}\}_n$ polymer, the pendant arm and the macrocycle do not coordinate with the same metal ion so that the pyrimidine ring protrudes outside, and the metal coordination positions not saturated by the macrocycle are occupied by exogenous species.

Electroneutrality is achieved by the presence of two perchlorate anions in the asymmetric unit. One of them strongly interacts with the nitroso pyrimidine group via anion−π interactions with three out of four oxygen atoms (Table S1). Remarkably, one of the strongest anion−π interactions ever observed was reported for a ligand (L) containing this nitroso-amino pyrimidine group functionalized with a tren (tris(2-aminoethyl)amine) moiety. In the crystal structure of the $\{H_4L[Co(CN)_6]\}\cdot 2H_2O$ compound, the nitrogen atom of a cyanide ion of $[Co(CN)_6]^{3-}$ was found 2.786 Å apart from the ring centroid.[9] In this structure, as well as in those obtained for the same ligand with $HgCl_4^{2-}$, $HgBr_4^{2-}$, and CdI_4^{2-}, the anions are pretty well localized above the ring centroid,[9] whereas in $[Cu(HL1)](ClO_4)_2$, the ClO_4^--pyrimidine interaction appears dominated by the contact of one perchlorate oxygen with the carbonyl C atom of the pyrimidine ring. The O11···C17 contact distance (2.872(8) Å) is almost coincident with the O···ring plane distance (2.882 Å). The O13 and O14 oxygen atoms are 3.238 and 3.813 Å apart from the ring centroid and can be considered localized on the ring periphery, having offsets of 0.81 and 2.13 Å, respectively.

Acid−Base Properties of HL3. Potentiometric (pH-metric) titrations performed in aqueous solution (0.1 M Me_4NCl, 298.1 K) in the pH range of 2.5−11.5 showed that HL3 contains four groups undergoing protonation and an acidic group that starts being deprotonated above pH 10. Table 2 lists the equilibrium constants determined for these processes in the form of protonation constants.

Table 2. Protonation Constants of Ligands HL1, HL2, and HL3 (L) in 0.1 M NMe_4Cl at 298.1 ± 0.1 K

	log *K*		
equilibria	HL1[a]	HL2[a]	HL3
$L^- + H^+ = HL$	11.13(4)[b]	11.21(5)	11.22(3)
$HL + H^+ = H_2L^+$	9.28(5)	9.71(4)	10.43(3)
$H_2L^+ + H^+ = H_3L^{2+}$	7.83(7)	8.64(6)	8.55(4)
$H_3L^{2+} + H^+ = H_4L^{3+}$	2.3(1)	7.51(6)	3.23(5)
$H_4L^{3+} + H^+ = H_5L^{4+}$	1.6(5)	2.2(1)	1.99(5)
$H_5L^{4+} + H^+ = H_6L^{5+}$		1.6(5)	

[a]Taken from ref 1. [b]Values in parentheses are standard deviations of the last significant figures.

For the sake of comparison, the table includes the protonation constants previously determined for HL1 and HL2. A distribution diagram of the protonated species formed as a function of pH is reported in Figure S1. The protonation behavior of HL3 is consistent with that of HL1 and HL2, in particular with that of HL1, which is structurally more similar to HL3 (Figure 1). Accordingly, the protonation stage occurring at the highest pH (log *K* = 11.22, Table 2) can be ascribed to the nitrogen atom of the chain directly connected to the pyrimidine ring, which is expected to be deprotonated at a high pH, whereas protonation occurring at the lowest pH (log *K* = 1.99, Table 2) involves the pyrimidine nitroso group. This behavior is confirmed by the pH dependence of the absorption spectra of HL3. Indeed, the near-UV spectra of HL3 are characterized by three bands centered at about 328, 276, and 230 nm (Figure 3) corresponding to allowed $\pi-\pi^*$ transitions between the π-orbitals of the pyrimidinic group and overlapping with the band at about 265 nm of the pyridinic one. The spectra show a significant pH dependence in acidic and alkaline solutions when protonation involves the pyrimidine chromophore, whereas they are almost invariant in the pH region 4.6−10 when protonation takes place on the non-chromogenic aliphatic amine groups. Very similar spectral features were found for HL1 and HL2.[1]

The highly protonated H_5L3^{4+} species is formed only in small amounts in the lower-pH region we have investigated (Figure S1). Nevertheless, the detection of this species is an important result revealing that, as previously observed for HL1 and HL2 as well as for HL3, three out of the four nitrogen atoms of the macrocyclic ring can undergo protonation in the studied pH range.

Formation of Metal Complexes in Solution. The equilibrium constants for the formation of Zn(II) and Cu(II) complexes with HL1, HL2, and HL3, determined in aqueous solution (0.1 M Me_4NCl, 298.1 K) by means of potentiometric (pH-metric) titrations, are listed in Table 3. In the case of the Cu(II) complexes with HL3, because of the slowness of both complexation and dissociation reactions, we were able to study the system in a restricted pH range (2.5−8) and after special manipulation of the samples (see Experimental Section). For this reason, larger errors were obtained for the determined stability constants. Distribution diagrams for the formation of these complexes are presented in Figure S2. In terms of the species formed, the three ligands (HL = HL1, HL2, HL3) give rise to identical complex systems with Zn(II), constituted by ZnL^+, $ZnHL^{2+}$, ZnH_2L^{3+}, and ZnLOH species, whereas in the case of Cu(II), there are some differences. In particular, HL1 forms $CuL1^+$, $CuHL1^{2+}$, CuH_4L1^{5+}, and CuL1OH, whereas HL2 forms $CuL2^+$, $CuHL2^{2+}$, CuH_2L2^{3+}, and CuH_5L2^{6+}. HL3

DOI: 10.1021/acsomega.7b00736
ACS Omega 2017, 2, 3868−3877

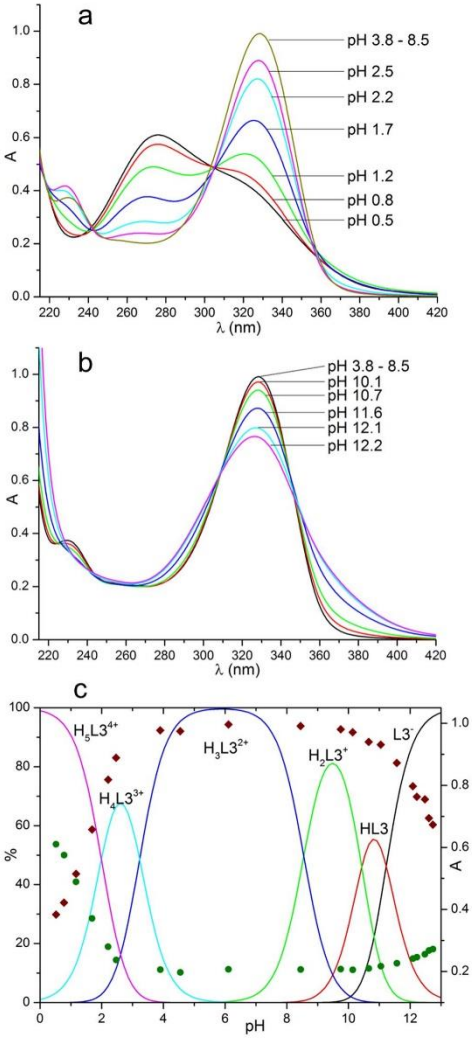

Figure 3. UV absorption spectra of HL3 at different pHs in aqueous solution: (a) pH 0.5−8.5, (b) pH 8.5−12.2, and (c) pH dependence of the 330 nm (red diamonds) and 265 nm (green dots) absorbances.

forms the same species of HL1 with the exclusion of the tetraprotonated one. Such differences are justified by the different numbers of donor atoms in the ligands and, in the case of Cu(II), by the greater stability of the complexes with HL3. Indeed, HL1 and HL3, which can provide at most five donor atoms, are not able to fulfill the coordination sphere of the metal ions, and deprotonation of a coordinated water molecule gives rise to MLOH complexes in alkaline media. On the other hand, HL2, containing one more donor atom, does not form a similar hydroxylate species with Cu(II), whereas the corresponding Zn(II) species is significantly less stable than the hydroxylated complexes formed by HL1 and HL3 (Table 3). The most peculiar feature of these complex systems, however, is the gap of protonation states observed for the Cu(II) systems between $CuHL1^{2+}$ and CuH_4L1^{5+}, in the case of HL1, and between CuH_2L2^{3+} and CuH_5L2^{6+}, for HL2 (Table 3, Figure S2). In CuH_4L1^{5+} and CuH_5L2^{6+}, the metal ion is expected to be bound by the pyrimidine group in a chelating mode similar to that observed in the crystal structure of $[Cu(HL1)](ClO_4)_2$, while the macrocyclic ring, being triprotonated, is not able to bind metal ions. As a matter of fact, these highly protonated complexes are formed in very acidic solutions. When the pH is increased and the macrocycle starts releasing the most acidic proton, Cu(II) migrates from the pyrimidine binding site to the macrocycle, forcing the deprotonation of the remaining ammonium groups. Most likely, such a triple deprotonation process does not occur in a single step but takes place through successive equilibria occurring in a pH range so tight that they are not distinguishable, at least by means of the potentiometric method. This is a case of pH-controlled metal translocation similar to that observed with macrocyclic ligands containing divergent binding sites.[10]

Table 3. Stability Constants of the Complexes Formed by HL1 and HL2 with Cu^{2+}, Zn^{2+}, and Pd^{2+} in 0.1 M NMe_4Cl at 298.1 ± 0.1 K

equilibria	log *K*		
L =	HL1	HL2	HL3
$L^- + Zn^{2+} = [ZnL]^+$	16.3(1)[a]	17.8(1)	19.0(1)
$HL + Zn^{2+} = [ZnHL]^{2+}$	12.62(5)	16.65(6)	13.1(1)
$H_2L^+ + Zn^{2+} = [ZnH_2L]^{3+}$	7.1(1)	11.3(1)	7.8(1)
$[ZnL]^+ + H^+ = [ZnHL]^{2+}$	7.4(1)	10.1(1)	5.3(1)
$[ZnHL]^{2+} + H^+ = [ZnH_2L]^{3+}$	3.8(1)	4.4(1)	5.1(1)
$[ZnL]^+ + OH^- = [ZnLOH]$	4.4(1)	2.8(1)	7.0(2)
$L^- + Cu^{2+} = [CuL]^+$	22.59(6)	21.2(1)	26.0(3)
$HL + Cu^{2+} = [CuHL]^{2+}$	15.65(5)	20.21(9)	18.6(3)
$H_2L^+ + Cu^{2+} = [CuH_2L]^{3+}$		14.74(7)	
$H_4L^{3+} + Cu^{2+} = [CuH_4L]^{5+}$	3.6(2)		
$[CuL]^+ + H^+ = [CuHL]^{2+}$	4.19(6)	10.2(1)	3.9(5)
$[CuHL]^{2+} + H^+ = [CuH_2L]^{3+}$		4.2(1)	
$H_5L^{4+} + Cu^{2+} = [CuH_5L]^{6+}$		3.7(2)	
$[CuL]^+ + OH^- = [CuLOH]$	4.16(8)		7.2(5)

[a]Values in parentheses are standard deviations of the last significant figures.

The UV spectra of the ligands in the presence of metal ions, recorded at various pH values, are shown in Figure 4 for HL2 with Zn(II) and in Figures S3−S5 for the other systems. A comparison of complex spectra with those of the metal-free ligands shows that the 330 nm absorbance is insensitive to the presence of metal ions, whereas the band at 265 nm, due to the pyridine moiety, is enhanced within the entire pH region in which metal complexation takes place, indicating that the pyridine nitrogen atom is involved in the formation of all complex species (Figures 5 and S6). In the case of Cu(II) complexes (Figures 5b and S6b), however, this enhancement is present even in very acidic solutions because, under such conditions, the formation of CuH_4L1^{5+} and CuH_5L2^{6+}, in which the metal ion is coordinated to the pyrimidine residue, enhances the absorbance due to this chromophoric group also occurring at about 260 nm. The profile of the pH dependence of this band is indicative of metal translocation occurring from

DOI: 10.1021/acsomega.7b00736
ACS Omega 2017, 2, 3868−3877

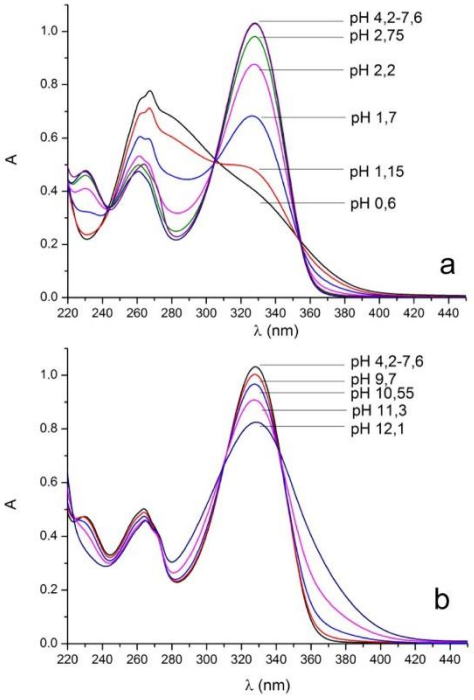

Figure 4. UV spectra of HL2 complexes with Zn^{2+} in the pH ranges 0.6−7.6 (a) and 7.6−12.1 (b). $[Zn^{2+}] = [HL2] = 5 \times 10^{-5}$ M. UV spectra for other complex systems are reported in Figures S3 and S4.

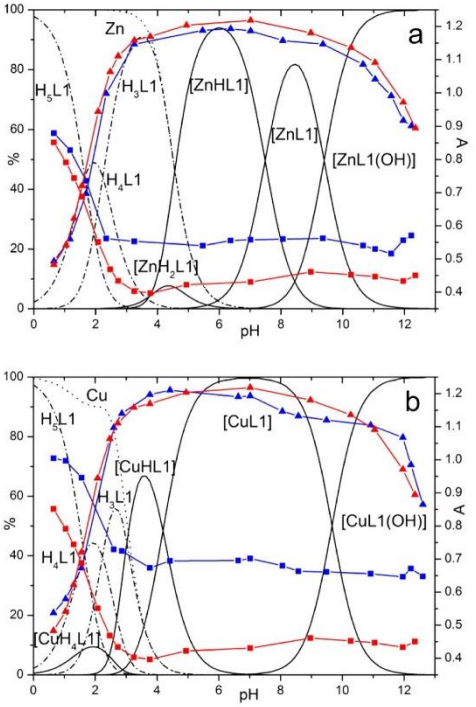

Figure 5. pH dependence of the 330 nm (triangles) and 265 nm (squares) absorbances of HL1 in the absence (red) and presence (blue) of Zn^{2+} (a) and Cu^{2+} (b) superimposed to the relevant species distribution diagrams. $[M^{2+}] = [L] = 5 \times 10^{-5}$ M. Species charges have been omitted for simplicity.

pyrimidine to the macrocyclic (pyridine) sites with increasing pH.

As already noted above, for HL3, we did not observe the formation of Cu(II) complexes in a high protonation state, such as CuH_4L1^{5+} for HL1, in which the metal ion is chelated by the pyrimidine group. Because of the greater stability of the complexes formed by HL3, a release of the Cu(II) ion from the macrocyclic ring takes place in more acidic solutions (below pH 3), relative to HL1. Accordingly, the hypothetical CuH_4L3^{5+} species, is not expected to form in appreciable amounts above pH 2.5, which is the lower pH limit useful for our pH-metric titrations. Nevertheless, we cannot exclude the formation of such species below pH 2.5, although under similar acidic conditions, protonation of the nitroso group becomes an additional impediment.

HL2 binds the two metal ions forming more stable complexes than HL1 and HL3 (Table 3), in agreement with the presence of one more amine group in its lateral chain. In the case of HL1, it is possible to perform a comparison with the coordination properties of the parent ligand **1**,[8c,11] evidencing that the stability of the $ZnHL1^{2+}$ ($\log K = 12.6$) and $CuHL1^{2+}$ ($\log K = 15.48$) complexes is significantly lower than that of the analogous complexes $Zn\mathbf{1}^{2+}$ ($\log K = 17.42$)[11] and $Cu\mathbf{1}^{2+}$ ($\log K = 20.43$, ref 8c), in agreement with the loss of coordinating ability experienced by the primary nitrogen of **1** (Figure 1) upon functionalization with the pyrimidine residue. As a matter of fact, in the crystal structure of $CuHL1(ClO_4)_2$, this amine group is not involved in the coordination to the metal ion, which completes its coordination environment by chelate binding of the pyrimidine residue of an adjacent complex molecule. Nonetheless, when this functionalized nitrogen undergoes deprotonation, enhancing its coordinating ability, the complex stability increases (Table 3). This phenomenon is much less evident for HL2, as the additional amine group in the lateral chain is already coordinated when the nitrogen atom directly bound to the pyrimidine group becomes deprotonated. The involvement of this deprotonated amine group in metal coordination can be assessed by comparing the equilibrium constants for the protonation of free and complexed ligands according to the general equilibria $L^- + H^+ = HL$ and $ML^+ + H^+ = MHL^{2+}$ (L = L1, L2, L3; M = Zn, Cu). In the case of HL2, complex protonation constants ($\log K = 10.42$ for $ZnL2^+$, $\log K = 10.5$ for $CuL2^+$, Table 3) are very similar to the protonation constant of $L2^-$ ($\log K = 11.25$, Table 2), indicating that the group being protonated is free, whereas in the case of HL1, a similar comparison shows that complex protonation takes place on a coordinated group ($\log K = 7.4$ for $ZnL1^+$, $\log K = 4.02$ for $CuL1^+$, $\log K = 5.3$ for $ZnL3^+$, $\log K =$

DOI: 10.1021/acsomega.7b00736
ACS Omega 2017, 2, 3868−3877

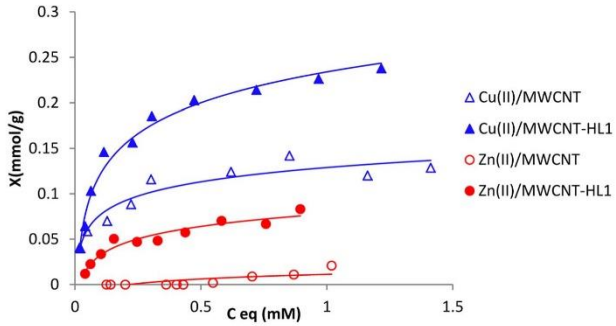

Figure 6. Adsorption isotherms of Cu(II) and Zn(II) on MWCNT and MWCNT-HL1 adsorbents at pH 5.0.

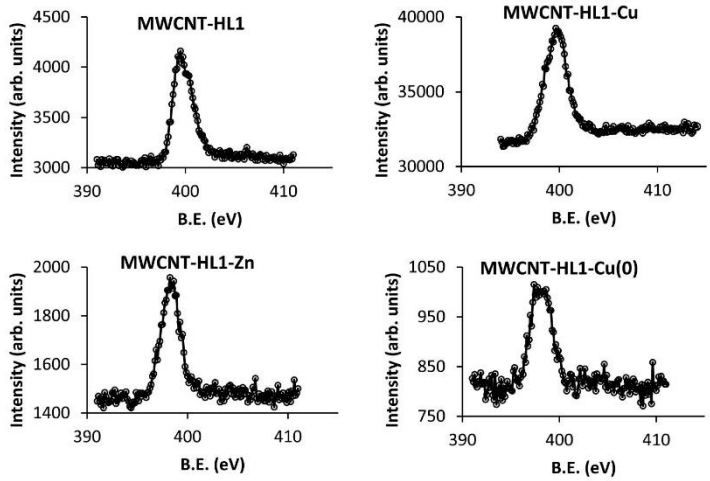

Figure 7. High-resolution XPS spectra in the N1s region.

3.9 for $CuL3^{+}$ vs $\log K$ = 11.13 for $L1^{-}$ and $\log K$ = 11.22 for $L3^{-}$).

Adsorption of Cu(II) and Zn(II) by MWCNT-HL1. To explore the ability of MWCNTs functionalized with these macrocyclic ligands to adsorb metal ions other than the already studied Pd(II), which forms very stable and inert complexes, we checked the MWCNT-HL1/Cu(II) and MWCNT-HL1/Zn-(II) systems. According to a reported procedure,[1] hybrid MWCNT-HL1 material, containing 0.36 mmol of HL1 per gram of MWCNT, was prepared by shaking at 298 K a suspension of MWCNT (0.5 g) in an aqueous 10^{-3} M HL1 solution (500 cm^3) at pH 7.5 for 3 days to reach the maximum load of HL1. The MWCNT-HL1 material, resulting after filtration of the equilibrated suspension, water washing, and drying, was employed for the Cu(II) and Zn(II) adsorption tests.

The adsorption isotherms of Cu(II) and Zn(II) ions on MWCNTs and MWCNT-HL1 adsorbents, obtained in water at 298.1 K and pH = 5.0, are shown in Figure 6. The analysis of the equilibrium solutions allowed us to check that HL1 was not desorbed in the experiments involving MWCNT-HL1. All of the adsorption isotherms were fit to the linear form of the Langmuir eq 1 (except that of the MWCNT/Zn(II) system, see below), where C_e is the adsorbate equilibrium concentration, X is the amount adsorbed, X_m is the maximum adsorption capacity, and K_L is the Langmuir constant.

$$\frac{1}{X} = \frac{1}{K_L X_m C_e} + \frac{1}{X_m} \quad (1)$$

As shown in Figure 6, at pH = 5.0, the pristine MWCNTs bind Cu(II) to a significant extent, with a maximum adsorption capacity, calculated from the above equation, X_m = 0.13(1) mmol/g of adsorbent. In contrast, in the case of Zn(II), the adsorption is insignificant. The results can be explained by considering that the adsorption of a metal ion from aqueous solution onto a graphene surface takes place by interactions of the Cπ(a soft base)−dπ type,[12] which is expected to be stronger for the acidic Cu(II) than for Zn(II).

The Cu(II) and Zn(II) loads increase significantly upon functionalization of the MWCNTs with HL1. In the case of

DOI: 10.1021/acsomega.7b00736
ACS Omega 2017, 2, 3868−3877

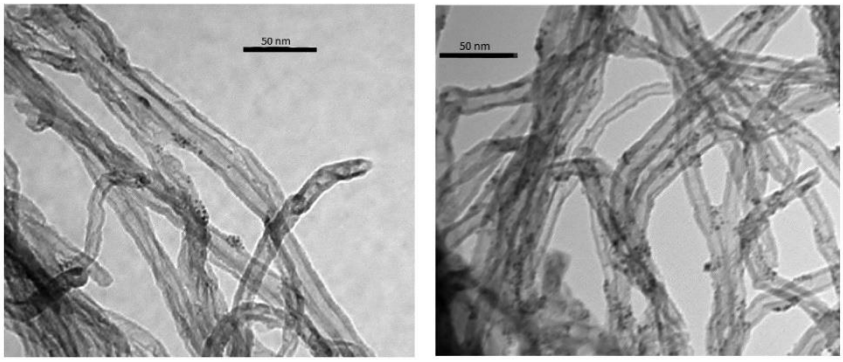

Figure 8. TEM Images of MWCNT-HL1-Cu(0).

Cu(II), the X_m value increases up to 0.24(1) mmol/g, relative to MWCNT-HL1, whereas in the case of Zn(II), it also increases significantly from ca. 0 to 0.080(4) mmol/g (Figure 6). In a previous work,[1] the characterization of MWCNT-HL1 showed that $\pi-\pi$ stacking interaction of the pyrimidine moiety of the adsorbed HL1 with the Cπ centers of MWCNT results in the loss of (Brönsted) basicity by the pyrimidine conjugate C(5)-NO group, whereas the basicity of the polyamine function is preserved to a good extent, allowing the adsorption, via complexation, of Pd(II) ions by MWCNT-HL1.[1] Accordingly, also the adsorptivity enhancement observed for MWCNT-HL1 with Cu(II) and Zn(II), relative to pristine MWCNT, is expected to occur via metal coordination to the macrocyclic moiety of HL1. Indeed, like in the case of Pd(II), upon adsorption of Cu(II) by MWCNT-HL1, the aliphatic component of the X-ray photoelectron spectroscopy (XPS) N1s signal corresponding to the polyamine moiety (Figure 7) shifts to higher binding energy (BE) values, compared to those of the metal-free MWCNT-HL1, in agreement with the high strength of the Cu(II)−polyamine interaction (Table 3). On the contrary, in the case of MWCNT-HL1-Zn(II), the N1s component of the XPS spectrum shifts to lower BE values. The latter effect, which is the opposite to that observed with Cu(II) and Pd(II),[1] can be ascribed to the fact that the binding of Zn(II) to HL1 polyamine nitrogen atoms in MWCNT-HL1-Zn is weaker than the binding of protons by MWCNT-HL1 at the working pH (5). In fact, the equilibrium data for the HL1-Zn(II) system (Table 3 and Figure 5) show that, at pH = 5, ligand protonation competes efficiently with Zn(II) coordination.

The presence, in the Cu2p range of the XPS spectrum of MWCNT-HL1-Cu(II), of a single peak at 933.6 eV with a satellite at 944.0 eV (corresponding to the release of $Cu2p_{3/2}$ electrons) and of another peak at 953.9 eV (assigned to $Cu2p_{1/2}$ electrons), typical of Cu(II),[13] discards any metal reduction during the adsorption process and suggests that all copper is adsorbed as Cu(II) coordinated to the polyamine (Supporting Information). In the case of MWCNT-HL1-Zn(II), the presence of Zn(II) is confirmed by a well-defined XPS signal at 1020.1 eV corresponding to the release of $Zn^2p_{3/2}$ electrons (Supporting Information).

According to the equilibrium data (Table 3) for the formation of HL1 complexes with Cu(II), the ligand environment of the coordinated Cu(II) in MWCNT-HL1-Cu(II) should be formed by four polyamine nitrogen atoms, which leave space for the additional coordination of water molecules or/and hydroxyl groups. The presence of hydroxyl ligands coordinated to Cu(II) in MWCNT-HL1-Cu(II) is suggested by the quantitative analysis of its XPS spectrum, which provides an atomic relationship, Cu/Cl ≈ 2/1. As charge neutrality requires two negative charges for each Cu(II) in the sample, it seems likely that the missing Cl^- ions were replaced by OH^- groups upon the repeated washing of MWCNT-HL1-Cu(II) performed in the final stage of its preparation (see Experimental Section). A similar conclusion is reached in the case of MWCNT-HL1-Zn(II), for which the Zn/Cl atomic relationship obtained from its XPS spectrum is also ≈2/1. Thus, Zn(II) adsorbed in this material should be complexed by the ligand polyamine moiety (although more weakly coordinated than in the case of Cu(II)) and by additional water molecules and/or hydroxyl groups.

Metal-ion adsorption by a polyamine-complexation mechanism explains that the X_m values of MWCNT-HL1 with Zn(II) and Cu(II) at pH = 5.0 follow the same trend of the corresponding effective stability constants (K_{eff})[14] at this pH ($\log K_{eff}$ = 4.48 for Zn(II) and $\log K_{eff}$ = 9.33 for Cu(II)). In the case of other metal ions, such as Pd(II), which is expected to form more stable complexes with HL1[1] than Zn(II) and Cu(II), the adsorption capacity of MWCNT-HL1 is also much higher.[1]

In previous works,[1,15] we studied the behavior of Pd catalysts based on Pd(0) nanoparticles and Pd(II) supported on: (i) an activated carbon functionalized with a tren-derivative ligand and (ii) the MWCNT-HL1 and MWCNT-HL2 materials used in this work. In these studies, it was found that the catalytic efficiency and the robustness of the catalysts increase with the binding ability of surface functions.[1,15] On this background and on account of the implication of Cu-based nanoparticles as catalysts in a wide range of reactions,[4] we found it interesting to test the possibility of obtaining functionalized MWCNTs with surface-stabilized Cu(0) nanoparticles using our hybrid materials. To this purpose, a MWCNT-HL1-Cu(II) sample was treated with $NaBH_4$ by following the procedure described in Experimental Section. The XPS of this sample showed the lack of Cu(II) peaks and the appearance of two peaks at 951.0 and 930.1 eV corresponding to $Cu(0)2p_{1/2}$ and $Cu(0)2p_{3/2}$,[13]

DOI: 10.1021/acsomega.7b00736
ACS Omega 2017, 2, 3868−3877

indicating a quantitative reduction of Cu(II) to Cu(0) (Supporting Information). This reduction is also accompanied by a loss of oxygen from 2.75 to 2.15 atom %, which can be ascribed to the removal of water and hydroxyl ligands. It is very significant that the nitrogen content after reduction remains unchanged (3.09 and 3.04 atom % for unreduced and reduced MWCNT-HL1-Cu, respectively) as also occurs for the Cu one (0.35 and 0.34 atom % for unreduced and reduced MWCNT-HL1-Cu, respectively). This shows that, despite the relatively drastic conditions used for the reduction, neither HL1 nor Cu lixiviate during sample reduction and successive repeated washing, pointing out a significant stability of the material. This is not surprising, according to the proven stability of the $\pi-\pi$ interactions in similar systems.[2] Concerning the Cu(0) nanoparticles, their interactions with the MWCNT surface, illustrated by the transmission electron microscopy (TEM) images in Figure 8, are reinforced by interaction with the polyamine residue of HL1 molecules protruding from the surface. As a matter of fact, shifting of the XPS N1s signal to a significantly lower BE, relative to MWCNT-HL1, suggests that the unprotonated polyamine residues of MWCNT-HL1-Cu(0) interact with the surface Cu(0) nanoparticles.[15] It is noteworthy that the result obtained by XPS analysis for the Cu(0) content of the reduced sample is equal to the Cu(II) content of the parent MWCNT-HL1-Cu(II), meaning that such Cu(0) nanoparticles should be very small. Actually, because of the low penetrating power of the radiation used in the XPS analysis, an accurate quantitative determination of metal from nanoparticles, by this technique, is only possible for very small nanoparticles (the bigger the nanoparticle, the lower the amount of metal detected compared to the real one). Indeed, the detected nanoparticles are smaller than 5 nm. This is illustrated in Figure 8, which also shows the uniformity of their size and distribution on the external surface of the MWCNTs.

The whole results obtained in this section show that the structural characteristics and the stability of both MWCNT-HL1-Cu(II) and MWCNT-HL1-Cu(0) make them promising Cu-based materials to be assayed as potentially active and robust solid catalysts.

CONCLUSIONS

In summary, the results of this work show that metal-ion adsorption by materials of the MWCNT-HL1 type represents a suitable procedure for the preparation of heterogeneous catalysts based on HL1−metal complexes adsorbed on the MWCNT surface. The preparation procedure, which is characterized by very mild, environmentally friendly conditions, provides an efficient control for MWCNT surface functionalization, which is a crucial factor for an efficient transfer of the catalytic properties of the HL1−metal complex to the MWCNT surface.

The adsorption results show how the reactivity of the polyamine function of HL1 toward Zn(II) and Cu(II) determines the preferential adsorption of these ions on MWCNT-HL1 via coordination to HL1. This determines a higher adsorption capacity for Cu(II) than for Zn(II) and gives rise to hybrid materials consisting of MWCNTs containing HL1-Cu(II) and HL1-Zn(II) complexes homogeneously distributed on the external graphene surface of the MWCNTs. In view of our previous results, showing high catalytic efficiency of an analogous Pd(II) derivative, and taking into account the high thermodynamic stability of the Cu(II) complex, we expect that MWCNT-HL1-Cu(II) might behave as a robust and reusable catalyst for reactions in which Cu(II)-based catalysts have proven their efficiency.[4] Moreover, reduction of MWCNT-HL1-Cu(II) provides a Cu(0)-nanostructured MWCNT hybrid material, whose structure and stability are very promising for its application in reactions requiring Cu(0)-based catalysts. This will be the focus of further research work.

EXPERIMENTAL SECTION

Materials. Unless otherwise specified, all starting materials were purchased from commercial sources and used as supplied. Thin MWCNTs with metal oxide content ≤5% were purchased from Nanocyl (Ref 3100). HL1 and HL2 were obtained according to a previously reported synthetic procedure.[1] The MWCNT-HL1 hybrid material was prepared as previously reported.[1]

Synthesis of HL3. HL3 was prepared by the reaction of 1,4,8,11-tetraazacyclotetradecane-1-ethanamine[16] (**3** in Figure 1) with 6-amino-3,4-dihydro-3-methyl-2-methoxy-5-nitroso-4-oxopyrimidine according to the procedure previously described[1] for the synthesis of HL1 and HL2. Yield 95%. $C_{18.5}H_{31}N_9O_{3.5}$ (HL3·0.5MeOH·H_2O): calcd C 51.02, H 7.18, N 28.94; found C 50.93, H 7.19, N 28.70. ^{1}H NMR D_2O: δ (ppm) 2.62−3.46 (m, 13H), 3.74 (t, 2H), 4.55 (s, 4H), 7.37 (d, 2H), 7.88 (t, 1H).

Synthesis of [Cu(HL1)](ClO$_4$)$_2$. Crystals of the complex suitable for X-ray analysis were obtained by slow evaporation at room temperature of an ethanolic solution containing HL1 and $Cu(ClO_4)_2\cdot 6H_2O$ in equimolar amounts. **Caution!** Perchlorate salts of metal complexes are potentially explosive. Only a small amount of material should be prepared and handled with care.

Potentiometric Measurements. Potentiometric (pH-metric) titrations, used to determine ligand protonation and complex stability constants, were performed in 0.1 M NMe_4Cl at 298.1 ± 0.1 K using an automated apparatus and a procedure previously described.[17] The combined Metrohm 6.0262.100 electrode was calibrated as a hydrogen-ion concentration probe by titrating previously standardized amounts of HCl with CO_2-free NaOH solutions and determining the equivalent point by Gran's method,[18] which gives the standard potential, $E°$, and the ionic product of water (pK_w = 13.83(1) in 0.1 M NMe_4Cl at 298.1 K). Computer program HYPERQUAD[19] was used to calculate ligand protonation and complex stability constants from potentiometric data. The concentration of the ligands was about 1×10^{-3} M, whereas the concentration of metal ions (M) was [M] ≈ 0.8[L]. The studied pH range was 2.5−11.5, unless otherwise noted. Both complex formation and dissociation reactions of HL3 with Zn(II) and Cu(II), occurring during the potentiometric titrations, appeared to be very slow, although the dissociation processes were much faster than the formation ones. For this reason, these systems were studied following complex dissociation, that is, by performing the potentiometric titrations from alkaline to acidic conditions. In the case of Zn(II), the alkaline solution of the complex was prepared in the potentiometric cell and the pH variation was monitored until equilibrium was reached (2 h). Then, the solution was titrated with a standardized HCl solution. A duration of 45 min was necessary to reach the equilibrium after each addition. In the case of Cu(II), 2 days were necessary to reach the equilibrium of the starting solution. Accordingly, the alkaline complex solution was prepared in a separate vessel, stored in an inert atmosphere, left to equilibrate for 2 days at 298 K, and then transferred into the titration cell. The measurement was performed as in the case of Zn(II) but with

DOI: 10.1021/acsomega.7b00736
ACS Omega 2017, 2, 3868−3877

an elapsed time of 2 h between successive titrant (acid) additions. In the case of Cu(II), the pH range investigated was 2.5−8. At least two measurements were performed for each system, both for ligand protonation and for metal-ion-complexation experiments. For all systems, the different titration curves were treated as separated curves without significant variations in the values of the calculated stability constants. Finally, the sets of data were merged and treated simultaneously to give the final stability constants. Different equilibrium models for the complex systems were generated by eliminating and introducing different species. Only those models for which the HYPERQUAD program furnished a variance of the residuals $\sigma^2 \leq 9$ were considered acceptable. Such a condition was unambiguously met by a single model for each system.

Spectrophotometric Measurements. Absorption spectra were recorded at 298 K on a Jasco V-670 spectrophotometer. The concentrations of both ligand and metal complex solutions were about 5×10^{-5} M. ^{1}H NMR spectra (400 MHz) in D_2O solution were recorded at 298 K on a 400 MHz Bruker Avance III spectrometer.

Crystallography. Crystallographic data for CuHL1-$(ClO_4)_2$: $C_{18}H_{27}Cl_{12}CuN_9O_{10}$, MW = 663.94, orthorhombic, *Pbca*, a = 14.2264(4) Å, b = 18.2109(5) Å, c = 18.9638(5) Å, V = 4913.1(2) Å^3, Z = 8, ρ_{calcd} = 1.795 g cm^{-3}, μ (Cu Kα) = 3.938 mm^{-1}, T = 150 K, $R1$ = 0.0595 (for 2479 reflections with $I > 2s(I)$), w$R2$ = 0.1010 (all data), and GOF = 1.025. The crystals gave poor diffraction, so the resolution was limited to theta max = 62°. Data collection was carried out using an Oxford Diffraction XcaliburPX instrument equipped with a copper anode (λ = 1.5418 Å). A summary of the crystallographic data is reported in Table S2. The integrated intensities were corrected for Lorentz and polarization effects and absorption correction was applied.[20] The structure was solved by direct methods (SIR92).[21] Refinement was performed by means of full-matrix least-squares using SHELXL-2014/7 program.[22] All nonhydrogen atoms were anisotropically refined. Hydrogen atoms were introduced in calculated positions, and their coordinates and isotropic displacement factors were refined in agreement with the linked carbon atoms.

Crystallographic data have been deposited with the Cambridge Crystallographic Data Center (CCDC 1553257).

Adsorption Measurements. Adsorption isotherms of Cu(II) and Zn(II) ions on MWCNTs and MWCNT-HL1 adsorbents were carried out at 298.1 K, according to the experimental procedure previously reported.[23] Under typical conditions, 0.050 g of each adsorbent were placed in contact with 25 mL of an aqueous solution of the corresponding metal dichloride at pH 5.0. The samples were shaken in a thermostated air incubator until equilibrium was reached (5 days). The adsorbate concentration ranged from 1×10^{-4} to 1.7×10^{-3} M. The concentration of the ions was determined by atomic absorption spectrometry using a PerkinElmer Analyst 800 equipment. The analysis of the equilibrium solutions allowed us to check that HL1 was not desorbed when the MWCNT-HL1 hybrid material was used as adsorbent.

Preparation of MWCNT-HL1-Cu(0). A sample (43.9 mg) of MWCNT-HL1-Cu (containing 0.157 mmol of Cu(II) per gram of MWCNT-HL1), which was obtained from the adsorption isotherm experiment (see above), was mixed with 10 mL of water, and the mixture was added to 22 mg of $NaBH_4$, (molar Cu(II)/$NaBH_4$ = 1/80). The mixture was left to react under stirring for 2 h at room temperature. After this, the resulting solid was separated by filtration, washed repeatedly with doubly distilled water, and dried in a desiccator under silica until a constant weight was obtained.

XPS Spectra. The XPS spectra of solid samples MWCNT-HL1-Cu, MWCNT-HL1-Cu(0), and MWCNT-HL1-Zn were recorded with a ESCA5701 instrument (Physical Electronics), using the Mg Kα 300 W, 15 kV radiation of the twin anode in the constant analyzer energy mode, with pass energies of 187.85 and 29.35 eV for the survey and high-resolution spectra, respectively. The pressure of the analysis chamber was maintained at 10^{-9} T, and the BE and the Auger kinetic energy scale were regulated by setting the C1s transition at 284.6 eV. The accuracy of BE values was 0.2 eV.

TEM Micrographs. TEM images of the MWCNT-HL1-Cu(0) sample have been obtained with a JEOL Mod. JEM-1010 equipment.

■ ASSOCIATED CONTENT

Supporting Information

The Supporting Information is available free of charge on the ACS Publications website at DOI: 10.1021/acsomega.7b00736.

Crystal and structure refinement data; geometric parameters for the anion−π contact; distribution diagrams for HL3 protonation and Cu(II) and Zn(II) complexation with HL1−HL3; UV spectra at variable pH values of Cu(II) and Zn(II) complexes with HL1 and HL2 and of Cu(II) complexes with HL3; high-resolution XPS spectra of MWCNT-HL1-Cu(II), MWCNT-HL1-Cu(0), and MWCNT-HL1-Zn(II) (PDF)

■ AUTHOR INFORMATION

Corresponding Authors

*E-mail: antonio.bianchi@unifi.it (A.B.).
*E-mail: enrique.garcia-es@uv.es (E.G.E.).
*E-mail: rlopez@ujaen.es (R.L.G.).

ORCID

Antonio Bianchi: 0000-0002-1082-3911

Notes

The authors declare no competing financial interest.

■ ACKNOWLEDGMENTS

Support from Italian MIUR (Project 2015MP34H3), MINECO (Project MAT2014-60104-C2-2-R), Autonomous Regional Government (Junta de Andalucía, Group PAIDI FQM273), University of Jaén (EI-FQM6_2017), Spanish Ministerio de Economía y Competitividad (projects CTQ2013-48917-C3-1-P, CTQ2016-78499-C6-1-R, and Unidad de Excelencia MDM 2015-0038), and Generalitat Valenciana (Project PROMETEOII2015-002) is gratefully acknowledged.

■ REFERENCES

(1) Savastano, M.; Arranz-Mascarós, P.; Bazzicalupi, C.; Clares, M. P.; Godino-Salido, M. L.; Gutíerrez-Valero, M. D.; Inclán, M.; Bianchi, A.; García-España, E.; Lopez-Garzón, R. Construction of Green Nanostructured Heterogeneous Catalysts via Non-Covalent Surface Decoration of Multi-Walled Carbon Nanotubes with Pd(II) Complexes of Azamacrocycles. *J. Catal.* **2017**, *000*, 000.

(2) López-Garzón, R.; Godino-Salido, M. L.; Gutíerrez-Valero, M. D.; Arranz-Mascarós, P.; Melguizo, M.; García, C.; Domingo-García, M.; López-Garzón, F. J. Supramolecular assembling of molecular ion-ligands on graphite-based solid materials directed to specific binding of metal ions. *Inorg. Chim. Acta* **2014**, *417*, 208−221.

(3) Bazzicalupi, C.; Bianchi, A.; García-España, E.; Delgado-Pinar, E. Metals in supramolecular chemistry. *Inorg. Chim. Acta* **2014**, *417*, 3−26.
(4) Gawande, M. B.; Goswami, A.; Felpin, F. X.; Asefa, T.; Huang, X.; Silva, R.; Zou, X.; Zboril, R.; Varma, R. S. Cu and Cu-Based Nanoparticles: Synthesis and Applications in Catalysis. *Chem. Rev.* **2016**, *116*, 3722−3811.
(5) (a) Nakatake, D.; Yokote, Y.; Matsushima, Y.; Yazakia, R.; Ohshima, T. A highly stable but highly reactive zinc catalyst for transesterification supported by a bis(imidazole) ligand. *Green Chem.* **2016**, *18*, 1524−1530. (B) Bencini, A.; Berni, E.; Bianchi, A.; Fedi, V.; Giorgi, C.; Paoletti, P.; Valtancoli, B. Carboxy and diphosphate ester hydrolysis promoted by dinuclear zinc(II) macrocyclic complexes. Role of Zn(II)-bound hydroxide as the nucleophilic function. *Inorg. Chem.* **1999**, *38*, 6323−6325. (c) Bazzicalupi, C.; Bencini, A.; Berni, E.; Bianchi, A.; Fornasari, P.; Giorgi, C.; Valtancoli, B. Zn(II) coordination to polyamine macrocycles containing dipyridine units. New insights into the activity of dinuclear Zn(II) complexes in phosphate ester hydrolysis. *Inorg. Chem.* **2004**, *43*, 6255−6265.
(6) Comerford, J. W.; Hart, S. J.; North, M.; Whitwood, A. C. Homogeneous and silica-supported zinc complexes for the synthesis of propylene carbonate from propane-1,2-diol and carbon dioxide. *Catal. Sci. Technol.* **2016**, *6*, 4824−4831.
(7) Bianchi, A.; Micheloni, M.; Paoletti, P. Thermodynamic aspects of the polyazacycloalkane complexes with cations and anions. *Coord. Chem. Rev.* **1991**, *110*, 17−113.
(8) (a) Clares, M. P.; Serena, C.; Blasco, S.; Nebot, A.; Del Castillo, L.; Soriano, C.; Domènech, A.; Sánchez-Sánchez, A. V.; Soler-Calero, L.; Mullor, J. L.; García-España, A.; García-España, E. Mn(II) complexes of scorpiand-like ligands. A model for the MnSOD active centre with high in vitro and in vivo activity. *J. Inorg. Biochem.* **2015**, *143*, 1−8. (b) Blasco, S.; Verdejo, B.; Clares, M. P.; Castillo, C. E.; Algarra, A. G.; Latorre, J.; Máñez, M. A.; Basallote, M. G.; Soriano, C.; García-España, E. Hydrogen and Copper Ion Induced Molecular Reorganizations in Two New Scorpiand-Like Ligands Appended with Pyridine Rings. *Inorg. Chem.* **2010**, *49*, 7016−7027. (c) Verdejo, B.; Ferrer, A.; Blasco, S.; Castillo, C. E.; González, J.; Latorre, J.; Máñez, M. A.; García Basallote, M.; Soriano, C.; García-España, E. Hydrogen and Copper Ion-Induced Molecular Reorganizations in Scorpionand-like Ligands. A Potentiometric, Mechanistic, and Solid-State Study. *Inorg. Chem.* **2007**, *46*, 5707−5719. (d) Inclán, M.; Albelda, M. T.; Frías, J. C.; Blasco, S.; Verdejo, B.; Serena, C.; Salat-Canela, C.; Díaz, M. L.; García-España, A.; García-España, E. Modulation of DNA Binding by Reversible Metal-Controlled Molecular Reorganizations of Scorpiand-like Ligands. *J. Am. Chem. Soc.* **2012**, *134*, 9644−9656.
(9) (a) Savastano, M.; Arranz-Mascarós, P.; Bazzicalupi, C.; Bianchi, A.; Giorgi, C.; Godino-Salido, M. L.; Gutiérrez-Valero, M. D.; López-Garzón, R. Binding and removal of octahedral, tetrahedral, square planar and linear anions in water by means of activated carbon functionalized with a pyrimidine-based anion receptor. *RSC Adv.* **2014**, *4*, 58505−58513. (b) Arranz, P.; Bianchi, A.; Cuesta, R.; Giorgi, C.; Godino, M. L.; Gutiérrez, M. D.; López, R.; Santiago, A. Binding and Removal of Sulfate, Phosphate, Arsenate, Tetrachloromercurate, and Chromate in Aqueous Solution by Means of an Activated Carbon Functionalized with a Pyrimidine-Based Anion Receptor (HL). Crystal Structures of $[H_3L(HgCl_4)]\cdot H_2O$ and $[H_3L(HgBr_4)]\cdot H_2O$ Showing Anion−π Interactions. *Inorg. Chem.* **2010**, *49*, 9321−9332.
(10) Anda, C.; Bazzicalupi, C.; Bencini, A.; Bianchi, A.; Fornasari, P.; Giorgi, C.; Valtancoli, B.; Lodeiro, C.; Parola, A. J.; Pina, F. Cu(II) and Ni(II) complexes with dipyridine-containing macrocyclic polyamines with different binding units. *Dalton Trans.* **2003**, 1299−1307. Bencini, A.; Bianchi, A.; Danesi, A.; Giorgi, C.; Mariani, P.; Valtancoli, B. pH-Controlled metal translocation outside/inside the cavity of a polyamine macrocycle. *J. Coord. Chem.* **2009**, *62*, 82−91.
(11) González, J.; Llinares, J. M.; Belda, R.; Pitarch, J.; Soriano, C.; Tejero, R.; Verdejo, B.; García-España, E. Tritopic phenanthroline and pyridine tail-tied aza-scorpiands. *Org. Biomol. Chem.* **2010**, *8*, 2367−2376.
(12) Biniak, S.; Pakula, M.; Szymansky, G. S.; Swiatkowski, A. Effect of Activated Carbon Surface Oxygen- and/or Nitrogen-Containing Groups on Adsorption of Copper(II) Ions from Aqueous Solution. *Langmuir* **1999**, *15*, 6117−6122.
(13) NIST data base. https://srdata.nist.gov/xps/main_search_menu.aspx.
(14) (a) Bazzicalupi, C.; Bianchi, A.; Giorgi, C.; Clares, M. P.; Garcia-España, E. Addressing selectivity criteria in binding equilibria. *Coord. Chem. Rev.* **2012**, *256*, 13−27. (b) Bianchi, A.; García-España, E. The use of calculated species distribution diagrams to analyze thermodynamic selectivity. *J. Chem. Educ.* **1999**, *76*, 1727−1732.
(15) Godino-Salido, M. L.; Gutiérrez-Valero, M. D.; López-Garzón, R.; Arranz-Mascarós, P.; Santiago-Medina, A.; Melguizo, M.; Domingo-García, M.; López-Garzón, F. J.; Abdelkader-Fernández, V. K.; Salinas-Martínez de Lecea, C.; Román-Martínez, M. C. New hybrid materials based on the grafting of Pd(II)-amino complexes on the graphitic surface of AC: preparation, structures and catalytic properties. *RSC Adv.* **2016**, *6*, 58247−58259.
(16) Pallavicini, P. S.; Perotti, A.; Poggi, A.; Seghi, B.; Fabbrizzi, L. N-(aminoethyl)cyclam: a tetraaza macrocycle with a coordinating tail (scorpiand). Acidity controlled coordination of the side chain to nickel(II) and nickel(III) cations. *J. Am. Chem. Soc.* **1987**, *109*, 5139−5144.
(17) Bazzicalupi, C.; Bianchi, A.; Biver, T.; Giorgi, C.; Santarelli, S.; Savastano, M. Formation of Double-Strand Dimetallic Helicates with a Terpyridine-Based Macrocycle. *Inorg. Chem.* **2014**, *53*, 12215−12224.
(18) Gran, G. Determination of the equivalence point in potentiometric titrations. Part II. *Analyst* **1952**, *77*, 661−671.
(19) Gans, P.; Sabatini, A.; Vacca, A. Investigation of equilibria in solution. Determination of equilibrium constants with the HYPERQUAD suite of programs. *Talanta* **1996**, *43*, 1739−1753.
(20) *CrysAlisPro*, version 1.171.35.11; Agilent Technologies, 2015.
(21) Altomare, A.; Cascarano, G.; Giacovazzo, C.; Guagliardi, A.; Burla, M. C.; Polidori, G.; Camalli, M. SIRPOW.92 − a program for automatic solution of crystal structures by direct methods optimized for powder data. *J. Appl. Crystallogr.* **1994**, *27*, 435−436.
(22) Sheldrick, G. M. Crystal structure refinement with SHELXL. *Acta Crystallogr., Sect. C: Struct. Chem.* **2015**, *71*, 3−8.
(23) Godino-Salido, M. L.; Santiago-Medina, A.; Arranz-Mascarós, P.; López-Garzón, R.; Gutiérrez-Valero, M. D.; Melguizo, M.; López-Garzón, F. J. Novel active carbon/crown ether derivative hybrid material for the selective removal of Cu(II) ions: the crucial role of the surface chemical functions. *Chem. Eng. Sci.* **2014**, *114*, 94−104.

DOI: 10.1021/acsomega.7b00736
ACS Omega 2017, 2, 3868−3877

RSC Advances

PAPER

Cite this: *RSC Adv.*, 2014, **4**, 58505

Binding and removal of octahedral, tetrahedral, square planar and linear anions in water by means of activated carbon functionalized with a pyrimidine-based anion receptor†

Matteo Savastano,[a] Paloma Arranz-Mascarós,[b] Carla Bazzicalupi,[a] Antonio Bianchi,*[a] Claudia Giorgi,[a] M. Luz Godino-Salido,[b] Maria Dolores Gutiérrez-Valero[b] and Rafael López-Garzón*[b]

Received 7th October 2014
Accepted 30th October 2014

DOI: 10.1039/c4ra11916a

www.rsc.org/advances

Binding of $S_2O_3^{2-}$, SeO_4^{2-}, $Pt(CN)_4^{2-}$, $Co(CN)_6^{3-}$, $Au(S_2O_3)_2^{3-}$ and $Fe(CN)_6^{4-}$ anions by the protonated (positively charged) forms of tren (tris(2-aminoethyl)amine) and of the tren-derivative (HL) containing a pyrimidine residue was studied by means of potentiometric measurements in 0.1 M NMe_4Cl solutions at 298.1 ± 0.1 K. Both ligands form stable complexes with these anions which appear to be mostly stabilized by electrostatic forces. In the case of HL, an anion–π interaction with the pyrimidine residue of the ligand also affords a significant contribution to complex stability. Some shape preference for tetrahedral and octahedral anions over square planar ones is observed. A hybrid AC/HL material obtained by adsorption of HL on commercial activated carbon (AC) was used to study the extraction of these anions from water. AC/HL shows enhanced adsorption capacity toward all the anions studied with respect to AC. This behavior is ascribed to the stronger interaction of anions with the HL function of AC/HL than with the Cπ-H_3O^+ sites of unfunctionalized AC. Of special interest is the enhancement of the adsorption capacities found for $Au(S_2O_3)_2^{3-}$ and $Pt(CN)_4^{2-}$, two anions of great relevance for the extraction of platinum and gold from ores and from metallic wastes.

Introduction

Anion coordination chemistry, the binding of negatively charged species *via* non covalent interactions with Lewis acid receptors, is a dynamic research area attracting growing interest as a fertile source of applications.[1–10] We have recently shown, for instance, that functionalization of an activated carbon (AC) with the polyamine molecule HL gives rise to a hybrid material (AC/HL) with marked affinity for various anions, thus providing a promising tool for anion sequestration and the remediation of contaminated media.[11]

The method used for the functionalization of a commercially available AC was based on the irreversible π-stacking interaction between the pyrimidine anchor of HL and the arene centres of the graphite domains of AC (Fig. 1).[11] The characteristics of the AC/HL material mostly relies on the properties of the functionalities implanted on the carbon surface that are transferred to the hybrid material.[13] HL contains a tren unit (L1) (Chart 1), whose protonated forms are efficient anion receptors,[14] and coherently also protonated forms of HL give rise to stable complexes with various anions, both inorganic and organic.[11,15–17] With the latter ligand, the participation of anion–π interactions, involving the pyrimidine residue, can furnish further contributions to complex stability in addition to charge–charge attraction and hydrogen bonding. Indeed, crystal structures of HL complexes with anions

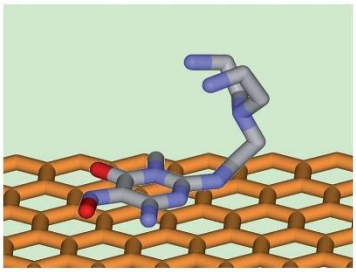

Fig. 1 Schematic representation of the interaction between the surface of activated carbon and the pyrimidine residue of HL.

[a]*Department of Chemistry "Ugo Schiff", University of Florence, Via della Lastruccia 3, 50019, Sesto Fiorentino, Italy. E-mail: antonio.bianchi@unifi.it*

[b]*Department of Inorganic and Organic Chemistry, University of Jaén 23071, Jaén, Spain. E-mail: rlopez@ujaen.es*

† Electronic supplementary information (ESI) available: Selectivity diagrams and conditional stability constant diagrams for complex systems. Tables of overall equilibrium constants for complexation reactions. See DOI: 10.1039/c4ra11916a

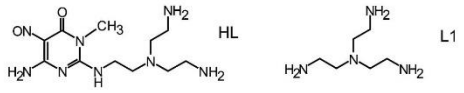

Chart 1 Tren (L1) and tren derivative (HL) studied in this work. The notation HL is used for the pyrimidine derivative since it can undergo deprotonation of the NH group linked to the pyrimidine ring.[12]

such as $HgCl_4^{2-}$, $HgBr_4^{2-}$, CdI_4^{2-} and $Co(CN)_6^{3-}$ showed very short (among the shortest ever reported) anion–π interactions.[11,17,18] Accordingly, the AC/HL material is an efficient sorbent for anions such as SO_4^{2-}, PO_4^{3-}, AsO_4^{3-}, CrO_4^{2-} and $HgCl_4^{2-}$ in water over rather wide pH ranges.[11] More recently, we showed that HL forms stable to very stable complexes with other tetrahedral anions ($S_2O_3^{2-}$, SeO_4^{2-}) and with anions of different geometries such as $P_2O_7^{4-}$, $P_3O_{10}^{5-}$ and $Co(CN)_6^{3-}$.[16,17]

In the present paper, we extend the study to metal complex anions such as $Pt(CN)_4^{2-}$, $Fe(CN)_6^{4-}$ and $Au(S_2O_3)_2^{3-}$ and we relate the stability of $S_2O_3^{2-}$, SeO_4^{2-}, $Pt(CN)_4^{2-}$, $Co(CN)_6^{3-}$, $Fe(CN)_6^{4-}$ and $Au(S_2O_3)_2^{3-}$ complexes of HL with the stability of the analogous species formed by the parent ligand tren. Furthermore, we analyse the sorption ability of the hybrid AC/HL material towards $S_2O_3^{2-}$, SeO_4^{2-}, $Pt(CN)_4^{2-}$, $Co(CN)_6^{3-}$, $Fe(CN)_6^{4-}$ and $Au(S_2O_3)_2^{3-}$ to enlarge the base of data correlating the sorption properties of AC/HL with the binding ability of HL and of its constituents. Of particular interest was the study involving $Pt(CN)_4^{2-}$ and $Au(S_2O_3)_2^{3-}$, since a successful adsorption of these anions on the hybrid AC/HL material could have important technological applications. Cyanide leaching of platinum-group metals (PGM) and gold followed by activated carbon adsorption of the resulting cyanide complexes is a technique currently in use, in particular for gold, and receives continuous attention for improvements and extensions for the recovery of these precious metals from ores or from metallic wastes such as automobile exhaust catalysts.[19–22] Improvements of the activated carbon adsorption method is, of course, desirable, as well as replacement of the very toxic cyanide with safer ligands is desirable. Thiosulfate could be an alternative, at least in the case of gold.[23] The very stable $Au(S_2O_3)_2^{3-}$ complex, for instance, is the main component obtained when thiosulfate is used as an alternative to cyanide for extraction of gold. Thiosulfate is essentially non-toxic and it is able to extract gold from ore types that are refractory to gold cyanidation, like carbonaceous or Carlin type ores. This alternative process, however, presents some drawbacks, the principal one being the lack of a suitable recovery technique, since $Au(S_2O_3)_2^{3-}$ is not efficiently adsorbed by activated carbon, which is the standard technique used in gold cyanidation to separate the gold complex from the ore slurry. As we will show later on in this paper, functionalization with HL enhances the ability of activated carbon to adsorb both $Au(S_2O_3)_2^{3-}$ and $Pt(CN)_4^{2-}$.

Experimental

Materials

The HL ligand[18] and the hybrid AC/HL material[11,24] were prepared and characterized as previously described. The commercial AC adsorbent supplied by Merck was also previously characterized.[23] The anions used for the potentiometric and the adsorption measurements were obtained as high purity $Na_2S_2O_3$, Na_2SeO_4, $Na_3[Au(S_2O_3)_2]$, $K_2[Pt(CN)_4]$, $K_3[Co(CN)_6]$ and $K_4[Fe(CN)_6]$ salts from commercial sources and were used without further purification.

Potentiometric measurements

pH-metric measurements ($pH = -\log[H^+]$) employed for the determination of equilibrium constants were carried out in 0.1 M NMe_4Cl solutions at 298.1 ± 0.1 K, by using the equipment and the methodology that has been already described.[25] The combined Hamilton glass electrode (LIQ-GLASS 238000/08) was calibrated as a hydrogen concentration probe by titrating known amounts of HCl with CO_2-free NMe_4OH solutions and determining the equivalent point by Gran's method[26] which allows one to determine the standard potential E^0 and the ionic product of water ($pK_w = 13.83(1)$ at 298.1 ± 0.1 K in 0.1 M NMe_4Cl). At least three measurements were performed for each system in the pH ranges 2.5–10.5. The computer program Hyperquad[27] was used to calculate the equilibrium constants from e.m.f. data. The concentration of the ligand was 1×10^{-3} M, while the concentration of anions [A] was in the range $[L] \leq [A] \leq 5[L]$. Ligand protonation constants used in calculations were previously determined,[11,14] while anion protonation constants were taken from the literature.[28] Three measurements were performed for each anion and the titration curves were treated both separately or as a unique set without significant variations in the calculated stability constants. The final stability constants were obtained by processing the whole set of curves.

Adsorption measurements

Equilibration times for anion adsorption measurements were preliminarily determined by means of independent experiments. For this purpose, different flasks containing 25 mL of 10^{-3} M anion solution and 25 mg of adsorbent were prepared, kept under stirring, and the anion concentration was measured at different times by means of ICP mass measurements in all cases except for $Pt(CN)_4^{2-}$ whose concentration was measured by UV absorbance at 255 nm.

The anion adsorption isotherms were obtained at 298.1 ± 0.1 K. Typically, 25 mg of adsorbent (AC or AC/HL) was added to a 100 mL plastic flask containing 25 mL of aqueous solution of the examined anion. Anion concentration was varied between 5×10^{-4} and 1.1×10^{-3} M, and the initial pH was adjusted to 6.0 by adding KOH or HCl solutions to the adsorbate solutions. The flasks were kept under stirring into a Selecta Unitronic-Orbital themostated air-bath and the anion concentration in the equilibrium solutions was determined as indicated above. UV measurements were previously performed to ascertain that no desorption of HL occurred in the presence of the studied anions under the experimental conditions employed, and blank experiments were performed to verify that neither the ligand nor the anions were adsorbed by the plastic flasks.

To obtain the theoretical maximum adsorption capacities of the corresponding sorbents toward the anions (X_m), the isotherm data X (mmols of anion adsorbed per gram of adsorbent) and C_{eq} (anion equilibrium concentrations) were fit to the linear form of the Langmuir equation[29] $1/X = 1/B \times X_m \times C_{eq} + 1/X_m$, where B is the Langmuir constant. This was done for all the adsorbent/adsorbate systems (R varying between 0.9661 and 0.9915) except for $S_2O_3^{2-}$ due to high dispersion of the experimental data obtained in this case.

XPS spectra of AC/$Pt(CN)_4^{2-}$ and AC/$Au(S_2O_3)_2^{3-}$ samples, obtained from the adsorption experiments of $Pt(CN)_4^{2-}$ and $Au(S_2O_3)_2^{3-}$ on AC, were registered with a ESCA5701 instrument (Physical Electronics), by using the Mgkα 300 W 15 kV radiation of twin anode in the constant analyzer energy mode, with pass energy of 187.85 eV (for the survey spectrum) and 29.35 eV (for narrow atomic ranges). Pressure of the analysis chamber was maintained at 4×10^{-9} Torr. The binding energy and the Auger kinetic energy scale were regulated by setting the C1s transition at 284.6 eV. The accuracy of BE values was ±0.2 eV.

Results and discussion

Anion complexation by HL and L1

The equilibrium constants for the interaction of $S_2O_3^{2-}$, SeO_4^{2-}, $Pt(CN)_4^{2-}$, $Co(CN)_6^{3-}$, $Fe(CN)_6^{4-}$ and $Au(S_2O_3)_2^{3-}$ with protonated forms of the pyrimidine derivative HL and the parent ligand tren (L1) were determined by means of computer analysis, performed by means of the Hyperquad[27] program, of potentiometric (pH-metric) titration data acquired in 0.1 M Me_4NCl aqueous solutions at 298.1 K. Their values are listed in Tables 1 and 2, respectively.

As can be seen from these tables, the stability constants of these complexes invariably increases as increasing positive charge accumulates on the ligands upon protonation. Only in the case of $Pt(CN)_4^{2-}$, the effect of ligand charge on complex stability is small or unappreciable within the experimental errors.

The two ligands display rather similar anion binding trends. For a given ligand charge, for instance, the tetrahedral anions $S_2O_3^{2-}$ and SeO_4^{2-} show very similar binding constants, and similar behaviors were previously found for SO_4^{2-}, HPO_4^{2-} and $HAsO_4^{2-}$.[11,14] Also the stability of complexes with the elongated $Au(S_2O_3)_2^{3-}$ anion, having tetrahedral terminations, are comparable with the stability of complexes with the above tetrahedral anions, despite its greater charge. The more charged octahedral $Co(CN)_6^{3-}$ and $Fe(CN)_6^{4-}$ anions form complexes of greater stability, relative to the less charged anions, $Fe(CN)_6^{4-}$ being the anion forming the most stable complexes. On the other hand, complexes of the square planar $Pt(CN)_4^{2-}$ with HL are less stable than the analogous species formed by the other dicharged anions, and reduced stability is also observed for the complex with H_3L1^{3+}.

Accordingly, anion binding by protonated forms of HL and L1 appears to be mostly regulated by electrostatic forces, and the ligands display some shape preference for tetrahedral and octahedral anions over square planar ones. Indeed, the crystal structures of the complexes formed by $HgCl_4^{2-}$, $HgBr_4^{2-}$ and CdI_4^{2-} with H_3L^{2+} and by $Co(CN)_6^{3-}$ with H_4L^{3+} showed a good complementarity between the interacting partners, the anions being anchored to the ligand *via* salt-bridges with ligand

Table 1 Equilibrium constants for the formation of anion complexes with HL determined by means of potentiometric measurements in 0.1 M Me_4NCl aqueous solution at 298.1 K

Equilibria	log K
$HL + S_2O_3^{2-} = [HL(S_2O_3)]^{2-}$	1.9(1)[a,b,c]
$H_2L^{+} + S_2O_3^{2-} = [H_2L(S_2O_3)]^{-}$	2.83(7)[b]
$H_3L^{2+} + S_2O_3^{2-} = [H_3L(S_2O_3)]$	3.34(8)[b]
$H_4L^{3+} + S_2O_3^{2-} = [H_4L(S_2O_3)]^{+}$	3.95(9)[b]
$HL + SeO_4^{2-} = [HL(SeO_4)]^{2-}$	2.1(1)[b,c]
$H_2L^{+} + SeO_4^{2-} = [H_2L(SeO_4)]^{-}$	2.68(6)[b]
$H_3L^{2+} + SeO_4^{2-} = [H_3L(SeO_4)]$	3.34(6)[b]
$H_4L^{3+} + SeO_4^{2-} = [H_4L(SeO_4)]^{+}$	3.96(8)[b]
$H_2L^{+} + Pt(CN)_4^{2-} = [H_2L(Pt(CN)_4)]^{-}$	2.24(6)[b]
$H_3L^{2+} + Pt(CN)_4^{2-} = [H_3L(Pt(CN)_4)]$	2.62(6)[b]
$H_4L^{3+} + Pt(CN)_4^{2-} = [H_4L(Pt(CN)_4)]^{+}$	2.74(5)[b]
$HL + Co(CN)_6^{3-} = [HL(Co(CN)_6)]^{3-}$	2.0(1)[b,c]
$H_2L^{+} + Co(CN)_6^{3-} = [H_2L(Co(CN)_6)]^{2-}$	2.72(6)[b]
$H_3L^{2+} + Co(CN)_6^{3-} = [H_3L(Co(CN)_6)]^{-}$	3.44(5)[b]
$H_4L^{3+} + Co(CN)_6^{3-} = [H_4L(Co(CN)_6)]$	4.24(6)[b]
$H_2L^{+} + Fe(CN)_6^{4-} = [H_2L(Fe(CN)_6)]^{3-}$	2.91(8)
$H_3L^{2+} + Fe(CN)_6^{4-} = [H_3L(Fe(CN)_6)]^{2-}$	3.65(6)
$H_4L^{3+} + Fe(CN)_6^{4-} = [H_4L(Fe(CN)_6)]^{-}$	5.08(9)
$H_4L^{3+} + HFe(CN)_6^{3-} = [H_4L(HFe(CN)_6)]$	4.21(8)
$H_2L^{+} + Au(S_2O_3)_2^{3-} = [H_2L(Au(S_2O_3)_2)]^{2-}$	2.33(7)
$H_3L^{2+} + Au(S_2O_3)_2^{3-} = [H_3L(Au(S_2O_3)_2)]^{-}$	3.31(5)
$H_4L^{3+} + Au(S_2O_3)_2^{3-} = [H_4L(Au(S_2O_3)_2)]$	3.86(6)

[a] Values in parentheses are standard deviations on the last significant figures. [b] Taken from ref. 17. [c] Determined by isothermal titration calorimetry.

Table 2 Equilibrium constants for the formation of anion complexes with tren (L1) determined by means of potentiometric measurements in 0.1 M Me_4NCl aqueous solution at 298.1 K

Equilibria	log K
$H_2L1^{2+} + S_2O_3^{2-} = [H_2L1(S_2O_3)]$	1.61(8)[a]
$H_3L1^{3+} + S_2O_3^{2-} = [H_3L1(S_2O_3)]^{+}$	2.08(7)
$H_4L1^{4+} + S_2O_3^{2-} = [H_4L1(S_2O_3)]^{2+}$	2.97(7)
$H_2L1^{2+} + SeO_4^{2-} = [H_2L1(SeO_4)]$	1.58(6)
$H_3L1^{3+} + SeO_4^{2-} = [H_3L1(SeO_4)]^{+}$	1.93(6)
$H_4L1^{4+} + SeO_4^{2-} = [H_4L1(SeO_4)]^{2+}$	3.28(4)
$HL1^{+} + Pt(CN)_4^{2-} = [HL1(Pt(CN)_4)]^{-}$	2.03(8)
$H_2L1^{2+} + Pt(CN)_4^{2-} = [H_2L1(Pt(CN)_4)]$	2.26(7)
$H_3L1^{3+} + Pt(CN)_4^{2-} = [H_3L1(Pt(CN)_4)]^{+}$	2.18(7)
$HL1^{+} + Co(CN)_6^{3-} = [HL1(Co(CN)_6)]^{2-}$	3.11(9)
$H_2L1^{2+} + Co(CN)_6^{3-} = [H_2L1(Co(CN)_6)]^{-}$	3.30(7)
$H_3L1^{3+} + Co(CN)_6^{3-} = [H_3L1(Co(CN)_6)]$	3.82(6)
$H_4L1^{4+} + Co(CN)_6^{3-} = [H_4L1(Co(CN)_6)]^{+}$	4.88(7)
$HL1^{+} + Fe(CN)_6^{4-} = [HL1(Fe(CN)_6)]^{3-}$	3.24(6)
$H_2L1^{2+} + Fe(CN)_6^{4-} = [H_2L1(Fe(CN)_6)]^{2-}$	3.42(7)
$H_3L1^{3+} + Fe(CN)_6^{4-} = [H_3L1(Fe(CN)_6)]^{-}$	3.99(8)
$H_4L1^{4+} + Fe(CN)_6^{4-} = [H_4L1(Fe(CN)_6)]$	5.47(6)
$H_2L1^{2+} + Au(S_2O_3)_2^{3-} = [H_2L1(Au(S_2O_3)_2)]^{-}$	2.23(5)
$H_3L1^{3+} + Au(S_2O_3)_2^{3-} = [H_3L1(Au(S_2O_3)_2)]$	2.47(8)
$H_4L1^{4+} + Au(S_2O_3)_2^{3-} = [H_4L1(Au(S_2O_3)_2)]^{+}$	2.66(6)

[a] Values in parentheses are standard deviations on the last significant figures.

ammonium groups and very strong anion–π interactions with the pyrimidine residue of HL acting as anion binding functionality (Fig. 2).[11,17,18] In particular, the $H_4L[Co(CN)_6]$ complex showed one of the strongest anion–π interactions so far reported.[17]

While in H_3L^{2+} protonation involves the two primary amine groups of the tren moiety, in H_4L^{3+} also the pyrimidine nitroso group is protonated. Since protonation of the nitroso group modifies its π-electron cloud, we expect that it also produces a significant alteration of the π-density on the pyrimidine ring, thus affecting the anion–π interactions occurring in these complexes. To get insight on this point, we performed a detailed analysis of the crystal structures deposited in the Cambridge Structural Database (CSD) for nitroso-pyrimidines containing nitroso groups in both neutral and protonated forms, by using the structure reported in Fig. 3a as a query for the database investigation and excluding metal coordinated NO groups. No limits to data quality were imposed. Visualization of these crystal structures evidences that protonation of the nitroso group determines, in addition to the expected lengthening of the N–O bonds and shortening of the adjacent N–C bonds, a significant elongation of the C–C distances of the pyrimidine ring. This is clearly shown in Fig. 3 by the correlations of N–C (Fig. 3b) and C–C (Fig. 3c) with N–O bond distances obtained from CSD. In this figure, data relative to the $\{H_4L[Co(CN)_6]\}\cdot 2H_2O$ complex[17] are displayed in red, while the yellow markers represent the mean value evaluated for the structures of complexes formed by H_3L^{2+} with $HgCl_4^{2-}$, $HgBr_4^{2-}$ and CdI_4^{2-}.[11,18] Accordingly, protonation of the nitroso group has an electron withdrawing effect on the pyrimidine π-electron density: the N–O bond acquires single bond character, the bond between the nitroso nitrogen and the linked carbon atom is shortened to a double bond distance, while the loss of π-electron density of the pyrimidine ring is particularly evident for the C–C bonds close to the nitroso group.

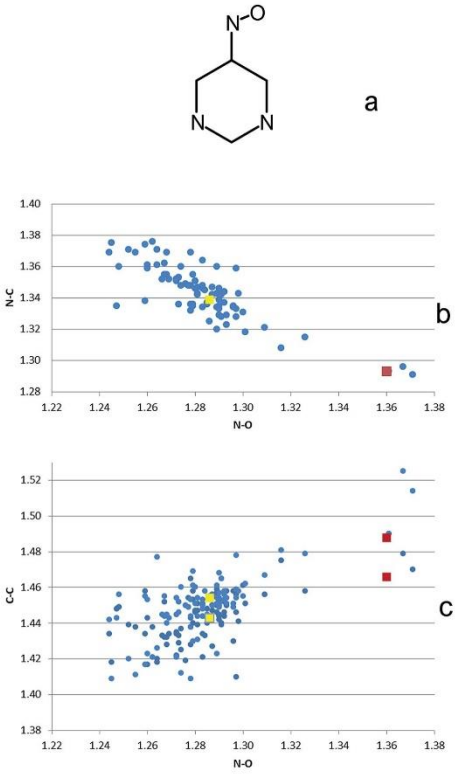

Fig. 3 (a) Basic structure used as a query for the database investigation; single, double, delocalized and aromatic bonds were considered. (b) N–C *vs.* N–O and (c) C–C *vs.* N–O bond lengths (blue markers: CSD data, red markers: $\{H_4L[Co(CN)_6]\}\cdot 2H_2O$ complex, yellow markers: mean values for the complexes formed by H_3L^{2+} with $HgCl_4^{2-}$, $HgBr_4^{2-}$ and CdI_4^{2-}.

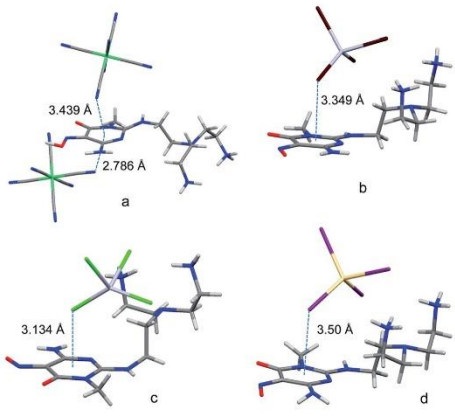

Fig. 2 Crystal structures of the complexes formed by H_4L^{3+} with $Co(CN)_6^{3-}$ (a)[17] and by H_3L^{2+} with $HgBr_4^{2-}$ (b) $HgCl_4^{2-}$ (c)[11] and CdI_4^{2-} (d)[18] (CSD refcodes IDIKAJ (a), AVISEE (b), AVISII (c), WASXAQ (d)).

To verify whether the change in π-electron density brought about by protonation of the nitroso group affects the anion–π interaction with our ligand in the solid state, we overlaid the nitroso-pyrimidine group in the crystal structures of the anion complexes with H_3L^{2+} and H_4L^{3+} and placed the anion atoms forming anion–π interactions in their relative positions to obtain the picture shown in Fig. 4. It is clearly visible that the interacting CN^- group in the $\{H_4L[Co(CN)_6]\}\cdot 2H_2O$ complex is more displaced from the center of the pyrimidine ring than any other anion, and that it points towards the C–C bonds where a lower π-electron density is localized.

Evidences that also in aqueous solution anion–π interactions contribute to stabilize these anion complexes were

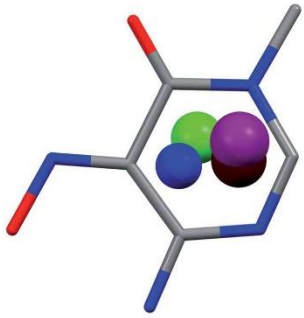

Fig. 4 Overlaid relative dispositions of the nitroso-pyrimidine group with the interacting anion atoms forming anion–π interactions in the crystal structures of H_4L^{3+} with $Co(CN)_6^{3-}$ (blue) and of H_3L^{2+} with $HgCl_4^{2-}$ (green), $HgBr_4^{2-}$ (brown) and CdI_4^{2-} (purple).

obtained by means of isothermal titration measurements and by linear correlation of complex stability constants with ligand charge, which provided evaluations of the equilibrium constants for SO_4^{2-}, $S_2O_3^{2-}$, SeO_4^{2-}, and $Co(CN)_6^{3-}$ association with the uncharged HL ligand to be in the range $\log K = 1.6$–2.2.[11,17] Values for $S_2O_3^{2-}$, SeO_4^{2-}, and $Co(CN)_6^{3-}$ complexes with HL are shown in Table 1.

As far as the anion binding abilities of the two ligands are compared, we observe that, for ligand species with the same positive charge, HL forms more stable complexes than L1, the complexes of $Co(CN)_6^{3-}$ and $Fe(CN)_6^{4-}$ with the monocharged H_2L^+ and $HL1^+$ receptors representing the unique exceptions to this trend (Tables 1 and 2). Most likely, the anion–π interactions and the less solvated environment provided by the pyrimidine residue of HL make the main contributions that enhance the ligand binding ability. Nevertheless, an interpretation of ligand binding ability in terms of binding selectivity cannot be performed by simply comparing the stability constants of analogous complexes, since the formation of these complexes is regulated by the protonation of ligands having different protonation properties. A useful method for the analysis of binding selectivity consists in considering a ternary system containing the anion and the two ligands, in equimolar amounts, and calculating the overall percentage of complexes formed by each ligand at different pH values.[30,31] The result of a similar analysis performed for the system $HL/L1/SeO_4^{2-}$ (millimolar concentrations) is reported in the diagram of Fig. 5a, showing that the anion is preferentially bound by HL over the entire pH range in which complexation occurs. Conversely, the same analysis performed for the $HL/L1/Fe(CN)_6^{4-}$ system reveals that L1 is the preferred ligand by $Fe(CN)_6^{4-}$ (Fig. 5b). The results obtained for the other anions are displayed in Fig. S1 of ESI.† While the hexacyanometallate anions undergo preferential binding with HL, all the other anions prefer L1. Analogous results (see Fig. S2†) are obtained by comparison of the conditional stability constants calculated for the complexation equilibria A(all forms) + L(all forms) = AB(all forms) and expressed as K_{AB}^{cond} = [AL(all forms)]/([A(all forms)][L(all forms)]), where A, L and AL are the anion, the ligand and the anion complex, respectively.[31]

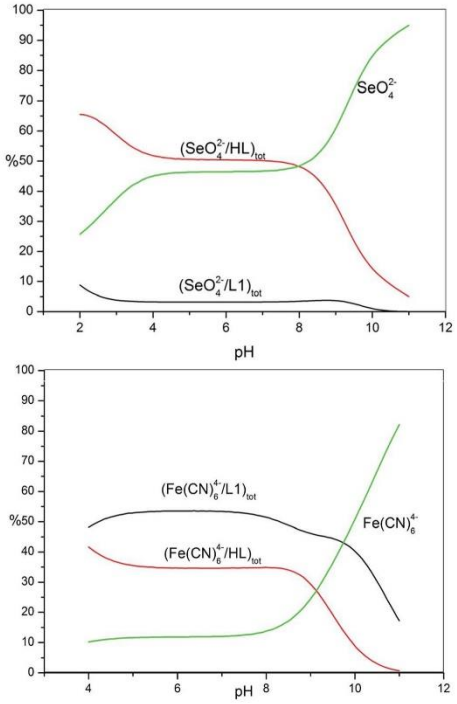

Fig. 5 Selectivity diagrams calculated for the systems (a) HL/L1/SeO_4^{2-}, (b) HL/L1/$Fe(CN)_6^{4-}$ showing the percentage of anion bound to each ligand as a function of pH. All reagents 1×10^{-3} M. Percentages are referred to total anion concentration.

In conclusion, the ligand tren (L1) maintains its anion binding properties upon functionalization to give its pyrimidine derivative HL. In some cases ($S_2O_3^{2-}$, SeO_4^{2-}, $Pt(CN)_4^{2-}$, $Au(S_2O_3)_2^{3-}$), HL displays enhanced binding ability relative to tren, while in few case ($Co(CN)_6^{3-}$, $Fe(CN)_6^{4-}$) it is less efficient than the parent ligand. Nevertheless, in all cases HL is a promising candidate for the preparation of hybrid AC/HL materials for recovery of these anions from aqueous media.

Adsorption studies

The use of AC-based adsorbents is important compared to other sorbents because of its large surface area, high adsorption capacity, porous structure, negligible environmental toxicity, low cost, and high purity.[21] In previous works it was established that the hybrid AC/HL material behaves as an efficient adsorbent for SO_4^{2-}, PO_4^{3-}, AsO_4^{3-}, $HgCl_4^{2-}$ and CrO_4^{2-} anions[11] as

well as for some metal cations.[18,24,32] Therefore, having in mind the binding data shown in the previous section, it seemed interesting to extend the adsorption study to $S_2O_3^{2-}$, SeO_4^{2-}, $Pt(CN)_4^{2-}$, $Co(CN)_6^{3-}$, $Au(S_2O_3)_2^{3-}$ and $Fe(CN)_6^{4-}$ anions, especially to $Pt(CN)_4^{2-}$ and $Au(S_2O_3)_2^{3-}$ because of the role they have, or might have, in precious metals extraction. To this purpose, we analyzed the adsorptivity toward the above set of anions of a commercial activated carbon (AC) and of the corresponding AC/HL hybrid material that was prepared as previously described.[11,24]

AC is a graphitized activated carbon with a surface area of 1062 $m^2\ g^{-1}$ and containing oxygen as the only heteroatom component present in significant amount (3.9%).[11,24] Most of the surface area (*ca.* 1000 $m^2\ g^{-1}$) is associated to narrow micropores (diameter < 2.5–3.0 nm) whereas the remaining area corresponds to mesopores (2.5–3 nm < diameter > 50 nm) and macropores (diameter > 50 nm).[33] AC surface mainly exhibits weak Brönsted basic character,[11] which is reflected in its ability to bind protons from water giving rise to the accumulation of net positive charge in the 3.0–9.2 pH range. The low proton affinities of the (few) oxygen groups on the AC surface (carboxyl acids, carbonyl, quinone, lactone and phenol groups) exclude these functions from acting as binding sites for protons in the 2.5–10.0 pH range. Consequently, most of proton binding sites at AC surface are expected to be the arene centers of the graphite sheets (Cπ), which interact with protons according to the Cπ + $H_3O^+ \rightarrow$ Cπ-H_3O^+ process.[11,34] The surface charge density, Q (mmol H^+ per gram of AC), decreases steadily from *ca.* 0.26 mmol H^+ per g, at pH 3.5, to 0.15 mmol of H^+ per g at pH = 6.0.[11]

The textural and surface chemical properties of AC/HL have been described previously. The hybrid material AC/HL contains 0.49 mmol of HL per gram of AC, irreversibly adsorbed in water in the pH range 2.5–10. The specific surface area, pore distribution and surface chemical properties of AC/HL were also determined previously.[11,33]

Attachment of HL to the surface of AC, by π–π stacking interaction of the aromatic residue of HL with the Cπ sites AC,[24] has two effects on the physico-chemical properties of the latter: (i) transference of the Brönsted base properties of the amine residue of HL to the AC surface, determining a sharp increase of the positive surface charge of AC/HL, relative to AC, in the whole pH range,[11] and (ii) blocking of the entrance to the more inner pores of AC by HL molecules that reduces the accessible surface area of AC/HL to 495 $m^2\ g^{-1}$.[33]

For the studies of anion adsorption, pH 6.0 was chosen as the most suitable for comparative purposes, since at this pH all these anions form the same unique H_3LA^{n-} (n = 0–2) complex (see Table 1). The adsorption isotherms on AC and AC/HL at pH 6.0 are shown in Fig. 6.

All the isotherms, except that of $S_2O_3^{2-}$, fit well to the Langmuir equation[29] (see Experimental section), which enabled to obtain the maximum adsorption capacities, X_{mAC} and $X_{mAC/HL}$, summarized in Table 3, although some deviation of experimental points from the calculated curves, that can be ascribed to the surface heterogeneity of the porous adsorbents, is observed. As can be seen in Fig. 6, the adsorption capacity of AC grows, in most of cases, when the anion charge increases. Since the AC surface charge is the same for all systems, it is likely that anion adsorption on AC is due to electrostatic attraction with the positive charges of the protonated arene centers of AC, even if some dispersive contribution is also expected. The good fitting to Langmuir equation of the experimental isotherms (except for $S_2O_3^{2-}$) is consistent with the existence of similar adsorbing sites on the adsorbent surface. The lowest adsorptivities are found for di-charged anions ($S_2O_3^{2-}$, SeO_4^{2-}), whereas intermediate adsorptivities correspond to the tri-charged $Co(CN)_6^{3-}$ and $Au(S_2O_3)_2^{3-}$ and the highest adsorptivity corresponds to the tetra-charged $Fe(CN)_6^{4-}$. In the last case, not only the higher negative charge, but also the possibility hydrogen bonding with –OH functions (from phenol groups) should be responsible for the higher adsorptivity observed for this anion.

It is worth commenting the adsorption of $Pt(CN)_4^{2-}$ and $Au(S_2O_3)_2^{3-}$. The adsorptivity on AC of the elongated tri-charged $Au(S_2O_3)_2^{3-}$ is higher than that of $Co(CN)_6^{3-}$, while adsorptivity of planar $Pt(CN)_4^{2-}$ is greater than that of all anions but $Fe(CN)_6^{4-}$. The absence of reduced Pt(0) and Au(0) in the XPS spectra of samples of AC/$Pt(CN)_4^{2-}$ and AC/$Au(S_2O_3)_2^{3-}$, respectively, rules out metal reduction as the cause of the high adsorptivities of these anions on AC. Three effects could contribute to the higher adsorptivities of this couple of anions: (i) their high hydrophobicity due to their high molecular sizes that determine lower water solubilities;[35] (ii) the existence of Cπ–dπ interactions between the arene centers of AC and the metal center of linear $Au(S_2O_3)_2^{3-}$ and planar $Pt(CN)_4^{2-}$ complexes,[36] although for $Au(S_2O_3)_2^{3-}$ such interactions should be somewhat hindered by the non-planar structure of $S_2O_3^{2-}$,[37] (iii) Cπ–C$\equiv$Nπ interactions between the arene centers of AC and the metal coordinated cyanide anions. Anyway, the influence of electrostatic components in anion interactions with the AC surface is clearly illustrated by the adsorptivity drop observed for $Pt(CN)_4^{2-}$ and $Co(CN)_6^{3-}$ from pH 2.5 to pH 6.0 (Fig. 6) as the positive net surface charge of AC decreases.

Also isotherms for anion adsorption at pH 6.0 on the hybrid AC/HL material (see Experimental section) are shown in Fig. 6, while the corresponding maximum adsorption capacities, $X_{mAC/HL}$, are summarized in Table 3. These data evidence that functionalization of AC with HL clearly improves its adsorption capacity. Assuming that most of HL molecules are anchored to AC through the pyrimidine moiety,[24,38] the enhanced adsorptivity of AC/HL can be ascribed to the high anion binding ability of the polyamine residue of HL.

In the cases of bi-anions $S_2O_3^{2-}$, SeO_4^{2-}, $Pt(CN)_4^{2-}$, the maximum adsorption capacities of AC/HL is about twice those of AC, which is consistent with the similar values of the stability constants of the H_3LA neutral complexes formed by these anions. In the cases of $Co(CN)_6^{3-}$ and $Au(S_2O_3)_2^{3-}$, we observed a lower enhancement. Although the stability constants of the H_3LA complexes formed by these tri-anions are similar to those of the bi-anions, the monoanionic character of $[H_3L(Co(CN)_6)]^-$ and $[H_3L(Au(S_2O_3)_2)]^-$ determines higher water solubility, thus explaining their lower adsorptivities. Finally, the adsorptivity of AC/HL for $Fe(CN)_6^{4-}$ is enhanced by a factor of *ca.* 3, relative to AC, in agreement with the higher stability of the

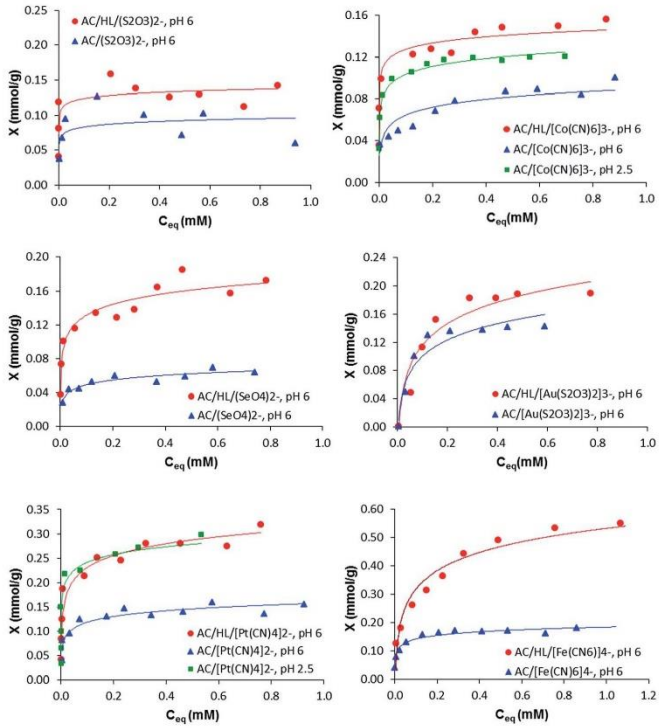

Fig. 6 Adsorption isotherms of the $S_2O_3^{2-}$, SeO_4^{2-}, $Pt(CN)_4^{2-}$, $Co(CN)_6^{3-}$, $Au(S_2O_3)_2^{3-}$ and $Fe(CN)_6^{4-}$ anions on AC and AC/HL. X = mmols of anion adsorbed per gram of adsorbent, C_{eq} = anion equilibrium concentration.

Table 3 Langmuir maximum anion adsorption capacities of AC, X_{mAC}, and of AC/HL, $X_{mAC/HL}$ (in mmol of anion per gram of adsorbent), and corresponding normalized X_{NmAC} and $X_{NmAC/HL}$ values

Anion species	X_{mAC} (mmol g^{-1})	$X_{mAC/HL}$ (mmol g^{-1})	Improvement factor	X_{NmAC} (mmol m^{-2})	$X_{NmAC/HL}$ (mmol m^{-2})	Normalized improvement factor
$S_2O_3^{2-}$	0.08[a]	0.12[a]	2	4.85×10^{-5}	2.02×10^{-4}	4.16
SeO_4^{2-}	0.060(2) [0.9690][b]	0.138(8) [0.9840][b]	2.30	5.7×10^{-5}(2)[c]	2.8×10^{-4}(2)	4.91
$Pt(CN)_4^{2-}$	0.142(4) [0.9719][b]	0.30(1) [0.9662][b]	2.11	1.34×10^{-4}(3)	6.1×10^{-4}(2)	4.55
$Au(S_2O_3)_2^{3-}$	0.157(6) [0.9664][b]	0.209(6) [0.9661][b]	1.33	1.48×10^{-4}(5)	4.2×10^{-4}(1)	2.84
$Co(CN)_6^{3-}$	0.098(6) [0.9795][b]	0.161(3) [0.9798][b]	1.65	9.2×10^{-5}(5)	3.26×10^{-4}(6)	3.54
$Fe(CN)_6^{4-}$	0.172(2) [0.9866][b]	0.54(2) [0.9915][b]	3.14	1.62×10^{-4}(2)	1.10×10^{-3}(4)	6.79

[a] Approximate values from the corresponding isotherms (Fig. 6). [b] Linear correlation coefficients (R). [c] Values in parentheses are standard deviations on the last significant figure.

$[H_3L(Fe(CN)_6)]^{2-}$complex formed at pH 6.0. Worth mentioning is the enhancement of the adsorption capacity observed for $Au(S_2O_3)_2^{3-}$ and $Pt(CN)_4^{2-}$ anions, since it may rise applicative interest for extraction and recovery of gold and platinum. The sequestering capacities of AC/HL toward these anions at pH 6.0 (39.4 and 58.7 mg g^{-1} of adsorbent, respectively) are comparable with or better than those obtained with other functionalized activated carbons.[39,40]

In summary, this study points out that functionalization of AC with the polyamine HL provides a hybrid material which

significantly improves the ability of AC in the sequestration of the studied anions. This effect is a consequence of the anion binding ability of HL that is basically preserved after its adsorption onto the AC surface. These results enlarge a previous data base that correlates the metal ion and anion adsorbing properties of hybrid materials of AC/HL type with the ability of the HL ligand to bind the same species,[11,18,24,32] and encourage further thorough research on the factors that could improve the adsorption capacity, *i.e.* (i) the influence of the textural characteristics of AC and (ii) the design of the polyamine HL function.

Regarding the textural properties, adsorption of HL on AC surface results in blocking the entrance to the more inner (narrower) pores, giving rise to a decrease of surface area from 1062 $m^2 g^{-1}$ for AC to 495 $m^2 g^{-1}$ for AC/HL,[33] thus reducing the accessible surface area for larger functionalization with HL and interaction with other small molecular species (such as the anions here studied). Accordingly, a more suitable information on the improvement of adsorptivity derived from AC functionalization with HL is provided by the comparison of the adsorption capacities of both adsorbents normalized with respect to the accessible areas, X_{mN}. The values of X_{mN} for AC and AC/HL, that appear in Table 3, were obtained by dividing the maximum adsorption capacities, X_{mAC} and $X_{mAC/HL}$, by the accessible surface areas of the corresponding adsorbents. The improvement factors obtained by using such normalized values (see Table 3) increase greatly, thus showing that activated carbons having most of their surface areas accessible to the receptors (highly meso- and macroporous activated carbons) are the most suitable for ion recovery purposes.

With respect to the second point, the use of receptors containing a larger number of amine groups than HL should improve the anion binding ability of the hybrid material, since a greater positive charge would be achievable on the surface of the hybrid material. Furthermore, appropriate synthesis of tailored polyamine ligands, in particular of macrocyclic and cleft-like structures, would afford hybrid materials with enhanced anion extraction selectivity.

References

1 (*a*) J. L. Sessler, P. A. Gale and W. S. Cho, *Anion Receptor Chemistry*, Royal Society of Chemistry, Cambridge, 2006; (*b*) *Supramolecular Chemistry of Anions*, ed. A. Bianchi, K. Bowman-James and E. Garcia-España, Wiley-VCH, New York, 1997; (*c*) J.-M. Lehn, *Supramolecular Chemistry, Concepts and Perspectives*, VCH, Weinheim, 1995.

2 H.-J. Schneider and A. K. Yatsimirsky, *Chem. Soc. Rev.*, 2008, **37**, 263.

3 E. Garcia-España, P. Díaz, J. M. Llinares and A. Bianchi, *Coord. Chem. Rev.*, 2006, **250**, 2952.

4 S. Kubik, C. Reyheller and S. Stüwe, *J. Inclusion Phenom. Macrocyclic Chem.*, 2005, **52**, 137.

5 (*a*) S. O. Kang, Md. A. Hossain and K. Bowman-James, *Coord. Chem. Rev.*, 2006, **250**, 3038; (*b*) V. McKee, J. Nelson and R. M. Town, *Chem. Soc. Rev.*, 2003, **32**, 309.

6 P. A. Gale, *Coord. Chem. Rev.*, 2001, **213**, 79.

7 P. D. Beer and E. J. Hayes, *Coord. Chem. Rev.*, 2003, **240**, 167.

8 R. Vilar, *Angew. Chem., Int. Ed.*, 2003, **42**, 1460.

9 J. M. Llinares, D. Powell and K. Bowman-James, *Coord. Chem. Rev.*, 2003, **240**, 57.

10 Special Issue on Anion Sensing*Top. Curr. Chem.*, 2005, **255**.

11 P. Arranz, A. Bianchi, R. Cuesta, C. Giorgi, M. L. Godino, M. D. Gutiérrez, R. López and A. Santiago, *Inorg. Chem.*, 2010, **49**, 9321.

12 HL behaves as a week acid with $pK_a = 10.94$ for the equilibrium $HL = L^- + H^+$ (see ref. 11).

13 R. López-Garzón, M. L. Godino-Salido, M. D. Gutiérrez-Valero, P. Arranz-Mascaros, M. Melguizo, C. García, M. Domingo-García and F. J. López-Garzón, *Inorg. Chim. Acta*, 2014, **417**, 208.

14 C. Bazzicalupi, A. Bencini, A. Bianchi, A. Danesi, C. Giorgi and B. Valtancoli, *Inorg. Chem.*, 2009, **48**, 2391.

15 P. Arranz Mascaros, C. Bazzicalupi, A. Bianchi, C. Giorgi, M. D. Gutiérrez Valero, R. López Garzón, M. L. Godino Salido and B. Valtancoli, *Chem. Commun.*, 2011, **47**, 2814.

16 P. Arranz Mascaros, C. Bazzicalupi, A. Bianchi, C. Giorgi, M. L. Godino Salido, M. D. Gutiérrez Valero, R. López Garzón and B. Valtancoli, *New J. Chem.*, 2011, **35**, 1883.

17 P. Arranz Mascaros, C. Bazzicalupi, A. Bianchi, C. Giorgi, M. L. Godino Salido, M. D. Gutiérrez Valero, R. López Garzón and M. Savastano, *J. Am. Chem. Soc.*, 2013, **135**, 102.

18 J. García Martín, R. López Garzón, M. L. Godino Salido, R. Cuesta, M. D. Gutiérrez Valero, P. Arranz Mascaros and H. Stoeckli- Evans, *Eur. J. Inorg. Chem.*, 2005, 3093.

19 J. C. Yannopoulos, *The Extractive Metallurgy of Gold*, Van Nostrand Reinhold, New York, 1991.

20 M. G. Aylmore and D. M. Muir, *Miner. Eng.*, 2001, **14**, 135.

21 C. A. Snyders, C. N. Mpinga, S. M. Bradshaw, G. Akdogan and J. J. Eksteen, *J. South. Afr. Inst. Min. Metall.*, 2013, **113**, 381.

22 C. Jing and H. Kun, *Hydrometallurgy*, 2006, **82**, 164–171.

23 H. Arima, T. Fujita and W.-T. Yen, *Mater. Trans.*, 2003, **44**, 2099.

24 J. García-Martín, R. López-Garzón, M. Godino-Salido, M. Gutiérrez-Valero, P. Arranz-Mascarós, R. Cuesta and F. Carrasco-Marín, *Langmuir*, 2005, **21**, 6908.

25 C. Bazzicalupi, A. Bianchi, C. Giorgi, P. Gratteri, P. Mariani and B. Valtancoli, *Inorg. Chem.*, 2013, **52**, 2125.

26 (*a*) G. Gran, *Analyst*, 1952, **77**, 661; (*b*) F. J. Rossotti and H. Rossotti, *J. Chem. Educ.*, 1965, **42**, 375.

27 P. Gans, A. Sabatini and A. Vacca, *Talanta*, 1996, **43**, 1739.

28 R. M. Smith and A. E. Martell, *NIST Stability Constants Database*, Version 4.0, National Institute of Standards and Technology, Washington, 1997.

29 M. D. Gutiérrez-Valero, P. Arranz-Mascarós, M. L. Godino-Salido, M. D. López-León, R. López-Garzón and R. Cuesta, *Micropor. Mesopor. Mat.*, 2008, **116**, 445.

30 A. Bianchi and E. Garcia-España, *J. Chem. Educ.*, 1999, **76**, 1727.

31 C. Bazzicalupi, A. Bianchi, C. Giorgi, M. P. Clares and E. García-España, *Coord. Chem. Rev.*, 2012, **256**, 13.

32 M. L. Godino-Salido, R. López-Garzón, P. Arranz-Mascarós, M. D. Gutiérrez-Valero, A. Santiago-Medina and J. García-Martín, *Polyhedron*, 2009, **28**, 3781.

33 M. D. Gutiérrez-Valero, P. Arranz-Mascarós, A. Peñas-Sanjuan, M. L. Godino-Salido, R. López-Garzón, A. Santiago-Medina, M. Melguizo-Guijarro, M. Pérez-Mendoza, F. J. López-Garzón and M. Domingo-García, *Mater. Chem. Phys.*, 2012, **134**, 608.
34 L. R. Radovic, C. Moreno-Castilla and J. Rivera-Utrilla, Carbon materials as adsorbents in aqueous solution, in *Chemistry and physics of carbon*, ed. L. R. Radovic, Marcel Dekker, New York, 2000, vol. 27, pp. 227–405.
35 G. Wulfsberg, *Inorganic Chemistry*, University Science Book, Herndon, VA, 2000, ch. 2.
36 N. V. Vorob'ev-Desyatovskii, S. A. Kubyshkin, R. I. Ibragimova, V. V. Kaichev, Y. A. Dubrovskii, V. N. Babakov and D. A. Pichugina, *Russ. J. Gen. Chem.*, 2012, **82**, 384.
37 R. F. Baggio and S. Baggio, *J. Inorg. Nucl. Chem.*, 1973, **35**, 3191.
38 M. D. Gutiérrez-Valero, M. L. Godino-Salido, P. Arranz-Mascarós, R. López-Garzón, R. Cuesta and J. García-Martín, *Langmuir*, 2007, **23**, 5995.
39 Z. Tu, S. Lu, X. Chang, Z. Li, Z. Hu, L. Zhang and H. Tian, *Microchim. Acta*, 2011, **173**, 231.
40 H. Kasaini, F. Mahange and K. K. Mbaya, *Proceedings of International Mineral Processing Congress*, ed. W. D. Duo, Beijing, China, 24th edn, 24–28 Sept. 2008, vol. 2, pp. 3117–3123.

Molecules **2015**, *20*, 3783-3790; doi:10.3390/molecules20033783

OPEN ACCESS

molecules

ISSN 1420-3049

www.mdpi.com/journal/molecules

Article

Inorganic Mercury Sequestration by a Poly(ethylene imine) Dendrimer in Aqueous Solution

Elena Salvador Serrano [1], Matteo Savastano [2] and Antonio Bianchi [2,*]

[1] Instituto de Ciencia Molecular, C/Catedrático José Beltrán 2, 46980 Paterna, Valencia, Spain; E-Mail: elena.salvador@uv.es

[2] Department of Chemistry "Ugo Schiff", via della Lastruccia 3, 50019 Sesto Fiorentino, Italy; E-Mail: msavastano@unifi.it

* Author to whom correspondence should be addressed; E-Mail: antonio.bianchi@unifi.it; Tel.: +30-055-4573254.

Academic Editor: Derek J. McPhee

Received: 26 January 2015 / Accepted: 15 February 2015 / Published: 26 February 2015

Abstract: The interaction of the G-2 poly(ethylene imine) dendrimer L, derived from ammonia as initiating core, with Hg(II) and $HgCl_4^{2-}$ was studied in aqueous solution by means of potentiometric (pH-metric) measurements. Speciation of these complex systems showed that L is able to form a wide variety of complexes including 1:1, 2:1, 3:1 and 3:2 metal-to-ligand species, of different protonation states, as well as the anion complexes $[(H_7L)HgCl_4]^{5+}$ and $[(H_8L)HgCl_4]^{6+}$. The stability of the metal complexes is very high, making L an excellent sequestering agent for Hg(II), over a large pH range, and a promising ligand for the preparation of functionalized activated carbons to be employed in the remediation and the prevention of environmental problems.

Keywords: mercury; dendrimers; poly(ethylene imine); contamination; remediation

1. Introduction

Mercury and most of its compounds are highly toxic. They can be absorbed through the skin and mucous membranes, while mercury vapours and volatile derivatives can be inhaled [1]. Mercury is mainly emitted into the air by industries that burn fossil fuels, particularly coal, and by incomplete incineration of wastes containing inorganic mercury. Over the years, however, different chemical

manufacturers and other industrial facilities, have contributed to mercury contamination of the environment. A famous environmental disaster occurred in Japan, where dumping of mercury compounds into Minamata Bay from 1932 to 1968 caused severe poisoning symptoms or death to more than 3000 people from what became known as Minamata disease [2]. Concentrations of mercury up to 3.6 μg/L were measured in seawater of Minamata Bay from 1960 to 1962, when mercury was still being discharged into the bay [3,4], and this caused contamination levels as high as 35.7 ppm in marine products in the bay, while extremely higher mercury levels were found in the tissues (up to 705 ppm in hair) of the poisoned coastline inhabitants [5]. Notwithstanding that, one of the largest sources of mercury intake by people is still a fish-based diet, since fishes, in particular large size ones, accumulate mercury from the aqueous environments where they live.

Hg(II), its chloride complexes present in seawater and methylmercury(II), which is formed in the environment by microbial metabolism and by abiotic chemical reactions involving inorganic mercury, are the main polluting forms of mercury [6–8]. Considering the severe problems generated by this metal to biological systems, it is an important task to find methods of removing these undesirable compounds from the environment and from toxic waste and to find efficient chelation therapies to treat contaminated human beings.

It was shown that activated carbon functionalized with polyamine molecules can be efficiently used for the recovery of both metal ions [9–11] and inorganic anions [12], including $HgCl_4^{2-}$, from aqueous media. Such particular behaviour is due to the dual nature of the polyamine functionalities that are able to coordinate metal ions when they are completely or partially deprotonated and to bind anions, through electrostatic and hydrogen bonds, when they are extensively protonated. Among polyamines, dendrimeric ones are able to coordinate large numbers of metal ions, forming stable complexes, thanks to the many amine groups they contain and to their branched structures. For instance, we have recently shown that even the small poly(ethylene imine) dendrimer L (Figure 1) can bind two metal ions such as Ni(II), Zn(II) and Cd(II) and up to three Cu(II) ions [13]. The same ligand is also able to bind inorganic and organic anions and to form ion-pair complexes [14,15]. Accordingly, polyamine dendrimers display the appropriate binding properties for the recovery of both metal ions and anions from aqueous solutions and, as a matter of fact, it has been demonstrated that activated carbons functionalized with polyalkylamines display excellent performance as Pd(II) scavengers in water [10].

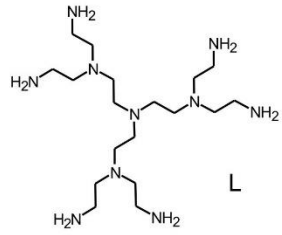

Figure 1. The G-2 poly(ethylene imine) dendrimer L.

For this reason, we have studied the interaction of L with Hg(II) and $HgCl_4^{2-}$ to assess the ability of this ligand to sequestrate these ions in view of a possible use of the dendrimer to prepare functionalized

activated carbons for the remediation of aqueous media contaminated by inorganic mercury. We describe here the results of this study.

2. Results and Discussion

Speciation of the Hg(II)/L systems and determination of the relevant stability constants were performed by means of pH-metric (potentiometric) titrations (0.1 M Me_4NCl, 298.1 ± 0.1 K) and analysis of the associated data by means of the computer program HYPERQUAD [16] which furnished the stability constants collected in Table 1. A medium containing high chloride concentration (0.1 M) was adopted both to facilitate the determination of the large stability constants of Hg(II) complexes and to furnish information about Hg(II) complexation by L in aqueous media with high chloride levels, like seawater.

Table 1. Equilibrium constants (with standard deviations in parentheses) for the complexes formed by L with Hg(II) and $HgCl_4^{2-}$, determined in 0.1 M Me_4NCl aqueous solution at 298.1 K.

Equilibria	log*K*
$L + Hg^{2+} = HgL^{2+}$	28.17(5)
$HgL^{2+} + H^+ = HgLH^{3+}$	9.64(6)
$HgLH^{3+} + H^+ = HgLH_2^{4+}$	8.91(7)
$HgLH_2^{4+} + H^+ = HgLH_3^{5+}$	8.45(5)
$HgLH_3^{5+} + H^+ = HgLH_4^{6+}$	6.13(4)
$HgLH_4^{6+} + H^+ = HgLH_5^{7+}$	4.85(5)
$L + 2Hg^{2+} = Hg_2L^{4+}$	48.38(8)
$Hg_2L^{4+} + H^+ = Hg_2LH^{5+}$	9.41(9)
$Hg_2LH^{5+} + H^+ = Hg_2LH_2^{6+}$	6.63(6)
$HgL^{2+} + Hg^{2+} = Hg_2L^{4+}$	20.21(9)
$2L + 3Hg^{2+} = Hg_3L_2^{6+}$	79.4(1)
$Hg_3L_2^{6+} + H^+ = Hg_3HL_2^{7+}$	10.4(2)
$Hg_3L_2H^{7+} + H^+ = Hg_3L_2H_2^{8+}$	9.0(2)
$Hg_2L^{4+} + HgL^{2+} = Hg_3L_2^{6+}$	2.9(2)
$L + 3Hg^{2+} = Hg_3L^{6+}$	66.74(5)
$Hg_3L^{6+} + OH^- = Hg_3LOH^{5+}$	4.83(8)
$Hg_2L^{4+} + Hg^{2+} = Hg_3L^{6+}$	18.36(8)
$H_7L^{7+} + HgCl_4^{2-} = [(H_7L)HgCl_4]^{5+}$	2.7(1)
$H_8L^{8+} + HgCl_4^{2-} = [(H_8L)HgCl_4]^{6+}$	2.8(1)

The results shown in the table evidence the ability of L to form a variety of complexes with Hg(II), including 1:1, 3:2, 2:1 and 3:1 metal-to-ligand species, of different protonation states, as well as the anion complexes $[(H_7L)HgCl_4]^{5+}$ and $[(H_8L)HgCl_4]^{6+}$. Cumulative species distribution diagrams calculated [17,18] for the formation of these complexes in 1:1, 3:2, 2:1 and 3:1 metal-to-ligand molar ratios (R), under the experimental conditions adopted for the potentiometric measurements, are shown in Figure 2. In these diagrams, the percentage of the overall concentration of complexes with a particular metal-to-ligand stoichiometry (all protonation states) are represented as a function of pH. Distribution diagrams showing the formation of the individual species are reported in the Supplementary Material (Figures S1–S4). As can be seen in Figure 2, in a solution containing Hg(II) and L in 1:1 molar ratio

(R = 1), the mononuclear complexes are the main species above pH 4.5 becoming the only species from pH 8 above (Figure 2a). Increasing R, complexes of higher nuclearity (greater number of metal ions) become of increasing importance (Figure 2b–d), until for R = 3 only trinuclear complexes are formed in alkaline media (Figure 2d). The adducts formed by the anionic $HgCl_4^{2-}$ species are always present in acidic solutions (pH < 5) and their formation increases with increasing R. It is interesting to note that, even for R > 1, mononuclear complexes are the main species in solution around pH 5. This is due to the very high stability of the HgL^{2+} complex (logK = 28.17) and to the high tendency of this complex to bear protonation forming stable species (Table 1) that strongly compete, in this pH region, with the binding of additional metal ions.

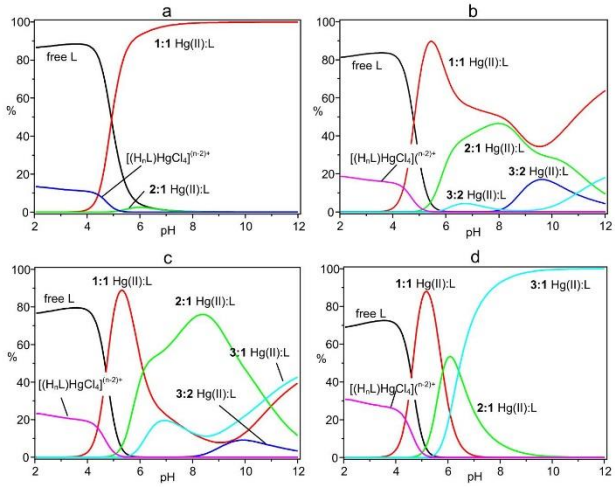

Figure 2. Cumulative distribution diagrams for the system Hg(II)/L. (**a**) [Hg(II)] = [L] = 1×10^{-3} M; (**b**) [Hg(II)] = 1.5×10^{-3} M, [L] = 1×10^{-3} M; (**c**) [Hg(II)] = 2×10^{-3} M, [L] = 1×10^{-3} M; (**d**) [Hg(II)] = 3×10^{-3} M, [L] = 1×10^{-3}M. [Cl^-] = 0.1 M in all cases.

Protonation of primary amine groups in the free ligand L was shown to occur with equilibrium constants log$K \geq 8.32$, while tertiary ones undergo protonation with log$K \leq 5.69$ [13]. Table 1 shows that the first three successive protonation constants of HgL^{2+} are greater than the limiting value (log$K \geq 8.32$) for protonation of primary nitrogens and, accordingly these three protonation stages should involve primary amine groups that are not engaged in metal coordination. The fourth protonation constant (log$K$ = 6.13 for $HgLH_3^{5+} + H^+ = HgLH_4^{6+}$, Table 1) is intermediate between the limiting log$K$ values for protonation of primary and tertiary amine groups of L. Nevertheless, considering that in the complex, the ligand is not able to expand its structure to minimize the electrostatic repulsion between positive charges as it is able to do it in its metal-free form, even this fourth protonation stage can be ascribed to an uncoordinated primary nitrogen. Successive protonation, the fifth one, has a log$K$ value typical of tertiary amine group. All in all, we can reasonably conclude that, in HgL^{2+}, the metal ion is coordinated to five ligand donor atoms, while four primary and one tertiary nitrogen atoms keep

uncoordinated. By similar reasoning, it is possible to draw some conclusions about the coordinated donor atoms in the different complexes and propose the coordination scheme depicted in Figure 3.

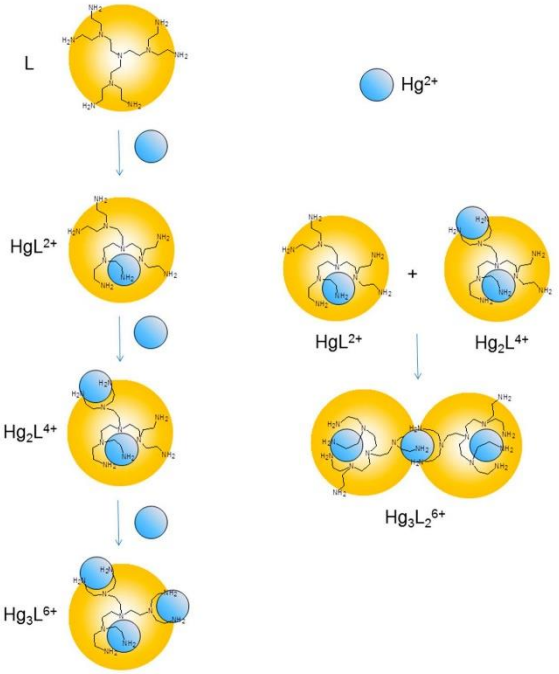

Figure 3. Schematic representation of the coordination environments suggested for the Hg(II) complexes formed by L in solution.

This coordination scheme is consistent with previous results obtained with Ni(II), Zn(II), Cd(II) and Cu(II) and with the crystal structures of the $Ni_3L_2^{6+}$ and Cu_3L^{6+} complexes [13]. It was reported that Ni(II), Zn(II), Cd(II) and Cu(II) form mono- and binuclear complexes with L, while only Cu(II) forms trinuclear species and Ni(II), Zn(II) and Cd(II) form 3:2 metal-to-ligand complexes [13]. Interestingly, Hg(II) forms the whole variety of species and all of them (HgL^{2+}, $Hg_3L_2^{6+}$, Hg_2L^{4+}, Hg_3L^{6+}) are considerably more stable than the corresponding complexes formed by the other metal ions.

As far as the sequestering ability of L toward Hg(II) is considered, we note that the stability constant of the HgL^{2+} complex ($\log K$ = 28.17, Table 1) ranks among the highest values shown by the most efficient chelating agents used for Hg(II) sequestration [19,20]. Furthermore, the ligand is able to sustain the coordination of two additional Hg(II) ions, the corresponding equilibrium constants being still very high ($\log K$ = 20.21 for $HgL^{2+} + Hg^{2+} = Hg_2L^{4+}$ and $\log K$ = 18.36 for $Hg_2L^{4+} + Hg^{2+} = Hg_3L^{6+}$, Table 1), thus making L an excellent sequestering agent for Hg(II). For instance, calculations performed by means of the computer program HYSS [21] show that upon addition of a millimolar amount of L to an aqueous solution of Hg(II), in a concentration corresponding to the maximum level recorded for the Minamata Bay seawater (3.6 μg/L) and in the presence of Cl^- at the common 0.6 M concentration of seawater, the

overall concentration of free mercury (Hg(II), $HgCl^+$, $HgCl_2$, $HgCl_3^-$, $HgCl_4^{2-}$) is reduced to 1.8 ng/L at pH 7, to 0.06 ng/L at pH 7.5 and to 0.02 ng/l at pH 8, despite the strong competitive effect of chloride. Furthermore, under the same conditions but in the absence of chloride, the concentration of free mercury at these pH values is negligible, becoming appreciable only in very acidic solutions (5×10^{-5} ng/L at pH 3). In more alkaline media (pH > 8) the binding ability of L is even greater.

3. Experimental Section

3.1. General

All starting materials were high purity compounds purchased from commercial sources and used as supplied. Ligand L was synthetized according to a previously described procedure [13].

3.2. Potentiometric Measurements

Potentiometric (pH-metric) titrations, used to determine equilibrium constants, were performed in 0.1 M Me_4NCl aqueous solution at 298.1 ± 0.1 K by using an automated system and a procedure already described [13]. The combined Metrohm 6.0262.100 electrode was calibrated as a hydrogen-ion concentration probe by titration of previously standardized amounts of HCl with CO_2-free NMe_4OH solutions and determining the equivalent point by Gran's method [22], which gives the standard potential, $E°$, and the ionic product of water (pK_w = 13.83(1) in 0.1 M Me_4NCl at 298.1 K). A chloride containing medium (0.1 M from the electrolyte) was adopted to take advantage from the competing coordinative effect of chloride in determining the high stability constants of Hg(II) complexes. The computer program HYPERQUAD [16] was used to calculate complex stability constants. Five titrations were performed in the pH range investigated (2.5–11.0) with 1×10^{-3} M ligand concentration and Hg^{2+} concentration in the range $0.5[L] \leq [Hg^{2+}] \leq 2.8[L]$. The different titration curves were treated as separated curves without significant variations in the values of the common stability constants. Finally, the sets of data were merged together and treated simultaneously to give the final stability constants. The hydrolysis of metal ion was considered in calculations. Different equilibrium models for the complex systems were generated by eliminating and introducing different species. Only those models for which the HYPERQUAD program furnished a variance of residuals $\sigma^2 \leq 9$ were accepted. This condition was unambiguously met by a single model. Ligand protonation constants (log$K$ = 10.16, 9.98, 9.25, 9.22, 8.57, 8.32, 5.69, 2.60) [13] and stability constants of Hg(II) chloride complexes [19] were taken from the literature.

4. Conclusions

The G-2 poly(ethylene imine) dendrimer L is able to bind Hg(II) forming complexes with 1:1, 3:2, 2:1 and 3:1 metal-to-ligand stoichiometries. In acidic solution and in the presence of chloride anions, the protonated species H_7L^{7+} and H_8L^{8+} interact with $HgCl_4^{2-}$ to form the $[(H_7L)HgCl_4]^{5+}$ and $[(H_8L)HgCl_4]^{6+}$ anion complexes. The stability of the Hg(II) complexes is very high, much higher than the stability previously found for the analogous complexes with Ni(II), Zn(II), Cd(II) and Cu(II), and ranks among the highest values shown by the most efficient chelating agents used for Hg(II) sequestration. High stability is also observed for protonated Hg(II) complexes with L, which makes this

polyamine dendrimer an excellent sequestering agent for Hg(II) from acidic to alkaline conditions. Accordingly, L is a promising ligand for the preparation of functionalized activated carbons to be employed in the decontamination of polluted waters containing Hg(II), even in the presence of high chloride concentrations, like in seawater, and in a wide pH range. The preparation of such hybrid material and its application will be the subject of a future study.

Supplementary Materials

Supplementary materials can be accessed at: http://www.mdpi.com/1420-3049/20/03/3783/s1.

Acknowledgments

Financial support from the University of Florence is acknowledged.

Author Contributions

Conceived and designed the experiments: E.S., M.S., A.B.; Performed the experiments: E.S., M.S.; Analyzed the data: E.S., M.S., A.B.; Wrote the paper: A.B.

Conflicts of Interest

The authors declare no conflict of interest.

References

1. Merian, E.; Anke, M.; Ihnat, M.; Stoeppler, M. (Eds.) *Elements and Their Compounds in the Environment*; Wiley-VCH: Weinheim, Germany, 2008; pp. 931–1005.
2. Normile, D. In Minamata, Mercury Still Divides. *Science* **2013**, *341*, 1446–1447.
3. Hosohara, K.; Uezuma, H.K.; Kawasaki, K.; Tsuruta, T. Studies on the total amount of mercury in sea waters. *Nippon Kagaku Zasshi* **1961**, *81*, 1479–1480.
4. Kumagai, M.; Nishimura, H. Mercury distribution in seawater in Minamata Bay and the origin of particulate mercury. *J. Oceanogr. Soc. Jpn.* **1978**, *34*, 50–56.
5. Harada, M. Minamata disease: Methylmercury poisoning in Japan caused by environmental pollution. *Crit. Rev. Toxicol*. **1995**, *25*, 1–24.
6. Gianguzza, A., Pellizzetti, E., Sammartano, S., Eds. *Chemistry of Marine Water and Sediments*; Springer: Berlin, Germany, 2002.
7. Gianguzza, A., Pellizzetti, E., Sammartano, S., Eds. *Chemical Processes in Marine Environments*; Springer: Berlin, Germany, 2000.
8. Global Mercury Assessment 2013, United Nations Environment Programme, Geneva, Switzerland. Available online: http://www.unep.org/publications/contents/pub_details_search.asp?ID=6282 (accessed on 23 February 2015).
9. López-Garzón, R.; Godino-Salido, M.L.; Gutiérrez-Valero, M.D.; Arranz-Mascarós, P.; Melguizo, M.; García, C.; Domingo-García, M.; López-Garzón, F.J. Supramolecular assembling of molecular ion-ligands on graphite-based solid materials directed to specific binding of metal ions. *Inorg. Chim. Acta* **2014**, *417*, 208–221.

10. Peñas-Sanjuán, A.; López-Garzón, R.; López-Garzón, J.; Pérez-Mendoza, M.; Melguizo, M. Preparation of a poly-alkylamine surface-functionalized carbon with excellent performance as a Pd(II) scavenger. *Carbon* **2012**, *50*, 2350–2352.
11. García-Martín, J.; López-Garzón, R.; Godino-Salido, M.L.; Cuests-Martos, R.; Gutiérrez-Valero, M.D.; Arranz-Mascarós, P.; Stoeckli-Evans, H. Adsorption of Zn^{2+} and Cd^{2+} from aqueous solution onto a carbon sorbent containing a pyrimidine–polyamine conjugate as ion receptor. *Eur. J. Inorg. Chem.* **2005**, *2005*, 3093–3103, doi:10.1002/ejic.200500071.
12. Arranz, P.; Bianchi, A.; Cuesta, R.; Giorgi, C.; Godino, M.L.; Gutiérrez, M.D.; López, R.; Santiago, A. Binding and removal of sulphate, phosphate, arsenate, tetrachloromercurate, and chromate in aqueous solution by means of an activated carbon functionalized with a pyrimidine-based anion receptor (HL). Crystal structures of $[H_3L(HgCl_4)]\cdot H_2O$ and $[H_3L(HgBr_4)]\cdot H_2O$ showing anion-π interactions. *Inorg. Chem.* **2010**, *49*, 9321–9332.
13. Bazzicalupi, C.; Bianchi, A.; Giorgi, C.; Gratteri, P.; Mariani, P.; Valtancoli, B. Metal ion binding by a G-2 poly(ethylene imine) dendrimer. Ion-directed self-assembling of hierearchical mono- and two-dimensional nanostructured materials. *Inorg. Chem.* **2013**, *52*, 2125–2137.
14. Bazzicalupi, C.; Bianchi, A.; Giorgi, C.; Gratteri, P.; Mariani, P.; Valtancoli, B. Anion and ion-pair binding by a G-2 poly(ethylene imine) dendrimer. *Dalton Trans.* **2013**, *42*, 12130–12138.
15. Bazzicalupi, C.; Bianchi, A.; Giorgi, C.; Valtancoli, B. Zn(II) enhances nucleotide binding and dephosphorylation in the presence of a 2 poly(ethylene imine) dendrimer. *Inorg. Chim. Acta* **2014**, *417*, 163–170.
16. Gans, P.; Sabatini, A.; Vacca, A. Investigation of equilibria in solution. Determination of equilibrium constants with the HYPERQUAD suite of programs. *Talanta* **1996**, *43*, 1739–1753.
17. Bianchi, A.; García-España, E. The Use of calculated species distribution diagrams in the analysis of thermodynamic selectivity. *J. Chem. Educ.* **1999**, *76*, 1727–1732.
18. Bazzicalupi, C.; Bianchi, A.; Giorgi, C.; Clares, M.P.; García-España, E. Addressing selectivity criteria in binding equilibria. *Coord. Chem. Rev.* **2012**, *256*, 13–27.
19. Smith, R.M.; Martell, A.E. *NIST Stability Constants Database, Version 4.0*; National Institute of Standards and Technology: Washington, DC, USA, 1997.
20. Crea, F.; de Stefano, C.; Foti, C.; Milea, D.; Sammartano, S. Chelating agents for the sequestration of mercury(II) and monomethyl mercury(II). *Curr. Med. Chem.* **2014**, *21*, 3819–3836.
21. Alderighi, L.; Gans, P.; Ienco, A.; Peters, D.; Sabatini, A.; Vacca, A. Hyperquad simulation and speciation (HySS): A utility program for the investigation of equilibria involving soluble and partially soluble species. *Coord. Chem. Rev.* **1999**, *184*, 311–318.
22. Gran, G. Determination of the equivalence point in potentiometric titration, Part II. *Analyst (Lond.)* **1952**, *77*, 661–671.

Sample Availability: Samples of L·10HCl are available from the authors.

ChemComm

COMMUNICATION

View Article Online
View Journal | View Issue

Cite this: *Chem. Commun.*, 2015, 51, 3907

Received 14th January 2015,
Accepted 30th January 2015

DOI: 10.1039/c5cc00350d

www.rsc.org/chemcomm

ATP dephosphorylation can be either enhanced or inhibited by pH-controlled interaction with a dendrimer molecule†

Carla Bazzicalupi,[a] Antonio Bianchi,*[a] Claudia Giorgi,[a] Matteo Savastano[a] and Fracisco Morales-Lara[b]

Synthetic polyammonium/polyamine receptors are known to enhance ATP dephosphorylation in solution. ATP interaction with a G-3 poly(ethylene imine) dendrimer shows an unprecedented behaviour, the dendrimer catalyst being able to enhance or inhibit dephosphorylation of the nucleotide depending on the solution pH.

Dendrimers are branched three-dimensional molecules commonly characterized by highly ordered, well defined structures produced by the iterative synthetic routes adopted to grow successive generations (G) of the dendritic architecture around a central core. Their structures can be thought to be characterized by three major parts: the core, the inner shell, and the surface. Lower generation dendrimers are flexible molecules with no appreciable inner regions, while medium sized dendrimers (G-3 or G-4) have an internal space that is essentially separated from the outer shell of the dendrimer. Very large (G-7 and greater) dendrimers are similar to solid particles, with very dense surfaces due to the crowding of branches in the outer shell.[1] The ability of dendrimer molecules to produce surface and/or inner shell binding, transport and release of a variety of chemical species encourages the continuous expansion of their applications in technological areas such as, among others, gene[2] and drug delivery,[3] medicinal chemistry,[4] sensing,[5] advanced materials[6] and catalysis (ref. 1*c*).

We have recently shown that protonated forms of the G-2 poly(ethylene imine) dendrimer L1 (Fig. 1) are able to form stable cation, anion and ion-pair complexes in aqueous solution.[7]

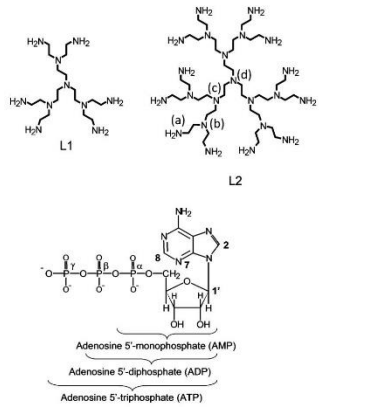

Fig. 1 G-2 (L1) and G3 (L2) poly(ethylene imine) dendrimers and nucleotides.

When the interaction occurs with the anionic forms of ATP (adenosine 5′-triphosphate), dephosphorylation of this nucleotide to form ADP and phosphate was observed to proceed 2–5 times faster, depending on the solution pH, than the uncatalysed process.[7*c*] The ability of polyammonium/polyamine receptors to induce catalytic processes, mimicking the behaviour of ATP-ases or kinases, has been observed for receptors of different molecular structures, including macrocyclic, linear and few branched molecules.[8] Although L1 is significantly less efficient than the abiotic receptors producing highest enhancements of ATP cleavage,[9] its catalytic effect falls within the range shown by most of the synthetic compounds that are able to enhance the activation of ATP dephosphorylation.[8,10]

We have now extended this study to the G-3 poly(ethylene imine) dendrimer L2 (Fig. 1),[11] obtained upon addition of a further generation of ethylamino residues to L1, and found an unprecedented behaviour consisting of the possibility of switching the catalytic action of L2 from enhancement to inhibition of ATP cleavage by changing the solution pH.

[a] *Department of Chemistry "Ugo Schiff", via della Lastruccia 3, 50019 Sesto Fiorentino, Italy. E-mail: antonio.bianchi@unifi.it*
[b] *Department of Inorganic Chemistry, University of Granada, 18071 Granada, Spain*

† Electronic supplementary information (ESI) available: Experimental details of potentiometric, NMR and modelling studies, table providing equilibrium constants for ligand protonation and complex formation with ATP, ADP, AMP, PO_4^{3-}, $P_2O_7^{4-}$ and $P_3O_{10}^{5-}$, and figures showing distribution diagrams of protonated L2 species and L2–ATP complexes, pH dependence of the effective stability constants for the complexes of L2 with PO_4^{3-}, $P_2O_7^{4-}$ and $P_3O_{10}^{5-}$, pH dependence of the ^{1}H NMR spectra of L2, ^{31}P NMR spectra of ATP in the absence and in the presence of L2, ^{31}P NMR data for ATP dephosphorylation and related kinetic fitting. See DOI: 10.1039/c5cc00350d

Potentiometric (pH-metric) titrations performed in water (see the ESI†) showed that tight association occurs between protonated forms of L2 (Table S1 and Fig. S1, ESI†) and the anionic species of ATP, ADP and AMP. An inspection of the equilibrium constants determined for the formation of L2 complexes with these nucleotides (Tables S2–S4, ESI†) evidences some general characteristics. Nucleotide complexation takes place over all the studied pH range (2.5–11) and involves a large number of ligand protonated species spanning from H_2L2^{2+} to $H_{17}L2^{17+}$. The complex stability is very high, even when the ligand is in low protonation states. Indeed, H_2L2^{2+} affords enough attraction to form anion complexes of considerable stability (*e.g.* $\log K$ = 4.21 for $H_2L2^{2+} + ATP^{4-} = [H_2L2(ATP)]^{2}$) while in the case of L1 a minimum of 4+ charge was necessary to form a weaker complex ($\log K$ = 3.72 for $H_4L1^{4+} + ATP^{4-} = [H_4L1(ATP)]$).[7c] Very likely, the G-3 polyamine-dendrimer L2, with its 12 primary and 10 tertiary amine groups, is able to establish a great number of hydrogen bond contacts with these anionic nucleotides even when it does not hold a great positive charge. Hydrogen bonds are known to play a crucial role in nucleotide–polyammonium receptor interactions.[8,12]

Another interesting aspect of these complex systems is the approximate invariance of stability displayed by complexes with the ligand in high protonation states (Tables S2–S4, ESI†). L2 is a large molecule; its successive protonation stages (Table S1, ESI†) take place in such a way that the generated ammonium groups are located as far as possible from each other, to minimize the electrostatic repulsion (see the ESI†), leading, as a further consequence, to progressive expansion and stiffening of the molecule. Then, in contrast to more preorganized molecules, such as macrocycles for instance, most of the binding sites in the protonated forms of L2 are divergent with respect to the interacting nucleotides. Large ligand dimensions, ligand rigidity and low preorganization make the nucleotide interact with a sector of the ligand, and therefore the adduct stability is poorly, or not at all affected by ligand protonation occurring far from the bound nucleotide.

On a comparative basis, L2 shows a binding preference for ADP over both AMP and ATP, for given protonation states of ligand and nucleotides, the general trend being ADP > ATP > AMP. That is, L2 performs a selective recognition of ADP, despite the greater negative charge of ATP species favouring the latter. Remarkably, another case of molecular recognition of ADP over ATP was recently reported for a pyrimidine derivative of tren (tris(2-aminoethyl)amine), the G-1 precursor of L2.[13] The binding behaviour of L2 toward the three nucleotides can be evidenced, over the entire pH range, by comparing the effective (conditional) stability constants calculated as a function of pH for these binding events. This is a practical computational method for the analysis of binding selectivity in competitive systems which balances all complex stability constants along with receptor and substrate basicity.[14] Plots of the effective stability constants, as a function of pH, for the nucleotide/L2 systems (Fig. 2) show that the ligand preference for ADP increases above pH 5, while ATP starts being competitive only below pH 9.

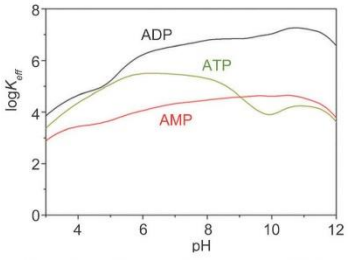

Fig. 2 Logarithms of the effective stability constants (K_{eff}) for the interaction of L2 with ATP, ADP and AMP calculated as a function of pH.

Analogous studies performed for the interaction of L2 with PO_4^{3-}, $P_2O_7^{4-}$ and $P_3O_{10}^{5-}$, which are the inorganic portions of AMP, ADP and ATP, respectively, showed that the binding features of the phosphate anions are consistent with those of the corresponding nucleotides, including some disadvantageous binding of $P_3O_{10}^{5-}$ in a limited region above pH 10, but below pH 10 the trend of binding stability expected on the basis of electrostatic considerations ($P_3O_{10}^{5-} > P_2O_7^{4-} > PO_4^{3-}$) is invariably observed (Fig. S2, ESI†). Accordingly, we can conclude that electrostatic and hydrogen bond interactions between the protonated forms of L2 and the phosphate chains of the nucleotides are the driving forces of these association processes, while the adenosine residue furnishes a significant regulation of the nucleotide–ligand interaction, determining the binding selectivity.

^{31}P NMR spectra recorded for ATP solutions at pH 3, 6 and 9, in the absence and in the presence of L2, showed a downfield shift of the ^{31}P NMR signals of ATP, in particular of P_β and P_γ, determined by interaction of the nucleotide with the positively charged ligand (Fig. S3, ESI†). At pH 9, only P_β shows a significant shift, P_α and P_γ being modestly affected, while greater coordination induced shifts are observed at lower pH. Accordingly, modelling calculations (see the ESI†) performed for the $[H_9L2(ATP)]^{5+}$ and $[H_{15}L2(H_2ATP)]^{13+}$ adducts, which are main species at pH 9 and 3 (Fig. S4, ESI†), respectively, showed that, in an implicit simulation of the aqueous environment, the nucleotide forms a greater number of salt–bridge interactions with the more charged ligand form (Fig. 3).

According to calculations, ATP is attracted under the dendrimer surface where the phosphate chain of the nucleotide is shielded from solvent interactions (Fig. 4).

The most outstanding feature of these nucleotide/L2 systems is the effect of L2 on ATP dephosphorylation to form ADP and inorganic phosphate. Depending on the solution pH, L2 can enhance or inhibit this process. ATP hydrolysis over time was followed at pH 3 and 9 by ^{31}P NMR at 343.1 K (Fig. S5, ESI†) with solutions 0.01 M of ATP and 0.001 M of L2. As shown in Table 1, the presence of L2 at pH 9 gives rise to an approximate 6-fold enhancement of the dephosphorylation rate, while at pH 3 the spontaneous ATP cleavage is slowed down by about 30% in the presence of the dendrimer. Such unprecedented behaviour is in

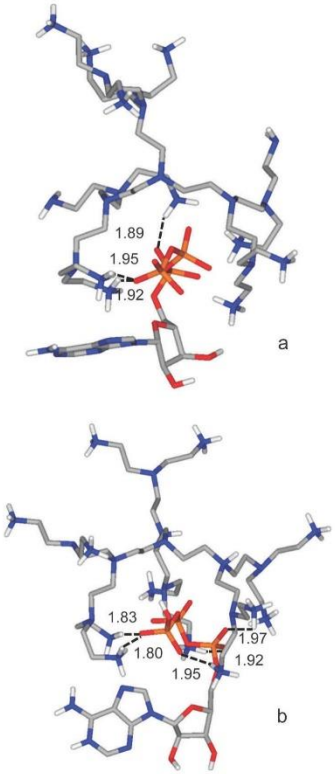

Fig. 3 Minimum energy structures calculated for the adducts $[H_9L2(ATP)]^{5+}$ (a) and $[H_{15}L2(H_2ATP)]^{13+}$ (b). Hydrogen bond distances are in Å. Only contacts shorter than 2.0 Å are shown.

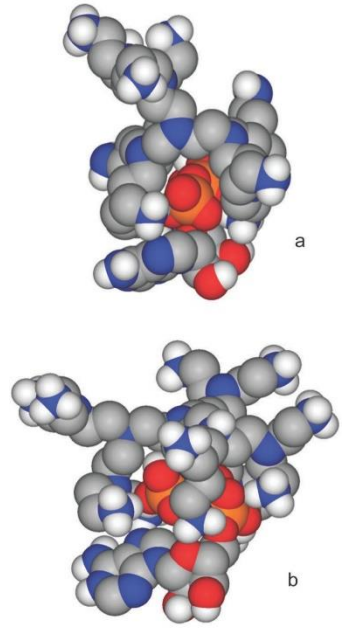

Fig. 4 Space filling views of the minimum energy structures calculated for the adducts $[H_9L2(ATP)]^{5+}$ (a) and $[H_{15}L2(H_2ATP)]^{13+}$ (b).

Table 1 Rate constants (k) determined at 343.1 K for ATP dephosphorylation in the absence and in the presence of L2

	pH	k ($min^{-1} \times 10^3$)
ATP	3	0.68(2)[a]
ATP	9	0.041(4)
L2 + ATP	3	0.48(4)
L2 + ATP	9	0.23(4)

[a] Values in parentheses are standard deviations on the last significant figures.

agreement with the different ATP adducts formed at the different pH values, with their calculated structures and with the location of ammonium groups in the protonated forms of L2 deduced by ^{1}H NMR spectra (Fig. S6, ESI†). The latter shows that the first 12 H^+ ions bind the 12 primary N(a) atoms (Fig. 1), which remain protonated in more acidic solutions. The 13th proton binds the central tertiary N(d) nitrogen, while in the two successive protonation stages, until the formation of $H_{15}L2^{15+}$, also N(c) nitrogen atoms get involved. Successive protonation causes a redistribution of protons over all tertiary amine groups.

It is known that when the polyamine receptor contains unprotonated amine groups, nucleotide dephosphorylation proceeds through the formation of a labile phosphoramidate intermediate.[9b,c,13–18] Indeed, in the principal ATP complex formed by L2 at pH 9, $[H_9L2(ATP)]^{5+}$, there are at least three unprotonated primary amine groups which are available for the formation of the phosphoramidate intermediate.

Conversely, in the complexes formed in acidic media, all surface amine groups are protonated while in the inner dendrimer region, where the phosphate ATP chain is attracted, there are only tertiary amine groups that are unable to form the phosphoramidate intermediate. In this environment, ATP, which is present at pH 3 as H_2ATP^{2-}, is protected from solvent interactions and its spontaneous dephosphorylation, that is thought to proceed through the formation of a labile monomeric metaphosphate intermediate,[19] becomes slower.

In conclusion, interaction of ATP with differently protonated forms of the G-3 poly(ethylene imine) dendrimer L2 produces opposite dephosphorylation effects in giving ADP and inorganic phosphate. In alkaline solutions, where ATP finds unprotonated primary amine groups of L2 that can trigger the phosphoramidate-mediated

hydrolytic mechanism, dephosphorylation is enhanced with respect to the spontaneous process, while in the acidic region, where unprotonated primary amine groups are no longer available, inclusion of the nucleotide phosphate chain into the inner dendrimer region protects ATP from the spontaneous dephosphorylation reaction, thus inhibiting the process. Previous studies of the effect of synthetic receptors on the process of ATP dephosphorylation have concentrated exclusively on the enhancement aspect and, to the best of our knowledge, a receptor capable of producing both enhancement and inhibition has never been found, neither has one been found that could produce just the inhibition.

The unprecedented behaviour shown by L2 is further evidence of the peculiar properties characterizing the inclusion compounds of dendrimer molecules.

Notes and references

1 (*a*) F. Vögtle, G. Richardt and N. Werner, *Dendrimer Chemistry*, Wiley-VCH, Weinheim, 2007; (*b*) U. Boas, J. B. Christensen and P. M. H. Heegaard, *Dendrimers in medicine and biotechnology: new molecular tools*, RSC Publishing, Cambridge, 2006; (*c*) *Dendrimer Catalysis*, Topics in Organometallic Chemistry, ed. L. H. Gade, Springer, Berlin, vol. 20, 2006; (*d*) G. R. Newkome, C. N. Moorefield and F. Vögtle, *Dendritic Molecules: Concepts, Syntheses, Perspectives*, VCH, Weinheim, 1996; (*e*) D. A. Tomalia, A. M. Naylor and W. A. Goddard III, *Angew. Chem., Int. Ed.*, 1990, **29**, 138–175; (*f*) G. Bergamini, E. Marchi and P. Ceroni, *Coord. Chem. Rev.*, 2011, **255**, 2458; (*g*) D. Konkolewicz, M. J. Monteiro and S. Perrier, *Macromolecules*, 2011, **44**, 7067; (*h*) H. Frey, C. Lach and K. Lorenz, *Adv. Mater.*, 1998, **10**, 279; (*i*) L. M. Bronstein and Z. B. Shifrina, *Chem. Rev.*, 2011, **111**, 5301.

2 (*a*) M. Guillot-Nieckowski, S. Eisler and F. Diederich, *New J. Chem.*, 2007, **31**, 1111; (*b*) D. Ferber, *Science*, 2001, **294**, 1638; (*c*) J. F. Kukowska-Latallo, A. U. Bielinska, J. Johnson, R. Spindler, D. A. Tomalia and J. R. Baker, *Proc. Natl. Acad. Sci. U. S. A.*, 1996, **93**, 4897.

3 R. J. Amir, L. Albertazzi, J. Willis, A. Khan, T. Kang and C. J. Hawker, *Angew. Chem., Int. Ed.*, 2011, **50**, 3425.

4 (*a*) R. Rupp, S. L. Rosenthal and L. R. Stanberry, *Int. J. Nanomed.*, 2007, **2**, 561; (*b*) R. Roy, *Curr. Opin. Struct. Biol.*, 1996, **6**, 692.

5 L. Albertazzi, B. Storti, L. Marchetti and F. Beltram, *J. Am. Chem. Soc.*, 2010, **132**, 18158.

6 (*a*) G. J. Tong, S. C. Hsiao, Z. M. Carrico and M. B. Francis, *J. Am. Chem. Soc.*, 2009, **131**, 11174; (*b*) S. Mann, *Nat. Mater.*, 2009, **8**, 781; (*c*) K. Okuro, K. Kinbara, K. Tsumoto, N. Ishii and T. Aida, *J. Am. Chem. Soc.*, 2009, **131**, 1626; (*d*) G. M. Whitesides and B. Grzybowski, *Science*, 2002, **295**, 2418.

7 (*a*) C. Bazzicalupi, A. Bianchi, C. Giorgi, P. Gratteri, P. Mariani and B. Valtancoli, *Inorg. Chem.*, 2013, **52**, 2125; (*b*) C. Bazzicalupi, A. Bianchi, C. Giorgi, P. Gratteri, P. Mariani and B. Valtancoli, *Dalton Trans.*, 2013, **42**, 12130; (*c*) C. Bazzicalupi, A. Bianchi, C. Giorgi and B. Valtancoli, *Inorg. Chim. Acta*, 2014, **417**, 163.

8 (*a*) E. García-España, R. Belda, J. Gonzalez, J. Pitarch and A. Bianchi, Receptors for nucleotides, in *Supramolecular Chemistry: From Molecules to Nanomaterials*, ed. P. A. Gale and J. W. Steed, John Wiley & Sons, New York, 2012, vol. 3; (*b*) C. Bazzicalupi, A. Bencini and V. Lippolis, *Chem. Soc. Rev.*, 2010, **39**, 3709; (*c*) E. Garcia-España, P. Díaz, J. M. Llinares and A. Bianchi, *Coord. Chem. Rev.*, 2006, **250**, 2952; (*d*) S. O. Kang, M. A. Hossain and K. Bowman-James, *Coord. Chem. Rev.*, 2006, **250**, 3038.

9 (*a*) M. W. Hosseini, J.-M. Lehn and M. P. Mertes, *Helv. Chim. Acta*, 1983, **66**, 2454; (*b*) A. Bencini, A. Bianchi, E. Garcia-España, E. C. Scott, L. Morales, B. Wang, T. Deffo, F. Takusagawa, M. P. Mertes, K. Bowman Mertes and P. Paoletti, *Bioorg. Chem.*, 1992, **20**, 8; (*c*) J. A. Aguilar, A. B. Descalzo, P. Díaz, V. Fusi, E. García-España, S. V. Luis, M. Micheloni, J. A. Ramírez, P. Romani and C. Soriano, *J. Chem. Soc., Perkin Trans. 2*, 2000, 1187.

10 (*a*) A. Andrés, J. Aragó, A. Bencini, A. Bianchi, A. Domenech, V. Fusi, E. García-España, P. Paoletti and J. A. Ramírez, *Inorg. Chem.*, 1993, **32**, 3418; (*b*) J. Aguilar, E. García-España, J. A. Guerrero, S. V. Luis, J. M. Llinares, J. F. Miravet, J. A. Ramírez and C. Soriano, *J. Chem. Soc., Chem. Commun.*, 1995, 2237; (*c*) J. Aguilar, E. García-España, J. A. Guerrero, S. V. Luis, J. M. Llinares, J. A. Ramírez and C. Soriano, *Inorg. Chim. Acta*, 1996, **246**, 287; (*d*) M. T. Albelda, M. A. Bernardo, E. García-España, M. L. Godino-Salido, S. V. Luis, M. J. Melo, F. Pina and C. Soriano, *J. Chem. Soc., Perkin Trans. 2*, 1999, 2545; (*e*) M. T. Albelda, J. Aguilar, S. Alves, R. Aucejo, P. Díaz, C. Lodeiro, J. C. Lima, E. García-España, F. Pina and C. Soriano, *Helv. Chim. Acta*, 2003, **86**, 3118; (*f*) A.-S. Delépine, R. Tripier, N. Le Bris, H. Bernard, A. Honraedt and H. Handel, *Inorg. Chim. Acta*, 2009, **362**, 3829; (*g*) Y. Guo, Q. Ge, H. Lin, H. Lin, S. Zhu and C. Zhou, *J. Mol. Recognit.*, 2003, **16**, 102; (*h*) Y. Guo, Q. Ge, H. Lin, H. Lin and S. Zhu, *Inorg. Chem. Commun.*, 2003, **6**, 308; (*i*) Y. Guo, Q. Ge, H. Lin, H. K. Lin, S. Zhu and C. Zhou, *Biophys. Chem.*, 2003, **105**, 119; (*j*) J. Aguilar, P. Díaz, F. Escartí, E. García-España, L. Gil, C. Soriano and B. Verdejo, *Inorg. Chim. Acta*, 2002, **339**, 307; (*k*) C. Bazzicalupi, A. Bencini, E. Berni, A. Bianchi, P. Fornasari, C. Giorgi, C. Marinelli and B. Valtancoli, *Dalton Trans.*, 2003, 2564.

11 L2 was synthetized according to the procedure reported in S. H. Lee, D.-J. Kim, C.-C. Chang, S. S. Hah and J. Suh, *Bull. Korean Chem. Soc.*, 1998, **19**, 1270.

12 A. Bianchi, M. Micheloni and P. Paoletti, *Inorg. Chim. Acta*, 1988, **151**, 269.

13 P. Arranz Mascaros, C. Bazzicalupi, A. Bianchi, C. Giorgi, M. D. Gutíerrez Valero, R. López Garzón, M. L. Godino Salido and B. Valtancoli, *Chem. Commun.*, 2011, **47**, 2814.

14 C. Bazzicalupi, A. Bianchi, C. Giorgi, M. P. Clares and E. Gracia-España, *Coord. Chem. Rev.*, 2012, **256**, 13.

15 *Supramolecular Chemistry of Anions*, ed. A. Bianchi, K. Bowman-James and E. García-España, Wiley-VCH, New York, 1997.

16 E. Kimura, M. Kodama and T. Yatsunami, *J. Am. Chem. Soc.*, 1982, **104**, 3182.

17 P. G. Yohannes, M. P. Mertes and K. Bowman James, *J. Am. Chem. Soc.*, 1985, **107**, 8288; M. W. Hosseini, J.-M. Lehn, S. R. Duff, K. Gu and M. P. Mertes, *J. Org. Chem.*, 1987, **52**, 1662.

18 (*a*) A. Andrés, C. Bazzicalupi, A. Bencini, A. Bianchi, V. Fusi, E. García-España, C. Giorgi, N. Nardi, P. Paoletti, J. A. Ramirez and B. Valtancoli, *J. Chem. Soc., Perkin Trans. 2*, 1994, 2367; (*b*) A. Bencini, A. Bianchi, C. Giorgi, P. Paoletti, B. Valtancoli, V. Fusi, E. García-España, J. M. Llinares and J. A. Ramírez, *Inorg. Chem.*, 1996, **35**, 1114; (*c*) C. Bazzicalupi, A. Bencini, A. Bianchi, A. Danesi, C. Giorgi, C. Lodeiro, F. Pina, S. Santarelli and B. Valtancoli, *Chem. Commun.*, 2005, 2630.

19 F. Ramirez and J. F. Marecek, *Pure Appl. Chem.*, 1980, **52**, 1021.

molecules

MDPI

Article

Cation, Anion and Ion-Pair Complexes with a G-3 Poly(ethylene imine) Dendrimer in Aqueous Solution

Matteo Savastano [1], Carla Bazzicalupi [1], Claudia Giorgi [1], Paola Gratteri [2] and Antonio Bianchi [1,*]

[1] Department of Chemistry "Ugo Schiff", via della Lastruccia 3, 50019 Sesto Fiorentino, Italy; matteo.savastano@unifi.it (M.S.); carla.bazzicalupi@unifi.it (C.B.); Claudia.giorgi@unifi.it (C.G.)

[2] NEUROFARBA Department, Pharmaceutical and Nutraceutical Section, and Laboratory of Molecular Modeling Cheminformatics & QSAR, University of Florence, Via Ugo Schiff 6, 50019 Sesto Fiorentino, Italy; paola.gratteri@unifi.it

* Correspondence: antonio.bianchi@unifi.it; Tel.: +39-055-457-3254

Academic Editor: Ashok Kakkar
Received: 12 April 2017; Accepted: 12 May 2017; Published: 16 May 2017

Abstract: The G-3 poly(ethylene imine) ligand L2 shows a multifaceted coordination ability, being able to bind metal cations, anions and ion-pairs. The equilibrium constants for the formation of metal (Cu^{2+}, Zn^{2+}), anion (SO_4^{2-}) and ion-pair (Cu^{2+}/SO_4^{2-}) complexes were determined in 0.1 M Me_4NCl aqueous solution at 298.1 ± 0.1 K by means of potentiometric titrations. Thanks to its dendrimeric nature, L2 can form highly nucleated metal complexes, such as Cu_5L2^{10+} and Zn_4L2^{8+}, in successive and well-defined complexation steps. Protonated forms of L2 give rise to relatively weak anion complexes with SO_4^{2-}, but the addition of Cu^{2+} significantly enhances the binding ability of the ligand toward this anion below pH 9. In more alkaline solutions, an opposite trend is observed. The coordination properties of L2 are discussed with the support of modelling calculations. According to results, L2 is a promising molecule for the preparation of solid supported materials for the recovery of cations and anions from aqueous media and/or for applications in heterogeneous catalysis.

Keywords: copper; zinc; dendrimers; poly(ethylene imine); polynuclear complexes; anion complexes; ion-pair complexes

1. Introduction

In recent papers, we showed that the G-2 poly(ethylene imine) dendrimer L1 (Figure 1) and its variously protonated forms are able to assemble stable cation, anion and ion-pair complexes in aqueous solution [1–4]. Such ability appears to be a propagation and an enhancement of the properties of the parent ligand tris(2-aminoethyl)amine (*tren*), which is historically known to bind metal complexes and, more recently, has also been accredited as a rather efficient anion receptor [5]. Indeed, regarding the coordination of metal ions, while *tren* forms stable mononuclear complexes, L1 can bind two metal ions such as Ni^{2+}, Zn^{2+} and Cd^{2+} and up to three Cu^{2+} and Hg^{2+} ions [1,4]. L1 and its metal complexes are also able to bind inorganic anions [2] as well as the anionic forms of AMP, ADP and ATP nucleotides acting as catalysts that enhance significantly ATP dephosphorylation in aqueous solution [3]. Construction of a third generation of ethylamino branches around L1 gave rise to the G-3 poly(ethylene imine) dendrimer L2 (Figure 1) that is also able to bind anions, such as PO_4^{3-}, $P_2O_7^{4-}$ and $P_3O_{10}^{5-}$, and AMP, ADP and ATP nucleotides. In particular, L2 showed an unprecedented behaviour toward ATP, the dendrimer being able to enhance or inhibit dephosphorylation of the nucleotide depending on the solution pH [6].

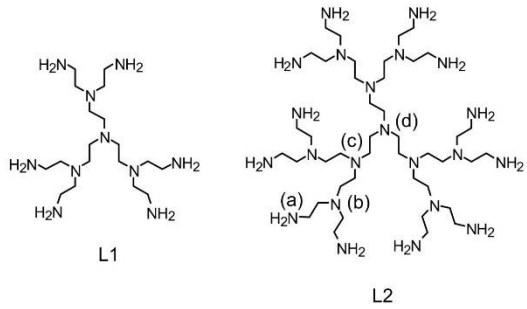

Figure 1. G-2 (**L1**) and G-3 (**L2**) poly(ethylene imine) dendrimers.

Despite the discovery of such properties towards nucleotide and phosphate type anions, the ability of L2 to bind metal cations, inorganic anions and ion-pairs remains unexplored. Actually, L2 is a very interesting ligand for the formation of metal complexes, in particular of polynuclear assemblies, since it contains a large number (22) of nitrogen donor atoms in its molecular structure, and accordingly, it should be able to form complexes of greater nuclearity than the smaller homologous L1. It is worth of note that there is a great deal of interest toward polynuclear metal complexes, especially for their catalytic properties and/or for their use in the generation of metal nanoparticle-based catalysts [7–10].

This has aroused our interest in performing a detailed analysis of the complexation equilibria involving L2, metal cations and anions in aqueous solution. As previously noted [1], to study similar complexation systems is an arduous task, due to the many equilibria involving the stepwise coordination of several metal ions involving several protonation states for each complexation step. Attempts to perform the speciation of complex systems and determining the equilibrium constants for complexation equilibria with other poly(ethylene imine) dendrimers were made by considering the repeating triamine units of the dendrimer as identical independent ligand molecules, under the implicit assumption that these repeating units were uniformly distributed in solution, in contrast to their actual localization within the same dendrimer molecule [11]. These studies were performed under conditions approaching the ligand coordinative saturation, the metal-to-triamine unit ratios being closed to 1:1 and extending it, at most, up to 1:4.

Despite such an approximation, the results of these studies can be functional for the purposes for which they are developed, although they furnish an incomplete picture of the complexation systems. In particular, this approach leads to the identification of a limited number of complex species relative to the many that these dendrimers can form. For instance, dendrimers containing large numbers of amino groups are expected to bind metal ions even when they are extensively protonated. Some of the missing species could have interesting properties, like the ability of highly protonated Zn(II) complexes with L1 to promote the binding and the dephosphorylation of ATP [3].

In this paper, we report the results of a detailed analysis of the complexation systems formed by L2 with Zn^{2+} and Cu^{2+} that led to the identification of 35 and 42 complex species for Zn^{2+} and Cu^{2+}, respectively, the ligand achieving the stepwise coordination of 4 Zn^{2+} or 5 Cu^{2+} ions. Once these complexation systems were clearly defined, we analysed the ability of L2 to interact with SO_4^{2-} both in the absence and in the presence of Cu^{2+}.

2. Results and Discussion

2.1. Formation of Metal Complexes

Speciation of L2/Cu^{2+} and L2/Zn^{2+} complex systems and determination of the relevant stability constants were performed by means of pH-metric (potentiometric) titrations (0.1 M Me_4NCl,

298.1 ± 0.1 K) and analysis of the associated data by means of the computer program HYPERQUAD [12] which furnished the stability constants collected in Tables 1 and 2 for Cu^{2+} and Zn^{2+}, respectively. Distribution diagrams of the complexes formed are reported in Figures S1 and S2.

As shown by these tables, the G-3 dendrimer L2 is able to bind in successive steps from one to five Cu^{2+} cations and from one to four Zn^{2+} ions. According to the presence of many (22) nitrogen donor atoms in the ligand, all complexes but Cu_5L2^{10+} are able to bind protons, and the number of protonated species they form decreases with increasing complex nuclearity. It was previously reported that protonation of the primary amine groups of L2 is associated with protonation constants log$K \geq 8.3$ [6]. Considering this value as the limiting value for protonation of primary amine groups also in L2 complexes, we can deduce from the equilibrium data in Table 1 that, in $CuL2^{2+}$, there are nine primary amine groups, out of 12, that are not involved in metal coordination. By similar reasoning, and taking into account the experimental errors on the determined equilibrium constants, the number of uncoordinated primary nitrogens can be reasonably estimated as six in Cu_2L2^{4+}, five in Cu_3L2^{6+}, three in Cu_4L2^{8+}, and none in Cu_5L2^{10+}. The equilibrium constants for the successive binding of the first and the second Cu^{2+} ions are very high (log$K$ = 23.66 and 22.9, Table 1) and consistent with the stability of hexacoordinated Cu^{2+} complexes of polyamines [13,14]. Accordingly, the first two Cu^{2+} ions binding L2 should be coordinated by three primary and three secondary amine groups near the surface of the G-3 dendrimer. The third coordination stage causes a greater involvement of the inner dendrimer region, since only one primary amine group is involved in the equilibrium $Cu_2L2^{4+} + Cu^{2+} = Cu_3L2^{6+}$. This appears to be a poorly favourable coordination step as shown by the surprisingly low value of the corresponding equilibrium constant (log$K$ = 10.0, Table 1).

Table 1. Stability constants of Cu^{2+} complexes with L2. 0.1 M Me_4NCl, 298.1 ± 0.1 K. Values in parentheses are standard deviation on the last significant figure.

Equilibria	log$K$	Equilibria	log$K$
$Cu^{2+} + L2 = CuL2^{2+}$	23.66 (5)	$Cu_2H_7L2^{11+} + H^+ = Cu_2H_8L2^{12+}$	7.46 (8)
$CuL2^{2+} + 2H^+ = CuH_2L2^{4+}$	22.88 (7)	$Cu_2H_8L2^{12+} + H^+ = Cu_2H_9L2^{13+}$	6.25 (8)
$CuH_2L2^{4+} + H^+ = CuH_3L2^{5+}$	9.93 (5)	$Cu_2H_9L2^{13+} + H^+ = Cu_2H_{10}L2^{14+}$	4.98 (7)
$CuH_3L2^{5+} + H^+ = CuH_4L2^{6+}$	10.07 (5)	$Cu_2H_{10}L2^{14+} + H^+ = Cu_2H_{11}L2^{15+}$	4.07 (7)
$CuH_4L2^{6+} + H^+ = CuH_5L2^{7+}$	9.42 (3)		
$CuH_5L2^{7+} + H^+ = CuH_6L2^{8+}$	9.21 (7)	$3Cu^{2+} + L2 = Cu_3L2^{6+}$	56.55 (7)
$CuH_6L2^{8+} + H^+ = CuH_7L2^{9+}$	9.09 (7)	$Cu_2L2^{4+} + Cu^{2+} = Cu_3L2^{6+}$	10.0 (1)
$CuH_7L2^{9+} + H^+ = CuH_8L2^{10+}$	8.63 (5)	$Cu_3L2^{6+} + 2H^+ = Cu_3H_2L2^{8+}$	22.72 (6)
$CuH_8L2^{10+} + H^+ = CuH_9L2^{11+}$	8.50 (4)	$Cu_3H_2L2^{8+} + H^+ = Cu_3H_3L2^{9+}$	10.31 (7)
$CuH_9L2^{11+} + H^+ = CuH_{10}L2^{12+}$	8.13 (4)	$Cu_3H_3L2^{9+} + H^+ = Cu_3H_4L2^{10+}$	8.87 (8)
$CuH_{10}L2^{12+} + H^+ = CuH_{11}L2^{13+}$	7.49 (4)	$Cu_3H_4L2^{10+} + H^+ = Cu_3H_5L2^{11+}$	8.50 (8)
$CuH_{11}L2^{13+} + H^+ = CuH_{12}L2^{14+}$	5.87 (4)	$Cu_3H_5L2^{11+} + H^+ = Cu_3H_6L2^{12+}$	7.39 (7)
$CuH_{12}L2^{14+} + H^+ = CuH_{13}L2^{15+}$	5.18 (4)	$Cu_3H_6L2^{12+} + H^+ = Cu_3H_7L2^{13+}$	6.82 (8)
$CuH_{13}L2^{15+} + H^+ = CuH_{14}L2^{16+}$	3.94 (5)	$Cu_3H_7L2^{13+} + H^+ = Cu_3H_8L2^{14+}$	5.81 (8)
$CuH_{14}L2^{16+} + H^+ = CuH_{15}L2^{17+}$	2.59 (5)		
$CuH_{15}L2^{17+} + H^+ = CuH_{16}L2^{18+}$	2.89 (6)	$4Cu^{2+} + L2 = Cu_4L2^{8+}$	72.6 (1)
		$Cu_3L2^{6+} + Cu^{2+} = Cu_4L2^{8+}$	16.0 (1)
$2Cu^{2+} + L2 = Cu_2L2^{4+}$	46.53 (7)	$Cu_4L2^{8+} + 2H^+ = Cu_4H_2L2^{8+}$	22.5 (1)
$CuL2^{2+} + Cu^{2+} = Cu_2L2^{4+}$	22.9 (1)	$Cu_4H_2L2^{10+} + H^+ = Cu_4H_3L2^{11+}$	8.54 (1)
$Cu_2L2^{4+} + H^+ = Cu_2HL2^{5+}$	11.51 (6)	$Cu_4H_3L2^{11+} + H^+ = Cu_4H_4L2^{12+}$	7.3 (1)
$Cu_2HL2^{5+} + H^+ = Cu_2H_2L2^{6+}$	10.20 (7)	$Cu_4H_4L2^{12+} + H^+ = Cu_4H_5L2^{13+}$	6.9 (1)
$Cu_2H_2L2^{6+} + H^+ = Cu_2H_3L2^{7+}$	9.24 (7)	$Cu_4H_5L2^{13+} + H^+ = Cu_4H_6L2^{14+}$	3.9 (1)
$Cu_2H_3L2^{7+} + H^+ = Cu_2H_4L2^{8+}$	9.61 (6)		
$Cu_2H_4L2^{8+} + H^+ = Cu_2H_5L2^{9+}$	8.31 (7)	$5Cu^{2+} + L2 = Cu_5L2^{10+}$	82.0 (2)
$Cu_2H_5L2^{9+} + H^+ = Cu_2H_6L2^{10+}$	8.22 (7)	$Cu_4L2^{8+} + Cu^{2+} = Cu_5L2^{10+}$	9.4 (3)
$Cu_2H_6L2^{10+} + H^+ = Cu_2H_7L2^{11+}$	8.18 (7)	$Cu_5L2^{10+} + 2OH^- = [Cu_5L2(OH)_2]^{8+}$	8.5 (2)

Such a drop of the metal ion binding constant is, most likely, determined by an important structural rearrangement that the very stable Cu_2L2^{4+} complex must bear to accommodate the third Cu^{2+} ion. Conversely, Cu_3L2^{6+} displays a greater binding ability toward Cu^{2+} than Cu_2L2^{4+} ($Cu_3L^{6+} + Cu^{2+} = Cu_4L^{8+}$, log$K$ = 16.0, Table 1), that is, the coordination of the third Cu^{2+} ion is not very favourable but generates the structural conditions for a favourable continuation of the

stepwise binding process. Two of the 5 free primary amine groups of Cu_3L2^{6+} become coordinated in Cu_4L2^{8+}, while no primary amine group appears to be available for protonation in Cu_5L2^{10+}. The formation of the latter from the tetranuclear complex is accompanied by a small equilibrium constant ($Cu_4L^{8+} + Cu^{2+} = Cu_5L^{10+}$, log*K* = 9.4, Table 1) in agreement with the high electrostatic repulsion exerting between the five metal ions and the reduced number of donor atoms remaining available for coordination in Cu_4L2^{8+}. As a matter of fact, the ligand is not able to fulfil the coordination sphere of all five metal ions in Cu_5L2^{10+} and facile dissociation of coordinated water molecules generates the hydroxo complex $[Cu_5L2(OH)_2]^{8+}$.

In contrast to Cu^{2+}, in the case of Zn^{2+} complexation, the equilibrium constants for the successive binding of metal ions to form $ZnL2^{2+}$, Zn_2L2^{4+}, Zn_3L2^{6+} and Zn_4L2^{8+} (log*K* = 17.8, 13.2, 11.0, 10.7, Table 2) display a more regular trend. The loss of stability from the mono- to the binuclear complex (log*K* = 17.8, 13.2, Table 2) is greater than for the corresponding equilibria with Cu^{2+}. Nevertheless, also the stability constants for the formation of $ZnL2^{2+}$ and Zn_2L2^{4+} are consistent with the stability of hexacoordinated Zn^{2+} complexes with polyamines [15,16]. According to the criterium based on complex protonation constants, the number of uncoordinated primary amine group should be 9 in $ZnL2^{2+}$ and 6 in Zn_2L2^{4+}, in agreement with a coordination sphere constituted by three primary and three tertiary nitrogen atoms for both metal ions. Binding of the third Zn^{2+} ion takes place with further decrease of stability ($Zn_2L2^{4+} + Zn^{2+} = Zn_3L2^{6+}$, log*K* = 11.0, Table 2). At this stage, another three primary amine groups become involved in metal binding, suggesting a similar hexacoordination for all three metal ions in Zn_3L2^{6+}. An insignificant decrease of binding constant is instead observed at the fourth coordination step ($Zn_3L2^{6+} + Zn^{2+} = Zn_4L2^{8+}$, log*K* = 10.7, Table 2) even though an important reorganization of the trinuclear complex must occur to accommodate the fourth Zn^{2+} ion. According to protonation data in Table 2, two primary nitrogen atoms should remain uncoordinated in Zn_4L2^{8+}.

Table 2. Stability constants of Zn^{2+} complexes with L2. 0.10 M Me_4NCl, 298.1 ± 0.1 K. Values in parentheses are standard deviation on the last significant figure.

Equilibria	log*K*	Equilibria	log*K*
$Zn^{2+} + L2 = ZnL2^{2+}$	17.18 (5)	$Zn_2H_6L2^{10+} + H^+ = Zn_2H_7L2^{11+}$	8.13 (8)
$ZnL2^{2+} + 2H^+ = ZnH_2L2^{4+}$	22.50 (8)	$Zn_2H_7L2^{11+} + H^+ = Zn_2H_8L2^{12+}$	7.36 (7)
$ZnH_2L2^{4+} + H^+ = ZnH_3L2^{5+}$	10.04 (5)	$Zn_2H_8L2^{12+} + H^+ = Zn_2H_9L2^{13+}$	6.47 (5)
$ZnH_3L2^{5+} + H^+ = ZnH_4L2^{6+}$	9.59 (6)		
$ZnH_4L2^{6+} + H^+ = ZnH_5L2^{7+}$	10.01 (7)	$3Zn^{2+} + L2 = Zn_3L2^{6+}$	41.36 (5)
$ZnH_5L2^{7+} + 2H^+ = ZnH_7L2^{9+}$	18.14 (7)	$Zn_2L2^{4+} + Zn^{2+} = Zn_3L2^{6+}$	11.0 (1)
$ZnH_7L2^{9+} + H^+ = ZnH_8L2^{10+}$	8.25 (6)	$Zn_3L2^{6+} + 2H^+ = Zn_3H_2L2^{8+}$	22.52 (6)
$ZnH_8L2^{10+} + H^+ = ZnH_9L2^{11+}$	8.64 (7)	$Zn_3H_2L2^{8+} + H^+ = Zn_3H_3L2^{9+}$	9.34 (8)
$ZnH_9L2^{11+} + H^+ = ZnH_{10}L2^{12+}$	7.97 (6)	$Zn_3H_3L2^{9+} + H^+ = Zn_3H_4L2^{10+}$	8.12 (8)
$ZnH_{10}L2^{12+} + H^+ = ZnH_{11}L2^{13+}$	6.92 (5)	$Zn_3H_4L2^{10+} + H^+ = Zn_3H_5L2^{11+}$	8.00 (8)
$ZnH_{11}L2^{13+} + H^+ = ZnH_{12}L2^{14+}$	5.75 (4)	$Zn_3H_5L2^{11+} + H^+ = Zn_3H_6L2^{12+}$	6.94 (6)
$ZnH_{12}L2^{14+} + H^+ = ZnH_{13}L2^{15+}$	5.38 (5)	$Zn_3H_6L2^{12+} + H^+ = Zn_3H_7L2^{13+}$	6.26 (6)
$2Zn^{2+} + L2 = Zn_2L2^{4+}$	30.35 (7)	$4Zn^{2+} + L2 = Zn_4L2^{8+}$	52.08 (8)
$ZnL2^{2+} + Zn^{2+} = Zn_2L2^{4+}$	13.2 (1)	$Zn_3L2^{6+} + Zn^{2+} = Zn_4L2^{8+}$	10.7 (1)
$Zn_2L2^{4+} + H^+ = Zn_2HL2^{5+}$	11.27 (8)	$Zn_4L2^{8+} + H^+ = Zn_4HL2^{9+}$	9.48 (8)
$Zn_2HL2^{5+} + H^+ = Zn_2H_2L2^{6+}$	11.44 (8)	$Zn_4HL2^{9+} + H^+ = Zn_4H_2L2^{10+}$	8.90 (8)
$Zn_2H_2L2^{6+} + H^+ = Zn_2H_3L2^{7+}$	9.53 (8)	$Zn_4H_2L2^{10+} + H^+ = Zn_4H_3L2^{11+}$	8.24 (8)
$Zn_2H_3L2^{7+} + H^+ = Zn_2H_4L2^{8+}$	9.54 (8)	$Zn_4H_3L2^{11+} + H^+ = Zn_4H_4L2^{12+}$	7.35 (9)
$Zn_2H_4L2^{8+} + H^+ = Zn_2H_5L2^{9+}$	8.80 (9)	$Zn_4L2^{8+} + OH^- = [Zn_4L2(OH)]^{7+}$	2.2 (1)
$Zn_2H_5L2^{9+} + H^+ = Zn_2H_6L2^{10+}$	8.60 (8)		

To get insight into the structural properties of these Zn^{2+} polynuclear complexes, we performed molecular modelling calculations on Zn_2L2^{4+}, Zn_3L2^{6+} and Zn_4L2^{8+} in a simulated implicit water environment. The lower energy structures obtained for these complexes are shown in Figure 2. According to these structures, in Zn_2L2^{4+} (Figure 2a) and Zn_3L2^{6+} (Figure 2b) each metal ion is coordinated, in a distorted octahedral environment, to six nitrogen atoms pertaining to one arm of the ligand originating from the central tertiary amine group. In agreement with the deductions drawn above from the equilibrium constants, the number of primary nitrogen atoms remaining not

coordinated is six in Zn_2L2^{4+} (Figure 2a) and three in Zn_3L2^{6+} (Figure 2b). Indeed, the addition of the fourth Zn^{2+} ion causes a major rearrangement of the trinuclear complex. The ligand displays a great ability to minimize the electrostatic repulsion between metal cations bringing them at long distance from each other (Figure 2c). Only one of the Zn^{2+} ions retains the octahedral coordination environment seen in the trinuclear complex, while the other three metal cations are: one pentacoordinated by ligand nitrogen atoms, one pentacoordinated by four ligand donors and a water molecule, one tetracoordinated by two ligand donors and two water molecules. The last coordination environment requires some cautionary considerations. In this complex unit, the ligand forms an 8-membered chelate ring including a not coordinated nitrogen atom. A similar arrangement is unlikely to occur in a real solution, since chelate rings of such size are poorly stable. In the simulated implicit water environment of our calculations, however, an overestimation of electrostatic repulsions could have forced the Zn^{2+} ion to stay as far as possible from the other three cations, instead of involving the third nitrogen atom in the formation of two stable 5-membered chelate rings, which is the situation that we expect to occur in water. Nevertheless, the calculated structure of Zn_4L2^{8+} (Figure 2c) seems very representative of the overall organization of this complex, as shown by the fact that it implicates the presence of two not coordinated primary nitrogen atoms in agreement with the results deduced above from equilibrium data.

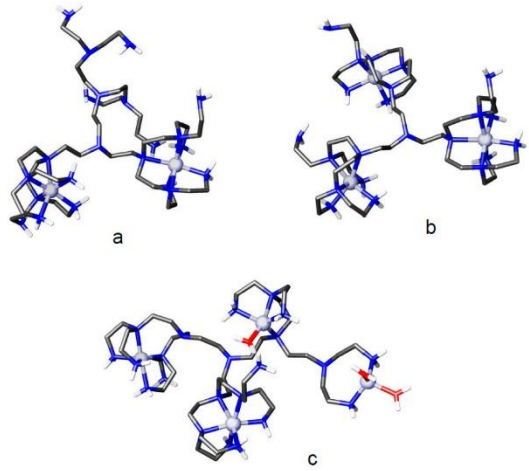

Figure 2. Minimum energy conformations calculated for (**a**) Zn_2L2^{4+}; (**b**) Zn_3L2^{6+} and (**c**) Zn_4L2^{8+}.

2.2. *Formation of Anion and Ion-Pair Complexes*

The detailed analysis of metal complexation equilibria with L2 makes it possible to further investigate such equilibrium systems. For instance, it is possible to analyse the ability of L2 complexes to interact with other species in the environment. We have already seen that protonated forms of L2 can bind PO_4^{3-}, $P_2O_7^{4-}$, $P_3O_{10}^{5-}$, and nucleotides (AMP, ADP, ATP) anions in solution [6], and we have already seen that the G-2 dendrimer L1 is able to form both anion and ion-pair complexes [2,3]. We have now studied the equilibria involving L2 and SO_4^{2-} both in the absence and in the presence of Cu^{2+} ions by means of pH-metric (potentiometric) titrations (0.1 M Me_4NCl, 298.1 $\pm$ 0.1 K). Indeed, the potentiometric data, treated with the computer program HYPERQUAD [12], revealed that many protonated forms of L2 are able to bind both the SO_4^{2-} anion alone and the Cu^{2+}/SO_4^{2-} ion-pair. The equilibrium constants for the formation of SO_4^{2-} complexes are reported in Table 3 (see Figure S3

for a distribution diagram). This table includes the overall constants (β values) for the binding of SO_4^{2-} along with the constants for the equilibria of anion binding by protonated ligand species ($H_nL2^{n+} + SO_4^{2-} = [H_nL2(SO_4)]^{(n-2)+}$) that could be calculated from the former by using the ligand protonation constants [6]. It is to be noted that the constants for the latter equilibria could not be calculated for complexes $[H_nL2(SO_4)]^{(n-2)+}$ with $n < 11$ (Table 3), since it was not possible to resolve as single proton binding processes the protonation equilibria involving H_nL2^{n+} species with $n < 11$ [6]. Nonetheless, the stability constants that are available for the binding of SO_4^{2-} to the protonated ligand forms show some peculiarities of this ligand. The stability of anion complexes of polyammonium ligands is generally determined by electrostatic attraction and hydrogen bonding [17–21]. Conversely, the ability of L2 to bind SO_4^{2-} appears to be unaffected by its positive charge, that is, by its protonation state. Actually, the equilibrium constants for the anion binding vary in a very reduced range and their values are very small, on consideration of the high positive ligand charge and in comparison with SO_4^{2-} complexes of other polyammonium ligands [22]. A similar behaviour was also observed for phosphate and phosphate-like anion complexes with L2, although, in several cases, the stability of these complexes was significantly higher, probably due to the greater hydrogen bond ability of phosphate-like anions [6]. Also the trend of stability is particular: the stability constants decrease from $H_{11}L2^{11+}$ (log$K$ = 3.10) to $H_{13}L2^{13+}$ (log$K$ = 2.46), then steadily increase up to the formation of the complex with $H_{18}L2^{18+}$ (log$K$ = 3.32).

Table 3. Stability constants of the anion complexes formed by L2 with SO_4^{2-}. 0.1 M Me_4NCl, 298.1 ± 0.1 K. Values in parentheses are standard deviation on the last significant figure.

Equilibria	log$K$	Equilibria	log$K$
$L2 + 3H^+ + SO_4^{2-} = [H_3L2(SO_4)]^+$	38.09 (5)	$H_{11}L2^{11+} + SO_4^{2-} = [H_{11}L2(SO_4)]^{9+}$	3.10 (7)
$L2 + 5H^+ + SO_4^{2-} = [H_5L2(SO_4)]^{3+}$	57.88 (5)	$H_{12}L2^{12+} + SO_4^{2-} = [H_{12}L2(SO_4)]^{10+}$	2.81 (7)
$L2 + 7H^+ + SO_4^{2-} = [H_7L2(SO_4)]^{5+}$	76.63 (5)	$H_{13}L2^{13+} + SO_4^{2-} = [H_{13}L2(SO_4)]^{11+}$	2.46 (7)
$L2 + 9H^+ + SO_4^{2-} = [H_9L2(SO_4)]^{7+}$	94.62 (5)	$H_{15}L2^{15+} + SO_4^{2-} = [H_{15}L2(SO_4)]^{13+}$	2.59 (7)
$L2 + 11H^+ + SO_4^{2-} = [H_{11}L2(SO_4)]^{9+}$	111.54 (5)	$H_{16}L2^{16+} + SO_4^{2-} = [H_{16}L2(SO_4)]^{14+}$	2.76 (7)
$L2 + 12H^+ + SO_4^{2-} = [H_{12}L2(SO_4)]^{10+}$	119.58 (5)	$H_{17}L2^{17+} + SO_4^{2-} = [H_{17}L2(SO_4)]^{15+}$	2.91 (7)
$L2 + 13H^+ + SO_4^{2-} = [H_{13}L2(SO_4)]^{11+}$	127.24 (5)	$H_{18}L2^{18+} + SO_4^{2-} = [H_{18}L2(SO_4)]^{16+}$	3.32 (7)
$L2 + 15H^+ + SO_4^{2-} = [H_{15}L2(SO_4)]^{13+}$	139.90 (5)		
$L2 + 16H^+ + SO_4^{2-} = [H_{16}L2(SO_4)]^{14+}$	145.53 (5)		
$L2 + 17H^+ + SO_4^{2-} = [H_{17}L2(SO_4)]^{15+}$	149.44 (5)		
$L2 + 18H^+ + SO_4^{2-} = [H_{18}L2(SO_4)]^{16+}$	152.12 (5)		

To get information about the possibility that such behaviour originates form the structural characteristics of the anion complexes, we performed a molecular modelling calculation on the $[H_6L2(SO_4)]^{4+}$, $[H_{12}L2(SO_4)]^{10+}$ and $[H_{15}L2(SO_4)]^{13+}$ species, assuming that the localization of H^+ ions in the protonated ligand forms is as previously established by ^{1}H-NMR spectroscopy [6], that is, the first 12 H^+ ions bind the 12 primary N(a) atoms (Figure 1), while in $H_{15}L2^{15+}$ the three additional protons involve the three tertiary N(c) nitrogen atoms. In $[H_6L2(SO_4)]^{4+}$, protonation was assumed to occur on primary amine groups located as far apart as possible from each other. The minimum energy structures calculated for these complexes, reported in Figure 3, show that the ligand molecule becomes increasingly expanded while becoming increasingly protonated, as a consequence of the increasing electrostatic repulsion exerting between the ammonium groups. In the minimum energy structures of $[H_6L2(SO_4)]^{4+}$ (Figure 3a) and $[H_{12}L2(SO_4)]^{10+}$ (Figure 3b), the SO_4^{2-} anion forms four salt-bridges (charge reinforced hydrogen bonds) with four ammonium groups of the ligand, while in $[H_{15}L2(SO_4)]^{13+}$ (Figure 3c) such interactions drop to three and become longer. Most likely, the two opposite trends developing with increasing ligand protonation, namely (i) the favourable contribution due to the increasing ligand charge; (ii) the unfavourable contribution determined by ligand expansion, are responsible for the particular trend of complex stability showing a minimum for SO_4^{2-} binding by $H_{13}L2^{13+}$ (log$K$ = 2.46, Table 3).

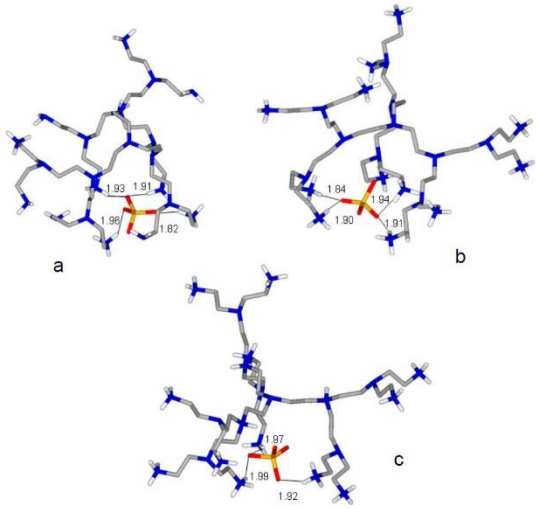

Figure 3. Minimum energy conformations calculated for (**a**) $[H_6L2(SO_4)]^{4+}$; (**b**) $[H_{12}L2(SO_4)]^{10+}$ and (**c**) $[H_{15}L2(SO_4)]^{13+}$. Distances are in Å.

As anticipated above, L2 can bind SO_4^{2-} and Cu^{2+}, simultaneously, forming ion-pair complexes. The equilibrium constants determined for such complexes are presented in Table 4 in the form of equilibrium constants for SO_4^{2-} binding the by Cu^{2+} complexes of L2 (see Figure S4 for a distribution diagram). The analysis of the L2/Cu^{2+}/SO_4^{2-} system was limited to the formation of ion-pair complexes containing a single metal ion (see the experimental section). Nevertheless, even under the appropriate conditions, the $[Cu_2L2(SO_4)]^{2+}$ complex was also found (Table 4), evidencing that more complex ion-pair species including more than one Cu^{2+} ion can be formed in solution. However, the analysis of such systems, requiring consideration of more than 92 equilibria, did not produced univocal results. This is the reason why we limited our study to ion-pair complexes with a single metal ion.

As can be seen from Table 4, the ability of the protonated Cu^{2+} complexes to bind SO_4^{2-} increases almost steadily with the positive charge of the metal complex, that is with its protonation state, the unique exception being represented by $[CuH_{10}L2(SO_4)]^{10+}$, whose formation constant appears to be a little bit smaller than that of $[CuH_9L2(SO_4)]^{9+}$. An assessment of the ability of the ligand to bind the anion in the absence or in the presence of Cu^{2+} ions can be performed by direct comparison of the equilibrium constants in Tables 3 and 4, limited to species with $H_{11}L2^{11+}$ to $H_{18}L2^{18+}$ ligand forms. Such comparison shows that the presence of Cu^{2+} enhances the ability of these ligand species to bind SO_4^{2-}, the increment growing with increasing ligand protonation. For instance, if we consider SO_4^{2-} binding by species with equal positive charge, such as $H_{18}L2^{18+}$ and $CuH_{16}L2^{18+}$, we observed an increase in stability from log$K$ = 3.32 ($H_{18}L2^{18+}$ + SO_4^{2-} = $[H_{18}L2(SO_4)]^{16+}$) to log$K$ = 5.20 ($CuH_{16}L2^{18+}$ + SO_4^{2-} = $[CuH_{16}L2(SO_4)]^{16+}$), corresponding to a free energy increment of 11 kJ/mol. For ligand species in lower protonation state than $H_{11}L2^{11+}$, a similar comparison cannot be performed due to the already mentioned impossibility of expressing in the form H_nL2^{n+} + SO_4^{2-} = $[H_nL2(SO_4)]^{(n-2)+}$ the formation constants of $[H_nL2(SO_4)]^{(n-2)+}$ complexes with $n < 11$. To overcome this problem, we can make use of the so called conditional (effective) stability constants that can be calculated for each system, as a function of pH, in the form $K_{eff} = \Sigma[AH_iL]/(\Sigma[H_jL] \times [A])$, for anion complexes (A = SO_4^{2-}), and $K_{eff} = \Sigma[CuAH_kL]/(\Sigma[CuH_lL] \times [A])$, for ion-pair complexes, where i, j, k and l are

the number of acidic protons on the ligand in the different species [23]. As can be seen from Figure 4, which shows the variation with pH of the effective stability constants calculated for SO_4^{2-} and ion-pair complexes, the presence of Cu^{2+} promotes the binding of SO_4^{2-} below pH 9, while in the range 9 < pH < 10.5 there is a preference for the metal-free ligand. This behaviour suggests the involvement of the metal ion in the binding of SO_4^{2-} in the ion-pair complexes of higher protonation state. At high pH values, the ligand is poorly protonated and thus it is able to fulfil the coordination sphere of Cu^{2+}, preventing metal coordination to SO_4^{2-}. The ligand wraps around the metal ion leaving less space for SO_4^{2-}. Upon protonation of the Cu^{2+} complex, the ligand becomes less involved in the coordination to the metal and the increasing positive charge of the complex expands its structure, thus making space for the anion to get in contact with Cu^{2+} and form an increasing number of salt-bridges with ligand ammonium groups. At the break point of these trends (pH 9), the main ion-pair species in solution is $[CuH_7L2(SO_4)]^{7+}$ (Figure S4). Below pH 6.5, the separation between the two curves in Figure 4, becomes about 2 logarithm units, which corresponds to the 11 kJ/mol free energy increment observed above for the binding of SO_4^{2-} to $CuH_{16}L2^{18+}$ relative to $H_{18}L2^{18+}$. The formation of contact ion-pair complexes was previously reported for the G-2 dendrimer L1, and is corroborated for L2 by the fact that the binuclear Cu_2L2^{4+} complex binds SO_4^{2-} (Table 4) in the absence of ligand ammonium groups (ligand protonation).

Table 4. Stability constants of the ion-pair complexes formed by L2 with Cu^{2+} and SO_4^{2-}. 0.1 M Me_4NCl, 298.1 ± 0.1 K. Values in parentheses are standard deviation on the last significant figure.

Equilibria	log*K*
$CuH_3L2^{5+} + SO_4^{2-} = [CuH_3L2(SO_4)]^{3+}$	3.10 (8)
$CuH_5L2^{7+} + SO_4^{2-} = [CuH_5L2(SO_4)]^{5+}$	3.33 (5)
$CuH_7L2^{9+} + SO_4^{2-} = [CuH_7L2(SO_4)]^{7+}$	3.51 (5)
$CuH_9L2^{11+} + SO_4^{2-} = [CuH_9L2(SO_4)]^{9+}$	3.62 (5)
$CuH_{10}L2^{12+} + SO_4^{2-} = [CuH_{10}L2(SO_4)]^{10+}$	3.44 (5)
$CuH_{11}L2^{13+} + SO_4^{2-} = [CuH_{11}L2(SO_4)]^{11+}$	3.69 (5)
$CuH_{12}L2^{14+} + SO_4^{2-} = [CuH_{12}L2(SO_4)]^{12+}$	3.96 (5)
$CuH_{13}L2^{15+} + SO_4^{2-} = [CuH_{13}L2(SO_4)]^{13+}$	4.31 (5)
$CuH_{14}L2^{16+} + SO_4^{2-} = [CuH_{14}L2(SO_4)]^{14+}$	4.64 (5)
$CuH_{16}L2^{18+} + SO_4^{2-} = [CuH_{16}L2(SO_4)]^{16+}$	5.20 (5)
$[CuH_{16}L2(SO_4)]^{16+} + H+ = [CuH_{17}L2(SO_4)]^{17+}$	2.78 (5)
$Cu_2L2^{4+} + SO_4^{2-} = [Cu_2L2(SO_4)]^{2+}$	4.01 (5)

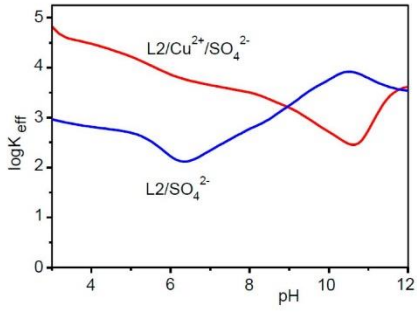

Figure 4. Logarithms of the conditional stability constants of anion (SO_4^{2-}) and ion-pair (Cu^{2+}/SO_4^{2-}) complexes with L2.

3. Materials and Methods

3.1. General Information

All starting materials were high purity compounds purchased from commercial sources and used as supplied. Ligand L2 was synthetized according to a previously described procedure [24].

3.2. Potentiometric Measurements

Potentiometric (pH-metric) titrations, employed to determine equilibrium constants, were performed in 0.1 M Me_4NCl aqueous solution at 298.1 ± 0.1 K by using an automated system and a procedure already described [25]. The combined Metrohm 6.0262.100 electrode (Metrohm AG, Herisau, Switzerland) was calibrated as a hydrogen-ion concentration probe by titration of previously standardized amounts of HCl with CO_2-free NMe_4OH solutions and determining the equivalent point by Gran's method [26], which gives the standard potential, E°, and the ionic product of water (pK_w = 13.83 (1) in 0.1 M Me_4NCl at 298.1 ± 0.1 K). The computer program HYPERQUAD [12] was used to calculate complex stability constants. All experiments were performed in the pH range 2.5–11.0 with 1×10^{-3} M ligand concentration. Six titrations in the case of Cu^{2+} complexation, and five in the case of Zn^{2+}, were performed with metal concentration varying in the ranges $0.5[L] \leq [Cu^{2+}] \leq 4.5[L]$ and $0.5[L] \leq [Zn^{2+}] \leq 3.5[L]$. Metal to ligand molar ratios greater than 5 for Cu^{2+} and 4 for Zn^{2+} were also tested: precipitation of metal hydroxide was observed in alkaline solution, while the analysis of the acidic branches of the titrations confirmed the maximum nuclearity of 5 for Cu^{2+} and 4 for Zn^{2+}. Three titrations were performed for anion binding with SO_4^{2-} concentration in the range $2[L] \leq [SO_4^{2-}] \leq 5[L]$. Three titrations were performed for ion-pair binding with $[Cu^{2+}] = 0.8[L]$ and SO_4^{2-} concentration $2[L] \leq [SO_4^{2-}] \leq 5[L]$. The different titration curves, obtained for metal, anion and ion-pair complexation experiments, respectively, were treated as separated curves without significant variations in the values of the common stability constants. Finally, the sets of data were merged together and treated simultaneously to give the final stability constants. Different equilibrium models for the complex systems were generated by eliminating and introducing different species. Only those models for which the HYPERQUAD program furnished a variance of residuals $\sigma^2 \leq 9$ were accepted. This condition was unambiguously met by a single model. Ligand protonation constants were taken from the literature [6].

3.3. Molecular Modelling

Molecular modelling investigations on $[H_6L2(SO_4)]^{4+}$, $[H_{12}L2(SO_4)]^{10+}$ and $[H_{15}L2(SO_4)]^{13+}$ complexes were performed by means of the empirical force field method AMBER3 as implemented in the Hyperchem 7.51 package [27], using an implicit simulation of aqueous environment (ε = 4 r) and atomic charged evaluated at the semiempirical level of theory (PM3) [28,29]. Potential energy surface of all the systems were explored by means of simulated annealing (T = 600 K, equilibration time = 10 ps, run time = 10 ps and cooling time = 10 ps, time step = 1.0 fs). For each studied system, 80 conformations were sampled.

As for the Zn(II) complexes, the trinuclear Zn_3L2^{6+} species was firstly analysed. Starting coordinates were built from the crystal structure of the Ni^{2+} complex of L1 [1], containing Ni^{2+} ions hexacoordinated in distorted octahedral environments to six out of the seven nitrogen atoms constituting a portion of L1 that is identical to the three branches of L2 growing from the central N(c) atom (Figure 1). The nitrogen atom remaining uncoordinated is a primary one. This structural motif was chosen taking into account that, according to the equilibrium data discussed before, all three metal ions of Zn_3L2^{6+} should be hexacoordinated and three primary amine groups of the complex should not be involved in metal coordination. This crystallographic structural unit was firstly modified by replacing Ni^{2+} with Zn^{2+} and completing each coordination environment with water molecules.

The starting coordinates for the binuclear Zn_2L2^{4+} complex were obtained by deleting one zinc ion in the QM minimized structure of Zn_3L2^{6+}. The tetranuclear Zn_4L2^{8+} complex was instead obtained

from the QM minimized binuclear complex by adding to its metal-free branch two QM minimized pentacoordinated Zn^{2+} complexes, one in square pyramidal and one in bipyramidal geometry, taken from the crystallographic structure of the trinuclear Cu^{2+} complex of L1 [1] and successively modified by replacing Cu^{2+} with Zn^{2+}.

The starting coordinates for each polynuclear complexes were firstly optimized by using the OPLS2005 forcefield implemented in the Impact software [30], with completely frozen metals and coordination environments. Then, each MM minimized structure was fully optimized at the DFT/M06 level of theory [31,32] by using the 6–31 g(tm) basis set [33–37] and the implicit simulation for the aqueous environment [38]. The nature of stationary points as true minima was checked by frequency calculations.

4. Conclusions

The ability of L2 to form stable highly nucleated complexes over a large pH range, as a consequence of its dendrimeric nature and of the many amine groups in its structure, make this compound a promising candidate for the preparation of solid supported materials to be used in the recovery of metal ions from aqueous media. This could find applications in both decontamination of waste waters and in the extraction of precious metals. Indeed, it was recently reported that activated carbon functionalized with randomly structured poly(ethylene imine) dendrimers are efficient scavenger of Pd^{2+} cations [39]. Moreover, L2 is also a promising candidate for catalytic purposes. The use of molecules with well-defined molecular structures, such as L2, has the advantage that with such molecules it is possible to perform a confident speciation of the complexes they form in solution, thus getting a fundamental instrument for the tailoring of appropriate receptors for substrates binding and activation. This is of special interest when the supported complex is used for catalytic purposes. Considering the ability of L2 to form complexes with many metal centres that may promote the binding of further species from the medium, we are particularly interested in developing carbon materials (activated carbons, carbon nanotubes, graphene) functionalized with L2 and testing them for catalytic applications in reaction for the formation of carbon-carbon bonds, such as the Sonogashira cross coupling.

Supplementary Materials: The following are available online: Figure S1: Distribution diagrams of the Cu^{2+} complexes of L2, Figure S2: Distribution diagrams of the Zn^{2+} complexes of L2, Figure S3: Distribution diagrams of the anion complexes formed by L2 with SO_4^{2-}, Figure S4: Distribution diagrams of the ion-pair complexes formed by L2 with Cu^{2+} and SO_4^{2-} complexes of L2.

Acknowledgments: Financial support from the Italian MIUR (project 2015MP34H3) is gratefully acknowledged.

Author Contributions: All authors conceived and designed the experiments; M.S. performed the synthesis and part of the potentiometric measurements; C.B. and P.G. performed the modelling calculations; C.G. performed part of the potentiometric measurements and took care of the graphical presentation of results; A.B. wrote the paper.

Conflicts of Interest: The authors declare no conflict of interest.

References

1. Bazzicalupi, C.; Bianchi, A.; Giorgi, C.; Gratteri, P.; Mariani, P.; Valtancoli, B. Metal ion binding by a G-2 Poly(ethylene imine) dendrimer. Ion-directed self-assembling of hierearchical mono- and two-dimensional nanostructured materials. *Inorg. Chem.* **2013**, *52*, 2125–2137. [CrossRef] [PubMed]
2. Bazzicalupi, C.; Bianchi, A.; Giorgi, C.; Gratteri, P.; Mariani, P.; Valtancoli, B. Anion and ion-pair binding by a G-2 Poly(ethylene imine) dendrimer. *Dalton Trans.* **2013**, *42*, 12130–12138. [CrossRef] [PubMed]
3. Bazzicalupi, C.; Bianchi, A.; Giorgi, C.; Valtancoli, B. Zn(II) enhances nucleotide binding and dephosphorilation in the presence of a Poly(ethylene imine) dendrimer. *Inorg. Chim. Acta* **2014**, *417*, 163–170. [CrossRef]
4. Salvador Serrano, E.; Savastano, M.; Bianchi, A. Inorganic Mercury Sequestration by a Poly(ethylene imine) Dendrimer in Aqueous Solution. *Molecules* **2015**, *20*, 3783–3790. [CrossRef] [PubMed]
5. Bazzicalupi, C.; Bencini, A.; Bianchi, A.; Danesi, A.; Giorgi, C.; Valtancoli, B. Anion Binding by Protonated Forms of the Tripodal Ligand Tren. *Inorg. Chem.* **2009**, *48*, 2391–2398. [CrossRef] [PubMed]

6. Bazzicalupi, C.; Bianchi, A.; Giorgi, C.; Savastano, M.; Morales-Lara, F. ATP dephosphorylation can be either enhanced or inhibited by pH-controlled interaction with a dendrimer molecule. *Chem. Commun.* **2015**, *51*, 3907–3910. [CrossRef] [PubMed]
7. Astruc, D.; Wang, D.; Deraedt, C.; Liang, L.; Ciganda, R.; Ruiz, J. Catalysis Inside Dendrimers. *Synthesis* **2015**, *47*, 2017–2031. [CrossRef]
8. Wang, D; Astruc, D. Dendritic catalysis—Basic concepts and recent trends. *Coord. Chem. Rev.* **2013**, *257*, 2317–2334. [CrossRef]
9. Myers, V.S.; Weir, M.G.; Carino, E.V.; Yancey, D.F.; Pande, S.; Crooks, R.M. Dendrimer-encapsulated nanoparticles: New synthetic and characterization methods and catalytic applications. *Chem. Sci.* **2011**, *2*, 1632–1646. [CrossRef]
10. Hwang, S.-H.; Shreiner, C.D.; Moorefield, C.N.; Newkome, G.W. Recent progress and applications for metallodendrimers. *New J. Chem.* **2007**, *31*, 1192–1217. [CrossRef]
11. Jarvis, N.V.; Wagener, J.M. Mechanistic studies of metal ion binding to water-soluble polymers using potentiometry. *Talanta* **1995**, *42*, 219–226. [CrossRef]
12. Gans, P.; Sabatini, A.; Vacca, A. Investigation of equilibria in solution. Determination of equilibrium constants with the HYPERQUAD suite of programs. *Talanta* **1996**, *43*, 1739–1753. [CrossRef]
13. Aragó, J.; Bencini, A.; Bianchi, A.; Garcia-España, E.; Micheloni, M.; Paoletti, P.; Ramirez, J.A.; Paoli, P. Interaction of "long" open-chain polyazaalkanes with hydrogen and copper(II) ions. *Inorg. Chem.* **1991**, *30*, 1843–1849. [CrossRef]
14. Bencini, A.; Bianchi, A.; Micheloni, M.; Paoletti, P.; Garcia-España, E.; Niño, M.A. Co-ordination tendency of [3*k*]aneN$_k$ polyazacycloalkanes. Thermodynamic study of solution equilibria. *J. Chem. Soc. Dalton Trans.* **1991**, 1171–1174. [CrossRef]
15. Aragó, J.; Bencini, A.; Bianchi, A.; Garcia-España, E.; Micheloni, M.; Paoletti, P.; Ramirez, J.A.; Rodriguez, A. Interaction of long polyazaalkanes with zinc(II) and cadmium(II) ions. A thermodynamic and ^{13}C nuclear magnetic resonance study. *J. Chem. Soc. Dalton Trans.* **1991**, 3077–3083. [CrossRef]
16. Bencini, A.; Bianchi, A.; Dapporto, P.; Garcia-España, E.; Micheloni, M.; Paoletti, P. Polynuclear zinc(II) complexes with large polyazacycloalkanes. 2. Equilibrium study and crystal structure of the binuclear complex $[Zn_2LCl_2](Cl)ClO_4 \cdot H_2O$ (L = 1,4,7,10,13,16,19,22-octaazacyclotetracosane). *Inorg. Chem.* **1989**, *28*, 1188–1191. [CrossRef]
17. *Anion Coordination Chemistry*; Bowman-James, K., Bianchi, A., García-España, E., Eds.; Wiley-VCH: New York, NY, USA, 2012.
18. Mateus, P.; Bernier, N.; Delgado, R. Recognition of anions by polyammonium macrocyclic and cryptand receptors: Influence of the dimensionality on the binding behavior. *Coord. Chem. Rev.* **2010**, *254*, 1726–1747. [CrossRef]
19. Bowman-James, K. Alfred Werner Revisited: The Coordination Chemistry of Anions. *Acc. Chem. Res.* **2005**, *38*, 671–678. [CrossRef] [PubMed]
20. Garcia-España, E.; Díaz, P.; Llinares, J.M.; Bianchi, A. Anion coordination chemistry in aqueous solution of polyammonium receptors. *Coord. Chem. Rev.* **2006**, *250*, 2952–2986. [CrossRef]
21. Bianchi, A.; Micheloni, M.; Paoletti, P. Supramolecular interaction between adenosine 5′-triphosphate (ATP) and polycharged tetraazamacrocycles. Thermodynamic and ^{31}P NMR studies. *Inorg. Chim. Acta* **1988**, *151*, 269–272. [CrossRef]
22. Arranz, P.; Bencini, A.; Bianchi, A.; Díaz, P.; Garcia-España, E.; Giorgi, C.; Luis, S.V.; Querol, M.; Valtancoli, B. Thermodynamics of sulfate anion binding by macrocyclic polyammonium receptors. *J. Chem. Soc. Perkin Trans.* **2001**, 1765–1770. [CrossRef]
23. Bazzicalupi, C.; Bianchi, A.; Giorgi, C.; Clares, M.P.; Garcia-España, E. Addressing selectivity criteria in binding equilibria. *Coord. Chem. Rev.* **2011**, *256*, 13–27. [CrossRef]
24. Lee, S.H.; Kim, D.-J.; Chang, C.-C.; Hah, S.S.; Suh, J. An efficient synthesis of ethylenimine dendrimer. *Bull. Korean Chem. Soc.* **1998**, *19*, 1270–1273.
25. Bazzicalupi, C.; Bianchi, A.; Biver, T; Giorgi, C.; Santarelli, S.; Savastano, M. Formation of double-strand dimetallic helicates with a terpyridine-based macrocycle. *Inorg. Chem.* **2014**, *53*, 12215–12224. [CrossRef] [PubMed]
26. Gran, G. Determination of the equivalence point in potentiometric titration, Part II. *Analyst* **1952**, *77*, 661–671. [CrossRef]

27. *Hyperchem, Release 7.51 for Windows MM System*; Hypercube, Inc.: Gainesville, FL, USA, 2002.
28. Stewart, J.J.P. Optimization of parameters for semiempirical methods I. Method. *J. Comput. Chem.* **1989**, *10*, 209–220. [CrossRef]
29. Stewart, J.J.P. Optimization of parameters for semiempirical methods II. Applications. *J. Comput. Chem.* **1989**, *10*, 221–264. [CrossRef]
30. Banks, J.L.; Beard, H.S.; Cao, Y.; Cho, A.E.; Damm, W.; Farid, R.; Felts, A.K.; Halgren, T.A.; Mainz, D.T.; Maple, J.R.; et al. Integrated Modeling Program, Applied Chemical Theory (IMPACT). *J. Comput. Chem.* **2005**, *26*, 1752–1780. [CrossRef] [PubMed]
31. Kohn, W.; Sham, L.J. Self-Consistent Equations Including Exchange and Correlation Effects. *Phys. Rev.* **1965**, *140*, A1133–A1138. [CrossRef]
32. Zhao, Y.; Truhlar, D.G. The M06 suite of density functionals for main group thermochemistry, thermochemical kinetics, noncovalent interactions, excited states, and transition elements: Two new functionals and systematic testing of four M06-class functionals and 12 other functionals. *Theor. Chem. Acc.* **2008**, *120*, 215–241.
33. Ditchfield, R.; Hehre, W.J.; Pople, J.A. Self-Consistent Molecular-Orbital Methods. IX. An Extended Gaussian-Type Basis for Molecular-Orbital Studies of Organic Molecules. *J. Chem. Phys.* **1971**, *54*, 724–728. [CrossRef]
34. Hehre, W.J.; Pople, J.A. Self-Consistent Molecular Orbital Methods. XIII. An Extended Gaussian Type Basis for Boron. *J. Chem. Phys.* **1972**, *56*, 4233–4234. [CrossRef]
35. Binkley, J.S.; Pople, J.A. Self-Consistent Molecular Orbital Methods. XIX. Split Valence Gaussian-type Basis Sets for Beryllium. *J. Chem. Phys.* **1977**, *66*, 879–880. [CrossRef]
36. Hariharan, P.C.; Pople, J.A. The Influence of Polarization Functions on Molecular Orbital Hydrogenation Energies. *Theor. Chim. Acta* **1973**, *28*, 213–222. [CrossRef]
37. Mitin, A.V.; Baker, J.; Pulay, P. An improved 6–31G* basis set for first-row transition metals. *J. Chem. Phys.* **2003**, *119*, 7775–7782. [CrossRef]
38. Cortis, M.C.; Friesner, R.A. Poisson-Boltzmann Calculations of Nonspecific Salt Effects on Protein-Protein Binding Free Energies. *J. Comput. Chem.* **1997**, *18*, 1591–1608. [CrossRef]
39. Peñas-Sanjuán, A.; López-Garzón, R.; López-Garzón, J.; Pérez-Mendoza, M.; Melguizo, M. Preparation of a poly-alkylamine surface-functionalized carbon with excellent performance as a Pd(II) scavenger. *Carbon* **2012**, *50*, 2350–2352. [CrossRef]

Sample Availability: Samples of the compound **L2** is available from the authors.

Journal of Catalysis 353 (2017) 239–249

Contents lists available at ScienceDirect

Journal of Catalysis

journal homepage: www.elsevier.com/locate/jcat

Construction of green nanostructured heterogeneous catalysts via non-covalent surface decoration of multi-walled carbon nanotubes with Pd (II) complexes of azamacrocycles

Matteo Savastano [a], Paloma Arranz-Mascarós [b], Carla Bazzicalupi [a], Maria Paz Clares [c], Maria Luz Godino-Salido [b], Maria Dolores Gutiérrez-Valero [b], Mario Inclán [c], Antonio Bianchi [a,*], Enrique García-España [c,*], Rafael López-Garzón [b,*]

[a] Department of Chemistry "Ugo Schiff", University of Florence, Italy
[b] Department of Inorganic and Organic Chemistry, University of Jaén, Spain
[c] Institute of Molecular Sciences, University of Valencia, Spain

ARTICLE INFO

Article history:
Received 14 March 2017
Revised 13 July 2017
Accepted 20 July 2017
Available online 9 August 2017

Keywords:
Palladium(II) catalysis
Sonogashira cross coupling
Multi-walled carbon nanotubes
Azamacrocycles
Hybrid materials
Non-covalent functionalization

ABSTRACT

Green nanostructured heterogeneous catalysts were prepared via a bottom-up strategy. Designed ligands were synthesized joining covalently an electrondeficient pyrimidine residue and a scorpiand azamacrocycle. The desired molecular properties were easily transferred to nanostructured materials in two steps: first, exploiting their spontaneous chemisorption onto multi-walled carbon nanotubes (MWCNTs) via the pyrimidinic moiety in water at room temperature, then, taking advantage of the easy coordination of Pd (II) to the azamacrocycle in the same conditions. An evenly distribution of catalytic centres was obtained on the MWCNTs surface. Catalytic properties of these materials were assessed toward the Cu-free Sonogashira cross-coupling, leading to significant improvements in terms of yields and reaction conditions, especially when considering the possibility to maintain yields of 90%, or above, in a feasible amount of time (2 h), while working under green conditions (water, 50 °C, aerobic atmosphere). The catalysts proved to be reusable for several cycles with good yields.

1. Introduction

Palladium-catalysed coupling reactions, leading to C—C, C—N and C—O bond formation, are highly significant to efficiently access products which would otherwise require far more impractical routes. The advantages they offer are relevant both in terms of costs (yields, reaction rates) and of required synthetic efforts (reaction conditions, selectivity) [1].

Although many of such processes have been developed employing homogeneous catalysts [1–3], successive research focused on the development of heterogeneous Pd-catalysts as a more practical solution, on a large scale, capable of overcoming the difficulties in recovering, and thus reusing, expensive homogeneous catalysts, which were moreover found as residuals in the final products. Several substrates have been proposed as possible solid supports, among which many carbon-based materials [4–8].

Carbon nanotubes (CNTs) have gathered a lot of attention in recent years due to their peculiar chemical and physical properties, which makes them suitable for catalytic processes [4,9]. Their non-covalent functionalization has become a topic of interest, as such approach offers not only an effective way to keep composite systems together, but also preserves CNTs unique electronic properties, otherwise widely disrupted through a covalent procedure [9]. Van der Waals forces, especially π-π stacking interactions, have been exploited to decorate CNTs with a variety of species, including nanoparticles [10,11], polymers [12–14], cyclodextrins [15,16], glycolipids [17,18] and biomolecules [19–22]. Porphyrins and phtalocyanines, among other candidates [23–27], have become the ligands of choice for inserting metal cations in such non-covalent assemblies, as they combine their ability to form stable complexes with an aromatic nature, thus giving rise to robust adducts [28–33].

In this paper, we use non-covalent π-π stacking interactions to functionalize commercial MWCNTs with two tetraazamacrocyclic ligands (Scheme 1): the macrocyclic functionalities were used to further decorate the obtained hybrid materials (MWCNT/HL1 and

* Corresponding authors.
E-mail addresses: antonio.bianchi@unifi.it (A. Bianchi), enrique.garcia-es@uv.es (E. García-España), rlopez@ujaen.es (R. López-Garzón).

http://dx.doi.org/10.1016/j.jcat.2017.07.023
0021-9517/

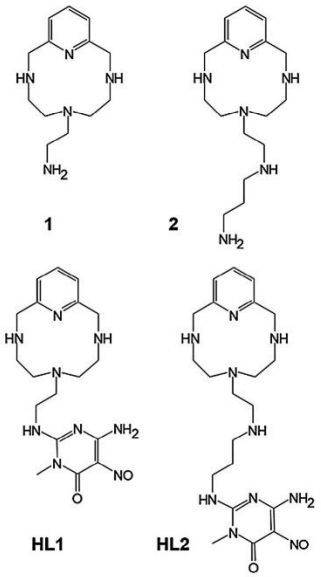

Scheme 1. The ligands HL1 and HL2 along with their precursor molecules **1** and **2**.

MWCNT/HL2, Fig. 1) with Pd(II) and the resulting compounds (MWCNT/HL1-Pd(II) and MWCNT/HL2-Pd(II)) were tested as heterogeneous catalysts for the Sonogashira cross coupling.

As some of us recently showed, pyrimidine residues can be employed as anchor groups for the non-covalent functionalization of activated carbon (AC), thanks to their ability to form strong π-π stacking interactions with the arene centres of such substrate [34]. In particular, the 6-amino-3,4-dihydro-3-methyl-5-nitroso-4-oxo pyrimidine group has proved particularly efficient to this purpose, as it allowed the irreversible attachment of several ligands of the Ar-S-F type (Scheme 2) on AC to obtain hybrid materials that were employed for the extraction of both metal cations [35–38] and anionic species [39,40] from aqueous media.

The mild conditions used in the preparation of the AC/Ar-S-F hybrid materials (the adsorption of Ar-S-F molecules on the AC at room temperature) [34] has two main advantages, (i) they preserve the structure of the AC, (ii) they allow strict control of the functionalization of the graphitic surface of the AC.

Furthermore, in a recent work [41], some of us assessed the catalytic properties toward the hydrogenation of 1-octene of three catalysts of the AC/Ar-S-F/Pd type which were prepared by adsorption of Ar-S-F on AC and subsequent Pd(II) binding by the AC/Ar-S-F hybrid. Two of these catalysts bore the triamine Tren (tris(2-aminoethyl)amine) and one bore lysine as active complexing functions F. Suitable fitting conditions of the adsorption experiments enables to control that all the adsorbed Pd(II) was complexed by the F functions. The study demonstrated that the anchored Ar-S-F-Pd complexes behave as highly efficient catalysts at low temperatures and the important role played by the nature of F functions in their stabilities, i.e. in the reuse of the catalysts.

The whole body of gathered experimental evidences, which guided us in the design of the new heterogeneous catalysts herein reported, points out several strong points of our approach. First, convenience and simplicity: with a proper choice of the anchoring group Ar (the 6-amino-3,4-dihydro-3-methyl-5-nitroso-4-oxopyri midine moiety in our case, see above), the grafting process should take place spontaneously when CNTs are suspended in an aqueous solution of the ligand at room temperature [34–41], the hydrophilic character of F function favouring the dispersion of CNTs in water. The mildness of the procedure should allow the preparation of CNT/Ar-S-F hybrids under conditions ensuring that the structures of both the support and the ligands are preserved. The same can be said for the coordination of metal cations [35–38] to the macrocyclic moiety of the grafted ligands, thermodynamics driving the system together effortlessly in such conditions. Second, the self-assembly of our systems not only allows a high degree of control over the chemical nature and amount of catalytic sites, but also ensures their homogeneous distribution on the supporting substrate [41].

The higher uniformity of the catalysts produced by the above route correlates well with their observed superior overall performances over other published systems. Such correlation stands out even more if one considers that many reported catalysts are prepared through direct deposition of Pd-nanoparticles (potentially more heterogeneous in size and nature than a molecular

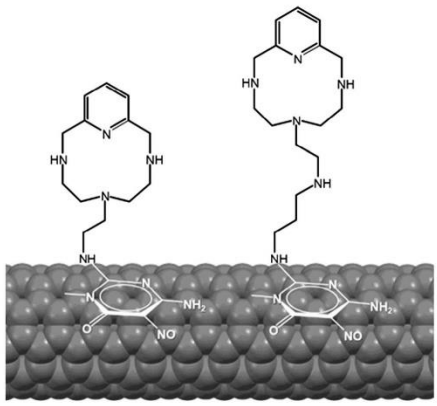

Fig. 1. Schematic representation of the non-covalent functionalization of a MWCNT with HL1 and HL2 to provide MWCNT/HL1 and MWCNT/HL2, respectively.

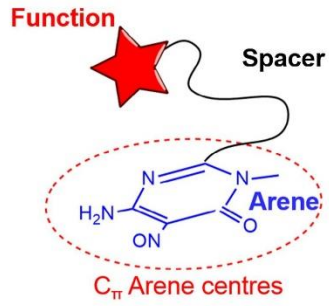

Scheme 2. General structure of an Ar-S-F ligand.

active site and surely harder to spread evenly on a surface), without assisting ligands or with ligands covalently linked to the substrate, often requiring pre-emptive surface modification [4].

In view of the previous remarks, also the choice of CNTs as supporting material can be fully explained: not only the chosen functionalization method is able to preserve their peculiar properties [4,9], but they stand out as a quasi-molecular material. Compared to AC, CNTs possess less defects and chemical functionalities and a wholly exposed surface area, lacking micropores that may limit the diffusion of reagents to the active sites, or trap the reaction products causing the poisoning of the catalyst over time [41].

The copper-free Sonogashira coupling has been chosen as catalytic test. In spite of the crucial role of Cu(I) in the Sonogashira reaction, in the last years there has been a growing interest in the development of experimental procedures working in the absence of Cu(I) [42,43], since the addition of Cu(I) salts may give rise to some drawbacks, such as induction of a Glaser type oxidative homocoupling of the terminal alkyne to yield the corresponding diene [44] and inhibitory effects [45,46]. The copper-free Sonogashira reaction has been largely conducted under homogeneous conditions in the presence of phosphine-palladium catalysts, $Pd(PPh_3)_4$ and $PdCl_2(PPh_3)_2$ being the most commonly used, although many other candidates have been explored, including palladium complexes with bidentate phosphines and polydentate ligands bearing nitrogen and oxygen donors [47]. The air sensitivity of phosphine ligands, which demands the use of an inert atmosphere, and the difficulty to recycle such homogeneous catalysts have hindered their large-scale application. Heterogeneous catalysts have attracted considerable interest, in the last years, as convenient alternatives to overcome such drawbacks, addressing the recovery of the catalyst by means of simple separation methods [47]. Several supporting materials have been proposed, such as silica [48,49], polymers [50–53], ionic liquids [50,54–56], metal organic frameworks (MOFs) [57,58] and CNTs [4,9,59–63], for the immobilization of metal (mostly palladium) complexes or metal nanoparticles [50,64–67].

Successfully, our heterogeneous MWCNT/HL1-Pd and MWCNT/HL2-Pd catalysts, herein reported, proved efficient in promoting the Sonogashira coupling between phenylacetylene and iodobenzene to give diphenylacetylene in water under aerobic conditions in almost quantitative yields, even at low temperatures. They are easily recoverable and reusable with appreciable conservation of their efficacy for at least four catalytic cycles. Accordingly, this type of catalysts, their preparation method and their application conditions are very promising to define new protocols for environmentally and economically sustainable carbon-carbon bond-making processes.

2. Experimental

2.1. Synthesis of HL1 and HL2

0.38 g (1,52 mmol) of 6-(2-aminoethyl)-3,6,9-triaza-1-(2,6)-pyridinecyclodecaphane [68] (**1**) dissolved in 20 cm^3 of methanol were reacted at room temperature with 0.35 g (1.73 mmol) of 6-amino-3,4-dihydro-3-methyl-2-methoxy-5-nitroso-4-oxopyrimidine [69]. The latter dissolves slowly over 8 h under stirring. The excess of pyrimidine was then converted into the insoluble 2,4-diamino-1-methyl-5-nitroso-6-oxopyrimidine derivative by reaction with ammonia (5 drops of 37% aqueous ammonia). After standing overnight in a fridge, the resulting suspension was filtered and the solution was evaporated to dryness under vacuum at room temperature to obtain HL1 as a deep purple solid compound. Yield 95%. $C_{18.5}H_{31}N_9O_{3.5}$ (HL1·0.5MeOH·H_2O): calcd. C 51.02, H 7.18, N 28.94; found C 50.93, H 7.19, N 28.70. ^{1}H NMR D_2O: δ (ppm) 2.62–3.46 (m, 13H), 3.74 (t, 2H), 4.55 (s, 4H), 7.37 (d, 2H), 7.88 (t, 1H).

HL2 was prepared by reaction of 6-(7-amino-3-azahexyl)-3,6,9-triaza-1-(2,6)-pyridinecyclodecaphane [70] (**2**) with 6-amino-3,4-dihydro-3-methyl-2-methoxy-5-nitroso-4-oxopyrimidine according to the procedure adopted for the synthesis of HL1. Yield 73%. $C_{22}H_{37}N_{10}O_4$ (HL2·MeOH·H_2O): calcd. C 51.95, H 7.93, N 27.53; found C 52.30, H 7.68, N 27.68. ^{1}H NMR D_2O: δ (ppm) 2.90–3.28 (m, 15H), 3.34 (s, 3H), 3.66 (t, 2H), 4.56 (s, 4H), 7.38 (d, 2H), 7.88 (t, 1H).

2.2. Potentiometric measurements

Potentiometric (pH-metric) titrations, employed to determine the protonation constants of the studied ligands and of their Pd (II) complexes, were performed in 0.1 M NMe_4Cl at 298.1 ± 0.1 K using an automated apparatus and a procedure previously described [71]. The combined Metrohm 6.0262.100 electrode was calibrated as a hydrogen-ion concentration probe by titration of previously standardized amounts of HCl with CO_2-free NaOH solutions and determining the equivalent point by Gran's method [72], which gives the standard potential, $E°$, and the ionic product of water (pK_w = 13.83(1) in 0.1 M NMe_4Cl at 298.1 K). The computer program HYPERQUAD [73] was used to calculate the stability constants from the potentiometric data. The concentration of ligands was about 1×10^{-3} M in all experiments. The studied pH range was 2.0–11.5. At least two measurements were performed for each system: at first, the different titration curves were treated as separated curves without significant variations in the values of the calculated stability constants; finally, the sets of data were merged together and treated simultaneously to give the final stability constants. Although it was not possible to determine the equilibrium constants for the formation of PdL^+ complexes with both ligands due to the slowness of the complexation reactions, these species proved to be very stable once formed and could be titrated in the pH range 2.5–11.5 according to fast protonation equilibria. Titrations were performed by means of the above method onto solutions containing L (L = HL1, HL2) and K_2PdCl_4 (1×10^{-3} M) equilibrated for 10 days at pH 3 and 298 K, thus making possible the determination of the complexes protonation constants. Different equilibrium models for the studied systems were generated by eliminating and introducing different species. Only those models for which the HYPERQUAD program furnished a variance of the residuals $\sigma^2 \leq 9$ were considered acceptable. Such condition was unambiguously met by a single model for each system.

2.3. Spectroscopic measurements

Absorption spectra were recorded at 298 K on a Jasco V-670 spectrophotometer. Both ligand and metal complex solutions were about 5×10^{-5} M. ^{1}H NMR spectra (400 MHz) in D_2O solution were recorded at 298 K on a 400 MHz Bruker Avance III spectrometer. XPS spectra were obtained in a Kratos Axis Ultra DLD spectrometer. Monochromatic Al/MgKα radiation from twin anode in constant analyzer energy mode with pass energy of 160 and 20 eV (for the survey and high resolution spectra, respectively) was used. The C1s transition at 284.6 eV was used as a reference to obtain the heteroatoms binding energies. The accuracy of the binding energy (BE) values was ±0.2 eV.

2.4. Determination of the molecular dimensions of HL1 and HL2

Theoretical calculations of the molecular dimensions of HL1 and HL2 were performed on model compounds with idealized geometries. Optimum geometries of the molecules were calculated from the conformations corresponding to the global minimum by using

the MM2 algorithm (ChemBats3D, CambridgeSoft Corp.) [74]. The geometry was optimized without any constraints, allowing all atoms, bonds, and dihedral angles to change simultaneously. The final RMS gradient was less than 0.001 kcal mol^{-1} $Å^{-1}$ for all the minimized structures.

2.5. Adsorption studies

The equilibrium time for the adsorption of HL1 and HL2 on CNTs was determined experimentally by kinetic measurements. The data points were obtained by mixing 0.0250 g of the adsorbent with 25 mL of a 10^{-3} M aqueous solution of the adsorbate at a given initial pH value. The obtained suspension was kept at 298.1 K under continuous shaking while concentration of the adsorbate was regularly monitored by checking its UV-absorbance at the isosbestic point, 302 nm in the case of HL1 and 304 nm in the case of HL2, until the equilibrium (3 days) was reached.

The adsorption isotherms were obtained under the same conditions (298.1 K, 0.0250 g of adsorbent suspended in 25 mL of the appropriate solution of the adsorbate at the chosen pH value). The ligand concentration values ranged from 8×10^{-5} M to 2×10^{-3} M. The samples were shaken in a thermostatic air-incubator until the determined equilibrium time was reached. Desorption isotherms of the ligands from the MWCNT/HL1 and MWCNT/HL2 hybrid materials were obtained point-by-point from the adsorption isotherms, recovering, drying, weighting and re-suspending the solid in water, maintaining a 1 mg of material/1 mL water ratio, then following a similar procedure to that described for the adsorption isotherms.

2.6. Determination of the surface charge density of MWCNT/HL1 and MWCNT/HL2

The surface charge density (Q in mmol H^+/g of adsorbent) of both materials was determined by a method based on potentiometric titration data [75,76], following an already described procedure [40]. Q was calculated by means of the equation $Q = \frac{1}{m}(V_0 + V_t)([H]_i - [OH]_i - [H]_e + [OH]_e)$, where V_0 and V_t are the volumes of initial solution and titrant, respectively, and m is the mass of the adsorbent. Subscripts i and e refer to the initial and equilibrium concentration of protons or hydroxyl ions. The proton isotherms are obtained by plotting Q vs equilibrium pHs.

2.7. Preparation of the catalysts

Easy characterization of the obtained Pd-catalysts based on MWCNT/HL hybrids is crucial for a better understanding of their catalytic behavior (one of the focus of this study). This fact was taken into account on electing the preparation procedure of the catalysts used in this work.

Due to the hydrophobic nature of their surface, CNTs tend to form bundles in water which hinder the exposure of the external surface to the adsorbates. Sample sonication could shorten the equilibrium time of the adsorption processes, but the harshness of this technique can cause damage to the CNTs and ligand structures (e.g., shortening their lengths and/or altering their chemical functions) [77,78]. Nevertheless, the adsorption on CNTs in water of Ar-S-F substrates bearing hydrophilic F functions facilitates dispersion of the latter in the medium, improving the efficiency of the process under mild conditions and avoiding significant damages to the materials. Accordingly, the two, MWCNT/HL1-Pd and MWCNT/HL2-Pd catalysts, were prepared following a two-step procedure, consisting in the adsorption of HL1 or HL2 on the MWCNT and the subsequent binding of Pd(II) at room temperature.

According to the above, we first prepared MWCNT/HL1 and MWCNT/HL2 materials, adsorbing the ligands on commercial CNTs (Thin MWCNTs Nanocyl, Ref 3100, Spain, with metal oxides content ≤5%). This was accomplished according to the following procedure for both ligands: 0.5 g of the adsorbent were mixed with 500 mL of 10^{-3} M aqueous solution of the ligand at pH = 7.5 in a plastic flask. This pH value was proved to be the optimum for the highest irreversible loading of the ligand. The flask was shaken in an air-thermostated bath at 298.1 K until the adsorption equilibrium was reached (3 days). The obtained solids, MWCNT/HL1 and MWCNT/HL2, were separated by filtration, washed repeatedly with distilled water and dried into a desiccator. The final amount of adsorbent per gram of adsorbate was quantified in 0.36 mmol of HL1 and 0.31 mmol of HL2 per g of CNT, respectively.

In the second step, MWCNT/HL1-Pd and MWCNT/HL2-Pd catalysts were prepared by coordination of Pd(II), as K_2PdCl_4, on the appropriate CNT/ligand material. Accordingly, 0.5 g of the corresponding CNT/ligand material were mixed in a suitable plastic flask with 500 mL of a 1 M KCl aqueous solution containing K_2PdCl_4 5×10^{-4} M, whose pH had been adjusted to 5.0 through HCl addition. pH 5.0 was selected as the best compromise between the minimization of proton competition toward the coordination of Pd(II) with the amino groups of the ligands and the avoidance of the formation of Pd(II) hydroxy-species, that, at this pH value, are not yet formed (i.e. all the Pd(II) is present as $[PdCl_4]^{2-}$) [79]. The suspensions were shaken in an air-thermostated bath at 298.1 K within four days until the adsorption equilibrium was reached (i.e. when the UV absorbance of the Pd(II) solution at λ = 474 nm remained constant over time). Finally, the amount of adsorbed Pd(II) was determined as the difference between initial and final absorbances at λ = 474 nm: 0.45 mmol Pd per gram of MWCNT/HL1 (4.8% in weight of Pd for MWCNT/HL1-Pd) and 0.40 mmol per gram of MWCNT/HL2 (4.3% in weight of Pd for MWCNT/HL2-Pd) were assessed.

2.8. General procedure for the Sonogashira reaction

A mixture of iodobenzene (1 mmol), phenylacetylene (1 mmol), Et_3N (2 mmol), H_2O (1 mL) and the catalyst (22 mg of MWCNT/HL1-Pd or 25 mg of MWCNT/HL2-Pd, relationship reactants/Pd (II) = 100) was stirred under aerobic conditions at a constant temperature (30, 50 or 70 °C). The progress of the reaction was monitored by gas chromatography (GC). Yields of reaction as a function of time were calculated to determine the equilibrium reaction times. After completion, $CHCl_3$ (10 mL) was added to the reaction mixture and the catalyst was recovered by filtration and washed with $CHCl_3$ (2 × 5 mL) and H_2O (2 × 5 mL). The aqueous and organic layers were separated through a separatory funnel. The organic layer was dried over anhydrous $MgSO_4$. The analysis of the reaction products in the organic phase was performed by GC using a 7820 A Agilent GC System chromatograph, with an Agilent 190915-433 column, 30 m × 250 μm × 25 μm and a flame ionization detector (FID). The recovered catalyst was reused for another batch of the same reaction. The process was repeated for three additional runs.

3. Results and discussion

3.1. Acid-base properties of HL1 and HL2

Potentiometric (pH-metric) titrations performed in aqueous solution (0.1 M Me_4NCl, 298.1 K) in the pH range 2.0–11.5 showed that HL1 and HL2 contain, respectively, four and five basic groups undergoing protonation, as well as an acidic group that starts being deprotonated above pH 10. The equilibrium constants determined

for these processes are reported in Table 1 in the form of protonation constants. Distribution diagrams of the protonated species formed as a function of pH are reported as supplementary materials (Fig. S1).

According to the properties of other amine derivatives with the same pyrimidine residue, the protonation stages occurring at the highest pH values (log$K$ = 11.13, 11.21, Table 1) should involve the amine groups directly connected to the pyrimidine ring, which are expected to be deprotonated at high pH, while the protonation stages corresponding to the log$K$ values of 2.3 and 2.2 (Table 1) should involve the pyrimidine nitroso groups. This assignment of the protonation sites is confirmed by the pH dependence of the adsorption spectra of both ligands.

As shown in Fig. 2 for HL1 and in Fig. S2 for HL2, the near-UV spectra are characterized by three bands centered at about 230, 265 and 330 nm corresponding to allowed π-π* transitions between π-orbitals of the pyrimidinic group and overlapping with the band at about 265 nm of the pyridinic one. The spectra of both HL1 and HL2 display a marked pH dependence in acidic and alkaline solution, when protonation involves the pyrimidine chromophore, while in the intermediate pH region (4.0–9.0 approximately) they are almost invariant since protonation takes place on the non-chromogenic aliphatic amine groups.

Interestingly, the equilibrium constants for the protonation stages involving the chromophores of the two ligands are equal, or almost equal, within the experimental errors, in agreement with protonation occurring on almost identical sites, while, for the remaining proton binding processes, HL2 demonstrates a greater basicity, in terms of values and number of the protonation constants, according to the presence of one more amine group in its structure. The highly protonated H_5L1^{4+} and H_6L2^{6+} species are formed only in small amounts in the lower pH region we have investigated (Fig. S1). Nevertheless, the discovery of their formation reveals that three out of the four nitrogen atoms of the macrocyclic ring of both ligands can undergo protonation in the studied pH range.

3.2. Formation of Pd(II) complexes in solution

The complexation of Pd(II) by the two ligands HL1 and HL2 takes place very slowly, however, once such complexes are formed, their protonation can be studied without kinetic problems above pH 2.5. Accordingly, we were able to determine the protonation constants for these complexes, shown in Table 2, by means of potentiometric (pH-metric) titration in aqueous solution (0.1 M Me_4NCl, 298.1 K). Distribution diagrams concerning these equilibria can be found in supplementary materials (Fig. S3).

$[PdL1]^+$ and $[PdL2]^+$ are involved in two and three protonation steps, respectively. The equilibrium constants corresponding to log$K$ = 9.46 and log$K$ = 10.19 for $[PdL1]^+$ and $[PdL2]^+$, respectively, are too high to be associated with protonation of metal-coordinated amine groups while they can be assigned to protonation of metal-free deprotonated amine groups, in agreement with the UV spectral variations observed for these complexes in the alkaline zone (Fig. S4). UV spectra also show that, in the acidic region, protonation corresponding to the smallest equilibrium constants (log$K$ = 2.2 and 2.5, Table 2) occurs on the pyrimidine group. In the case of $[PdL2]^+$, there is an intermediate protonation step (log$K$ = 7.0) corresponding to protonation of the additional amine group in the chain connecting the macrocycle and the pyrimidine moieties of HL2, which is expected not to be coordinated, as the basicity of this amine group in the complex is relatively close to that of the same group in the free ligand (log$K$ = 8.64, Table 1).

An interesting point regards the number of donor atoms used by HL1 and HL2 to bind Pd(II). In the case of the Cu(II) complexes, crystal structures of the $[CuL]^{2+}$ complexes of the precursor molecules 1 ad 2 (Scheme 1) show that the metal is coordinated to all

Table 1
Protonation constants of ligands HL1 and HL2 (L) in 0.1 M NMe_4Cl at 298.1 ± 0.1 K.

Equilibria	log$K$	
	HL1	HL2
$L^- + H^+ = HL$	11.13(4)[a]	11.21(5)
$HL + H^+ = H_2L^+$	9.28(5)	9.71(4)
$H_2L^+ + H^+ = H_3L^{2+}$	7.83(7)	8.64(6)
$H_3L^{2+} + H^+ = H_4L^{3+}$	2.3(1)	7.51(6)
$H_4L^{3+} + H^+ = H_5L^{4+}$	1.6(5)	2.2(1)
$H_5L^{4+} + H^+ = H_6L^{5+}$		1.6(5)

[a] Values in parentheses are standard deviations on the last significant figures.

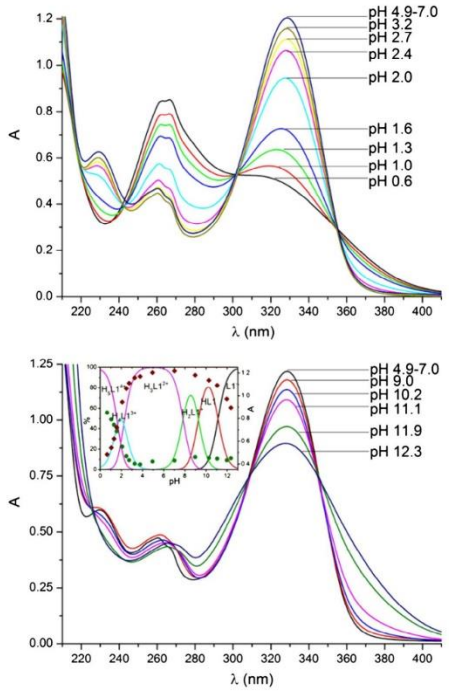

Fig. 2. UV absorption spectra of HL1 at different pH in aqueous solution: pH 0.6–7.0 (top), pH 4.9–12.3 (bottom). Inset (bottom): pH dependence of the 330 nm (red diamonds) and 265 nm (green dots) absorbances.

Table 2
Protonation constants of the $[LPd]^+$ complexes formed by HL1 and HL2 in 0.1 M NMe_4Cl at 298.1 ± 0.1 K.

Equilibria	log$K$	
HL =	HL1	HL2
$[PdL]^+ + H^+ = [PdHL]^{2+}$	9.46(6)[a]	10.19(7)
$[PdHL]^{2+} + H^+ = [PdH2L]^{3+}$	2.2(2)	7.0(1)
$[PdH_2L]^{3+} + H+ = [PdH_3L]^{4+}$		2.5(2)

[a] Values in parentheses are standard deviation on the last significant figures.

An interesting point regards the number of donor atoms used by HL1 and HL2 to bind Pd(II). In the case of the Cu(II) complexes, crystal structures of the $[CuL]^{2+}$ complexes of the precursor molecules 1 ad 2 (Scheme 1) show that the metal is coordinated to all

four nitrogen atoms of the macrocycle and to all the nitrogen atoms of the pending arm [68,70]. The crystal structures of the $[ML]^{2+}$ (M = Mn(II), Ni(II), Zn(II)) complexes of 2 are isostructural to $[Cu2]^{2+}$ [80,81]. In all these structures the macrocycle adopts a folded conformation. As observed above, in the case of the square planar Pd(II) complexes it seems that there is no participation of donor atoms of the appended chains in metal coordination, thus, if the macrocyclic ring of the ligand would assume the expected folded conformation, only three out of the four macrocyclic nitrogen atoms would be coordinated to Pd(II) (Fig. 3).

To get information on this point, solutions containing equimolar quantities of ligand and $[PdCl_4]^{2-}$ were equilibrated at pH 4 and 298 K within ten days, for both HL1 and HL2. The UV–Vis spectra of the mixtures were monitored daily: no variations were observed after four days. The concentration of free Cl^- was then determined by means of ion chromatography evidencing that only three chloride anions were released by $[PdCl_4]^{2-}$ upon coordination. Accordingly, we must assume that in these complexes Pd(II) is coordinated to three macrocyclic nitrogen atoms and one Cl^- anion, as sketched out in Fig. 3 for the case of HL1.

3.3. Characterization of the catalysts

The data on the bare graphitic support are sketched below: for a detailed analysis of the properties of the employed MWCNTs the reader is addressed to a previous paper [82]. The used MWCNTs have C as the main constituent (~96.0%), H (~0.3%) and little oxygen content as the only heteroatomic component (~3.6%). Negligible amounts of various metal oxides residues, such as chromium, nickel and cobalt, are also presents [83].

The adsorption-desorption isotherms of N_2, determined at 77 K, on MWCNT/HL1-Pd and MWCNT/HL2-Pd, together with the one for the bare MWCNT, appear in Fig. S5. Although little N_2 adsorptions are observed at very low pressures, as in type I isotherms, they are of no account, indicating that the microporosity of the material is irrelevant [83]. Instead, a strong increasing adsorption prevails with a hysteresis loop at high relative pressures, which is typical of type II isotherms, indicating the existence of meso- and macropores with wide distribution sizes, which is consistent with the aggregation of CNTs in bundles. The BET external surface area (determined by applying the BET equation to the N_2 adsorption data) associated to the wide pores of the pristine CNTs, 221 m^2/g, decreases upon adsorption of the ligands, to 198 m^2/g in the case of HL1 and 188 m^2/g in the HL2. These data are consistent with the adsorption of the ligands by π-π interactions of their pyrimidine residues with the arene centres of the external surface of the CNTs [36,37]. Despite the slightly smaller molar amount of adsorbed HL2 per gram of CNTs (0.31 mmol/g) compared to HL1 (0.36 mmol/g), the larger molecular size of the former determines the observed lower BET surface area of MWCNT/HL2 in respect to MWCNT/HL1.

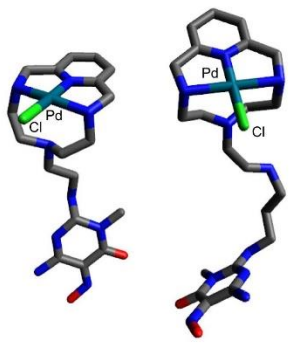

Fig. 3. Outline of the proposed coordination mode for Pd(II) to HL1 and HL2.

According to previous studies [84], other adsorption mechanisms, such as interaction with the scarce oxygen functions located at the edges of open ends and surface hole-defects of MWCNTs (determined by the analysis of TEM micrographs and data of D and G bands of Raman spectra [83]) are not expected to influence the adsorption of these Ar-S-F ligands. Unfortunately, a statistical analysis of MWCNT openings was not possible, because of the inadequate quality of some TEM images, but the information given by these images points out that some adsorption of the ligands can also take place on the arene centres at the internal surface of the MWCNTs.

The determined mean diameter of the internal cavity of the MWCNTs used in this work (4.5 nm [83]) corresponds to the mesopores range where ligands of Ar-S-F type with similar dimensions to HL1 and HL2 (box containing HL1: 5.2 Å, 6.6 Å, 14.6 Å; box containing HL2: 5.2 Å, 6.9 Å, 17.9 Å,) are easily adsorbed [85].

The adsorption and desorption isotherms of HL1 and HL2 on CNTs at pH 4.0 and 7.5 can be found in supplementary materials (Fig. S6): the manifest high irreversibility of the adsorption processes indicates strong ligand-CNT surface interaction. All adsorption isotherms fit the type L of the Giles classification [86], indicating a predominant adsorption mechanism. One can also see how the adsorption capacity of CNTs increases slightly with pH for both ligands: this is due to the number of protonated groups in the polyaminic chains attached to the pyrimidine, which decrease, along with the strength of the ligand-solvent interaction, as the pH increases. These features are consistent with the adsorption of the ligands by π-π interactions between the heterocyclic moiety of the ligands and the arene centres, C_π, at the CNT surface as previously observed for analogous ligands on graphitized ACs [40].

Profiles of surface charge density Q (mmol(H^+)/g) versus pH are reported in Fig. S7 for both functionalized materials, MWCNT/HL1 and MWCNT/HL2, and pristine MWCNTs. Applying the SAIEUS method [87] the respective p*K*a versus pH profiles were obtained. The plot obtained for pristine CNTs is consistent with the existence of carboxyl groups (p*K*a ≈ 3) and weakly acidic phenol, lactone and anhydride functions (p*K*a ≈ 9–10) [84]. Furthermore, the peak at p*K*a ≈ 6.5 is due to the protonation of the arene centres of the CNTs surface [39,40]. Concerning the hybrid materials, the Q vs pH plots already show how their positive surface charge densities are higher than that of the bare CNTs in a wide pH range (3–10), due to the protonation of the polyamine functions of the anchored ligands. The pKa *vs* pH profiles of MWCNT/HL1 and MWCNT/HL2 (Fig. S7), approximately investigated in the 3.0–10.5 pH range, show no signs of the protonation of C(5)-NO groups of the pyrimidine moieties of the adsorbed ligands (log*K* 2.3 and 2.2 for the free ligands HL1 and HL2, respectively, see Table 1): such evidences suggest that the protonation of those sites is probably hindered due to π-π interactions. Concerning the other protonation steps of the polyamine moieties of the adsorbed ligands, they take place at substantially lower pH values than those observed for the free molecules in solution, indicating a decreasing of the overall basicity of such moieties (cf. Table 1 and Fig. S7). This can probably be rationalized in terms of different conformation of the ligands in solution and at CNTs surface, where an elongated arrangement is required to optimize the stacking interactions, thus hampering to some extent the protonation of such groups.

The XPS spectra of the ligands in the N1s region (Fig. S8) consist of a main peak at about 397.0 eV, pertaining to the aliphatic nitrogen atoms, with shoulders (398.1 eV and 397.5 eV for HL1 and HL2 respectively) relating to the aromatic nitrogen atoms. After adsorption of the ligands on CNTs surface, both components of the N1s signal shift to higher binding energy values (Fig. S8). In the case of the aromatic components, referring to both the pyridine and pyrimidine rings, the shift may indicate a strong plane-to-plane Cπ-pyrimidine interaction, the interacting sites being compressed one onto the other resulting in local repulsion of the adjoined π clouds of both moieties, thus deshielding the N atoms of the pyrimidine. This hypothesis is reinforced by the observation of similar shifts in the binding energies of the C and O atoms of the pyrimidinic ring. These effects are similar to those previously observed with other analogous ligands when adsorbed on graphitized ACs [36,37] and CNTs (Fig. S9). The shift of the aliphatic N atoms, together with the pyridinic component of the aromatic ones, indicates a change in their chemical environments due to the adsorption process, suggesting changes in the protonation degree of such moieties.

After adsorption of $[PdCl_4]^{2-}$ on the hybrid materials, the binding energy values of the aromatic subunits are almost unmodified, whereas those of the aliphatic moieties increase from 399.6 eV to 400.6 eV for MWCNT/HL1 and from 399.7 eV to 400.6 eV for MWCNT/HL2 (Fig. S8). This points out that Pd(II) ions are complexed by the polyaminic portions of the adsorbed ligands, the increased deshielding of the aliphatic nitrogen atoms being due to the coordination of the metal cations.

Concerning the oxidation state of Pd, XPS spectra of MWCNT/HL1-Pd and MWCNT/HL2-Pd (Fig. 4) show two signals in the Pd3d region (343.5 and 338.2 eV) which are characteristics of Pd (II), discarding any reduction to Pd(0).

As the molar amounts of adsorbed Pd(II) are always close to those of adsorbed ligand, for both HL1 and HL2, it is safe to conclude that most, if not all, $[PdCl_4]^{2-}$ is adsorbed via complexation of the palladium ion to the polyamine moieties of the ligands. Inspection of Cl/Pd molar ratio, from Pd and Cl signals of the XPS spectra of both catalysts (Fig. 4), reveals that such ratio is invariably very close to 2, reinforcing the idea that the metal is bound to the ligand. Moreover, further insight into the nature of the formed complex could be gained by close inspection of Cl XPS spectra. The two peaks at 198.0 and 199.6 eV, assigned to electrons from $2p_{3/2}$ and $2p_{1/2}$ states respectively, both possess a shoulder peak of higher energy (198.5 and 200.1 eV severally) (Fig. 4); the twofold nature of such peaks correlates with the presence of two distinct chloride anions: the first bound to Pd(II) ions, acting as its fourth donor, the latter being retained upon complexation of Pd(II) to guarantee charge neutrality. This, corroborated by the evidences from the coordination behavior observed in the solution studies of the free ligands, proofs that both HL1 and HL2, adsorbed on CNTs or not, function as N-tridentate ligands toward Pd (II), leading to complexes with an activated position occupied by a chloride anion.

The values of the BET surface areas of the functionalized materials reveal changes in the conformations of the polyaminic chains upon Pd(II) complexation. In the case of MWCNT/HL1, the BET surface area diminishes significantly after the coordination of the metal (from 198 m^2/g of the precursor to 179 m^2/g), while for MWCNT/HL2 there is barely a detectable difference (from 188 to 183 m^2/g). This can be rationalized considering the tendency of the formed square-planar Pd(II) complexes to interact with CNTs surface by Cπ-dπ interactions, which should result in a decrease of the BET surface area. Such interaction justifies both the data for HL1 and HL2: for the first ligand, the required folding of the polyaminic chain is not hindered, resulting in the interaction of the Pd(II)-macrocycle complex with the graphitic surface which actively reduces the surface area; in the case of HL2, the possible formation of such interactions is thought to be hindered both by

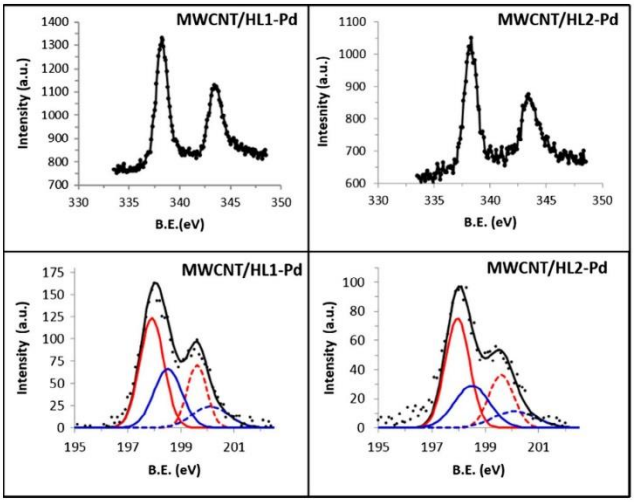

Fig. 4. High resolution XPS spectra of the catalysts useful for the assessment of the nature of the anchored Pd-complex species: top, spectra in the Pd $3d_{5/2}$ and Pd $3d_{3/2}$ regions, bottom, spectra in the Cl $2p_{3/2}$ and Cl $2p_{1/2}$ regions, showing the deconvolution of the twofold peaks into distinct signals.

the electrostatic interaction with the additional ammonium group in the side chain, which in Pd(II) adsorption conditions (pH 5.0) is expected to be protonated ($\log K = 7.0$ for the free complex, see Table 2), and by the higher loss of conformational entropy of the chain required to establish Cπ-dπ contacts compared to the shorter HL1. Thus, in this latter case, the variation of the BET surface area upon Pd(II) complexation is found to be very modest.

3.4. The Sonogashira carbon-carbon coupling reaction

The catalytic activity of MWCNT/HL1–Pd and MWCNT/HL2–Pd materials toward the copper-free Sonogashira reaction between iodobenzene and phenylacetylene (1:1 M ratio), using water as solvent and triethylamine as base, was tested at three different temperatures (30, 50, 70 °C). The catalytic process proceeds in all cases, although with significant differences (Table 3).

At 30 °C, the reaction was not completed in 3 days (Fig. S10). This high reaction time could be attributed to the extreme insolubility of the reactants in water, preventing their diffusion to the polar active-centres. Then, the reaction was assayed at 50 °C. The kinetic plots of the reaction at this temperature were collected in Fig. S11. Although the solubility of the reactants in water at 50 °C is still poor, probably acting as a limiting kinetic factor, the C—C coupling reaction was completed in 2 h: 90% of conversion of the reactants into diphenyl acetylene was achieved in the case of MWCNT/HL1-Pd and 94% for MWCNT/HL2-Pd (see Fig. S11), moreover without formation of any other by-product. The TOF values (mmol of reactants/mmol Pd(II)-amino complexes transformed per second) calculated for MWCNT/HL1-Pd (0.021 s^{-1}) and MWCNT/HL2-Pd (0.024 s^{-1}) show a better catalytic activity relative to similar catalysts previously used for the reaction studied here [90]. The shortened equilibrium times, even at lower temperature, than most proposed Pd(II)-based heterogeneous catalysts, (see Table 4) along with the high yields obtained, are probably due to the easy accessibility of the catalytic active centres, reinforced by their homogeneous dispersion over the whole external surface of the CNTs.

It should also be mentioned that, after recovering the catalysts by simple filtration methods and washing them with chloroform and water, their XPS spectra still showed traces of adsorbed iodobenzene. This points out that the partial adsorption of iodobenzene on the CNTs surface likely prevents that 100% conversion is reached in both cases.

To explore the influence of higher temperatures on the coupling, tests were also carried out at 70 °C (Fig. S12). In the case of both catalysts, the yields, although satisfactory, were not better than those at 50 °C. Moreover, in the case of MWCNT/HL2-Pd, a significant lixiviation of the anchored complex was observed which becomes evident as a pink colour appeared in the aqueous phase. For these reasons, the catalysts were not reused for additional cycles at this temperature. Nevertheless, this should be regarded as an important result, since such behavior demonstrates the heterogeneous nature of the catalyst, as an increased desorption of the Pd-HL2 complex not only does not improve the yield, but lowers it. In the case of MWCNT/HL1-Pd, containing the smaller and less protonated HL1, no lixiviation was noticed, but neither the yields (84% of diphenylacetylene formed) nor the equilibrium time (2 h) improved from the 50 °C assay. For these reasons, assays on reused catalysts were only carried out at 50 °C.

The studied C—C coupling reaction, was also carried out i) without any catalyst, ii) with the MWCNTs used as support of the catalysts, iii) with MWCNT/HL1 and MWCNT/HL2, but no reaction was observed in any of such cases. Assays with HL1-Pd and HL2-Pd complexes were not performed because we were unable to isolate complex samples of good quality. In addition, the catalytic activity of a MWCNT/$[PdCl_4]^{2-}$ material, consisting of $[PdCl_4]^{2-}$ directly adsorbed on CNTs, was assessed at 50 °C. In this case, the C—C coupling reaction did take place, with an equilibrium time of 24 h, after which a 78% of conversion of the reactants in diphenylacetylene was reached.

Table 3
Yields (% of product formation) measured at the equilibrium times corresponding to the catalytic assays of fresh and reused catalysts toward the Cu-free Sonogashira coupling between iodobenzene and phenylacetylene (1 mmol of each, 1 ml H_2O, Et_3N 2 mmol, 1% mol Pd).

Catalyst	T (°C)	Cycle	Equilibrium reaction times	Yield (%)
MWCNT/HL1-Pd	30	1	>3 d	88
	50	1	2 h	90
		2	8 h	86
		3	8 h	80
		4	24 h	80
	70	1	2 h	84
MWCNT/HL2-Pd	30	1	3 d	87
	50	1	2 h	94
		2	16 h	92
		3	24 h	76
		4	24 h	66
	70[a]	1	2 h	83

[a] At this temperature desorption of the anchored HL2-Pd complex was observed.

3.5. Reusability of the catalysts

The reusability of the two heterogeneous catalysts was tested for the above Sonogashira coupling reaction under the same conditions: three additional runs were carried out after the first one. After each cycle the catalysts were separated by filtration, washed thoroughly with chloroform and water and dried before reusing. As one can see in Table 3, the catalysts maintain a good catalytic activity through the four reaction cycles. In the second reaction cycle the yields of the reactions are close to those of the first run. For MWCNT/HL1-Pd catalyst, the yield decreases to 80% in the third cycle, value which is maintained in the fourth reaction. In the case of MWCNT/HL2-Pd, a higher decrease of the catalytic activity is observed after the second reaction, as the yields start to decrease with each cycle. Parallel to the above, the kinetic data (Fig. S12) show a significant increase of the equilibrium times for both catalysts after the first run, this effect being again sharper for MWCNT/HL2-Pd than for MWCNT/HL1-Pd.

To get insight into the possible causes of this behavior, the catalysts were characterized after each cycle to detect any possible modification occurring under their repeated use. The elemental analyses of the catalysts reveal nitrogen losses with each use, obviously involving lixiviation of the corresponding HL1-Pd and HL2-Pd complexes, which is more substantial for MWCNT/HL2-Pd than for MWCNT/HL1-Pd (Table S1), probably due to the higher solubility of HL2 in water. Such decreasing is sharper in the earliest cycles, after which the nitrogen content almost remains stable. It should be noted how the catalytic activities of the material decreases in parallel with the nitrogen losses they suffer.

Representative TEM images of the reused catalysts appear in Fig. 5. Despite some metal traces are present in the pristine MWCNTs used in this work (see above), they were not observed in their TEM micrographs [83]. Thus, the very scarce amount of nanoparticles observed in the TEM images of the reused MWCNT/HL1-Pd catalyst should correspond to Pd(0). In contrast, Pd(0) nanoparticles were not found in MWCNT/HL2-Pd (Fig. 5). Interestingly, most of the few particles formed in the MWCNT/HL1-Pd catalyst appear at the inner surface, where they might not contribute to the catalytic reaction. This might be caused by the fact that complexes adsorbed in relatively tight nanotube-

Table 4
Catalytic performances of MWCNT/HL1-Pd and MWCNT/HL2-Pd and selected carbon-based catalysts assessed for Cu-free Sonogashira Coupling.

Catalyst/support	Pd%[a]	T (°C)	Time (h)	Base	Solvent[b]	Molar ratio[c]	Atmosphere	Yield (%)	Ref
Pd(II)-HL1 complex/MWCNT	1	50	2	Et_3N	H_2O (1 mL)	1:1:2	Aerobic	90	[d]
Pd(II)-HL2 complex/MWCNT	1	50	2	Et_3N	H_2O (1 mL)	1:1:2	Aerobic	94	[d]
Pd(II)-Schiff base complex/MWCNT	1.2	27 55 90	24 6 1	Et_3N	H_2O (2 mL)	1:1.5:2	Aerobic	64 81 95	[63]
Pd(0) NPs/pramipexole-MWCNT	0.1 0.1	80 80	2 12	Et_3N K_2CO_3	DMF (3 mL) H_2O (3 mL)	1:1.2:2 1:1.2:2	Unspecified	96 55	[88]
Electrodeposited Pd(0) NPs/MWCNT	1	Reflux	2.5	K_2CO_3	MeOH/H_2O (3 mL:1 mL)	1:1.2:1.5	Aerobic	71	[89]
Pd(0) NPs/Iminopyridine-MWCNT	1	120	0.5	K_2CO_3	DMF (4 mL)	1:1:1	Unspecified	98	[60]
Pd(0) NPs/Nanoporous CHT	0.23	80	10–18	Cs_2CO_3	DMF (5 mL)	1:1.5:1.5	Inert	85	[90]

[a] 100(mol Pd/mol reagent).
[b] mL solvent/mmol Iodobenzene.
[c] Iodobenzene: Phenylacetylene:Base.
[d] This study.

holes may suffer stereochemical restrictions (as previously observed in the case of ACs for analogous Ar-S-F ligands [85]) that could decrease their stability, favoring their reduction to Pd(0). This would explain why most of Pd(0) nanoparticles are formed inside the tubes. On the other hand, a higher stability of the HL2-Pd complex, relative to HL1-Pd, could explain why no Pd(0) nanoparticles were observed in the reused MWCNT/HL2-Pd catalyst. According to the proposed mechanism for the copper-free Sonogashira reaction [43,47], the presence of Pd(0) should be related to the formation of a Pd(0) complex as an intermediate species during the catalyzed process. Nevertheless, the XPS spectra of the materials in the Pd region, collected after each cycle (Fig. S13), show signals at similar values than in the fresh catalysts, *i.e.* 343.5 and 338.2 eV, discarding the reduction of Pd(II) to Pd(0) as a possible cause of the deactivation of the catalysts, which seems better to be related to nitrogen losses.

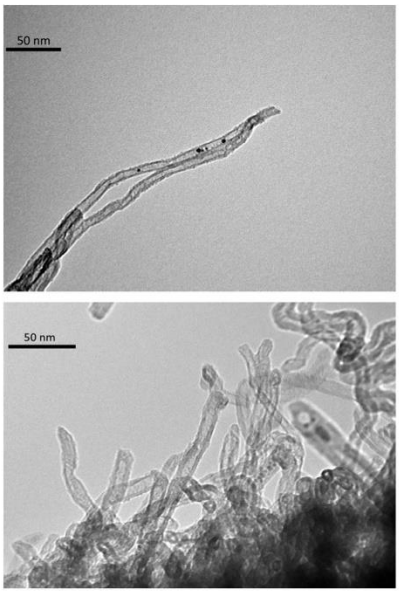

Fig. 5. TEM Images of MWCNT/HL1-Pd 4th cycle (top) and MWCNT/HL2-Pd 4th cycle (bottom).

Furthermore, the ratio between the intensities of N1s and Pd3d signals in the XPS spectra of reused catalysts remains similar to that of the fresh ones. This clearly suggests that the deactivation of the catalysts is due to the lixiviation of the anchored HL1-Pd and HL2-Pd complexes during the reactions. The mechanism of loss of catalytic centres, however, appears different from what some of us previously observed in the case of hydrogenation reactions with AC-supported Pd(II) amino complexes [41], where pyrimidine residues stuck to the graphitic walls while the appended chains were partially lost due to solvolysis of the C$(2)_{pyrimidine}$-NH bond. In those cases, the solvolysis was thought to be promoted by the stereochemical restrictions suffered by molecules adsorbed in the micropores of the carbon support. The lack of microporosity in our CNTs-based systems, along with the steady N/Pd ratio observed, lead to the conclusion that the partial lixiviation of catalytic centres observed in this study should be attributed to the competition of the hydrophobic molecules (phenylbenzene, iodobenzene and phenylacetylene) with the adsorbed HL1-Pd and HL2-Pd complexes for the C_π centres of the CNT surface.

4. Conclusions

The gathered experimental evidences strongly support the assayed MWCNT/HL1-Pd and MWCNT/HL2-Pd materials as valuable catalysts for the Cu-free Sonogashira coupling reaction: as one can easily see comparing the obtained results with other candidates (Table 4), our systems not only rank among the first in terms of yields and reaction times, but the conditions (solvent and temperature) in which they are capable of such performances are unprecedented; such finding deserves to be underlined, especially in an era striving for green, sustainable and energy-saving chemical processes. Accordingly, also the choices of a carbonaceous support and of a single Pd(II) ion as catalytic active site should be stressed as environmentally friendly solutions, adding to the convincing heterogeneous nature of our catalysts.

As documented above, the strong points underlying their striking catalytic activity reside in the uniformity of the catalytic sites, both in terms of surface distribution and chemical environment, which is granted by the preparation method.

Another feature worth mentioning is the choice of the polyaminic ligands, which are not only capable of coordinating Pd(II) strongly, forming a macrocyclic complex which is mostly stable under re-use even under stern alkaline conditions, but also manage to maintain an activated position, occupied by a chloride anion in the free complex and in the fresh catalyst, in the metal's first coordination sphere, which is probably crucial for the observed catalytic activity.

These promising results encourage the extension of this research to ligands possessing more than one pyrimidine moiety to ensure a firmer sorption and improve the overall re-usability of these materials, while maintaining the observed high catalytic performances.

Uncited references

[88,89].

Acknowledgements

Financial support from the following institutions is gratefully acknowledged: MIUR (project 2015MP34H3), Spanish MICINN and MEC and FEDER funds from the European Union (grants CTQ2013-14892 and CTQ2016-78499-C6-1-R), Unidad de Excelencia María de Maeztu MDM-15-0538), Generalitat Valenciana (PROMETEO II 2015-002), Spanish MINECO (Project MAT2014-60104-C2-2-R), the Autonomous Regional Government Junta de Andalucía (Group PAIDI FQM273) and the University of Jaén (EI-FQM6_2017).

The assistance of Dr. R. Cuesta in the determination of the molecular dimensions of HL1 and HL2 is gratefully acknowledged.

Appendix A. Supplementary materials

Supplementary data associated with this article can be found, in the online version, at http://dx.doi.org/10.1016/j.jcat.2017.07.023.

References

[1] C.C.C. Johansson Seechurn, M.O. Kitching, T.J. Colacot, V. Snieckus, Angew. Chem. Int. Ed. 51 (2012) 5062–5085.
[2] The Nobel Prize in Chemistry 2010 - Advanced Infor-mation, Nobelprize.org. Nobel Media AB 2014. Web. 13 Dec 2016.<http://www.nobelprize.org/nobel_prizes/chemistry/laureates/2010/advanced.html>.
[3] S.A. Timofeeva, M.A. Kinzhalov, E.A. Valishina, K.V. Luzyanin, V.P. Boyarskiy, T. M. Buslaeva, M. Haukka, V.Y. Kukushkin, J. Catal. 329 (2015) 449–456.
[4] P. Serp, B. Machado, Nanostructured Carbon Materials for Catalysis, RSC Catalysis Series No. 23, The Royal Society of Chemistry, Cambridge, 2015, pp. 370–375.
[5] L. Yin, J. Liebscher, Chem. Rev. 107 (2007) 133–173.
[6] A. Fihri, M. Bouhrara, B. Nekoueishahraki, J.-M. Basset, V. Polshettiwar, Chem. Soc. Rev. 40 (2011) 5181–5203.
[7] J. Guerra, M.A. Herrero, Nanoscale 2 (2010) 1390–1400.
[8] Q. Zhao, Y. Zhu, Z. Sun, Y. Li, G. Zhang, F. Zhang, X. Fan, J. Mater. Chem. A 3 (2015) 2609–2616.
[9] W. Maser, A.M. Benito, E. Muñoz, M.T. Martinez, in: Functionalized Nanoscale Materials, Devices and Systems, Springer, Dordrecht, The Netherlands, 2008, pp. 101–119.
[10] T.A. Saleh, V.K. Gupta, in: A. Tiwari, S.K. Shukla (Eds.), Advanced Carbon Materials and Technology, Wiley Online Library, 2014, pp. 317–330.
[11] L. Hu, Y.-L. Zhao, K. Ryu, C. Zhou, J.F. Stoddart, G. Grüner, Adv. Mater. 20 (2008) 939–946.
[12] T. Fujigaya, N. Nakashima, Sci. Tech. Adv. Mat. 16 (2015) 1–21.
[13] P. Bilalis, D. Katsigiannopoulos, A. Avgeropoulos, G. Sakellariou, RSC Adv. 4 (2014) 2911–2934.
[14] D. Ravelli, D. Merli, E. Quartarone, A. Profumo, P. Mustarelli, M. Fagnoni, RSC Adv. 3 (2013) 13569–13582.
[15] G. Zhu, X. Zhang, P. Gai, X. Zhang, J. Chen, Nanoscale 4 (2012) 5703–5709.
[16] Y.-L. Zhao, L. Hu, J.F. Stoddart, G. Grüner, Adv. Mater. 20 (2008) 1910–1915.
[17] M. Assali, M.P. Leal, I. Fernandez, N. Khiar, Nanotechnology 24 (2013), 085604/1–085604/12.
[18] M. Assali, M.P. Leal, I. Fernandez, R. Baati, C. Mioskowski, N. Khiar, Soft Matter. 5 (2009) 948–950.
[19] S. Marchesan, M. Prato, Chem. Commun. 51 (2015) 4347–4359.
[20] P. Yadav, V. Rastogi, A.K. Mishra, A. Verma, Drug Deliv. Lett. 4 (2014) 156–169.
[21] A. Battigelli, C. Menard-Moyon, T. Da Ros, M. Prato, A. Bianco, Adv. Drug Deliv. Rev. 65 (2013) 1899–1920.
[22] G. Lamanna, A. Battigelli, C. Menard-Moyon, A. Bianco, Nanotechnol. Rev. 1 (2012) 17–29.
[23] B.I.K. Kharisov, O.V. Kharissova, J. Coord. Chem. 67 (2014) 3769–3808.
[24] S.F. Liu, S. Lin, T.M. Swager, ACS Sens. 1 (2016) 354–357.
[25] C.C. Gheorghiu, C. Salinas-Martinez de Lecea, M.C. Roman-Martinez, Appl. Cat. A 478 (2014) 194–203.
[26] P. Gou, N.D. Kraut, I.M. Feigel, A. Star, Macromolecules 46 (2013) 1376–1383.
[27] V.A. Basiuk, L.V. Henao-Holguin, E. Alvarez-Zauco, M. Bassiouk, E.V. Basiuk, Appl. Surf. Sci. 270 (2013) 634–647.
[28] G. Bottari, O. Trukhina, M. Ince, T. Torres, Coord. Chem. Rev. 256 (2012) 2453–2477.
[29] F. D'Souza, O. Ito, Chem. Soc. Rev. 41 (2012) 86–96.
[30] F. Vialla, G. Delport, Y. Chas-Sagneux, Ph. Roussignol, J.S. Lauret, C. Voisin, Nanoscale 8 (2016) 2326–2332.
[31] S.F. Liu, L.C.H. Moh, T.M. Swager, Chem. Mater. 27 (2015) 3560–3563.
[32] E. Ma-ligaspe, A.S.D. Sandanayaka, T. Hasobe, O. Ito, F. D'Souza, J. Am. Chem. Soc. 132 (2010) 8158–8164.
[33] B. Wang, X. Zhou, Y. Wu, Z. Chen, C. He, Sensor. Actuat. B-Chem. 171–172 (2012) 398–404.
[34] R. López-Garzón, M.L. Godino-Salido, M.D. Gutierrez-Valero, P. Arranz-Mascarós, M. Melguizo, C. García, M. Domingo-García, F.J. López-Garzón, Inorg. Chim. Acta 417 (2014) 208–221.
[35] J. García-Martín, M.L. Godino-Salido, R. López-Garzón, M.D. Gutiérrez-Valero, P. Arranz-Mascarós, H. Stoeckli-Evans, Eur. J. Inorg. Chem. (2008) 1095–1106.
[36] M.D. Gutiérrez-Valero, M.L. Godino-Salido, P. Arranz-Mascarós, R. López-Garzón, R. Cuesta, J. García-Martín, Langmuir 23 (2007) 5995–6003.
[37] J. García-Martín, R. López-Garzón, M.L. Godino-Salido, M.D. Gutiérrez-Valero, P. Arranz-Mascarós, R. Cuesta, F. Carrasco-Marín, Langmuir 21 (2005) 6908–6914.
[38] J. García-Martín, R. López-Garzón, M.L. Godino-Salido, R. Cuesta-Martos, M.D. Gutiérrez-Valero, P. Arranz-Mascarós, H. Stoeckli-Evans, Eur. J. Inorg. Chem. (2005) 3093–3103.
[39] M. Savastano, P. Arranz-Mascarós, C. Bazzicalupi, A. Bianchi, C. Giorgi, M.L. Godino-Salido, M.D. Gutiérrez-Valero, R. López-Garzón, RSC Adv. 4 (2014) 58505–58513.
[40] P. Arranz, A. Bianchi, R. Cuesta, C. Giorgi, M.L. Godino, M.D. Gutiérrez, R. López, A. Santiago, Inorg. Chem. 49 (2010) 9321–9332.
[41] M.L. Godino-Salido, M.D. Gutiérrez-Valero, R. López-Garzón, P. Arranz-Mascarós, A. Santiago-Medina, M. Melguizo, M. Domingo-García, F.J. López-Garzón, V.K. Abdelkader-Fernández, C. Salinas-Martínez de Lecea, M.C. Román-Martínez, RSC Adv. 6 (2016) 58247–58259.
[42] S.K. Das, M. Sarmah, U. Bora, Tetrahedron Lett. 58 (2017) 2094–2097.
[43] M. Karak, L.C. Barbosa, G.C. Hargaden, RSC Adv. 4 (2014) 53442–53466, and references therein.
[44] P. Siemsen, R.C. Livingston, F. Diederich, Angew. Chem. Int. Ed 39 (2000) 2632–2657.
[45] D. Gelman, S. Buchwals, Angew. Chem., Int. Ed. 42 (2003) 5993–5996.
[46] M. Aufiero, P. Proutiere, F. Schoenebeck, Angew. Chem. Int. Ed. 51 (2012) 7226–7230.
[47] R. Chinchilla, C. Nájera, Chem. Soc. Rev. 40 (2011) 5084–5121, and references therein.
[48] M. Opanasenko, P. Stepnicka, J. Cejka, RSC Adv. 4 (2014) 65137–65162.
[49] V. Polshettiwar, C. Len, A. Fihri, Coord. Chem. Rev. 253 (2009) 2599–2626.
[50] A. Kumbhar, R. Salunkhe, Curr. Org. Chem. 19 (2015) 2075–2121.
[51] M. Bakherad, S. Jajarmi, J. Mol. Catal. A-Chem. 370 (2013) 152–159.
[52] A. Alonso, A. Shafir, J. Mascanás, A. Vallribera, M. Muñoz, D.N. Muraviev, Catal. Today 193 (2012) 200–206.
[53] Z.J. Wang, S. Ghasimi, K. Landfester, K.A.I. Zhang, Chem. Mater. 27 (2015) 1921–1924.
[54] R. Munirathinam, J. Huskens, W. Verboom, Adv. Synth. Catal. 357 (2015) 1093–1123.
[55] J.C. Hierso, M. Beauperin, S. Saleh, A. Job, J. Andrieu, M. Picquet, C. R. Chim. 16 (2013) 580–596.
[56] T. Miao, L. Wang, P.H. Li, J.C. Yan, Synthesis (2008) 3828–3834.
[57] C.I. Ezugwu, B. Mousavi, M.A. Asraf, Z. Luo, F. Verpoort, J. Catal. 344 (2016) 445–454.
[58] J. Huang, W. Wang, H. Li, ACS Catal. 3 (2013) 1526–1536.
[59] J. John, E. Gravel, I.N.N. Namboothiri, E. Doris, Nanotechnol. Rev. 1 (2012) 515–539.
[60] H. Veisi, M. Adib, R. Karimi-Nami, New J. Chem. 40 (2016) 4945–4951.
[61] A. Ohtaka, J.M. Sansano, C. Najera, I. Miguel-Garcia, A. Berenguer-Murcia, D. Cazorla-Amoros, ChemCatChem 7 (2015) 1841–1847.
[62] C. Rossy, J. Majimel, Tréguer M. Delapierre, E. Fouquet, F.-X. Felpin, Appl. Catal. A-Gen. 482 (2014) 157–162.
[63] M. Navidi, N. Rezaei, B. Mo-vassegh, J. Organomet. Chem. 743 (2013) 63–69.
[64] A.J. Reay, I.J.S. Fairlamb, Chem. Commun. 51 (2015) 16289–16307.
[65] M.O. Sydnes, Curr. Org. Chem. 18 (2014) 312–326.
[66] A. Ohtaka, Chem. Rec. 13 (2013) 274–285.
[67] A. Balanta, C. Godard, C. Claver, Chem. Soc. Rev. 40 (2011) 4973–4985.

[68] B. Verdejo, A. Ferrer, S. Blasco, C.E. Castillo, J. González, J. Latorre, M.A. Máñez, M. García Basallote, C. Soriano, E. García-España, Inorg. Chem. 46 (2007) 5707–5719.
[69] N.J. Low, M.D. López, P. Arranz, J. Cobo, M.L. Godino, R. López, M.D. Gutiérrez, M. Melguizo, G. Ferguson, C. Glidewell, Acta Cryst. B 56 (2000) 882–892.
[70] M. Inclán, M.T. Albelda, J.C. Frías, S. Blasco, B. Verdejo, C. Serena, C. Salat-Canela, M.L. Díaz, A. García-España, E. García-España, J. Am. Chem. Soc. 134 (2012) 9644–9656.
[71] C. Bazzicalupi, A. Bianchi, T. Biver, C. Giorgi, S. Santarelli, M. Savastano, Inorg. Chem. 53 (2014) 12215–12224.
[72] G. Gran, Analyst (London) 77 (1952) 661–671.
[73] P. Gans, A. Sabatini, A. Vacca, Talanta 43 (1996) 1739–1753.
[74] M.J. Dudek, J.W. Ponder, J. Comput. Chem. 16 (1995) 791–816.
[75] T.J. Bandosz, J. Jagiello, C. Contescu, J.A. Schwarz, Carbon 31 (1993) 1193–1202.
[76] J. Jagiello, T.J. Bandosz, J.A. Schwarz, Carbon 32 (1994) 1026–1028.
[77] D.-Q. Yang, J.F. Rochette, E. Sacher, J. Phys. Chem. B 109 (2005) 7788–7794.
[78] D.B. Holt, M.C. McCorry, P.D. Boyer, K.N. Dahl, M.F. Islam, Nanoscale 4 (2012) 7425–7434.
[79] C.F. Baes, R.E. Mesmer, The Hydrolysis of Cations, John Wiley and Sons, New York, 1976.
[80] M.P. Clares, C. Serena, S. Blasco, A. Nebot, L. del Castillo, C. Soriano, A. Domènech, A.V. Sánchez-Sánchez, L. Soler-Calero, J.L. Mullor, A. García-España, E. García-España, J. Inorg. Biochem. 143 (2015) 1–8.
[81] S. Blasco, Complejos Metálicos de Compuestos Poliaminicos y su Aplicación como Miméticos de Enzimas Protec-toras Antioxidantes Ph. D. Thesis, University of Valencia, 2011.
[82] F. Morales-Lara, M.J. Perez-Mendoza, D. Altmajer-Vaz, M. García-Roman, M. Melguizo, F.J. Lopez-Garzón, M. Domingo-García, J. Phys. Chem. C 117 (2013) 11647–11655.
[83] V.K. Abdelkader-Fernández, Hyperbranched structures on carbon nanotubes to obtain supported metal nanoparticles: attachment by means of halogenated functions and direct functionalization Ph. D. Thesis, University of Granada, Spain, 2015.
[84] M.L. Godino-Salido, R. López-Garzón, M.D. Gutiérrez-Valero, P. Arranz-Mascarós, M. Melguizo-Guijarro, M.D. López de la Torre, V. Gómez-Serrano, M. Alexandre-Franco, D. Lozano-Castelló, D. Cazorla-Amorós, M. Domingo-García, Mat. Chem. Phys. 143 (2014) 1489–1499.
[85] M.D. Gutiérrez-Valero, P. Arranz-Mascarós, A. Peñas-Sanjuan, M.L. Godino-Salido, R. López-Garzón, A. Santiago-Medina, M. Melguizo-Guijarro, M. Pérez-Mendoza, F.J. López-Garzón, M. Domingo-García, Mat. Chem. and Phys. 134 (2012) 608–615.
[86] C.H. Giles, T.H. MacEwan, S.N. Nakhwa, D. Smith, J. Chem. Soc. (1960) 3973–3993.
[87] J. Jagiello, T. Bandosz, K. Putyera, J. Schwarz, J. Colloid Interface Sci. 172 (1995) 341–346.
[88] S. Abbasi, M. Hekmati, Appl. Organomet. Chem. DOI: 10.1002/aoc.3600.
[89] M. Radtke, S. Stumpf, B. Schröter, S. Höppener, U.S. Schu-bertb, A. Ignaszak, Tetrahedron Lett. 56 (2015) 4084–4087.
[90] A. Modak, A. Bhaumik, J. Mol. Catal. A-Chem. 425 (2016) 147–156.

Inorganic Chemistry

Article

pubs.acs.org/IC

Anion Complexes with Tetrazine-Based Ligands: Formation of Strong Anion−π Interactions in Solution and in the Solid State

Matteo Savastano,[†] Carla Bazzicalupi,[†] Claudia Giorgi,[†] Celeste García-Gallarín,[‡] Maria Dolores López de la Torre,[‡] Fabio Pichierri,[§] Antonio Bianchi,*[,†] and Manuel Melguizo*[,‡]

[†]Department of Chemistry "Ugo Schiff", University of Florence, Via della Lastruccia 3, 50019 Sesto Fiorentino, Italy

[‡]Department of Inorganic and Organic Chemistry, University of Jaén, 23071 Jaén, Spain

[§]Department of Applied Chemistry, Graduate School of Engineering, Tohoku University, 980-8579 Sendai, Japan

Supporting Information

ABSTRACT: Ligands **L1** and **L2**, consisting of a tetrazine ring decorated with two morpholine pendants of different lengths, show peculiar anion-binding behaviors. In several cases, even the neutral ligands, in addition to their protonated HL^+ and H_2L^{2+} (L = **L1** and **L2**) forms, bind anions such as F^-, NO_3^-, PF_6^-, ClO_4^-, and SO_4^{2-} to form stable complexes in water. The crystal structures of H_2**L1**$(PF_6)_2\cdot 2H_2O$, H_2**L1**$(ClO_4)_2\cdot 2H_2O$, H_2**L2**$(NO_3)_2$, H_2**L2**$(PF_6)_2\cdot H_2O$, and H_2**L2**$(ClO_4)_2\cdot H_2O$ show that anion−π interactions are pivotal for the formation of these complexes, although other weak forces may contribute to their stability. Complex stability constants were determined by means of potentiometric titration in aqueous solution at 298.1 K, while dissection of the free-energy change of association ($\Delta G°$) into its enthalpic ($\Delta H°$) and entropic ($T\Delta S°$) components was accomplished by means of isothermal titration calorimetry measurements. Stability constants are poorly regulated by anion−ligand charge−charge attraction. Thermodynamic data show that the formation of complexes with neutral ligands, which are principally stabilized by anion−π interactions, is enthalpically favorable ($-\Delta G°$, 11.1−17.5 kJ/mol; $\Delta H°$, −2.3 to −0.5 kJ/mol; $T\Delta S°$, 9.0−17.0 kJ/mol), while for charged ligands, enthalpy changes are mostly unfavorable. Complexation reactions are invariably promoted by large and favorable entropic contributions. The importance of desolvation phenomena manifested by such thermodynamic data was confirmed by the hydrodynamic results obtained by means of diffusion NMR spectroscopy. In the case of **L2**, complexation equilibria were also studied in a 80:20 (v/v) water/ethanol mixture. In this mixed solvent of lower dielectric constant than water, the stability of anion complexes decreases, relative to water. Solvation effects, mostly involving the ligand, are thought to be responsible for this peculiar behavior.

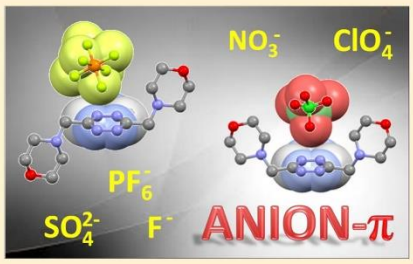

INTRODUCTION

Anion coordination chemistry has sparked considerable interest in recent years because of the ubiquitous presence of anions in biological and environmental systems, the roles they play in various biochemical processes, and their involvement in many technological areas. Consequently, scientists from all areas of chemistry and beyond have joined forces to explore this relatively young field. However, the design of receptors for the binding of anions in solution, in particular in water, can be very challenging because the noncovalent interactions employed to anchor the anions to the receptor are weak, they must prevail over the competing anion−solvent interactions, and structural features that provide them are often difficult to build into the receptor framework. Fortunately, while individual noncovalent interactions are weak, collectively they could be made sufficiently powerful to afford polyfunctional receptors capable of strong and selective anion binding.[1]

Anion−π interactions are among the most recently recognized noncovalent forces.[2−7] In spite of the fact that experimental observations were already reported as early as 1987 by Hiraoka et al.,[7] their importance was underappreciated for a long time by the scientific community, most likely because it seems rather counterintuitive to expect that an attraction may arise between a negatively charged species and common aromatic rings characterized by negative quadrupole moments. However, these quadrupole moments can be inverted upon insertion of either strongly electron-withdrawing substituents or heteroatoms able to accumulate more positive charge toward the ring center, turning parent aromatic systems into π acids able to attract anions.[8] Indeed, reviews of archived crystallographic data showed that anion−π interactions in the solid phase are more frequent than one might have expected,[3,9]

Received: May 10, 2016
Published: July 25, 2016

DOI: 10.1021/acs.inorgchem.6b01138
Inorg. Chem. 2016, 55, 8013−8024

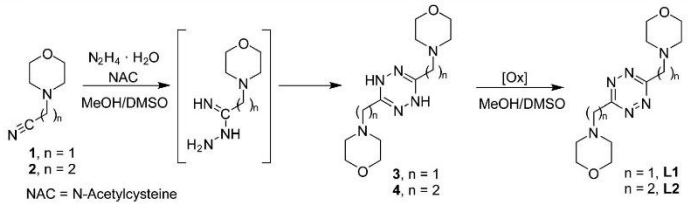

Figure 1. Synthetic scheme for the preparation of tetrazine ligands **L1** and **L2**.

evidencing that different geometries of the anion−arene interaction should be considered for a correct interpretation of the interaction itself (ref 9c). Further structural studies were undertaken to characterize such interactions in the solid state,[8,10] while theoretical and experimental investigations were made to analyze their properties in the gas phase and in solution.[3,8,10g−k,11,12]

Because of the elusive character of anion−π interactions in solution, their functional relevance was demonstrated only very recently in a study on anion transport in bilayer membranes.[13] Further conclusive evidence of anion−π interactions at work appeared for transport,[10g,12j,14] catalytic,[15] and anion recognition[10h] processes. Another intriguing matter concerns the thermodynamics of anion−π interactions in solution. Some attempts at the determination of stability constants[8,10k,12] and a few binding enthalpies[12d,e,16] for the association processes that involved anion−π interactions were reported, but the results obtained did not provide a clear-cut picture. All the same, they stimulated further attempts to determine energetic parameters that control such interactions in solution and to clarify their very definition. Measurement of the thermodynamic parameters for a pure anion−π interaction in solution is a highly challenging task and, to date, not a single anion−receptor pair is known, which is surely kept together exclusively by a single interaction of this type that would allow a direct measurement of the corresponding interaction energy. Commonly, the components are paired because of multiple contacts, and partitioning of the association free energy into its constituent contributions is not justified thermodynamically, except under severe restrictions and approximations.[17]

Theoretical studies have placed the binding energies of the anion−π interactions in the gas phase in the range 17−71 kJ/mol,[18] although measured values as high as 125 kJ/mol have been reported.[12b] For the anion−π interaction in solution, a recent review of the experimental results concluded that the binding free energy ($-\Delta G°$) for this attractive force in organic solvents is typically less than 4 kJ/mol per single phenyl ring−halide anion interaction, although larger values have also been reported.[8g] Such estimates of the anion−π contribution are often made by subtracting (with the aid of reference systems) from the combined effect of anion−π and hydrogen-bonding interactions (sometimes multiple) the latter, under the implicit and, generally, arbitrary assumption that free-energy changes are additive.[17] Furthermore, model structures and solvation effects may affect the magnitude of the measured term.[12h]

Recently, we have reported that protonated forms of the polyfunctional ligand NAP-T, assembled from the tripodal amine tris(2-aminoethyl)amine (tren, T) and nitrosoaminopyrimidine (NAP), form complexes with a range of anions. Crystal structures of the complexes revealed the anions to be tightly anchored to the ligand by both salt bridges to T and very short anion−π interactions with NAP.[10p,12e] The neutral (unprotonated) NAP-T and variously protonated species of NAP-T formed complexes with anions in water. The fact that the neutral NAP-T, which is unable to form salt bridges, and the isolated NAP residue both form complexes of very similar stability with the studied anions [SO_4^{2-}, SeO_4^{2-}, $S_2O_3^{2-}$, $Co(CN)_6^{3-}$] corroborated the idea that the anion−π interaction is the major contribution to the anion−receptor binding energy in these complexes. Accordingly, the associated free-energy changes ($-\Delta G°$ values were in the range 9−12 kJ/mol) were taken as good estimates of such anion−π interactions in water.[12e] Isothermal titration calorimetry (ITC) measurements revealed that these anion−π interactions were almost athermic ($\Delta H°$ values were in the range −2 to +3 kJ/mol) and were driven by large entropic contributions ($T\Delta S°$ terms were in the range 8−15 kJ/mol).[12e] Higher thermal effects were measured in acetonitrile for the complexes of monoanions, where multiple anion−π and hydrogen-bonding interactions were present.[12d,16] The majority of them were exothermic, and the relevant complexation processes were accompanied by either negligible[12d] or favorable[16a] entropic contributions; in other cases,[16b] the coordination enthalpies were endothermic, and the processes of complex formation were promoted by favorable entropy changes.

Taking into account that the introduction of anion−π interactions into the makeup of anion receptors, anion carriers, catalysts, and new functional systems in general has become of great interest, we have undertaken the task of advancing the understanding of these weak forces by developing a new type of anion receptor (Figure 1). These new receptors include a tetrazine ring decorated with two morpholine pendants of variable length. We have characterized their ability to bind inorganic anions such as F^-, NO_3^-, PF_6^-, ClO_4^-, and SO_4^{2-} both in solution and in the solid state. The latter included elucidation of the crystal structures of NO_3^-, PF_6^-, and ClO_4^- complexes by single-crystal X-ray diffraction analysis, while solution studies were concerned with determination of the thermodynamic parameters ($\Delta G°$, $\Delta H°$, and $T\Delta S°$) for the formation such complexes in water. Furthermore, improved solubility of **L2** made it possible to extend the solution studies to a mixed solvent [80:20 (v/v) water/ethanol] and to establish how the stability of these complexes is affected by the solvent polarity.

Ligands **L1** and **L2** (Figure 1) were designed to deliver the tetrazine ring into an aqueous medium without the addition of structural elements that might offer strong anchorage to anions in addition to the anion−π interaction. *s*-Tetrazine is a molecule with a high and positive quadrupole moment (Q_{zz} = 10.7 B) and a high molecular polarizability ($\alpha_{\parallel}$ = 58.7 au);

DOI: 10.1021/acs.inorgchem.6b01138
Inorg. Chem. 2016, 55, 8013−8024

therefore, both electrostatic and ion-induced polarization terms contribute to make it a strong π acid.[10r] Accordingly, tetrazine ligands are amenable to anion–π interactions, but usually they have low water solubility.[8c−f,m,10f,19a] Functionalization with two morpholine groups makes **L1** and **L2** sufficiently soluble in water to be studied by means of our thermodynamic techniques. In particular, both ligands are well soluble in an acidic aqueous medium because of protonation of the morpholine nitrogen atoms. In general, the phenomenon of ligand protonation in the study of anion–π interactions is undesirable because the protonated ligands may also form strong salt bridges with the anions. However, in this particular case, our crystallographic studies revealed a poor tendency of the protonated ligands to bind anions through the salt bridge interactions. Furthermore, while for a weaker π-acid ligand preorganization is fundamental for successful anion binding,[20] the localization of anions over the tetrazine ring of **L1** and **L2** appears to be independent of the ligand conformation.

■ RESULTS AND DISCUSSION

Synthesis of L1 and L2. The preparation of ligands **L1** and **L2** (Figure 1) was achieved following a two-step, classical Pinner synthesis, consisting of reaction of the morpholinylnitriles **1** and **2** with hydrazine hydrate to generate the corresponding dihydro-1,2,4,5-tetrazine intermediates **3** and **4**, which upon easy (although slowly) air oxidation yielded the fully aromatic *s*-tetrazines. Notably, the synthesis of **L1** and **L2** is one of the few nonmetal-catalyzed Pinner syntheses of 3,6-dialkyl-*s*-tetrazine derivatives reported to date. Indeed, it is historically accepted that Pinner's procedures are of general applicability to the preparation of 3,6-diaryl-substituted *s*-tetrazines but not to the synthesis of 3,6-dialkyl derivatives.[19] Only recently was a variant of the Pinner synthesis to prepare 3,6-dialkyl-*s*-tetrazines with a wide scope of application reported, but it was based on the use of anhydrous hydrazine and a metal Lewis acid catalyst,[21] with the drawback of needing intensive purification to remove metal traces in the case of products containing good transition-metal binding moieties such as the morpholinyl groups in our molecules. On the other hand, in our preparations, the safer hydrazine hydrate is used together with *N*-acetylcysteine (NAC) as the catalyst, with acceptable results in terms of isolated yields. Because the catalytic effect of NAC in the general preparation of amidines from primary amines and both alkyl- and arylnitriles is known,[22] we attribute the success of our preparations to the role of NAC as a catalyst in the reactions between the morpholinylnitriles **1** and **2** hydrazine to give the corresponding amidrazone intermediates. The subsequent formation of dihydro-1,2,4,5-tetrazine derivatives by dimerization of amidrazones is a well-known process,[23] which, in our case, leads to the isolable intermediates **3** and **4**.

Crystal Structure of H_2L1$(PF_6)_2\cdot 2H_2O$. In this crystal structure, the diprotonated H_2**L1**$^{2+}$ ligand lies on an inversion center and assumes an overall symmetric chair conformation (Figure 2). The tetrazine ring forms two anion–π interactions with the symmetry related PF_6^- ions, with one of the fluorine atoms of these anions being only 2.94(9) Å apart from the ring centroid. Interestingly, the ammonium groups of the ligand are not involved in the binding of the PF_6^- anions but interact via hydrogen bonding with cocrystallized water molecules [N···OW 2.686(6) Å]. As a consequence, the anion is held in the crystal packing by the anion–π interaction with contributions

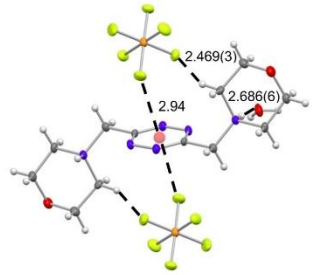

Figure 2. Crystal structure of H_2**L1**$(PF_6)_2\cdot 2H_2O$. Distances are in angstroms.

from CH···F bonds [2.469(3) Å] and van der Waals interactions.

Crystal Structure of H_2L1$(ClO_4)_2\cdot 2H_2O$. In this complex, the ligand assumes a boatlike conformation, with both morpholine pendants protruding from the same side of the tetrazine ring (Figure 3). The aromatic group forms anion–π

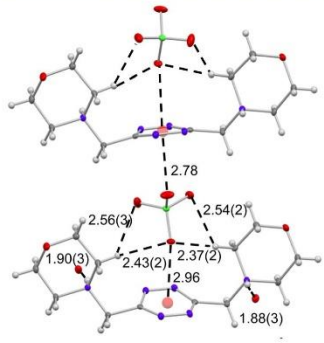

Figure 3. Crystal structure of H_2**L1**$(ClO_4)_2\cdot 2H_2O$. Distances are in angstroms.

interactions with the oxygen atoms of two symmetry-related ClO_4^- anions. As in the previous structure, the anions are located almost above the center of the tetrazine ring with O··· centroid distances of 2.96(3) and 2.78(3) Å, respectively. Accordingly, this anion is sandwiched between the tetrazine rings of two ligand molecules, while the other ClO_4^- anion, not shown in Figure 3, is hydrogen-bonded to water molecules interacting with ligand ammonium groups [NH···OW 1.88(3) Å; NH···OW 1.90(3) Å]. It is worth noting that, also in this complex, the sandwiched anion is held in place only by anion–π interactions and CH···O hydrogen bonds (Figure 3).

Crystal Structure of H_2L2$(PF_6)_2\cdot H_2O$. The crystal structure of the PF_6^- complex with H_2**L2**$^{2+}$ contains two centrosymmetric crystallographically independent ligand molecules (Figure 4). One of them assumes a chair conformation similar to that found in the structure of H_2**L1**$(PF_6)_2\cdot 2H_2O$, while the other one is almost planar. Also in H_2**L2**$(PF_6)_2\cdot H_2O$, the tetrazine rings give rise to anion–π interactions with PF_6^-. Different kinds of interactions are established between the

DOI: 10.1021/acs.inorgchem.6b01138
Inorg. Chem. 2016, 55, 8013−8024

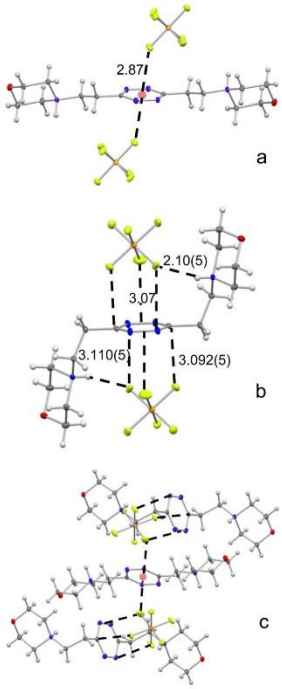

Figure 4. Crystal structure of H_2**L2**$(PF_6)_2 \cdot H_2O$. Distances are in angstroms. Views of the ligand and of its anion···π contacts: (a) planar and (b) chair conformations and (c) a portion of the crystal packing.

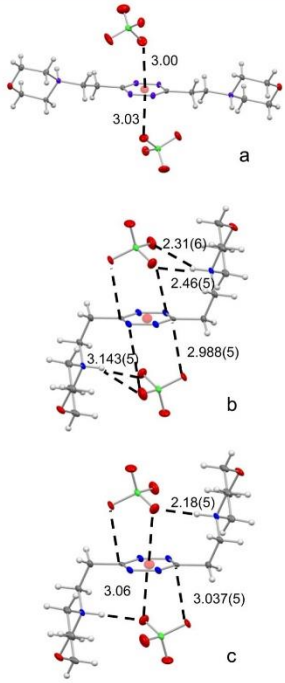

Figure 5. Crystal structure of H_2**L2**$(ClO_4)_2 \cdot H_2O$. Distances are in angstroms. Views of the ligand and of its anion···π contacts: (a) planar and (b and c) chair conformations.

fluorine atoms of PF_6^- and the tetrazine groups. Actually, one of the fluorine atoms is located pretty well above the tetrazine ring centroid of the planar ligand [F···centroid 2.87(6) Å; Figure 4a], governed by the ion−dipole attraction, while three cofacial fluorine atoms face the other tetrazine ring, forming F··· N, F···C, and F···N−N contacts [3.110(5), 3.092(5), and 3.07 Å, respectively; Figure 4b]. Because of the enhanced flexibility of the ethylenic chains connecting the tetrazine and morpholine rings, the ligand in the chair conformation is able to form a salt bridge with the anion [NH···F 2.10(5) Å], in contrast to the behavior of **L1**, featuring shorter methylenic chains. It is to be underlined, however, that in this structure only one PF_6^- is in contact with the tetrazine rings, bridging the two ligands to form infinite zigzag chains of anion−π contacts (Figure 4c). The second PF_6^- anion only interacts with a water molecule hydrogen-bonded to an ammonium group of the planar H_2**L2**$^{2+}$ ligand form.

Crystal Structure of H_2L2$(ClO_4)_2 \cdot H_2O$. This crystal structure contains three crystallographically independent diprotonated ligand molecules H_2**L2**$^{2+}$. One of them assumes an almost planar arrangement (Figure 5a), while the other two, lying around a crystallographic center, adopt chair conformations (Figure 5b,c). Like in the crystal structure of H_2**L2**$(PF_6)_2 \cdot H_2O$, several types of anion···tetrazine interactions contribute to stabilizing the crystal (O···centroid, O···C, and O···N in Figure 5) and the overall crystal packing contains infinite zigzag chains of alternating ligand and perchlorate units (Figure S1). In particular, in the adducts shown in Figures 5a,c, one of the anion oxygen atoms is located almost above the ring centroid. However, while in the case of the planar ligand no other relevant interactions are observed in addition to such O··· centroid contacts (Figure 5a), in the case of the complex in Figure 5c, additional O···C interactions contribute to strengthening the anion−tetrazine binding.

As in the previous structure, each ligand molecule in the chair conformation forms a salt bridge with ClO_4^- [NH···O 2.31(6) and 2.46(5) Å, Figure 5b; NH···O 2.18(5) Å, Figure 5c]. The crystal packing is further stabilized by additional hydrogen bonds involving the two remaining ClO_4^- and lattice water molecules.

Crystal Structure of H_2L2$(NO_3)_2$. Among the crystal structures obtained for anion complexes with **L2**, the NO_3^- complex is the one having more similarities with the structures seen for the shorter **L1** ligand. Actually, the packing contains a single centrosymmetric ligand molecule in the chair conformation, interacting with NO_3^- through the tetrazine ring (Figure 6). The planar anion is arranged almost parallel above the tetrazine group [dihedral angle 21.9(2)°], with an oxygen atom close to the ring centroid [O···ring centroid 2.850(2) Å]. The same oxygen atom forms a salt bridge with a ligand

DOI: 10.1021/acs.inorgchem.6b01138
Inorg. Chem. 2016, 55, 8013−8024

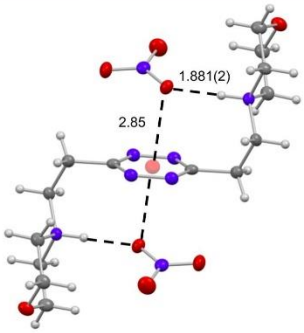

Figure 6. Crystal structure of H_2**L2**$(NO_3)_2$. Distances are in angstroms.

ammonium group [NH···O 1.881(2) Å]. Obviously, all groups and interactions are duplicated below the tetrazine ring by the inversion center, but no chains based on repeated anion−π interactions are observed in this crystal.

Analysis of the Anion−Tetrazine Ring Interaction in the Crystal Structures. It was recently shown for the interaction of halides with electron-deficient arenes that, when the anion lies above the plane of the π system, both centered and off-center interaction geometries are common.[9c] In the latter case, the anion is positioned over the periphery of the ring and charge-transfer (CT) complexes can be formed thanks to a certain covalent character of the interaction with ring atoms. Conversely, in the former case, the anion lies above the centroid of the ring where the CT contribution to the anion−π interaction is expected to be negligible. The geometric parameters d_{offset}, $d_{centroid}$, and d_{plane} (Figure 7a) were used to describe the location of the anion above the ring.[9c] The d_{plane} parameter is the distance from the mean ring plane and defines

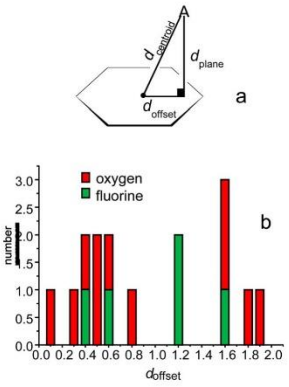

Figure 7. (a) Displacement of an atom A from the center (centroid) of the tetrazine ring. (b) Histogram of d_{offset} values (rounded to one decimal place) for the crystal structures reported here. Red and green bars refer respectively to oxygen and fluorine atom interactions with tetrazine rings.

d_{offset}, which has a value of 0 Å for a perfectly centered anion−π complex and a value of 1.4 Å when the anion is exactly located above a ring atom.

A similar analysis of the crystal structures herewith reported, performed by considering oxygen and fluorine atoms within 4 Å from the tetrazine centroid, shows a preference of the studied polyatomic anions for centered interactions (in 50% of the cases, $d_{offset} \leq 0.6$ Å), although a significant number of off-center interactions nearby the ring atoms (31% of the cases are in the range 1.2 Å $\leq d_{offset} \leq$ 1.6 Å) are also present (Figure 7b). PF_6^- and ClO_4^- complexes form only centered interactions with **L1**, while for **L2** complexes, a greater dispersion of d_{offset} values is observed (Table S2): oxygen atoms tend to form centered interactions, while three out of the five ring−fluorine contacts are off-center (Figure 7b). All structures show anion−tetrazine contacts slightly shorter than the sum of the van der Waals radii of the interacting atoms (Table S3).

Anion Binding in Solution. Protonated forms of **L1** and **L2** and, in some cases, even the neutral ligands give rise to detectable interactions with anions in water. Analysis, by means of the computer program *HYPERQUAD*,[24] of potentiometric (pH-metric) titrations performed for the various ligand−anion systems afforded the stability constants of the anion complexes reported in Table 1. As reported in the experimental

Table 1. Equilibrium Constants (log *K*) for Ligand Protonation and Anion Complex Formation Determined at 298.1 ± 0.1 K in a 0.1 M Me_4NCl Aqueous Solution or a 80:20 (v/v) Water/Ethanol Mixture

	water		80:20 (v/v) water/ethanol
	L1	**L2**	**L2**
$L + H^+ = HL^+$	4.45(3)	6.19(1)	6.04(2)
$HL^+ + H^+ = H_2L^{2+}$	3.45 (3)	5.37(1)	5.19(2)
$HL^+ + F^- = [HLF]$	n.d.	1.58(8)	1.16(7)
$H_2L^{2+} + F^- = [H_2LF]^+$	n.d.	1.97(3)	1.26(5)
$HL^+ + NO_3^- = [HL(NO_3)]$	1.43(5)	1.8(1)	1.72(7)
$H_2L^{2+} + NO_3^- = [H_2L(NO_3)]^+$	1.66(6)	2.32(4)	2.18(3)
$L + SO_4^{2-} = [L(SO_4)]^{2-}$		2.18(3)	
$HL^+ + SO_4^{2-} = [HL(SO_4)]^-$	1.65(8)	2.31(3)	1.68(7)
$H_2L^{2+} + SO_4^{2-} = [H_2L(SO_4)]$	2.08(3)	2.48(3)	2.29(3)
$L + ClO_4^- = [L(ClO_4)]^-$		1.98(5)	
$HL^+ + ClO_4^- = [HL(ClO_4)]$	2.07(9)	2.26(5)	1.55(8)
$H_2L^{2+} + ClO_4^- = [H_2L(ClO_4)]^+$	2.31(8)	2.51(4)	1.83(5)
$L + PF_6^- = [L(PF_6)]^-$	1.96(8)	3.07(8)	
$HL^+ + PF_6^- = [HL(PF_6)]$	2.67(7)	3.17(7)	1.67(9)
$H_2L^{2+} + PF_6^- = [H_2L(PF_6)]^+$	2.98(7)	3.39(8)	2.22(8)

procedures (Supporting Information), it was not possible to study the interaction of **L1** with F^- because of the low basicity of this ligand forming protonated species at enough low pH values to make F^- reactive toward the glass components of the measurement cell. Because these measurements were performed in the presence of 0.10 M Me_4NCl, we must assume that all of the equilibria in this table are potentially affected by the competitive ligand interaction with Cl^-.

Although the crystal structures of the anion complexes previously described show the diprotonated ligand forms

DOI: 10.1021/acs.inorgchem.6b01138
Inorg. Chem. 2016, 55, 8013−8024

(H_2L^{2+}) interacting with pairs of anions, the 1:1 stoichiometry of the complexes in solution was unambiguously ascertained by computer analysis of the titration curves. The stability of these complexes invariably increases with ligand protonation (increasing positive charge), even though the relevant association processes are poorly controlled by electrostatic forces. As a matter of fact, the mean increment of the complexation free-energy change associated with the variation of a single positive charge of the ligand, 1.8 kJ/mol (0.4 kcal/mol), is considerably smaller than the value 5 ± 1 kJ/mol expected for the formation of a single salt bridge in water.[25] Accordingly, forces other than salt bridges are expected to furnish the decisive contribution making such association events favorable This is in agreement with the previously described crystal structures of anion complexes, showing that, in the solid phase, the ligands can bind anions without resorting to salt bridges. The same crystal structures show that, both in the absence and in the presence (few cases) of salt bridges, the anions are located over the tetrazine rings, forming anion−π interactions. Actually, the most remarkable binding characteristic observed in the five crystal structures is that the anions invariably choose the tetrazine ring as the preferential binding site, despite the presence of two ammonium groups. Indeed, density functional theory (DFT) calculations showed that the lowest unoccupied molecular orbital (LUMO) of the free ligands is localized on the tetrazine ring, which might accept the electronic charge of the interacting anion, while the highest occupied molecular orbital (HOMO) is localized on the atoms of both morpholine rings, excluding the positively charged NH groups (Figure S2). However, a natural population analysis[42] of the complexes indicates that the CT contribution is modest in our systems.

We can reasonably expect that similar binding features are maintained in solution, where the modest increment of the complex stability with increasing ligand protonation is clear evidence of the weak increment of electrostatic attraction exerted on the anion by ligand ammonium groups. Furthermore, anion contacts with aliphatic CH groups are not expected to furnish much stabilization because aliphatic CH groups are known to be very poor hydrogen-bond donors in comparison to water[26] and the studied anions, except F^-, are not good hydrogen-bond acceptors because they are the conjugated bases of strong acids. Accordingly, no evidence of similar CH···anion interactions was found in the ^{1}H NMR spectra of the complexes recorded at different pH values. Above all, these anions are not willing to replace hydrogen bonds to water molecules with hydrogen bonds to aliphatic CH groups. Accordingly, the main contribution to the stability of these complexes in solution should be provided by anion−π interactions that would become the most effective (almost unique) binding forces in the anion complexes of uncharged (not protonated) ligands. The free-energy changes ($-\Delta G^\circ$) for formation of the latter are in the range 11.3−12.4 kJ/mol for the complexes of **L1** with PF_6^- and of **L2** with ClO_4^- and SO_4^{2-}, while a somewhat greater value, $-\Delta G^\circ$ = 17.5 kcal/mol, was determined for the PF_6^- complex with **L2** (Table 1). These values well compare with the free-energy changes ($-\Delta G^\circ$ = 8.6−12 kJ/mol) previously determined for anion complexes, formed in water by SO_4^{2-}, SeO_4^{2-}, $S_2O_3^{2-}$, and $Co(CN)_6^{3-}$ with pyrimidine ligands, in which the anion−π interaction is thought to be the almost unique binding force.[12e] Of course, such free-energy changes refer to association processes including solvent effects. DFT calculations performed on the complexes of these anions with protonated and neutral ligands in a continuum water environment showed that all complexes are stabilized by an interplay of different weak forces, among which anion−π interactions are invariably present. In agreement with the above solution data, binding energies calculated for the formation of such anion complexes point out that even complexes with neutral ligands are significantly stable. Even the plain tetrazine ring, deprived of morpholine residues, forms stable complexes with the anions, with the anion−π interaction being the unique bonding interaction; for instance, the calculated binding energies for the interaction of ClO_4^- with 1,2,4,5-tetrazine and 3,6-dimethyl-1,2,4,5-tetrazine are 9.1 and 10.1 kJ/mol, respectively (Figure S3). However, the calculated binding energies increase faster with the ligand charge (ligand protonation state) than the free-energy changes determined in the real solutions, probably because of the lack of explicit solvent effects in our DFT calculations. A comprehensive theoretical analysis of these binding processes will be the subject of a separate paper.

It is interesting to note that **L2** forms complexes of greater stability than **L1**. Unfortunately, the comparison between complexes of neutral ligands is only possible for PF_6^- because neutral ligand complexes of **L1** were not detected with the other anions. Most likely, they are formed in very small amounts, not detectable with the potentiometric method.

Greater insight into the thermodynamic aspects governing the formation of these complexes was gained by dissecting the complexation free-energy changes in their enthalpic and entropic contributions by means of ITC. The determined enthalpy changes are reported in Table 2 along with the derived entropy terms. Regrettably, only some calorimetric data were obtained for the anion complexes with **L1**, owing to insufficient solubility of the ligand and complexes. Data in Table 2, however, clearly show that these anion-binding equilibria are invariably promoted by large and favorable entropic contributions, while the relevant enthalpy changes are mostly unfavorable (endothermic). However, in the cases of anion

Table 2. Thermodynamic Parameters (kJ/mol) for Ligand Protonation and Anion Complex Formation Determined at 298.1 ± 0.1 K in a 0.1 M Me_4NCl Aqueous Solution

	ΔG°	ΔH°	$T\Delta S^\circ$
L1 + H^+ = $HL1^+$	−25.4(2)	−4.6(4)	20.8(4)
$HL1^+$ + H^+ = H_2L1^{2+}	−19.7(2)	4.6(4)	24.3(4)
L2 + H^+ = $HL2^+$	−35.32(6)	−26.8(4)	8.5(4)
$HL2^+$ + H^+ = H_2L2^{2+}	−30.64(6)	−18.4(4)	12.2(4)
H_2L1^{2+} + ClO_4^- = $[H_2L1(ClO_4)]^+$	−13.2(5)	−0.8(4)	12.4(6)
L1 + PF_6^- = $[L1(PF_6)]^-$	−11.1(5)	n.d.	n.d.
$HL1^+$ + PF_6^- = $[HL1(PF_6)]$	−15.2(4)	−5.9(4)	9.3(6)
H_2L1^{2+} + PF_6^- = $[H_2L1(PF_6)]^+$	−17.0(4)	0.8(4)	17.8(6)
$HL2^+$ + NO_3^- = $[HL2(NO_3)]$	−10.3(6)	9.1(3)	19.4(7)
H_2L2^{2+} + NO_3^- = $[H_2L2(NO_3)]^+$	−13.2(2)	6.4(3)	19.6(4)
L2 + SO_4^{2-} = $[L2(SO_4)]^{2-}$	−12.4(2)	−0.6(3)	11.8(4)
$HL2^+$ + SO_4^{2-} = $[HL2(SO_4)]^-$	−13.2(2)	27.2(4)	40.4(4)
H_2L2^{2+} + SO_4^{2-} = $[H_2L2(SO_4)]$	−14.12(2)	17.0(4)	31.1(4)
L2 + ClO_4^- = $[L2(ClO_4)]^-$	−11.3(3)	−2.3(2)	9.0(4)
$HL2^+$ + ClO_4^- = $[HL2(ClO_4)]$	−12.9(3)	9.6(4)	22.5(5)
H_2L2^{2+} + ClO_4^- = $[H_2L2(ClO_4)]^+$	−14.3(2)	6.7(4)	21.0(4)
L2 + PF_6^- = $[L2(PF_6)]^-$	−17.5(5)	−0.5(3)	17.0(6)
$HL2^+$ + PF_6^- = $[HL2(PF_6)]$	−18.1(4)	12.5(3)	30.6(5)
H_2L2^{2+} + PF_6^- = $[H_2L2(PF_6)]^+$	−19.3(5)	5.5(3)	24.8(6)

DOI: 10.1021/acs.inorgchem.6b01138
Inorg. Chem. 2016, 55, 8013−8024

binding by the neutral (unprotonated) **L2** ligand, in which anion−π interactions should make the major contributions, the complexation reactions are not hampered by thermal effects because the measured enthalpy changes are favorable, although very small ($\Delta H°$ in the range −0.5 to −2.3 kJ/mol). A similar enthalpy and entropy dependence of binding equilibria is typical of association processes controlled by desolvation phenomena. Indeed, charge neutralization occurring upon interaction of charged species causes an important release of solvent molecules, that is, an endothermic process accompanied by a large entropy increase. When the anion binds an uncharged ligand, a smaller desolvation is expected to occur with respect to the association with a charged one, and, accordingly, the reaction is expected to be less endothermic and less exoentropic, as was actually found for our systems (Table 2).

To get more information on solvent effects, the formation of anion complexes with the more soluble **L2** ligand was also studied in the 80:20 (v/v) water/ethanol mixture, displaying a lower dielectric constant (ε = 69.05 at 25 °C) with respect to pure water (ε = 78.56 at 25 °C).[27] The stability constants of the complexes formed in the solvent mixture are listed in Table 1. These data show that the addition of ethanol to water causes a general lowering of the stability for complexes with protonated ligand forms, while complexes of the unprotonated, uncharged ligand were not detected. At first glance, these results might be surprising because one could reasonably expect that the association between charged species becomes stronger as the polarity of the solvent decreases. Nevertheless, when the association takes place between charged and neutral species, the stability of the assembly may increase with increasing solvent polarity. As a matter of fact, the protonation constants of **L2** are smaller in 80:20 (v/v) water/ethanol than in pure water, as generally happens[28] for many other amines. Instructive examples, in this sense, are given by the protonation properties of molecules containing both neutral and negatively charged protonation sites, such as amino acids.[28,29] In these cases, as the solvent polarity decreases (upon the addition of ethanol to water), the protonation constants of the carboxylate groups increase while the protonation constants of the amine groups decrease, as a consequence of the selective solvation occurring in the solvent mixture, with water and ethanol molecules being preferentially attracted respectively by charged groups and neutral functionalities. Accordingly, the lower stability of our anion complexes in the solvent mixture corroborates our previous conclusion that in pure water the anion complexation processes studied here are essentially controlled by forces other than charge−charge attractions.

Also, anions can be subjected to selective solvation.[30] F^-, for instance, in 80:20 (v/v) water/ethanol, is selectively hydrated, with no ethanol molecules in its first solvation sphere. Upon an increase of the anion size, also the involvement of ethanol molecules in anion solvation increases, and for ClO_4^-, the composition of the first solvation sphere approaches the composition of the bulk solvents.[30b] Taking into account, however, that in the 80:20 (v/v) water/ethanol mixture there is one ethanol molecule every 13 water molecules, even for ClO_4^- the participation of ethanol molecules in the solvation sphere is still modest. Then, anion desolvation occurring upon interaction with **L2** is not expected to be at the origin of the difference of the complex stability between water and the water/ethanol mixture, and, accordingly, different ligand solvation should be responsible for the observed difference in the binding constants. Consistent with this general drop in the stability, complexes of anions with the neutral **L2** ligand are not formed or their formation is too scarce to be detected.

Unfortunately, our attempts to identify significant changes in the NMR spectra (^1H, ^{13}C, and ^{15}N and also ^{19}F and ^{31}P for PF_6^-) of the species involved in the anion−π complexation equilibria were unfruitful in both D_2O and acetonitrile-d_3. However, interesting information about the formation of such anion complexes in water was obtained by pulsed gradient spin−echo (PGSE) ^{19}F and ^1H NMR diffusion spectroscopy,[31] following variation of the diffusion coefficients of PF_6^- and $H_2\mathbf{L2}^{2+}$ occurring upon complexation. Because the exchange between complexed and uncomplexed species in the anion−π complexation equilibrium is a fast process on the time scale of the (relatively slow) NMR measurements, the diffusion coefficient measured by PGSE NMR for a particular species is the weighted average of the diffusion coefficients of its uncomplexed and complexed forms. That is, for the equilibrium $H_2\mathbf{L2}^{2+} + PF_6^- = [H_2\mathbf{L2}(PF_6)]^+$, the observed diffusion coefficient for PF_6^-, $\overline{D}_{PF_6}$, can be expressed as $\overline{D}_{PF_6} = (1 - \alpha) D_{PF_6} + \alpha D_{\mathbf{L2}PF_6}$, where D_{PF_6} and $D_{\mathbf{L2}PF_6}$ represent the diffusion coefficients of the uncomplexed and complexed forms of PF_6^-, respectively, and α is the mole fraction of complexed PF_6^-. As shown in Figure 8a, the addition of increasing amounts of

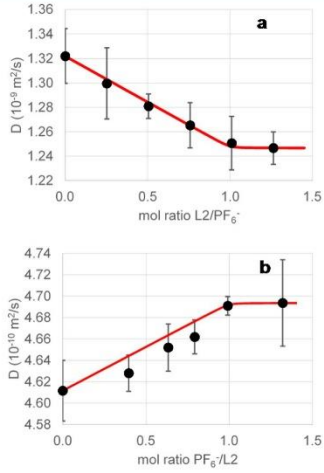

Figure 8. Average diffusion coefficients of (a) PF_6^- in the presence of increasing concentrations of $H_2\mathbf{L2}^{2+}$, measured by means of ^{19}F NMR. (b) $H_2\mathbf{L2}^{2+}$ in the presence of increasing concentrations of PF_6^-, measured by means of ^1H NMR. Red lines represent the trends expected on the basis of the stability constant (log K = 3.39; Table 1) measured for the $[H_2\mathbf{L2}(PF_6)]^+$ complex.

$H_2\mathbf{L2}^{2+}$ to a solution of PF_6^- causes a significant decrease of the observed diffusion coefficient of the anion. According to the Stokes−Einstein equation $\overline{D} = k_BT/6\pi\eta r$, such a variation of $\overline{D}$ can be ascribed to the increase of the hydrodynamic radius (r) of the measured species occurring when PF_6^- becomes increasingly associated with $H_2\mathbf{L2}^{2+}$. Furthermore, this figure also reveals a good agreement between the evolution of the

DOI: 10.1021/acs.inorgchem.6b01138
Inorg. Chem. 2016, 55, 8013−8024

observed diffusion coefficient $\bar{D}_{PF_6}$ upon increasing concentrations of $H_2\mathbf{L2}^{2+}$ (black dots) and the evolution expected according to the value of the stability constant (log K = 3.39; Table 1) measured by the potentiometry for the $[H_2\mathbf{L2}(PF_6)]^+$ complex, represented by the red line. This line was calculated by assuming D_{PF_6} equal to the value of $\bar{D}_{PF_6}$ measured for the sample containing pure PF_6^- (i.e., α = 0), and D_{L2PF_6} equal to the value of $\bar{D}_{PF_6}$ obtained for a $[H_2\mathbf{L2}^{2+}]/[PF_6^-]$ ratio greater than 1:1, at which $\bar{D}_{PF_6}$ appears to become invariant (Figure 8a).

The evolution of the average diffusion coefficient of $H_2\mathbf{L2}^{2+}$, $\bar{D}_{L2}$ (Figure 8b), gives rise to a less accurate fitting of the expected trend (red line calculated according to the above-described procedure for $\bar{D}_{PF_6}$), but it shows a noteworthy feature. When PF_6^- is gradually added to $H_2\mathbf{L2}^{2+}$, the average diffusion coefficient of $H_2\mathbf{L2}^{2+}$ increases (Figure 8b), denoting that the complex has a smaller size than the free ligand, a phenomenon that can be rationalized by considering that an extensive desolvation occurs upon interaction of the two oppositely charged species, with the volume of lost water molecules being greater than the gained volume of the bound anion, in agreement with the important entropy increase derived for anion binding from the above thermodynamic data. Additionally, also a conformational change of the ligand upon complexation, consisting of an inward folding of the two ligand arms to interact with the anion, might contribute to the shrinking of the hydrodynamic radius. Nevertheless, although the occurrence of a similar conformation change is possible, its contribution to the overall phenomenon does not seem to be decisive because it would be accompanied by a loss of entropy in contrast to the highly exoentropic character of the complexation process.

Furthermore, taking into account that both theoretical[32] and experimental[33] works coincide in that the interaction of PF_6^- with water molecules is extremely weak, the desolvation phenomenon occurring upon formation of the $[H_2L(PF_6)]^+$ complex should be mostly due to ligand desolvation.

■ CONCLUSIONS

Crystallographic data obtained for five crystal structures of anion complexes formed by the diprotonated forms of **L1** and **L2** show that the anions invariably choose the tetrazine ring as the preferential binding site, forming short anion−π contacts, despite the presence of two ammonium groups. Nevertheless, weak anion contacts with aliphatic CH groups and, in a few cases, salt bridge interactions with the ammonium groups also contribute to the complex stability in the solid state. According to DFT calculations, the LUMO of the free ligands is localized on the tetrazine ring, which is able to bind anions via anion−π interactions even in the absence of supplementary binding groups.

Equilibrium data reveal that anion binding takes place in aqueous solution with the ligands in different protonation states. In some cases, even the neutral (unprotonated) ligands form stable anion complexes. The main characteristic of these binding events is that the stability of the formed complexes is poorly related to the ligand charge, indicating that formation of these complexes is not governed by the dominating charge−charge attraction that is normally observed in the formation of anion complexes with positively charged ligands. The enthalpic ($\Delta H°$) and entropic ($T\Delta S°$) parameters for the binding equilibria, experimentally determined by dissecting the complexation free-energy changes ($\Delta G°$) by means of ITC measurements, clearly show that these anion-binding processes are invariably promoted by large and favorable entropic contributions, while the relevant enthalpy changes are mostly unfavorable (endothermic). A similar enthalpy and entropy dependence of the binding equilibria is typical of association processes controlled by desolvation phenomena (desolvation is typically endothermic and exoentropic). The occurrence of a significant desolvation upon the formation of these complexes is corroborated by diffusion NMR spectroscopy data, which led to the unprecedented observation that the ligand undergoes a significant shrinkage in size (increase of the diffusion coefficient) upon interaction with PF_6^-.

A somewhat different behavior is observed for anion binding by the neutral ligand, in which anion−π interactions should make the major contribution. In this case, the complexation reactions ($-\Delta G°$ in the range 11.1−17.5 kJ/mol) are still favored by dominant entropic contributions ($T\Delta S°$ in the range 9.0−17.0 kJ/mol) but are accompanied by favorable, although very small, enthalpy changes ($\Delta H°$ in the range −0.5 to −2.3 kJ/mol). Interestingly, these thermodynamic parameters are strongly consistent with previous values ($-\Delta G°$, 9−12 kJ/mol; $\Delta H°$, −2 to +3 kJ/mol; $T\Delta S°$, 8−15 kJ/mol)[12e] experimentally determined in water for the formation of various anion complexes with the two receptors NAP and NAP-T, cited above, which are thought to be almost exclusively stabilized by anion−π interactions.

Equilibrium data for the formation of anion complexes in a 80:20 (v:v) water/ethanol mixture showed that a decrease of the dielectric constant of the medium (ε = 78.56 for pure water and ε = 69.05 for the mixture at 25 °C)[25] causes a general lowering of the stability for complex with protonated ligand forms, while complexes of the unprotonated ligand are no longer detectable. Taking into account that the presence of 20% ethanol affects very little the solvation sphere of the anions,[29] the loss of stability observed in the aqueous ethanolic solution, relative to pure water, can be reasonably ascribed to stronger ligand solvation in the mixed solvent. Once again, solvation effects seem to play a fundamental role.

■ EXPERIMENTAL PROCEDURES

Materials. All reagents and solvents were of reagent-grade purity or higher. They were purchased from commercial sources and used without further purification unless otherwise stated. The anions used for potentiometric and microcalorimetric measurements were obtained as high-purity NaF, $NaNO_3$, Na_2SO_4, $NaClO_4$, and $NaPF_6$ salts from commercial sources and were used without further purification. Crystals of **L1**, $H_2\mathbf{L1}(PF_6)_2\cdot 2H_2O$, $H_2\mathbf{L1}(ClO_4)_2\cdot 2H_2O$, $H_2\mathbf{L2}(NO_3)_2$, $H_2\mathbf{L2}(PF_6)_2\cdot H_2O$, and $H_2\mathbf{L2}(ClO_4)_2\cdot H_2O$ suitable for single-crystal X-ray diffraction analysis were obtained by slow evaporation at room temperature of aqueous solutions of the components. In the case of PF_6^- salts, the solutions were made by adding ligands and appropriate amounts of HCl and $NaPF_6$.

*Synthesis of **L1** and **L2**.* Tetrazine-based ligands **L1** and **L2** were prepared according to Pinner's synthetic scheme from the corresponding morpholinylnitriles (Figure 1). The morpholinylnitrile derivatives, **1** and **2**, were prepared according to literature procedures.[34] ^1H and ^{13}C NMR spectra of ligands and intermediates are reported in Figures S4−S15.

*Synthesis of 3,6-Bis(morpholin-4-ylmethyl)-1,2,4,5-tetrazine, **L1**.* Hydrazine (50% aqueous solution, 1.9 mL, 30.5 mmol) was added dropwise to a solution of morpholin-4-ylacetonitrile (**1**; 1.500 g, 11.9 mmol) and *N*-acetyl-L-cysteine (1.942 g, 11.9 mmol) in methanol (12 mL), and the resulting solution was stirred at room temperature under

DOI: 10.1021/acs.inorgchem.6b01138
Inorg. Chem. 2016, 55, 8013−8024

an argon atmosphere for 48 h. The solid in suspension was collected by filtration, washed with methanol, and dried to afford 0.711 g (2.5 mmol, 42%) of a white compound identified as the dihydrotetrazine intermediate **3**. Mp: 194 °C (dec). IR (neat, ATR): ν/cm^{-1} 3285, 2972, 2926, 2901, 2860, 2812, 1661, 1450, 1398, 1111. ^{1}H NMR (DMSO-d_6, 400 MHz): δ 7.71 (s, 2 H), 3.57 (t, J = 4.5 Hz, 8 H), 2.95 (s, 4 H), 2.40−2.32 (m, 8 H). ^{13}C NMR (DMSO-d_6, 100 MHz): δ 147.1, 66.0, 56.7, 52.9. This solid was subjected to air oxidation without further purification. Thus, a suspension of **3** (n = 1) (0.511 g, 1.8 mmol) in dimethyl sulfoxide (DMSO; 5 mL) was stirred at room temperature under an air atmosphere for 4 days. The resulting red solid was filtered, washed with methanol, and dried to afford **L1** (0.417 g, 83% referred to **3**. Mp: 145 °C (dec). IR (neat, ATR): ν/cm^{-1} 2970, 2951, 2891, 2878, 2855, 2812, 2801, 1460, 1443, 1331, 1105. UV−vis [H_2O, pH 2; λ_{max}, nm (ε, M^{-1} cm^{-1})]: 520 (430), 298 (290, sh), 267 (2475). ^{1}H NMR ($CDCl_3$, 400 MHz): δ 4.22 (s, 4 H), 3.77 (t, J = 4.6 Hz, 9 H), 2.75−2.70 (m, 8 H). ^{13}C NMR ($CDCl_3$, 100 MHz): δ 167.0, 66.8, 60.9, 53. HRMS (EI). Calcd for $C_{12}H_{20}N_6O_2$ (M^+): m/z 280.1642. Found: m/z 280.1648.

Synthesis of 3,6-Bis(morpholin-4-ylethyl)-1,2,4,5-tetrazine, ***L2***. Hydrazine (50% aqueous solution, 3.0 mL, 48.2 mmol) was added dropwise to a solution of 3-(morpholin-4-yl)propanenitrile (**2**; 1.400 g, 10.0 mmol) and *N*-acetyl-L-cysteine (1.632 g, 10.0 mmol) in a 1:2 (v/v) methanol/DMSO mixture (6 mL), and the resulting solution was stirred at room temperature under an argon atmosphere for 72 h. The resulting solid was filtered, washed with a methanol/ethyl ether mixture (1:2, v/v), and pumped dry to afford **4** containing some DMSO residue, as shown by NMR spectra. ^{1}H NMR ($CDCl_3$, 400 MHz): δ 7.76 (s, 2 H), 3.68 (t, J = 4.6 Hz, 8 H), 2.54 (t, J = 6.1 Hz, 4 H), 2.50−2.41 (m, 8 H), 2.29 (t, J = 6.1 Hz, 4 H). ^{13}C NMR ($CDCl_3$, 100 MHz): δ 151.4, 66.7, 55.3, 53.3, 26.1. This solid was subjected to oxidation without further purification. Thus, a suspension of **4** in a mixture of methanol (3 mL) and DMSO (0.2 mL) was stirred for 2 days under an air atmosphere. The resulting pink solid was collected by filtration, dissolved in chloroform, and filtered to remove insoluble impurities. The filtrate was evaporated to dryness to afford **L2** as a pink solid (0.612 g, 2.0 mmol, 40%, referred to as **3**). Mp: 110 °C. IR (neat, ATR): ν/cm^{-1} 2961, 2922, 2878, 2845, 2824, 1460, 1443, 1414, 1115. UV−vis [H_2O, pH 7; λ_{max}, nm (ε, M^{-1} cm^{-1})]: 518 (435), 329 (300, sh), 275 (2550). ^{1}H NMR ($CDCl_3$, 400 MHz): δ 3.63 (t, J = 4.6 Hz, 8 H), 3.50 (t, J = 7.1 Hz, 4 H), 3.01 (t, J = 7.2 Hz, 4 H), 2.54 (t, J = 4.6 Hz, 8 H). ^{13}C NMR ($CDCl_3$, 100 MHz): δ 169.0, 66.9, 56.5, 53.3, 32.2. HRMS (EI). Calcd for $C_{14}H_{24}N_4O_2$ ($M^{\bullet+}$): m/z 308.1961. Found: m/z 308.1964.

Potentiometric Measurements. Potentiometric (pH-metric) titrations employed for determination of the equilibrium constants were carried out in 0.1 M NMe_4Cl aqueous and 80:20 (v/v) water/ethanol solutions at 298.1 ± 0.1 K by using previously described equipment and procedures.[35] The determined ionic product of water was pK_w = 13.83(1) in water and pK_w = 13.89(1) in the water/ethanol mixture at 298.1 ± 0.1 K in 0.1 M Me_4NCl. The computer program *HYPERQUAD*[24] was used to calculate the equilibrium constants from potentiometric data. The concentration of ligands was 5 × 10^{-4} M, while the anion (A) concentration was varied in the range [L] ≤ [A] ≤ 5[L]. The studied pH range was 2.5−9 for all systems. Only in the case of F^- complexation with **L2** was the pH range reduced to 4.5−9 to avoid significant formation of HF. Nevertheless, protonation of F^- was taken into account in calculations by using literature constants (log K = 2.95 for $H^+ + F^- = HF$ and log K = 3.55 for $H^+ + 2F^- = HF_2^-$),[36] for measurements in water, and constants [log K = 3.49(1) for $H^+ + F^- = HF$ and log K = 4.28(1) for $H^+ + 2F^- = HF_2^-$] determined by us in the water/ethanol mixture by means of the above method. In the case of **L1**, the interaction with F^- was not studied because complete protonation of the poorly basic ligand takes place well below pH 4.5 and, under similar conditions, HF is formed in a significant amount and reacts with the glass components of the titration cell.

ITC. Ligand protonation and anion (NO_3^-, PF_6^-, ClO_4^-, and SO_4^{2-}) complexation enthalpies were determined in 0.10 M Me_4NCl aqueous solutions at 298.1 K by using previously described equipment and procedures.[2] Examples of titration curves are shown in Figure S16 for ligand protonation. Measurements with fluoride were avoided to prevent corrosion of the calorimeter components. In a typical experiment, a NMe_4OH solution (0.10 M, addition volumes 15 μL) was added to acidic solutions of the ligands (5 × 10^{-3} M, 1.5 cm^3), containing 5-fold excess of the anion in the binding experiments. Because of solubility problems, it was not possible to study the systems **L1**/NO_3^- and **L1**/SO_4^{2-} and partly also **L1**/ClO_4^-. A different type of ITC measurements was performed to confirm the enthalpy changes for the interaction of anions with the unprotonated **L2** ligand by adding a solution of the anion to solutions containing **L2** at pH 8. A 10:1 anion-to-ligand molar ratio was reached. The same procedure performed for the system **L1**/PF_6^- was unsuccessful because of precipitation occurring during the measurements. At least two titrations were performed for each system and each titration procedure. The computer program *HypΔH*[37] was used to calculate the reaction enthalpies from calorimetric data. Corrections for the heats of dilution were applied.

Diffusion NMR Spectroscopic Measurements. NMR experiments were performed on samples with a fixed concentration of PF_6^- (5.6 × 10^{-3} M) and increasing concentrations of **L2** (from 0 to 1.4 × 10^{-2} M) in D_2O at pH 1.5, as well as on a sample of pure **L2** (7.1 × 10^{-3} M) in D_2O at pH 1.5 (Figures S17−S20). The samples were conditioned in standard 5-mm-o.d. NMR tubes and thermally equilibrated inside the NMR probe, for at least 10 min, prior to data acquisition. The PGSE NMR experiments were performed with a Bruker Avance 500 spectrometer equipped with a Bruker broad-band BBI probe with a Z-gradient coil. For each sample, sets of 32 1D NMR spectra were acquired at different values of the Z-gradient intensity, linearly varied from 2% up to 95% of the maximum gradient intensity, using the standard *ledbpgp2s* Bruker pulse sequence. The values of the average diffusion coefficients $\bar{D}$ (Tables S4 and S5) were obtained after fitting of the signal decay by nonlinear least-squares regression analysis (Figures S21−S32) to the Stejstal−Tanner equation (1),[38] performed by means of a Bruker routine based on *SimFit*.

$$I = I_0 e^{-[D\gamma^2 g^2 \delta^2 (\Delta - \delta/3)]} \quad (1)$$

In eq 1, I is the intensity of the measured signal, I_0 is the intensity of the signal without applied gradients, D is the value of the average diffusion coefficient, γ is the gyromagnetic ratio, and Δ and δ are the parameters of the *ledbpgp2s* pulse program known as the diffusion time and diffusion gradient length, respectively. The values of Δ and δ were set at 70 ms and 4000 μs, respectively, for **L2** PGSE ^{1}H NMR measurements and at 80 ms and 2300 μs, respectively, for PF_6^- PGSE ^{19}F NMR measurements.

X-ray Structure Analyses. Pink single crystals of H_2**L1**$(PF_6)_2\cdot 2H_2O$ (a), H_2**L1**$(ClO_4)_2\cdot 2H_2O$ (b), and H_2**L2**$(NO_3)_2$ (e) and red single crystals of H_2**L2**$(PF_6)_2\cdot H_2O$ (c) and H_2**L2**$(ClO_4)_2\cdot H_2O$ (d) were used for X-ray diffraction analysis. A summary of the crystallographic data is reported in Table S1. The integrated intensities were corrected for Lorentz and polarization effects, and an empirical absorption correction was applied.[39] The structures were solved by direct methods (*SIR92*).[40] Refinements were performed by means of full-matrix least squares using the *SHELX-97* program.[41] All of the non-hydrogen atoms were anisotropically refined. Hydrogen atoms were usually introduced in calculated positions, and their coordinates were refined according to the linked atoms, with the exception of the acidic protons linked to the ligand tertiary nitrogen atoms for (b)−(d) and of the cocrystallized water hydrogen atoms for (a) and (d). All crystallographic data were deposited in the CCDC database with the deposition numbers 1473254−1473258.

Quantum-Chemical Calculations. Quantum-chemical DFT calculations were performed with the *Gaussian 09* software package.[42] The B3LYP hybrid functional of Becke,[43] in combination with the 6-31G(d,p) basis set,[44] and the dispersion-corrected ωB97X-D functional of Chai and Head-Gordon,[45] in combination with the 6-31+G(d,p) basis set, were employed. Given that complexes are formed between charged ions, their geometry optimizations were performed in a continuum water environment with the polarization continuum model of Tomasi and co-workers.[46] The binding energy (expressed as

DOI: 10.1021/acs.inorgchem.6b01138
Inorg. Chem. 2016, 55, 8013−8024

a positive number) was corrected for the basis-set superposition error using the counterpoise correction method of Boys and Bernardi.[47]

■ ASSOCIATED CONTENT

Supporting Information

The Supporting Information is available free of charge on the ACS Publications website at DOI: 10.1021/acs.inorgchem.6b01138.

Crystallographic data (Table S1), geometric parameters (Table S2), normalized anion−tetrazine interaction distances (Table S3), measured mean diffusion coefficients (Tables S4 and S5), a portion of the packing of the crystal structure of H_2**L2**$(ClO_4)_2 \cdot H_2O$ (Figure S1), calculated HOMO and LUMO orbitals of H_2**L1**$^{2+}$ and H_2**L2**$^{2+}$ (Figure S2), optimized geometries of the complexes between ClO_4^- and 2,3,5,6-tetrazine and 2,3,5,6-dimeth-1,4-yltetrazine (Figure S3), ^{1}H and ^{13}C NMR spectra of ligands and synthetic intermediates (Figures S4−S15), profiles calorimetric ligand titrations (Figure S16), ^{1}H, ^{1}H DOSY, ^{19}F, and ^{19}F DOSY NMR spectra of **L2** and PF_6^- at pH 1.5 (Figures S17−S20), and nonlinear fittings of the signal decay in PGSE experiments (Figures S21−S32) (PDF)

X-ray crystallographic data in CIF format (CIF)

■ AUTHOR INFORMATION

Corresponding Authors

*E-mail: antonio.bianchi@unifi.it.

*E-mail: mmelgui@ujaen.es.

Notes

The authors declare no competing financial interest.

■ ACKNOWLEDGMENTS

F.P. thanks the Department of Applied Chemistry of the Graduate School of Engineering of Tohoku University for financial support. The Centre of Instrumental Facilities, STI, of the University of Jaén is acknowledged for technical assistance.

■ REFERENCES

(1) (a) *Anion Coordination Chemistry*; Bowman-James, K., Bianchi, A., Garcia-España, E., Eds.; Wiley-VCH: New York, 2012. (b) Sessler, J. L.; Gale, P. A.; Cho, W. S. *Anion Receptor Chemistry*; Monographs in Supramolecular Chemistry; RSC Publishing: Cambridge, U.K., 2006.

(2) Quiñonero, D.; Frontera, A.; Deyà, P. M. Anion−π Interactions in Molecular Recognition. In *Anion Coordination Chemistry*; Bowman-James, K., Bianchi, A., García-España, E., Eds.; Wiley-VCH: New York, 2012.

(3) Quiñonero, D.; Garau, C.; Rotger, C.; Frontera, A.; Ballester, P.; Costa, A.; Deyà, P. M. *Angew. Chem., Int. Ed.* **2002**, *41*, 3389−3392.

(4) Schneider, H.−J. *Angew. Chem., Int. Ed.* **2009**, *48*, 3924−3977.

(5) Mascal, M.; Armstrong, A.; Bartberger, M. D. *J. Am. Chem. Soc.* **2002**, *124*, 6274−6276.

(6) (a) Alkorta, I.; Blanco, F.; Deyà, P.; Elguero, J.; Estarellas, C.; Frontera, A.; Quiñonero, D. *Theor. Chem. Acc.* **2010**, *126*, 1−14. (b) Alkorta, I.; Rozas, I.; Elguero, J. *J. Am. Chem. Soc.* **2002**, *124*, 8593−8598.

(7) Hiraoka, K.; Mizuse, S.; Yamabe, S. *J. Phys. Chem.* **1987**, *91*, 5294−5297.

(8) (a) Giese, M.; Albrecht, M.; Rissanen, K. *Chem. Commun.* **2016**, *52*, 1778−1795. (b) Giese, M.; Albrecht, M.; Rissanen, K. *Chem. Rev.* **2015**, *115*, 8867−8895. (c) Wheeler, S. E.; Bloom, J. W. G. *J. Phys. Chem. A* **2014**, *118*, 6133−6147. (d) Gamez, P. *Inorg. Chem. Front.* **2014**, *1*, 35−43. (e) Wheeler, S. E.; Bloom, J. W. G. *Chem. Commun.* **2014**, *50*, 11118−11121. (f) Chifotides, H. T.; Dunbar, K. R. *Acc. Chem. Res.* **2013**, *46*, 894−906. (g) Ballester, P. *Acc. Chem. Res.* **2013**, *46*, 874−884. (h) Watt, M. M.; Collins, M. S.; Johnson, D. W. *Acc. Chem. Res.* **2013**, *46*, 955−966. (i) Schneider, H.−J. *Acc. Chem. Res.* **2013**, *46*, 1010−1019. (j) Wheeler, E. S. *Acc. Chem. Res.* **2013**, *46*, 1029−1038. (k) Frontera, A.; Gamez, P.; Mascal, M.; Mooibroek, T. J.; Reedijk, J. *Angew. Chem., Int. Ed.* **2011**, *50*, 9564−9583. (l) Salonen, L. M.; Ellermann, M.; Diederich, F. *Angew. Chem., Int. Ed.* **2011**, *50*, 4808−4842. (m) Berryman, O. B.; Johnson, D. W. *Chem. Commun.* **2009**, 3143−3153. (n) Caltagirone, C.; Gale, P. A. *Chem. Soc. Rev.* **2009**, *38*, 520−563. (o) Schottel, B. L.; Chifotides, H. T.; Dunbar, K. R. *Chem. Soc. Rev.* **2008**, *37*, 68−83. (p) Hay, B. P.; Bryantsev, V. S. *Chem. Commun.* **2008**, 2417−2428.

(9) (a) Robertazzi, A.; Krull, F.; Knapp, E.-W.; Gamez, P. *CrystEngComm* **2011**, *13*, 3293−3300. (b) Mooibroek, T. J.; Black, C. A.; Gamez, P.; Reedijk, J. *Cryst. Growth Des.* **2008**, *8*, 1082−1093. (c) Berryman, O. B.; Bryantsev, V. S.; Stay, D. P.; Johnson, D. W.; Hay, B. P. *J. Am. Chem. Soc.* **2007**, *129*, 48−58. (d) Gamez, P.; Mooibroek, T. J.; Teat, S. J.; Reedijk, J. *Acc. Chem. Res.* **2007**, *40*, 435−444. (e) Ahuja, R.; Samuelson, A. G. *CrystEngComm* **2003**, *5*, 395−399.

(10) For recent structural studies, see: (a) Canellas, S.; Bauza, A.; Lancho, A.; Garcia-Raso, A.; Fiol, J. J.; Molins, E.; Ballester, P.; Frontera, A. *CrystEngComm* **2015**, *17*, 5987−5997. (b) Giese, M.; Albrecht, M.; Valkonen, A.; Rissanen, K. *Chem. Sci.* **2015**, *6*, 354−359. (c) Orvay, F.; Bauza, A.; Barcelo-Oliver, M.; Garcia-Raso, A.; Fiol, J. J.; Costa, A.; Molins, E.; Mata, I.; Frontera, A. *CrystEngComm* **2014**, *16*, 9043−9053. (d) Giese, M.; Albrecht, M.; Repenko, T.; Sackmann, J.; Valkonen, A.; Rissanen, K. *Eur. J. Org. Chem.* **2014**, *12*, 2435−2442. (e) Savastano, M.; Arranz-Mascarós, P.; Bazzicalupi, C.; Bianchi, A.; Giorgi, C.; Godino-Salido, M. L.; Gutiérrez-Valero, M. D.; López-Garzón, R. *RSC Adv.* **2014**, *4*, 58505−58513. (f) Chifotides, H. T.; Giles, I. D.; Dunbar, K. R. *J. Am. Chem. Soc.* **2013**, *135*, 3039−3055. (g) Adriaenssens, L.; Estarellas, C.; Vargas Jentzsch, A.; Martinez Belmonte, M.; Matile, S.; Ballester, P. *J. Am. Chem. Soc.* **2013**, *135*, 8324−8330. (h) Wang, D.-X.; Wang, M.-X. *J. Am. Chem. Soc.* **2013**, *135*, 892−897. (i) Giese, M.; Albrecht, M.; Krappitz, T.; Peters, M.; Gossen, V.; Raabe, G.; Valkonen, A.; Rissanen, K. *Chem. Commun.* **2012**, *48*, 9983−9985. (j) Canellas, P.; Bauza, A.; García-Raso, A.; Fiol, J. J.; Deyà, P. M.; Molins, E.; Mata, I.; Frontera, A. *Dalton Trans.* **2012**, *41*, 11161−11169. (k) Li, S.; Fa, S.-X.; Wang, Q.-Q.; Wang, D.-X.; Wang, M.-X. *J. Org. Chem.* **2012**, *77*, 1860−1867. (l) Yong, G.-P.; Zhang, Y.-M.; She, W.-L. *CrystEngComm* **2012**, *14*, 3923−3929. (m) Mooibroek, T. J.; Gamez, P. *CrystEngComm* **2012**, *14*, 1027−1030. (n) Qin, L.; Yao, L.-Y.; Yu, S.-Y. *Inorg. Chem.* **2012**, *51*, 2443−2453. (o) Giles, I. D.; Chifotides, H. T.; Shatruk, M.; Dunbar, K. R. *Chem. Commun.* **2011**, *47*, 12604−12606. (p) Arranz, P.; Bianchi, A.; Cuesta, R.; Giorgi, C.; Godino, M. L.; Gutiérrez, M. D.; López, R.; Santiago, A. *Inorg. Chem.* **2010**, *49*, 9321−9332;(q) *Inorg. Chem.* **2012**, *51*, 4883−4883. (r) Schottel, B. L.; Chifotides, H. T.; Shatruk, M.; Chouai, A.; Pérez, L. M.; Bacsa, J.; Dunbar, K. R. *J. Am. Chem. Soc.* **2006**, *128*, 5895−5912.

(11) For recent computational studies, see: (a) Wang, K.; Lv, J.; Miao, J. *Theor. Chem. Acc.* **2015**, *134*, 1−6. (b) Mezei, P. D.; Csonka, G. I.; Ruzsinszky, A.; Sun, J. *J. Chem. Theory Comput.* **2015**, *11*, 360−371. (c) Bauza, A.; Quinonero, D.; Deya, P. M.; Frontera, A. *Chem. - Eur. J.* **2014**, *20*, 6985−6990. (d) Wheeler, S. E.; Bloom, J. W. G. *Chem. Commun.* **2014**, *50*, 11118−11121. (e) Bretschneider, A.; Andrada, D. M.; Dechert, S.; Meyer, S.; Mata, R. A.; Meyer, F. *Chem. - Eur. J.* **2013**, *19*, 16988−17000. (f) Bauzá, A.; Quiñonero, D.; Deyà, P. M.; Frontera, A. *Comput. Theor. Chem.* **2012**, *998*, 20−25. (g) Quiñonero, D.; Frontera, A.; Deyà, P. M. *Comput. Theor. Chem.* **2012**, *998*, 51−56. (h) Evans, J. D.; Hollis, C. A.; Hack, S.; Gentleman, A. S.; Hoffmann, P.; Buntine, M. A.; Sumby, C. J. *J. Phys. Chem. A* **2012**, *116*, 8001−8007. (i) Estarellas, C.; Frontera, A.; Quiñonero, D.; Deyà, P. M. *ChemPhysChem* **2011**, *12*, 2742−2750. (j) Lao, K.−U.; Yu, C.−H. *J. Comput. Chem.* **2011**, *32*, 2716−2726. (k) Ali, Md. E.; Oppeneer, P. M. *J. Phys. Chem. Lett.* **2011**, *2*, 939−943. (l) Sánchez-Lozano, M.; Otero, N.; Hermida-Ramón, J. M.; Estévez, C. M.; Mandado, M. *J. Phys. Chem. A* **2011**, *115*, 2016−2025.

DOI: 10.1021/acs.inorgchem.6b01138
Inorg. Chem. 2016, 55, 8013−8024

(12) (a) Hafezi, N.; Holcroft, J. M.; Hartlieb, K. J.; Dale, E. J.; Vermeulen, N. A.; Stern, C. L.; Sarjeant, A. A.; Stoddart, J. F. *Angew. Chem., Int. Ed.* **2014**, *54*, 456−461. (b) Zhang, J.; Zhou, B.; Sun, Z.-R.; Wang, X.-B. *Phys. Chem. Chem. Phys.* **2015**, *17*, 3131−3141. (c) Chang, K.-C.; Minami, T.; Koutnik, P.; Savechenkov, P. Y.; Liu, Y.; Anzenbacher, P. *J. Am. Chem. Soc.* **2014**, *136*, 1520−1525. (d) Adriaenssens, L.; Gil-Ramírez, G.; Frontera, A.; Quiñonero, D.; Escudero-Adán, E. C.; Ballester, P. *J. Am. Chem. Soc.* **2014**, *136*, 3208−3218. (e) Arranz-Mascarós, P.; Bazzicalupi, C.; Bianchi, A.; Giorgi, C.; Godino-Salido, M. L.; Gutierrez-Valero, M. D.; Lopez-Garzón, R.; Savastano, M. *J. Am. Chem. Soc.* **2013**, *135*, 102−105. (f) Barceló-Oliver, M.; Bauzá, A.; Baquero, B. A.; García-Raso, A.; Terrón, A.; Molins, E.; Frontera, A. *Tetrahedron Lett.* **2013**, *54*, 5355−5360. (g) Watt, M. M.; Zakharov, L. N.; Haley, M. M.; Johnson, D. W. *Angew. Chem., Int. Ed.* **2013**, *52*, 10275−10280. (h) Baldridge, K. K.; Cozzi, F.; Siegel, J. S. *Angew. Chem., Int. Ed.* **2012**, *51*, 2903−2906. (i) Chudzinski, M. G.; McClary, C. A.; Taylor, M. S. *J. Am. Chem. Soc.* **2011**, *133*, 10559−10567. (j) Vargas Jentzsch, A.; Emery, D.; Mareda, J.; Metrangolo, P.; Resnati, G.; Matile, S. *Angew. Chem., Int. Ed.* **2011**, *50*, 11675−11678. (k) Guha, S.; Goodson, F. S.; Roy, S.; Corson, L. J.; Gravenmier, C. A.; Saha, S. *J. Am. Chem. Soc.* **2011**, *133*, 15256−15259. (l) Sakai, N.; Mareda, J.; Vauthey, E.; Matile, S. *Chem. Commun.* **2010**, *46*, 4225−4237. (m) Chifotides, H. T.; Schottel, B. L.; Dunbar, K. R. *Angew. Chem., Int. Ed.* **2010**, *49*, 7202−7207. (n) Guha, S.; Saha, S. *J. Am. Chem. Soc.* **2010**, *132*, 17674−17677. (o) Wang, D.-X.; Wang, Q.-Q.; Han, Y.; Wang, Y.; Huang, Z.-T.; Wang, M.-X. *Chem. - Eur. J.* **2010**, *16*, 13053−13057. (p) Mareda, J.; Matile, S. *Chem. - Eur. J.* **2009**, *15*, 28−37. (q) Gil-Ramírez, G.; Escudero-Adán, E. C.; Benet-Buchholz, J.; Ballester, P. *Angew. Chem., Int. Ed.* **2008**, *47*, 4114−4118. (r) Berryman, O. B.; Sather, A. C.; Hay, B. P.; Meisner, J. S.; Johnson, D. W. *J. Am. Chem. Soc.* **2008**, *130*, 10895−10897. (s) Wang, D.-X.; Zheng, Q.-Y.; Wang, Q.-Q.; Wang, M.-X. *Angew. Chem., Int. Ed.* **2008**, *47*, 7485−7488. (t) Berryman, O. B.; Hof, F.; Hynes, M. J.; Johnson, D. W. *Chem. Commun.* **2006**, 506−508. (u) Maeda, H.; Morimoto, T.; Osuka, A.; Furuta, H. *Chem. - Asian J.* **2006**, *1*, 832−844.

(13) Dawson, R. E.; Hennig, A.; Weimann, D. P.; Emery, D.; Ravikumar, V.; Montenegro, J.; Takeuchi, T.; Gabutti, S.; Mayor, M.; Mareda, J.; Schalley, C. A.; Matile, S. *Nat. Chem.* **2010**, *2*, 533−538.

(14) (a) Jentzsch, A. V.; Matile, S. *Top. Curr. Chem.* **2014**, *358*, 205−39. (b) Vargas Jentzsch, A.; Matile, S. *J. Am. Chem. Soc.* **2013**, *135*, 5302−5303. (c) Vargas Jentzsch, A.; Hennig, A.; Mareda, J.; Matile, S. *Acc. Chem. Res.* **2013**, *46*, 2791−2800. (d) Jentzsch, A. V.; Emery, D.; Mareda, J.; Nayak, S. K.; Metrangolo, P.; Resnati, G.; Sakai, N.; Matile, S. *Nat. Commun.* **2012**, *3*, 905. (e) Misek, J.; Vargas Jentzsch, A.; Sakurai, S.; Emery, D.; Mareda, J.; Matile, S. *Angew. Chem., Int. Ed.* **2010**, *49*, 7680−7683.

(15) (a) Zhao, Y.; Benz, S.; Sakai, N.; Matile, S. *Chem. Sci.* **2015**, *6*, 6219−6223. (b) Zhao, Y.; Sakai, N.; Matile, S. *Nat. Commun.* **2014**, *5*, 3911. (c) Zhao, Y.; Beuchat, C.; Domoto, Y.; Gajewy, J.; Wilson, A.; Mareda, J.; Sakai, N.; Matile, S. *J. Am. Chem. Soc.* **2014**, *136*, 2101−2111. (d) Lu, T.; Wheeler, S. E. *Org. Lett.* **2014**, *16*, 3268−3271. (e) Phuengphai, P.; Youngme, S.; Mutikainen, I.; Reedijk, J. *Inorg. Chem. Commun.* **2012**, *24*, 129−133. (f) Estarellas, C.; Frontera, A.; Quiñonero, D.; Deyá, P. M. *Angew. Chem., Int. Ed.* **2011**, *50*, 415−418. (g) Rojas, C. M.; Rebek, J., Jr. *J. Am. Chem. Soc.* **1998**, *120*, 5120−5121.

(16) (a) Dutta, R.; Ghosh, P. *Eur. J. Inorg. Chem.* **2012**, *21*, 3456−3462. (b) Xu, Z.; Singh, N. J.; Kim, S. K.; Spring, D. R.; Kim, K. S.; Yoon, J. *Chem. - Eur. J.* **2011**, *17*, 1163−1170.

(17) (a) Bianchi, A.; Garcia-España, E. Thermodynamic Aspects of Anion Coordination. In *Anion Coordination Chemistry*; Bowman-James, K., Bianchi, A., Garcia-España, E., Eds.; Wiley-VCH: New York, 2012. (b) Schneider, H.-J.; Yatsimirsky, A. *Principle and Methods in Supramolecular Chemistry*; John Wiley & Sons: Chichester, U.K., 2000.

(18) (a) Frontera, A.; Saczewski, F.; Gdaniec, M.; Dziemidowicz-Borys, E.; Kurland, A.; Deyá, P. M.; Quiñonero, D.; Garau, C. *Chem. - Eur. J.* **2005**, *11*, 6560−6567. (b) Garau, C.; Frontera, A.; Quiñonero, D.; Ballester, P.; Costa, A.; Deyá, P. M. *Chem. Phys. Lett.* **2004**, *392*, 85−89. (c) Garau, C.; Frontera, A.; Quiñonero, D.; Ballester, P.; Costa, A.; Deyá, P. M. *J. Phys. Chem. A* **2004**, *108*, 9423−9427.

(19) (a) Clavier, G.; Audebert, P. *Chem. Rev.* **2010**, *110*, 3299−3314. (b) Tolshchina, S. G.; Rusinov, G. L.; Charushin, V. N. *Chem. Heterocycl. Compd.* **2013**, *49*, 66−91.

(20) Miros, F. N.; Zhao, Y.; Sargsyan, G.; Pupier, M.; Besnard, C.; Beuchat, C.; Mareda, J.; Sakai, N.; Matile, S. *Chem. - Eur. J.* **2016**, *22*, 2648−2657.

(21) Yang, J.; Karver, M. R.; Li, W.; Sahu, S.; Devaraj, N. K. *Angew. Chem., Int. Ed.* **2012**, *51*, 5222−5225.

(22) Lange, U. E. W.; Schäfer, B.; Baucke, D.; Buschmann, E.; Mack, H. *Tetrahedron Lett.* **1999**, *40*, 7067−7070.

(23) (a) Neunhoeffer, H. In Tetrazines and Pentazines. *Comprehensive Heterocyclic Chemistry*; Rees, A. R. K. W., Ed.; Pergamon: Oxford, U.K., 1984; Volume 2.21; p 565. (b) Sagot, E.; Le Roux, A.; Soulivet, C.; Pasquinet, E.; Poullain, D.; Girard, E.; Palmas, P. *Tetrahedron* **2007**, *63*, 11189−11194.

(24) Gans, P.; Sabatini, A.; Vacca, A. *Talanta* **1996**, *43*, 1739−1753.

(25) (a) Schneider, H.-J. *Chem. Soc. Rev.* **1994**, *23*, 227−234. (b) Schneider, H.-J.; Blatter, T.; Eliseev, A.; Rüdiger, V.; Raevsky, O. A. *Pure Appl. Chem.* **1993**, *65*, 2329−2334. (c) Schneider, H.-J.; Schiestel, T.; Zimmermann, P. *J. Am. Chem. Soc.* **1992**, *114*, 7698−7703. (d) Schneider, H.-J. *Angew. Chem., Int. Ed. Engl.* **1991**, *30*, 1417−1436. (e) Schneider, H.-J.; Theis, I. *Angew. Chem., Int. Ed. Engl.* **1989**, *28*, 753−754.

(26) Gilli, G.; Gilli, P. *The Nature of the Hydrogen Bond*; Oxford University Press: New York, 2009.

(27) (a) Faraji, M.; Farajtabar, A.; Gharib, F. *J. Appl. Chem. Res.* **2009**, *9*, 7−12. (b) Åkerlöf, G. *J. Am. Chem. Soc.* **1932**, *54*, 4125−4139.

(28) Petit, L. D. *IUPAC Stability Constants Data Base*; Academic Software: 1997.

(29) (a) Shamel, A.; Saghiri, A.; Jaberi, F.; Farajtabar, A.; Mofidi, F.; Khorrami, S. A.; Gharib, F. *J. Solution Chem.* **2012**, *41*, 1020−1032. (b) Doğan, A.; Kılıç, E.; Özel, A. D. *Amino Acids* **2009**, *36*, 373−379. (c) Canel, E.; Gültepe, A.; Doğan, A.; Kılıç, E. *J. Solution Chem.* **2006**, *35*, 5−19.

(30) (a) Marcus, Y. *Ion Solvation*; Wiley: New York, 1985. (b) Marcus, Y. *J. Chem. Thermodyn.* **2007**, *39*, 1338−1345.

(31) Cohen, Y.; Avram, L.; Frish, L. *Angew. Chem., Int. Ed.* **2005**, *44*, 520−554.

(32) Wang, Y.; Li, H.; Han, S. *J. Phys. Chem. B* **2006**, *110*, 24646−24651.

(33) Dominguez-Vidal, A.; Kaun, N.; Ayora-Cañada, M. J.; Lendl, B. *J. Phys. Chem. B* **2007**, *111*, 4446−4452.

(34) (a) Marrero, J. G.; Harwood, L. M. *Tetrahedron Lett.* **2009**, *50*, 3574−3576. (b) Hatakeyama, J.; Kobayashi, T.; Watanabe, T. U.S. Patent 0115018A1, 2002. (c) Ranu, B. C.; Banerjee, S. *Tetrahedron Lett.* **2007**, *48*, 141−143. (d) Xu, J.; Wu, Q.; Zhang, Q.; Zhang, F.; Lin, X. *Eur. J. Org. Chem.* **2007**, *2007*, 1798−1802.

(35) Bazzicalupi, C.; Bianchi, A.; Giorgi, C.; Gratteri, P.; Mariani, P.; Valtancoli, B. *Inorg. Chem.* **2013**, *52*, 2125−2137.

(36) Smith, R. M.; Martell, A. E. *NIST Stability Constants Database*, version 4.0; National Institute of Standards and Technology: Washington, DC, 1997.

(37) Gans, P.; Sabatini, A.; Vacca, A. *J. Solution Chem.* **2008**, *37*, 467−476.

(38) Stejskal, E. O.; Tanner, J. E. *J. Chem. Phys.* **1965**, *42*, 288−292.

(39) *CrysAlisPro*, version 1.171.35.11; Agilent Technologies: Oxfordshire, England, 2015.

(40) Altomare, A.; Cascarano, G.; Giacovazzo, C.; Guagliardi, A.; Burla, M. C.; Polidori, G.; Camalli, M. *J. Appl. Crystallogr.* **1994**, *27*, 435−436.

(41) Sheldrick, G. M. *Acta Crystallogr., Sect. A: Found. Crystallogr.* **2008**, *64*, 112−122.

(42) Frisch, M. J.; Trucks, G. W.; Schlegel, H. B.; Scuseria, G. E.; Robb, M. A.; Cheeseman, J. R.; Scalmani, G.; Barone, V.; Mennucci, B.; Petersson, G. A.; Nakatsuji, H.; Caricato, M.; Li, X.; Hratchian, H. P.; Izmaylov, A. F.; Bloino, J.; Zheng, G.; Sonnenberg, J. L.; Hada, M.; Ehara, M.; Toyota, K.; Fukuda, R.; Hasegawa, J.; Ishida, M.; Nakajima,

DOI: 10.1021/acs.inorgchem.6b01138
Inorg. Chem. 2016, 55, 8013−8024

T.; Honda, Y.; Kitao, O.; Nakai, H.; Vreven, T.; Montgomery, J. A., Jr.; Peralta, J. E.; Ogliaro, F.; Bearpark, M.; Heyd, J. J.; Brothers, E.; Kudin, K. N.; Staroverov, V. N.; Kobayashi, R.; Normand, J.; Raghavachari, K.; Rendell, A.; Burant, J. C.; Iyengar, S. S.; Tomasi, J.; Cossi, M.; Rega, N.; Millam, J. M.; Klene, M.; Knox, J. E.; Cross, J. B.; Bakken, V.; Adamo, C.; Jaramillo, J.; Gomperts, R.; Stratmann, R. E.; Yazyev, O.; Austin, A. J.; Cammi, R.; Pomelli, C.; Ochterski, J. W.; Martin, R. L.; Morokuma, K.; Zakrzewski, V. G.; Voth, G. A.; Salvador, P.; Dannenberg, J. J.; Dapprich, S.; Daniels, A. D.; Farkas, Ö.; Foresman, J. B.; Ortiz, J. V.; Cioslowski, J.; Fox, D. J. *Gaussian 09*, revision C.01; Gaussian, Inc.: Wallingford, CT, 2009.

(43) Becke, A. D. *J. Chem. Phys.* **1993**, *98*, 5648−5652.

(44) Hehre, W. J.; Ditchfield, R.; Pople, J. A. *J. Chem. Phys.* **1972**, *56*, 2257−2261.

(45) Chai, J.-D.; Head-Gordon, M. *Phys. Chem. Chem. Phys.* **2008**, *10*, 6615−6620.

(46) Tomasi, J.; Mennucci, B.; Cammi, R. *Chem. Rev.* **2005**, *105*, 2999−3093.

(47) Boys, S. F.; Bernardi, F. *Mol. Phys.* **1970**, *19*, 553−566.

DOI: 10.1021/acs.inorgchem.6b01138
Inorg. Chem. 2016, 55, 8013−8024

Volume 46 | Number 14 | 14 April 2017 | Pages 4469–4862

Dalton Transactions

An international journal of inorganic chemistry

rsc.li/dalton

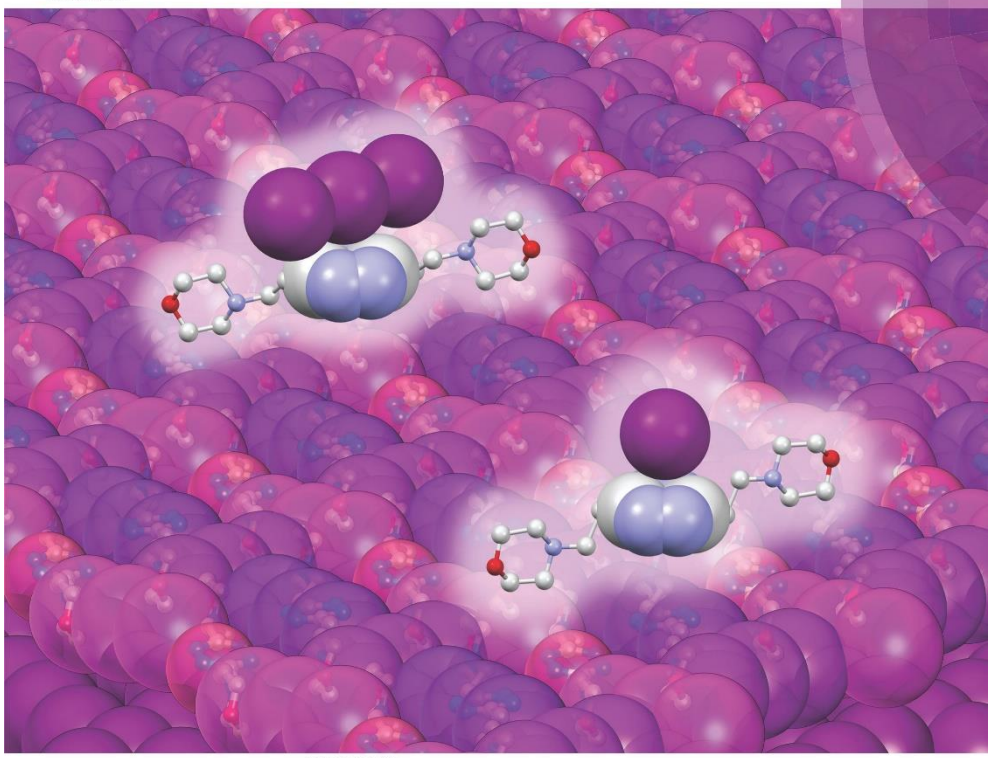

ISSN 1477-9226

ROYAL SOCIETY OF CHEMISTRY

PAPER

Antonio Bianchi, Manuel Melguizo *et al.*

Iodide and triiodide anion complexes involving anion–π interactions with a tetrazine-based receptor

Dalton Transactions

PAPER

View Article Online
View Journal | View Issue

Cite this: *Dalton Trans.*, 2017, **46**, 4518

Iodide and triiodide anion complexes involving anion–π interactions with a tetrazine-based receptor†

Matteo Savastano,[a] Carla Bazzicalupi,[a] Celeste García,[b] Cristina Gellini,[a] María Dolores López de la Torre,[b] Palma Mariani,[a] Fabio Pichierri,[c] Antonio Bianchi*[a] and Manuel Melguizo*[b]

Protonated forms of the tetrazine ligand L2 (3,6-bis(morpholin-4-ylethyl)-1,2,4,5-tetrazine) interact with iodide in aqueous solution forming relatively stable complexes ($\Delta G°$ = −11.6(4) kJ mol^{-1} for $HL2^+ + I^-$ = (HL2)I and $\Delta G°$ = −13.4(2) kJ mol^{-1} for $H_2L2^{2+} + I^-$ = $[(H_2L2)I]^+$). When solutions of $[(H_2L2)I]^+$ are left in contact with air, crystals of the oxidation product $(H_2L2)_2(I_3)_3I\cdot 4H_2O$ are formed. Unfortunately, the low solubility of I_3^- complexes prevents the determination of their stability constants. The crystal structures of $H_2L2I_2\cdot H_2O$ (**1**), $H_2L2(I_3)_2\cdot 2H_2O$ (**2**) and $(H_2L2)_2(I_3)_3I\cdot 4H_2O$ (**3**) were determined by means of X-ray diffraction analyses. In all crystal structures, it was found that the interaction between I^- and I_3^- with H_2L2^{2+} is dominated by anion interactions with the π electron density of the receptor. Only in the case of **1**, the iodide anions involved in close anion–π interactions with the ligand tetrazine ring form an additional H-bond with the protonated morpholine nitrogen of an adjacent ligand molecule. Conversely, in crystals of **2** and **3** there are alternate segregated planes which contain only protonated ligands hydrogen-bonded to cocrystallized water molecules or I_3^- and I^- forming infinite two-dimensional networks established through short interhalogen contacts, making these crystalline products good candidates to behave as solid conductors. In the solid complexes, the triiodide anion displays both end-on and side-on interaction modes with the tetrazine ring, in agreement with density functional theory calculations indicating a preference for the alignment of the I_3^- molecular axis with the molecular axis of the ligand. Further information about geometries and structures of triiodide anions in **2** and **3** was acquired by the analysis of their Raman spectra.

Received 12th January 2017,
Accepted 20th February 2017

DOI: 10.1039/c7dt00134g

rsc.li/dalton

Introduction

Anion binding has gained much attention because of the crucial role played by anionic species in biological and chemical systems.[1] As with all areas of supramolecular chemistry, anion binding is governed by weak forces, mostly electrostatic attraction, hydrogen bonding and/or hydrophobic effects. Nevertheless, also the weak attractive forces exerted between anions and the π-system of electron-deficient arenes, the so called anion–π interactions, have gained increasing consideration in recent years,[2,3] and are now included among the most appealing forces for the make-up of new functional materials,[4] anion receptors,[3a,5] carriers[6] and catalysts,[7] while their biological relevance[3a,b] is increasingly valued.

Within the multifaceted chemistry of anions, iodide and polyiodides occupy a special position, as a wide spectrum of structures, ranging from isolated units to complicated three-dimensional networks, passing through linear chains and two-dimensional assemblies, can be generated from three simple building blocks: I_2, I^- and I_3^-. This kind of structural feature is made possible by the ability of iodine to concatenate *via* donor–acceptor interactions, the character of each assembly being regulated by its chemical environment.[8] In the solid state, for instance, polyiodides of variable structures can be generated by using different countercations.[9]

The understanding of such a structural variety is an interesting challenge, especially when considering that the hypervalency exhibited by several large polyiodides is not easily justi-

[a]*Department of Chemistry "Ugo Schiff", University of Florence, Via della Lastruccia 3, 50019 Sesto Fiorentino, Italy. E-mail: antonio.bianchi@unifi.it*
[b]*Department of Inorganic and Organic Chemistry, University of Jaén 23071, Jaén, Spain. E-mail: mmelgui@ujaen.es*
[c]*Department of Applied Chemistry, Graduate School of Engineering, Tohoku University, Sendai 980-8579, Japan. E-mail: fabio@che.tohoku.ac.jp*

†Electronic supplementary information (ESI) available: Crystal packing of compound **1**. Superimposition of the ligand and water molecules of the crystalline structures **2** and **3**. CCDC 1518137–1518139. For ESI and crystallographic data in CIF or other electronic format see DOI: 10.1039/c7dt00134g

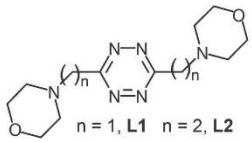

Fig. 1 The tetrazine ligands L1 and L2.

fied by simple covalent bonding models and, accordingly, the nature of bonding in polyiodide anions has been the object of intense theoretical consideration.[10] Furthermore, the particular electrical conductivity[11–13] and redox properties of polyiodide systems have attracted interest toward their application for the development of dye-sensitized solar cells[14] and solar batteries,[15] where they have been incorporated in many different forms, including aqueous solutions,[16,17] ionic liquid electrolytes,[18] gel polymer electrolytes[14a,19–21] or even solid state crystalline conductors (ref. 22–24).

We have recently reported that ligands L1 and L2, constituted by a tetrazine ring decorated with two morpholine pendants of different lengths (Fig. 1), are able to form stable anion complexes in solution. All crystal structures we obtained for such complexes (PF_6^- and ClO_4^- complexes with H_2L1^{2+} and NO_3^-, PF_6^- and ClO_4^- complexes with H_2L2^{2+}) invariably showed that the anions are involved in anion–π interactions with the tetrazine group, in agreement with the strong π-acid character of this ring.[25] These results encouraged us to further investigate the anion binding ability of these ligands, and the iodide/polyiodide system seemed to be an intriguing medium to explore new effects of these anion receptor molecules. Unfortunately, it was not possible to test L1 toward this anionic system, as it undergoes rapid degradation in the presence of I^-, even in slightly acidic media, but as shown in the following section, protonated forms of L2 do interact with I^- in aqueous solution, from which the crystalline iodide complex $H_2L2I_2{\cdot}H_2O$ (**1**) can be isolated, and depending on the medium conditions, the mixed iodide/triiodide $(H_2L2)_2(I_3)_3I{\cdot}4H_2O$ (**2**) and the triiodide $H_2L2(I_3)_2{\cdot}2H_2O$ (**3**) complexes can also be obtained. In these two latter structures, the segregation of the anion iodine species into distinct layers that alternate with the layers formed exclusively by protonated ligands and water molecules is remarkable. All crystal structures of these complexes show that anion–π interactions with the tetrazine ring of L2 are widespread elements of such crystalline assemblies in which the anions show different binding modes and aggregation patterns.

Experimental procedures

Materials

L2 (3,6-bis(morpholin-4-ylethyl)-1,2,4,5-tetrazine) was synthesized as previously described.[25] Deep pink crystals of $H_2L2I_2{\cdot}H_2O$ were obtained upon evaporation, at room temperature under a nitrogen atmosphere, of an aqueous solution of L (0.01 M) at pH 3 containing a fivefold excess of I^-. When maintained in contact with the mother liquor and exposed to air, these crystals slowly re-dissolve while poorly soluble brownish orange crystals of $(H_2L2)_2(I_3)_3I{\cdot}4H_2O$ grow. Highly insoluble dark brown crystals of $H_2L2(I_3)_2{\cdot}2H_2O$ were obtained by slow diffusion, in a H-shaped tube, of initially separated aqueous solution of L2 and I_3^- at pH 3. Merck Suprapur grade NaI was used for the potentiometric measurement.

Potentiometric measurements

Potentiometric (pH-metric) titrations employed for the determination of equilibrium constants were carried out in 0.1 M Me_4NCl degassed aqueous solutions at 298.1 ± 0.1 K by using previously described equipment and procedures.[26] The determined ionic product of water was pK_w = 13.83(1) (298.1 ± 0.1 K, 0.1 M Me_4NCl). The computer program HYPERQUAD[27] was used to calculate equilibrium constants from potentiometric data derived from three independent titration experiments. The ligand concentration was 5×10^{-4} M, while the I^- concentration was 2.5×10^{-3} M. The studied pH range was 4–9.

X-ray structure analyses

Pink crystals of $H_2L2I_2{\cdot}H_2O$ (**1**), dark orange crystals of $H_2L2(I_3)_2{\cdot}2H_2O$ (**2**) and dark brown crystals of $(H_2L2)_2(I_3)_3I{\cdot}4H_2O$ (**3**) were used for X-ray diffraction analysis. A summary of the crystallographic data is reported in Table 1. The integrated intensities were corrected for Lorentz and polarization effects, and an empirical absorption correction was applied.[28] The structures were solved by direct methods (SHELXS-86).[29] Refinements were performed by means of full-matrix least-squares using the SHELX Version 2014/7 program.[30] All the non-hydrogen

Table 1 Crystal data and structure refinement for $H_2L2I_2{\cdot}H_2O$ (**1**), $H_2L2(I_3)_2{\cdot}2H_2O$ (**2**) and $(H_2L2)_2(I_3)_3I{\cdot}4H_2O$ (**3**)

	(1)	(2)	(3)
Empirical formula	$C_{14}H_{28}I_2N_6O_3$	$C_{14}H_{30}I_6N_6O_4$	$C_{14}H_{34}I_5N_6O_4$
Formula weight	582.22	1107.84	984.97
Temperature (K)	150	100	100
Space group	$P\bar{1}$	$P\bar{1}$	$P2_1/c$
a (Å)	7.7303(6)	7.5053(6)	14.3403(3)
b (Å)	7.7864(6)	13.5410(7)	14.3161(2)
c (Å)	22.022(2)	14.5928(9)	13.8619(3)
α (°)	86.949(7)	99.590(5)	90
β (°)	87.158(7)	102.045(6)	106.228(2)
γ (°)	60.575(8)	94.974(5)	90
Volume (Å^3)	1152.5(2)	1418.74(16)	2732.42(9)
Z	2	2	4
Independent reflections/R(int)	3664/0.0450	4334/0.0986	5256/0.1171
μ (mm^{-1})	2.751/(Mo-Kα)	6.598/(Mo-Kα)	5.720/(Mo-Kα)
R indices $[I > 2\sigma(I)]^a$	R_1 = 0.0517 wR_2 = 0.0628	R_1 = 0.1013 wR_2 = 0.2418	R_1 = 0.0660 wR_2 = 0.1706
R indices (all data)^a	R_1 = 0.0857 wR_2 = 0.0793	R_1 = 0.1201 wR_2 = 0.2694	R_1 = 0.0927 wR_2 = 0.2053

^{a} $R_1 = \sum||F_o| - |F_c||/\sum|F_o|$; $wR_2 = [\sum w(F_o^2 - F_c^2)^2/\sum wF_o^4]^{1/2}$.

atoms were anisotropically refined. Hydrogen atoms were usually introduced in the calculated position and their coordinates were refined according to the linked atoms, with the exception of the cocrystallized water molecules. In all cases, analysis of the ΔF map didn't allow the localization of the water hydrogen atoms. In some cases, residual electron density remained at the end of refinements close to iodine atoms most likely due to series truncation errors.

Raman spectroscopy

The Raman spectra of **2** and **3** were recorded with a Bruker MultiRAM FT-Raman spectrometer equipped with a Nd-YAG laser emitting at 1064 nm as the excitation source. The spectra were recorded for the pure compounds, pressed in solid pellets, with 4 cm^{-1} slits, 100 mW power and acquiring 1000 scans. The lower slit width gave only a worse signal-to-noise ratio without increasing the resolutions.

Computational chemistry

Density functional theory (DFT) calculations were performed with the Gaussian09 quantum chemistry package[31] using the dispersion-corrected ωB97X-D functional of Chai and Head-Gordon[32] in combination with the all-electron DGDZVP basis set (ref. 33 and 34). Geometry optimizations were carried out with the integral equation formalism–polarization continuum model (IEF-PCM) of Tomasi and coworkers[35] to simulate an implicit water environment surrounding the tetrazine-anion complexes. Binding energies (B_e) for the tetrazine-anion complexes were corrected for the basis-set superposition error (BSSE) using the counterpoise method of Boys and Bernardi.[36] Atom charges were obtained with a natural population analysis[37] of the solvated complexes. The topological analyses of the electronic charge densities of the complexes were carried out with the aid of the AIMAll software[38] which implements the theoretical concepts of Bader's quantum theory of atoms in molecules (QTAIM[39]).

Results and discussion

In a previous paper we showed that the protonated $HL2^+$ and H_2L2^{2+} forms and, in some cases, even the uncharged (not protonated) L2 ligand are able to bind anions, such as F^-, NO_3^-, PF_6^-, ClO_4^-, and SO_4^{2-}, forming 1 : 1 anion-to-ligand complexes in aqueous solution.[25] Thermodynamic data obtained for these binding equilibria, in particular those concerning the formation of anion complexes with the uncharged ligand, suggested that anion–π interactions afford prominent contributions to the interplay of weak forces stabilizing these complexes in solution, while crystallographic data exhibited the relevance of anion–π interactions in defining the relative position of the two interacting partners in crystalline complexes. Also I^- forms 1 : 1 complexes with both $HL2^+$ and H_2L2^{2+} but fails to interact, at least within the detection limits of the potentiometric measurements, with the neutral ligand. Similar results were obtained for the interaction with F^-,[25] although this anion forms complexes of slightly lower stability than I^- (Table 2). These results might seem rather surprising, since F^- has a greater charge density and a greater propensity to form hydrogen bonds than I^-, but these are actually in line with previous evidence that electrostatic attraction and hydrogen bonding are not the principal forces pushing together the partners of the anion complexes formed by this ligand,[25] although such forces appear to be of upmost importance in promoting the formation of anion complexes with most of the ammonium receptors.[40] It was previously inferred, however, that solvation effects, principally involving the ligand, afford a significant contribution to the stability of such anion complexes.[25] Anion solvation, on the other hand, could make the difference in determining the binding energy of different anions. In the particular case of I^- and F^- complexes with L2, the considerably lower hydration free energy of the former is expected to make an important contribution to the greater stability of its complexes.

In line with previous results,[25] also in the case of I^-, complex stability is poorly correlated with the ligand charge, the binding free energy increasing by only 1.8 kJ mol^{-1} from HL^+ to H_2L^{2+} (Table 2).

Crystals of $(H_2L2)I_2{\cdot}H_2O$ (**1**) suitable for single crystal X-ray analysis were obtained by slow evaporation of an aqueous solution containing L and I^- at pH 3, in an anaerobic atmosphere at room temperature. Microcrystalline samples of the same compound can be obtained even under aerobic conditions provided that crystallization occurs in a few hours, otherwise complex $(H_2L2)_2(I_3)_3I{\cdot}4H_2O$ (**3**) is obtained. The crystal packing of **1** is built up by alternate planes of two sets of symmetry independent H_2L2I_2 adducts developing in the (001) and the (002) crystallographic planes, respectively. In each H_2L2I_2 adduct (Fig. 2 and 3), the ligand is placed around an inversion centre, giving rise to anion–π interactions with two iodide anions placed one above and one below its tetrazine ring (I···ring centroid/offset distances 3.70/0.32 Å – (001) plane – and 3.67/0.27 Å – (002) plane). Moreover, each iodide is H-bonded to two adjacent ligand molecules, through the protonated morpholine nitrogen on one side and a CH hydrogen bond on the other side (N···I 3.451(8) Å and C···I 4.010(8) Å – (001) plane, Fig. 2b– and N···I 3.485(6) Å and C···I 4.046(3) Å – (002) plane Fig. 3b–). In the (001) plane, the NH···I contacts are directed along the *b* axis, while, in the (002) plane, the

Table 2 Equilibrium constants and relevant $-\Delta G°$ values for anion complex formation with L2 determined at 298.1 ± 0.1 K in 0.1 M Me_4NCl aqueous solution

	log *K*	$-\Delta G°$ (kJ mol^{-1})
$HL2^+ + I^- = (HL2)I$	2.03(7)[a]	11.6(4)
$H_2L2^{2+} + I^- = [(H_2L2)I]^+$	2.35(4)	13.4(2)
$HL2^+ + F^- = (HL2)F$	1.58(8)[b]	9.0(5)[b]
$H_2L2^{2+} + F^- = [(H_2L2)F]^+$	1.97(3)[b]	11.2(2)[b]

[a] Values in parentheses are standard deviation in the last significant figure. [b] Taken from ref. 25.

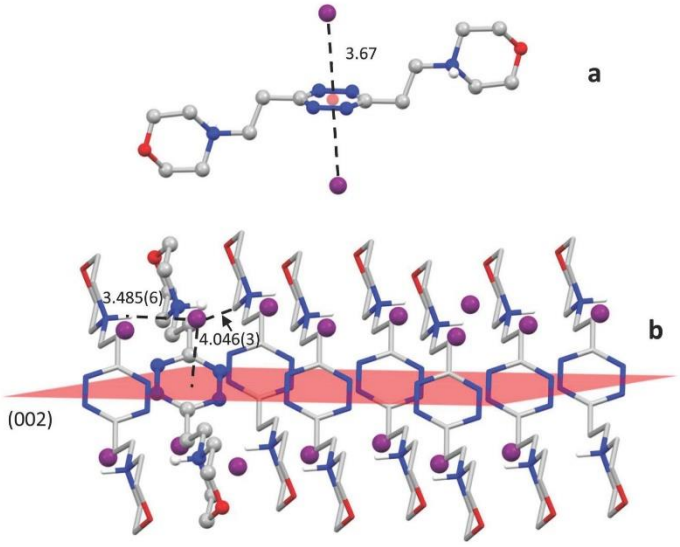

Fig. 2 Crystal structure of $(H_2L2)I_2{\cdot}H_2O$ (**1**): ligand conformation and anion···π contacts (a) in the H_2L2I_2 adduct developing in the (001) crystallographic plane (b). Distances are in Å.

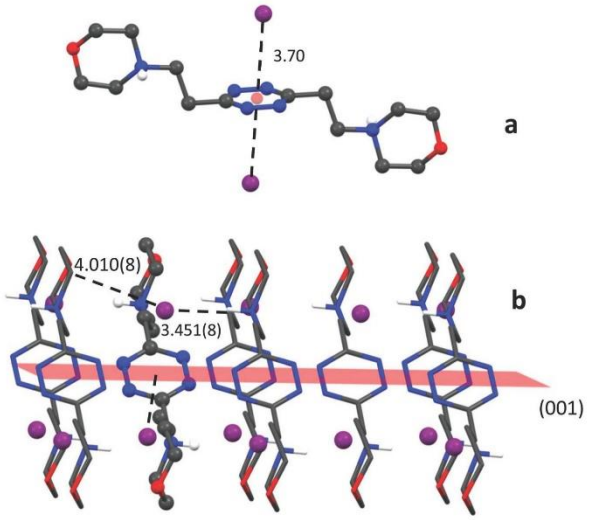

Fig. 3 Crystal structure of $(H_2L2)I_2{\cdot}H_2O$ (**1**): ligand conformation and anion···π contacts (a) in the H_2L2I_2 adduct developing in the (002) crystallographic plane (b). Distances are in Å.

analogous contacts point in the [100] direction. Actually, both ligand conformations and relative anion/receptor spatial dispositions are very similar, and the major reason for the lack of additional crystallographic symmetries is the presence of a co-crystallized water molecule which joins the two H_2L2I_2 systems, forming stronger interactions with the one developing in the (002) plane (OW1···C9 3.68(1) Å, Fig. S1†).

In both planes, the conformation assumed by the ligand can be considered as an intermediate between the planar and the chair conformations previously observed in the crystal structures of H_2L2^{2+} complexes with ClO_4^-, PF_6^- and NO_3^- anions.[25] Interestingly, in most of these complexes, as well as in all crystal structures solved until now for the anion complexes with L1, the anion and receptor almost exclusively form anion–π contacts, without the contribution of additional H-bonds from the protonated nitrogen atoms, which, instead, are very often in contact with water solvent molecules.

In analogy with the behaviour seen in these structures, we can hypothesize that, even in H_2L2I_2, the anion–π interaction strongly contributes to stabilize the complex. As a matter of fact, the anion is very well placed above the ring centroid, and the anion···centroid distance (3.67 and 3.70 Å) is significantly short with respect to the iodide ionic radius (2.20 Å).

When crystals of **1** are left in contact with the mother liquor and exposed to air, they slowly re-dissolve while crystals of $(H_2L2)_2(I_3)_3I{\cdot}4H_2O$ (**3**) are formed as a consequence of the spontaneous air oxidation of I^- to I_2 (I_3^-). Crystals of **3** are also the product of slow evaporation of acidic solutions of L2, not protected from air, in the presence of I^-. No further air oxidation of this compound was observed over several months. The highly insoluble $H_2L2(I_3)_2{\cdot}2H_2O$ (**2**) complex was obtained from the components by using a diffusion method (see the Experimental section).

The crystal structures of **2** and **3** show close analogies, despite that the crystals of these complexes belong to different space groups and crystal systems (Table 1). In the case of **2**, the asymmetric unit contains two half ligand molecules, each interacting with triiodide through the tetrazine ring. In particular, as shown in Fig. 4a and b, both end-on (a) and side-on (b) binding modes are found. In the case of triiodide (a), the I···ring centroid distance is 3.60 Å with an offset of 0.45 Å. This triiodide is almost symmetric and linear (I–I 2.94(2) and 2.91(2) Å, I–I–I angle 178.28(6)°). Instead, the anion (b) is strongly asymmetric, bent (I–I 2.796(2) and 3.098(2) Å, I–I–I angle 174.25(6)°) and almost aligned along the C–C axis. The central iodine atom is almost perfectly placed above a tetrazine nitrogen. The I···N distance is only 3.64(2) Å, significantly shorter than the sum of the van der Waals radii (3.7 Å) and, together with the overall asymmetry of the anion and its remarkable deviation from linearity, could be a consequence of charge-transfer or coulombic interactions taking place within the crystal.

In the structure of **3**, the three symmetry independent triiodide anions lie on crystallographic inversion centres. Two of them are in contact with the ligand tetrazine ring, both giving side-on interaction (Fig. 5a). Nevertheless, while one of them is very well placed above the ring centroid (I···ring centroid/offset distances 3.57/0.30 Å), the other one is more displaced toward the ring periphery (I···ring centroid/offset distances 3.61/0.80 Å). Interestingly, this second triiodide places its

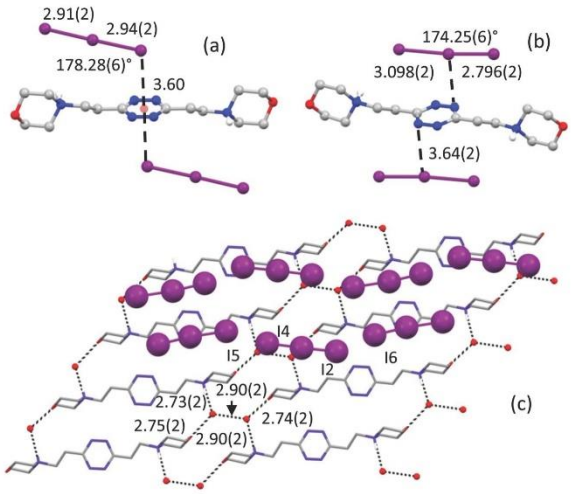

Fig. 4 Crystal structure of $H_2L2(I_3)_2{\cdot}2H_2O$ (**2**): end-on (a) and side-on (b) I_3^-···π contacts; honeycomb-like network given by protonated ligands and co-crystallized water molecules and zig-zag chains of triiodide anions (c). Distances are in Å.

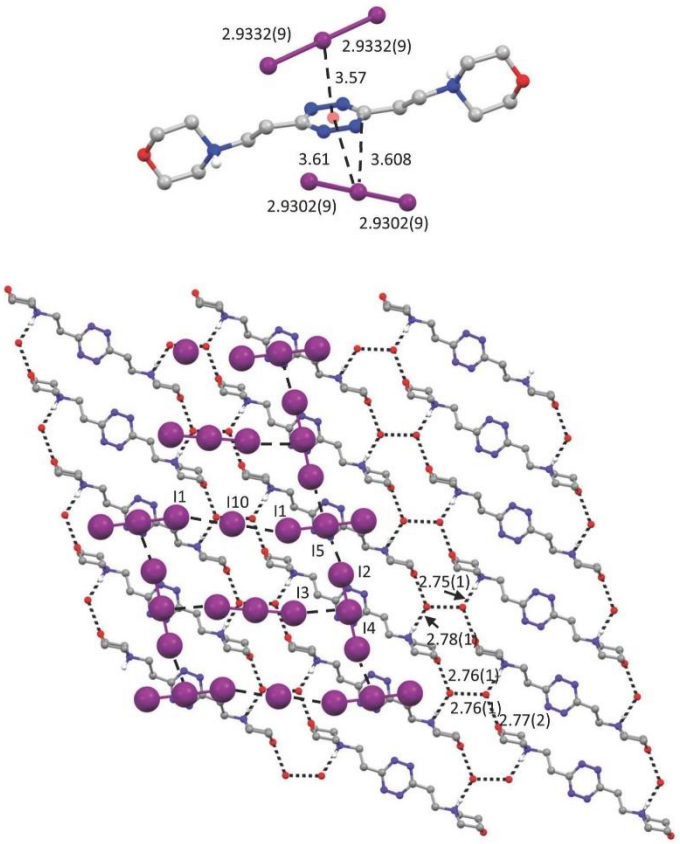

Fig. 5 Crystal structure of $(H_2L2)_2(I_3)_3I{\cdot}4H_2O$ (**3**): ligand conformation and $I_3^-\cdots\pi$ contacts (a); honeycomb-like network given by protonated ligands and co-crystallized water molecules and T-shaped pattern of triiodide anions (c). Distances are in Å.

central iodine just above a C–N aromatic bond, resulting in η^2-type binding. Differently from what found in the structure **2**, the crystallographic symmetry imposes both linearity and equal I–I bond distances to all anions (I–I bond distances in the three triiodides are 2.930, 2.933 and 2.937 Å).

The anion···ring centroid distances in these adducts are very similar to those found in the crystal structures reported by Rissanen for the I_3^- anion in the complex with pentafluorobenzylammonium and *N*-(pentafluorobenzyl)pyridinium receptors.[9a] Nevertheless, in the structures reported by Rissanen, the I_3^- anions are trapped in cavities, completely surrounded by the aromatic groups of the receptors, while in **2** and **3** there are segregate planes which contain only protonated ligands hydrogen-bonded to cocrystallized water molecules or only triiodide anions.

Regarding the analogies of structures **2** and **3**, in both crystalline structures, the ligand assumes almost the same conformation, the protonated nitrogen atoms of the morpholine rings pointing toward opposite directions and establishing water assisted contacts with the oxygen atoms of adjacent ligands (Fig. 4c and 5b). Protonated ligands and cocrystallized water molecules define honeycomb-like networks developing parallel to the (100) planes both in **2** and **3**. The similarity between these two structures goes even further, since the tridimensional arrangement attained by the ligand molecules is practically the same in both, as evidenced by the graphical

superimposition of the ligand components of the crystalline structure (Fig. S2†). Thus, the prime differences between structures **2** and **3** are the number of iodine atoms and their arrangement into discrete anions, leading to different interhalogen contact networks in the anionic planar layers sandwiched between two successive planes of protonated ligands. Some contacts of the iodine anions with the aliphatic hydrogen atoms (H···I distances in the range 3.0–3.21 Å) contribute to stabilize the interplanar interaction. In particular, in **2**, parallel zig-zag chains are formed by the head-to-tail disposition of the anions (Fig. 4c). Interestingly, the I···I contacts in these chains (I2···I6 3.530(2) and I4···I5 3.578(2) Å) can be regarded as secondary bonds, since they are shorter than typical I···I van der Waals contacts (3.8–3.9 Å).[8] In the mixed I^-/I_3^- system **2**, iodide and triiodide anions arrange alternately giving the T-shaped pattern shown in Fig. 5b. This structure features longer I···I contacts ranging from 4.0230(9) to 4.3413(9) Å.

In view of the mechanisms currently accepted to interpret the conductivity showed by polyiodides[11–13] and the precedents of conductive crystalline structures containing such species,[22,24,41] it was reasoned that structures **2** and **3** are good candidates to show electrical conductivity by virtue of the segregation of the iodine anions in separate layers and their interconnections into infinite networks through I···I short contacts, thus the conductivity of the polyiodide complexes **2** and **3** is currently under evaluation.

Further information about geometries and structures of the different triiodide anions of **2** and **3** were acquired by the analysis of their Raman spectra (Fig. 6) in the frequency region below 250 cm^{-1} which is characterized by vibrations involving the I_3^- units. In complex **3**, a single prominent band is observed at 110 cm^{-1} (Fig. 6a), although, as shown by the inset in Fig. 6a, a lower intensity structure is present with weak shoulders at 60, 75 and a broad one at 154 cm^{-1}, respectively, and an additional very weak band at 221 cm^{-1}. Crystals of **2** show a more structured spectrum, where the main band centered at 112 cm^{-1} is surrounded by a few medium intensity peaks, indicating that I_3^- anions have lower symmetry than in the case of **3**.

In crystals of **3** ($(H_2L2)_2(I_3)_3I{\cdot}4H_2O$, Fig. 5), three kinds of I_3^- anions were identified, displaying linear and symmetric structures but with slightly different I–I bond lengths. For each anion, three vibrational modes are expected (one twofold), among which only the symmetric stretching is Raman active. Therefore, the intense band at 110 cm^{-1} can be assigned to this vibration (ν_1). The presence of the very weak band at 221 cm^{-1}, assigned as $2\nu_1$, supports the linear structure of the ions.[42] However, small deviations from linearity, when randomly occurring, can be compatible with an observed overall centrosymmetric lattice. In such a case, bending and asymmetric stretching would become Raman active, even though with very weak intensities. Most likely, the shoulders at about 75 cm^{-1} and 154 cm^{-1} have a similar origin and can be related to the bending (ν_2) and asymmetric stretching (ν_3), respectively.[10j,43] The latter has been previously observed around 140–145 cm^{-1}.[9g,10j,43,44] The difference in the present data may be ascribed to the difficulty in accurately locating the maximum position because of the convolution with the very intense ν_1.

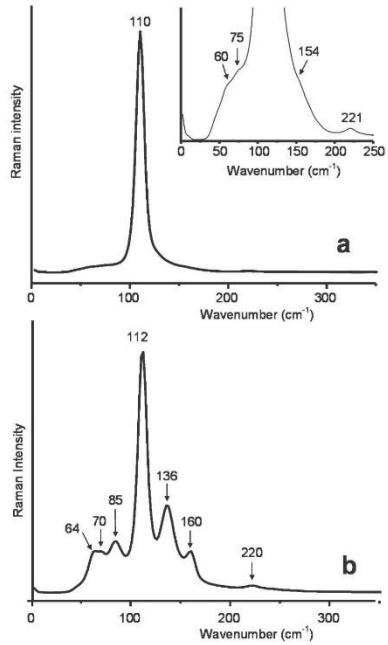

Fig. 6 Raman spectra of $(H_2L2)2(I_3)3I{\cdot}4H_2O$ (a) and $H_2L2(I_3)2{\cdot}2H_2O$ (b).

The 60 cm^{-1} shoulder can be attributed considering that, at room temperature, excited low frequency vibrational modes may be populated, hence $\nu(1–2)$ vibrational transitions other than the fundamental $\nu(0–1)$ can also be observed. For this reason, the 60 cm^{-1} shoulder is probably a hot band transition of the bending vibration ν_2. Alternatively, it could be considered as a lattice vibration (*i.e.* I_3^- with respect to the ligand),[10j,43,45] but in our opinion 60 cm^{-1} is a too high value for lattice modes.

As shown before, crystals of **2** ($H_2L2(I_3)_2{\cdot}2H_2O$, Fig. 4) contain two differently conformed I_3^- anions, (a) and (b), featuring end-on and side-on interaction modes, respectively, with the tetrazine ring. Both are non-linear, the bending angle of (b) being larger than that of (a). Moreover, the I–I distances are not symmetric with respect to the central atom and this is more evident in (b) than in (a), the latter being more similar to the symmetric I_3^- anions of complex **3**. Due to the loss of symmetry of (a) and (b), all three vibrational modes become Raman active accounting for the higher number of bands in the spectrum and for their increased intensities (Fig. 6, Table 3). Furthermore, the deviation from linearity of these

Table 3 Observed Raman frequencies of crystalline $H_2L2(I_3)_2{\cdot}2H_2O$ [(a) and (b)] and $(H_2L2)_2(I_3)_3I{\cdot}4H_2O$ (**3**) complexes

2(a)	2(b)	3	Assignment
64 mw		60 vw	Bending ν_2 ν(1–2)
70 w		75 vw	Bending ν_2 ν(0–1)
112 s		110 vs	Symmetric stretch ν_1
136 ms		154 bs	Asymmetric stretch ν_3
220 w		221 vw	$2\nu_1$
	85 m		Stretching $I_2\cdots I^-$
	160 m		Stretching $I\text{–}I\cdots I^-$

anions causes a lowering of the force constant of bending vibrations, justifying, in the (a) case, the frequency shift toward lower energies (75/70 cm^{-1}; 145–140/136 cm^{-1}) observed for the relevant bands.

In (b), the I–I bond distances from the central iodine atom, although still below the limit reported for intramolecular distances in polyiodide systems (3.3 Å),[8,46] are rather different, giving this triiodide anion some similarity with a $I_2\cdots I^-$ system.[9g,47,48] This may help in the assignment of the 160 cm^{-1} and 85 cm^{-1} bands. Actually, the band at 160 cm^{-1} can be assigned to an I–I stretching "perturbed" by the presence of a close I^- ion, as already reported for systems with I–I distances comparable to (b),[9g,49] while the $I_2\cdots I^-$ stretching should be found at lower frequency because of its longer bond distance (3.098 Å *vs.* 2.796 Å, Fig. 4). The 85 cm^{-1} band can be attributed to this vibration. The bending is not observed, which is likely hidden under this low frequency spectral feature.

In order to compare the relative strength of interaction of iodide and triiodide anions with the tetrazine moiety of L2, we investigated the four complexes shown in Fig. 7. Complex I is characterized by a binding energy (B_e) of 6.7 kJ mol^{-1} (here a positive value of B_e indicates the formation of a stable complex) which results from the anion–π interaction established between iodide and tetrazine with an $I^-\cdots$centroid distance of 3.884 Å. Regarding the triiodide anion, three high-symmetry orientations above the molecular plane of tetrazine were conceived: one where I_3^- is oriented normal to the plane (complex II), a second one (complex III) where I_3^- is oriented parallel to the plane and aligned along the C–C axis, and a third one (complex IV) where the bond axis of I_3^- bisects the N–N bonds of tetrazine. Interestingly, complex III possesses both the lowest total electronic energy and the highest value of B_e (15.1 kJ mol^{-1}) among the triiodide complexes shown in Fig. 7. A rotation of the I_3^- anion about the (central I)–centroid axis by 90.0° yields complex IV which, in spite of having the same I–centroid distance of 3.742 Å of complex III, is characterized by a slightly lower B_e value (13.1 kJ mol^{-1}) with respect to the former. The most disfavoured orientation is the vertical one corresponding to complex II which is characterized by a B_e value (6.7 kJ mol^{-1}) that is the same as that of the complex with the iodide anion.

As far as the possibility of a charge transfer process is concerned, the results of our natural population analysis indicate that almost no charge is transferred from the anion to tetrazine. For instance, $q(I^-) = -0.99e$ in complex I while similar net charges were calculated for the complexes with the triiodide anion. Interestingly, however, the negative charge accumulates on the terminal iodine atoms of I_3^- while the charge of the central atom is close to zero. This result suggests that the terminal iodine atoms of I_3^- are likely favoured to interact electrostatically with the counter-cations both in solution and in the crystals. Nevertheless, it is to be underlined that the contacts found in our models are longer than the sum of the van der Waals radii and always significantly longer than those found in the solid state.

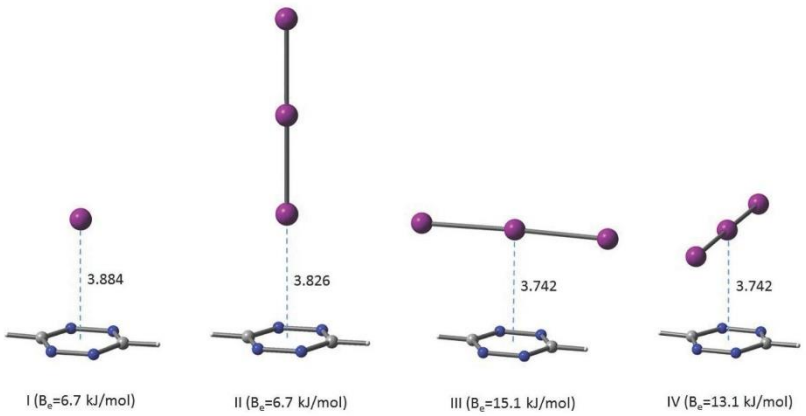

Fig. 7 DFT-optimized geometries of four tetrazine-anion complexes. Distances are in Å.

To unravel the nature of the intermolecular interactions that are operative within the I_3^- complexes both in the solid-state and in water, we have performed a topological analysis of the computed electronic charge density of the trimeric $(H_2L2^{2+})(I_3^-)_2$ complex displayed in Fig. 4b. The molecular graph obtained for the geometry corresponding to the crystal structure is shown in Fig. 8a. Each I_3^- anion interacts with the diprotonated ligand *via* five bond paths, four of which are concerned with C–H···I interactions and the fifth one with an N···I interaction. The latter is likely associated with an anion–π interaction rather than with halogen bonding interaction since it occurs in the direction normal to the tetrazine plane which is populated by π-electrons. The values of the electronic charge densities at the bond critical points, BCP(3,–1), indicate that the complex in the crystal is C_i symmetric. The binding energy associated with the interaction of two I_3^- anions with the dicationic ligand corresponds to 65.2 kJ mol^{-1}. Hence, half of this energy (32.6 kJ mol^{-1}) corresponds to the interaction of one I_3^- anion with the ligand. Upon replacement of both morpholinic arms with hydrogen atoms, the binding energy associated with the interaction of one I_3^- anion to the ligand becomes 10.2 kJ mol^{-1}, which is about twice the mean contribution from each of the four CH···I contacts. This value is slightly lower than those calculated for complexes III and IV in Fig. 7. Hence, this result indicates that the parallel orientation of the I_3^- anion with respect to the tetrazine plane is still favoured over the vertical orientation (complex II) even when the triiodide anion is translated away from its centroid.

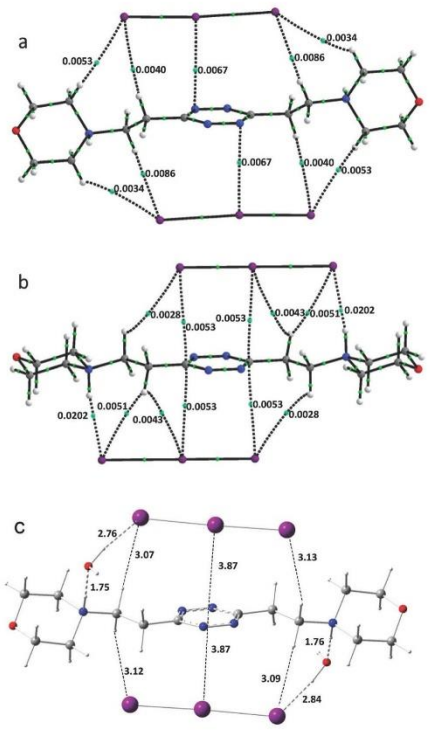

Fig. 8 Molecular graphs for (a) the $H_2L2(I_3)_2$ complex in the molecular crystal and (b) the same complex after geometry optimization in a continuum water environment. The values of the charge density at selected BCP(3,–1) are reported (in a.u.) whereas both RCPs and CCPs are not shown. (c) The optimized geometry of the complex with two explicit water molecules. Distances are in Å.

As noted above, we were not able to obtain information about I_3^- complexes in aqueous solution because they are poorly soluble. To remedy this lack of information, details of the possible geometry of the complex in water were obtained by optimization at the IEF-PCM(H_2O)-ωB97X-D/DGDZVP level of theory of the trimeric $(H_2L2^{2+})(I_3^-)_2$ complex and of the same system solvated by two explicit water molecules. The charge density of the former complex was analysed with QTAIM and the corresponding molecular graph is shown in Fig. 8b. Each I_3^- anion is now characterized by six bond paths connecting it to the diprotonated ligand. The new bond path topology results from the translation of the I_3^- anions in opposite directions, toward the positive ligand charges, nearly oriented along the C–C axis of the tetrazine ring. In addition to three C–H···I and one N–H···I bond paths, each I_3^- anion is now characterized by two I···C bond paths connecting the central and one terminal iodine atoms of I_3^- with the carbon atoms of the tetrazine ring. The increased number of bonding interactions in this model is in line with the enhancement of the computed binding energy, by ~40 kJ mol^{-1}, from 65.2 kJ mol^{-1} to 105.6 kJ mol^{-1}. Interestingly, in the solvated system with two explicit water molecules (Fig. 8c), the charge assisted NH···I hydrogen bonds are lost and each NH group points toward a water molecule which forms a bridge between the morpholinic arm and I_3^-. We note that in this model both I···π and CH···I interactions still do play a role in stabilizing the adduct.

Conclusions

Protonated forms of the tetrazine-based ligand L2 are able to form I^-, I_3^-, and mixed I^-/I_3^- anion complexes in the solid state. X-ray structures of these complexes showed that the anions are invariably located over the positive electrostatic potential of the ligand's tetrazine ring forming anion–π interactions. In the I^- complex, further noncovalent forces contribute to hold the anions in place, while in the case of I_3^- solid complexes, constituted by alternate segregated planes containing only protonated ligands and cocrystallized water molecules or only iodide and triiodide anions forming halogen–halogen contacts, forces other than anion–π interactions appear to make a modest contribution to the anion–ligand association. In the solid complexes, the triiodide anion displays both end-

on and side-on interaction modes with the tetrazine moieties, the I_3^- axis being aligned parallel to the ligand axis. DFT calculations substantiated that the side-on arrangement of I_3^- over the tetrazine ring corresponds to the most stable interaction mode among those computationally explored. Furthermore, calculations evidenced that, even when the ligand is deprived of the two morpholinium residues and in the presence of a simulated implicit water environment, the tetrazine ring is still able to promote the association with I^- and I_3^-, the side-on orientation of I_3^-, relative to the aromatic ring, remaining the most stable conformation. The infinite two-dimensional networks established between I_3^- and I_3^-/I^- anions through I···I short contacts make these crystalline structures good candidates to behave as solid conductors. While I_3^- complexes are of very low solubility, the I^- ones are soluble enough to allow the interaction of I^- with mono- and di-protonated forms of L2 to be studied. The stability of the complexes formed with $HL2^+$ and $H_2L_2^{2+}$ are very similar, the free energy change of association ($-\Delta G°$) being in the range 12–13 kJ mol^{-1}, in agreement with previous data[25] showing that anion association with L2 in aqueous solution is almost independent of the ligand charge, suggesting that anion–π interactions prevail over electrostatic attraction. In the case of I_3^-, the formation of solution complexes was modelled with the aid of quantum chemistry methods that showed the anion lying at a short distance over the tetrazine ring shifted toward a protonated morpholine nitrogen. Our calculations suggest that a pair of water molecules are likely to form bridges between the two anions and the diprotonated ligand thus stabilizing the whole complex.

Acknowledgements

Financial support from the Italian MIUR (project 2015MP34H3) is gratefully acknowledged. The centre of instrumental facilities, STI, of the University of Jaén is acknowledged for technical assistance. FP thanks the Department of Applied Chemistry of the Graduate School of Engineering of Tohoku University for financial support.

Notes and references

1 (*a*) *Anion Coordination Chemistry*, ed. K. Bowman-James, A. Bianchi and E. García-España, Wiley-VCH, New York, 2012; (*b*) J. L. Sessler, P. A. Gale and W.-S. Cho, *Anion Receptor Chemistry (Monographs in Supramolecular Chemistry)*, RSC Publishing, Cambridge, 2006.

2 D. Quiñonero, A. Frontera and P. M. Deyà, in *Anion Coord. Chem*, ed. E. Bowman-James, K. Bianchi and A. García-España, Wiley-VCH, New York, 2012, pp. 321–361.

3 (*a*) M. Giese, M. Albrecht and K. Rissanen, *Chem. Commun.*, 2016, **52**, 1778–1795; (*b*) X. Lucas, A. Bauza, A. Frontera and D. Quinonero, *Chem. Sci.*, 2016, **7**, 1038–1050; (*c*) M. Giese, M. Albrecht and K. Rissanen, *Chem. Rev.*, 2015, **115**, 8867–8895; (*d*) S. E. Wheeler and J. W. G. Bloom, *J. Phys. Chem. A*, 2014, **118**, 6133–6147; (*e*) P. Gamez, *Inorg. Chem. Front.*, 2014, **1**, 35–43; (*f*) H. T. Chifotides and K. R. Dunbar, *Acc. Chem. Res.*, 2013, **46**, 894–906; (*g*) P. Ballester, *Acc. Chem. Res.*, 2013, **46**, 874–884; (*h*) M. M. Watt, M. S. Collins and D. W. Johnson, *Acc. Chem. Res.*, 2013, **46**, 955–966; (*i*) H.-J. Schneider, *Acc. Chem. Res.*, 2013, **46**, 1010–1019; (*j*) P. Arranz-Mascaros, C. Bazzicalupi, A. Bianchi, C. Giorgi, M.-L. Godino-Salido, M.-D. Gutierrez-Valero, R. Lopez-Garzon and M. Savastano, *J. Am. Chem. Soc.*, 2013, **135**, 102–105; (*k*) S. E. Wheeler, *Acc. Chem. Res.*, 2013, **46**, 1029–1038; (*l*) A. Frontera, P. Gamez, M. Mascal, T. J. Mooibroek and J. Reedijk, *Angew. Chem., Int. Ed.*, 2011, **50**, 9564–9583; (*m*) L. M. Salonen, M. Ellermann and F. Diederich, *Angew. Chem., Int. Ed.*, 2011, **50**, 4808–4842; (*n*) I. Alkorta, F. Blanco, P. M. Deyà, J. Elguero, C. Estarellas, A. Frontera and D. Quiñonero, *Theor. Chem. Acc.*, 2010, **126**, 1–14; (*o*) O. B. Berryman and D. W. Johnson, *Chem. Commun.*, 2009, 3143–3153; (*p*) C. Caltagirone and P. A. Gale, *Chem. Soc. Rev.*, 2009, **38**, 520–563; (*q*) H.-J. Schneider, *Angew. Chem., Int. Ed.*, 2009, **48**, 3924–3977; (*r*) B. L. Schottel, H. T. Chifotides and K. R. Dunbar, *Chem. Soc. Rev.*, 2008, **37**, 68–83; (*s*) B. P. Hay and V. S. Bryantsev, *Chem. Commun.*, 2008, 2417–2428; (*t*) D. Quiñonero, C. Garau, C. Rotger, A. Frontera, P. Ballester, A. Costa and P. M. Deya, *Angew. Chem., Int. Ed.*, 2002, **41**, 3389–3392; (*u*) M. Mascal, A. Armstrong and M. D. Bartberger, *J. Am. Chem. Soc.*, 2002, **124**, 6274–6276; (*v*) I. Alkorta, I. Rozas and J. Elguero, *J. Am. Chem. Soc.*, 2002, **124**, 8593–8598; (*w*) K. Hiraoka, S. Mizuse and S. Yamabe, *J. Phys. Chem.*, 1987, **91**, 5294–5297.

4 (*a*) Z. Aliakbar Tehrani and K. S. Kim, *Int. J. Quantum Chem.*, 2016, **116**, 622–633; (*b*) J.-Z. Liao, H.-L. Zhang, S.-S. Wang, J.-P. Yong, X.-Y. Wu, R. Yu and C.-Z. Lu, *Inorg. Chem.*, 2015, **54**, 4345–4350; (*c*) M. Savastano, P. Arranz-Mascarós, C. Bazzicalupi, A. Bianchi, C. Giorgi, M. L. Godino-Salido, M. D. Gutiérrez-Valero and R. López-Garzón, *RSC Adv.*, 2014, **4**, 58505–58513; (*d*) P. Arranz, A. Bianchi, R. Cuesta, C. Giorgi, M. L. Godino, M. D. Gutierrez, R. Lopez and A. Santiago, *Inorg. Chem.*, 2010, **49**, 9321–9332; P. Arranz, A. Bianchi, R. Cuesta, C. Giorgi, M. L. Godino, M. D. Gutierrez, R. Lopez and A. Santiago, *Inorg. Chem.*, 2012, **51**, 4883.

5 (*a*) P. A. Gale and C. Caltagirone, *Chem. Soc. Rev.*, 2015, **44**, 4212–4227; (*b*) N. H. Evans and P. D. Beer, *Angew. Chem., Int. Ed.*, 2014, **53**, 11716–11754.

6 (*a*) A. Vargas Jentzsch and S. Matile, *Top. Curr. Chem.*, 2015, **358**, 205–239; (*b*) A. Vargas Jentzsch and S. Matile, *J. Am. Chem. Soc.*, 2013, **135**, 5302–5303; (*c*) A. Vargas Jentzsch, A. Hennig, J. Mareda and S. Matile, *Acc. Chem. Res.*, 2013, **46**, 2791–2800; (*d*) A. V. Jentzsch, D. Emery, J. Mareda, S. K. Nayak, P. Metrangolo, G. Resnati, N. Sakai and S. Matile, *Nat. Commun.*, 2012, **3**, 905; (*e*) J. Misek, A. V. Jentzsch, S. Sakurai, D. Emery, J. Mareda and S. Matile, *Angew. Chem., Int. Ed.*, 2010, **49**, 7680–7683; (*f*) L. Adriaenssens, C. Estarellas, A. Vargas Jentzsch, M. Martínez Belmonte, S. Matile and P. Ballester, *J. Am.*

Chem. Soc., 2013, **135**, 8324–8330; (*g*) A. Vargas Jentzsch, D. Emery, J. Mareda, P. Metrangolo, G. Resnati and S. Matile, *Angew. Chem., Int. Ed.*, 2011, **50**, 11675–11678.

7 (*a*) Y. Zhao, S. Benz, N. Sakai and S. Matile, *Chem. Sci.*, 2015, **6**, 6219–6223; (*b*) Y. Zhao, N. Sakai and S. Matile, *Nat. Commun.*, 2014, **5**, 3911; (*c*) Y. Zhao, C. Beuchat, Y. Domoto, J. Gajewy, A. Wilson, J. Mareda, N. Sakai and S. Matile, *J. Am. Chem. Soc.*, 2014, **136**, 2101–2111; (*d*) T. Lu and S. E. Wheeler, *Org. Lett.*, 2014, **16**, 3268–3271; (*e*) C. Estarellas, A. Frontera, D. Quiñonero and P. M. Deyà, *Angew. Chem., Int. Ed.*, 2011, **50**, 415–418; (*f*) C. M. Rojas and J. J. Rebek, *J. Am. Chem. Soc.*, 1998, **120**, 5120–5121.

8 P. H. Svensson and L. Kloo, *Chem. Rev.*, 2003, **103**, 1649–1684.

9 (*a*) M. Giese, M. Albrecht, T. Repenko, J. Sackmann, A. Valkonen and K. Rissanen, *Eur. J. Org. Chem.*, 2014, 2435–2442; (*b*) M. D. Garcia, J. Marti-Rujas, P. Metrangolo, C. Peinador, T. Pilati, G. Resnati, G. Terraneo and M. Ursini, *CrystEngComm*, 2011, **13**, 4411–4416; (*c*) M. Müler, M. Albrecht, V. Gossen, T. Peters, A. Hoffmann, G. Raabe, A. Valkonen and K. Rissanen, *Chem. – Eur. J.*, 2010, **16**, 12446–12453; (*d*) H. Chow, P. A. W. Dean, D. C. Craig, N. T. Lucas, M. L. Scudder and I. G. Dance, *New J. Chem.*, 2003, **27**, 704–713; (*e*) H. Paulsson, M. Berggrund, A. Fischer and L. Kloo, *Eur. J. Inorg. Chem.*, 2003, 2352–2355; (*f*) A. J. Blake, R. O. Gould, W.-S. Li, V. Lippolis, S. Parsons, C. Radek and M. Schroder, *Angew. Chem., Int. Ed.*, 1998, **37**, 293–296; (*g*) A. J. Blake, W.-S. Li, V. Lippolis, M. Schroder, F. A. Devillanova, R. O. Gould, S. Parsons and C. Radek, *Chem. Soc. Rev.*, 1998, **27**, 195–206; (*h*) A. J. Blake, V. Lippolis, S. Parsons and M. Shroeder, *Chem. Commun.*, 1996, 2207–2208; (*i*) R. D. Bailey and W. T. Pennington, *Chem. Commun.*, 1998, 1181–1182; (*j*) A. J. Blake, R. O. Gould, S. Parsons, C. Radek and M. Schroeder, *Angew. Chem., Int. Ed. Engl.*, 1995, **34**, 2374–2376.

10 (*a*) K. Lamberts, P. Handels, U. Englert, E. Aubert and E. Espinosa, *CrystEngComm*, 2016, **18**, 3832–3841; (*b*) D. Tristant, P. Puech and I. C. Gerber, *Phys. Chem. Chem. Phys.*, 2015, **17**, 30045–30051; (*c*) Y. Wang, Y. Xue, X. Wang, Z. Cui and L. Wang, *J. Mol. Struct.*, 2014, **1074**, 231–239; (*d*) R. D. Walsh, J. M. Smith, T. W. Hanks and W. T. Pennington, *Cryst. Growth Des.*, 2012, **12**, 2759–2768; (*e*) G. Manca, A. Ienco and C. Mealli, *Cryst. Growth Des.*, 2012, **12**, 1762–1771; (*f*) M. Otsuka, H. Mori, H. Kikuchi and K. Takano, *Comput. Theor. Chem.*, 2011, **973**, 69–75; (*g*) M. Groessl, Z. Fei, P. J. Dyson, S. A. Katsyuba, K. L. Vikse and J. S. McIndoe, *Inorg. Chem.*, 2011, **50**, 9728–9733; (*h*) A. Asaduzzaman and G. Schreckenbach, *Theor. Chem. Acc.*, 2009, **122**, 119–125; (*i*) V. T. Calabrese and A. Khan, *J. Phys. Chem. A*, 2000, **104**, 1287–1292; (*j*) P. H. Svensson and L. Kloo, *J. Chem. Soc., Dalton Trans.*, 2000, 2449–2455; (*k*) S. B. Sharp and G. I. Gellene, *J. Phys. Chem. A*, 1997, **101**, 2192–2197; (*l*) G. A. Landrum, N. Goldberg and R. Hoffmann, *J. Chem. Soc., Dalton Trans.*, 1997, 3605–3613.

11 C. L. Bentley, A. M. Bond, A. F. Hollenkamp, P. J. Mahon and J. Zhang, *J. Phys. Chem. C*, 2014, **118**, 22439–22449.

12 R. Thapa and N. Park, *J. Phys. Chem. Lett.*, 2012, **3**, 3065–3069.

13 W. Yourey, L. Weinstein and G. G. Amatucci, *Solid State Ionics*, 2011, **204**, 80–86.

14 (*a*) J. Wu, Z. Lan, J. Lin, M. Huang, Y. Huang, L. Fan and G. Luo, *Chem. Rev.*, 2015, **115**, 2136–2173; (*b*) A. Hagfeldt, G. Boschloo, L. Sun, L. Kloo and H. Pettersson, *Chem. Rev.*, 2010, **110**, 6595–6663; (*c*) M. Grätzel, *Chem. Lett.*, 2005, **34**, 8–13; (*d*) M. Grätzel, *Nature*, 2001, **414**, 338–344.

15 M. Yu, W. D. McCulloch, Z. Huang, B. B. Trang, J. Lu, K. Amine and Y. Wu, *J. Mater. Chem. A*, 2016, **4**, 2766–2782.

16 F. Bella, S. Galliano, M. Falco, G. Viscardi, C. Barolo, M. Gratzel and C. Gerbaldi, *Chem. Sci.*, 2016, **7**, 4880–4890.

17 F. Bella, C. Gerbaldi, C. Barolo and M. Gratzel, *Chem. Soc. Rev.*, 2015, **44**, 3431–3473.

18 (*a*) Z. Fei, F. D. Bobbink, E. Păunescu, R. Scopelliti and P. J. Dyson, *Inorg. Chem.*, 2015, **54**, 10504–10512; (*b*) H.-C. Chang, J.-C. Jiang, M.-H. Kuo, D.-T. Hsu and S. H. Lin, *Phys. Chem. Chem. Phys.*, 2015, **17**, 21143–21148; (*c*) H. Santa-Nokki, S. Busi, J. Kallioinen, M. Lahtinen and J. Korppi-Tommola, *J. Photochem. Photobiol., A*, 2007, **186**, 29–33; (*d*) R. Kawano and M. Watanabe, *Chem. Commun.*, 2005, 2107–2109.

19 E. Yilmaz, E. B. Olutas, G. Barim, J. Bandara and O. Dag, *RSC Adv.*, 2016, **6**, 97430–97437.

20 P. E. Marchezi, G. G. Sonai, M. K. Hirata, M. A. Schiavon and A. F. Nogueira, *J. Phys. Chem. C*, 2016, **120**, 23368–23376.

21 K. Prabakaran, A. K. Palai, S. Mohanty and S. K. Nayak, *RSC Adv.*, 2015, **5**, 66563–66574.

22 J. Li and Z.-S. Wang, *RSC Adv.*, 2015, **5**, 56967–56973.

23 H. Wang, J. Li, F. Gong, G. Zhou and Z.-S. Wang, *J. Am. Chem. Soc.*, 2013, **135**, 12627–12633.

24 H. Wang, H. Li, B. Xue, Z. Wang, Q. Meng and L. Chen, *J. Am. Chem. Soc.*, 2005, **127**, 6394–6401.

25 M. Savastano, C. Bazzicalupi, C. Giorgi, C. García-Gallarín, M. D. López de la Torre, F. Pichierri, A. Bianchi and M. Melguizo, *Inorg. Chem.*, 2016, **55**, 8013–8024.

26 C. Bazzicalupi, A. Bianchi, T. Biver, C. Giorgi, S. Santarelli and M. Savastano, *Inorg. Chem.*, 2014, **53**, 12215–12224.

27 P. Gans, A. Sabatini and A. Vacca, *Talanta*, 1996, **43**, 1739–1753.

28 Agilent, *CrysAlys PRO (Version 1.171.35.11)*, Agilent Technologies Ltd, Yarnton, Oxfordshire, England, 2014.

29 G. M. Sheldrick, *Acta Crystallogr., Sect. A: Fundam. Crystallogr.*, 1990, **46**, 467–473.

30 G. M. Sheldrick, *Acta Crystallogr.*, 2015, **71**, 3–8.

31 M. J. Frisch, G. W. Trucks, H. B. Schlegel, G. E. Scuseria, M. A. Robb, J. R. Cheeseman, G. Scalmani, V. Barone, B. Mennucci, G. A. Petersson, H. Nakatsuji, M. Caricato, X. Li, H. P. Hratchian, A. F. Izmaylov, J. Bloino, G. Zheng, J. L. Sonnenberg, M. Hada, M. Ehara, K. Toyota, R. Fukuda, J. Hasegawa, M. Ishida, T. Nakajima, Y. Honda, O. Kitao,

H. Nakai, T. Vreven, J. A. Montgomery, J. E. Peralta, F. Ogliaro, M. Bearpark, J. J. Heyd, K. N. Kundin, V. N. Staroverov, R. Kobayashi, J. Normand, K. Raghavachari, A. Rendell, J. C. Burant, S. S. Iyengar, J. Tomasi, M. Cossi, N. Rega, J. M. Millam, M. Klene, J. E. Knox, J. B. Cross, V. Bakken, C. Adamo, J. Jaramillo, R. Gomperts, R. E. Stratmann, O. Yazyev, A. J. Austin, R. Cammi, C. Pomelli, J. W. Ochterski, R. L. Martin, K. Morokuma, V. G. Zakrzewski, G. A. Voth, P. Salvador, J. J. Dannenberg, S. Dapprich, A. D. Daniels, Ö. Farkas, J. B. Foresman, J. V. Ortiz, J. Ciolowski and D. J. Fox, *Gaussian 09, Revision C.01*, Gaussian, Inc., Wallingford CT, 2009.

32 J.-D. Chai and M. Head-Gordon, *Phys. Chem. Chem. Phys.*, 2008, **10**, 6615–6620.

33 N. Godbout, D. R. Salahub, J. Andzelm and E. Wimmer, *Can. J. Chem.*, 1992, **70**, 560–571.

34 C. Sosa, J. Andzelm, B. C. Elkin, E. Wimmer, K. D. Dobbs and D. A. Dixon, *J. Phys. Chem.*, 1992, **96**, 6630–6636.

35 J. Tomasi, B. Mennucci and R. Cammi, *Chem. Rev.*, 2005, **105**, 2999–3093.

36 S. F. Boys and F. Bernardi, *Mol. Phys.*, 1970, **19**, 553–566.

37 A. E. Reed, L. A. Curtiss and F. Weinhold, *Chem. Rev.*, 1988, **88**, 899–926.

38 T. A. Keith, *AIMAll (Version 12.06.03, Professional)*, 2012.

39 F. W. Bader, *Atoms in Molecules: A Quantum Theory*, Oxford Univ. Press, Oxford, 1994.

40 (*a*) P. Mateus, N. Bernier and R. Delgado, *Coord. Chem. Rev.*, 2010, **254**, 1726–1747; (*b*) K. Bowman-James, *Acc. Chem. Res.*, 2005, **38**, 671–678; (*c*) E. Garcia-España, P. Díaz, J. M. Llinares and A. Bianchi, *Coord. Chem. Rev.*, 2006, **250**, 2952–2986; (*d*) A. Bianchi, M. Micheloni and P. Paoletti, *Inorg. Chim. Acta*, 1988, **151**, 269–272.

41 S. Madhu, H. A. Evans, V. V. T. Doan-Nguyen, J. G. Labram, G. Wu, M. L. Chabinyc, R. Seshadri and F. Wudl, *Angew. Chem., Int. Ed.*, 2016, **55**, 8032–8035.

42 R. Swietlik, D. Schweitzer and H. J. Keller, *Phys. Rev. B: Condens. Matter*, 1987, **36**, 6881–6888.

43 L. Kloo, P. H. Svensson and M. J. Taylor, *J. Chem. Soc., Dalton Trans.*, 2000, 1061–1065.

44 P. Deplano, F. A. Devillanova, J. R. Ferraro, F. Isaia, V. Lippolis and M. L. Mercuri, *Appl. Spectrosc.*, 1992, **46**, 1625–1629.

45 J. S. Zambounis, E. I. Kamitsos, A. P. Patsis and G. C. Papavassiliou, *J. Raman Spectrosc.*, 1992, **23**, 81–85.

46 P. Coppens, in *Ext. Linear Chain Compd.*, Plenum, 1982, vol. 1, pp. 333–356.

47 F. Bigoli, P. Deplano, F. A. Devillanova, V. Lippolis, M. L. Mercuri, M. A. Pellinghelli and E. F. Trogu, *Inorg. Chim. Acta*, 1998, **267**, 115–121.

48 L. Kloo, J. Rosdahl and P. H. Svensson, *Eur. J. Inorg. Chem.*, 2002, 1203–1209.

49 F. Groenewald, C. Esterhuysen and J. Dillen, *Theor. Chem. Acc.*, 2012, **131**, 1–12.

ARTICLE IN PRESS

Inorganica Chimica Acta xxx (2017) xxx–xxx

Contents lists available at ScienceDirect

Inorganica Chimica Acta

journal homepage: www.elsevier.com/locate/ica

Research paper

Interplay between salt bridge, hydrogen bond and anion-π interactions in thiocyanate binding ☆

Matteo Savastano [a], Celeste García [b], Maria Dolores López de la Torre [b], Fabio Pichierri [c], Carla Bazzicalupi [a,*], Antonio Bianchi [a,*], Manuel Melguizo [b,*]

[a] Department of Chemistry "Ugo Schiff", University of Florence, Via della Lastruccia 3, 50019, Sesto Fiorentino, Italy
[b] Department of Inorganic and Organic Chemistry, University of Jaén, 23071 Jaén, Spain
[c] Department of Applied Chemistry, Graduate School of Engineering, Tohoku University, Sendai 980-8579, Japan

ARTICLE INFO

Article history:
Received 21 February 2017
Received in revised form 12 April 2017
Accepted 14 April 2017
Available online xxxx

Keywords:
Anion complexes
Anion receptors
Anion-π interaction
Weak forces
DFT calculations
Tetrazine
Thiocyanate

ABSTRACT

The L2 ligand (3,6-bis(morpholin-4-ylethyl)-1,2,4,5-tetrazine) is constituted by a tetrazine ring decorated with two morpholine pendants. The crystal structure of the $H_2L2(SCN)_2$ anion complex shows the thiocyanate anion interacting with the ligand, protonated on the morpholine groups, through the formation of salt-bridge, anion-π and hydrogen bond interactions. The SCN^- anion lies over the tetrazine ring, with the nitrogen atom in proximity to the ring centroid, in a sort of π-π stacking binding mode. Density Functional Theory (DFT) calculations performed on the interaction of SCN^- with the plain tetrazine ring showed that the anion-π attraction alone is sufficient to form the complex, even in a simulated implicit water environment. The arrangement of the interacting partners in the DFT-optimized geometry of the most stable complex is very similar to the one actually assumed in the crystal structure. Potentiometric titrations performed in water (0.1 M Me_4NCl, 298.1 ± 0.1 K) revealed that not only the protonated ligand forms, but even the neutral L2 molecule is able to bind SCN^- in solution. The stability of the complexes formed is almost insensitive to ligand charge, revealing that, even in water, anion-π interactions are of major importance in the interplay of weak forces contributing to the formation of similar anion complexes.

1. Introduction

Anion coordination chemistry is a well-established area of supramolecular chemistry that is gathering a large deal of interest because of the importance and the specificity of the roles played by anions in abiotic and biological systems. In addition to strong electrostatic attractions with positively charged receptors, that fostered the birth of anion coordination chemistry, a plethora of weaker forces, including hydrogen bond, anion-dipole, halogen bond and anion-π interactions, as well as solvent effects, also proved to be efficient in promoting the formation of anion-receptor assemblies [1]. Anion-π interactions, exerting between anions and the π-system of electron-deficient arenes, have become rather popular, despite their relatively recent recognition [2,3], and are now used as design tools for the construction of new functional materials [4], anion receptors [3a, 5], carriers [6], sensors [7] and catalysts [8], while we observed an increasing appreciation of their biological relevance [3a,b].

We have recently shown that protonated forms of the tetrazine-based molecules L1 and L2, decorated with two morpholine pendants of different lengths (Fig. 1), bind several inorganic anions of different geometries, such as spherical F^- and I^-, trigonal NO_3^-, tetrahedral ClO_4^- and SO_4^{2-}, and octahedral PF_6^-, forming stable complexes in aqueous solution. Crystallographic information obtained for some solid samples of these complexes showed that the anions are invariably involved in anion-π interactions with the tetrazine group, in agreement with the strong π-acid character of this ring [9]. Also the triiodide anion (I_3^-) forms complexes with H_2L2^{2+} in the solid state, where the linear anion assumes both end-on and side-on interaction modes with the tetrazine moieties. Density Functional Theory (DFT) calculations substantiated that the side-on arrangement corresponds to the most stable interaction mode among those computationally explored in the presence of simulated aqueous environment [9b]. Unfortunately, because of the very low solubility of compounds formed by I_3^- with protonated

☆ This paper is dedicated to Dr. Carlo Mealli.

* Corresponding authors.
E-mail addresses: carla.bazzicalupi@unifi.it (C. Bazzicalupi), antonio.bianchi@unifi.it (A. Bianchi), mmelgui@ujaen.es (M. Melguizo).

http://dx.doi.org/10.1016/j.ica.2017.04.029
0020-1693/

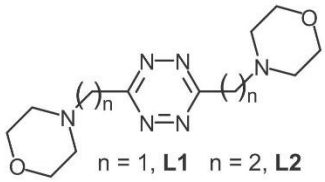

Fig. 1. The tetrazine ligands L1 and L2.

forms of L1 and L2, we could not manage to study the formation of I_3^- complexes in solution. For this reason, and with the aim of extending solution studies to complexes of similar ligands with linear anions, we investigated the interaction of L2 with thiocyanate (SCN^-) in aqueous solution.

In this paper, we report the result of this study along with a crystallographic analysis of the crystalline $H_2L2(SCN)_2$ complex in which SCN^- anions are bound to the ligand through salt-bridge and anion-π interactions. This is one of the very few cases of anion complexes including a receptor selected for involving anion-π interactions in the binding of SCN^- anions [10].

2. Experimental procedure

2.1. Materials

L2 (3,6-bis(morpholin-4-ylethyl)-1,2,4,5-tetrazine) was synthesized as previously described [9a]. Pink crystals of $H_2L2(NCS)_2$ were obtained upon slow evaporation at room temperature of an aqueous solution containing the ligand and an excess of the anion at pH 3. High purity NaSCN (Merck) was used for all experimental procedures.

2.2. Potentiometric measurements

Potentiometric (pH-metric) titrations employed for the determination of equilibrium constants were carried out in degassed aqueous solutions at 298.1 ± 0.1 K, with a 0.1 M ionic strength, by using previously described equipment and procedures [11]. The determined ionic product of water was $pK_w = 13.83(1)$ (298.1 ± 0.1 K, 0.1 M Me_4NCl). Ligand concentration was about 8×10^{-4} M, while SCN^- concentration was about 2.4×10^{-3} M. The ionic strength was adjusted to 0.1 M by the addition of Me_4NCl. The studied pH range was 2.7–9.0. The computer program HYPERQUAD [12] was used to calculate equilibrium constants from potentiometric data deriving from three independent titration experiments. Ligand protonation constants used in calculation were previously determined [9a].

2.3. X-ray structure analysis

A suitable pink crystal of $H_2L2(NCS)_2$ was used for X-ray diffraction analysis. A summary of the crystallographic data is reported in Table 1. The integrated intensities were corrected for Lorentz and polarization effects and an empirical absorption correction was applied [13]. The structure was solved by direct methods (Olex2) [14]. Refinements were performed by means of full-matrix least-squares using SHELX Version 2014/7 program [15]. All the non-hydrogen atoms were anisotropically refined. Hydrogen atoms were usually introduced in calculated position and their coordinates were refined according to the linked atoms.

Table 1
Refinement and crystallographic parameters for $H_2L2(NCS)_2$.

Empirical formula	$C_{16}H_{26}N_8O_2S_2$
Formula weight	426.57
Temperature (K)	293
Space group	$P\,2_1/c$
a (Å)	12.334(2)
b (Å)	6.816(1)
c (Å)	12.497(2)
β (°)	96.61(1)
Volume (Å^3)	1043.5(3)
Z	2
Independent reflections/R(int)	1834/0.0689
μ (mm^{-1})	2.566/(Cu-kα)
R indices [I > 2σ(I)]*	R1 = 0.0791 w*R2* = 0.2092
R indices (all data)*	R1 = 0.1215 w*R2* = 0.2731

2.4. Computational chemistry

DFT calculations were performed with the Gaussian 09 quantum chemistry package [16] using the dispersion-corrected ωB97X-D functional of Chai and Head-Gordon [17] in combination with the 6-31+G(d) basis set of Pople and coworkers [18,19]. Geometry optimizations were performed with the integral equation formalism – polarization continuum model (IEF-PCM) of Tomasi and co-workers [20] to simulate an implicit water environment surrounding the tetrazine-thiocyanate complexes. The binding energies (B_e) computed for the tetrazine-thiocyanate complexes were corrected for the basis-set superposition error (BSSE) using the counterpoise method proposed by Boys and Bernardi [21]. Atom charges were obtained from a natural population analysis (NPA) [22] of the solvated complexes. NPA charges were selected because they overcome some of the limitations observed in the charges calculated from the default Mulliken population analysis [23].

3. Results and discussion

The crystal structure of the $H_2L2(SCN)_2$ compound contains centrosymmetric diprotonated ligand molecules interacting with two symmetry related thiocyanate anions (Fig. 2). The ligand assumes a chair-type conformation, similar to that previously reported for its ClO_4^-, NO_3^-, PF_6^- complexes, in which the morpholine pendant arms are in trans position with respect to the tetrazine ring. The two SCN^- anions are localized in a side-on conformation just above and below the tetrazine ring, almost aligned along the C–C axis. The projection of the sulfur atom of each anion on the tetrazine plane lies completely outside the ring, while both nitrogen and carbon positions are representative of an anion-π interactions with the electron-poor aromatic group, the distance from the aromatic ring plane being 3.16 Å for N and 3.31 Å for C (distances from ring centroid/offset 3.19/0.46 Å for N and 3.35/0.72 Å for C). Furthermore, the thiocyanate nitrogen forms a strong H-bond (H···N distance 1.75(7) Å, N-H···N angle 174(6)°) with the morpholine protonated nitrogen. Interestingly, the H···N-C angle featuring the H-bond (161(2)°), as well the N-C intra-ion bond distance (1.187(8) Å), suggest the presence of a triple bond between nitrogen and carbon in the thiocyanate anion. This connectivity implies that some negative charge should be localized on the sulfur atom, which, as a matter of fact, is in contact with a hydrogen atoms of a CH_2 group linked to the tetrazine ring (H···S distance 2.861(1) Å).

Interesting comparisons can be done with some of the crystal structures previously reported for the $[(H_2L2)X]^+$ systems, with X = ClO_4^-, NO_3^-, PF_6^- and I_3^-. Fig. 3, for instance, shows the SCN^-

Please cite this article in press as: M. Savastano et al., Inorg. Chim. Acta (2017), http://dx.doi.org/10.1016/j.ica.2017.04.029

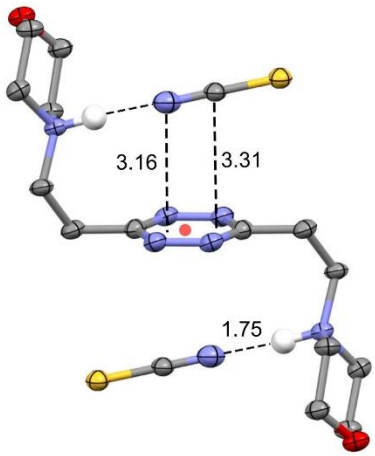

Fig. 2. ORTEP drawing of $H_2L2(NCS)_2$. Thermal ellipsoids plotted at 40% probability level. Distances are in Å. Colors code: grey, C; white, H; blue, N; red, O; yellow, S. (For interpretation of the references to colour in this figure legend, the reader is referred to the web version of this article.)

ion superimposed to the side-on (A) and to the end-on (B) H_2L2I_3 species found in the crystal of $H_2L2(I_3)_2{\cdot}2H_2O$ [9b]. As in the case of the SCN^- anion, also the end-on I_3^- is approximately aligned along the C–C interatomic axis of the tetrazine, while the side-on one is displaced toward the N-N side edge of the tetrazine ring. Notably, in the end-on $H_2L2I_3^+$ adduct, the main force taking triiodides in place is the anion-π interaction [9b], while in the case of the side-on $[H_2L2(SCN)]^+$ an additional salt-bridge interaction, linking together the morpholine protonated nitrogen with the nitrogen atom of SCN^-, contributes to strengthen the assembly. Most likely, the stronger propensity to form H-bonds of nitrogen induces the H_2L2^{2+} ligand to assume the chair conformation, which in the adduct with triiodide seems less favoured than the planar one. Nevertheless, such considerations do not take into account the effect of crystal packing forces, that could be important in determining the overall arrangement of these anion complexes.

Conversely, in $[(H_2L2)X]^+$ complexes with ClO_4^-, NO_3^- or PF_6^-, H_2L^{2+} assumes the chair conformation [9a], in analogy with the SCN^- complex. Fig. 4 offers an overlaid vision of H_2L^{2+} molecules from SCN^- and PF_6^- complexes. The superposition has been calculated for all the non-hydrogen atoms, except the tetrazine rings. It is evident that the pendant arms in the two structures are almost equal, but the similarity is even greater for ClO_4^-, NO_3^- compounds. Actually the calculated Root Mean Square Deviation is 0.48 Å in the case of PF_6^- and at most 0.2 and 0.1 Å for NO_3^- and ClO_4^-, respectively. The tetrazine rings are never coplanar, dihedral angles ranging from 11.2° for NO_3^- to 21.4° for ClO_4^-. For all these adducts as well as for the SCN^- one, H-bonds involving the protonated morpholine nitrogen atoms and anion-π interactions are recognized.

To our knowledge, no crystal structures of SCN^- complexes with tetrazine ligands have been reported so far, while only two papers containing crystallographic structures include receptors expressly selected for involving anion-π interactions in the binding of SCN^- [10]. In these papers, both end-on [10a] and side-on [10b] binding modes were found for the thiocyanate anion. In particular, the end-on binding mode is established in the adduct between

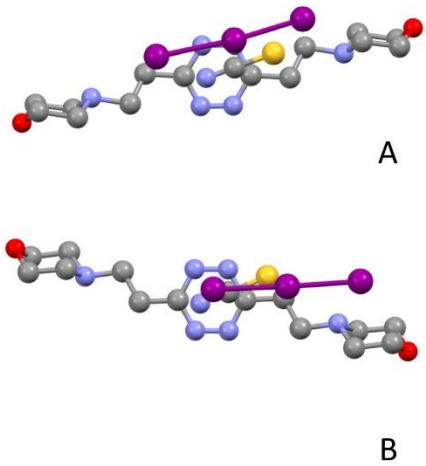

Fig. 3. NCS^- ion superimposed to the side-on (A) and the end-on (B) H_2L2I_3 species found in the crystal of $H_2L2(I_3)_2{\cdot}2H_2O$. Structures obtained overlapping the tetrazine rings.

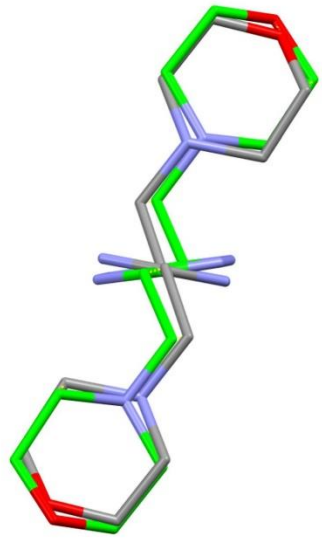

Fig. 4. L2 from the SCN^- complex (gray carbons) overlaid on ligand L2 from the PF_6^- complex [9a] (green carbons). Superposition calculated for all the non-hydrogen atoms, except the tetrazine rings. (For interpretation of the references to colour in this figure legend, the reader is referred to the web version of this article.)

Please cite this article in press as: M. Savastano et al., Inorg. Chim. Acta (2017), http://dx.doi.org/10.1016/j.ica.2017.04.029

SCN^- and a V-shaped calix[2]arene[2]triazine molecule, where arene and triazine alternate in the calix ring. In this structure the anion is pinched between the two triazines, respectively interacting with nitrogen and sulfur on opposite sides [10a]. The side-on binding mode is instead found for the adducts formed with tetracyanopyrazine or trinitrobenzene rings. In the two adducts, the SCN^- anion shows different orientations, tetracyanopyrazine and trinitrobenzene interacting with thiocyanate nitrogen and sulfur atoms, respectively [10b]. The tetracyanopyrazine adduct is structurally very similar to our complex, having the projection of the sulfur atom completely outside the ring and the nitrogen in contact with the aromatic ring. Nevertheless, the N···centroid distances and related offsets seem to indicate weaker interactions than in our complex (N···centroid distances ranging from 3.3 to 3.5 Å, offsets ranging from 1.2 to 1.4 Å).

As noted above, no crystal structures of SCN^- complexes with tetrazine ligands have been reported, while only three structures are available for triazine complexes of this anion [10a, 22]. In all these structures, SCN^- is involved in concomitant end-on interaction of both N and S atoms with different aromatic rings.

Further information on the SCN^--L2 interaction was obtained by performing a series of DFT calculations on complexes of SCN^- with the bare tetrazine ring, that is with L2 deprived of the morpholine residues. The calculations performed in a simulated implicit water environment showed that in the most stable adduct the anion forms an end-on anion-π interaction with the electron-deficient ring via the N atom (Fig. 5a) characterized by a B_e of 10.04 kJ/mol (here a positive value of B_e indicates a stabilizing interaction). This complex, which also possesses the lowest energy, is characterized by a tetrazine centroid (X)–N atom distance of 3.168 Å; the SCN^- anion is almost parallel to the tetrazine ring as evinced by the X–N–C angle of 93.4° formed by the anion with the N-centroid segment. When the SCN^- anion is oriented normal to the tetrazine molecular plane (X–N–C = 180°), the X–N distance (2.962 Å) is slightly shorter than the above value but B_e reduces to 7.11 kJ/mol (Fig. 5c). This result indicates that the complex shown in Fig. 5c lacks the extra-stabilization due to the π–π interaction that operates in the complex of Fig. 5a.

A similar trend is observed for the interaction of thiocyanate via the terminal S atom (Fig. 5b,d). Interestingly, the parallel complex

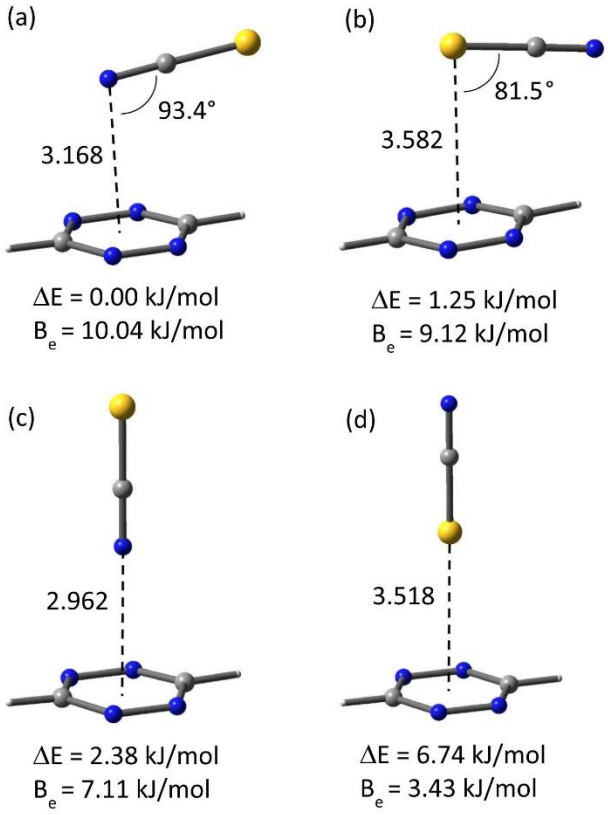

Fig. 5. DFT-optimized geometries of four tetrazine-SCN^- complexes. ΔE is the energy difference with respect to the lowest-energy complex. Distances are in Å.

Please cite this article in press as: M. Savastano et al., Inorg. Chim. Acta (2017), http://dx.doi.org/10.1016/j.ica.2017.04.029

Table 2
CSD search results for the thiocyanate···π contacts. (hits/obs = number of structure/number of measurements; Δ upper quantile = upper quantile for the difference between the distances from the ring plane of the contact and the carbon atoms; <dist> = average contact atom-ring centroid distance; <offset> = mean value for the calculated offset of the contact atom).

	N contact atom				S contact atom			
	hits/obs	Δupper quantile	⟨dist⟩	⟨offset⟩	hits/obs	Δupper quantile	⟨dist⟩	⟨offset⟩
Only C atoms in the ring	17/25	0.23	3.7(2)	1.2(7)	21/27	1.52	3.7(2)	1.2(4)
At least one N in the ring	44/57	0.47	3.6(2)	1.3(7)	40/58	1.43	3.7(2)	1.1(6)

Table 3
Equilibrium constants and relevant $-\Delta G^{\circ}$ values for anion complex formation determined at 298.1 ± 0.1 K in 0.1 M Me_4NCl aqueous solution.

	log K	$-\Delta G^{\circ}$kJ/mol
$L2 + SCN^- = [(L2)SCN]^-$	1.66(8)[a]	9.5(5)
$HL2^+ + SCN^- = [(HL2)SCN]$	1.87(8)	10.7(5)
$H_2L2^{2+} + SCN^- = [(H_2L2)SCN]^+$	1.90(7)	10.8 (4)

[a] Values in parentheses are standard deviation on the last significant figure.

(Fig. 5b) has only a slightly smaller B_e (9.12 kJ/mol) than the complex with the N-interacting anion (Fig. 5a), while the B_e of the vertical one (Fig. 5d) is considerably smaller (3.43 kJ/mol). Also, we notice that the X–S distances are always longer than 3.5 Å. This result appears to be in good agreement with our crystallographic findings, even in the absence of the additional salt-bridge and hydrogen bond contributions present in the crystal structure of $H_2L2(SCN)_2$. Interestingly, an analysis of the Cambridge Structural Database (CSD) [24] evidenced that SCN⁻···π contacts established by S and N atoms are similarly recurrent, and distances from ring centroids and offsets have comparable mean values. Nevertheless, when the contact implies nitrogen atoms, the end-on binding mode seems more frequent than the side-on one (Table 2).

Finally, the natural population analysis indicates that there is practically no charge transfer from the anion to the tetrazine ring, the natural charges of the three atoms of free SCN⁻ anion being almost same as those of the anion in the complexes shown in Fig. 5. The negative charge within the (free) SCN⁻ anion, however, is localized mainly on the terminal atoms with q(N) = −0.597*e* and q(S) = −0.460*e*. The larger magnitude of q(N) thus favours the end-on coordination of SCN⁻ via the nitrogen atom which results in the formation of a stronger monopole-quadrupole interaction with the tetrazine ring.

DFT and crystallographic results denote an important interplay of salt-bridge, hydrogen bond and anion-π interactions in stabilizing the thiocyanate complex. Nevertheless, salt-bridge interactions seem to have no effect when the complex is formed in aqueous solution. Equilibrium data determined for the formation of SCN⁻ complexes with neutral L2 and its protonated (charged) forms ($HL2^+$, H_2L2^{2+}) in water furnished association free energies that are almost independent of ligand charge, being 9.5(5), 10.7(5) and 10.8(4) kJ/mol for the formation of [(L2)SCN] , [(HL2)SCN] and $[(H_2L2)SCN]^+$, respectively (Table 3). A similar behaviour, although not so marked, was previously observed for the binding of other anions by L2 and the analogous L1 molecule [9], and suggests that anion-π interactions afford a prominent contribution to the stability of these complexes in a solvent, such as water, which has a high dielectric constant and is very competitive in the formation of hydrogen bonds. SCN⁻ ranks among the most hydrophobic anions of the Hofmeister series [1,25] and, accordingly, its association with the aromatic ligand moiety, resembling a π–π stacking interaction, is not expected to be much hampered by the polar solvent. As a matter of fact, it was previously shown that lowering the dielectric constant of water by addition of ethanol results in a drop of stability of L2 complexes with several anions [9a]. As already observed for other anion complexes with L2 [9], also in the presence of SCN⁻ only 1:1 anion:ligand species were detected in solution with the potentiometric method, despite the fact that, in the solid state, the ligand gives rise to symmetrical 2:1 assemblies. This is a common circumstance in the formation of weak complexes in solution, especially in water, the binding of the second anion not affording enough stabilization energy to become a detectable process.

4. Conclusions

Polyfunctional ligands are striking receptors of anions since they take advantage from multiple weak binding forces. In the crystal structure of $H_2L2(SCN)_2$, the protonated ligand furnishes a firm anchorage to SCN⁻ anions via salt-bridge, anion-π and hydrogen bond interactions. The resulting binding mode of SCN⁻, resembling a π–π stacking interaction with the tetrazine ring, is apparently determined by the interplay of these forces. Nevertheless, DFT calculations performed in a simulated implicit water environment showed that, even in the absence of other concurring binding forces, anion-π interactions afford enough stabilization for complex formation. In the most stable complex, the SCN⁻ anion and the tetrazine ring acquire a π–π stacking interaction mode with the N atom of the anion over the aromatic ring as in the crystal structure.

Moreover, thermodynamic data obtained for SCN⁻ binding with neutral L2 and its protonated forms ($HL2^+$, H_2L2^{2+}) showed that the stability of the resulting complexes is poorly correlated with ligand charge, further suggesting that anion-π interactions give a prominent contribution to the stability of these complexes. This is a peculiarity of L2 (and L1), since salt-bridge and hydrogen bond interactions are known to be of upmost importance in promoting the formation of anion complexes with most of ammonium receptors [26].

Acknowledgements

Italian MIUR (project 2015MP34H3) is gratefully acknowledged for financial support. The centre of instrumental facilities, STI, of the University of Jaén is acknowledged for technical assistance. FP thanks the Department of Applied Chemistry of the Graduate School of Engineering of Tohoku University for financial support.

Appendix A. Supplementary data

CCDC 1533369 contains the crystallographic data of the structural analysis. These data can be obtained free of charge from the Cambridge Crystallographic Data Centre via the www.ccdc.cam.ac.uk/data_request/cif. Supplementary data associated with this article can be found, in the online version, at http://dx.doi.org/10.1016/j.ica.2017.04.029.

References

[1] (a)K. Bowman-James, A. Bianchi, E. Garcia-España (Eds.), Anion Coordination Chemistry, Wiley-VCH, New York, 2012;
(b) J.L. Sessler, P.A. Gale, W.S. Cho, Anion Receptor Chemistry (Monographs in Supramolecular Chemistry), RSC Publishing, Cambridge, 2006.

[2] D. Quiñonero, A. Frontera, P.M. Deyà, Anion-π interactions in molecular recognition, in: K. Bowman-James, A. Bianchi, E. Garcia-España (Eds.), Anion Coordination Chemistry, Wiley-VCH, New York, 2012.
[3] (a) M. Giese, M. Albrecht, K. Rissanen, Chem. Comm. 52 (2016) 1778–1795; (b) X. Lucas, A. Bauzá, A. Frontera, D. Quiñonero, Chem. Sci. 7 (2016) 1038–1050; (c) M. Giese, M. Albrecht, K. Rissanen, Chem. Rev. 115 (2015) 8867–8895; (d) S.E. Wheeler, J.W.G. Bloom, J. Phys. Chem. A 118 (2014) 6133–6147; (e) P. Gamez, Inorg. Chem. Front. 1 (2014) 35–43; (f) H.T. Chifotides, K.R. Dunbar, Acc. Chem. Res. 46 (2013) 894–906; (g) P. Ballester, Acc. Chem. Res. 46 (2013) 874–884; (h) M.M. Watt, M.S. Collins, D.W. Johnson, Acc. Chem. Res. 46 (2013) 955–966; (i) H.-J. Schneider, Acc. Chem. Res. 46 (2013) 1010–1019; (j) P. Arranz-Mascarós, C. Bazzicalupi, A. Bianchi, C. Giorgi, M.L. Godino-Salido, M.D. Gutierrez-Valero, R. Lopez-Garzón, M. Savastano, J. Am. Chem. Soc. 135 (2013) 102–105; (k) E.S. Wheeler, Acc. Chem. Res. 46 (2013) 1029–1038; (l) A. Frontera, P. Gamez, M. Mascal, T.J. Mooibroek, J. Reedijk, Angew. Chem. Int. Ed. 50 (2011) 9564–9583; (m) L.M. Salonen, M. Ellermann, F. Diederich, Angew. Chem. Int. Ed. 50 (2011) 4808–4842; (n) I. Alkorta, F. Blanco, P. Deyà, J. Elguero, C. Estarellas, A. Frontera, D. Quiñonero, Theor. Chem. Acc. 126 (2010) 1–14; (o) O.B. Berryman, D.W. Johnson, Chem. Commun. (2009) 3143–3153; (p) C. Caltagirone, P.A. Gale, Chem. Soc. Rev. 38 (2009) 520–563; (q) H.-J. Schneider, Angew. Chem. Int. Ed. 48 (2009) 3924–3977; (r) B.L. Schottel, H.T. Chifotides, K.R. Dunbar, Chem. Soc. Rev. 37 (2008) 68–83; (s) B.P. Hay, V.S. Bryantsev, Chem. Commun. (2008) 2417–2428; (t) D. Quiñonero, C. Garau, C. Rotger, A. Frontera, P. Ballester, A. Costa, P.M. Deyà, Angew. Chem., Int. Ed. 41 (2002) 3389–3392; (u) M. Mascal, A. Armstrong, M.D. Bartberger, J. Am. Chem. Soc. 124 (2002) 6274–6276; (v) I. Alkorta, I. Rozas, J. Elguero, J. Am. Chem. Soc. 124 (2002) 8593–8598; (w) K. Hiraoka, S. Mizuse, S. Yamabe, J. Phys. Chem. 91 (1987) 5294–5297.
[4] (a) Z.A. Tehrani, K.S. Kim, Int. J. Quantum Chem. 116 (2016) 622–633; (b) J.-Z. Liao, H.-L. Zhang, S.-S. Wang, J.-P. Yong, X.-Y. Wu, R. Yu, C.-Z. Lu, Inorg. Chem. 54 (2015) 4345–4350; (c) M. Savastano, P. Arranz-Mascarós, C. Bazzicalupi, A. Bianchi, C. Giorgi, M.L. Godino-Salido, M.D. Gutiérrez-Valero, R. López-Garzón, RSC Adv. 4 (2014) 58505–58513; (d) P. Arranz, A. Bianchi, R. Cuesta, C. Giorgi, M.L. Godino, M.D. Gutiérrez, R. López, A. Santiago, Inorg. Chem. 49 (2010) 9321–9332; Inorg. Chem. 51 (2012) 4883.
[5] (a) P.A. Gale, C. Caltagirone, Chem. Soc. Rev. 44 (2015) 4212–4227; (b) N.H. Evans, P.D. Beer, Angew. Chem. Int. Ed. 53 (2014) 11716–11754.
[6] (a) A. Vargas Jentzsch, S. Matile, Top. Curr. Chem. 358 (2015) 205–239; (b) A. Vargas Jentzsch, S. Matile, J. Am. Chem. Soc. 135 (2013) 5302–5303; (c) A. Vargas Jentzsch, A. Hennig, J. Mareda, S. Matile, Acc. Chem. Res. 46 (2013) 2791–2800; (d) A. Vargas Jentzsch, D. Emery, J. Mareda, S.K. Nayak, P. Metrangolo, G. Resnati, N. Sakai, S. Matile, Nat. Commun. 3 (2012) 905; (e) J. Misek, A. Vargas Jentzsch, S. Sakurai, D. Emery, J. Mareda, S. Matile, Angew. Chem. Int. Ed. 49 (2010) 7680–7683; (f) L. Adriaenssens, C. Estarellas, A. Vargas Jentzsch, M. Martinez Belmonte, S. Matile, P. Ballester, J. Am. Chem. Soc. 135 (2013) 8324–8330; (g) A. Vargas Jentzsch, D. Emery, J. Mareda, P. Metrangolo, G. Resnati, S. Matile, Angew. Chem. Int. Ed. 50 (2011) 11675–11678.
[7] (a) L.E. Solis-Delgado, A. Ochoa-Teran, A.K. Yatsimirsky, G. Pina-Luis, Anal. Lett. 49 (2016) 2301–2311; (b) J. Sabek, L. Adriaenssens, T. Guinovart, E.J. Parra, F.X. Rius, P. Ballester, P. Blondeau, Chem. Eur. J. 21 (2015) 448–454; (c) M.M. Watt, L.N. Zakharov, M.M. Haley, D.W. Johnson, Angew. Chem. Int. Ed. 52 (2013) 10275–10280; (d) S. Guha, S. Saha, J. Am. Chem. Soc. 132 (2010) 17674–17677; (e) H.T. Chifotides, B.L. Schottel, K.R. Dunbar, Angew. Chem. Int. Ed. 49 (2010) 7202–7207; (f) J. Yoo, M.-S. Kim, S.-J. Hong, J.L. Sessler, C.-H. Lee, J. Org. Chem. 74 (2009) 1065–1069; (g) M. Mascal, I. Yakovlev, E.B. Nikitin, J.C. Fettinger, Angew. Chem. Int. Ed. 46 (2007) 8782–8784; (h) M. Mascal, Angew. Chem. Int. Ed. 45 (2006) 2890–2893.
[8] (a) C. Wang, F.N. Miros, J. Mareda, N. Sakai, S. Matile, Angew. Chem. Int. Ed. 55 (2016) 14422–14426; (b) L. Liu, Y. Cotelle, A.-J. Avestro, N. Sakai, S. Matile, J. Am. Chem. Soc. 138 (2016) 7876–7879; (c) Y. Zhao, S. Benz, N. Sakai, S. Matile, Chem. Sci. 6 (2015) 6219–6223; (d) Y. Zhao, N. Sakai, S. Matile, Nat. Commun. 5 (2014) 3911; (e) Y. Zhao, C. Beuchat, Y. Domoto, J. Gajewy, A. Wilson, J. Mareda, N. Sakai, S. Matile, J. Am. Chem. Soc. 136 (2014) 2101–2111; (f) T. Lu, S.E. Wheeler, Org. Lett. 16 (2014) 3268–3271; (g) P. Phuengphai, S. Youngme, I. Mutikainen, J. Reedijk, Inorg. Chem. Commun. 24 (2012) 129–133; (h) C. Estarellas, A. Frontera, D. Quiñonero, P.M. Deyà, Angew. Chem. Int. Ed. 50 (2011) 415–418.
[9] (a) M. Savastano, C. Bazzicalupi, C. García, M.D. López de la Torre, F. Pichierri, A. Bianchi, M. Melguizo, Inorg. Chem. 55 (2016) 8013–8024; (b) M. Savastano, C. Bazzicalupi, C. García, M.D. López de la Torre, P. Mariani, F. Pichierri, A. Bianchi, M. Melguizo, Dalton Trans. 46 (2017) 4518–4529.
[10] (a) W. De-Xian, W. Mei-Xiang, J. Am. Chem. Soc. 135 (2013) 892–897; (b) H. Bing, L. Jianjiang, K.K. Jay, Cryst. Growth Des. 8 (2008) 1327–1334.
[11] C. Bazzicalupi, A. Bianchi, T. Biver, C. Giorgi, S. Santarelli, M. Savastano, Inorg. Chem. 53 (2014) 12215–12224.
[12] P. Gans, A. Sabatini, A. Vacca, Talanta 43 (1996) 1739–1753.
[13] CrysAlisPro, Agilent Technologies, Version 1.171.38.41r.
[14] O.V. Dolomanov, L.J. Bourhis, R.J. Gildea, J.A.K. Howard, H. Puschmann, J. Appl. Cryst. 42 (2009) 339–341.
[15] G.M. Sheldrick, Acta Crystallogr. C71 (2015) 3–8.
[16] Gaussian 09, Revision D.01, M.J. Frisch, G.W. Trucks, H.B. Schlegel, G.E. Scuseria, M.A. Robb, J.R. Cheeseman, G. Scalmani, V. Barone, B. Mennucci, G.A. Petersson, H. Nakatsuji, M. Caricato, X. Li, H.P. Hratchian, A.F. Izmaylov, J. Bloino, G. Zheng, J.L. Sonnenberg, M. Hada, M. Ehara, K. Toyota, R. Fukuda, J. Hasegawa, M. Ishida, T. Nakajima, Y. Honda, O. Kitao, H. Nakai, T. Vreven, J.A. Jr. Montgomery, J.E. Peralta, F. Ogliaro, M. Bearpark, J.J. Heyd, E. Brothers, K.N. Kudin, V.N. Staroverov, R. Kobayashi, J. Normand, K. Raghavachari, A. Rendell, J. C. Burant, S.S. Iyengar, J. Tomasi, M. Cossi, N. Rega, J.M. Millam, M. Klene, J.E. Knox, J.B. Cross, V. Bakken, C. Adamo, J. Jaramillo, R. Gomperts, R.E. Stratmann, O. Yazyev, A.J. Austin, R. Cammi, C. Pomelli, J.W. Ochterski, R.L. Martin, K. Morokuma, V.G. Zakrzewski, G.A. Voth, P. Salvador, J.J. Dannenberg, S. Dapprich, A.D. Daniels, Ö. Farkas, J.B. Foresman, J.V. Ortiz, J. Cioslowski, D.J. Fox, Gaussian, Inc., Wallingford CT, 2009.
[17] J.-D. Chai, M. Head-Gordon, Phys. Chem. Chem. Phys. 10 (2008) 6615–6620.
[18] R. Ditchfield, W.J. Hehre, J.A. Pople, J. Chem. Phys. 54 (1971) 724–728.
[19] W.J. Hehre, R. Ditchfield, J.A. Pople, J. Chem. Phys. 56 (1972) 2257–2261.
[20] J. Tomasi, B. Mennucci, R. Cammi, Chem. Rev. 105 (2005) 2999–3093.
[21] S.F. Boys, F. Bernardi, Mol. Phys. 19 (1970) 553–566.
[22] A.E. Reed, L.A. Curtiss, F. Weinhold, Chem. Rev. 88 (1988) 899–926.
[23] F. Jensen, Introduction to Computational Chemistry, second ed., Wiley, Chichester, 2007.
[24] CSD version 5.37, last update Feb 2016.
[25] F. Hofmeister, Arch. Exp. Patol. Pharmakol. 24 (1888) 247–260.
[26] (a) P. Mateus, B. Bernier, R. Delgado, Coord. Chem. Rev. 254 (2010) 1726–1747; (b) K. Bowman-James, Acc. Chem. Res. 38 (2005) 671–678; (c) E. Garcia-España, P. Díaz, J.M. Llinares, A. Bianchi, Coord. Chem. Rev. 250 (2006) 2952–2986; (d) A. Bianchi, M. Micheloni, P. Paoletti, Inorg. Chim. Acta 151 (1988) 269–272.

7 ACKNOWLEDGEMENTS (*REDDITE CAESARI*)

Many are the people I am indebted to for this thesis project as well as for my growth, both personal and as a chemist.

I have to begin with my *Ph.D.* advisor, supervisor of this project, Professor Antonio Bianchi. Despite *Professore* (Professor) being his legitimate title, I mostly think of him as a *Maestro*: don't be fooled, the English "master" cannot really render the nuance of the Italian word. Sure, a *maestro* is a teacher and a true master of the art, but is also a person to whom you are attached and that feels affection for you as well (which is why children use *maestro* in the everyday sense to refer to their elementary teachers). *"A caring mentor, possessing full expertise in its own area and gladly willing to share"*, would not be a totally bad translation.

In my experience within the Academia I had the chance of meeting many Professors, thou coming across a *Maestro* is something that happens maybe once in a lifetime.

Maestro, is also a term reminiscent of the old times, especially here in Florence, as the title was not reserved to scholars, but also master artisans: the world-famous master painters and sculptors of the Renaissance bore that title as well. When I look back at these years, an old way of saying comes to mind: *"andare a bottega"* which translates approximately into *"going to the studio"* or *"going to the workshop"*. This saying really dates back to Renaissance, when families sent gifted children to work and live with a Maestro, a famous artist, helping him in his workshop while getting the chance of learning from the best at the same time. At times, payment was not even required, as true masters recognized talented children and offered the parents to educate their sons for free, lest their gift would else be wasted. Theory and practice blended together, studying perspective and grinding the pigments being equally important to ultimately master the art. In this sense, Chemistry is no different, proceeding at the same time from the knowledge in our brains and the skill in our hands.

I am grateful beyond words for the time and efforts Professor Bianchi profusely dedicated to my education and training, in general, and to this thesis project in particular. I learned much and yet have much to learn, looking forward to prosecuting my growth under his guidance. Lastly, I want to thank him for the kindness and friendship he invariably demonstrated.

Second, the esteemed friends from the Carbon group of the University of Jaén, Spain, which gladly hosted me as a graduate student and disclosed their surface functionalization techniques. Hospitality and gratitude tie me to Professors Rafael López Garzón, Paloma Arranz Mascarós, María Luz Godino Salido and María Dolores

Gutiérrez Valero. The number of papers published together through these years speaks for a long-lasting collaboration and friendship.

Probability would say there is a limited number of awesome people you may expect to come across in just one trip: apparently Jaén challenges the law of large numbers.

In fact, the aforementioned people are not the only "*jienenses*" I have had the pleasure to meet and subsequently work with. Professors Celeste García Gallarín, María Dolores López de la Torre and Manuel Melguizo Guijarro are gratefully acknowledged. Sure, tetrazine-based ligands would not have seen the light without them, but they deserve credit also for the throughout fruitful discussion. Professor Manuel Melguizo Guijarro, with whom I had the chance and pleasure to be more in contact with on the spot, is also a prime example of the kindness and hospitality you would like to encounter when going abroad.

After spending some time there, one cannot help but realizing that the famous warmth of Andalucía is really not a matter of sun, but comes straight from the kind heart of its inhabitants.

I do not need to spend much words on the Florence research group, which is of course acknowledged, as there will be plenty of occasions to show my appreciation. Considering the amount of solved crystal structures, which despite the long-lasting collaboration helped us getting in touch on a more personal level in the last three years, Professor Carla Bazzicalupi, our crystallographic supervisor, has well-deserved an explicit mention. Once more, giving credit for the crystallographic work is exceedingly restrictive: scientific discussion with international experts is always a good thing, having one just a few steps away from your doorway really allows for a continuous and fruitful exchange, for which I wish to thank Professor Carla Bazzicalupi once more.

Timewise, we arrive at my most recent host, Professor Enrique García-España Monsonís and his renown Supramolecular Chemistry Group based in Valencia, Spain, where I spent almost six months during the Ph.D. program. The well-known Spanish hospitality, a widespread trait of the Mediterranean Europe I guess, was once more well-represented. Beyond expressing my gratitude to him and the whole research group, several of them being or going to become co-authors in a number of papers, I want to spend a few words praising our collaboration. It is no mystery that Professor Bianchi and Professor García-España are longstanding co-workers and, beyond chemistry, long-time friends. I consider myself a "Brussel sprout", in the sense that I fully belong to that pan-European generation who got struck down by the recent reappearance of individual nationalisms and by the Brexit event. Being part of a long lasting scientific partnership, eventually contributing to build-up the

second generation of a healthy cooperation by cultivating fruitful relationships with my Valencian peers (thinking especially of Elena and Lluís), really makes me appreciate the “Good Science”, able to bring together experts from around the globe beyond any restriction imposed by national boundaries.

In thanking the Supramolecular Chemistry Group of Valencia once more, I wish them and myself many other years of good friendship and first-rate science.

Speaking of the ability of Science to promote worldwide collaboration, our furthest co-worker, Prof. Fabio Pichierri, based in Tohoku University in Sendai, Japan, needs to be thankfully acknowledged. Prof. Pichierri is in charge of the computational quantum chemistry part of the anion studies, with much of his work being disseminated through these pages.

We end the institutional part of these acknowledgements by thanking all the co-authors and the people I had the pleasure to work with within the framework of this thesis project.

On a more personal side, my parents need to be mentioned. Set aside the affection and the human participation, when I look back at my studies I clearly realize that, if the journals allowed, “M.S. wishes to acknowledge financial contribution from his own parents” should legitimately appear on every paper. Thank you for everything you have done for me through the years.

The chemical part of these acknowledgements is really not over, blending with the most private part of them in expressing my gratitude to Giulia.

She has been by my side from the very beginning of this *Ph.D.*, I clearly remember the joy when together we discovered I was awarded the grant and the position, up to now, laying next to me as I write these final lines, showing patience despite the last months of thesis writing; not even my Valencian adventure could divide us, as She generously placed me before herself, working much harder on her studies to be able to come with me. Beyond her love and caring attentions, which never failed to support me through the years (and cannot be really payed off with a thank), I am much indebted to her in many other ways. I am passionate about my job and I tend to be (as my Reader should have realised by now) a bit long-winded: coming home and finding a chemist like her, invariably exposes Giulia to my never-ending accounts, reasonings and outbursts. She could not be more concerned and patient, yet steady in supporting me, valuable in scientific discussion and irremovable from pointing out the right way to follow and bringing me back on it whenever I am going astray.

I do not consider myself an easy to handle person either, being a joker in disguise most of the time, while dramatically in need of others appreciation to be able to recognize my own worth when I am blue: She can magic all the unease away, always finding the words to make me smile again. Usually, one does not thank his own life support systems (finding lungs or cardiovascular system properly acknowledged would freak out any sane Reader), yet Giulia has had that kind of importance for me: I guess that is the proper effect the soul mate has.

Thank you, Giulia.

Last but not least, I want to thank you, Reader, the more so if you reached these final words without taking any shortcuts: I hope you have found in the text what you had been looking for, and eventually something more. Thank you for your time.